U.S. CENTERS FOR DISEASE CONTROL AND PREVENTION

EMERGING INFECTIOUS DISEASES®

Parasitic Diseases

September 2024

Winslow Homer (1836–1910). *On the Trail* (1889). Watercolor over graphite on wove paper, 12 5/8 in × 19 7/8 in/32.1 cm × 50.5 cm. Gift of Ruth K. Henschel in memory of her husband, Charles R. Henschel. National Gallery of Art, Washington, DC, USA. Open access image.

EMERGING INFECTIOUS DISEASES®

Emerging Infectious Diseases is published monthly by the Centers for Disease Control and Prevention, 1600 Clifton Rd NE, Mailstop H16-2, Atlanta, GA 30329-4018, USA. Telephone 404-639-1960; email, eideditor@cdc.gov

EMERGING INFECTIOUS DISEASES®

Parasitic Diseases **September 2024**

On the Cover

Winslow Homer (1836–1910). *On the Trail* (1889). Watercolor over graphite on wove paper, 12 5/8 in × 19 7/8 in/32.1 cm × 50.5 cm. Gift of Ruth K. Henschel in memory of her husband, Charles R. Henschel. National Gallery of Art, Washington, DC, USA. Open access image.

About the Cover p. 1982

Synopses

Research

Medscape EDUCATION ACTIVITY

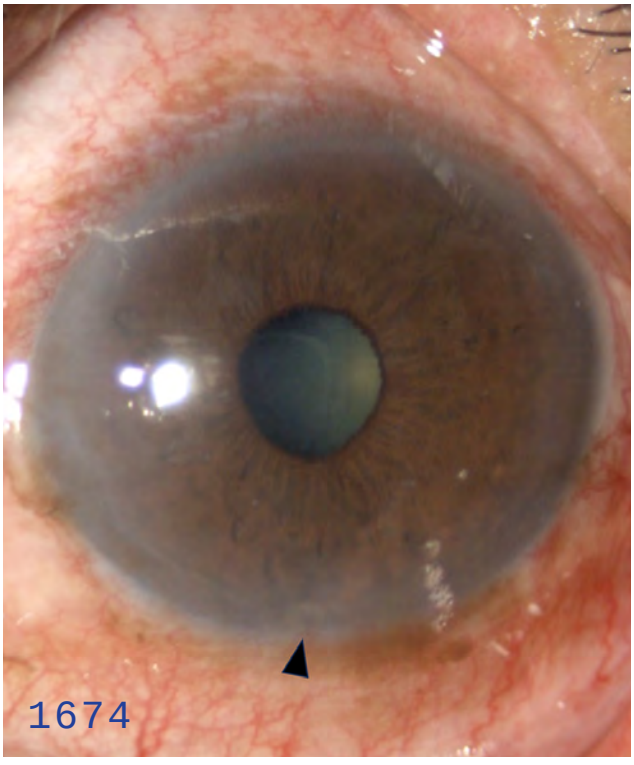

EMERGING INFECTIOUS DISEASES®
September 2024

Dispatches

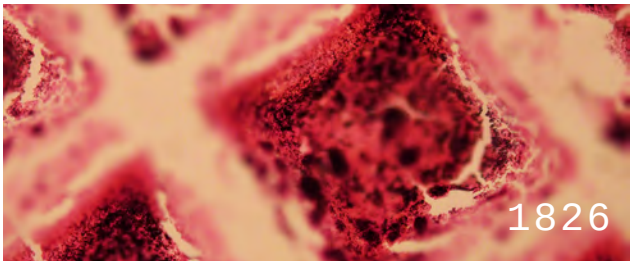

Photo Quiz

Research Letters

EMERGING INFECTIOUS DISEASES®
September 2024

Emerging Infections Network Letter

In Memoriam

About the Cover

Corrections

Vol. 30, No. 5 **1980**
The name of author Glenn Patriquin was misspelled in Case Series of Jamestown Canyon Virus Infections with Neurologic Outcomes, Canada, 2011–2016 (V. Meier-Stephenson et al.).

Vol. 30, No. 8 **1980**
The name of author Carlos E. Sanz-Rodriguez was misspelled in Outbreak of Intermediate Species *Leptospira venezuelensis* Spread by Rodents to Cows and Humans in *L. interrogans*–Endemic Region, Venezuela (L. Caraballo et al.).

Emerging Infectious Diseases
Photo Quiz Articles

Volume 14, Number 9
September 2008

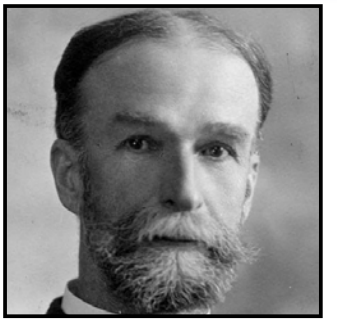

Volume 14, Number 12
December 2008

Volume 15, Number 9
September 2009

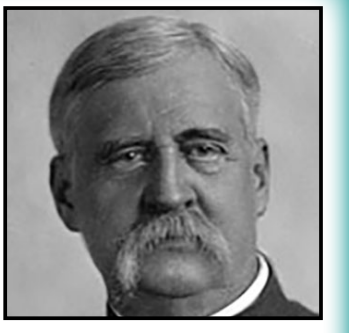

Volume 15, Number 10
October 2009

Volume 16, Number 6
June 2010

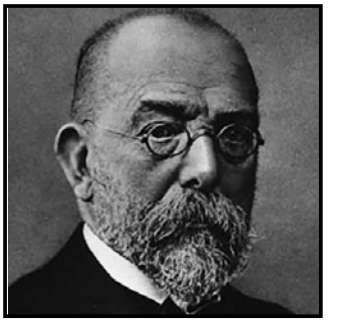

Volume 17, Number 3
March 2011

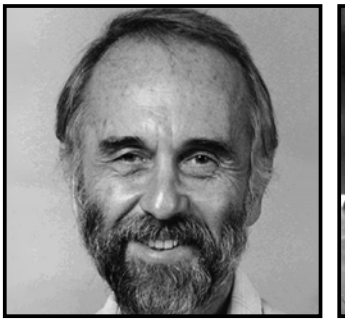

Volume 17, Number 12
December 2011

Volume 19, Number 4
April 2013

Volume 20, Number 5
May 2014

Volume 21, Number 9
September 2015

Volume 22, Number 8
August 2016

Volume 28, Number 3
March 2022

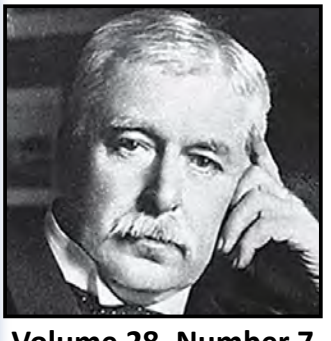

Volume 28, Number 7
July 2022

Click on the link below to read about the people behind the science.

https://bit.ly/3LN02tr

See requirements for submitting a photo quiz to EID.

https://bit.ly/3VUPqfj

EID Journal

Onward Virus Transmission after Measles Secondary Vaccination Failure

Isaac Tranter, Nicolas Smoll, Colleen L. Lau, Dusty-Lee Williams, Deborah Neucom, Donna Barnekow, Amalie Dyda

Measles in persons with secondary vaccination failure (SVF) may be less infectious than cases in unvaccinated persons. Our systematic review aimed to assess transmission risk for measles after SVF. We searched PubMed, Embase, and Web of Science databases from their inception dates. Inclusion criteria were articles describing persons who were exposed to measles-infected persons who had experienced SVF. Across the included 14 studies, >3,030 persons were exposed to measles virus from SVF cases, of whom 180 were susceptible, indicating secondary attack rates of 0%–6.25%. We identified 109 cases of SVF from the studies; 10.09% (n = 11) of case-patients transmitted the virus, resulting in 23 further cases and yielding an effective reproduction number of 0.063 (95% CI 0.0–0.5). These findings suggest a remarkably low attack rate for SVF measles cases, suggesting that, In outbreak situations, public health management of unvaccinated persons could be prioritized over persons with SVF.

Measles virus is one of the most infectious pathogenic agents and has a basic reproduction number (R_0) of 12–18, indicating that each infected person could infect 12–18 other susceptible persons (*1*). In 2022, measles caused an estimated 136,000 deaths globally and predominantly affected unvaccinated persons and undervaccinated children ≤5 years of age (*1*). Despite the number of deaths, measles vaccination has averted an estimated 57 million deaths in the 22 years since 2000 (*1*). Because of exclusive interhuman transmission, the existence of an effective and safe live attenuated vaccine, and the absence of healthy carriers, measles is inherently an eradicable disease. By 2023, a total of 82 countries had achieved measles elimination through high immunization coverage (*2*).

Despite the effectiveness of measles-containing vaccines, infection remains possible in immunized persons. This phenomenon has come to be known as vaccination failure. Two types of vaccination failure have been documented. Primary vaccination failure (PVF) results from a person's failure to produce any humoral response to viral antigen (nonseroconversion) and is thought to occur in 5% of vaccinees (*3*). Secondary vaccination failure (SVF) seems to occur 6–26 years after the last vaccine dose and is a result of waning or incomplete immunity. SVF occurs in 2%–10% of vaccinated persons (*4*).

Measles infection after SVF, also known as modified measles, is generally milder (i.e., less cough, coryza, conjunctivitis, or fever), is associated with lower viral loads, and has lower risk for complicated disease (*5*). This form of measles is thought to occur because of insufficient but not absent immune response. Stated differently, immunity is sufficient to curtail symptoms and viral replication but insufficient to prevent infection. Muted symptoms in this scenario makes identification of measles cases on the basis of classical features unreliable.

In the postelimination setting, cases of measles after vaccination failure make up a higher proportion of total cases. This situation occurs when fewer unvaccinated persons exist to acquire the infection and the only remaining susceptible persons are those experiencing vaccination failure (*6*). In addition, in settings where measles does not commonly circulate, vaccinated persons are not exposed to wild virus and hence do not receive a natural booster (*7*). In the endemic setting, vaccinated persons make up 3%–8% of measles cases (*4*), in contrast to 14%–57% of cases

Author affiliations: University of Queensland, Herston, Queensland, Australia (I. Trantner, N. Smoll, C.L. Lau, A. Dyda); Sunshine Coast Hospital and Health Service, Maroochydore, Queensland, Australia (N. Smoll, D.-L. Williams, D. Neucom, D. Barnekow)

DOI: https://doi.org/10.3201/eid3009.240150

in postelimination settings (*4*). This gap is likely the product of SVF because of waning immunity and the absence of natural immune boosters, rather than a primary vaccination failure, which would not be affected by the prevalence of circulating virus.

No universally agreed upon definition for measles SVF exists; however, several methods of classification have been suggested. The best methods remain the serum detection of IgG after vaccination but before infection and the avidity enzyme immunoassay. Measles IgG develops later in the course of infection (typically 7–10 days postinfection) and persists for long periods (generally for life) (*8*). IgG avidity index can determine recent (low avidity IgG, <40%) or past (high avidity, IgG >60%) exposure to the measles virus (*9*). Persons experiencing SVF are characterized by early production of IgG (before day 7 of infection) with a high avidity index (*10*). IgM may be produced in both novel and breakthrough measles infections. However, the absence of IgM in the presence of IgG within 7 days of infection is indicative of prior exposure and is another indicator of SVF (*9*).

Persons with SVF cases have lower measles viral loads in bodily fluids than do unvaccinated persons. Cycle threshold (Ct) values of real-time reverse transcription PCR are a semiquantitative measure of measles RNA loads (*11*). Higher Ct values equate to lower numbers of measles RNA copies in a sample and hence lower transmissibility (*11*).

It has been hypothesized that, because of reduced symptomatology and lower viral loads, SVF patients are less likely to transmit the measles virus (*11*–*14*). Our review aimed to determine the risk for transmission by persons with SVF for 2 key reasons: measles occurring post-SVF will increasingly make up a greater proportion of total cases in the postelimination setting, and an understanding of the different transmission dynamics in preelimination versus postelimination settings will enable more precise design and implementation of outbreak responses.

Methods

This systematic review followed a study protocol registered with the International Prospective Register of Systematic Reviews before the date of first search. We followed the Preferred Reporting Items for Systematic review and Meta-analyses guidelines for reporting (*15*).

Eligibility

This review included original, nonreview articles, published in English or French. The report must have described a person or cohort of persons who were exposed to a laboratory-confirmed measles-infected person who had experienced SVF. We defined confirmed measles through 3 methods: PCR detection of measles virus, detection of a ≥4-fold increase in measles IgG titer in the absence of recent vaccination with a measles-containing vaccine, or detection of measles IgM in the absence of recent vaccination with a measles-containing vaccine. We defined recent vaccination as administration of a measles-containing vaccine within the preceding 8 days–8 weeks. Given the unreliable nature of clinical signs and symptoms in measles SVF cases, we did not include signs and symptoms in the case definition for the purpose of this analysis.

We defined SVF as measles infection despite serologic immunity after documented or reported immunization with a measles-containing vaccine. Evidence of serologic immunity included documentation of a positive measles IgG result before exposure, high avidity measles IgG postinfection (>60%), concurrent positive IgG and negative IgM results within 7 days of infection, or early positive IgG alone within 7 days of infection. For inclusion we required that the report specify the number of exposed persons who then had a laboratory-confirmed case of measles within the next 21 days.

The original study protocol sought only to included articles that reported an attack rate post-SVF. However, to ensure transmission risk was fully reviewed, we completed an amendment to the study protocol to include any study that discussed onward transmission.

Search Strategy and Study Selection

We searched PubMed, Embase, and Web of Science databases from their respective dates of inception through May 31, 2023, when the search was conducted (Appendix 1, https://wwwnc.cdc.gov/EID/article/30/9/24-0150-App1.pdf). We also searched citation lists of review articles and studies that met inclusion criteria for articles not already included. We also sought input from subject matter experts to minimize the chances of relevant studies being missed. We uploaded all articles found through these search processes to Covidence software (https://www.covidence.org), and 2 authors (I.T. and A.D.) screened titles and abstracts and then full texts. We resolved conflicts through collaborative discussion and referral to a third reviewer when required.

Data Extraction and Quality Assessment

One author (I.T.) extracted data from studies meeting the inclusion criteria. The data extracted

included study setting, location, SVF case definition, SVF case numbers, onward transmissions, exposure population sizes, and susceptible population size (i.e., persons who had not received ≥1 dose of measles-containing vaccine, had not received postexposure prophylaxis [PEP], were immunocompromised, or had unknown vaccination status). In addition, we recorded data on the administration of PEP with either measles-containing vaccine or measles immunoglobulin to all contacts involved in the outbreak rather than only those in contact with the SVF case-patient. We used PEP data to serve as a proxy for the strength of public health response taken. We recorded Ct value and IgG avidity data, where available, as the mean value of SVF cases in the dataset. A second author (A.D.) checked extracted data; we resolved discrepancies through discussion.

We used Joanna Briggs Institute methodological quality of case series studies critical appraisal tool to assess both quality and risk for bias of the studies included (Appendix 2 Table 1, https://wwwnc.cdc.gov/EID/article/30/9/24-0150-App2.xlsx). We assessed publication bias by using a quasi-funnel plot with the point estimate of effective reproduction number (R_{eff}) on the x-axis and total cases of SVF on the y-axis. We assessed the presence of bias on the basis of distribution of results.

Data Analysis

R_{eff} Calculation

R_{eff} is the expected number of secondary cases produced by a typical infected person during their entire infectious period. R_{eff} is used in situations where the exposed population has a nonzero proportion of nonsusceptible persons (by natural immunity or vaccination) or public health measures are in place (e.g., movement restrictions and PEP requirements) (*16*). This situation is often observed in the SVF studies performed in high-income countries with high vaccination rates.

Directly Calculated R_{eff}

We estimated R_{eff} after SVF by using the direct calculation approach. To ensure this estimate was robust, we demonstrated that this methodology is equivalent to traditional methods of estimating reproductive numbers (e.g., survivor function and ordinary differential equations) (Appendix 1). We calculated the direct R_{eff} by using simple division of the total number of secondary measles cases by the total number of primary SVF cases.

Estimated R_{eff}

We calculated the direct R_{eff} from each study in which SVF cases and total transmissions were reported. We then obtained the estimated R_{eff} by using bootstrapped median and bootstrapped 95% CIs (2.5%–97.5%). We used that method because there is no known sampling distributions for the direct R_{eff} and the intervals were not expected to be symmetric.

Secondary Attack Rate

We calculated the secondary attack rate by using the number of new measles cases arising from exposure to an SVF case-patient as the numerator. We used the susceptible population exposed to this SVF case-patient as the denominator.

Results

The search yielded 1,327 articles, of which we removed 18 duplicates (Figure 1). We screened a total of 1,309 articles for inclusion, of which we excluded 1,295. We included a total of 14 studies in the final analysis. Three articles reported sufficient information from which to derive an attack rate (*17*–*19*). An additional 11 articles discussed transmission after measles SVF (Appendix 2 Table 2).

Nine studies were conducted in the healthcare setting, 1 in a military environment (*20*), and 4 in a community setting (*13*,*18*,*21*,*22*); 1 made reference to household contacts (*12*). All 14 studies were conducted in high-income or upper-middle–income countries.

Seven studies reported the administration of PEP with either measles-containing vaccine or measles immunoglobulin. Four of those studies reported administration of measles-containing vaccine (*12*,*13*,*20*,*23*), 3 studies reported measles immunoglobulin (*12*,*13*,*17*), and 2 studies reported administration of PEP but did not specify type (*18*,*19*).

Across the 14 studies, 109 cases of measles SVF had been identified (*4*,*12*,*13*,*17*–*27*). Of those cases, 11 (10.09%) were in persons who transmitted the virus, resulting in a total of 23 further measles cases (1–8 onward infections per transmitting case-patient) (*12*,*18*–*22*,*28*). Through the direct calculation method, those data yielded an R_{eff} of 0.211. The estimated R_{eff} was 0.063 (95% CI 0.0–0.5).

In the 6 studies that reported exposure population data, >3,030 persons were exposed to an SVF-affected person with measles during the infectious period (*17*–*20*,*23*,*27*); of those, 180 were considered susceptible (*17*–*19*). From the susceptible population, 5 infections occurred (*17*–*19*). We calculated a secondary

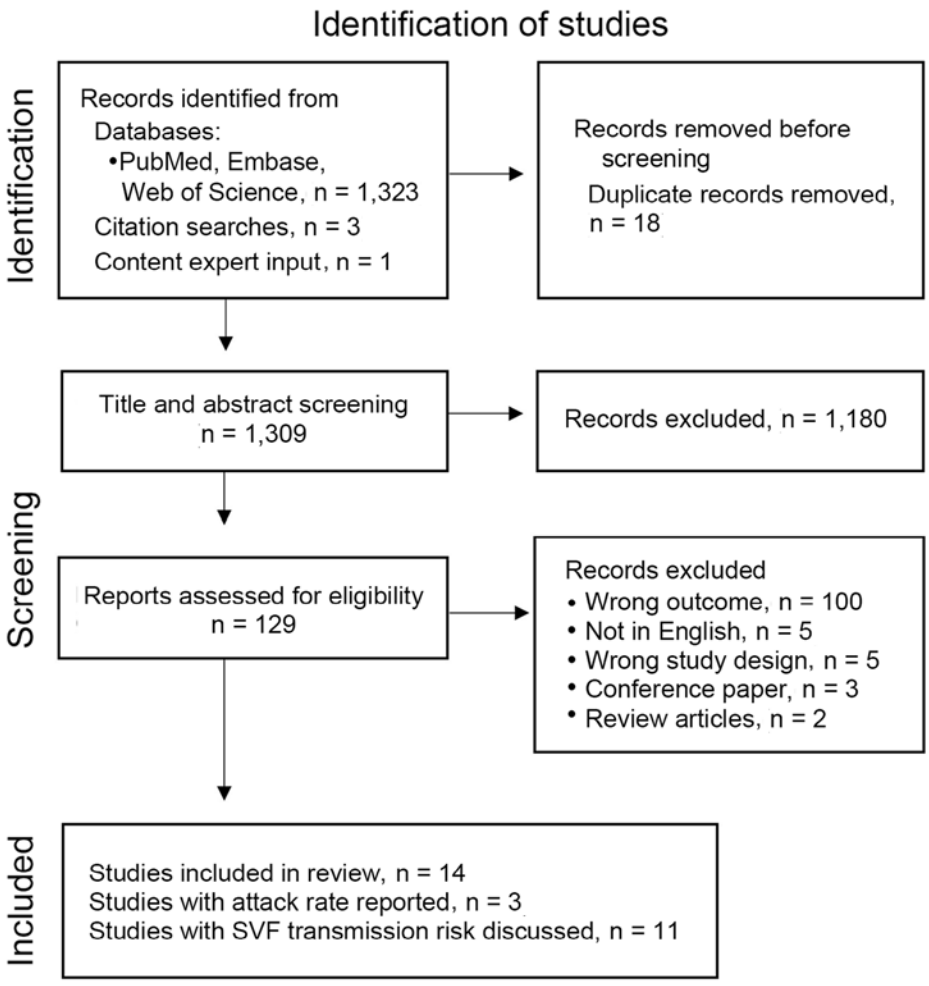

Figure 1. Flowchart of retrieved, excluded, and included items during systemic review of cases of onward virus transmission after measles SVF, as of March 31, 2023 (*15*). SVF, secondary vaccination failure.

attack rate from the 3 studies for which sufficient data were provided. The attack rate ranged from 0% (0/68) (*17*) to 6.25% (1/16) (*19*).

SVF was defined differently between studies. The most common method was high IgG avidity (77 persons) (*12*,*13*,*18*–*22*,*26*–*28*), followed by an IgM-negative or IgG-positive serologic profile (18 persons) (*24*,*25*). Thirteen persons had recorded measles IgG positivity before illness onset (*12*,*23*,*26*), and 1 person was classified on the basis of an early measles IgG result (day 2) (*17*).

Four studies reported Ct values from oropharyngeal samples, which ranged from 30.3 to 33.7 (*4*,*13*,*25*,*26*). Ten studies used IgG avidity to characterize SVF; 7 of those reported avidity values of 70.83%–88.6% (*12*,*13*,*18*–*20*,*22*,*26*).

We demonstrated the potential presence of publication bias as reviewed visually in the form of a quasi-funnel plot (Figure 2). Underreporting of outbreaks with large numbers of SVF cases with multiple transmission events may have occurred.

Sensitivity analyses (Figure 3), in which the SVF case definition, measles case definition, and report type were varied, yielded similar results to the main analysis. Isolation of studies where PEP was provided to susceptible populations also yielded similar results to the main analysis.

Discussion

This systematic review reports the attack rate and R_{eff} after measles SVF. We found 14 studies that reported the risk for measles infection after exposure to a person who experienced SVF. All included studies reported a very low attack rate (0%–6.25%) and R_{eff} (0.063 [95% CI 0.0–0.5]). Those findings suggests that persons with measles SVF have a very low risk for transmitting the disease.

Our findings are in keeping with the results of Gastañaduy et al. (*14*), who looked at the factors associated with measles transmission. Although they did not disaggregate PVF and SVF, they found an R_{eff} of 0.17 for persons who had received 1 dose of

a measles-containing vaccine and an R_{eff} of 0.27 for those who received ≥2 doses of a measles-containing vaccines. That finding was in contrast to a R_{eff} of 0.76 for unvaccinated persons (*14*).

Although the overall attack rate for persons exposed to SVT case-patients appears to be low, prolonged exposure and confined settings probably result in higher risk for transmission. The presence of acutely unwell patients in healthcare settings appears to be the most likely scenario to result in infection (*12*,*13*,*17*–*19*,*22*,*23*,*26*,*27*). This probability stands to reason given the close and prolonged exposure that medical and nursing staff have with their patients, proximity to other patients, and the highly aerosolizing symptoms (i.e., cough) that brought those patients to seek medical care. Moreover, having household contacts, living in confined housing situations (e.g., military barracks, residential dormitories) (*12*,*20*,*29*), and being in educational settings (e.g., schools, universities) have also been documented as potentially high risk for transmission (*29*,*30*).

Ct values attained from our review compare appropriately with those found in other studies. Pacenti et al. (*31*) found vaccination failure (both PVF and SVF) Ct values of 27.6 (SD ±4.8), whereas other authors reported median values of 32 (*13*). When comparing our result and those of other authors with unvaccinated controls (Ct 19.0–22.7) (*13*,*31*), we found that incidents of vaccine failure are more likely to have higher Ct values. These lower viral loads may be part of the explanation for the low attack rates attributable to SVF patients.

Another implication of this review is the observation that the attack rate after SVF appears to be exceptionally low. Although maintaining vigilance and appropriate measures remains crucial, the exceedingly low attack rate suggests that public health responses after SVF in high vaccination coverage regions could be implemented by using a transmission risk stratification approach. Because SVF case-patients are much less likely to transmit the virus, outbreak-control resources could be directed toward vaccine-naive and PVF-affected persons as a matter of priority. Public health follow-up will still be required for SVF-affected persons; however, such follow-up could occur once high transmission risk case-patients are managed. This approach would ensure the efficient use of resources, particularly during large outbreaks.

However, to properly inform any future public health responses, enhanced data collection and reporting surrounding the transmission dynamics after SVF is needed. Our study shows that data in this area are limited. To strengthen the evidence base, we advocate first for the development of a robust measles SVF case definition, then routine reporting of cases that meet that definition (*9*). In addition, reporting of exposed populations and attack rates is essential to create a more nuanced understanding of measles transmission from SVF case-patients. Standardizing data collection in this manner will render

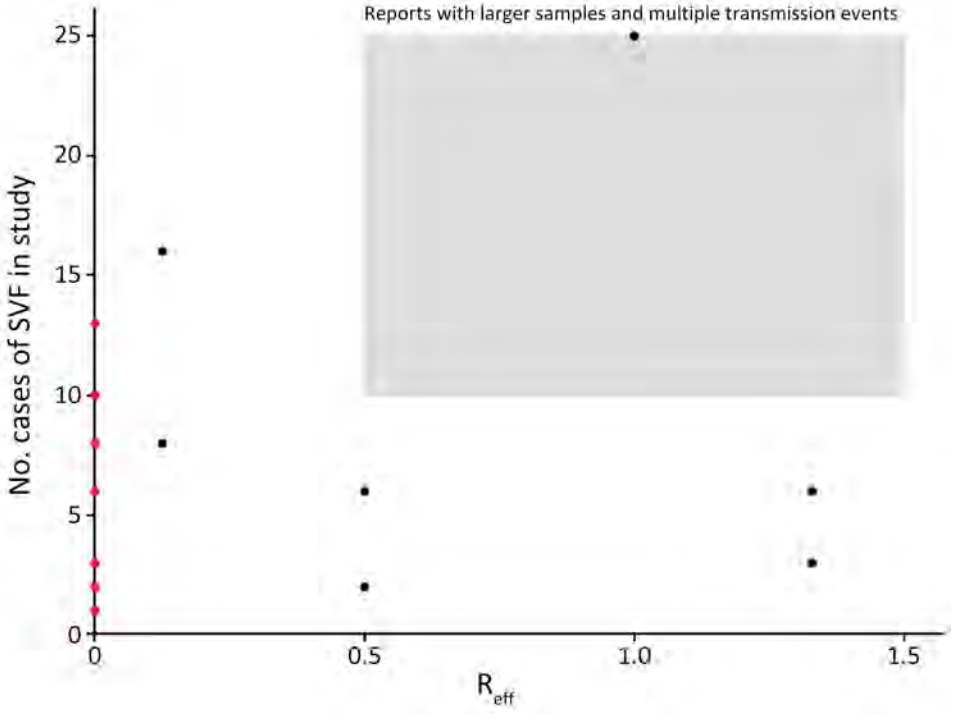

Figure 2. Study-specific effect size by total reported measles SVF cases identified during systemic review of cases of onward virus transmission after measles SVF, as of March 31, 2023. R_{eff}, effective reproduction number; SVF, secondary vaccination failure.

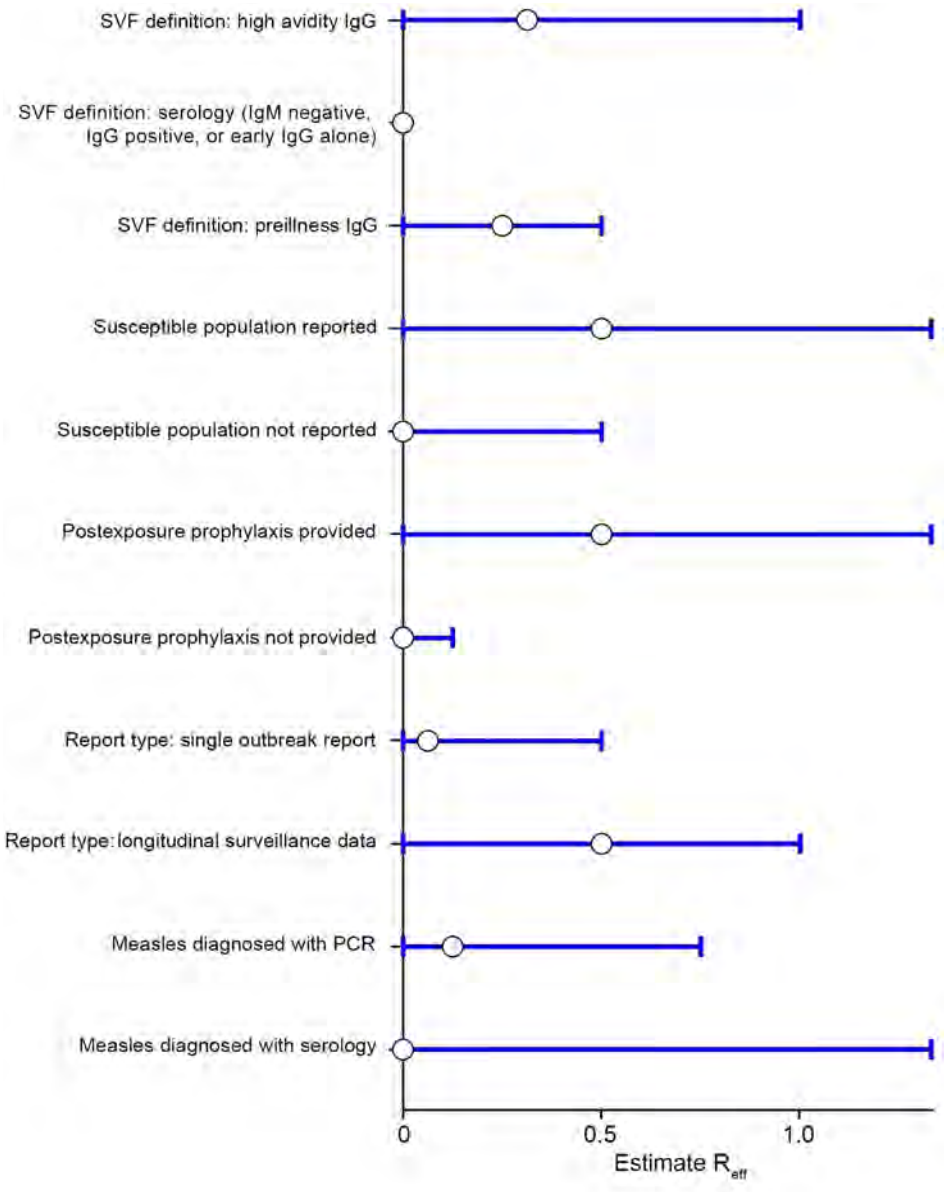

Figure 3. Sensitivity analysis of measles SVF cases identified during systemic review of cases of onward virus transmission after measles SVF, as of March 31, 2023. Error bars indicate 95% CIs. R_{eff}, effective reproduction number; SVF, secondary vaccination failure; –ve, negative; +ve, positive.

future research endeavors better equipped to analyze and interpret the implications of SVF, ultimately contributing to more effective and efficient public health strategies.

A key limitation of our study is potential publication bias. Underreporting of outbreaks that have high numbers of SVF but few or no reported transmission events is possible (Figure 2). This likelihood is consistent with investigators failing to report typical outbreaks (i.e., where persons with SVF transmit like persons without SVF). Another limitation of our analysis is the small sample size of studies available for analysis, which can make generalizability and confidence in the findings difficult and may not fully capture the variability and nuances of transmission after SVF. The lack of standardized criteria for defining SVF resulted in the exclusion of several potentially relevant studies from our analysis. The standard for defining SVF is the use of IgG avidity testing or preinfection serologic testing (*9*). Unfortunately, not all included studies had access to those diagnostic tools, instead relying on early infection course serologic test. Moreover, the reporting of exposed populations was deficient in many studies, limiting our ability to calculate an accurate attack rate. Of the studies that did report data on exposure populations, prior vaccination status was difficult to attain. In those instances, we classified persons who were unimmunized, were immunocompromised, or had any unknown vaccination

status as susceptible. Thus, persons with unknown vaccinations status might have been vaccinated and therefore nonsusceptible, which could have led to an overestimation of this susceptible population size and an underestimation of the calculated attack rate. Furthermore, the studies included in our analysis were predominantly conducted in postelimination settings, which may limit the generalizability of our findings to measles-endemic settings. On the other hand, this fact may also be a strength, given that SVF is far more common in the postelimination setting, meaning those studies may more accurately reflect real-world scenarios.

Our findings suggest that the risk for onward transmission from persons with measles SVF is very low but not zero. In large outbreak situations, public health management of measles cases in unvaccinated persons could be prioritized before SVF cases. In postelimination settings, routine serologic testing for SVF, in addition to the standard PCR tests, may be a useful adjunct for risk stratification during outbreak management.

About the Author

Dr. Tranter is a general practitioner and public health registrar at the University of Queensland. His primary research interests include qualitative and quantitative research methods that support communicable disease control.

References

1. World Health Organization. Measles. 2024 Jul 12 [cited 2024 Aug 1]. https://www.who.int/news-room/fact-sheets/detail/measles
2. Patel MK, Goodson JL, Alexander JP Jr, Kretsinger K, Sodha SV, Steulet C, et al. Progress toward regional measles elimination—worldwide, 2000–2019. MMWR Morb Mortal Wkly Rep. 2020;69:1700–5. https://doi.org/10.15585/mmwr.mm6945a6
3. Anders JF, Jacobson RM, Poland GA, Jacobsen SJ, Wollan PC. Secondary failure rates of measles vaccines: a metaanalysis of published studies. Pediatr Infect Dis J. 1996;15:62–6. https://doi.org/10.1097/00006454-199601000-00014
4. Fappani C, Gori M, Canuti M, Terraneo M, Colzani D, Tanzi E, et al. Breakthrough infections: a challenge towards measles elimination? Microorganisms. 2022;10:1567. https://doi.org/10.3390/microorganisms10081567
5. Hubiche T, Brazier C, Vabret A, Reynaud S, Roudiere L, Del Giudice P. Measles transmission in a fully vaccinated closed cohort: data from a nosocomial clustered cases in a teenage psychiatric unit. Pediatr Infect Dis J. 2019;38:e230–2. https://doi.org/10.1097/INF.0000000000002372
6. Arima Y, Oishi K. Letter to the editor: measles cases among fully vaccinated persons. Euro Surveill. 2018;23:1800449.
7. Markowitz LE, Preblud SR, Fine PE, Orenstein WA. Duration of live measles vaccine-induced immunity. Pediatr Infect Dis J. 1990;9:101–10. https://doi.org/10.1097/00006454-199002000-00008
8. Gastañaduy PA, Clemmons N, Redd SB, Clemmons NK, Lee AD, Hickman CJ, et al. Measles [chapter 7]. In: Roush SW, Baldy LM, editors. Manual for the surveillance of vaccine-preventable diseases. Atlanta: Centers for Disease Control and Prevention; 2019 [cited 2024 May 16]. https://www.cdc.gov/vaccines/pubs/surv-manual/chpt07-measles.html
9. Mercader S, Garcia P, Bellini WJ. Measles virus IgG avidity assay for use in classification of measles vaccine failure in measles elimination settings. Clin Vaccine Immunol. 2012;19:1810–7. https://doi.org/10.1128/CVI.00406-12
10. Javelle E, Colson P, Parola P, Raoult D. Measles, the need for a paradigm shift. Eur J Epidemiol. 2019;34:897–915. https://doi.org/10.1007/s10654-019-00569-4
11. Seto J, Ikeda T, Tanaka S, Komabayashi K, Matoba Y, Suzuki Y, et al. Detection of modified measles and super-spreader using a real-time reverse transcription PCR in the largest measles outbreak, Yamagata, Japan, 2017 in its elimination era. Epidemiol Infect. 2018;146:1707–13. https://doi.org/10.1017/S095026881800211X
12. Kurata T, Kanbayashi D, Egawa K, Kinoshita M, Yoshida H, Miyazono M, et al. A measles outbreak from an index case with immunologically confirmed secondary vaccine failure. Vaccine. 2020;38:1467–75. https://doi.org/10.1016/j.vaccine.2019.11.075
13. Sundell N, Dotevall L, Sansone M, Andersson M, Lindh M, Wahlberg T, et al. Measles outbreak in Gothenburg urban area, Sweden, 2017 to 2018: low viral load in breakthrough infections. Euro Surveill. 2019;24:1900114. https://doi.org/10.2807/1560-7917.ES.2019.24.17.1900114
14. Gastañaduy PA, Funk S, Lopman BA, Rota PA, Gambhir M, Grenfell B, et al. Factors associated with measles transmission in the United States during the postelimination era. JAMA Pediatr. 2020;174:56–62. https://doi.org/10.1001/jamapediatrics.2019.4357
15. Liberati A, Altman DG, Tetzlaff J, Mulrow C, Gøtzsche PC, Ioannidis JPA, et al. The PRISMA statement for reporting systematic reviews and meta-analyses of studies that evaluate health care interventions: explanation and elaboration. PLoS Med. 2009;6:e1000100. https://doi.org/10.1371/journal.pmed.1000100
16. Gostic KM, McGough L, Baskerville EB, Abbott S, Joshi K, Tedijanto C, et al. Practical considerations for measuring the effective reproductive number, R_t. PLOS Comput Biol. 2020;16:e1008409. https://doi.org/10.1371/journal.pcbi.1008409
17. Jones J, Klein R, Popescu S, Rose K, Kretschmer M, Carrigan A, et al. Lack of measles transmission to susceptible contacts from a health care worker with probable secondary vaccine failure—Maricopa County, Arizona, 2015. MMWR Morb Mortal Wkly Rep. 2015;64:832–3. https://doi.org/10.15585/mmwr.mm6430a5
18. Rosen JB, Rota JS, Hickman CJ, Sowers SB, Mercader S, Rota PA, et al. Outbreak of measles among persons with prior evidence of immunity, New York City, 2011. Clin Infect Dis. 2014;58:1205–10. https://doi.org/10.1093/cid/ciu105
19. Zhang Z, Chen M, Ma R, Pan J, Suo L, Lu L. Outbreak of measles among persons with secondary vaccine failure, China, 2018. Hum Vaccin Immunother. 2020;16:358–62. https://doi.org/10.1080/21645515.2019.1653742
20. Avramovich E, Indenbaum V, Haber M, Amitai Z, Tsifanski E, Farjun S, et al. Measles outbreak in a highly vaccinated population—Israel, July–August 2017. MMWR Morb Mortal Wkly Rep. 2018;67:1186–8. https://doi.org/10.15585/mmwr.mm6742a4

21. Iwamoto M, Hickman CJ, Colley H, Arciuolo RJ, Mahle CE, Deocharan B, et al. Measles infection in persons with secondary vaccine failure, New York City, 2018–19. Vaccine. 2021;39:5346–50. https://doi.org/10.1016/j.vaccine.2021.07.078
22. Santibanez S, Prosenc K, Lohr D, Pfaff G, Jordan Markocic O, Mankertz A. Measles virus spread initiated at international mass gatherings in Europe, 2011. Euro Surveill. 2014;19:6–15. https://doi.org/10.2807/1560-7917.ES2014.19.35.20891
23. Gohil SK, Okubo S, Klish S, Dickey L, Huang SS, Zahn M. Healthcare workers and post-elimination era measles: lessons on acquisition and exposure prevention. Clin Infect Dis. 2016;62:166–72. https://doi.org/10.1093/cid/civ802
24. Edmonson MB, Addiss DG, McPherson JT, Berg JL, Circo SR, Davis JP. Mild measles and secondary vaccine failure during a sustained outbreak in a highly vaccinated population. JAMA. 1990;263:2467–71. https://doi.org/10.1001/jama.1990.03440180073035
25. Gibney KB, Attwood LO, Nicholson S, Tran T, Druce J, Healy J, et al. Emergence of attenuated measles illness among IgG-positive/IgM-negative measles cases: Victoria, Australia, 2008–2017. Clin Infect Dis. 2020;70:1060–7. https://doi.org/10.1093/cid/ciz363
26. Hahné SJM, Nic Lochlainn LM, van Burgel ND, Kerkhof J, Sane J, Yap KB, et al. Measles outbreak among previously immunized healthcare workers, the Netherlands, 2014. J Infect Dis. 2016;214:1980–6. https://doi.org/10.1093/infdis/jiw480
27. Rota JS, Hickman CJ, Sowers SB, Rota PA, Mercader S, Bellini WJ. Two case studies of modified measles in vaccinated physicians exposed to primary measles cases: high risk of infection but low risk of transmission. J Infect Dis. 2011;204(Suppl 1):S559–63. https://doi.org/10.1093/infdis/jir098
28. Bianchi S, Gori M, Fappani C, Ciceri G, Canuti M, Colzani D, et al. Characterization of vaccine breakthrough cases during measles outbreaks in Milan and surrounding areas, Italy, 2017–2021. Viruses. 2022;14:141068. https://doi.org/10.3390/v14051068
29. Paunio M, Peltola H, Valle M, Davidkin I, Virtanen M, Heinonen OP. Explosive school-based measles outbreak: intense exposure may have resulted in high risk, even among revaccinees. Am J Epidemiol. 1998;148:1103–10. https://doi.org/10.1093/oxfordjournals.aje.a009588
30. Smith J, Banu S, Young M, Francis D, Langfeldt K, Jarvinen K. Public health response to a measles outbreak on a university campus in Australia, 2015. Epidemiol Infect. 2018;146:314–8. https://doi.org/10.1017/S0950268817003089
31. Pacenti M, Maione N, Lavezzo E, Franchin E, Dal Bello F, Gottardello L, et al. Measles virus infection and immunity in a suboptimal vaccination coverage setting. Vaccines (Basel). 2019;7:199. https://doi.org/10.3390/vaccines7040199
32. Heesterbeek JAP, Dietz K. The concept of R_0 in epidemic theory. Stat Neerl. 1996;50:89–110. https://doi.org/10.1111/j.1467-9574.1996.tb01482.x
33. Heffernan JM, Smith RJ, Wahl LM. Perspectives on the basic reproductive ratio. J R Soc Interface. 2005;2:281–93. https://doi.org/10.1098/rsif.2005.0042
34. Li J, Blakeley D, Smith RJ. The failure of R_0. Comput Math Methods Med. 2011;2011:527610. https://doi.org/10.1155/2011/527610

Address for correspondence: Isaac Tranter, University of Queensland, Faculty of Medicine, Level 2, Mayne Medical Building, 288 Herston Rd, Herston, QLD 4006, Australia; email: i.tranter@uq.edu.au

Clinical Significance, Species Distribution, and Temporal Trends of Nontuberculous Mycobacteria, Denmark, 1991–2022

Victor Naestholt Dahl, Andreas Arnholdt Pedersen, Anders Norman, E. Michael Rasmussen, Jakko van Ingen, Aase Bengaard Andersen, Christian Morberg Wejse,[1] Troels Lillebaek[1]

Nontuberculous mycobacteria (NTM) are emerging as notable causative agents of opportunistic infections. To examine clinical significance, species distribution, and temporal trends of NTM in Denmark, we performed a nationwide register-based study of all unique persons with NTM isolated in the country during 1991–2022. We categorized patients as having definite disease, possible disease, or isolation by using a previously validated method. The incidence of pulmonary NTM increased throughout the study period, in contrast to earlier findings. *Mycobacterium malmoense*, *M. kansasii*, *M. szulgai*, and *M. avium* complex were the most clinically significant species based on microbiologic findings; *M. avium* dominated in incidence. This study shows the need for surveillance for an emerging infection that is not notifiable in most countries, provides evidence to support clinical decision-making, and highlights the importance of not considering NTM as a single entity.

Nontuberculous mycobacteria (NTM) are emerging as important causative agents of opportunistic infections globally (*1*). NTM can cause a wide spectrum of disease, leading to various clinical manifestations depending on the exposure, species virulence, host immunity, and site of infection (*2*). Clinical management and studies of pulmonary NTM infections are often challenged by difficulties in discriminating between transient NTM findings in nonsterile body sites after environmental exposure (often referred to as colonization, contamination, or isolation) as opposed to true NTM disease, because positive NTM cultures do not necessarily reflect disease.

For NTM pulmonary disease, the diagnostic criteria are based on the presence of symptoms along with radiologic and microbiologic findings (*3*). Although those criteria have been widely implemented, the application still relies on the individual clinician's subjective assessment and decision. As an alternative strategy, previous studies have validated infections by using microbiologic data only as a proxy for clinically significant pulmonary NTM disease, dividing NTM into categories reflecting the likelihood of disease (*4*–*6*). In Denmark and elsewhere, data on the clinical significance of NTM, including specific NTM species, is sparse. Consequently, in this nationwide study, we examined the clinical significance, species distribution, and temporal trends of NTM isolates over 32 years.

Methods

For decades, mycobacterial diagnostics and surveillance in Denmark have been centralized at the International Reference Laboratory of Mycobacteriology (IRLM) at Statens Serum Institut in Copenhagen. IRLM stores nationwide data and cultures from patients tested for mycobacterial infections as the only such laboratory in the country. In this nationwide register-based study, we combined mycobacteriologic data from IRLM with population data from Statistics Denmark (https://www.dst.dk).

Author affiliations: Statens Serum Institut, Copenhagen, Denmark (V.N. Dahl, A. Norman, E.M. Rasmussen, T. Lillebaek); Aarhus University Hospital, Aarhus, Denmark (V.N. Dahl, C.M. Wejse); Aarhus University, Aarhus (V.N. Dahl, C.M. Wejse); Odense University Hospital, Odense, Denmark (A.A. Pedersen); Lillebaelt Hospital, Vejle, Denmark (A.A. Pedersen); Radboud University Medical Center, Nijmegen, the Netherlands (J. van Ingen); Rigshospitalet, Copenhagen (A.B. Andersen); University of Copenhagen, Copenhagen (T. Lillebaek)

DOI: https://doi.org/10.3201/eid3009.240095

[1]These authors contributed equally to this article.

We evaluated the clinical significance of NTM isolates in Denmark by using only microbiologic data for all persons in Denmark who had ≥1 NTM isolate identified during 1991–2022. We only counted an incident case of NTM once and thereafter excluded the affected person from the population at risk for NTM infection. We excluded from our study patients with *Mycobacterium gordonae* isolates only, because that species is considered a clinically irrelevant contaminant (*6*,*7*). We also excluded patients with multiple NTM isolated concomitantly.

As part of routine diagnostics, samples were cultured on liquid media with BACTEC MGIT 960 (BD Diagnostic Systems, https://www.bd.com) and on solid Löwenstein–Jensen slants (Statens Serum Institut Diagnostica, https://ssidiagnostica.com) for up to 8 weeks. Throughout the study period, NTM species were identified using different methods, including AccuProbe (Gen-Probe, https://www.hologic.com) and supplementary biochemical tests during 1991–2001, InnoLipa Mycobacteria version 2 (InnoGenetics, https://www.fujirebio.com) during 2001–2012, GenoType Mycobacterium CM/AS (Hain Lifescience, https://www.hain-lifescience.de) during 2012–2022, and GenoType NTM-DR (Hain Lifescience) during 2016–2022. Supplementary species identification also was used, targeting the 16S (2006–2022) and internal transcribed spacer (2015–2022) regions with Sanger sequencing.

Using a previously validated method and modifying guideline criteria (*3*), we categorized patients as having either definite disease, possible disease, or isolation (*4*,*5*). For pulmonary NTM, including gastric lavages, we defined definite disease as either >3 positive samples, 3 positive samples including ≥1 obtained by bronchoscopy or pleurocentesis, or ≥1 positive sample from a lung or transbronchial biopsy. We defined NTM isolation as only 1 positive NTM sample and categorized the remaining patients as having possible disease. We defined all patients with a positive NTM sample from an extrapulmonary location as having definite disease, except for patients with only 1 sample of urine or feces, who we categorized as possible disease. We categorized patients with samples from both pulmonary and extrapulmonary locations as having disseminated disease. We grouped species by using phylogenetic classifications described by Tortoli et al. (*7*). As we considered the discrimination of NTM species identification within a complex or group to have changed much over time, we grouped NTM species for main analyses.

We compiled descriptive statistics by using counts and percentages for categorical data and medians and interquartile ranges (IQRs) for continuous data. As an illustration of the clinical significance of pulmonary NTM, we calculated the number and corresponding percentage of patients fulfilling the modified disease criteria by each species for definite disease only and for definite and possible disease combined. We calculated annual incidence rates (IRs) as the number of new patients with NTM in the numerator and the total number of patients in Denmark in the denominator for the given year. We evaluated trends over time by using a Poisson model with age groups, sex, and calendar year as explanatory variables, and we calculated IRs by using the population of Denmark as response variables. We conducted statistical analyses and generated figures by using R version 4.2.3 (The R Project for Statistical Computing, https://www.r-project.org). The study was approved by Denmark's Data Protection Agency through the Department of Compliance at Statens Serum Institut, Copenhagen (approval no. 22/00845).

Results

A total of 4,123 unique patients had a positive NTM culture, excluding 896 with *M. gordonae* and 34 with multiple species isolated concomitantly, equaling 129 new patients annually on average. Median patient age was 59 years (IQR 33–72 years); 1,977 (48%) were female and 2,146 (52%) male, and 3,673 (89%) were born in Denmark.

Most samples were pulmonary (2,851 [69%]), whereas approximately one fourth were extrapulmonary (1,106 [27%]); few patients had disseminated NTM (166 [4.0%]) (Table). The most frequent isolates were *M. avium* complex (MAC) (2,547 [62%]), whereas other species were seen much less frequently. *M. avium* (2,046 [80%]) and *M. intracellulare* (334 [13%]) accounted for most cases of MAC.

Approximately half of patients had definite disease (2,158 [52%]), whereas 26% (1,060) had possible disease and 22% (905) had isolation. One third of patients with pulmonary samples had definite disease (932 [33%]) and one third had possible disease (1,014 [36%]). We assessed clinical significance by species for patients with pulmonary samples (Figure 1). *M. malmoense* (55%), *M. kansasii* (46%), and MAC (36%) were most often associated with definite pulmonary NTM disease, whereas *M. kansasii* (86%), *M. malmoense* (81%), and *M. szulgai* (78%) were the most significant species when combing definite and possible disease. We also assessed the clinical significance of NTM isolation by species for any sample type and by age group and sex (Appendix Table 1, Figures 1, 2, https://wwwnc.cdc.gov/EID/article/30/9/24-0095-App1.pdf).

Table. Disease localization, species distribution, and clinical significance for patients with nontuberculous mycobacteria, Denmark 1991–2022*

Characteristic	Total	Years			
		1991–1998	1999–2006	2007–2014	2015–2022
No. patients	4,123 (100)	948 (100)	793 (100)	1,027 (100)	1,355 (100)
Disease localization					
Pulmonary	2,851 (69)	495 (52)	523 (66)	769 (75)	1,064 (79)
Extrapulmonary	1,106 (27)	341 (36)	255 (32)	242 (24)	268 (20)
Disseminated†	166 (4.0)	112 (12)	15 (1.9)	16 (1.6)	23 (1.7)
Mycobacteria species group‡					
M. avium complex	2,547 (62)	634 (67)	433 (55)	592 (58)	888 (66)
M. avium	2,046 (80)	575 (91)	370 (85)	467 (79)	634 (71)
M. chimaera	119 (4.7)	0	0	2 (0.3)	117 (13)
M. intracellulare	334 (13)	59 (9.3)	62 (14)	114 (19)	99 (11)
Other or unspecified	48 (1.9)	0	1 (0.2)	9 (1.5)	38 (4.3)
M. abscessus-chelonae complex	275 (6.7)	49 (5.2)	50 (6.3)	86 (8.4)	90 (6.6)
M. xenopi group	231 (5.6)	37 (3.9)	45 (5.7)	52 (5.1)	97 (7.2)
M. fortuitum-smegmatis group	202 (4.9)	57 (6.0)	48 (6.1)	34 (3.3)	63 (4.6)
M. malmoense	168 (4.1)	38 (4.0)	45 (5.7)	54 (5.3)	31 (2.3)
M. marinum	128 (3.1)	23 (2.4)	25 (3.2)	41 (4.0)	39 (2.9)
M. celatum group	117 (2.8)	13 (1.4)	19 (2.4)	45 (4.4)	40 (3.0)
M. kansasii	81 (2.0)	11 (1.2)	12 (1.5)	32 (3.1)	26 (1.9)
M. simiae complex	43 (1.0)	11 (1.2)	10 (1.3)	15 (1.5)	7 (0.5)
M. parascrofulaceum/scrofulaceum	40 (1.0)	10 (1.1)	3 (0.4)	10 (1.0)	17 (1.3)
M. szulgai	39 (0.9)	7 (0.7)	10 (1.3)	12 (1.2)	10 (0.7)
M. interjectum	22 (0.5)	4 (0.4)	5 (0.6)	8 (0.8)	5 (0.4)
M. terrae group	18 (0.4)	6 (0.6)	3 (0.4)	5 (0.5)	4 (0.3)
M. phocaicum/mucogenicum	17 (0.4)	0	7 (0.9)	3 (0.3)	7 (0.5)
Other§	195 (4.7)	48 (5.1)	78 (9.8)	38 (3.7)	31 (2.3)
Clinical significance					
Isolation	905 (22)	216 (23)	212 (27)	202 (20)	275 (20)
Possible disease	1,060 (26)	111 (12)	132 (17)	258 (25)	559 (41)
Definite disease	2,158 (52)	621 (66)	449 (57)	567 (55)	521 (38)

*All values are no. (%).
†Patients with samples from both pulmonary and extrapulmonary locations were categorized as having disseminated disease.
‡Species were grouped by using phylogenetic classifications described by Tortoli et al. (*7*).
§Defined as *Mycobacteria* spp. and species with <15 cases reported throughout the study period.

In all disease categories, MAC isolates were highly predominant, accounting for 68% (1,478/2,158) of definite disease cases and 65% (692/1,060) of possible disease cases but was slightly less common for isolation cases (42% [377/905]) (Appendix Table 1). *M. phocaicum/mucogenicum*, *M. parascrofulaceum/scrofulaceum*, and *M. terrae* group more often represented isolation cases. Disseminated NTM infections were mainly caused by MAC (87% [144/166]) (Appendix Table 2). All NTM species and groups were mostly isolated from pulmonary samples except for *M. marinum*, which was only found in extrapulmonary samples. *M. marinum* was the second-most common NTM isolated from extrapulmonary samples after MAC.

After adjustment for age and sex group differences, annual IRs of a positive NTM culture per 100,000 persons increased throughout the period (0.8%/year; p<0.001). This increase was driven mainly by an increase in patients with pulmonary NTM (2.3%/year; p<0.001), whereas the rate of extrapulmonary (−1.7%/year; p<0.001) and disseminated NTM (−9.5%/year; p<0.001) decreased (Figure 2, panel A). For pulmonary NTM, we also calculated annual IRs by disease categories (Figure 2, panel B). Annual IRs of patients with definite and possible pulmonary MAC increased over time (4.6%/year; p<0.001) (Figure 3), whereas the incidence of extrapulmonary and disseminated MAC decreased (Figure 4). These changes were mainly caused by subspecies *M. avium* (Appendix Figure 3). Infections attributable to *M. celatum* group (4.9%/year; p<0.001), *M. kansasii* (3.8%/year; p = 0.012), and *M. xenopi* (2.2%/year; p = 0.0152) also increased over time for definite and possible pulmonary NTM combined. The annual species distribution was comparable throughout the study period with discrete variations (Table).

Discussion

Using nationwide mycobacteriologic data from Denmark during a 32-year period, we found that 52% of patients in whom NTM were isolated had clinically significant disease (i.e., definite); that percentage increased to 78% when possible disease was included. Species most often associated with definite NTM pulmonary disease, on the basis of microbiologic findings, were *M. malmoense*, *M. kansasii*, and MAC, whereas *M. kansasii*, *M. malmoense*, and *M. szulgai* were the most clinically significant species when possible disease

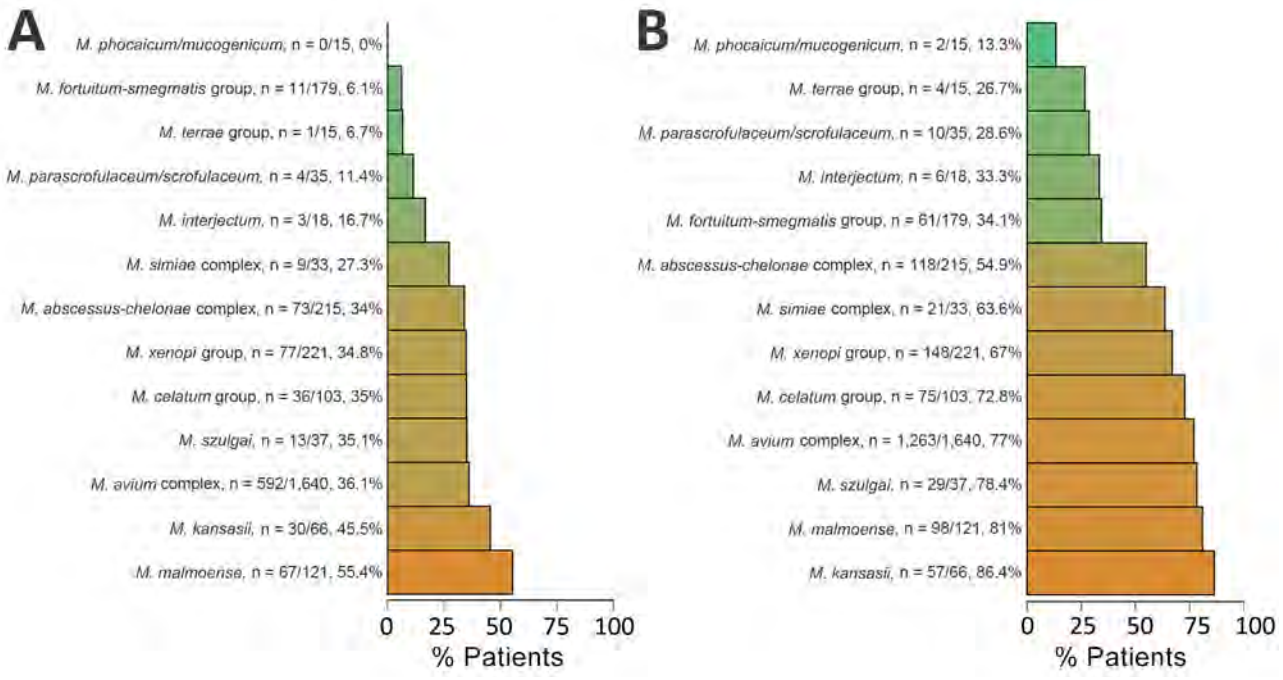

Figure 1. Absolute numbers and corresponding percentages of patients fulfilling modified criteria for nontuberculous mycobacteria pulmonary disease, based on microbiologic data only, Denmark, 1991–2022. A) Definite disease; B) definite and possible disease combined. Species were grouped by using phylogenetic classifications described by Tortoli et al. (*7*).

was included as a sensitivity analysis. MAC infections, mainly attributable to *M. avium*, were predominant across disease categories and localizations, underscoring its status as the clinically most important species. However, the considerable differences in clinical significance and epidemiology identified in our study highlight that NTM should not be considered a single entity. We observed that pulmonary NTM incidence has been increasing in Denmark during the study period, in contrast to earlier reports (*4*,*5*).

Comparable to our findings, a previous study from Denmark that included data from a clinical survey found that approximately half of pulmonary NTM patients (31/58 [53.4%]) received treatment with ≥2 antimycobacterial drugs or were considered to have clinically significant NTM infection on the basis of signs and symptoms (*8*). Slightly less than half of those patients (39/85 [45.9%]) fulfilled clinical, radiologic, and microbiologic criteria for disease for those that had information available on all criteria.

Identifying NTM species, including to subspecies level, is crucial for selection of a treatment regimen and because different species are associated with varying clinical significance and outcomes (i.e., severity)

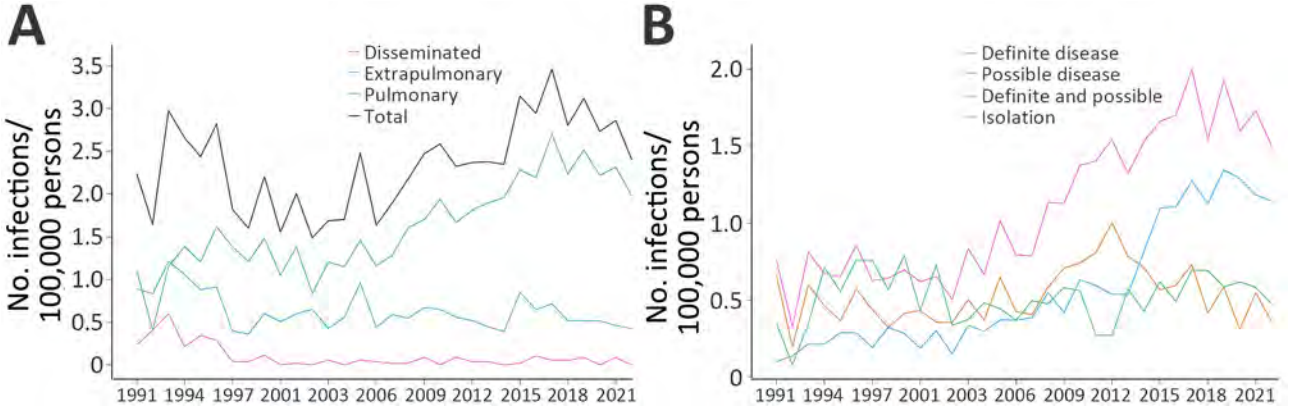

Figure 2. Annual incidence rates (infections/100,000 persons) of unique patients with a first culture positive for nontuberculous mycobacteria, by disease localization (A) and disease category for patients with pulmonary isolates only (B), Denmark, 1991–2022. Patients with samples from both pulmonary and extrapulmonary locations were categorized as having disseminated disease.

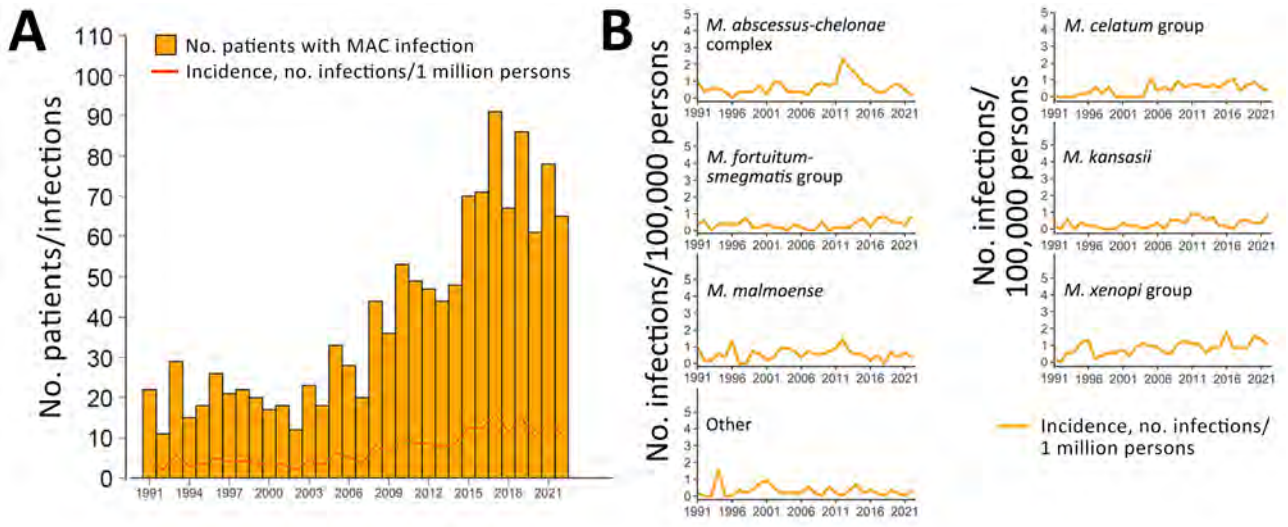

Figure 3. Annual absolute number of patients with a first culture positive for MAC, corresponding incidence rates, and annual incidence rates for the most frequent nontuberculous mycobacteria species for patients with definite and possible pulmonary disease combined, Denmark, 1991–2022. A) Numbers of first MAC cases by year and annual incidence (infections/1 million persons). B) Annual incidence rates (infections/1 million persons) of the most frequent nontuberculous mycobacteria species. Species were grouped by using phylogenetic classifications described by Tortoli et al. (*7*). Other was defined as *Mycobacteria* spp. and species with <15 cases reported throughout the study period. MAC, *Mycobacterium avium* complex.

(*9*–*11*). Several studies have investigated the clinical significance of NTM species (*12*–*20*), predominantly smaller studies with clinical data, whereas the larger studies have been based on laboratory data without clinical information. Many of those laboratory studies use the microbiologic component of the international guide criteria by the American Thoracic Society, European Respiratory Society, European Society of Clinical Microbiology and Infectious Diseases, and Infectious Diseases Society of America (*3*,*17*,*21*–*24*). Jankovic et al. found the positive predictive value of the microbiologic component compared with the full criteria was 59.8% (*17*); however, that value increased to 93.3% when a stricter definition was applied (*25*).

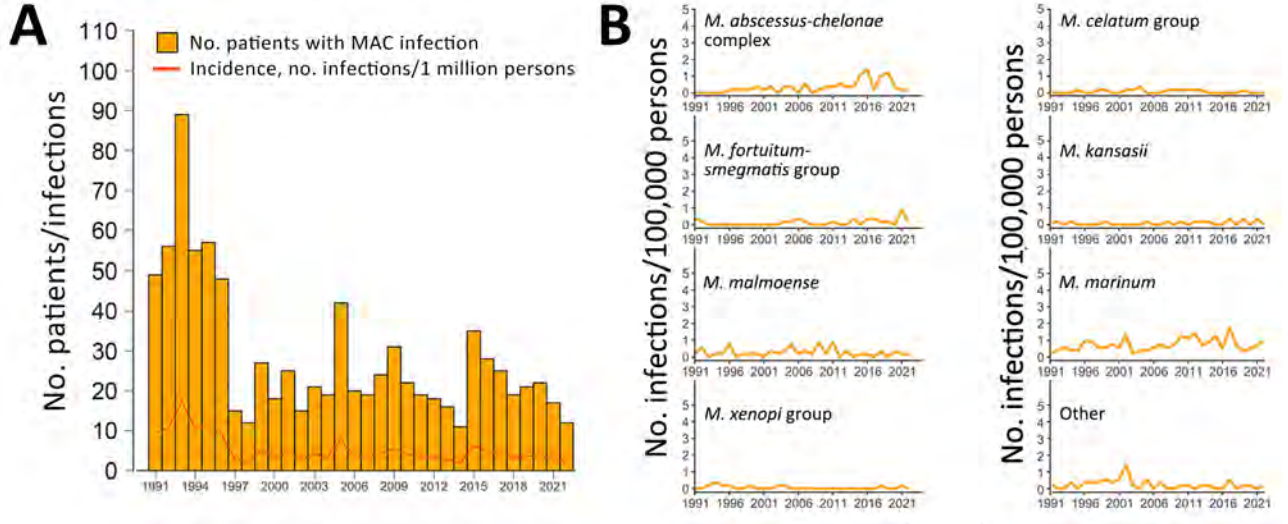

Figure 4. Annual absolute number of patients with a first culture positive for MAC, corresponding incidence rates, and annual incidence rates for the most frequent nontuberculous mycobacteria species for extrapulmonary and disseminated nontuberculous mycobacteria, Denmark, 1991–2022. Patients with samples from both pulmonary and extrapulmonary locations were categorized as having disseminated disease. A) Numbers of first MAC cases by year and annual incidence (infections/1 million persons). B) Annual incidence rates (infections/1 million persons) of the most frequent nontuberculous mycobacteria species. Species were grouped by using phylogenetic classifications described by Tortoli et al. (*7*). Other was defined as *Mycobacteria* spp. and species with <15 cases reported throughout the study period. MAC, *Mycobacterium avium* complex.

Because many epidemiologic NTM studies use different approaches for defining NTM infection and disease (*26*), a consensus for reporting surveillance data is warranted to enable fair comparisons across countries and regions.

In our study, we applied stricter criteria than those used in many other studies, enabling comparisons with previous studies (*4*,*5*). Those criteria have been shown to have high positive predictive values for clinically significant disease (*4*). We found that 33% of patients with pulmonary NTM had definite disease, comparable to the number of patients fulfilling American Thoracic Society and Infectious Diseases Society of America criteria in other studies, albeit slightly higher (*12*,*15*,*20*). A previous study of pulmonary NTM in eastern Asia found that 31% (582/1,744) of patients fulfilled those criteria (*16*). In studies from northwestern Europe, *M. kansasii*, *M. szulgai*, and *M. malmoense* have been associated with a high degree of clinical significance (>70%) (*27*,*28*). In other regions of the world, those species are considered less clinically significant, demonstrating that clinical significance varies with geography.

MAC was the most predominant group of pulmonary NTM (58%) in Denmark (*5*). In contrast, *M. xenopi* (7.8%) and *M. kansasii* were rare (2.3%) compared with findings in eastern and southern Europe, whereas *M. malmoense* was much more incident (4.2%) than in countries outside Scandinavia (*29*,*30*). *M. abscessuschelonae* complex accounted for the second-most frequently observed NTM group (7.5%). We observed clear differences in trends over time for the different species. For instance, the incidence of *M. malmoense* has previously been shown to rise in northern Europe (*31*), and although we did not observe an increase (–1.3%/year; p = 0.113), we could confirm the relative significance in our region, finding similar proportions of clinical significance (up to 81%) as reported in a systematic review of clinical data (70%–80%) (*31*). The abundance of *M. malmoense* in northern Europe, compared with southern Europe (0.6% of 3,696 isolates) and rest of the world (1% of ≈20,000 isolates), remains unexplained (*30*). The most extensive evaluations of geographic differences in the distribution of NTM species are older (*30*,*32*), and because NTM epidemiology is clearly changing over time, reevaluations of geographic differences are necessary.

Until recently, no increasing trends in NTM incidence had been reported in Denmark (*4*,*5*), in contrast to most other parts of the world (*33*). However, recent studies based on diagnostic codes from the International Classification of Diseases, 10th Revision, a potential proxy for NTM-treated patients, also found that NTM incidence and prevalence have been increasing in Denmark (*34*,*35*). Again, those findings show that temporal and geographic differences are essential when evaluating NTM epidemiology, underlining the need for surveillance. Diagnostic codes may have a lower sensitivity but a good positive predictive value (*36*), suggesting that combining the different approaches could be useful. Our study, showing an increase of pulmonary NTM incidence over time but not of extrapulmonary and disseminated NTM, suggests that structural lung disease and advancing age could be among the main determinants for those changes. This hypothesis is supported by the fact that structural lung disease is the strongest risk factor for NTM pulmonary disease (*37*). Still, sampling for NTM from pulmonary sites probably evolved over time, especially with increasing awareness of chronic lung conditions predisposing to NTM, whereas sampling from extrapulmonary sites is mainly based on disease manifestations (*37*). Hence, in the past decade, or even longer, patients living with chronic lung disease might have had cultures examined regularly as part of standard of care, leading to a higher number of positive NTM cultures. Further discussion of potential explanations for the increasing trends is available elsewhere (*1*,*33*).

One limitation of our study is the lack of clinical information, including data on symptoms, underlying conditions, risk factors for NTM, radiologic findings, and treatment. Although the use of microbiologic data as a measure of clinical significance may be flawed, lacking clinical information and a description of sampling strategy, we believe microbiologic data are a useful proxy for NTM disease and a valuable tool for NTM surveillance (*33*).

In conclusion, *M. malmoense*, *M. kansasii*, *M. szulgai*, and MAC are the most clinically significant NTM in Denmark based on microbiologic findings, with *M. avium* being of greatest importance because of its dominance in incidence. In contrast to earlier findings, the incidence of pulmonary NTM has been increasing in Denmark. This study shows the critical need for surveillance for an emerging infection that is not notifiable in most countries, provides evidence to support clinical decision-making, and highlights the importance of not considering NTM as a single entity.

Acknowledgments

We thank biostatistician Morten Overgaard for providing essential advice on statistical analyses. Responsibility and interpretations of the statistical analyses remain solely with the authors.

This study, performed as part of a PhD project, has been funded by a 2024 grant from the European Society of Clinical Microbiology and Infectious Diseases (to V.N.D.). In addition, V.N.D. received funding from the Department of Public Health, Aarhus University, Fonden af 17-12-1981, Skibsreder Per Henriksen, R. og hustrus fond, Health Research Foundation of Central Denmark Region, Christian Larsen og dommer Ellen Larsens Legat, Helga og Peter Kornings Fond, Beckett Foundation, the A.P. Moller Foundation (Fonden for Lægevidenskabens Fremme) and Denmark's Ministry of Higher Education and Science (Elite Research Travel Grant, 2023). The funders of the study had no role in study design, data collection, data analysis, data interpretation, or writing of the report.

About the Author

Dr. Dahl is a medical doctor and PhD student in the Department of Infectious Diseases, Aarhus University Hospital, Aarhus, Denmark. He is interested in complicated respiratory infections, such as tuberculosis and nontuberculous mycobacteria infections, and mainly works with clinical epidemiology and systematic reviews.

References

1. Dahl VN, Mølhave M, Fløe A, van Ingen J, Schön T, Lillebaek T, et al. Global trends of pulmonary infections with nontuberculous mycobacteria: a systematic review. Int J Infect Dis. 2022;125:120–31. https://doi.org/10.1016/j.ijid.2022.10.013
2. Griffith DE, Aksamit T, Brown-Elliott BA, Catanzaro A, Daley C, Gordin F, et al.; ATS Mycobacterial Diseases Subcommittee; American Thoracic Society; Infectious Disease Society of America. An official ATS/IDSA statement: diagnosis, treatment, and prevention of nontuberculous mycobacterial diseases. Am J Respir Crit Care Med. 2007; 175:367–416. https://doi.org/10.1164/rccm.200604-571ST
3. Daley CL, Iaccarino JM, Lange C, Cambau E, Wallace RJ Jr, Andrejak C, et al. Treatment of nontuberculous mycobacterial pulmonary disease: an official ATS/ERS/ESCMID/IDSA clinical practice guideline. Eur Respir J. 2020; 56:2000535. https://doi.org/10.1183/13993003.00535-2020
4. Andréjak C, Thomsen VO, Johansen IS, Riis A, Benfield TL, Duhaut P, et al. Nontuberculous pulmonary mycobacteriosis in Denmark: incidence and prognostic factors. Am J Respir Crit Care Med. 2010;181:514–21. https://doi.org/10.1164/rccm.200905-0778OC
5. Hermansen TS, Ravn P, Svensson E, Lillebaek T. Nontuberculous mycobacteria in Denmark, incidence and clinical importance during the last quarter-century. Sci Rep. 2017;7:6696. https://doi.org/10.1038/s41598-017-06931-4
6. Winthrop KL, McNelley E, Kendall B, Marshall-Olson A, Morris C, Cassidy M, et al. Pulmonary nontuberculous mycobacterial disease prevalence and clinical features: an emerging public health disease. Am J Respir Crit Care Med. 2010;182:977–82. https://doi.org/10.1164/rccm.201003-0503OC
7. Tortoli E, Fedrizzi T, Meehan CJ, Trovato A, Grottola A, Giacobazzi E, et al. The new phylogeny of the genus *Mycobacterium*: the old and the news. Infect Genet Evol. 2017;56:19–25. https://doi.org/10.1016/j.meegid.2017.10.013
8. Thomsen VO, Andersen AB, Miörner H. Incidence and clinical significance of non-tuberculous mycobacteria isolated from clinical specimens during a 2-y nationwide survey. Scand J Infect Dis. 2002;34:648–53. https://doi.org/10.1080/00365540210147813
9. Kwak N, Dalcolmo MP, Daley CL, Eather G, Gayoso R, Hasegawa N, et al. *Mycobacterium abscessus* pulmonary disease: individual patient data meta-analysis. Eur Respir J. 2019;54:1801991. https://doi.org/10.1183/13993003.01991-2018
10. Diel R, Ringshausen F, Richter E, Welker L, Schmitz J, Nienhaus A. Microbiological and clinical outcomes of treating non–*Mycobacterium avium* complex nontuberculous mycobacterial pulmonary disease: a systematic review and meta-analysis. Chest. 2017;152:120–42. https://doi.org/10.1016/j.chest.2017.04.166
11. Diel R, Nienhaus A, Ringshausen FC, Richter E, Welte T, Rabe KF, et al. Microbiologic outcome of interventions against *Mycobacterium avium* complex pulmonary disease: a systematic review. Chest. 2018;153:888–921. https://doi.org/10.1016/j.chest.2018.01.024
12. van Ingen J, Bendien SA, de Lange WC, Hoefsloot W, Dekhuijzen PN, Boeree MJ, et al. Clinical relevance of non-tuberculous mycobacteria isolated in the Nijmegen-Arnhem region, The Netherlands. Thorax. 2009;64:502–6. https://doi.org/10.1136/thx.2008.110957
13. Vande Weygaerde Y, Cardinaels N, Bomans P, Chin T, Boelens J, André E, et al. Clinical relevance of pulmonary non-tuberculous mycobacterial isolates in three reference centres in Belgium: a multicentre retrospective analysis. BMC Infect Dis. 2019;19:1061. https://doi.org/10.1186/s12879-019-4683-y
14. Al-Mahruqi SH, van-Ingen J, Al-Busaidy S, Boeree MJ, Al-Zadjali S, Patel A, et al. Clinical relevance of nontuberculous mycobacteria, Oman. Emerg Infect Dis. 2009;15:292–4. https://doi.org/10.3201/eid1502.080977
15. Schiff HF, Jones S, Achaiah A, Pereira A, Stait G, Green B. Clinical relevance of non-tuberculous mycobacteria isolated from respiratory specimens: seven year experience in a UK hospital. Sci Rep. 2019;9:1730. https://doi.org/10.1038/s41598-018-37350-8
16. Simons S, van Ingen J, Hsueh PR, Van Hung N, Dekhuijzen PN, Boeree MJ, et al. Nontuberculous mycobacteria in respiratory tract infections, eastern Asia. Emerg Infect Dis. 2011;17:343–9. https://doi.org/10.3201/eid170310060
17. Jankovic M, Samarzija M, Sabol I, Jakopovic M, Katalinic Jankovic V, Zmak L, et al. Geographical distribution and clinical relevance of non-tuberculous mycobacteria in Croatia. Int J Tuberc Lung Dis. 2013;17:836–41. https://doi.org/10.5588/ijtld.12.0843
18. Gerogianni I, Papala M, Kostikas K, Petinaki E, Gourgoulianis KI. Epidemiology and clinical significance of mycobacterial respiratory infections in Central Greece. Int J Tuberc Lung Dis. 2008;12:807–12.
19. Dabó H, Santos V, Marinho A, Ramos A, Carvalho T, Ribeiro M, et al. Nontuberculous mycobacteria in respiratory specimens: clinical significance at a tertiary care hospital in the north of Portugal. J Bras Pneumol. 2015;41:292–4. https://doi.org/10.1590/S1806-37132015000000005
20. Al-Harbi A, Al-Jahdali H, Al-Johani S, Baharoon S, Bin Salih S, Khan M. Frequency and clinical significance of respiratory isolates of non-tuberculous mycobacteria

in Riyadh, Saudi Arabia. Clin Respir J. 2016;10:198–203. https://doi.org/10.1111/crj.12202
21. Brode SK, Marchand-Austin A, Jamieson FB, Marras TK. Pulmonary versus nonpulmonary nontuberculous mycobacteria, Ontario, Canada. Emerg Infect Dis. 2017;23:1898–901. https://doi.org/10.3201/eid2311.170959
22. Russell CD, Claxton P, Doig C, Seagar AL, Rayner A, Laurenson IF. Non-tuberculous mycobacteria: a retrospective review of Scottish isolates from 2000 to 2010. Thorax. 2014; 69:593–5. https://doi.org/10.1136/thoraxjnl-2013-204260
23. Prevots DR, Shaw PA, Strickland D, Jackson LA, Raebel MA, Blosky MA, et al. Nontuberculous mycobacterial lung disease prevalence at four integrated health care delivery systems. Am J Respir Crit Care Med. 2010;182:970–6. https://doi.org/10.1164/rccm.201002-0310OC
24. Wetzstein N, Dahl VN, Lillebaek T, Lange C. Clinical spectrum and relevance of *Mycobacterium malmoense*: Systematic review and meta-analysis of 859 patients. J Infect. 2024;89:106203. https://doi.org/10.1016/j.jinf.2024.106203
25. Jankovic M, Sabol I, Zmak L, Jankovic VK, Jakopovic M, Obrovac M, et al. Microbiological criteria in non-tuberculous mycobacteria pulmonary disease: a tool for diagnosis and epidemiology. Int J Tuberc Lung Dis. 2016;20:934–40. https://doi.org/10.5588/ijtld.15.0633
26. Marras TK, Nelson P, Peci A, Richard-Greenblatt M, Brode S, Sullivan A, et al. Pulmonary nontuberculous mycobacteria, Ontario, Canada, 2020. Emerg Infect Dis. 2023;29:1415–9. https://doi.org/10.3201/eid2907.230216
27. van Ingen J. Microbiological diagnosis of nontuberculous mycobacterial pulmonary disease. Clin Chest Med. 2015;36:43–54. https://doi.org/10.1016/j.ccm.2014.11.005
28. Yan M, Brode SK, Marras TK. Treatment of the less common nontuberculous mycobacterial pulmonary disease. Clin Chest Med. 2023;44:799–813. https://doi.org/10.1016/j.ccm.2023.06.011
29. Dahl VN, Laursen LL, He Y, Zhang YA, Wang MS. Species distribution among patients with nontuberculous mycobacteria pulmonary disease in Europe. J Infect. 2023;87:469–72. https://doi.org/10.1016/j.jinf.2023.03.010
30. Hoefsloot W, van Ingen J, Andrejak C, Angeby K, Bauriaud R, Bemer P, et al.; Nontuberculous Mycobacteria Network European Trials Group. The geographic diversity of nontuberculous mycobacteria isolated from pulmonary samples: an NTM-NET collaborative study. Eur Respir J. 2013;42:1604–13. https://doi.org/10.1183/09031936.00149212
31. Hoefsloot W, Boeree MJ, van Ingen J, Bendien S, Magis C, de Lange W, et al. The rising incidence and clinical relevance of *Mycobacterium malmoense*: a review of the literature. Int J Tuberc Lung Dis. 2008;12:987–93.
32. Zweijpfenning SMH, Ingen JV, Hoefsloot W. Geographic distribution of nontuberculous mycobacteria isolated from clinical specimens: a systematic review. Semin Respir Crit Care Med. 2018;39:336–42. https://doi.org/10.1055/s-0038-1660864
33. Prevots DR, Marshall JE, Wagner D, Morimoto K. Global epidemiology of nontuberculous mycobacterial pulmonary disease: a review. Clin Chest Med. 2023;44:675–721. https://doi.org/10.1016/j.ccm.2023.08.012
34. Dahl VN, Fløe A, Wejse C. Nontuberculous mycobacterial infections in a Danish region between 2011 and 2021: evaluation of trends in diagnostic codes. Infect Dis (Lond). 2023;55:439–43. https://doi.org/10.1080/23744235.2023.2194411
35. Pedersen AA, Løkke A, Fløe A, Ibsen R, Johansen IS, Hilberg O. Nationwide increasing incidence of nontuberculous mycobacterial diseases among adults in Denmark: eighteen years of follow-up. Chest. 2024;S0012-3692(24)00393-3.
36. Mejia-Chew C, Yaeger L, Montes K, Bailey TC, Olsen MA. Diagnostic accuracy of health care administrative diagnosis codes to identify nontuberculous mycobacteria disease: a systematic review. Open Forum Infect Dis. 2021;8:ofab035. https://doi.org/10.1093/ofid/ofab035
37. Loebinger MR, Quint JK, van der Laan R, Obradovic M, Chawla R, Kishore A, et al. Risk factors for nontuberculous mycobacterial pulmonary disease: a systematic literature review and meta-analysis. Chest. 2023;164:1115–24. https://doi.org/10.1016/j.chest.2023.06.014

Address for correspondence: Victor Næstholt Dahl, Department of Infectious Diseases, Aarhus University Hospital, Palle Juul-Jensens Blvd 99, DK-8200, Aarhus, Denmark; email: victor.dahl@rm.dk

Morphologic and Molecular Identification of Human Ocular Infection Caused by *Pelecitus* Nematodes, Thailand

Ploysai Rujkorakarn, Pukkapol Suvannachart, Samadhi Patamatamkul, Tongjit Thanchomnang, Pairot Pramual, Weerachai Saijuntha, Wanchai Maleewong, Shigehiko Uni

Nematodes of the Onchocercidae family, such as *Pelecitus* spp., are filarial parasites of medical and veterinary importance. Although infections are widely distributed among avian species, only 2 cases of human *Pelecitus* ocular infection, both in South America, have been reported. We describe a 61-year-old man in northeast Thailand diagnosed with an ocular infection. Morphologic characteristics suggested the causative agent was a female *Pelecitus* nematode: coiled body, rounded anterior and posterior extremities, a distinct preesophageal cuticular ring, lateral alae, a postdeirid, and a protuberant vulva. Sequences of the 12S rDNA gene indicated 95%–96% identity and *cox*1 gene 92%–96% identity with published *P. copsychi* sequences. P-distance for *cox*1 sequences between the causative agent and *P. copsychi* was 6.71%. Phylogenetic trees of 12S rDNA and *cox*1 genes indicated the species differed from but is closely associated with *P. copsychi*. Healthcare providers should be aware of the threat of ocular infection from *Pelecitus* spp. nematodes.

Ocular parasitosis is relatively rare, and causative agents vary by geographic area (*1*). Manifestations vary according to the parasite's location. A live parasite in the anterior chamber of the eye can lead to anterior uveitis or secondary glaucoma. Various parasites, such as representatives of the genera *Gnathostoma*, *Onchocerca*, and *Angiostrongylus*, have been reported in the literature to cause similar conditions (*1*). In Southeast Asia, ocular gnathostomiasis and angiostrongyliasis often manifest with a live parasite in the anterior chamber (*2*,*3*).

The nematode genus *Pelecitus* belongs to the Onchocercidae family, which includes filariae of medical and veterinary importance. Among the 21 species of *Pelecitus* nematodes, 18 are found in birds and 3 in mammals (*4*,*5*), most distributed in Africa and South America (*4*). Birds serve as definitive hosts or reservoirs. *Pelecitus* spp. nematodes are transmitted by blood-sucking arthropods, such as mosquitoes, chewing lice, and tabanids (*6*).

Within the Indomalayan realm, *P. ceylonensis*, *P. galli*, and *P. copsychi* nematodes have been identified in animal hosts in Sri Lanka and Malaysia (*5*,*7*,*8*). In humans, 2 cases of *Pelecitus* infection have been discovered in Colombia and Brazil (*9*,*10*). However, in both reports, the parasites were identified on the basis of morphologic characteristics only.

In this study, we identified the causative agent of intraocular infection in a patient outside South America as a nematode species of the genus *Pelecitus*. We subsequently corroborated the preliminary identification based on morphologic characteristics using molecular studies of the mitochondrial 12S ribosomal RNA and the cytochrome *c* oxidase subunit 1 (*cox*1) genes (*11*,*12*). This study provides a morphologic description and details concerning the phylogenetic position of the *Pelecitus* sp. nematode identified in this article. Our case report was approved by the ethics committee of Mahasarakham University (approval no. 181-200/2023).

Methods

Case Report

An otherwise healthy 61-year-old man in Thailand sought treatment for gradually increasing eye pain, redness, light sensitivity, and slight vision loss in his

Author affiliations: Prince of Songkla University, Songkhla, Thailand (P. Rujkorakarn); Mahasarakham University, Maha Sarakham, Thailand (P. Rujkorakarn, P. Suvannachart, S. Patamatamkul, T. Thanchomnang, P. Pramual, W. Saijuntha); Khon Kaen University, Khon Kaen, Thailand (P. Suvannachart, W. Maleewong); Universiti Malaya, Kuala Lumpur, Malaysia (S. Uni); Kobe Women's University, Kobe, Japan (S. Uni)

DOI: https://doi.org/10.3201/eid3009.231692

left eye. Symptoms persisted for ≈1 month. He was a farmer in northeastern Thailand and had not traveled outside the country. He regularly consumed traditional dishes containing raw and partially cooked ingredients, including beef and fish. He was diagnosed with an intraocular parasite at a private clinic, where staff performed an Nd:YAG (neodymium-doped yttrium aluminum garnet) laser procedure to immobilize the parasite before the patient was referred to the hospital. We postulate that the infection in this patient might have resulted from a bite from a hematophagous arthropod.

Upon examination, the patient had best-corrected visual acuity of 20/20 in the right eye and 20/40 in the left eye. Intraocular pressure measurements were 18 mm Hg in the right eye and 14 mm Hg in the left. The right eye examination was unremarkable, but the left eye showed ciliary injection (Figure 1, panel A) and grade 1+ anterior chamber cells. A live, moving parasite was observed in the inferior anterior chamber, more distinctly during gonioscopic examination (Figure 1, panel B). The posterior segment was within reference limits. Complete blood count results showed leukocytosis of 12,640 cells/mm^3 and eosinophilia of 5.5% (absolute eosinophil count 695.2 cells/mm^3). Fecal examination did not reveal parasites or eggs.

We performed urgent surgical removal to prevent posterior or extraocular migration. After the operation, we treated the patient with prednisolone acetate 1% eye drops (every 2 h), moxifloxacin 0.5% eye drops (4×/d), and oral albendazole (400 mg 2×/d for 5 d). At 1-month follow-up, the patient returned with a reduction in pain and redness. The best-corrected visual acuity was 20/30 and the intraocular pressure 10 mm Hg in the left eye. We found no active inflammation upon slit-lamp examination. Prednisolone acetate 1% eye drops were gradually tapered. At the 1-year follow-up, the patient was doing well without recurrence of ocular symptoms. We did not perform a blood test at follow-up.

Morphologic Identification of the Parasite

We fixed the causative agent in 70% ethanol and subsequently cleared it in lactophenol (R & M Chemicals, https://www.evergreensel.com.my) for morphologic examination under a compound microscope equipped with an Olympus U-DA camera lucida (https://www.olympus-global.com). We extracted DNA from the caudal part of the causative agent (0.2 mm) using the Nucleospin Tissue kit (Macherey-Nagel, https://www.mn-net.com) according to manufacturer instructions. We performed a conventional PCR to amplify the targeted mitochondrial 12S rRNA and *cox*1 genes, according to instructions for specific primers and PCR conditions described elsewhere (*13*–*15*). Afterward, we sequenced the PCR products using the Applied Biosystems DNA Analyzer (ThermoFisher, https://www.thermofisher.com). We compared the 12S rDNA and *cox*1 sequences with public sequences in the GenBank database by using BLASTn (https://blast.ncbi.nlm.nih.gov).

We performed multiple sequence alignment of DNA sequences from the 12S rRNA and *cox*1 genes with ClustalW (http://www.clustal.org) using MEGA-X (https://www.megasoftware.net). We constructed phylogenetic trees using the maximum-likelihood method with 1,000 bootstrap resamplings as implemented in MEGA-X (*16*). We used publicly available sequences from different nematode species

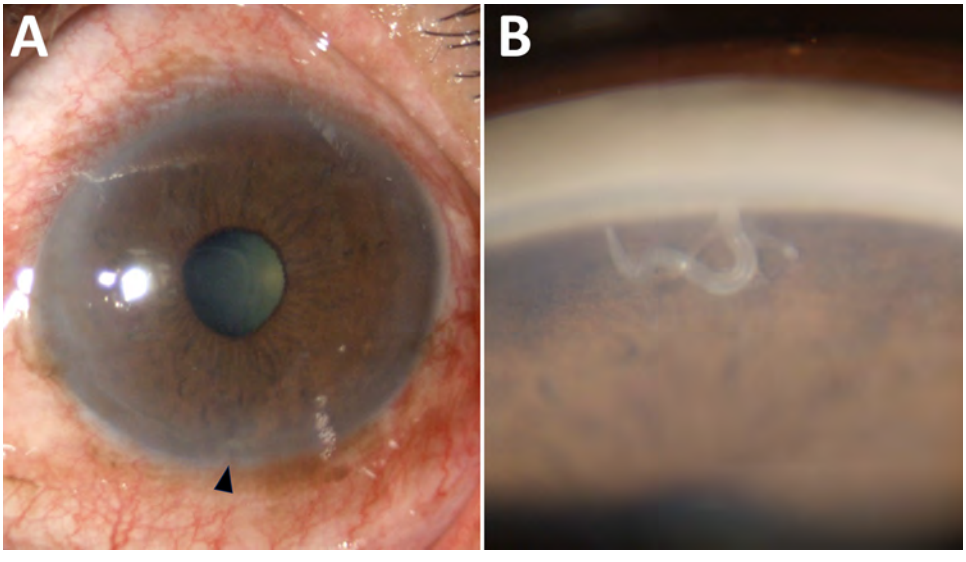

Figure 1. Slit-lamp examination of the left eye of a 61-year-old man in Thailand with ocular parasitosis. A) Ciliary injection and a live parasite in the inferior part of the anterior chamber (arrowhead). B) Gonioscopic view revealing a parasite in the inferior anterior chamber angle, lodged in the iris fibers. Precise magnification levels are not available.

Figure 2. Light micrographs of *Pelecitus* sp. nematode isolated from the left eye of a 61-year-old man in Thailand. A) Curled female, 3.5 mm in length and 198 μm in width. Head (arrow) and tail (arrowhead) are indicated. Scale bar = 250 μm. B) Rounded anterior extremity with preesophageal cuticular ring (arrows). Scale bar = 10 μm. C) Postdeirid (arrowhead) at the posterior left side and lateral alae (arrows) at the posterior part. Scale bar = 50 μm. D) Rounded posterior extremity (arrowhead). Scale bar = 100 μm.

for comparison. We selected the Hasegawa–Kishino–Yano model as a suitable substitution model (*17*).

Results

Morphologic Identification

The surgically removed female nematode had a coiled body, 3.5 mm long and 198 μm wide at the midbody (Figure 2, panel A). The head was bluntly rounded and the preesophageal cuticular ring (6.3 μm wide × 2.5 μm high) was distinct (Figure 2, panel B). Labial and cephalic papillae, arranged in 4 submedian pairs, were not markedly protuberant. Amphids were small, lateral, and not salient. A slight neck was found 69 μm from the anterior extremity. The nerve ring was situated 138 μm from the anterior extremity. The esophagus was 608 μm long, and its diameter slightly widened in the posterior half. The vulva was located at the level of the posterior half of the esophagus, 395 μm from the anterior extremity. No microfilariae were present in the uteri. A postdeirid was found on the left side, 300 μm from the caudal extremity (Figure 2, panel C). Lateral alae were present, broadening toward the posterior extremity. At the level of the postdeirid, the ala was 28 μm wide. The intestine was filled with brown pigments. The cuticle was thick, 5–10 μm wide, at the postdeirid level. The tail extremity was rounded (Figure 2, panel D). We deposited the specimen (MNHN-114YT) in the Muséum National d'Histoire Naturelle, Paris, France (https://www.mnhn.fr).

Molecular Analyses

Based on the best match in BLAST, the 12S rDNA sequence (468 bp) (Figure 3) showed 95%–96% identity with *P. copsychi* (GenBank accession nos. OK480976 and OK480977) and the *cox*1 sequence (611 bp) (Figure 4) showed 92%–96% identity with *P. copsychi* (GenBank accession nos. OK480041 and OK480043). The calculated p-distance for *cox*1 sequences between this causative agent and *P. copsychi* was 6.71%. We submitted sequences generated in this study to GenBank (accession nos. OR346706 [*cox*1] and OR396900 [12S rRNA]).

Discussion

The parasite specimen removed from this patient had a coiled body, rounded anterior and posterior extremities, distinct preesophageal cuticular ring, lateral alae, and a postdeirid. In addition, the vulva opened in the esophageal region. Those morphologic characteristics, along with the described morphometrics,

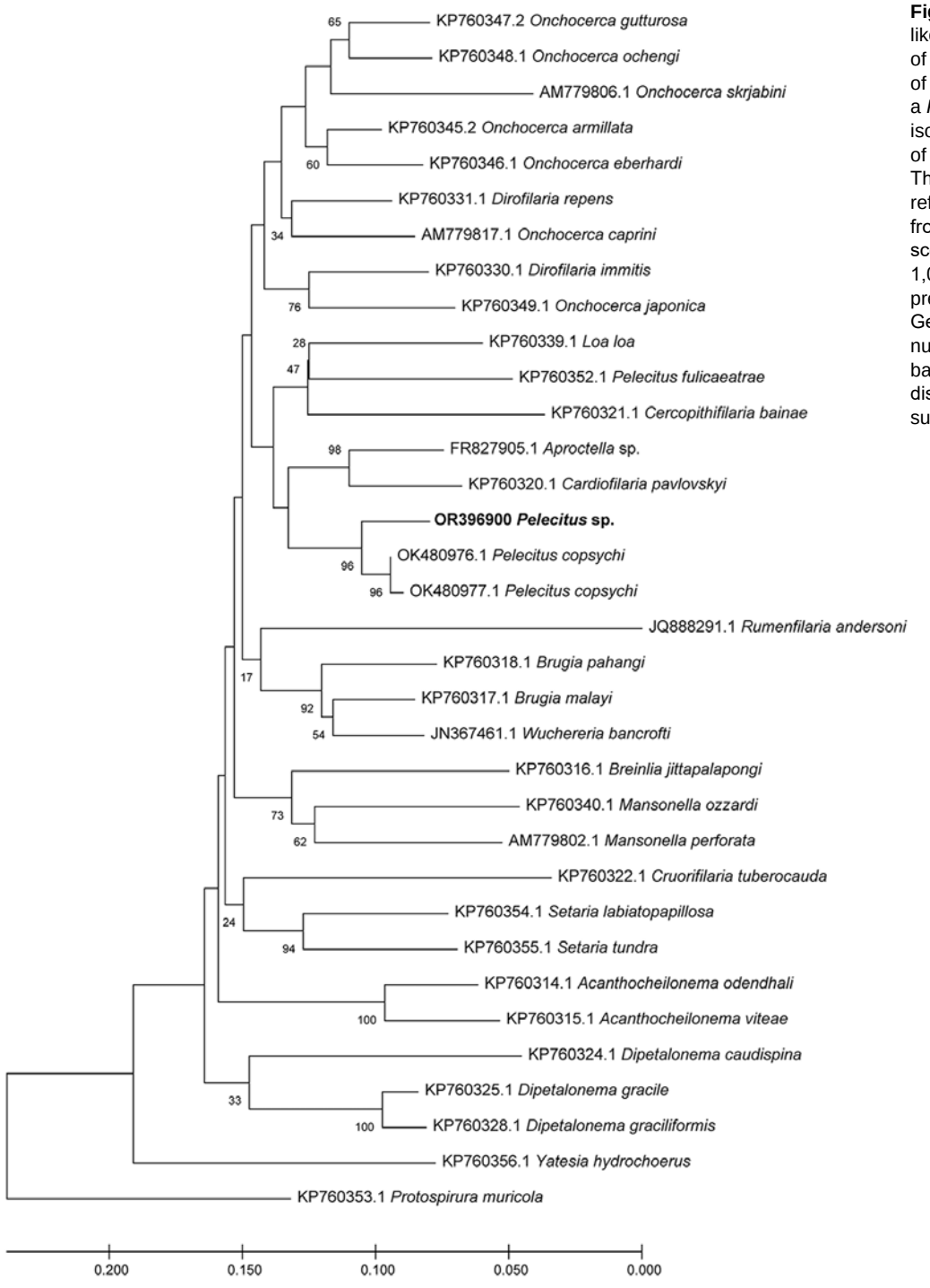

Figure 3. Maximum-likelihood reconstruction of phylogeny on the basis of 12S rDNA sequences of a *Pelecitus* sp. nematode isolated from the left eye of a 61-year-old man in Thailand (bold text) and reference sequences from GenBank. Bootstrap scores (percentages of 1,000 replications) are presented for each node. GenBank accession numbers are shown. Scale bar refers to a phylogenetic distance of 0.05 nucleotide substitutions per site.

indicated that the causative agent was a young, unmated female nematode of the genus *Pelecitus* (*5*,*18*). We compared that specimen with *P. copsychi*, *P. ceylonensis*, and *P. galli* nematodes from avian hosts in the Indomalayan realm (*5*,*7*,*8*). The specimen from our patient showed greater similarity to *P. copsychi* nematode than to the other 2 species, particularly in terms of body length. However, the esophagus of the specimen from our patient was shorter, only half the length of the *P. copsychi* esophagus. Although the morphometrics of microfilariae would have been necessary to differentiate species, the female nematode harbored no microfilariae. Nevertheless, we inferred that the taxonomic species of the specimen from our patient differed from *P. copsychi*.

Our molecular analyses positioned the specimen from our patient near *P. copsychi* taxonomically

(Figures 3, 4). The calculated p-distance for *cox*1 gene sequences between the specimen from our patient and *P. copsychi* was 6.71%. Filarial nematodes can be considered of the same species if the genetic distance based on their *cox*1 sequences is <2% (*19*). Interspecific distances are >4.8% in filariae. A 2017 study confirmed this distance threshold in the *Onchocerca* species (*20*). Therefore, genetic distances suggested the specimen from our patient differed from *P. copsychi* at the species level. However, because the specimen from our patient possessed the general morphologic characteristics of *Pelecitus* nematodes and was

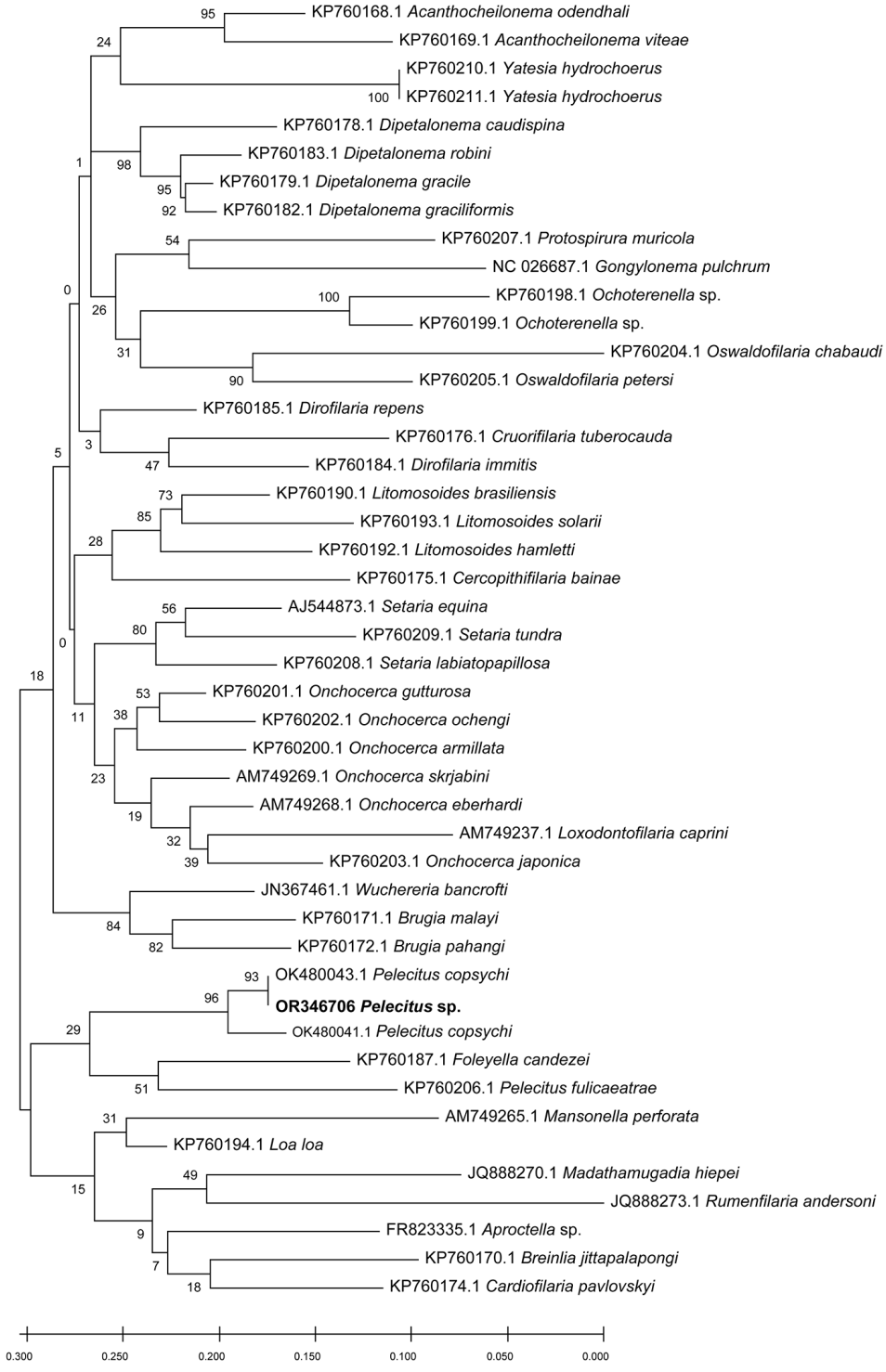

Figure 4. Maximum-likelihood reconstruction of phylogeny on the basis of *cox*1 sequences of *Pelecitus* sp. nematode isolated from the left eye of a 61-year-old man in Thailand (bold text) and reference sequences from GenBank. Bootstrap scores (percentages of 1,000 replications) are presented for each node. GenBank accession numbers are shown. Scale bar refers to a phylogenetic distance of 0.05 nucleotide substitutions per site.

positioned near *P. copsychi* in the phylogenetic trees, we concluded that it is a congener, currently identified only as *Pelecitus* sp.

Previously, 2 cases of zoonotic ocular infections possibly caused by *Pelecitus* spp. nematodes have been described in humans (*9*,*10*). The specimen from our patient was similar to the *Pelecitus* sp. nematode isolated from the iris fibers of a man in Brazil (*10*). The specimen from Brazil was a male worm with a preesophageal cuticular ring, lateral alae, and a postdeirid. In another case in Colombia, a male specimen of the genus *Loaina* was observed in the anterior chamber of the patient's eye (*9*) but was later suggested to be of the genus *Pelecitus* (*4*,*10*). The study from Brazil (*10*) also stated that 2 specimens from humans in Colombia and Brazil were *Pelecitus* nematodes from birds. However, in the previous reports, no DNA sequences were obtained (*9*,*10*). Hence, we were unable to compare the sequences from our study with species from previous human ocular *Pelecitus* infections.

Several modalities in the treatment of ocular parasitic infections have been described elsewhere. Lasers, including argon, Nd:YAG, and diode, are recommended to immobilize and kill the parasite before removal (*21*), but surgical removal is the mainstay of treatment options (*2*,*3*). Data are lacking regarding the efficacy of available anthelmintics for the treatment of *Pelecitus* infections (*22*). In animal studies, use of ivermectin, either alone or in combination with systemic steroids, may be effective against *Pelecitus* infection in macaws (*23*). In our case-patient, the intracameral parasite was successfully removed through surgery followed by treatment of the patient with postoperative topical antimicrobials and steroids. No recurrence occurred during the 1-year follow-up period.

In conclusion, we report a case of human intraocular infection caused by a *Pelecitus* sp. nematode in Thailand. This finding expands the known geographic range of human infection with this zoonotic nematode, formerly reported only in South America. Guided by an initial morphologic analysis, molecular methods such as PCR can be useful for identifying rare infections such as *Pelecitus* sp. nematodes in humans, offering a rapid and accurate diagnostic approach. Healthcare providers should consider *Pelecitus* spp. nematodes as a possible causative agent in cases of small-to-moderate–sized helminths lodged in iris tissue.

Acknowledgments

We gratefully acknowledge the valuable assistance of Kerstin Junker in the preparation of this manuscript.

This research project was financially supported by Mahasarakham University.

About the Author

Dr. Rujkorakarn is a vitreoretinal specialist at the Department of Ophthalmology, Faculty of Medicine, Mahasarakham University, Thailand. Her primary research interests are in the fields of ocular infection and inflammation, as well as retinal diseases.

References

1. Nimir AR, Saliem A, Ibrahim IAA. Ophthalmic parasitosis: a review article. Interdiscip Perspect Infect Dis. 2012;2012:587402. https://doi.org/10.1155/2012/587402
2. Sinawat S, Trisakul T, Choi S, Morley M, Sinawat S, Yospaiboon Y. Ocular angiostrongyliasis in Thailand: a retrospective analysis over two decades. Clin Ophthalmol. 2019;13:1027–31. https://doi.org/10.2147/OPTH.S204380
3. Kongwattananon W, Wiriyabanditkul T, Supwatjariyakul W, Somkijrungroj T. Intracameral gnathostomiasis: a case report and literature review. Ocul Immunol Inflamm. 2023;31:1092–6. https://doi.org/10.1080/09273948.2022.2073239
4. Bartlett CM, Greiner EC. A revision of *Pelecitus* Railliet & Henry, 1910 (Filarioidea, Dirofilariinae) and evidence for the "capture" by mammals of filarioids from birds [in French]. Bull Mus Nat Hist. 1986;8:47–99. https://doi.org/10.5962/p.287619
5. Uni S, Mat Udin AS, Tan PE, Rodrigues J, Martin C, Junker K, et al. Description and molecular characterisation of *Pelecitus copsychi* Uni, Mat Udin & Martin n. sp. (Nematoda: Onchocercidae) from the white-rumped shama *Copsychus malabaricus* (Scopoli) (Passeriformes: Muscicapidae) of Pahang, Malaysia. Curr Res Parasitol Vector Borne Dis. 2022;2:100078. https://doi.org/10.1016/j.crpvbd.2022.100078
6. Anderson RC. Nematode parasites of vertebrates: their development and transmission. 2nd ed. Wallingford (UK): CAB International; 2000.
7. Dissanike AS, Fernando MA. *Pelecitus galli* n. sp. from the Malayan jungle fowl *Gallus gallus spadiceus*. J Helminthol. 1974;48:199–203. https://doi.org/10.1017/S0022149X00022847
8. Dissanike AS. *Pelecitus ceylonensis* n. sp., from the chick and ash-dove experimentally infected with larvae from *Mansonia crassipes*, and from naturally-infected crows in Ceylon. Ceylon J Sci. 1967;7:96–104.
9. Botero D, Aguledo LM, Uribe FJ, Esslinger JH, Beaver PC. Intraocular filaria, a *Loaina* species, from man in Colombia. Am J Trop Med Hyg. 1984;33:578–82. https://doi.org/10.4269/ajtmh.1984.33.578
10. Bain O, Otranto D, Diniz DG, dos Santos JN, de Oliveira NP, Frota de Almeida IN, et al. Human intraocular filariasis caused by *Pelecitus* sp. nematode, Brazil. Emerg Infect Dis. 2011;17:867–9. https://doi.org/10.3201/eid1705.101309
11. Chan AHE, Chaisiri K, Morand S, Saralamba N, Thaenkham U. Evaluation and utility of mitochondrial ribosomal genes for molecular systematics of parasitic nematodes. Parasit Vectors. 2020;13:364. https://doi.org/10.1186/s13071-020-04242-8
12. Chan AHE, Chaisiri K, Dusitsittipon S, Jakkul W, Charoennitiwat V, Komalamisra C, et al. Mitochondrial ribosomal genes as novel genetic markers for discrimination of closely related species in the *Angiostrongylus*

cantonensis lineage. Acta Trop. 2020;211:105645. https://doi.org/10.1016/j.actatropica.2020.105645
13. Casiraghi M, Anderson TJ, Bandi C, Bazzocchi C, Genchi C. A phylogenetic analysis of filarial nematodes: comparison with the phylogeny of *Wolbachia* endosymbionts. Parasitology. 2001;122 (Pt 1):93–103. https://doi.org/10.1017/S0031182000007149
14. Casiraghi M, Bain O, Guerrero R, Martin C, Pocacqua V, Gardner SL, et al. Mapping the presence of *Wolbachia pipientis* on the phylogeny of filarial nematodes: evidence for symbiont loss during evolution. Int J Parasitol. 2004;34:191–203. https://doi.org/10.1016/j.ijpara.2003.10.004
15. Sobotyk C, Foster T, Callahan RT, McLean NJ, Verocai GG. Zoonotic *Thelazia californiensis* in dogs from New Mexico, USA, and a review of North American cases in animals and humans. Vet Parasitol Reg Stud Rep. 2021;24:100553. https://doi.org/10.1016/j.vprsr.2021.100553
16. Kumar S, Stecher G, Li M, Knyaz C, Tamura K. MEGA X: molecular evolutionary genetics analysis across computing platforms. Mol Biol Evol. 2018;35:1547–9. https://doi.org/10.1093/molbev/msy096
17. Hasegawa M, Kishino H, Yano T. Dating of the human-ape splitting by a molecular clock of mitochondrial DNA. J Mol Evol. 1985;22:160–74. https://doi.org/10.1007/BF02101694
18. Gibbons LM. Keys to the nematode parasites of vertebrates. Supplementary volume. Wallingford (UK): CAB International; 2010.
19. Ferri E, Barbuto M, Bain O, Galimberti A, Uni S, Guerrero R, et al. Integrated taxonomy: traditional approach and DNA barcoding for the identification of filarioid worms and related parasites (*Nematoda*). Front Zool. 2009;6:1. https://doi.org/10.1186/1742-9994-6-1
20. Lefoulon E, Giannelli A, Makepeace BL, Mutafchiev Y, Townson S, Uni S, et al. Whence river blindness? The domestication of mammals and host-parasite co-evolution in the nematode genus Onchocerca. Int J Parasitol. 2017;47:457–70. https://doi.org/10.1016/j.ijpara.2016.12.009
21. Murugan SB. Commentary: *Angiostrongylus cantonensis* in anterior chamber. Indian J Ophthalmol. 2019;67:161–2. https://doi.org/10.4103/ijo.IJO_1511_18
22. Morishita TY, Schaul JC. Parasites of birds. In: Baker DG, editor. Flynn's parasites of laboratory animals. Ames (IA): Blackwell Publishing; 2007. p. 217–301.
23. Allen JL, Kollias GV, Greiner EC, Boyce W. Subcutaneous filariasis (*Pelecitus* sp.) in a yellow-collared macaw (*Ara auricollis*). Avian Dis. 1985;29:891–4. https://doi.org/10.2307/1590686

Address for correspondence: Pukkapol Suvannachart, 296 Nakhornsawan Rd, Department of Ophthalmology, Suddhavej Hospital, Faculty of Medicine, Mahasarakham University, Maha Sarakham 44000, Thailand; email: pakkapol22@gmail.com

Clinical Aspects and Disease Severity of *Streptococcus dysgalactiae* Subspecies *equisimilis* Bacteremia, Finland[1]

Viivi Nevanlinna, Janne Aittoniemi, Reetta Huttunen, Tiina Luukkaala, Sari Rantala

Medscape CME Activity

In support of improving patient care, this activity has been planned and implemented by Medscape, LLC and Emerging Infectious Diseases. Medscape, LLC is jointly accredited with commendation by the Accreditation Council for Continuing Medical Education (ACCME), the Accreditation Council for Pharmacy Education (ACPE), and the American Nurses Credentialing Center (ANCC), to provide continuing education for the healthcare team.

Medscape, LLC designates this Journal-based CME activity for a maximum of 1.00 ***AMA PRA Category 1 Credit(s)™***. Physicians should claim only the credit commensurate with the extent of their participation in the activity.

Successful completion of this CME activity, which includes participation in the evaluation component, enables the participant to earn up to 1.0 MOC points in the American Board of Internal Medicine's (ABIM) Maintenance of Certification (MOC) program. Participants will earn MOC points equivalent to the amount of CME credits claimed for the activity. It is the CME activity provider's responsibility to submit participant completion information to ACCME for the purpose of granting ABIM MOC credit.

All other clinicians completing this activity will be issued a certificate of participation. To participate in this journal CME activity: (1) review the learning objectives and author disclosures; (2) study the education content; (3) take the post-test with a 75% minimum passing score and complete the evaluation at https://www.medscape.org/qna/processor/72389?showStandAlone=true&src=prt_jcme_eid_mscpedu; and (4) view/print certificate. For CME questions, see page 1985.

NOTE: It is Medscape's policy to avoid the use of Brand names in accredited activities. However, in an effort to be as clear as possible, trade names are used in this activity to distinguish between the mixtures and different tests. It is not meant to promote any particular product.

Release date: August 22, 2024; Expiration date: August 22, 2025

Learning Objectives

Upon completion of this activity, participants will be able to:

1. Distinguish the most common clinical presentation in cases of *Streptococcus dysgalactiae* subspecies equisimilis (SDSE) bacteremia
2. Assess antibiotic therapy of SDSE bacteremia in the current study
3. Evaluate outcomes of SDSE bacteremia
4. Analyze predictors of severe SDSE bacteremia

CME Editor

Susan Zunino, PhD, Technical Writer/Editor, Emerging Infectious Diseases. *Disclosure: Susan Zunino, PhD, has no relevant financial relationships.*

CME Author

Charles P. Vega, MD, Health Sciences Clinical Professor of Family Medicine, University of California, Irvine School of Medicine, Irvine, California. *Disclosure: Charles P. Vega, MD, has the following relevant financial relationships: served as consultant or advisor for Boehringer Ingelheim; GlaxoSmithKline.*

Authors

Viivi Nevanlinna, MD; Janne Aittoniemi, MD, PhD; Reetta Huttunen, MD, PhD; Tiina H. Luukkaala, MSc; Sari Rantala, MD, PhD.

Author affiliations: Tampere University, Tampere, Finland (V. Nevanlinna, R. Huttunen, T. Luukkaala, S. Rantala); Tampere University Hospital, Tampere (V. Nevanlinna, R. Huttunen, T. Luukkaala, S. Rantala); Fimlab Laboratories, Tampere (J. Aittoniemi)

DOI: https://doi.org/10.3201/eid3009.240278

[1]Preliminary results from this study were presented at the European Congress of Clinical Microbiology and Infectious Diseases; April 27–30, 2024; Barcelona, Spain.

We conducted a prospective study of 159 cases of *Streptococcus dysgalactiae* subspecies *equisimilis* (SDSE) bacteremia in 157 patients at 2 hospitals in Finland during November 2015–November 2019. Cellulitis was associated with nonsevere disease (p = 0.008); necrotizing fasciitis was associated with severe disease (p = 0.004). Fifty percent of patients had ≥1 clinical characteristic associated with risk for death. The case-fatality rate was 6%, and 7% of patients were treated in an intensive care unit. Blood leukocyte counts on days 2 (p = 0.032) and 3 (p = 0.020) and C-reactive protein levels on days 3 (p = 0.030) and 4 (p = 0.009) after admission were predictors of severe disease. The Pitt bacteremia score was an accurate predictor of death. Using the Pitt bacteremia score, leukocyte counts, and CRP responses during initial treatment can improve treatment strategies and survival for patients with SDSE.

Streptococcus dysgalactiae subspecies *equsimilis* (SDSE) is a β-hemolytic *Streptococcus* species mainly expressing Lancefield antigens C or G (*1*). The incidence of SDSE bacteremia has been increasing, and SDSE has surpassed *S. pyogenes* as the primary cause of β-hemolytic streptococcal bacteremia in several countries (*2*–*4*).

The clinical manifestations of SDSE bacteremia resemble those caused by *S. pyogenes*, such as cellulitis, pneumonia, endocarditis, and necrotizing fasciitis (*5*). Death associated with SDSE bacteremia has varied from 8% to 20% (*6*–*9*), reaching 33% in patients with more severe clinical manifestations (*10*). Nevertheless, only a few studies provide data on disease severity of SDSE bacteremia (*8*,*11*–*15*), and information on factors contributing to severe disease is lacking. In a study from Canada, 70% of SDSE bacteremia episodes were associated with severe disease, involving admission to an intensive care unit (ICU) or the need for vasopressor or ventilator support (*11*).

Endocarditis has been observed in 6%–7% of SDSE bacteremia patients; 29% of those patients required ICU treatment, and embolic complications developed in 45%–46% (*11*,*16*,*17*). Although necrotizing fasciitis has been relatively uncommon among SDSE bacteremia patients, a large multicenter study on necrotizing soft tissue infections identified SDSE as the second most common causative agent after *S. pyogenes*, contributing to 7% of cases (*18*). Septic shock developed in 41% of patients with necrotizing soft tissue infections caused by SDSE, and 89% of those required mechanical ventilation (*18*).

The Pitt bacteremia score (PBS) is a clinical scoring system used to assess the severity of acute illness in patients with bloodstream infections (*19*). PBS uses a scale ranging from 0 to 14 points; patients with a PBS score ≥4 are categorized as critically ill and have a high death risk. Compared with other scores that determine acute severity of illness, PBS has performed well and is simple to use because it is solely derived from variables identified during the initial physical examination. PBS has been extensively assessed in bloodstream infections and also in nonbacteremic infections; however, the accuracy of the score has not been evaluated for SDSE bacteremia (*19*–*21*).

We conducted a prospective study on clinical aspects and disease severity in patients with SDSE bacteremia. The aim of this study was to examine clinical manifestations of the disease, antibiotic treatment and susceptibility, laboratory test results associated with severe disease, and clinical manifestations requiring ICU treatment. Furthermore, we used the Pitt bacteremia score to assess severity of acute illness in SDSE bacteremia.

Methods

Tampere University Hospital (TAUH) in Tampere, Finland, is the second-largest tertiary-care hospital in Finland, serving a catchment population of ≈535,000 residents within the Pirkanmaa health district. We included adult patients with ≥1 SDSE-positive blood culture who were hospitalized at TAUH or Hatanpää City Hospital in Tampere during November 2015–November 2019 in the study population. At the beginning of 2017, Hatanpää City Hospital was integrated with TAUH. During the study period, we excluded 3 cases of *S. canis* infection, and 2 patients declined to participate. Consequently, the final study population consisted of 159 episodes involving 157 patients with SDSE bacteremia. The study was approved by the Regional Ethics Committee of Tampere University Hospital.

Blood samples were collected in the emergency room at Tampere University Hospital and were studied and cultivated at Fimlab Laboratories in Tampere. During November 2015–October 2017, blood samples were collected into BacT/Alert FA Plus aerobic and FN Plus anaerobic blood culture bottles and incubated in an automated BacT/Alert 3D microbial detection system (bioMérieux). During November 2017–November 2019, blood samples were collected in BD BACTEC Plus Aerobic/F and Lytic/10 Anaerobic/F culture vials and incubated in a BD BACTEC FX blood culture system (Becton Dickinson).

We identified SDSE primarily on the basis of typical large colony-forming growth and β-hemolysis on blood agar plates. Until February 2017, we identified bacteria by using latex bead agglutination to determine Lancefield grouping (PathoDxtra Strep

Grouping Kit; Thermo Fisher Scientific) and confirmed identity by using API 20 Strep (bioMérieux) or matrix-assisted laser desorption/ionization time-of-flight (MALDI-TOF) mass spectrometry (VITEK MS instrument; bioMérieux). Since March 2017, MALDI-TOF mass spectrometry has been the primary method for identification. MALDI-TOF analysis provided results for *S. dysgalactiae* subsp. *dysgalactiae/equisimilis*, which was interpreted as *S. dysgalactiae* subsp. *equisimilis* associated with human disease.

During the study period, a clinical microbiologist (J.A. or T.S.) contacted an infectious disease specialist (S.R.) regarding all SDSE-positive blood cultures. Concurrently, the specialist kept track of SDSE-positive blood cultures in Finland's register for hospital infections and antimicrobial drug use, where all positive blood cultures in Finland are recorded, and contacted SDSE bacteremia patients to obtain informed consent for study participation. In cases where the patient was unable to provide informed consent because of deteriorating condition, we obtained informed consent from the patient's first-degree relatives. We gathered clinical data through a combination of patient interviews and examinations. In addition, we conducted a review of the patients' medical records both during and after hospitalization.

The variables included in the PBS were measured at hospital admission, and we calculated the score for each patient. We defined hypotension as a systolic blood pressure of <90 mm Hg or the need for vasopressors. Mechanical ventilation refers to the use of invasive mechanical support. We categorized mental status as disoriented or unconscious upon admission. Because no specific data on unconsciousness existed at admission, we considered a patient to be unconscious if their mental status deteriorated after admission and the patient was recorded as unconscious during the first 2 days of hospitalization. Body temperature was measured at hospital admission. Data on cardiac arrests were unavailable and were excluded from the score.

We analyzed clinical manifestations and laboratory test results in relation to severe disease, which we defined as treatment in ICU or death within 30 days after hospital admission. We analyzed categorical data by using the χ^2 or Fisher exact test, as appropriate, and analyzed nonparametric data by using the Mann-Whitney U test. We evaluated whether laboratory test results and the PBS predicted death by using receiver operating characteristic (ROC) curves (22). For the ROC method, the area under the curve (AUC) is 1.0 if both sensitivity and specificity of the test are 100% and 0.5 if the test has no diagnostic value. We used the Youden index (sensitivity + specificity – 1) to determine optimal cutoff levels for PBS and laboratory test results that had statistically significant AUCs predicting severe disease or death. We calculated odds ratios (ORs) and 95% CIs and considered p values of <0.05 statistically significant. We performed all statistical analyses by using SPSS Statistics for Mac version 29 (IBM).

Results

The study comprised 159 SDSE bacteremia episodes in 157 patients during November 2015–November 2019. The median patient age was 71 (range 28–93) years, and 95% of patients had underlying conditions. Sixty percent of patients were male and 40% female; 71% percent of patients with severe disease were male and 29% female. The most common clinical manifestations in all patients were cellulitis (69%), purulent skin infections (19%), and pneumonia (15%) (Table 1). Cellulitis was associated with nonsevere disease (p = 0.008), whereas necrotizing fasciitis was associated with severe disease (p = 0.004). Endocarditis was diagnosed in 5 patients, but none of those patients experienced embolic complications, died, or needed intensive care or surgical treatment.

Intravenous antimicrobial drugs were administered as the initial treatment for all episodes. The initial antimicrobial drug treatment was second-generation cephalosporin for 73% of patients with nonsevere disease and 47% of patients with severe disease. In 35% of patients with severe disease, the initial antimicrobial drug treatment was ceftriaxone. The initial antimicrobial drug treatments were effective for all episodes. After 2 days, the antimicrobial drug treatment was narrowed to penicillin G for 43% of all patients: 24% of those patients had severe disease, and 46% had nonsevere disease. Clindamycin treatment was provided to 29% of patients with severe disease and 10% of patients with nonsevere disease. No association was observed between clindamycin treatment and death rate. The median length of intravenous antimicrobial drug treatment was 10 (range 0–45) days. None of the patients received intravenous immunoglobulin therapy. All SDSE isolates were susceptible to penicillin and cephalosporins. Clindamycin resistance was found in 4 (3%) isolates. Erythromycin resistance was found in 16% of isolates, and 3% of isolates had intermediate sensitivity to erythromycin.

The 30-day case-fatality rate for all patients was 6% (9 patients). The 2-day case-fatality rate was 3%, and the 7-day case-fatality rate was 4%. The median age of deceased patients was 77 (range 69–88) years; 56% were male and 44% female. Associations between

Table 1. Clinical manifestations and disease severity in patients with *Streptococcus dysgalactiae* subspecies *equisimilis* bacteremia during November 2015–November 2019, Finland*

Infection type†	Nonsevere disease, n = 142	Severe disease, n = 17	p value
Skin/soft tissue infection	107 (75)	10 (59)	0.154
Cellulitis	103 (73)	7 (41)	0.008
Purulent skin infection	27 (19)	4 (24)	0.746
Necrotizing fasciitis	1 (1)	3 (18)	0.004
Deep abscess	13 (9)	2 (12)	0.664
Bursitis	2 (1)	0	NA
Bone and joint infection	16 (11)	2 (12)	1.000
Osteomyelitis, all	7 (5)	1 (6)	1.000
Spondylitis	7 (5)	1 (6)	1.000
Arthritis, all	10 (7)	2 (12)	0.620
Periprosthetic joint infection	6 (4)	0	NA
Pneumonia	19 (13)	5 (29)	0.141
Empyema	1 (1)	0	NA
Endocarditis	5 (4)	0	NA
Aortitis	0	1 (6)	NA
Foreign body infection	3 (2)	0	NA
Puerperal sepsis	4 (3)	0	NA
Intraabdominal infection	2 (1)	0	NA
Endophthalmitis	2 (1)	0	NA
Bacteremia without defined focus	14 (10)	3 (18)	0.397

*Values are no. (%) except as indicated. Severe disease was defined as treatment in the intensive care unit or death within 30 days after hospital admission. NA, not applicable.
†One patient might have ≥1 clinical manifestations.

clinical characteristics and risk for death were studied (Table 2); 50% of all patients (48% of survivors and 78% of nonsurvivors [p = 0.094]) had ≥1 clinical characteristic significantly associated with risk factors for death, which included admission to an ICU, hypotension, need for vasopressors, lowered level of consciousness, septic shock, multiorgan failure, or surgical intervention. The case-fatality rates were high for patients who experienced unconsciousness (43%), multiorgan failure (33%), and septic shock (28%). Surgical intervention was needed for 24% of all patients. The most commonly required surgical interventions were amputation (5%), abscess drainage (5%), joint aspiration or lavage (3%), and prosthetic joint replacement or removal (3%). Most (84%) patients showed their first symptoms within 24 hours before hospital admission. We did not observe a significant difference in the median duration of symptoms before hospital admission between nonsurvivors and survivors (p = 0.858). Among survivors, 17 (11%) patients had nosocomial infections (symptoms manifested after prior discharge from inpatient care or ≥48 hours after hospitalization). In contrast, all patients who died had community-acquired SDSE bacteremia (p = 0.599).

We calculated PBS for each patient and found it was a significant predictor of death (Table 3; Figure). ROC analysis indicated PBS had an AUC of 0.775 (95% CI 0.555–0.995; p = 0.014). The optimal cutoff determined by the Youden index was PBS ≥3; PBS was strongly associated with 30-day mortality at

Table 2. Disease severity among 159 episodes of *Streptococcus dysgalactiae* subspecies *equisimilis* bacteremia during November 2015–November 2019, Finland*

Characteristic	Total, n = 159	Survivors, n = 150	Nonsurvivors, n = 9	p value
Admitted to intensive care unit	11 (7)	8 (5)	3 (33)	0.017
Needed mechanical ventilation	3 (2)	2 (1)	1 (11)	0.161
Needed continuous renal replacement therapy	1 (1)	1 (1)	0	NA
Needed hemodialysis	1 (1)	1 (1)	0	NA
Needed vasopressors	15 (9)	12 (8)	3 (33)	0.041
Lowered level of consciousness†	37 (23)	31 (21)	6 (67)	0.005
Unconscious	7 (4)	4 (3)	3 (33)	0.004
Hypotension‡	36 (23)	30 (20)	6 (67)	0.005
Septic shock§	18 (11)	13 (9)	5 (56)	0.001
Disseminated intravascular coagulation¶	6 (4)	5 (3)	1 (11)	0.299
Multiorgan failure#	12 (8)	8 (5)	4 (44)	0.002
Underwent surgical intervention	38 (24)	33 (22)	5 (56)	0.037

*Values are no. (%) except as indicated; p values compare survivors and nonsurvivors. NA, not applicable.
†Lowered level of consciousness (unconscious or confusion) ≥1 time during the first 2 days after positive blood culture.
‡Systolic blood pressure <90 mm Hg ≥1 time during days 0–2 after positive blood culture.
§Use of vasopressor and blood lactate level >2 mmol/L ≥1 time during days 0–2 after positive blood culture.
¶Platelet counts $<100 \times 10^9$/L.
#Observed ≥3 concomitant organ failures.

Table 3. Variables included in the Pitt bacteremia score in study of clinical aspects and disease severity of *Streptococcus dysgalactiae* subspecies *equisimilis* bacteremia, Finland*

Variable	Point allocation
Hypotension†	2
Mechanical ventilation	2
Mental status	
Disoriented	1
Unconscious	4
Body temperature, °C	
35.1–36 or 39–39.9	1
≤35.0 or ≥40.0	2

*All variables recorded at hospital admission.
†Systolic blood pressure <90 mm Hg or vasopressor required.

this cutoff, having 78% sensitivity and 87% specificity (OR 22.84 [95% CI 4.41–118.22]; p<0.001). A PBS ≥4 was also associated with 30-day mortality but had 44% sensitivity and 95% specificity (OR 15.54 [95% CI 3.41–70.96]; p = 0.002).

Eleven patients with SDSE bacteremia were admitted to an ICU (Table 4). Their median age was 68 (range 35–85) years, and the median length of ICU stay was 3 (range 1–7) days; 2 patients were female and 9 male. Three of the 11 patients died, 10 manifested general deterioration, 9 had fever, and 6 had dyspnea. Cellulitis was the most common clinical manifestation in 5 patients, but several patients had ≥1 clinical sign. Eight patients were hypotensive and needed vasopressors, 3 patients needed mechanical ventilation, and 1 required continuous renal replacement therapy. All patients treated in an ICU had elevated blood lactate and procalcitonin levels. The median lactate level in blood was 3.5 (range 0.5–4.9) mmol/L; the median procalcitonin level in blood was 11.8 (range 2.1–88.5) μg/L.

We determined associations between laboratory test results from SDSE bacteremia patients and nonsevere or severe disease (Table 5). Decreases in leukocyte counts and C-reactive protein (CRP) levels in blood during the first days of treatment were less for patients with severe disease than those with nonsevere disease. The leukocyte counts were significantly higher on days 2 and 3, and CRP levels were higher on days 3 and 4 after admission in patients with severe disease than those with nonsevere disease. Blood creatinine levels were higher in patients with severe disease than those with nonsevere disease at admission and during the first day of hospitalization.

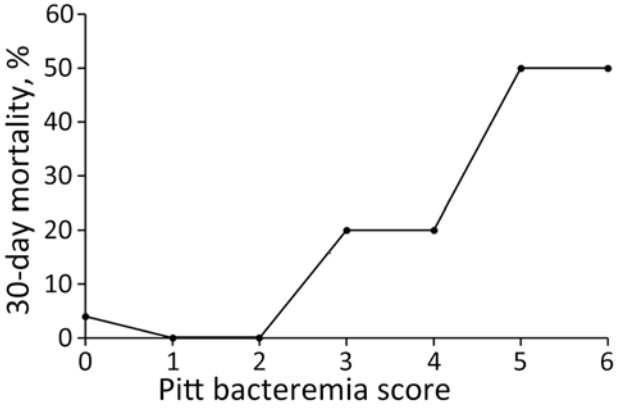

Figure. Association between 30-day mortality and Pitt bacteremia scores in study of clinical aspects and disease severity of *Streptococcus dysgalactiae* subspecies *equisimilis* bacteremia, Finland. Pitt bacteremia score was a significant predictor of death for infected patients with bacteremia.

We analyzed the predictive value of laboratory test results for severe disease by using ROC curves. The leukocyte counts on days 2 and 3, the CRP levels on days 3 and 4, and the highest level of alanine aminotransferase (ALT) during days 0–4 after admission were significant predictors of severe disease. The AUC for leukocyte counts was 0.680 (95% CI 0.522–0.839; p = 0.026) on day 2 and 0.713 (95% CI 0.584–0.877; p = 0.011) on day 3. The AUC for CRP was 0.697 (95% CI 0.553–8.62; p = 0.019) on day 3 and 0.740 (95% CI 0.569–0.991; p = 0.006) on day 4. The AUC of the highest ALT level during days 0–4 was 0.674 (95% CI 0.501–0.848; p = 0.049).

We determined optimal cutoff levels for laboratory test results predicting severe disease by using the Youden index. A leukocyte count >14.1 × 10^9 cells/L on day 2 had a 64% sensitivity and 74% specificity (OR 4.48 [95% CI 1.37–14.61]; p = 0.021). A leukocyte count >12.5 × 10^9 cells/L on day 3 had a 64% sensitivity and 80% specificity (OR 6.78 [95% CI 1.83–25.08]; p = 0.004). CRP levels >199 mg/L on day 3 had a 64% sensitivity and 72% specificity (OR 4.50 [95% CI 1.24–16.33]; p = 0.035). CRP levels >163 mg/L on day 4 had a 73% sensitivity and 75% specificity (OR 8.00 [95% CI 1.97–32.42]; p = 0.002). The highest measured ALT level during days 0–4 that was >53 U/L had a 67% sensitivity and 79% specificity (OR 7.65 [95% CI 2.06–28.44]; p = 0.002).

Discussion

We observed an association between cellulitis and nonsevere disease in SDSE, whereas necrotizing fasciitis was associated with severe disease. A previous study also indicated that cellulitis, which is a clinical manifestation of β-hemolytic streptococcal bacteremia, predicted a favorable prognosis (*8*). In this study, 3 of 4 patients with necrotizing fasciitis had severe disease, and 2 of those patients died. Mortality rates of 19%–33% have been reported for patients with necrotizing fasciitis caused by SDSE (*10*,*18*). Endocarditis caused by SDSE

has a high prevalence of embolic complications and high mortality rates, similar to that for endocarditis caused by *Staphylococus aureus* (*16*,*17*,*23*). Our findings diverge from those previous studies; all 5 patients with endocarditis had nonsevere disease, and none experienced embolic complications or required surgical intervention. Pneumonia seemed to be associated with severe disease, although statistical significance was not reached. No data on the association between pneumonia and death in patients with SDSE bacteremia are available, but pneumonia has been associated with marked mortality rates for patients with group A *Streptococcus* bacteremia (*24*,*25*). In contrast to previous studies, patients without a defined disease focus had relatively favorable outcomes.

In our study, 50% of patients manifested ≥1 clinical characteristic associated with risk for death. Despite this finding, the case-fatality rate (6%) remained relatively low. In previous studies of SDSE bacteremia, 6%–24% of patients required treatment in an ICU, 7%–19% required vasopressors, and 0%–17% required ventilation support (*12*–*14*). In another study, 70% of SDSE episodes were associated with markers of severe disease, including ICU admission and the need for vasopressors or ventilation support (*11*).

Surgical intervention was required for 24% of all SDSE bacteremia patients and 55% of patients treated in an ICU. In previous studies on SDSE bacteremia, the reported need for surgical intervention showed substantial variability, ranging from 18% to as high as 58.8% (*11*,*12*,*26*,*27*). For patients with group A *Streptococcus* bacteremia, surgical intervention was required in 37% of patients overall (*28*) and 61% of patients treated in an ICU (*24*).

Case-fatality rates ranging from 2% to 21% have been reported for patients with SDSE bacteremia (*12*,*29*), but no consistent trend in case-fatality rates has been identified. However, in a previous study from the Pirkanmaa health district, the case-fatality rates were 22% for patients with group C and 15% for those with group G *Streptococcus* bacteremia (*8*). For all bloodstream infections in Finland, case-fatality rates have remained stable at 13% since 2004 (*30*). The

Table 4. Clinical synopses of 11 patients with *Streptococcys dysgalactiae* subspecies *equisimilis* bacteremia who were treated in an intensive care unit during November 2015–November 2019, Finland

Patient no.	Age, y*/sex	Symptoms	Clinical syndrome	Continuous renal replacement therapy	Mechanical ventilation	Vasopressors	ICU stay, d	Outcome
1	80/M	Fever, general deterioration, dyspnea, cough	Cellulitis, pneumonia	No	No	No	3	Survived
2	60/F	Fever, general deterioration, dyspnea	Arthritis	No	Yes	No	3	Survived
3	71/M	Fever, pain, general deterioration, altered mental status, dyspnea	Cellulitis, pneumonia	No	No	Yes	3	Died
4	69/F	Fever, general deterioration, nausea, altered mental status, dyspnea	Purulent skin infection	No	No	Yes	4	Died
5	68/M	General deterioration, dyspnea	No defined focus	No	No	Yes	1	Survived
6	85/M	Fever, general deterioration, nausea, dyspnea	Cellulitis	No	No	Yes	1	Survived
7	43/M	General deterioration	Cellulitis, spondylitis, arthritis, osteomyelitis	No	No	Yes	2	Survived
8	59/M	Fever, general deterioration, altered mental status	Cellulitis	Yes	No	No	4	Survived
9	82/M	Fever, pain, general deterioration, altered mental status	Necrotizing fasciitis	No	Yes	Yes	2	Died
10	35/M	Fever, pain, nausea	Necrotizing fasciitis, abscess	No	No	Yes	2	Survived
11	66/M	Fever, general deterioration, nausea, altered mental status	Pneumonia	No	Yes	Yes	7	Survived

*Age at hospital admission.

Table 5. Laboratory test results of patients with *Streptococcus dysgalactiae* subspecies *equisimilis* bacteremia in relation to nonsevere and severe disease during November 2015–November 2019, Finland*

Laboratory test	Nonsevere disease, n = 142	Severe disease, n = 17	p value
Leukocyte count, × 10^9 cells/L			
Day 0	16 (11–19)	14 (11–21)	0.973
Day 1	13 (10–18)	15 (11–23)	0.370
Day 2	11 (8–15)	15 (10–21)	0.032
Day 3	10 (7–12)	15 (10–16)	0.020
Highest†	17 (12–21)	19 (12–25)	0.488
C-reactive protein, mg/L			
Day 0	70 (20–179)	196 (21–344)	0.093
Day 1	177 (123–274)	195 (94–360)	0.439
Day 2	207 (124–283)	256 (120–348)	0.329
Day 3	149 (79–217)	217 (124–305)	0.030
Day 4	99 (51–163)	193 (100–260)	0.009
Highest‡	237 (163–320)	328 (162–385)	0.202
Creatinine, μmol/L			
Day 0	94 (78–122)	113 (84–203)	0.046
Day 1	93 (81–121)	135 (89–182)	0.043
Day 2	94 (73–121)	103 (80–175)	0.137
Platelet count, × 10^9/L			
Day 0	196 (159–234)	169 (143–216)	0.178
Day 2	183 (146–217)	142 (105–212)	0.175
Highest ALT,§ U/L	26 (18–41)	58 (25–69)	0.052

*Values are median (interquartile range) except as indicated. Severe disease was defined as treatment in the intensive care unit or death within 30 days after hospital admission. ALT, alanine aminotransferase.
†Highest count during days 0–3.
‡Highest level during days 0–4.
§Highest level during days 0–4.

relatively low case-fatality rates in our study could be partly attributed to early recognition of the disease and enhanced treatment protocols.

In this study, we showed a clinical overview of ICU-treated SDSE bacteremia. Most patients admitted to an ICU exhibited nonspecific symptoms, such as general deterioration, fever, and dyspnea. Among the patients treated in an ICU, 2 had necrotizing fasciitis, which was identified as a risk factor for severe disease. However, most ICU-treated patients manifested nonnecrotizing soft tissue infections or pneumonia. Although data on ICU treatment for patients with SDSE bacteremia are lacking, studies on ICU-treated group A *Streptococcus* bacteremia indicated cellulitis and pneumonia were the most common clinical manifestations (*24*,*25*). However, in ICU-treated group A *Streptococcus* bacteremia, the proportion of necrotizing fasciitis cases has been substantially higher than that for SDSE bacteremia (*24*,*31*). In our study, most ICU-treated patients survived, possibly because of effective treatment but also careful patient selection practice, which excluded those with a very poor prognosis. Furthermore, TAUH has high-dependency units, where treatments such as vasopressor support are administered, lowering the need for ICU treatment.

The PBS has been used for >30 years to assess mortality risk for bloodstream infections (*32*). Our findings indicate that PBS serves as an accurate predictor of death from SDSE bacteremia. Although the previously validated cutoff value of ≥4 had high specificity in our study, it was achieved at the expense of sensitivity. In contrast to previous studies, we identified an optimal PBS cutoff point of ≥3, which achieved a maximum balance between sensitivity and specificity. This deviation from previous findings might be attributed to the relatively small number of patients in our study who died. In addition, excluding cardiac arrest from the score might have partly contributed to the relatively low overall scores.

We observed erythromycin resistance in 16% and clindamycin resistance in 3% of SDSE isolates. Increasing SDSE resistance to erythromycin or clindamycin have been reported. In Norway, resistance to both clindamycin and erythromycin, which was absent before 2009, increased to 12% during 2016–2018 (*33*). Similarly, in Japan, macrolide resistance increased from 10.3% during 2003–2005 to 18.5% during 2010–2013 (*4*,*34*).

We did not observe significant associations between leukocyte counts or CRP levels and disease severity at admission. However, significant associations with severe disease were identified on days 2 and 3 for leukocyte counts and on days 3 and 4 for CRP levels after admission. In an SDSE bacteremia study in Japan, an insufficient leukocyte response and thrombocytopenia at admission were linked to poor outcomes, but CRP levels were not predictive at admission, which agrees with our findings (*13*). Confirming our findings, another study on the association between CRP levels and death in patients

with sepsis showed that a CRP value >100 mg/dL on day 3 after hospital admission was linked to a fatal outcome (*35*). Our findings suggest that monitoring leukocyte and CRP responses during the initial days of treatment is crucial. If an adequate response is not observed after a few days of treatment, heightened attention to more intensive treatment is warranted.

A major strength of this study is the prospective design, enabling the systematic and reliable collection of a broad range of clinical data. All data were consistently gathered by the same infectious disease specialist, and the study encompassed a relatively large population. However, some data used to determine PBS in previous studies were unavailable in our study. Although scoring performed well in predicting death, limited available data might have contributed to the comparatively lower scores observed in our study. Data collected from laboratory test results were also limited.

In conclusion, this prospective study on SDSE bacteremia revealed necrotizing fasciitis is a risk factor for severe disease, whereas cellulitis is associated with a favorable prognosis. Despite a substantial proportion of patients manifesting characteristics associated with mortality risk, the overall mortality rate remained relatively low, underscoring the importance of prompt and effective treatment. The PBS accurately predicted death of patients with SDSE bacteremia. Leukocyte counts and CRP responses during the initial days of treatment emerged as valuable indicators of disease severity. Clinicians should consider using the PBS, leukocyte counts, and CRP responses during initial treatment with antimicrobial drugs to improve treatment strategies and survival of patients with SDSE.

Acknowledgments

We thank Tapio Seiskari for contributing to SDSE isolate collection.

This study was supported by research funding from Tampere University (to V.N.) and Tampere University Hospital (to S.R.) and by grants from the Orion Research Foundation (to V.N.), the Finnish Medical Foundation (to S.R.), and the Tampere Tuberculosis Foundation (to S.R.). The authors used GPT-3.5, produced by OpenAI, to enhance the language and readability of this manuscript.

About the Author

Dr. Nevanlinna is a physician and PhD candidate in the Faculty of Medicine and Health Technology at Tampere University, Finland. Her academic interests include invasive *S. dysgalactiae* subsp. *equisimilis* infections.

References

1. Facklam R. What happened to the streptococci: overview of taxonomic and nomenclature changes. Clin Microbiol Rev. 2002;15:613–30. https://doi.org/10.1128/CMR.15.4.613-630.2002
2. Nevanlinna V, Huttunen R, Aittoniemi J, Luukkaala T, Rantala S. Incidence, seasonal pattern, and clinical manifestations of *Streptococcus dysgalactiae* subspecies *equisimilis* bacteremia; a population-based study. Eur J Clin Microbiol Infect Dis. 2023;42:819–25. https://doi.org/10.1007/s10096-023-04607-8
3. Oppegaard O, Glambek M, Skutlaberg DH, Skrede S, Sivertsen A, Kittang BR. *Streptococcus dysgalactiae* bloodstream infections, Norway, 1999–2021. Emerg Infect Dis. 2023;29:260–7. https://doi.org/10.3201/eid2902.221218
4. Wajima T, Morozumi M, Hanada S, Sunaoshi K, Chiba N, Iwata S, et al. Molecular characterization of invasive *Streptococcus dysgalactiae* subsp. *equisimilis*, Japan. Emerg Infect Dis. 2016;22:247–54. https://doi.org/10.3201/eid2202.141732
5. Rantala S. *Streptococcus dysgalactiae* subsp. *equisimilis* bacteremia: an emerging infection. Eur J Clin Microbiol Infect Dis. 2014;33:1303–10. https://doi.org/10.1007/s10096-014-2092-0
6. Oppegaard O, Mylvaganam H, Kittang BR. Beta-haemolytic group A, C and G streptococcal infections in western Norway: a 15-year retrospective survey. Clin Microbiol Infect. 2015; 21:171–8. https://doi.org/10.1016/j.cmi.2014.08.019
7. Broyles LN, Van Beneden C, Beall B, Facklam R, Shewmaker PL, Malpiedi P, *et al.* Population-based study of invasive disease due to β-hemolytic streptococci of groups other than A and B. Clin Infect Dis. 2009;48:706–12. https://doi.org/10.1086/597035
8. Rantala S, Vuopio-Varkila J, Vuento R, Huhtala H, Syrjänen J. Predictors of mortality in beta-hemolytic streptococcal bacteremia: a population-based study. J Infect. 2009;58:266–72. https://doi.org/10.1016/j.jinf.2009.01.015
9. Laupland KB, Pasquill K, Parfitt EC, Steele L. Bloodstream infection due to β-hemolytic streptococci: a population-based comparative analysis. Infection. 2019;47:1021–5. https://doi.org/10.1007/s15010-019-01356-9
10. Bruun T, Kittang BR, de Hoog BJ, Aardal S, Flaatten HK, Langeland N, et al. Necrotizing soft tissue infections caused by *Streptococcus pyogenes* and *Streptococcus dysgalactiae* subsp. *equisimilis* of groups C and G in western Norway. Clin Microbiol Infect. 2013;19:E545–50. https://doi.org/10.1111/1469-0691.12276
11. Lother SA, Demczuk W, Martin I, Mulvey M, Dufault B, Lagacé-Wiens P, et al. Clonal clusters and virulence factors of group C and G *Streptococcus* causing severe infections, Manitoba, Canada, 2012–2014. Emerg Infect Dis. 2017;23:1079–88. https://doi.org/10.3201/eid2307.161259
12. Kittang BR, Bruun T, Langeland N, Mylvaganam H, Glambek M, Skrede S. Invasive group A, C and G streptococcal disease in western Norway: virulence gene profiles, clinical features and outcomes. Clin Microbiol Infect. 2011;17:358–64. https://doi.org/10.1111/j.1469-0691.2010.03253.x
13. Takahashi T, Sunaoshi K, Sunakawa K, Fujishima S, Watanabe H, Ubukata K; Invasive Streptococcal Disease Working Group. Clinical aspects of invasive infections with *Streptococcus dysgalactiae* ssp. *equisimilis* in Japan:

differences with respect to *Streptococcus pyogenes* and *Streptococcus agalactiae* infections. Clin Microbiol Infect. 2010; 16:1097–103. https://doi.org/10.1111/j.1469-0691.2009.03047.x
14. Shinohara K, Murase K, Tsuchido Y, Noguchi T, Yukawa S, Yamamoto M, et al. Clonal expansion of multidrug-resistant *Streptococcus dysgalactiae* subspecies *equisimilis* causing bacteremia, Japan, 2005–2021. Emerg Infect Dis. 2023;29:528–39. https://doi.org/10.3201/eid2903.221060
15. Ikebe T, Murayama S, Saitoh K, Yamai S, Suzuki R, Isobe J, et al.; Working Group for Streptococci in Japan. Surveillance of severe invasive group-G streptococcal infections and molecular typing of the isolates in Japan. Epidemiol Infect. 2004;132:145–9. https://doi.org/10.1017/S0950268803001262
16. Bläckberg A, Nilson B, Özenci V, Olaison L, Rasmussen M. Infective endocarditis due to *Streptococcus dysgalactiae*: clinical presentation and microbiological features. Eur J Clin Microbiol Infect Dis. 2018;37:2261–72. https://doi.org/10.1007/s10096-018-3367-7
17. Lother SA, Jassal DS, Lagacé-Wiens P, Keynan Y. Emerging group C and group G streptococcal endocarditis: a Canadian perspective. Int J Infect Dis. 2017;65:128–32. https://doi.org/10.1016/j.ijid.2017.10.018
18. Bruun T, Rath E, Madsen MB, Oppegaard O, Nekludov M, Arnell P, et al.; INFECT Study Group. Risk factors and predictors of mortality in streptococcal necrotizing soft-tissue infections: a multicenter prospective study. Clin Infect Dis. 2021;72:293–300. https://doi.org/10.1093/cid/ciaa027
19. Chow JW, Yu VL. Combination antibiotic therapy versus monotherapy for gram-negative bacteraemia: a commentary. Int J Antimicrob Agents. 1999;11:7–12. https://doi.org/10.1016/S0924-8579(98)00060-0
20. Battle SE, Augustine MR, Watson CM, Bookstaver PB, Kohn J, Owens WB, et al. Derivation of a quick Pitt bacteremia score to predict mortality in patients with gram-negative bloodstream infection. Infection. 2019;47:571–8. https://doi.org/10.1007/s15010-019-01277-7
21. Henderson H, Luterbach CL, Cober E, Richter SS, Salata RA, Kalayjian RC, et al. The Pitt bacteremia score predicts mortality in nonbacteremic infections. Clin Infect Dis. 2020;70:1826–33. https://doi.org/10.1093/cid/ciz528
22. Harrell FE Jr, Califf RM, Pryor DB, Lee KL, Rosati RA. Evaluating the yield of medical tests. JAMA. 1982;247:2543–6. https://doi.org/10.1001/jama.1982.03320430047030
23. Oppegaard O, Mylvaganam H, Skrede S, Jordal S, Glambek M, Kittang BR. Clinical and molecular characteristics of infective β-hemolytic streptococcal endocarditis. Diagn Microbiol Infect Dis. 2017;89:135–42. https://doi.org/10.1016/j.diagmicrobio.2017.06.015
24. Mehta S, McGeer A, Low DE, Hallett D, Bowman DJ, Grossman SL, et al. Morbidity and mortality of patients with invasive group A streptococcal infections admitted to the ICU. Chest. 2006;130:1679–86. https://doi.org/10.1016/S0012-3692(15)50887-8
25. Lamagni TL, Neal S, Keshishian C, Alhaddad N, George R, Duckworth G, et al. Severe *Streptococcus pyogenes* infections, United Kingdom, 2003–2004. Emerg Infect Dis. 2008;14:202–9. https://doi.org/10.3201/eid1402.070888
26. Sylvetsky N, Raveh D, Schlesinger Y, Rudensky B, Yinnon AM. Bacteremia due to beta-hemolytic *Streptococcus* group G: increasing incidence and clinical characteristics of patients. Am J Med. 2002;112:622–6. https://doi.org/10.1016/S0002-9343(02)01117-8
27. Leitner E, Zollner-Schwetz I, Zarfel G, Masoud-Landgraf L, Gehrer M, Wagner-Eibel U, et al. Prevalence of *emm* types and antimicrobial susceptibility of *Streptococcus dysgalactiae* subsp. *equisimilis* in Austria. Int J Med Microbiol. 2015;305:918–24. https://doi.org/10.1016/j.ijmm.2015.10.001
28. Vilhonen J, Vuopio J, Vahlberg T, Gröndahl-Yli-Hannuksela K, Rantakokko-Jalava K, Oks J. Group A streptococcal bacteremias in Southwest Finland 2007–2018: epidemiology and role of infectious diseases consultation in antibiotic treatment selection. Eur J Clin Microbiol Infect Dis. 2020; 39:1339–48. PubMed https://doi.org/10.1007/s10096-020-03851-6
29. Ekelund K, Skinhøj P, Madsen J, Konradsen HB. Invasive group A, B, C and G streptococcal infections in Denmark 1999–2002: epidemiological and clinical aspects. Clin Microbiol Infect. 2005;11:569–76. https://doi.org/10.1111/j.1469-0691.2005.01169.x
30. Kontula KSK, Skogberg K, Ollgren J, Järvinen A, Lyytikäinen O. Population-based study of bloodstream infection incidence and mortality rates, Finland, 2004–2018. Emerg Infect Dis. 2021;27:2560–9. https://doi.org/10.3201/eid2710.204826
31. Björck V, Påhlman LI, Bodelsson M, Petersson AC, Kander T. Morbidity and mortality in critically ill patients with invasive group A streptococcus infection: an observational study. Crit Care. 2020;24:302. https://doi.org/10.1186/s13054-020-03008-z
32. Al-Hasan MN, Baddour LM. Resilience of the Pitt bacteremia score: 3 decades and counting. Clin Infect Dis. 2020;70:1834–6. https://doi.org/10.1093/cid/ciz535
33. Oppegaard O, Skrede S, Mylvaganam H, Kittang BR. Emerging threat of antimicrobial resistance in β-hemolytic streptococci. Front Microbiol. 2020;11:797. https://doi.org/10.3389/fmicb.2020.00797
34. Sunaoshi K, Murayama SY, Adachi K, Yagoshi M, Okuzumi K, Chiba N, et al. Molecular *emm* genotyping and antibiotic susceptibility of *Streptococcus dysgalactiae* subsp. *equisimilis* isolated from invasive and non-invasive infections. J Med Microbiol. 2010;59:82–8. https://doi.org/10.1099/jmm.0.013201-0
35. Devran O, Karakurt Z, Adıgüzel N, Güngör G, Moçin OY, Balcı MK, et al. C-reactive protein as a predictor of mortality in patients affected with severe sepsis in intensive care unit. Multidiscip Respir Med. 2012;7:47. https://doi.org/10.1186/2049-6958-7-47

Address for correspondence: Viivi Nevanlinna, Department of Internal Medicine, Tampere University Hospital, Elämänaukio 2, Tampere 33520, Finland; email: viivi.nevanlinna@tuni.fi

Loop-Mediated Isothermal Amplification Assay to Detect Invasive Malaria Vector *Anopheles stephensi* Mosquitoes

Cristina Rafferty, Gloria Raise, JeNyiah Scaife, Bernard Abongo, Seline Omondi, Sylvia Milanoi, Margaret Muchoki, Brenda Onyango, Eric Ochomo, Sarah Zohdy

Spread of the *Anopheles stephensi* mosquito, an invasive malaria vector, threatens to put an additional 126 million persons per year in Africa at risk for malaria. To accelerate the early detection and rapid response to this mosquito species, confirming its presence and geographic extent is critical. However, existing molecular species assays require specialized laboratory equipment, interpretation, and sequencing confirmation. We developed and optimized a colorimetric rapid loop-mediated isothermal amplification assay for molecular *An. stephensi* species identification. The assay requires only a heat source and reagents and can be used with or without DNA extraction, resulting in positive color change in 30–35 minutes. We validated the assay against existing PCR techniques and found 100% specificity and analytical sensitivity down to 0.0003 ng of genomic DNA. The assay can successfully amplify single mosquito legs. Initial testing on samples from Marsabit, Kenya, illustrate its potential as an early vector detection and malaria mitigation tool.

In 2012, *Anopheles stephensi*, a primary malaria vector in South Asia, was detected in Djibouti, a country in Africa that was approaching malaria preelimination status (*1*). Unlike typical malaria vectors in Africa, *An. stephensi* mosquitoes can thrive in both urban and rural environments. After the detection in Djibouti, *An. stephensi* mosquitoes were reported in Ethiopia and Sudan in 2016, Somalia in 2019, Nigeria in 2020, Kenya in 2022, and Ghana and Eritrea in 2023 (*2*). The initial detection in Djibouti came during a malaria outbreak (*1*), after which a 36-fold increase in malaria was reported from 2012 to 2020 (*3*). In Dire Dawa, the second largest city in Ethiopia, an unusual dry season outbreak of malaria was reported in 2022, and epidemiologic and entomologic investigations incriminated *An. stephensi* mosquitoes as driving the outbreak (*4*). Furthermore, the species' insecticide resistance status and unique bionomics present a challenge to proven malaria vector control tools, such as insecticide-treated bed nets and indoor residual spraying (*5*,*6*). Modeling studies have predicted that if *An. stephensi* mosquitoes continue to spread throughout Africa, an additional 126 million persons, predominantly in urban areas, will be at risk for malaria (*7*,*8*). To respond to this threat, the World Health Organization (WHO) launched an initiative to halt the spread of *An. stephensi* mosquitoes (*9*), and global organizations (*10*) and countries have released action plans to encourage enhanced surveillance for the species for early detection in new locations and rapid response to halt spread and mitigate impacts.

Despite efforts to enhance surveillance for *An. stephensi* mosquitoes in Africa, the species was not included in morphologic keys until 2020 (*11*). Therefore, the mosquitoes be missed in routine surveillance activities, and *An. stephensi* mosquitoes could be misidentified as the more common malaria vector *An. gambiae* sensu lato if morphological identification is inadequate (*3*). In addition, reporting a detection of *An. stephensi* mosquitoes in a new country to WHO requires molecular confirmation, which can be challenging in resource-limited settings. Surveillance for *An. stephensi* mosquitoes often requires larval surveys

Author affiliations: US President's Malaria Initiative, Centers for Disease Control and Prevention, Atlanta, Georgia, USA (C. Rafferty, S. Zohdy); Centers for Disease Control and Prevention, Atlanta (C. Rafferty, G. Raise, J. Scaife, S. Zohdy); Kenya Medical Research Institute (KEMRI), Kisumu, Kenya (B. Abongo, S. Omondi, S. Milanoi, M. Muchoki, B. Onyango, E. Ochomo)

DOI: https://doi.org/10.3201/eid3009.240444

(*12*) because routine malaria vector adult collections are not optimal for the species (*6*) and currently a validated key to identify *An. stephensi* larvae is not available, so larval samples that do not emerge to adults may also require molecular confirmation.

In 2023, a PCR protocol for *An. stephensi* species identification was released and shown to detect *An. stephensi* mosquitoes even among pooled samples, presenting a promising avenue for molecular detection (*13*). However, PCR can be time consuming and limited by molecular laboratory capacity, access to reagents, trained personnel, and assay specificity and interpretation.

Loop-mediated isothermal amplification (LAMP) assays have been used since the 1990s for rapid amplification of gene targets (*14*), resulting in a visual change through fluorescence, turbidity, or color that provides a qualitative indicator of positivity. In this way, LAMP assays function like conventional PCRs, which yield a band (positive) or no band (negative). However, instead of requiring temperature cycling like PCR, LAMP assays produce copies through looped primer sets at 1 consistent temperature, removing the need for a thermal cycler and instead requiring only a heat block, water bath, or any other device that keeps temperature constant. One study even used hand-warmers and a Styrofoam cup to conduct a LAMP assay (*15*). Because the COVID-19 pandemic increased the need for rapid diagnostics, LAMP technology evolved to include colorimetric and dipstick assays (*16*).

To address the challenges that invasive *An. stephensi* mosquito surveillance and corresponding molecular confirmation present, the aim of this study was to develop an easy-to-interpret, rapid colorimetric LAMP-based *Anopheles stephensi* species (CLASS) identification assay, specifically designed and optimized for use in resource-limited settings or for rapid high-throughput screening. To ensure accuracy and feasibility for deployment of the developed assay, we sought to design optimal primers and assay conditions, determine assay sensitivity and pooling strategies, determine assay specificity when compared with congeners or conspecifics, develop direct sample amplification approaches without the need for DNA extraction, compare results between the existing PCR protocol and CLASS assay, and evaluate CLASS on wild-caught, sequence-confirmed invasive *An. stephensi* mosquitoes from Kenya.

Methods

LAMP Primer Design and Optimization

We designed the LAMP primers by using the NEB LAMP Primer Design Tool version 1.4.1 (New England Biolabs, https://www.neb.com) (*17*). We used the internal transcribed spacer 2 rDNA region unique to *An. stephensi* species, using a sequence from GenBank (accession no. MW732931.1) (*18*). One LAMP primer set contains 5 primers as follows: an outer forward primer (F3), an inner forward primer (FIP), an outer backward primer (B3), an inner backward primer (BIP), and a loop primer (Figure 1) (*19*,*20*). Attempts to set fixed primers resulted in no possible loop primer combinations by the program; therefore, we used default parameters and allowed the program to choose primers.

Of 4 possible primer sets, 2 contained primers in the species-specific region. We tested those primers across a temperature gradient using 2 sets of differing concentrations. Initial test concentrations were adapted from NEB kit manufacturer recommendations, and primer concentrations were based on an *An. gambiae* species identification LAMP assay (*21*).

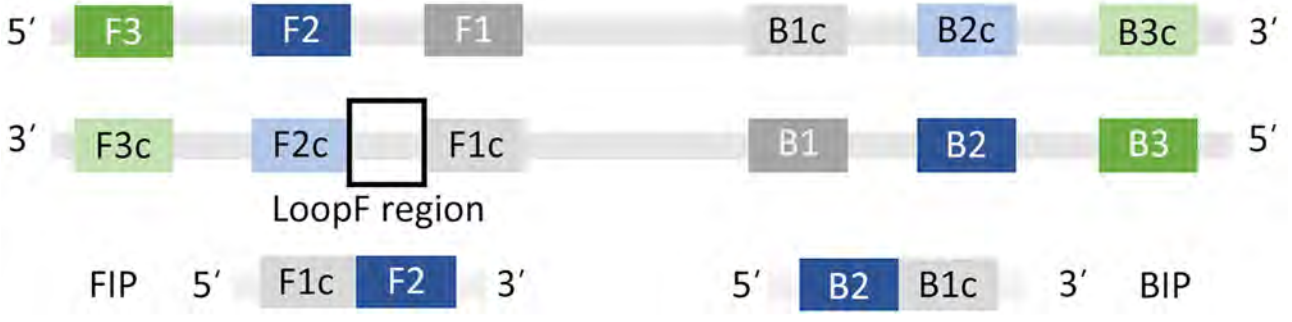

Figure 1. Schematic showing primer design for development of a colorimetric loop-mediated isothermal amplification assay to detect invasive malaria vector *Anopheles stephensi* mosquitoes. Primers were designed by using the NEB LAMP Primer Design Tool version 1.4.1 (New England Biolabs, https://www.neb.com) (*17*). One LAMP primer set contains 5 primers as follows: an outer forward primer (F3), an inner forward primer (FIP), an outer backward primer (B3), an inner backward primer (BIP), and a loop primer (*19*,*20*). Attempts to set fixed primers resulted in no possible loop primer combinations by the program; therefore, we used default parameters and allowed the program to choose primers.

One primer set showed positive, consistent results and minimum cross-reactivity to other species. We then further optimized that primer set for maximum specificity (Table 1; Figure 1).

Insectary-Reared *An. stephensi* and Other Mosquito Species

We obtained larvae and adult insectary-reared and maintained colony mosquitoes from 8 distinct non–*An. stephensi Anopheles* species, 3 strains of *An. stephensi* mosquitoes of different origins (STE2 from India, SDA 500 from Pakistan, UCI from India), and one *Aedes* (*Ae. aegypti*) mosquito. Mosquitoes came from the Malaria Research and Reference Reagent Resource Center through BEI Resources (Table 2) (*22*).

DNA Extraction

We extracted DNA from whole adult, single mosquito leg, and whole third instar larva by using the Extracta DNA Prep for PCR Kit (Quantabio Beverly, https://www.quantabio.com), adapted as follows: mosquito material added to a tube containing either 25 μL (for a single leg) or 50 μL (for a whole adult or larva) of Quantabio Extraction Reagent and incubated at 95°C for 30 minutes. We added an equal volume of Quantabio Stabilization Buffer and stored DNA at −20°C until further analysis. For the pooled species sample, we combined 1 μL of DNA from 9 DNA extractions of non–*An. stephensi* mosquitoes and 1 μL of DNA extracted from *An. stephensi* mosquitoes (STE2) in a microfuge tube and mixed contents.

CLASS Assay

We carried out CLASS reactions by using the NEB WarmStart Colorimetric LAMP 2X Master Mix (New England Biolabs), according to manufacturer recommendations but optimized as follows: 1 μL of genomic DNA was added to 12.5 μL of WarmStart Colorimetric LAMP 2X Master Mix and 10X primers at final concentrations of 5 μM of B3 and F3 primers, 20 μM of BIP and FIP primers, and 10 μM of LF primer. We added molecular-grade water to reach a final volume of 25 μL. We placed reaction tubes in a thermal cycler at 65°C for 30 minutes and inspected visually for color change, where positive amplification appears yellow and negative remains pink. We tested primers on extracted DNA from 12 assorted insectary-reared adults and larvae, including 3 *An. stephensi* strains (STE2, SDA500, and UCI), 14 field-collected specimens including 3 sequence-confirmed *An. stephensi* mosquitoes, and DNA from pooled species. We included a no-DNA control in each run of the assay.

Analytical Sensitivity

To test analytical sensitivity, we made a serial dilution (1:10) of DNA extract from a whole UCI *An. stephensi* mosquito and determined starting DNA concentration by using a NanoDrop 2000c spectrophotometer (Thermo Scientific, https://www.thermofisher.com) on 1 μL of DNA extract. For each concentration, no color change (pink) indicated a negative result and color change (yellow) a positive result. We ran samples from the dilution series in triplicate with no full change detected and 2 additional dilutions to determine the sensitivity cutoff.

Specificity Determination

We tested optimized primers against 12 laboratory anopheline strains that included 3 *An. stephensi* strains (SDA500, STE2, UCI) and 1 *Ae. aegypti* strain (Table 2). We subsequently tested the assay against 96 individual mosquitoes from each *An. stephensi* laboratory strain and 48 *An. gambiae*, *An. coluzzii*, *An. arabiensis*, *An. funestus*, and *Ae. aegypti* laboratory-reared samples for specificity and cross reactivity. We ran all reactions in triplicate to generate data on cross-reactivity with other species and specificity to *An. stephensi.* We included 3 *An. stephensi* strains to determine variations in target specificity across *An. stephensi* mosquitoes of different origins.

Table 1. Looped primers designed by using the NEB LAMP Primer Design Tool targeting *Anopheles stephensi* mosquito ITS2 sequence regions for development of colorimetric LAMP assay to detect invasive malaria vector *An. stephensi* mosquitoes*

Sequence	5′	3′	Primer sequence	Primer concentration
F3	333	351	ATTGCACGGGGACTTCCA	5 μM
B3	504	524	GCCTACAGACTCCACTGTCA	5 μM
FIP			CGACTGCAACTGTATGCGAGGACGGGTCGAGTAACACTTGC	20 μM
BIP			CCGTGTGGGTGAGTGAGGTTAGAATGATGCGACGGGAGAAG	20 μM
LF	383	401	AAGATACGAGCGCGTTGGG	10 μM
F1c†	402	423	CGACTGCAACTGTATGCG	
F2†	359	380	GGACGGGTCGAGTAACACTTGC	
B2†	439	461	CCGTGTGGGTGAGTGAGGTTAG	
B1c†	485	502	AATGATGCGACGGGAGAAG	

*ITS, internal transcribed spacer; LAMP, loop-mediated isothermal amplification; NEB, New England Biolabs, https://www.neb.com.
†Primers not needed for LAMP assay.

Table 2. Mosquito species and corresponding strains and catalog numbers used in development of colorimetric loop-mediated isothermal amplification assay to detect invasive malaria vector *Anopheles stephensi* mosquitoes*

Species	MRA BEI reference no.	Strain name
Anopheles gambiae sensu stricto	112	G3
An. gambiae s.s./*An. coluzzii* hybrid	334	RSP
An. coluzzii	1280	AKDR
An. arabiensis	856	DONGOLA
An. stephensi	1323	UCI
An. stephensi	NA	SDA500
An. funestus s.s	NA	FANG
An. quadriannulatus	1155	SANGWE
An. dirus	700	WRAIR
An. merus	1156	MAF
An. stephensi	128	STE2
Aedes aegypti	734	ROCK

*BEI, BEI Resources, https://www.beiresources.org; MRA, Malaria Repository Acquisition; NA, not applicable.

Samples for LAMP Amplification

To determine whether DNA extract is needed to run the CLASS assay or if tissue (mosquito leg, full larva, full adult mosquito) or pooled DNA amplify, we inserted single legs from insectary-reared mosquitoes directly into the master mix and compared the results with DNA extracted from a single leg. Because *An. stephensi* samples are often collected as larvae, we also tested the assay by immersing a whole larva into the master mix and using extracted DNA from a single larva. We also partially tested eDNA by using 1 µL using larval pan water in lieu of extracted DNA. We further tested the assay against whole adult mosquitoes and compared results with whole adult mosquito DNA. In addition, we tested pooled DNA extract from whole adult mosquitoes and from individual legs from 9 mosquito strains and 1 *An. stephensi* strain.

Conventional PCR Comparison

We compared CLASS results with those from a conventional *An. stephensi* species identification PCR assay by using previously described methods (*13*). We adapted the method as follows: 2X Quantabio Accustart PCR mix, 10 µM of each primer, molecular water to reach a final volume of 20 µL, and 1 µL of the extracted DNA from same species used in the CLASS assay.

CLASS Assay Validation on *An. stephensi* Mosquitoes from Kenya

We ran sequence-confirmed DNA extracted from wild-caught *An. stephensi* mosquitoes from Kenya (GenBank accession nos. OQ275144–6 and OQ878216–8) using the CLASS assay (*23*). We additionally tested 55 wild-caught samples collected from Marsabit, Kenya, in 2023 that previously failed to amplify via conventional PCR (*24*). DNA extracted at the Kenya laboratory was dried and shipped to the US Centers for Disease Control and Prevention (Atlanta, Georgia, USA), where samples were resuspended in 25 µL of PCR-grade water and stored at −20°C until processed.

Results

LAMP Primer Design and Assay Optimization

We tested the 4 primer sets suggested by the NEB LAMP Primer Design Tool version 1.4.1 against extracted DNA from 3 *An. stephensi* insectary strains and 8 other *Anopheles* species: *An. gambiae* s.s., *An. coluzzii*, *An. arabiensis*, *An. gambiae/coluzzii* hybrid, *An. funestus*, *An. quadriannulatus*, *An. dirus*, and *An. merus* (*17*). We tested the 2 primer sets (P2L-45 and P26L2) that showed color change for *An. stephensi* samples and minimum cross-reactivity among other species with varying concentrations at 3 incubation times: 15,

Table 3. Primer set candidates tested with different concentrations to determine effects on sensitivity and specificity of colorimetric loop-mediated isothermal amplification assay to detect invasive malaria vector *Anopheles stephensi* mosquitoes

Concentration combination	Primer concentration					Primer set* P26L2		Primer set* P2L-45	
	F3	B3	FIP	B IP	Loop primer	Sensitivity	Specificity	Sensitivity	Specificity
A1	2 µM	2 µM	16 µM	16 µM	4 µM	X	✓	X	X
A2	4 µM	4 µM	16 µM	16 µM	4 µM	✓	X	X	X
A3	2 µM	2 µM	32 µM	32 µM	4 µM	✓	X	X	X
A4	2 µM	2 µM	16 µM	16 µM	8 µM	X	✓	X	X
B1	5 µM	5 µM	40 µM	40 µM	10 µM	✓	X	✓	X
B2	2.5 µM	2.5 µM	40 µM	40 µM	10 µM	✓	X	X	✓
B3	5 µM	5 µM	20 µM	20 µM	10 µM	✓	✓	X	X
B4	5 µM	5 µM	40 µM	40 µM	5 µM	✓	X	X	X

*For each primer set, a check mark indicates consistent results and an X inconsistent results.

30, and 45 minutes. No color change was detected at 15 minutes, but specificity was affected at 45 minutes, confirming 30 minutes as the ideal assay incubation time. We analyzed 384 reactions in duplicate (768 total reactions) using 8 different primer concentration combinations, and we chose primer set P26L2 for its consistent sensitivity and specificity (Table 3). We tested the chosen primers and respective concentration combinations using a temperature gradient (57°C, 61°C, 65°C, 69°C, 73°C, and 83°C) through 176 separate reactions. Results confirmed that primer concentration combination B3 at 65°C yielded the most consistent and specific results (Table 3). Amplification occurred at 69°C and 73°C, but specificity was inconsistent. We observed no amplification at higher or lower temperatures.

Repeated time-interval testing of 384 samples with the chosen primers showed no amplification before 25 minutes, optimum amplification at 30 minutes, and a decrease of specificity after 35 minutes. Consequently, we adopted a 30-minute incubation period for the assay. Once incubation stopped (by removal from the heat source), the product and color change remained stable and unaltered at room temperature for ≥12 weeks.

CLASS Assay Analytical Sensitivity

To test the sensitivity of the CLASS assay, we performed serial dilutions (1:10) of initial DNA extract to a concentration of 311.6 ng, which resulted in 100% positive color change to yellow. Positive color change was repeatedly observed at ≥0.0003 ng; concentrations <0.0003 ng yielded positive color change, but changes occurred inconsistently (33.3% of the time). Because lower concentrations did not yield 100% color change, the assay sensitivity threshold established in this study is as low as 0.0003 ng, 1,000 times lower than what is found in typical DNA extract from a single leg (Table 4).

CLASS Assay Specificity and Cross-Reactivity

We tested the optimized P26L2 primers (Table 1) against extracted DNA from 11 insectary strains, including 3 *An. stephensi* mosquitoes. We ran the assay 11 separate times with different extracted DNA from single whole-colony mosquitoes for a total of 132 reactions (Figure 2). We further assessed specificity by testing DNA from 96 individual mosquitoes from each *An. stephensi* laboratory strain; 100% of the samples yielded a positive result. We determined cross-reactivity by sampling DNA from 48 *An. gambiae*, 48 *An. coluzzii*, 48 *An. arabiensis*, 48 *An. funestus*, and 48 *Ae. aegypti* whole mosquitoes and analyzing. None (0%) of the non–*An. stephensi* strains showed color change. We ran all specificity assays in triplicate (Table 5).

CLASS Assay Testing of Mosquito Tissue, DNA Extract, and DNA Pooling

Using DNA extract from a single leg resulted in color change in *An. stephensi* mosquitoes, with no cross-reactivity with other tested species. Inserting a single mosquito leg straight into the master mix also successfully amplified after optimization, but at a 35-minute incubation time (Figure 3). When testing a whole larva or whole adult mosquito, the assay had low specificity, and yielded cross-reactivity; however, the use of DNA extract from a single larva or mosquito from 11 *Anopheles* colony strains, including 3 *An. stephensi* strains and 1 *Ae. aegypti* strain, resulted in species-appropriate color change (Figure 3). Limited testing on larval pan water yielded inconclusive results. Although the CLASS assay was able to identify *An. stephensi* from larval pan water and not from other anopheline larval water, results showed cross-reactivity with *Ae. aegypti*.

CLASS Assay Specificity in Field Samples and Comparison with Conventional PCR

Sequence-confirmed *An. stephensi* samples from Kenya positively amplified using CLASS, and no cross-reactivity was seen with other *Anopheles* species. *An. stephensi* sampled in pooled DNA from 9 colony-reared species (*An. gambiae* s.s., *An. coluzzii*, *An. gambiae/coluzzii* hybrid, *An. arabiensis*, *An. funestus*, *An. quadriannulatus*, *An. merus*, *An. dirus*, and *Ae. aegypti*) and 1 *An. stephensi* sample (SDA 500) also amplified using CLASS. Conventional PCR resulted in difficult-

Table 4. Assessment of assay sensitivity for development of colorimetric loop-mediated isothermal amplification assay to detect invasive malaria vector *Anopheles stephensi* mosquitoes*

Template dilution	Template concentration, ng	UCI
NTC	NA	3/3 negative
1	311.6	3/3 positive
10	31.16	3/3 positive
1×10^2	3.12	3/3 positive
1×10^3	0.312	3/3 positive
1×10^4	0.031	3/3 positive
1×10^5	0.003	3/3 positive
1×10^6	0.0003	3/3 positive
1×10^7	0.00003	1/3 positive, 2/3 negative

*Assessment was done using a serial (1:10) dilution from DNA extract containing 311.6 ng of *Anopheles stephensi* (UCI) whole mosquito DNA and resulted in 100% positive color change down to 0.0003 ng. Each dilution test was performed in triplicate. Color change at 1×10^7 was inconsistent, and samples with DNA concentrations <0.0003 were less likely to result in a positive color change and did not display as clear pink or yellow. NA, not applicable; NTC, no template control; UCI, *An. stephensi* laboratory colony (BEI Resources, https://www.beiresources.org).

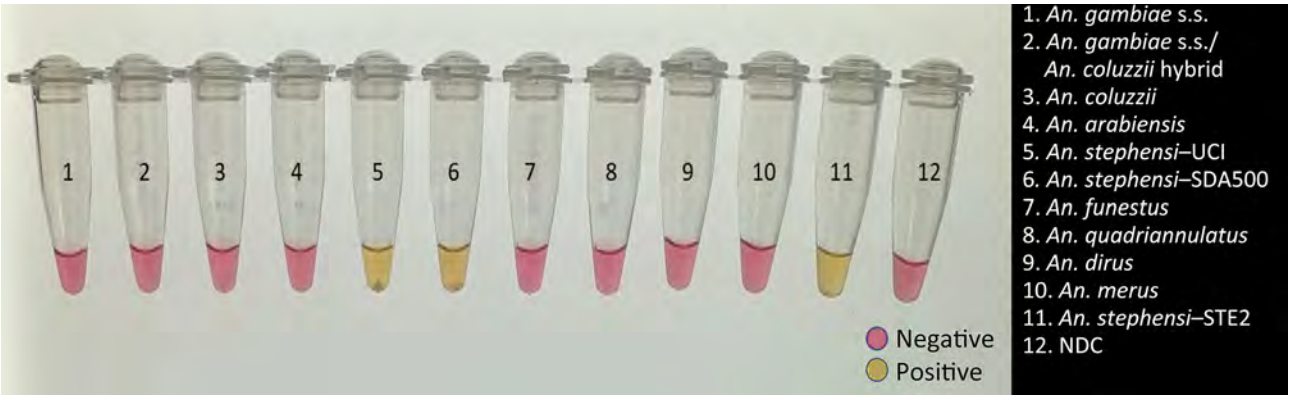

Figure 2. Visualization of testing using a colorimetric loop-mediated isothermal amplification assay to detect invasive malaria vector *Anopheles stephensi* mosquitoes. Positive samples show a color change to yellow, whereas negative samples and control remain pink. Samples were visualized on a white background and photographed on a standard light box. NDC, no DNA template control; UCI, *An. stephensi* laboratory colony (BEI Resources, https://www.beiresources.org).

to-interpret gel bands for *An. longipalpis* C, *Ae. aegypti*, and *An. coustani* samples, similar to *An. stephensi* samples, and inconsistently produced double bands (positive detection) on sequence-confirmed *An. stephensi* samples from Kenya (Figure 4, panel B).

CLASS Assay Testing of Field Samples from Marsabit, Kenya

CLASS assay testing of 55 wild-caught *Anopheles* samples from Marasabit, Kenya, successfully identified the 9 cytochrome c oxidase subunit I sequence-confirmed *An. stephensi* samples. Furthermore, no cross-reactivity was observed with the other species or unknown samples (Table 6). Twelve nonamplified samples in the sample set during barcoding also tested negative by the CLASS assay.

Discussion

Molecular species identification of malaria vectors is pivotal for effective control and elimination strategies, particularly because malaria-vector mosquitoes often cannot be morphologically identified to the species level. Of increasing complexity is the introduction of invasive species, such as *An. stephensi*, that are not included in traditional identification keys (*25*) and thus can be easily misidentified. In addition, to confirm the presence of *An. stephensi* mosquitoes on the WHO *An. stephensi* Threats Map (*26*), molecular confirmation through Sanger sequencing (*9*) is required.

We developed a rapid 1-step colorimetric LAMP assay for species identification of *An. stephensi* mosquitoes to accelerate tracking this species across Africa or in locations where it is endemic. The CLASS identification assay provides a precise and reliable means of *An. stephensi* identification. Our findings indicate high sensitivity and specificity of the assay, whether *An. stephensi* samples were mixed in a pool of 10 other species or validated against 8 species, including 3 unique insectary-reared strains and individual wild-caught invasive *An. stephensi* samples. No false positives or false negatives were observed. When we conducted a dilution series to determine analytical sensitivity, even at 0.0003 ng of DNA, the CLASS assay detected *An. stephensi* DNA. Thus far, the specificity remains 100% when other species are processed through the assay. The ability to differentiate

Table 5. Specificity testing for colorimetric loop-mediated isothermal amplification assay to detect invasive malaria vector *Anopheles stephensi* mosquitoes*

Species	Colony name	No. mosquitoes	Experiment 1	Experiment 2	Experiment 3
An. stephensi	STE2	96	Positive (96/96)	Positive (96/96)	Positive (96/96)
An. stephensi	SDA500	96	Positive (96/96)	Positive (96/96)	Positive (96/96)
An. stephensi	UCI	96	Positive (96/96)	Positive (96/96)	Positive (96/96)
An. gambiae senso stricto	G3	48	Negative (0/48)	Negative (0/48)	Negative (0/48)
An. coluzzii	AKDR	48	Negative (0/48)	Negative (0/48)	Negative (0/48)
An. arabiensis	DONGOLA	48	Negative (0/48)	Negative (0/48)	Negative (0/48)
An. funestus s.s	FANG	48	Negative (0/48)	Negative (0/48)	Negative (0/48)
Aedes aegypti	ROCK	48	Negative (0/48)	Negative (0/48)	Negative (0/48)
Total no. samples		528			
Total no. reactions				1,584	

*To determine specificity, we ran the essay in triplicate on extracted DNA from 96 individual mosquitoes from each of the 3 *An. stephensi* insectary strains and DNA extracted from 48 individual mosquitoes from each species of *An. gambiae* sensu stricto, *An. coluzzii*, *An. arabiensis*, *An. funestus*, and *Ae. aegypti*.

between various *Anopheles* species, especially those with differing vectorial capacities or behaviors, is indispensable for tailoring interventions to specific vector populations (*27*).

The CLASS assay can be run using a single mosquito leg or DNA extract from an adult or larval mosquito (Figure 3). DNA extracted from a leg is preferable so specimens can remain largely intact for further curation, sequencing, and storage. The use of an entire mosquito or larva is highly discouraged because it yields nonspecific results and prevents further follow-up and species confirmation. For WHO submission and confirmation, sequencing-positive specimens are still encouraged; however, the CLASS assay provides a rapid, high-throughput, field-friendly screening tool for an initial detection of *An. stephensi* mosquitoes. Although initial testing of larval pan water yielded inconclusive results, possibly because of *Aedes* excessive larval shedding in the water, findings suggest the potential for additional exploration using CLASS to examine environmental DNA or large pools of specimens to yield further information about potential cross-reactivity with other species in natural settings.

A conventional PCR to support molecular detection of *An. stephensi* mosquitoes exists (*13*); however, in settings where facilities and trained personnel are limited, conventional PCR can be challenging. That PCR also has multiple primers, and thus, interpreting results can be a challenge if one or both bands are absent. In our study, insectary and field *Anopheles* samples run through the conventional PCR showed gel bands that could be misinterpreted as false-positive or -negative. Even insectary-reared *An. stephensi* samples produced inconclusive results using that assay (Figure 4, panel B). External laboratories have also reported nonamplification using the assay on samples later confirmed to be *An. stephensi* through sequencing (*23*). Follow-up PCR and Sanger sequencing validation are still critical, but our findings support the

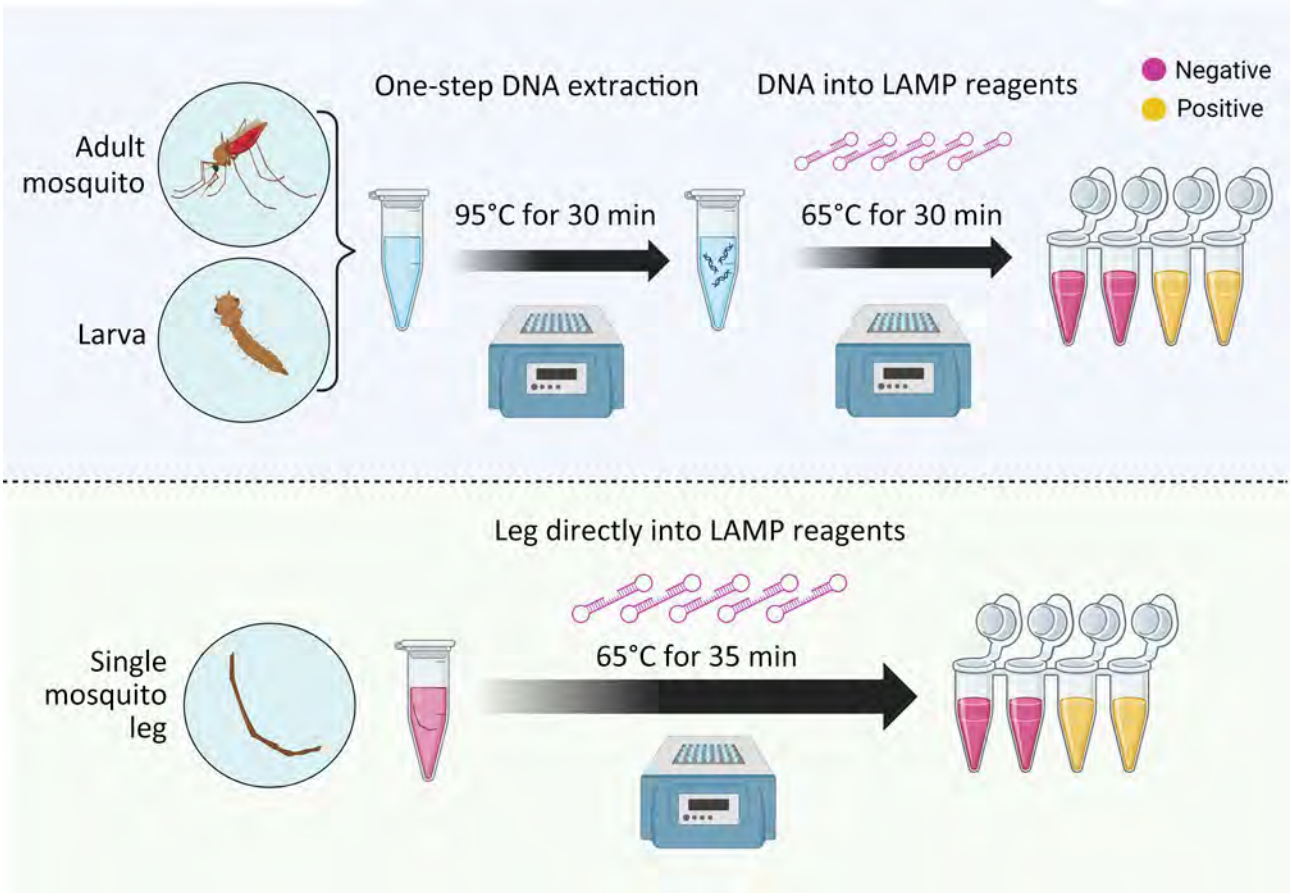

Figure 3. Schematic for colorimetric loop-mediated isothermal amplification assay to detect invasive malaria vector *Anopheles stephensi* mosquitoes. Top: DNA from any mosquito source directly placed in the colorimetric master mix are incubated at 65°C for 30 minutes to obtain a yellow color change, showing a positive sample. The assay shows high sensitivity and specificity when DNA extract from adult or larval mosquitoes is used. Bottom: Assay can also be used directly on a single mosquito leg, without the need for DNA extraction, by adding a 5-minute extension to incubation time (i.e., 35 minutes). Schematic produced using Biorender (https://www.biorender.com).

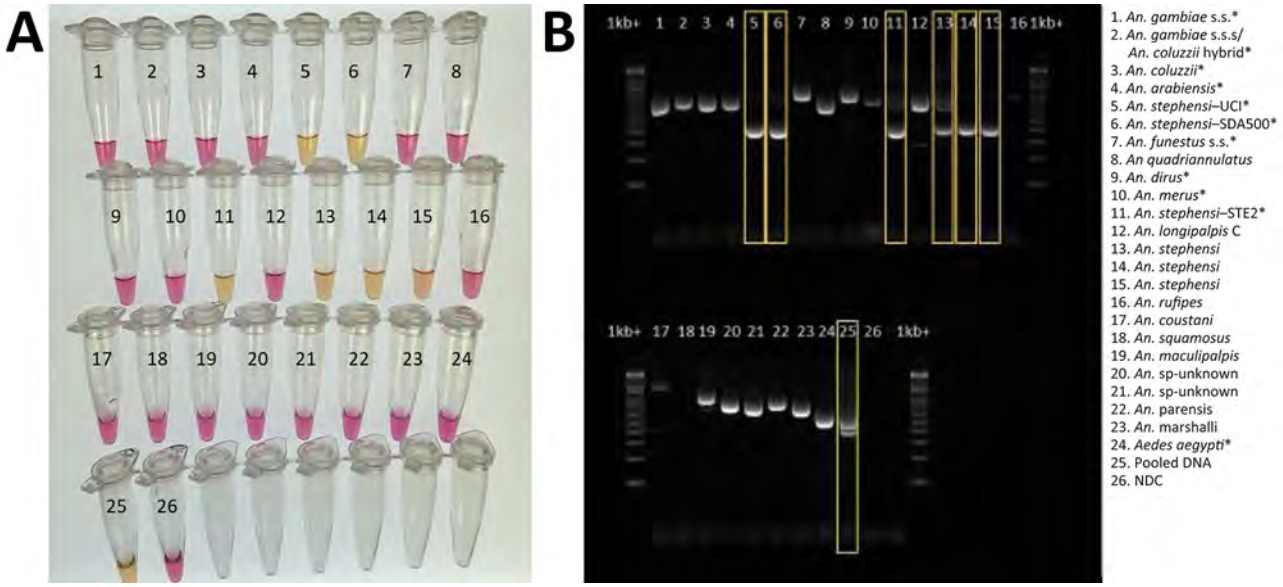

Figure 4. Validation of colorimetric loop-mediated isothermal amplification assay to detect invasive malaria vector *Anopheles stephensi* mosquitoes. A) Results using new assay. B) Results using existing *An. stephensi* PCR (*13*); yellow boxes indicate *An. stephensi* products. Conventional PCR resulted in difficult-to-interpret gel bands for *An. longipalpis* C, *Aedes aegypti*, and *An. coustani* samples, similar to *An. stephensi* samples, and inconsistently produced double bands (positive detection) on sequence-confirmed *An. stephensi* samples from Kenya. Asterisks (*) in key indicate samples from insectary-reared mosquitoes. Samples 12–23 came from sequence-confirmed field-collected specimens. Sample 25 contained a pool of assorted mosquito DNA species, in which *An. stephensi* was represented 1:10. For both assays, 1 µL extracted DNA was used. NDC, no DNA template control; UCI, *An. stephensi* laboratory colony (BEI Resources, https://www.beiresources.org).

need for a robust *An. stephensi* assay that is simple to interpret.

The CLASS assay showed promising results when field-caught samples from Kenya were tested. Although testing on those samples used DNA, this assay's ability to test single legs without extraction and using simple equipment suggests potential for screening large numbers of wild mosquitoes in remote settings. With additional field deployment and validation, data may be generated to potentially consider the CLASS assay as a species confirmation tool if confirmed sensitivity and specificity continue to fall within an 85% CI. In addition, alternate LAMP detection chemistries using the primers we describe could be adapted to ensure assay capacity in all settings without relying on a single company and master mix and without concern for reagent quality affecting pH change.

LAMP assay technology improved because of the need for rapid cost-effective diagnostics during the COVID-19 pandemic. Because phenol-based colorimetric LAMP assays are now widely adaptable, opportunities exist beyond *An. stephensi* species identification, such as for *An. arabiensis*, a common malaria vector in Africa currently requiring PCR for species confirmation (*28*). In some locations, *An. arabiensis* mosquitoes are the primary malaria vector, and a colorimetric LAMP screening tool could be used to rapidly distinguish non–*An. arabiensis* samples for further molecular confirmation. The first detection of *An. stephensi* mosquitoes in Ethiopia occurred when *An. gambiae* sensu lato mosquitoes did not amplify as *An. arabiensis* mosquitoes and sequencing revealed invasive *An. stephensi* mosquitoes instead (*29*).

Molecular species identification provides crucial data for epidemiologic surveillance. Real-time data on vector distribution and density guide the implementation of vector control methods, such as insecticide-treated bed nets and indoor residual spraying, ensuring that resources are used effectively to curb malaria transmission (*30*). Early detection, assisted by rapid assays like the CLASS assay, is critical for initiating timely responses to invasive vector populations (*7*).

The significance of accurate molecular identification of vector species extends beyond invasive *An. stephensi*. Long-term research and malaria program initiatives, guided by species identification data, enable program managers and scientists to study vector biology, behavior, and genetics. Such insights are invaluable for developing effective control tools and strategies. In addition, policy formulation relies heavily on accurate surveillance data. Molecular surveillance of vectors like *An. stephensi* informs policy

decisions at regional, national, and international levels, ensuring a coordinated and effective response to malaria (*31*). Accurate molecular identification not only aids in understanding the geographic distribution of vectors but also assists in predicting potential disease outbreaks, enabling public health authorities to proactively allocate resources and plan interventions (*32*).

Table 6. Testing of wild *Anopheles* spp. mosquitoes collected in Marsabit, Kenya, in 2022 and 2023 that failed to amplify during routine species assays as part of development of colorimetric LAMP assay to detect invasive malaria vector *Anopheles stephensi* mosquitoes*

Site	Collection method	Date of collection	Sequence-confirmed species	Colorimetric LAMP assay result
Marsabit	Light trap	2023 Feb	*An. gambiae* senus lato	Negative (0/2)
Marsabit	Light trap	2023 Feb	*An. gambiae* s.l.	Negative (0/2)
Marsabit	Larvae	2023 Feb	*An. dthali*	Negative (0/2)
Marsabit	Larvae	2023 Feb	*An. gambiae* s.l.	Negative (0/2)
Marsabit	Larvae	2023 Feb	*An. dthali*	Negative (0/2)
Marsabit	Larvae	2023 Feb	*Culex peresiguus*	Negative (0/2)
Marsabit	Larvae	2023 Feb	*An. dthali*	Negative (0/2)
Marsabit	Adults	2022 Dec	NA	Negative (0/2)
Marsabit	Adults	2022 Dec	*An. gambiae* s.l.	Negative (0/2)
Marsabit	Adults	2022 Dec	*An. stephensi*	Positive (2/2)
Marsabit	Adults	2022 Dec	NA	Negative (0/2)
Marsabit	Adults	2022 Dec	*An. gambiae* s.l.	Negative (0/2)
Marsabit	Adults	2022 Dec	*An. dthali*	Negative (0/2)
Marsabit	Adults	2022 Dec	*An. gambiae* s.l.	Negative (0/2)
Marsabit	Adults	2022 Dec	NA	Negative (0/2)
Marsabit	Adults	2022 Dec	NA	Negative (0/2)
Marsabit	Adults	2022 Dec	NA	Negative (0/2)
Marsabit	Adults	2022 Dec	*An. dthali*	Negative (0/2)
Marsabit	Adults	2022 Dec	*An. stephensi*	Positive (2/2)
Marsabit	Adults	2022 Dec	NA	Negative (0/2)
Marsabit	Adults	2022 Dec	NA	Negative (0/2)
Marsabit	Adults	2022 Dec	*An. gambiae* s.l.	Negative (0/2)
Marsabit	Adults	2022 Dec	Other	Negative (0/2)
Marsabit	Adults	2022 Dec	NA	Negative (0/2)
Marsabit	Larvae	2023 May	*An. gambiae* s.l.	Negative (0/2)
Marsabit	Larvae	2023 May	*An. pretoriensis*	Negative (0/2)
Marsabit	Larvae	2023 May	*An. stephensi*	Positive (2/2)
Marsabit	Larvae	2023 May	*An. gambiae* s.l.	Negative (0/2)
Marsabit	Larvae	2023 May	*An. pretoriensis*	Negative (0/2)
Marsabit	Larvae	2023 May	NA	Negative (0/2)
Marsabit	Larvae	2023 May	*An. gambiae* s.l.	Negative (0/2)
Marsabit	Larvae	2023 May	*An. gambiae* s.l.	Negative (0/2)
Marsabit	Larvae	2023 May	*An. stephensi*	Positive (2/2)
Marsabit	Larvae	2023 May	*An. stephensi*	Positive (2/2)
Marsabit	Larvae	2023 May	Other	Negative (0/2)
Marsabit	Larvae	2023 May	*An. gambiae* s.l.	Negative (0/2)
Marsabit	Larvae	2023 May	*An. stephensi*	Positive (2/2)
Marsabit	Larvae	2023 May	*An. gambiae* s.l.	Negative (0/2)
Marsabit	Larvae	2023 May	*An. stephensi*	Positive (2/2)
Marsabit	Larvae	2023 May	NA	Negative (0/2)
Marsabit	Larvae	2023 May	*An. pretoriensis*	Negative (0/2)
Marsabit	Larvae	2023 May	*An. pretoriensis*	Negative (0/2)
Marsabit	Larvae	2023 May	*An. pretoriensis*	Negative (0/2)
Marsabit	Larvae	2023 May	NA	Negative (0/2)
Marsabit	Larvae	2023 May	*An. stephensi*	Positive (2/2)
Marsabit	Larvae	2023 May	*An. gambiae* s.l.	Negative (0/2)
Marsabit	Larvae	2023 May	*An. stephensi*	Positive (2/2)
Marsabit	Larvae	2023 May	*An. gambiae* s.l.	Negative (0/2)
Marsabit	Larvae	2023 May	*An. pretoriensis*	Negative (0/2)
Marsabit	Larvae	2023 May	Other	Negative (0/2)
Marsabit	Larvae	2023 May	*An. gambiae* s.l.	Negative (0/2)
Marsabit	Larvae	2023 May	NA	Negative (0/2)
Marsabit	Larvae	2023 May	*An. gambiae* s.l.	Negative (0/2)
Marsabit	Larvae	2023 May	*An. pretoriensis*	Negative (0/2)
Marsabit	Larvae	2023 May	*An. pretoriensis*	Negative (0/2)

*Samples were sequenced using cytochrome c oxidase subunit I sequence testing to confirm species identification, and then DNA extract from the samples was run in duplicate through the colorimetric LAMP assay. Results showed 100% concurrence between the LAMP assay results and Sanger sequencing in determining which specimens were *An. stephensi* and which were not. LAMP, loop-mediated isothermal amplification; NA, no amplification occurred; other, other (non-*Anopheles*) mosquito species.

In conclusion, molecular species identification of malaria vectors, particularly in the context of invasive species such as *An. stephensi*, is indispensable to ensure gains made in global malaria control and elimination over the last few decades are not lost. Developing rapid, cost-effective assays, such as the CLASS assay, marks a substantial advancement in the ability to detect *An. stephensi* mosquitoes early in new locations, enabling rapid vector control response. This assay has potential as a screening tool to monitor the spread of the vector species. This tool is field adaptable and can be used in resource-limited settings so that laboratory capacity is not a bottleneck preventing countries from detecting and reporting the presence of *An. stephensi* mosquitoes. By combining accurate molecular identification of *An. stephensi* mosquitoes with adaptive interventions, policymakers, researchers, and public health officials can work collaboratively to mitigate the effect of this invasive malaria vector and continue to work toward a malaria-free future.

This article was preprinted at https://www.biorxiv.org/content/10.1101/2024.02.06.579110v1.

Acknowledgments

We thank the Malaria Research and Reference Reagent Resource Center and staff at the Centers for Disease Control and Prevention (CDC) Entomology Branch, particularly Laura Leite and Catherine Steele, for their help and support rearing and providing colony mosquito material for this study. We thank Biorender.com for the support in generating figures for the study. We thank Sue Visser, Jessica Sweeney, Anne Powers, Holley Hooks, the CDC Division of Vector-Borne Diseases, and the CDC National Center for Emerging and Zoonotic Infectious Diseases for the Public Health Entomology for All program. We also thank John Gimnig, Ellen Dotson, Audrey Lenhart, Lisa Reimer, and the CDC Entomology Branch for thoughtful and crucial feedback on the concept and assay development.

G.R. and J.S. were funded through Public Health Entomology for All, a partnership with the Entomological Society of America and CDC. Financial support for C.R. and S.Z. was provided by the US President's Malaria Initiative.

About the Author

Ms. Rafferty is a molecular biologist with the US President's Malaria Initiative in the Entomology Branch, Division of Parasitic Diseases and Malaria, National Center for Emerging and Zoonotic Infectious Diseases, Centers for Disease Control and Prevention, Atlanta, Georgia, USA. Her work focuses on molecular approaches for vector surveillance and control.

References

1. Faulde MK, Rueda LM, Khaireh BA. First record of the Asian malaria vector *Anopheles stephensi* and its possible role in the resurgence of malaria in Djibouti, Horn of Africa. Acta Trop. 2014;139:39–43. https://doi.org/10.1016/j.actatropica.2014.06.016
2. World Health Organization. WHO initiative to stop the spread of *Anopheles stephensi* in Africa. 2023 update [cited 2023 Aug 15]. https://www.who.int/publications/i/item/WHO-UCN-GMP-2022.06
3. World Health Organization. Vector alert: *Anopheles stephensi* invasion and spread: Horn of Africa, the Republic of the Sudan and surrounding geographical areas, and Sri Lanka: information note. 2019 [cited 2019 Sep 1]. https://iris.who.int/handle/10665/326595
4. Emiru T, Getachew D, Murphy M, Sedda L, Ejigu LA, Bulto MG, et al. Evidence for a role of *Anopheles stephensi* in the spread of drug- and diagnosis-resistant malaria in Africa. Nat Med. 2023;29:3203–11. https://doi.org/10.1038/s41591-023-02641-9
5. Faulde MK, Pages F, Uedelhoven W. Bioactivity and laundering resistance of five commercially available, factory-treated permethrin-impregnated fabrics for the prevention of mosquito-borne diseases: the need for a standardized testing and licensing procedure. Parasitol Res. 2016;115:1573–82. https://doi.org/10.1007/s00436-015-4892-2
6. Balkew M, Mumba P, Yohannes G, Abiy E, Getachew D, Yared S, et al. An update on the distribution, bionomics, and insecticide susceptibility of *Anopheles stephensi* in Ethiopia, 2018–2020. Malar J. 2021;20:263. https://doi.org/10.1186/s12936-021-03801-3
7. Sinka ME, Pironon S, Massey NC, Longbottom J, Hemingway J, Moyes CL, et al. A new malaria vector in Africa: predicting the expansion range of *Anopheles stephensi* and identifying the urban populations at risk. Proc Natl Acad Sci U S A. 2020;117:24900–8. https://doi.org/10.1073/pnas.2003976117
8. Hamlet A, Dengela D, Tongren JE, Tadesse FG, Bousema T, Sinka M, et al. The potential impact of *Anopheles stephensi* establishment on the transmission of *Plasmodium falciparum* in Ethiopia and prospective control measures. BMC Med. 2022;20:135. https://doi.org/10.1186/s12916-022-02324-1
9. World Health Organization. Vector alert: *Anopheles stephensi* invasion and spread in Africa and Sri Lanka. 2022 [cited 2022 Oct 15]. https://iris.who.int/handle/10665/365710
10. US President's Malaria Initiative. Responding to *Anopheles stephensi* [cited 2023 Feb 22]. https://www.pmi.gov/what-we-do/entomological-monitoring/anstephensi
11. Coetzee M. Key to the females of Afrotropical *Anopheles* mosquitoes (Diptera: Culicidae). Malar J. 2020;19:70. https://doi.org/10.1186/s12936-020-3144-9
12. Ahmed A, Irish SR, Zohdy S, Yoshimizu M, Tadesse FG. Strategies for conducting *Anopheles stephensi* surveys in non-endemic areas. Acta Trop. 2022;236:106671. https://doi.org/10.1016/j.actatropica.2022.106671
13. Singh OP, Kaur T, Sharma G, Kona MP, Mishra S, Kapoor N, et al. Molecular tools for early detection of invasive malaria vector *Anopheles stephensi* mosquitoes. Emerg Infect Dis. 2023;29:36–44. https://doi.org/10.3201/eid2901.220786
14. Garg N, Ahmad FJ, Kar S. Recent advances in loop-mediated isothermal amplification (LAMP) for rapid and efficient detection of pathogens. Curr Res Microb Sci. 2022;3:100120. https://doi.org/10.1016/j.crmicr.2022.100120
15. Hatano B, Maki T, Obara T, Fukumoto H, Hagisawa K, Matsushita Y, et al. LAMP using a disposable pocket warmer for anthrax detection, a highly mobile and reliable method

for anti-bioterrorism. Jpn J Infect Dis. 2010;63:36–40. https://doi.org/10.7883/yoken.63.36
16. Dao Thi VL, Herbst K, Boerner K, Meurer M, Kremer LP, Kirrmaier D, et al. A colorimetric RT-LAMP assay and LAMP-sequencing for detecting SARS-CoV-2 RNA in clinical samples. Sci Transl Med. 2020;12:eabc7075. https://doi.org/10.1126/scitranslmed.abc7075
17. New England Biolabs. NEB LAMP primer design tool version 1.4.1 [cited 2023 May 1]. https://www.neb.com/en-us/neb-primer-design-tools/neb-primer-design-tools
18. Mishra S, Sharma G, Das MK, Pande V, Singh OP. Intragenomic sequence variations in the second internal transcribed spacer (ITS2) ribosomal DNA of the malaria vector *Anopheles stephensi*. PLoS One. 2021;16:e0253173. https://doi.org/10.1371/journal.pone.0253173
19. Notomi T, Okayama H, Masubuchi H, Yonekawa T, Watanabe K, Amino N, et al. Loop-mediated isothermal amplification of DNA. Nucleic Acids Res. 2000;28:E63. https://doi.org/10.1093/nar/28.12.e63
20. Nagamine K, Hase T, Notomi T. Accelerated reaction by loop-mediated isothermal amplification using loop primers. Mol Cell Probes. 2002;16:223–9. https://doi.org/10.1006/mcpr.2002.0415
21 Bonizzoni M, Afrane Y, Yan G. Loop-mediated isothermal amplification (LAMP) for rapid identification of *Anopheles gambiae* and *Anopheles arabiensis* mosquitoes. Am J Trop Med Hyg. 2009;81:1030–4. https://doi.org/10.4269/ajtmh.2009.09-0333
22. BEI Resources Malaria Research and Reference Reagent Resource Center (MR4) [cited 2023 Jun 15]. https://www.beiresources.org/About/MR4Home.aspx
23. Ochomo EO, Milanoi S, Abong'o B, Onyango B, Muchoki M, Omoke D, et al. Detection of *Anopheles stephensi* mosquitoes by molecular surveillance, Kenya. Emerg Infect Dis. 2023;29:2498–508. https://doi.org/10.3201/eid2912.230637
24. Folmer O, Black M, Hoeh W, Lutz R, Vrijenhoek R. DNA primers for amplification of mitochondrial cytochrome c oxidase subunit I from diverse metazoan invertebrates. Mol Mar Biol Biotechnol. 1994;3:294–9.
25. Gillies MT, Coetzee M. A supplement to the Anophelinae of Africa South of the Sahara. Publ South African Institute for Medical Research Journal. 1987;55:1–143.
26. World Health Organization. Malaria threats map [cited 2023 Aug 7]. https://apps.who.int/malaria/maps/threats
27. Sherrard-Smith E, Skarp JE, Beale AD, Fornadel C, Norris LC, Moore SJ, et al. Mosquito feeding behavior and how it influences residual malaria transmission across Africa. Proc Natl Acad Sci U S A. 2019;116:15086–95. https://doi.org/10.1073/pnas.1820646116
28. Scott JA, Brogdon WG, Collins FH. Identification of single specimens of the *Anopheles gambiae* complex by the polymerase chain reaction. Am J Trop Med Hyg. 1993;49:520–9. https://doi.org/10.4269/ajtmh.1993.49.520
29. Carter TE, Yared S, Gebresilassie A, Bonnell V, Damodaran L, Lopez K, et al. First detection of *Anopheles stephensi* Liston, 1901 (Diptera: culicidae) in Ethiopia using molecular and morphological approaches. Acta Trop. 2018;188:180–6. https://doi.org/10.1016/j.actatropica.2018.09.001
30. Chitnis N, Smith T, Steketee R. A mathematical model for the dynamics of malaria in mosquitoes feeding on a heterogeneous host population. J Biol Dyn. 2008;2:259–85. https://doi.org/10.1080/17513750701769857
31. Yakob L, Yan G. Modeling the effects of integrating larval habitat source reduction and insecticide treated nets for malaria control. PLoS One. 2009;4:e6921. https://doi.org/10.1371/journal.pone.0006921
32. Dye C. The analysis of parasite transmission by bloodsucking insects. Annu Rev Entomol. 1992;37:1–19. https://doi.org/10.1146/annurev.en.37.010192.000245

Address for correspondence: Sarah Zohdy, Centers for Disease Control and Prevention, 1600 Clifton Rd NE, Mailstop H23-11, Atlanta, GA 30329-4018, USA; email: ykr2@cdc.gov

Mortality Rate and Cause of Death in Adults with Extrapulmonary Nontuberculous Mycobacteria Infection, Denmark

Andreas A. Pedersen, Victor N. Dahl, Anders Løkke, Inge K. Holden, Andreas Fløe, Rikke Ibsen, Ole Hilberg, Isik S. Johansen

Medscape CME Activity

In support of improving patient care, this activity has been planned and implemented by Medscape, LLC and Emerging Infectious Diseases. Medscape, LLC is jointly accredited with commendation by the Accreditation Council for Continuing Medical Education (ACCME), the Accreditation Council for Pharmacy Education (ACPE), and the American Nurses Credentialing Center (ANCC), to provide continuing education for the healthcare team.

Medscape, LLC designates this Journal-based CME activity for a maximum of 1.00 ***AMA PRA Category 1 Credit(s)™***. Physicians should claim only the credit commensurate with the extent of their participation in the activity.

Successful completion of this CME activity, which includes participation in the evaluation component, enables the participant to earn up to 1.0 MOC points in the American Board of Internal Medicine's (ABIM) Maintenance of Certification (MOC) program. Participants will earn MOC points equivalent to the amount of CME credits claimed for the activity. It is the CME activity provider's responsibility to submit participant completion information to ACCME for the purpose of granting ABIM MOC credit.

All other clinicians completing this activity will be issued a certificate of participation. To participate in this journal CME activity: (1) review the learning objectives and author disclosures; (2) study the education content; (3) take the post-test with a 75% minimum passing score and complete the evaluation at https://www.medscape.org/qna/processor/72395?showStandAlone=true&src=prt_jcme_eid_mscpedu; and (4) view/print certificate. For CME questions, see page 1986.

NOTE: It is Medscape's policy to avoid the use of Brand names in accredited activities. However, in an effort to be as clear as possible, trade names are used in this activity to distinguish between the mixtures and different tests. It is not meant to promote any particular product.

Release date: August 21, 2024; Expiration date: August 21, 2025

Learning Objectives

Upon completion of this activity, participants will be able to:

1. Distinguish differences in mortality rates among adults with extrapulmonary nontuberculous mycobacterial (E-NTM) disease and control participants
2. Analyze causes of death associated with E-NTM vs controls participants
3. Assess the demographic data of mortality outcomes among adults with E-NTM and control participants

CME Editor

Jill Russell, BA, Technical Writer/Editor, Emerging Infectious Diseases. *Disclosure: Jill Russell, BA, has no relevant financial relationships.*

CME Author

Charles P. Vega, MD, Health Sciences Clinical Professor of Family Medicine, University of California, Irvine School of Medicine, Irvine, California. *Disclosure: Charles P. Vega, MD, has the following relevant financial relationships: served as consultant or advisor for Boehringer Ingelheim; GlaxoSmithKline.*

Authors

Andreas A. Pedersen, MD; Victor N. Dahl, MD; Anders Løkke, MD, DMSc; Inge K. Holden, MD, MPH, PhD; Andreas Fløe, MD, PhD; Rikke Ibsen, MSc; Ole Hilberg MD, DMSc; Isik S. Johansen MD, DMSc.

Author affiliations: University of Southern Denmark, Odense, Denmark (A.A. Pedersen, A. Løkke, I.K. Holden, O. Hilberg, I.S. Johansen); Lillebaelt Hospital, Vejle, Denmark (A.A. Pedersen, A. Løkke, R. Ibsen, O. Hilberg); Mycobacterial Centre for Research Southern Denmark, Odense (A.A. Pedersen, I.K. Holden, O. Hilberg, I.S. Johansen); Odense University Hospital, Odense (A.A. Pedersen, I.K. Holden, I.S. Johansen); Aarhus University Hospital, Aarhus, Denmark (V.N. Dahl, A. Fløe)

DOI: https://doi.org/10.3201/eid3009.240475

Evidence on mortality rates and causes of death associated with extrapulmonary nontuberculous mycobacteria (NTM) infection is limited. This nationwide register-based study in Denmark used diagnostic codes to match adult patients with extrapulmonary NTM infection 1:4 to controls. During 2000–2017, we identified 485 patients, who had significantly more comorbidities than controls. The 5-year mortality rate for patients was 26.8% (95% CI 23.1%–31.0%) and for controls, 10.9% (95% CI 9.6%–12.4%). The median age at death was 76 (interquartile range 63–85) years for patients and 84 (interquartile range 73–90) years for controls. The adjusted hazard rate of death for patients was 1.34 (95% CI 1.10–1.63; p = 0.004). Patients and controls mainly died of cardiovascular disease and solid malignant neoplasms. Hematologic malignancies and HIV were more frequently causes of death in patients. Mortality rates are substantial among patients with extrapulmonary NTM infection, predominantly caused by underlying conditions.

Extrapulmonary nontuberculous mycobacteria (NTM) infection potentially affects any organ; lymph nodes, skin, and soft tissue are the most commonly affected (*1*,*2*). The severity of disease varies considerably from uncomplicated lymphadenitis with favorable prognosis among children to disseminated disease in immunocompromised patients (*3*–*5*). Still, a substantial knowledge gap remains regarding outcomes of extrapulmonary NTM disease (*6*).

Historically associated with HIV and AIDS, incidence of extrapulmonary NTM infection has been increasing and represents a growing healthcare challenge (*1*–*3*,*7*). This increase has been attributed to several factors, such as the intensified use of immunosuppressants, increased life expectancy, and increased awareness of the disease (*1*,*3*,*8*,*9*). Furthermore, extrapulmonary NTM has been implicated in iatrogenic infections and healthcare-related outbreaks (*10*–*13*). In addition, the discontinuation of the bacillus Calmette-Guérin (BCG) vaccine in areas with low tuberculosis incidence might have contributed to this increase, possibly because of reduced nonspecific immune protection previously provided by the vaccine (*14*)

Studies on extrapulmonary NTM–related deaths are scarce, and reported mortality rates vary widely. In a US cohort of 365 NTM infections, the mortality rate for extrapulmonary NTM was 2% and for disseminated NTM disease was 50% (*15*). In contrast, another US study of 831 extrapulmonary NTM patients from 2009–2014 reported an overall crude mortality rate of 5% (11% disseminated disease and 2% skin and soft tissue infections) (*16*). In patients with hematologic cancers, 30-day mortality has been reported at 15% in NTM-infected persons, compared with only 2% in noninfected persons (*17*).

In summary, extrapulmonary NTM represents a highly heterogeneous disease entity in terms of clinical manifestation and host factors, and knowledge of its associated mortality rates and causes of death among persons with extrapulmonary NTM disease is limited. To address this knowledge gap, we investigated mortality rates associated with diagnosis of extrapulmonary NTM infection and describe the causes of death.

Methods

Study Design

This study was a nationwide retrospective register-based cohort study from Denmark. The healthcare system is based on tax-funded universal healthcare. Different types of registers can be linked by using a unique 10-digit personal identification number issued to all citizens (*18*).

Data Sources and Measurement

The Danish Register of Causes of Death contains data on time, place, and cause of death using the International Classification of Diseases, 10th Revision (ICD-10), for all deaths occurring in Denmark (*19*). We identified all patients with extrapulmonary NTM infection using International Classification of Diseases, 8th Revision (ICD-8), and ICD-10 diagnostic codes from the National Patient Register. The register contains the ICD-8 and ICD-10 diagnostic codes and procedural codes on all inpatients from 1977 and all outpatients since 1995 (*20*). To evaluate the effects of baseline comorbidities on mortality, we calculated a Charlson Comorbidity Index (CCI) as described by Quan et al. (*21*) using ICD-10 codes from the National Patient Register.

Study Subjects

We included patients >18 years of age with a first-time extrapulmonary NTM disease ICD-10 code (A31.1, A31.8, or A31.9) during 2000–2017. The date of the first registered extrapulmonary NTM code was considered the index date. For persons without an extrapulmonary NTM–specific ICD-10 code (A31.1), we used procedural codes for specific examinations and treatments to differentiate between extrapulmonary NTM and other NTM disease manifestations in windows of 1 year on either side of the index date

(Appendix Table, https://wwwnc.cdc.gov/EID/article/30/9/24-0475-App1.pdf). Patients and controls were censored from the study at death, migration, or end of data. We matched patients with extrapulmonary NTM disease to controls at a ratio of 1:4 at index. Controls were randomly selected from the total population of Denmark and matched by birth year, sex, marital status, and municipality of residence. The controls entered the study at the same date as the case-patient to whom they were matched. We excluded persons with an ICD-8 or ICD-10 code of A31 from the possible control population to ensure a nonbiased representative sample.

Statistical Analysis and Variables

We present absolute numbers and percentages or medians with interquartile ranges (IQRs) as appropriate. We evaluated differences between groups using the χ^2 test and median age differences using the Wilcoxon-Mann-Whitney nonparametric test. Because of legislation in Denmark, descriptive variables with <3 observations were not reported to ensure patient privacy. We evaluated mortality rates using a cumulative mortality plot and tested differences using a log-rank test. We used the Cox proportional hazards model to estimate unadjusted hazard ratios (HRs) of death and adjusted for CCI (*21*). Because HRs were not constant over time (nonproportional), we estimated annual and average HRs in the study period (*22*). To investigate the effects of HIV and AIDS on mortality, we performed a sensitivity analysis by excluding patients with HIV from the analyses. We post hoc categorized comorbidities into 3 groups (overall burden of comorbidities, break in barrier function, and impaired immunity) on the basis of existing knowledge of risk factors for NTM infection to investigate the association of comparable comorbidities and morbidity (*9*,*10*,*12*,*23*–*25*). We examined causes of death using the 21 World Health Organization ICD-10 classification groups for cases and controls and qualified them using detailed data on causes of death for the most common groups for extrapulmonary NTM compared with controls. We performed statistical analyses using Stata version 16.1 (StataCorp LLC, https://www.stata.com) and SAS version 9.4 TS Level 1M5 (SAS Institute Inc., https://www.sas.com). We applied a significance level of 0.05 for all tests.

Ethics Statement

Ethics approval is not required for register studies according to Danish law. The Region of Southern Denmark (jr. no. 22/10240) approved the study.

Results

Patient Demographics

For the period spanning 2000–2017, we identified 485 patients with extrapulmonary NTM disease. Their median age at index was 57 (IQR 41–73) years; 40.4% of patients were women and 59.6% men, and 49.6% were married or cohabiting (Table 1). The median follow-up duration was 5 (IQR 3–10) years for extrapulmonary NTM patients and 6 (IQR 3–11) years for controls. NTM diagnostic codes for cutaneous infection accounted for 29.7% (*Mycobacterium marinum* in 13.2%, *M. ulcerans* in 1%), whereas 70.3% were reported as other or not otherwise specified.

Mortality Rates

The median age at death from all causes was 76 (IQR 63–85) years for extrapulmonary NTM patients compared with 84 (IQR 73–90) years in controls. In total, 158 (32.6%) of 485 extrapulmonary NTM patients died during the study period. Extrapulmonary NTM patients had a significantly higher mortality rate than did matched controls (mortality HR 1.9, 95% CI 1.58–2.29; p<0.0001); the largest difference occurred in the first 3 years after diagnosis. The cumulative 1-year mortality rate for extrapulmonary NTM patients was 9.3% (95% CI 7.0%–12.2%), compared with 3.1% (95% CI 2.4%–4.0%) for controls. The cumulative 5-year mortality rate was 26.8% (95% CI 23.1%–31.0%) for extrapulmonary NTM patients and 10.9% (95% CI 9.6%–12.4%) for controls (Figure).

The increased mortality rate remained after adjusting for baseline CCI with an HR of 1.34 (95% CI 1.10–1.63; p<0.01). The effect was most pronounced in the first 3 years (Table 2). After 4 years of follow-up, the hazards of death did not differ between extrapulmonary NTM patients and controls. The hazards of death remained higher for extrapulmonary NTM patients even when excluding persons with HIV from the analysis (HR 1.4, 95% CI 1.2–1.7).

Causes of Death

Patients with extrapulmonary NTM disease died more frequently from infectious diseases (10.8%, 95% CI 6.4–16.7) than did controls (2.1%, 95% CI 0.1–4.2). Cardiovascular disease and solid malignant neoplasms were the 2 most common causes of death for extrapulmonary NTM patients and for controls (Table 3). Cardiovascular disease was the cause of death for 17.7% of extrapulmonary NTM patients and 24.0% of controls, whereas solid malignant neoplasms caused 13.9% of deaths for extrapulmonary NTM patients

Table 1. Characteristics of patients and controls in study of mortality rates and cause of death in adults with extrapulmonary NTM infection, Denmark*

Characteristic	Extrapulmonary NTM	Controls
No. persons	485	1,935
Sex		Matched
F	196 (40.4)	
M	289 (59.6)	
Median age, y (IQR)	57 (41–73)	Matched
Age group, y		
18–29	46 (9.5)	
30–39	61 (12.6)	
40–49	77 (15.9)	
50–59	81 (16.7)	
60–69	79 (16.3)	
≥70	141 (29.1)	
Marital status		Matched
Married/cohabiting	282 (49.6)	
Not married/cohabiting	203 (50.4)	
Immigration status†		
Non-Western origin	46 (9.5)	111 (5.7)
Western/Danish origin	438 (90.3)	1,822 (94.2)
NTM diagnostic codes		
Cutaneous mycobacterial infection NOS	75 (15.5)	
Cutaneous infection with *Mycobacterium marinum*	64 (13.2)	
Cutaneous infection with *Mycobacterium ulcerans*	5 (1.0)	
Other mycobacterial infections	73 (15.1)	
Mycobacterial infection NOS	268 (55.3)	
CCI		
Mean CCI (SD)	1 (1.83)	0.26 (0.81)
CCI group		
0	313 (64.5)	1,694 (87.5)
1	48 (9.9)	74 (3.8)
2	58 (12.0)	127 (6.6)
≥3	66 (13.6)	40 (2.1)

*Values are no. (%) except as indicated. CCI, Charlson Comorbidity Index; IQR, interquartile range; NOS, not otherwise specified; NTM, nontuberculous mycobacteria.
†Unknown status for extrapulmonary NTM n = 1 and control n = 2.

and 16.5% of deaths for controls. Deaths caused by hematologic malignancies were significantly more common among extrapulmonary NTM patients (7.6%, 95% CI 4.0%–12.9%) than among controls (3.5%, 95% CI 1.9%–5.9%; p<0.05). Other bacterial diseases, a grouping that potentially includes NTM disease, accounted for 5.7% (95% CI 2.6%–10.5%) of deaths but was not reported for controls.

Comorbidities

Overall Burden of Comorbidities

Persons with extrapulmonary NTM infection had higher CCI scores and an overall significantly higher burden of comorbidities than did controls (Table 1). In particular, the burden of cardiovascular diseases was significantly higher in extrapulmonary NTM patients at 38.8% (95% CI 34.4%–43.3%) than among controls at 19.3% (95% CI 17.6%–21.2%). The burden of chronic lower respiratory diseases was also significantly higher in extrapulmonary NTM patients at 6.2% (95% CI 4.2%–8.7%) than among controls at 2.5% (95% CI 1.9%–3.3%) (Table 4). Metabolic disorders, benign neoplasms, diseases of the male genitalia, and diseases of the gastrointestinal tract were also more common in extrapulmonary NTM patients.

Break in Barrier Function

Several comorbidities related to break in barrier function were more common in extrapulmonary NTM patients than in controls. One third of extrapulmonary NTM patients (29.3%, 95% CI 25.3%–33.6%) had injuries to the head and musculoskeletal system, compared with 17.1% (95% CI 15.4–18.8) of controls. Complications from surgical and medical care were more common in extrapulmonary NTM patients: 7.8% (95% CI 5.6%–10.6%) from surgical care and 2.5% (95% CI 1.9%–3.3%) from medical care. Extrapulmonary NTM patients also experienced higher rates of skin and soft tissue diseases (17.1%, 95% CI 13.9%–20.8%) and diseases of veins and lymphatic tissues (6.4%, 95% CI 4.4%–9.0%). Extrapulmonary NTM patients had a higher proportion of urinary system disease at 21.0% (95% CI 17.5%–24.9%); of those, 8.8% (95% CI 4.1%–16.1%) had been treated with BCG intravesically before diagnosis.

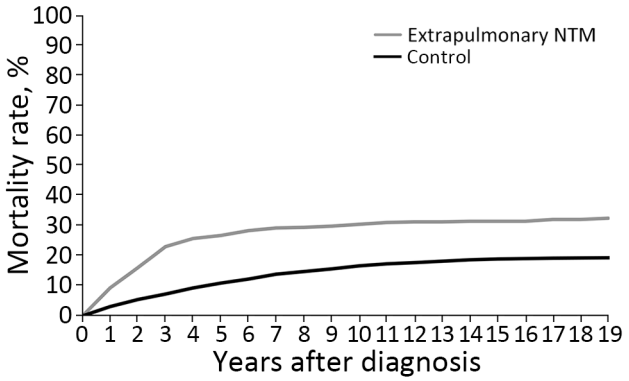

Figure. Cumulative mortality rate for patients with extrapulmonary NTM infection compared with matched controls in study of mortality and cause of death in adults with extrapulmonary NTM infection, Denmark. log-rank p<0.001. NTM, nontuberculous mycobacteria.

Impaired Immunity

Pneumonia and other bacterial diseases were significantly more common in extrapulmonary NTM patients at 21.2% (95% CI 17.7%–25.2%) than among controls at 2.9% (95% CI 2.2%–3.8%). The same discrepancy applied to diabetes mellitus (9.5%, 95% CI 7.0%–12.5%), HIV (2.5%, 95% CI 1.3%–4.3%), and hematologic malignancies (2.5%, 95% CI 1.3%–4.3%). Last, the proportion of inflammatory polyarthropathies was higher in extrapulmonary NTM patients (12.2%, 95% CI 9.4%–15.4%) than in controls (3.7% 95% CI 2.9%–4.6%) (Table 4).

Discussion

We present a comprehensive characterization of mortality rates among persons with extrapulmonary NTM infection and a unique description of causes of death in this nationwide register-based cohort study over an 18-year period. Patients with extrapulmonary NTM disease had higher all-cause mortality and died more often of hematologic malignancies and HIV than did controls.

Patients with extrapulmonary NTM infection had a higher mortality rate than controls in the first 3 years, and that difference persisted when controlling for comorbidities. Men and women with extrapulmonary NTM infection had similar all-cause mortality rates. The overall mortality rate was 32.6%, which is considerably higher than the rate of 4% reported in a recent Australia study of 73 patients with extrapulmonary NTM disease (*10*). That dissimilarity is likely because of differences in the 2 populations' sample sizes, demographics, burden of comorbidities, and disease manifestations.

Previous studies have shown that mortality rates among patients with extrapulmonary NTM infection are lower than that associated with pulmonary NTM disease and that mortality varies by localization, patient population, and NTM species (*26*). Disseminated infections with *M. chimaera* from heater–cooler units have been associated with a case-fatality rate of 45.5% (*12*). Comparable high mortality rates have been reported in different extrapulmonary NTM studies on peritonitis in immunosuppressed persons, patients with central nervous system infection, and persons who have undergone renal or allogeneic stem cell transplant (21%–50%) (*27*–*30*).

Understanding the cause of death for persons with extrapulmonary NTM disease is essential to identify patients who could benefit from earlier intervention (*31*). In this study, extrapulmonary NTM patients most often died of an underlying comorbidity, and only 5.7% of deaths were attributable to other bacterial diseases, potentially including NTM disease. Deaths caused by hematologic malignancies and HIV were more common in persons with extrapulmonary infection, and those diseases are also considered risk factors for NTM disease (*2*,*10*). Still, when excluding persons with HIV from our analyses, the mortality rate remained higher among patients with extrapulmonary infection. We did not observe significant differences in the 2 most common causes of death for persons with extrapulmonary NTM disease and controls.

Persons with extrapulmonary NTM infection had a significantly higher burden of comorbidities than did controls. That finding was evident when investigating the CCI and common categories of comorbidities in the years before the diagnosis. The higher proportion of cardiovascular disease, metabolic disorders, and chronic lower respiratory disease in extrapulmonary NTM patients may indicate

Table 2. Cox hazard regression for patients with extrapulmonary NTM infection compared with matched controls adjusted for Charlson Comorbidity Index and nonproportionality over time in study of mortality and cause of death in adults, Denmark*

	Extrapulmonary NTM versus controls	
Category	HR (95% CI)	p value
Total	1.34 (1.1–1.6)	0.004
Year after diagnosis		
1	2.07 (1.6–2.7)	
2	1.83 (1.3–2.5)	
3	1.61 (1.1–2.4)	
4	1.43 (0.9–2.2)	
5	1.26 (0.8–2.1)	
6	1.11 (0.6–1.9)	
7	0.98 (0.5–1.8)	
8	0.87 (0.4–1.7)	
9	0.77 (0.4–1.6)	
10	0.68 (0.3–1.5)	

*HR, hazard ratio for death; NTM, nontuberculosis mycobacteria.

Table 3. Causes of death for patients with extrapulmonary NTM infection and controls, Denmark*

	Extrapulmonary NTM		Controls	
Category	Cause of death	No. (%)	Cause of death	No. (%)
All causes	Total	158 (32.6)	Total	375 (19.4)
	Male	97 (33.6)	Male	256 (22.2)
	Female	61 (31.1)	Female	119 (15.2)
Rank				
1	Cardiovascular disease	28 (17.7)	Cardiovascular disease	90 (24.0)
2	Solid malignant neoplasms	22 (13.9)	Solid malignant neoplasms	62 (16.5)
3	Hematologic malignancies	12 (7.6)	Organic mental disorders	18 (4.8)
4	Other bacterial diseases†	9 (5.7)	Influenza and pneumonia	16 (4.3)
5	Respiratory diseases	8 (5.1)	Respiratory diseases	13 (3.5)
6	HIV	6 (3.8)	Hematological malignancies	13 (3.5)
	Others	73 (46.2)	Others	163 (43.5)

*NTM, nontuberculosis mycobacteria.
†Codes A30–A49, including mycobacterial diseases, in International Classification of Diseases, 8th Revision or 10th Revision.

a higher degree of frailty, leading to an increased incidence of extrapulmonary NTM infection. Cardiovascular disease has previously been identified as a risk factor for pulmonary NTM disease but, to our knowledge, has not been identified as such for extrapulmonary infection (*25*).

Several comorbidities, which might provide a port of entry for mycobacteria because of compromised barrier function, were more common in patients with extrapulmonary NTM disease. Those patients experienced higher proportions of injuries; skin and subcutaneous tissue disease; and diseases of the veins, lymphatic vessels, and lymph nodes that all expose skin and soft tissues to risk for infection. Surgical and medical complications were also more common, indicating that extrapulmonary NTM infection can be seen as iatrogenic, which has been described consistently (*10*,*11*).

We observed a higher proportion of benign neoplasms before NTM disease was diagnosed. Invasive procedures in the diagnostic process or the neoplasms itself could lead to compromised barrier function. Neoplasms could also to some degree be misclassifications that are in fact granulomatous formation caused by NTM. Diseases of the urinary system and male genital organs were significantly more common in extrapulmonary NTM patients. Only a few of those patients (9/102) had intravesical BCG installation, which could have been a confounder, because BCG installations are known to cause BCGitis (*32*). NTM infections of the genitourinary tract are extremely rare and are unlikely to explain the

Table 4. Numbers and percentages of comorbidities 3 years before diagnosis in study of mortality and cause of death in adults with extrapulmonary NTM infection, Denmark*

	Patients with extrapulmonary NTM		Controls	
Comorbidity	No.	% (95% CI)	No.	% (95% CI)
Cardiovascular disease	188†	38.8 (34.4–43.3)	373	19.3 (17.6–21.2)
Head and musculoskeletal injuries	142†	29.3 (25.3–33.6)	330	17.1 (15.4–18.8)
Other bacterial diseases including pneumonia‡	103†	21.2 (17.7–25.2)	57	2.9 (2.2–3.8)
Urinary system diseases and symptoms	102†	21.0 (17.5–24.9)	109	5.6 (4.6–6.8)
Gastrointestinal system diseases and symptoms	85†	17.5 (14.2–21.2)	122	6.3 (5.3–7.5)
Skin and soft tissue diseases	83†	17.1 (13.9–20.8)	82	4.2 (3.4–5.2)
Arthrosis and inflammatory polyarthropathies	59†	12.2 (9.4–15.4)	71	3.7 (2.9–4.6)
Metabolic disorders	51†	10.5 (7.9–13.6)	65	3.4 (2.6–4.3)
Infections of the skin and subcutaneous tissue	48†	9.9 (7.4–12.9)		
Diabetes mellitus	46†	9.5 (7.0–12.5)	67	3.5 (2.7–4.4)
Benign neoplasms	42†	8.7 (6.3–11.5)	55	2.8 (2.1–3.7)
Complications of surgical and medical care	38†	7.8 (5.6–10.6)	49	2.5 (1.9–3.3)
Circulatory and respiratory symptoms	37†	7.6 (5.4–10.4)	67	3.5 (2.7–4.4)
Diseases of veins, lymphatic vessels, and lymph nodes	31†	6.4 (4.4–9.0)		
Anemia	30†	6.2 (4.2–8.7)	NA	NA
Chronic lower respiratory diseases	30†	6.2 (4.2–8.7)	49	2.5 (1.9–3.3)
Other disorders of the ear	28§	5.8 (3.9–8.2)	89	4.6 (3.7–5.6)
Male genital organ diseases	28†	5.8 (3.9–8.2)	49	2.5 (1.9–3.3)
HIV	19†	3.9 (2.4–6.1)	4	0.2 (0.06−0.52)
Hematologic malignancies	12¶	2.5 (1.3–4.3)	18	0.9 (0.6–1.5)

*NA, not available; NTM, nontuberculosis mycobacteria.
†p<0.001.
‡Codes A30–A49 (excluding A31) in International Classification of Diseases, 8th Revision or 10th Revision.
§Not significant.
¶p<0.01.

large proportion of genitourinary diseases in our population (*33*). Disease in the genitourinary tract might indicate impaired mucosa barrier function or poor overall health, which increases the risk for extrapulmonary NTM. In addition, gastrointestinal diseases and symptoms were more prevalent in patients with extrapulmonary NTM infection, which could suggest compromised barrier function in the intestines. However, the extrapulmonary NTM disease could be localized to the gastrointestinal tract, as is the case with *M. genavense* (*34*).

Immunosuppression is strongly associated with extrapulmonary NTM (*35*,*36*). Immunosuppression in patients with any manifestation of NTM has been associated with an increased risk for death (HR 3.5 [95% CI 1.5–8.4]), but only 13 of 118 patients had an extrapulmonary NTM diagnosis (*37*). In our study, extrapulmonary NTM patients had a significantly higher proportion of hematological malignancies, which implies a higher risk for infection because of impaired immunity. Patients with extrapulmonary infection had higher proportions of anemia, HIV/AIDS, and diabetes mellitus, which are also associated with impaired immunity (*2*,*25*,*38*). Our study confirms an association with immunosuppression and HIV infection, which was also shown in an Australia study (*10*). Still, HIV generally seems to be rare in patients with NTM in our setting.

The higher proportion of inflammatory polyarthropathies in extrapulmonary NTM patients could be related to the use of immunosuppressants. Anti–tumor necrosis factor α treatment and corticosteroids are well-described risk factors for mycobacterial disease (*9*,*25*,*39*). A high mortality rate has been reported among patients treated with biological agents who have concomitant NTM infections (*9*).

The significantly higher proportion of extrapulmonary NTM patients with other bacterial diseases and pneumonia could be associated with an increased likelihood of immune dysfunction (*40*). Pneumonia is also a risk factor for pulmonary NTM (*25*). However, that finding could also be because of misdiagnoses and erroneous use of diagnostic codes.

This study was based on national registers, and the data entered in those registers imply an inherent risk for underreporting, overreporting, and misclassification. Treatment of extrapulmonary NTM disease is centralized in 6 hospitals in Denmark with specialized centers for mycobacterial diseases, and we are confident that the diagnoses have a high rate of accuracy. Previous validations of diagnostic codes in our registers have shown a high positive predictive value (*41*,*42*). The ICD-10 codes pertaining to extrapulmonary NTM manifestation and species are only specific for skin infections with *M. marinum* and *M. ulcerans*, and the registers used in this study do not contain data on microbiology or all relevant risk factors (e.g., type of immunosuppressants). This factor limited our ability to precisely describe the type, localization, and pathogenicity of NTM infections, including species. Nevertheless, the percentage of extrapulmonary NTM skin infections in our study (29.7%) is comparable to those in a US culture-based study (32%) (*16*). We assume that using ICD-10 codes for extrapulmonary NTM disease correlates well with clinically relevant disease compared with relying on microbiologic data alone. Furthermore, the inclusion of *M. ulcerans* patients could be debated, because *M. ulcerans* might not be considered as a separate disease entity, although it is genetically very similar to *M. marinum* (*6*,*43*,*44*).

Data on the causes of death are registered by the physician who verifies the death. However, those physicians might not be familiar with the patient's entire medical history or with complex infections, making it difficult to differentiate between causes of death in this comorbid population. The low number of autopsies conducted in Denmark calls into question the validity of the death certificates; however, that issue appears to be common in other settings (*31*).

In conclusion, patients with extrapulmonary NTM infection have a significantly higher burden of comorbidities than do matched controls. The mortality rate remained higher for persons with extrapulmonary NTM infection than for matched controls after adjusting for a comorbidity severity index. In addition, patients with extrapulmonary NTM disease often die from underlying comorbidities, such as hematologic malignancies and HIV, not from extrapulmonary NTM disease.

Data are not publicly available due to local legislative limitations.

This work was supported by The Region of Southern Denmark, A.P. Møller Foundation (to A.A.P.), Eva Merete Falck Crones Foundation (to A.A.P.), and Lillebaelt Hospital (to A.A.P.). The study funders had no role in study design, data collection, data analysis, data interpretation, or manuscript writing.

A.A.P., O.H., I.S.J., A.F., I.K.H., V.N.D., and A.L. designed the study. R.I. and A.A.P. performed the analysis. A.A.P. drafted the manuscript. All authors have critically reviewed and approved the final version of the manuscript.

About the Author

Dr. Pedersen is a PhD student and infectious diseases trainee in the region of Southern Denmark. His research interests are mycobacterial diseases, focusing on epidemiology and mycobacterial-related immunodeficiency.

References

1. Kiselinova M, Naesens L, Huis In 't Veld D, Boelens J, Van Braeckel E, Vande Weygaerde Y, et al. Management challenges of extrapulmonary nontuberculous mycobacterial infection: a single-center case series and literature review. Pathogens. 2023;13:12. https://doi.org/10.3390/pathogens13010012
2. Grigg C, Jackson KA, Barter D, Czaja CA, Johnston H, Lynfield R, et al. Epidemiology of pulmonary and extrapulmonary nontuberculous mycobacteria infections at 4 US emerging infections program sites: a 6-month pilot. Clin Infect Dis. 2023;77:629–37. https://doi.org/10.1093/cid/ciad214
3. Bhanushali J, Jadhav U, Ghewade B, Wagh P. Unveiling the clinical diversity in nontuberculous mycobacteria (NTM) infections: a comprehensive review. Cureus. 2023;15:e48270. https://doi.org/10.7759/cureus.48270
4. Reuss A, Drzymala S, Hauer B, von Kries R, Haas W. Treatment outcome in children with nontuberculous mycobacterial lymphadenitis: a retrospective follow-up study. Int J Mycobacteriol. 2017;6:76–82. https://doi.org/10.4103/2212-5531.201898
5. Jensen FN, Nielsen AB, Dungu KHS, Poulsen A, Schmidt G, Hjuler T, et al. Distinct clinical parameters were associated with shorter spontaneous resolution in children with non-tuberculous mycobacterial lymphadenitis. Acta Paediatr. 2024;apa.17104. https://doi.org/10.1111/apa.17104
6. Daley CL, Iaccarino JM, Lange C, Cambau E, Wallace RJ Jr, Andrejak C, et al. Treatment of nontuberculous mycobacterial pulmonary disease: an official ATS/ERS/ESCMID/IDSA clinical practice guideline. Clin Infect Dis. 2020;71:e1–36. https://doi.org/10.1093/cid/ciaa241
7. Pedersen AA, Løkke A, Fløe A, Ibsen R, Johansen IS, Hilberg O. Nationwide increasing incidence of nontuberculous mycobacterial diseases among adults in Denmark—eighteen years of follow-up. Chest. 2024 Mar 16; [Epub ahead of print].
8. Henkle E, Winthrop KL. Nontuberculous mycobacteria infections in immunosuppressed hosts. Clin Chest Med. 2015;36:91–9. https://doi.org/10.1016/j.ccm.2014.11.002
9. Ashizawa H, Takazono T, Kawashiri SY, Nakada N, Ito Y, Ashizawa N, et al. Risk factor of non-tuberculous *Mycobacterium* infection in patients with rheumatoid arthritis and other autoimmune diseases receiving biologic agents: a multicenter retrospective study. Respir Investig. 2024;62:322–7. https://doi.org/10.1016/j.resinv.2024.02.005
10. Nohrenberg M, Wright A, Krause V. Non-tuberculous mycobacterial skin and soft tissue infections in the Northern Territory, Australia, 1989–2021. Int J Infect Dis. 2023;135:125–31. https://doi.org/10.1016/j.ijid.2023.07.031
11. Malhotra AM, Arias M, Backx M, Gadsby J, Goodman A, Gourlay Y, et al. Extrapulmonary nontuberculous mycobacterial infections: a guide for the general physician. Clin Med (Lond). 2024;24:100016. https://doi.org/10.1016/j.clinme.2024.100016
12. Wetzstein N, Kohl TA, Diricks M, Mas-Peiro S, Holubec T, Kessel J, et al. Clinical characteristics and outcome of Mycobacterium chimaera infections after cardiac surgery: systematic review and meta-analysis of 180 heater-cooler unit-associated cases. Clin Microbiol Infect. 2023;29:1008–14. https://doi.org/10.1016/j.cmi.2023.03.005
13. Buser GL, Laidler MR, Cassidy PM, Moulton-Meissner H, Beldavs ZG, Cieslak PR. Outbreak of nontuberculous mycobacteria joint prosthesis infections, Oregon, USA, 2010–2016. Emerg Infect Dis. 2019;25:849–55. https://doi.org/10.3201/eid2505.181687
14. Shah JA, Lindestam Arlehamn CS, Horne DJ, Sette A, Hawn TR. Nontuberculous mycobacteria and heterologous immunity to tuberculosis. J Infect Dis. 2019;220:1091–8. https://doi.org/10.1093/infdis/jiz285
15. Hannah CE, Ford BA, Chung J, Ince D, Wanat KA. Characteristics of nontuberculous mycobacterial infections at a midwestern tertiary hospital: a retrospective study of 365 patients. Open Forum Infect Dis. 2020;7:ofaa173.
16. Ricotta EE, Adjemian J, Blakney RA, Lai YL, Kadri SS, Prevots DR. Extrapulmonary nontuberculous mycobacteria infections in hospitalized patients, United States, 2009–2014. Emerg Infect Dis. 2021;27:845–52. https://doi.org/10.3201/eid2703.201087
17. Chen CY, Sheng WH, Lai CC, Liao CH, Huang YT, Tsay W, et al. Mycobacterial infections in adult patients with hematological malignancy. Eur J Clin Microbiol Infect Dis. 2012;31:1059–66. https://doi.org/10.1007/s10096-011-1407-7
18. Schmidt M, Pedersen L, Sørensen HT. The Danish Civil Registration System as a tool in epidemiology. Eur J Epidemiol. 2014;29:541–9. https://doi.org/10.1007/s10654-014-9930-3
19. Helweg-Larsen K. The Danish register of causes of death. Scand J Public Health. 2011;39(Suppl):26–9. https://doi.org/10.1177/1403494811399958
20. Schmidt M, Schmidt SA, Sandegaard JL, Ehrenstein V, Pedersen L, Sørensen HT. The Danish National Patient Registry: a review of content, data quality, and research potential. Clin Epidemiol. 2015;7:449–90. https://doi.org/10.2147/CLEP.S91125
21. Quan H, Li B, Couris CM, Fushimi K, Graham P, Hider P, et al. Updating and validating the Charlson comorbidity index and score for risk adjustment in hospital discharge abstracts using data from 6 countries. Am J Epidemiol. 2011;173:676–82. https://doi.org/10.1093/aje/kwq433
22. Borucka J. Extensions of Cox model for non-proportional hazards purpose. Ekonometria. 2014;3(45).
23. Omori K, Kitagawa H, Yamaguchi K, Sakamoto S, Horimasu Y, Masuda T, et al. Clinical characteristics of extrapulmonary nontuberculous mycobacteria infections in comparison with pulmonary infections: a single-center, retrospective study in Japan. J Infect Chemother. 2023;29:875–81. https://doi.org/10.1016/j.jiac.2023.05.013
24. Hamed KA, Tillotson G. A narrative review of nontuberculous mycobacterial pulmonary disease: microbiology, epidemiology, diagnosis, and management challenges. Expert Rev Respir Med. 2023;17:973–88. https://doi.org/10.1080/17476348.2023.2283135
25. Loebinger MR, Quint JK, van der Laan R, Obradovic M, Chawla R, Kishore A, et al. Risk factors for nontuberculous mycobacterial pulmonary disease: a systematic literature review and meta-analysis. Chest. 2023;164:1115–24. https://doi.org/10.1016/j.chest.2023.06.014
26. Mirsaeidi M, Machado RF, Garcia JG, Schraufnagel DE. Nontuberculous mycobacterial disease mortality in the United States, 1999–2010: a population-based comparative study. PLoS One. 2014;9:e91879. https://doi.org/10.1371/journal.pone.0091879

27. Baldolli A, Daurel C, Verdon R, de La Blanchardière A. High mortality in peritonitis due to *Mycobacterium avium* complex: retrospective study and systematic literature review. Infect Dis (Lond). 2019;51:81–90. https://doi.org/10.1080/23744235.2018.1519639
28. Cinicola BL, Ottaviano G, Hashim IF, Zainudeen ZT, Hamid IJA, Elfeky R. Prevalence and characteristics of non-tuberculous mycobacteria (NTM) infection in recipients of allogeneic hematopoietic stem cell transplantation: a systematic review and meta-analysis. J Clin Immunol. 2023;44:23. https://doi.org/10.1007/s10875-023-01615-3
29. Song Y, Zhang L, Yang H, Liu G, Huang H, Wu J, et al. Non-tuberculous mycobacterium infection in renal transplant recipients: a systematic review. Infect Dis (Lond). 2018;50:409–16. https://doi.org/10.1080/23744235.2017.1411604
30. Meena DS, Kumar D, Meena V, Bohra GK, Tak V, Garg MK. Epidemiology, clinical presentation, and predictors of outcome in nontuberculous mycobacterial central nervous system infection: a systematic review. Trop Med Health. 2023;51:54. https://doi.org/10.1186/s41182-023-00546-4
31. Griffith DE, Marras TK. Nontuberculous mycobacterial disease epidemiology: you can see the stars and still not see the light. Clin Infect Dis. 2021;73:e327–9. https://doi.org/10.1093/cid/ciaa1096
32. Larsen ES, Nordholm AC, Lillebaek T, Holden IK, Johansen IS. The epidemiology of bacille Calmette-Guérin infections after bladder instillation from 2002 through 2017: a nationwide retrospective cohort study. BJU Int. 2019;124:910–6. https://doi.org/10.1111/bju.14793
33. Huang CT, Chen CY, Chen HY, Chou CH, Ruan SY, Lal CC, et al. Genitourinary infections caused by nontuberculous mycobacteria at a university hospital in Taiwan, 1996–2008. Clin Microbiol Infect. 2010;16:1585–90.
34. Wetzstein N, Kessel J, Bingold TM, Carney J, Graf C, Koch BF, et al. High overall mortality of *Mycobacterium genavense* infections and impact of antimycobacterial therapy: systematic review and individual patient data meta-analysis. J Infect. 2022;84:8–16. https://doi.org/10.1016/j.jinf.2021.10.027
35. Sexton P, Harrison AC. Susceptibility to nontuberculous mycobacterial lung disease. Eur Respir J. 2008;31:1322–33. https://doi.org/10.1183/09031936.00140007
36. Lake MA, Ambrose LR, Lipman MCI, Lowe DM. "Why me, why now?" Using clinical immunology and epidemiology to explain who gets nontuberculous mycobacterial infection. BMC Med. 2016;14:54.
37. Chai J, Han X, Mei Q, Liu T, Walline JH, Xu J, et al. Clinical characteristics and mortality of non-tuberculous mycobacterial infection in immunocompromised vs. immunocompetent hosts. Front Med (Lausanne). 2022;9:884446. https://doi.org/10.3389/fmed.2022.884446
38. Oh TK, Song K-H, Song I-A. History of anemia and l ong-term mortality due to infection: a cohort study with 12 years follow-up in South Korea. BMC Infect Dis. 2021;21:674.
39. Winthrop KL, Baxter R, Liu L, Varley CD, Curtis JR, Baddley JW, et al. Mycobacterial diseases and antitumour necrosis factor therapy in USA. Ann Rheum Dis. 2013;72:37–42. https://doi.org/10.1136/annrheumdis-2011-200690
40. Chapel H, Lucas M, Lee M, Bjorkander J, Webster D, Grimbacher B, et al. Common variable immunodeficiency disorders: division into distinct clinical phenotypes. Blood. 2008;112:277–86. https://doi.org/10.1182/blood-2007-11-124545
41. Bølling-Ladegaard E, Dreier JW, Christensen J. Identification of drug resistance in a validated cohort of incident epilepsy patients in the Danish National Patient Register. Epilepsia. 2023;64:2604–16. https://doi.org/10.1111/epi.17732
42. Albaek Jacobsen H, Jess T, Larsen L. Validity of inflammatory bowel disease diagnoses in the Danish National Patient Registry: a population-based study from the North Denmark Region. Clin Epidemiol. 2022;14:1099–109. https://doi.org/10.2147/CLEP.S378003
43. Guglielmetti L, Mougari F, Lopes A, Raskine L, Cambau E. Human infections due to nontuberculous mycobacteria: the infectious diseases and clinical microbiology specialists' point of view. Future Microbiol. 2015;10:1467–83. https://doi.org/10.2217/fmb.15.64
44. Turenne CY. Nontuberculous mycobacteria: insights on taxonomy and evolution. Infect Genet Evol. 2019;72:159–68. https://doi.org/10.1016/j.meegid.2019.01.017

Address for correspondence: Andreas Arnholdt Pedersen, Department of Medicine, Lillebaelt Hospital, Beriderbakken 4, 7100 Vejle, Denmark; email: andreas.arnholdt.pedersen@rsyd.dk

Mpox Epidemiology and Risk Factors, Nigeria, 2022

Dimie Ogoina, Mahmmod Muazu Dalhat, Ballah Akawu Denue, Mildred Okowa, Nneka Marian Chika-Igwenyi, Sebastine Oseghae Oiwoh, Ekaete Alice Tobin, Hakeem Abiola Yusuff, Anastacia Okwudili Ojimba, Umenzekwe Chukwudi Christian, John-Tunde Aremu, Simji Samuel Gomerep, Kambai Lalus Habila, Sati Klein Awang, Olukemi Adekanmbi, Michael Iroezindu, Asukwo Onukak, Olanrewaju Falodun, Mogaji Sunday, Simon Mafuka Johnson, Abimbola Olaitan, Chizaram Onyeaghala, Datonye Alasia, Juliet Mmerem, Uche Unigwe, Vivian Kwaghe, Mukhtar Abdulmajid Adeiza, on behalf of Nigerian Infectious Diseases Society (NIDS) mpox study group[1]

To investigate epidemiology of and risk factors for laboratory-confirmed mpox during the 2022 outbreak in Nigeria, we enrolled 265 persons with suspected mpox. A total of 163 (61.5%) were confirmed to have mpox; 137 (84.0%) were adults, 112 (68.7%) male, 143 (87.7%) urban/semi-urban dwellers, 12 (7.4%) self-reported gay men, and 3 (1.8%) female sex workers. Significant risk factors for adults were sexual and nonsexual contact with persons who had mpox, as well as risky sexual behavior. For children, risk factors were close contact with an mpox-positive person and prior animal exposure. Odds of being mpox positive were higher for adults with HIV and lower for those co-infected with varicella zoster virus (VZV). No children were HIV-seropositive; odds of being mpox positive were higher for children with VZV infection. Our findings indicate mpox affects primarily adults in Nigeria, partially driven by sexual activity; childhood cases were driven by close contact, animal exposure, and VZV co-infection.

Human mpox is a zoonotic disease caused by 2 distinct clades (I and II) of the monkeypox virus (MPXV) (*1*). Clade I primarily affects children and adolescents in Central Africa, especially in the Democratic Republic of Congo (DRC) (*1*,*2*). Clade IIa was responsible for the 2003 human outbreak of mpox in the United States, and clade IIb caused the 2017–2019 mpox outbreak in Nigeria and the 2022 global outbreak (*1*); ≈92,000 confirmed cases and 171 deaths were reported in 116 countries as of December 22, 2023 (*3*).

The epidemiologic characteristics of mpox during the 2022 outbreak have been described (*4*–*8*). The evidence suggests that ≈96% of mpox cases during the 2022 outbreak were in men, mostly 20–41 years of age, and the predominant mode of transmission (≈80%) was sexual encounter. Furthermore, the most frequent independent predictors of laboratory-confirmed mpox

Author affiliations: Niger Delta University/Niger Delta University Teaching Hospital, Bayelsa, Nigeria (D. Ogoina); Infectious Diseases Control Centre, Kaduna State, Nigeria (M.M. Dalhat); University of Maiduguri, Maiduguri, Nigeria (B.A. Denue); Ministry of Health, Asaba, Nigeria (M. Okowa); Alex Ekwueme Federal University Teaching Hospital, Abakaliki, Nigeria (N.M. Chika-Igwenyi); Irrua Specialist Teaching Hospital, Irrua, Nigeria (S. Oiwoh, E.A. Tobin); Ministry of Health, Abeokuta, Nigeria (H.A. Yusuff); Federal Medical Centre, Asaba (A.O. Ojimba); Nnamdi Azikiwe University Teaching Hospital, Nnewi, Nigeria (U.C. Christian); Federal Teaching Hospital, Gombe, Nigeria (J.T. Aremu); Jos University Teaching hospital/University of Jos, Jos, Nigeria (S.S. Gomerep); Kaduna State Emergency Medical Services and Ambulance System, Kaduna, Nigeria (K.L. Habila); Modibo Adamawa University Teaching Hospital, Yola, Nigeria (S.K. Awang); University of Ibadan College of Medicine, Ibadan, Nigeria (O. Adekanmbi); University of Nigeria Teaching Hospital, Enugu, Nigeria (M. Iroezindu, J Mmerem, U. Unigwe); University of Uyo, Uyo, Nigeria (A. Onukak); National Hospital Abuja, Abuja, Nigeria (O. Falodun); Federal Medical Centre Ebute-Metta, Lagos, Nigeria (M. Sunday); Federal University Teaching Hospital, Imo, Nigeria (S.M. Johnson); Olabisi Onabanjo University Teaching Hospital, Sagamu, Nigeria (A. Olaitan); University of Port Harcourt Teaching Hospital, Port Harcourt, Nigeria (C. Onyeaghala, D. Alasia); University of Abuja Teaching Hospital, Gwagalada, Nigeria (V. Kwaghe); Ahmadu Bello University Teaching Hospital, Zaria, Nigeria (M.A. Adeiza)

DOI: https://doi.org/10.3201/eid3009.240135

[1]Additional members of the NIDS study group Nigeria who are co-authors and contributed data to this work are listed at the end of this article.

during the 2022 mpox outbreak have been identified as being male; being gay, bisexual, and other men who have sex with men (GBMSM); being a person living with HIV (PLHIV); having multiple sex partners; and having lesions in the anogenital area (*9*–*14*).

The 2017–2019 mpox outbreak in Nigeria predominantly affected young urban adults; human-to-human and zoonotic-related transmissions were suspected (*15*). Confirmed cases were reported among prison inmates, household and sexual contacts, and persons exposed to wildlife (*15*). The 2017–2019 outbreak provided the first documented evidence of mpox transmission via sexual contact and of mpox being associated with having multiple sex partners or advanced HIV disease (*16*–*18*). However, in ≈60% of cases, the risk factors or sources of exposure for mpox were unknown, suggesting a substantial knowledge gap in the epidemiology of mpox in Nigeria (*15*).

During the 2022 mpox outbreak, ≈1,400 cases were reported in Africa, of which Nigeria accounted for 42% (*3*). However, only a few studies from Africa discuss the epidemiology of and risk factors for laboratory-confirmed mpox infections during that outbreak. A case series from Nigeria described the interplay of mpox with varicella zoster virus (VZV) but was limited to southern Nigeria (*19*), suggesting the need to explore the co-infection on a national scale. Since 2023, the DRC has reported increasing mpox cases, including those caused by the sexually transmitted clade I strain (*20*,*21*). That change in the epidemiology is concerning and calls for concerted action and more information about the epidemiology of and risk factors for mpox in countries in Africa where the disease was previously endemic.

To investigate the epidemiology of and risk factors for laboratory-confirmed mpox in Nigeria during the 2022 outbreak, we conducted an observational cross-sectional study to address existing knowledge gaps and provide insights that can be used to develop public health strategies and interventions to control future mpox outbreaks.

Methods

Ethics Statement

We obtained ethics approval for the study from the National Health Research Ethics Committee, Nigeria (NHREC/01/01/2007–25/10/2022). All participants gave informed consent to participate in the study.

Study Participants

Our cross-sectional study included persons with suspected mpox who attended mpox treatment centers and outpatient clinics across Nigeria during June 1–December 30, 2022. We defined a suspected case of mpox by using the Nigeria Centre for Disease Control and Prevention guidelines, as previously described (*22*). On the basis of an average of 12 suspected cases of mpox seen monthly during January–April 2022 in Nigeria, we estimated a minimum sample size of 158 participants, including a 10% dropout rate. We invited all mpox treatment centers and outpatient clinics across Nigeria to participate in the study and consecutively enrolled persons with suspected mpox who attended study sites and gave informed verbal or written consent. Suspected mpox was diagnosed by PCR at the National Reference Laboratory of the Nigeria Centre for Disease Control and Prevention as previously described (*23*). We defined an mpox-positive participant as an mpox-suspected participant for whom MPXV infection was confirmed by real-time PCR. Because of lack of laboratory diagnoses, we excluded probable cases of mpox (Appendix, https://wwwnc.cdc.gov/EID/article/30/9/24-0135-App1.pdf).

To document epidemiologic and clinical variables of all study participants, we used a structured case report form, which was developed from existing mpox literature review (*4*,*15*,*18*,*23*–*25*) and included variables such as patient age, sex, occupation, sexual orientation, and potential routes and risk factors for mpox transmission (e.g., animal exposure, close contact, and sexual behavior). Sexual history was not obtained for all children. We also documented comorbidities (e.g., HIV and VZV co-infections) (Appendix). All variables were documented at manifestation or at the time of participant recruitment.

We analyzed study data by using the SPSS Statistics 26 (IBM, https://www.ibm.com). We summarized categorical variables as frequencies and percentages and summarized continuous variables by using median and interquartile ranges (IQRs) because of nonnormal distribution. We used χ^2 for categorical variables (or Fisher exact tests when assumptions for χ^2 were not met because of small sample size) and Mann-Whitney tests (comparing median values) to determine variables associated with being mpox positive. We determined independent predictors of mpox positivity separately by using logistic regression models that included significant epidemiologic variables on univariate analysis and other relevant variables known to be theoretically associated with mpox infection from prior literature. We deleted missing variables pairwise without replacements. We excluded educational level from the model because of strong correlation with age group. Because of missing

data, we did not include HIV and VZV data in the logistic models. The logistic regression tables detail the variables included in each model. In view of differences in epidemiologic characteristics across age groups, we assessed the risk factors for mpox positivity for the entire study population and separately for children (<18 years of age) and adults. We reported results as crude odd ratios (ORs) and adjusted odds ratios (aORs) with 95% CIs. We considered $p<0.05$ (2-tailed) as statistically significant.

Results

Study Population

We enrolled 280 persons with suspected cases of mpox during the study period, among whom we excluded 15 (5.4%) from the final analysis because of missing data related to sociodemographic and epidemiologic characteristics. We enrolled 265 study participants, 28 days–69 years of age (median 27 years, IQR 14–36 years) across 23 states and the Federal Capital Territory in Nigeria (Figure). Of the 265 participants, 163 (61.5%) were mpox positive and 102 (38.5%) were mpox negative (Table 1). The mpox-positive participants (median age 30 years [IQR 22–37 years]) were older than the mpox-negative participants (median age 19 years [IQR 8–32 years]; $p<0.0001$).

Demographic and Epidemiologic Characteristics of Mpox-Positive Participants

Of the 163 mpox-positive participants, 137 (84.0%) were adults, 112 (68.7%) were male, 143 (87.7%) were urban/semi-urban dwellers, 12 (7.4%) were self-reported GBMSM, and 3 (1.8%) were female sex workers (Appendix Table). Among the 163 mpox-positive participants, exposure was unknown for 87 (53.4%) and ≥1 exposure was reported for 76 (46.6%). Specifically, 59 (36.2%) had contact with a person with a suspected case, 36 (22.1%) had close contact with a person with a confirmed case, 35 (21.5%) reported animal exposure, and 35 (21.5%) had sexual contact with a person with a suspected case. Of the 46 mpox-positive participants who provided information about

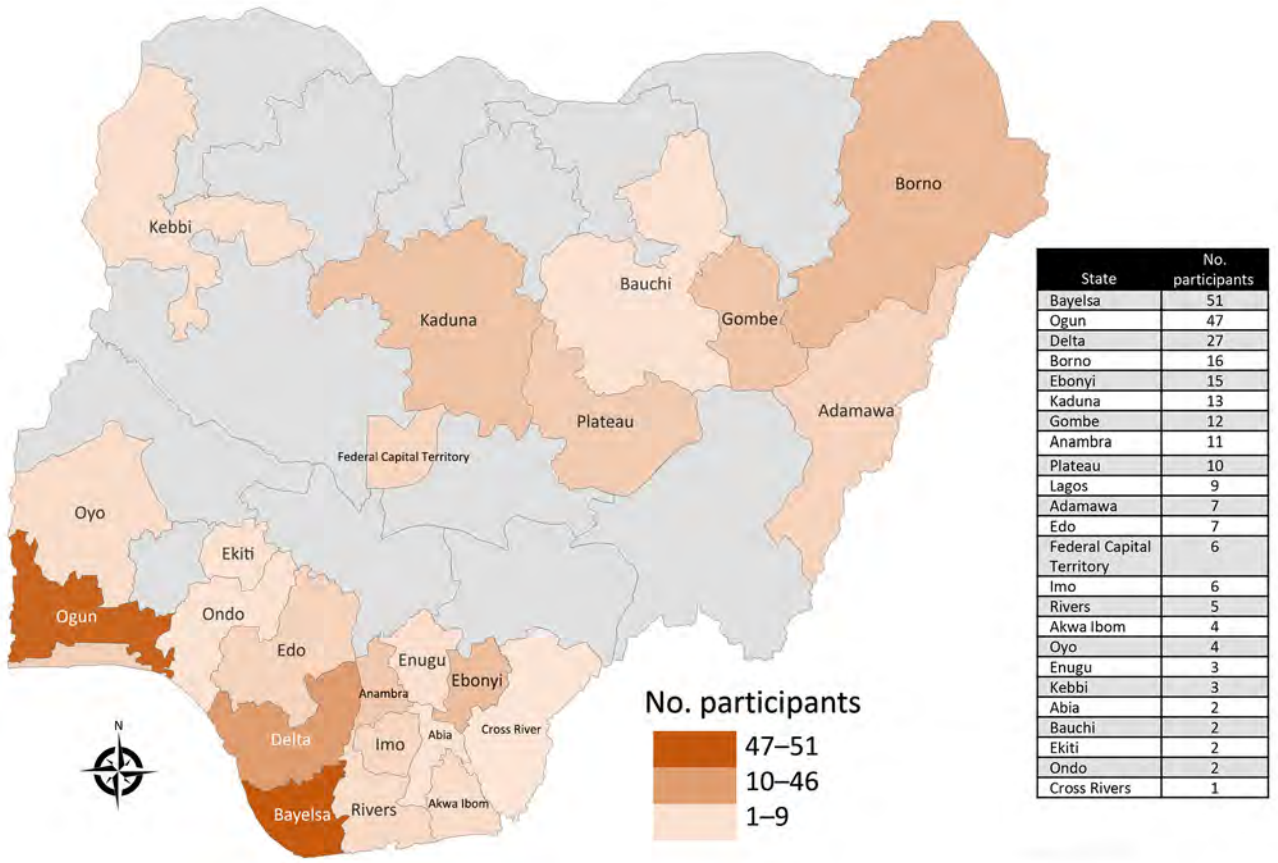

State	No. participants
Bayelsa	51
Ogun	47
Delta	27
Borno	16
Ebonyi	15
Kaduna	13
Gombe	12
Anambra	11
Plateau	10
Lagos	9
Adamawa	7
Edo	7
Federal Capital Territory	6
Imo	6
Rivers	5
Akwa Ibom	4
Oyo	4
Enugu	3
Kebbi	3
Abia	2
Bauchi	2
Ekiti	2
Ondo	2
Cross Rivers	1

Figure. Geographic distribution of sites in Nigeria participating in a study of epidemiology and risk factors for laboratory-confirmed mpox during the mpox outbreak, Nigeria, 2022. A total of 265 study participants were enrolled from all geopolitical zones of the country, across 23 states and the Federal Capital Territory in Nigeria.

possible places of exposure, 23 (50%) were exposed at home, 20 (43.5%) in the community, and 3 (6.5%) in the hospital. Among the mpox-positive participants tested for HIV and VZV co-infections, 35.9% (55/153) had VZV co-infection, 18.0% (24/133) had HIV co-infection, and 6.0% (8/133) had both HIV and VZV co-infections. Among the 102 mpox-negative participants, 31 (30.4%) were VZV positive, 52 (50.9%) were VZV negative, and 19 (18.6%) were missing data on VZV status. We did not investigate the causes of

n

Table 1. Demographic characteristics and epidemiologic risk factors for PCR-confirmed mpox among adults and children during mpox outbreak, Nigeria, 2022*

	No. (%) patients			Univariate analysis		Multivariate analysis	
Study variable	Total	Mpox-pos	Mpox-neg	cOR (95% CI)	p value†	aOR (95% CI)	p value†
Age group							**<0.0001**
Child, <18 y	73 (27.5)	26 (16.0)	47 (46.1)	Referent		Referent	
Young adult, 18–35 y	125 (47.2)	88 (54.0)	37 (36.3)	4.30 (2.33–7.94)	**<0.0001**	3.93 (2.06–7.50)	**<0.0000**
Older adult, >35 y	67 (25.3)	49 (30.0)	18 (17.6)	4.92 (2.39–10.13)	**<0.0001**	4.75 (2.23–10.13)	**<0.0001**
Sex at birth							
M	174 (65.7)	112 (68.7)	62 (60.8)	1.42 (0.84–2.38)	0.186	1.38 (0.77–2.48)	0.284
F	91 (34.3)	51 (31.3)	40 (39.2)	Referent		Referent	
Local travel							
Yes	34 (12.8)	28 (17.2)	6 (5.9)	3.32 (1.32–8.33)	**0.007**	2.02 (0.76–5.34)	0.158
No	231 (87.2)	135 (82.8)	96 (94.1)	Referent		Referent	
Close contact with person with confirmed mpox							
Yes	46 (17.4)	36 (22.1)	10 (9.8)	2.61 (1.21–5.52)	**0.010**	2.96 (1.26–6.96)	**0.013**
No	219 (82.6)	127 (77.9)	92 (90.2)	Referent		Referent	
Prior animal exposure							
Yes	43 (16.2)	35 (21.5)	8 (7.8)	3.21 (1.30–7.24)	**0.003**	2.35 (0.97–5.66)	0.058
No	222 (83.8)	128 (78.5)	94 (92.2)	Referent		Referent	
Residence							
Urban/semi-urban	231 (87.2)	143 (87.7)	88 (86.3)	1.14 (0.55–2.37)	0.73		
Rural	34 (12.8)	20 (12.3)	14 (13.7)	Referent			
Married‡							
Ever	95 (49.5)	70 (51.1)	25 (45.5)	1.25 (0.67–2.35)	0.48		
Never	97 (50.5)	67 (48.9)	30 (54.5)	Referent			
Education							
None	59 (22.3)	35 (21.5)	24 (41.4)	Referent			
Primary	32 (12.1)	12 (7.4)	20 (34.5)	0.41 (0.17–0.99)	**0.003**		
Secondary	68 (25.7)	39 (23.9)	29 (50)	0.92 (0.45–1.87)			
Tertiary	106 (40.0)	77 (47.2)	29 (50)	1.82 (0.93–3.57)			
International travel							
Yes	3 (1.1)	1 (0.6)	2 (2)	0.31 (0.03–3.45)	0.561§		
No	262 (98.9)	162 (99.4)	100 (98)	Referent			
Close contact with person with suspected mpox							
Yes	78 (29.4)	59 (36.2)	19 (18.6)	2.48 (1.37–4.48)	**0.002**		
No	187 (70.6)	104 (63.8)	83 (81.4)	Referent			
Care of person with suspected mpox							
Yes	5 (1.9)	4 (2.5)	1 (1)	2.54 (0.28–23.06)	0.652§		
No	260 (98.1)	159 (97.5)	101 (99)	Referent			
Prior smallpox vaccine							
Yes	13 (4.9)	9 (5.5)	4 (3.9)	1.43 (0.43–4.79)	0.557		
No	252 (95.1)	154 (94.5)	98 (96.1)	Referent			
Past chickenpox¶							
Yes	23 (16.6)	16 (17.4)	7 (12.7)	1.44 (0.55–3.77)	0.451		
No	124 (84.4)	76 (82.6)	48 (87.3)	Referent			
HIV-status¶							
Positive	26 (12.2)	24 (18.0)	2 (2.5)	8.59 (1.97–37.4)	**0.001**		
Negative	187 (87.8)	109 (82.0)	78 (97.5)	Referent			
VZV status¶							
Positive	86 (36.4)	55 (35.9)	31 (37.3)	0.94 (0.54–1.64)	0.831		
Negative	150 (63.6)	98 (64.1)	52 (62.7)	Referent			
Other comorbidities#							
Yes	13 (4.9)	10 (6.1)	3 (2.9)	2.16 (0.58–8.03)	0.241		
No	252 (95.1)	153 (93.9)	99 (97.1)	Referent			

*Boldface indicates statistical significance. aOR, adjusted odds ratio; neg, negative; pos, positive; cOR, crude odd ratio; VZV, varicella zoster virus.
†p values determined by χ^2 tests except as indicated.
‡Marital status data included adults only.
§Fisher exact test.
¶Some past chickenpox, VZV, and HIV status data were missing.
#Other comorbidities include type 2 diabetes mellitus, hypertension, and sickle cell disease.

Table 2. Demographic characteristics and epidemiologic risk factors for PCR-confirmed mpox among adults during the mpox outbreak, Nigeria, 2022*

Variables	No. (%) patients			Univariate analysis		Multivariate analysis	
	Total	Mpox-pos	Mpox-neg	cOR (95% CI)	p value†	aOR (95% CI)	p value†
Age group,							
Young adult, 18–35 y	125 (65.1)	88 (64.2)	37 (67.3)	0.87 (0.45–1.70)	0.69	1.36 (0.66– 2.80)	0.409
Older adult, >35 y	67 (34.9)	49 (35.8)	18 (32.7)	Referent		Referent	
Sex at birth							
M	131 (68.2)	95 (69.3)	36 (65.5)	1.19 (0.61–2.32)	0.601	1.29 (0.59– 2.79)	0.523
F	61 (31.8)	42 (30.7)	19 (34.5)	Referent		Referent	
Nonsexual contact with person with suspected mpox							
Yes	17 (8.90)	15 (10.9)	2 (3.6)	3.26 (0.72–14.75)	0.158	5.50 (1.12–27.14)	**0.036**
No	175 (91.1)	122 (89.1)	53 (96.4)	Referent		Referent	
Sexual contact with person with suspected mpox							
Yes	41 (21.4)	35 (25.5)	6 (10.9)	2.80 (1.10–7.11)	**0.025**	2.81 (1.01–7.79)	**0.048**
No	151 (78.6)	102 (74.5)	49 (89.1)	Referent		Referent	
Risky sexual behavior‡							
Yes	113 (58.9)	90 (65.7)	23 (41.8)	2.66 (1.40–5.06)	**0.002**	2.808 (1.40–5.3)	**0.004**
No	79 (41.1)	47 (34.3)	32 (58.2)	Referent		Referent	
Animal exposure							
Yes	36 (18.8)	30 (21.9)	6 (10.9)	2.29 (0.89–5.86)	0.078	1.79 (0.66–4.88)	0.255
No	156 (81.2)	107 (78.1)	49 (89.1)	Referent		Referent	
Local travel							
Yes	33 (17.2)	27 (19.7)	6 (10.9)	2.00 (0.78–5.17)	0.144	1.74 (0.64–4.72)	0.28
No	159 (82.8)	110 (80.3)	49 (89.1)	Referent		Referent	
Residence							
Urban/semi-urban	170 (88.5)	122 (89.1)	48 (87.3)	1.19 (0.46–3.09)	0.727		
Rural	22 (11.5)	15 (10.9)	7 (12.7)	Referent			
Married							
Ever	95 (49.5)	70 (51.1)	25 (45.5)	1.25 (0.67–2.35)	0.48		
Never	97 (50.5)	67 (48.9)	30 (54.5)	Referent			
Education							
None	25 (13.0)	21 (15.3)	4 (7.3)	Referent			
Primary	8 (4.20)	5 (3.60)	3 (5.5)	0.32 (0.05–1.90)	0.21		
Secondary	54 (28.1)	34 (24.8)	20 (36.4)	0.32 (0.10–1.08)	0.07		
Tertiary	105 (54.7)	77 (56.2)	28 (50.9)	0.53 (0.17–1.66)	0.27		
International travel							
Yes	3 (1.60)	1 (0.70)	2 (3.6)	0.19 (0.02–2.19)	0.198§		
No	189 (98.4)	136 (99.3)	53 (96.4)	Referent			
Close contact with confirmed mpox							
Yes	33 (17.2)	29 (21.2)	4 (7.3)	3.42 (1.14–10.26)	**0.021**		
No	159 (82.8)	108 (78.8)	51 (92.7)	Referent			
GBMSM							
No	146 (76.0)	107 (78.1)	39 (70.9)	Referent			
Yes	15 (7.80)	12 (8.80)	3 (5.5)	1.46 (0.39–5.44)	0.575		
Unknown	31 (16.1)	18 (13.1)	13 (23.6)	0.51 (0.23–1.13)	0.095		
Care of person with suspected mpox							
Yes	5 (2.60)	4 (2.90)	1 (1.8)	1.02 (0.18–14.86)	0.999§		
No	187 (97.4)	133 (97.1)	54 (98.2)	Referent			
Prior smallpox vaccine							
Yes	13 (6.80)	9 (6.60)	4 (7.3)	0.90 (0.26–3.04)	0.999§		
No	179 (93.2)	128 (93.4)	51 (92.7)	Referent			
Comorbidities¶							
Yes	13 (6.80)	10 (7.30)	3 (5.5)	0.87 (0.23–3.30)	0.761§		
No	179 (93.2)	127 (92.7)	52 (94.5)	Referent			
HIV status#							
Positive	26 (18.3)	24 (22.4)	2 (5.7)	4.71 (1.07–21.34)	**0.026**		
Negative	116 (81.7)	83 (77.6)	33 (94.3)	Referent			
VZV status							
Positive	62 (36.0)	40 (31.0)	22 (51.2)	0.43 (0.21–0.87)	**0.017**		
Negative	110 (64.0)	89 (69.0)	21 (48.8)	Referent			

*Boldface indicates statistical significance, Empty cells indicate not applicable. aOR, adjusted odds ratio; cOR, crude odds ratio; GBMSM, gay and bisexual and men who have sex with men; neg, negative; pos, positive; VZV, varicella zoster virus.
†p values determined by χ^2 tests except as indicated.
‡Risky sexual behavior is defined as ≥1 of the following in the 3 mo before illness onset: condomless casual sex; multiple sexual partners (≥2 more concurrent sex partners); treatment for sexually transmitted infections; transactional sex (payment for sex); sex with a sex worker.
§Fisher exact test.
¶Comorbidities include type 2 diabetes mellitus, hypertension, and sickle cell disease.
#Some HIV and VZV status data were missing.

Table 3. Univariate analysis of associated between sexual histories of adults and mpox-PCR status during mpox outbreak, Nigeria, 2022*

Variables†	No. (%) Mpox positive	Mpox negative	Total	cOR (95% CI)	p value‡
Condomless casual sex, n = 166					
Yes	77 (62.1)	19 (45.2)	96 (57.8)	1.98 (0.98–4.02)	0.056
No	47 (37.9)	23 (54.8)	70 (42.2)		
Multiple sexual partners, n = 170					
Yes	65 (50.8)	10 (23.8)	75 (44.1)	3.30 (1.50–7.28)	**0.002**
No	63 (49.2)	32 (76.2)	95 (55.9)		
Sex with sex worker, n = 166					
Yes	23 (18.5)	4 (9.5)	27 (16.3)	2.16 (0.70–6.67)	0.228
No	101 (81.5)	38 (90.5)	139 (83.7)		
Transactional sex, n = 103					
Yes	6 (8.10)	2 (6.9)	8 (7.80)	1.19 (0.23–6.27)	0.99
No	68 (91.9)	27 (93.1)	95 (92.2)		
Sex in prior month, n = 192					
Yes	101 (73.7)	30 (54.5)	131 (68.2)	2.34 (1.22–4.49)	**0.010**
No	36 (26.3)	25 (45.5)	61 (31.8)		
Prior treatment for STI, n = 158					
Yes	37 (31.6)	12 (29.30)	49 (31.0)	1.12 (0.51–2.43)	0.779
No	80 (68.4)	29 (70.70)	109 (69.0)		
Risky sexual behavior, n = 192§					
Yes	90 (65.7)	23 (41.8)	113 (58.9)	2.66 (1.40–5.06)	**0.002**
No	47 (34.3)	32 (58.2)	79 (41.1)		

*Boldface indicates statistical significance. cOR, crude odds ratio; STI, sexually transmitted infection.
†Variables are defined in the Appendix (https://wwwnc.cdc.gov/EID/article/30/9/24-0135-App1.pdf).
‡p values determined by χ^2 tests.
§Risky sexual behavior is defined as ≥1 of the following in the 3 mo before illness onset: condomless casual sex; multiple sexual partners (≥2 more concurrent sex partners); treatment for sexually transmitted infections; transactional sex (payment for sex); sex with a sex worker.

skin rash among participants who were VZV-negative and those for whom VZV status was missing.

Among the 23 study participants who reported a history of chickenpox (Table 1), 7 (30.4%) were VZV positive; 2 were mpox-negative adults and 5 were mpox positive (a 16-year-old adolescent and 4 adults), all of whom were probably experiencing reactivated herpes zoster infection. Among the 2 mpox-negative adults with probable reactivated herpes zoster infection was a recently diagnosed 63-year-old man living with HIV whose CD4 cell count was unknown/missing.

Epidemiologic Risk Factors for Mpox Positivity

Univariate analysis indicated that the epidemiologic risk factors associated with mpox positivity among the 265 study participants were history of prior animal exposure, age group, close contact with a person with confirmed mpox, educational level, and local travel (Table 1). In a logistic regression model that included age group, sex, animal exposure, close contact with confirmed case and local travel, the independent predictors of mpox positivity were age group and close contact with a person with confirmed mpox (Table 1). The odds of being mpox positive were significantly higher among younger adults (18–35 years of age) (aOR 3.93, 95% CI 2.06–7.50) and older adults (>35 years of age) (aOR 4.75, 95% CI 2.23–10.13) than among children. Odds of being mpox positive were significantly higher among participants who had reported close contact with a person with confirmed mpox than among those who had not (aOR 2.96, 95% CI 1.26–6.96). Among 213 participants with known HIV status, odds of being mpox positive were greater among PLHIV than among those who were HIV negative (OR 8.59, 95% CI 1.97–37.40; p = 0.001).

Epidemiologic Risk Factors among Adults

Univariate analysis indicated that among the 192 adult participants, the variables associated with being mpox positive were prior sexual and nonsexual contact with a person with suspected mpox and recent history of risky sexual behavior (Table 2). The independent predictors among adults for being mpox positive included recent history of risky sexual behavior (aOR 2.81, 95% CI 1.40–5.63), nonsexual contact with a person with a suspected case (aOR 5.50, 95% CI 1.12–27.14), and sexual contact with a person with a suspected case (aOR 2.81, 95% CI 1.01–7.79) (Table 2). Among the 142 adults with known HIV status and the 172 with known VZV status, the odds of being mpox positive were significantly higher among PLHIV (OR 4.77, 95% CI 1.07–21.34) and significantly lower among those who were VZV positive (OR 0.43, 95% CI 0.21–0.87). History of having had multiple sex partners, having had sex recently, and having engaged in risky sexual behaviors were significantly associated with being mpox positive (Table 3).

Epidemiologic Risk Factors among Children

All 71 children with known HIV status tested negative for HIV. Multivariate analysis indicated that the predictors of mpox positivity among children were contact with animals (aOR 9.97, 95% CI 1.27–78.34) and close contact with a person with a confirmed case (aOR 4.76, 95% CI 1.14–19.87) (Table 4). We did not include VZV in the model because of the high numbers of missing data. However, among the 64 children with known VZV status, the odds of being mpox positive were significantly higher among those who were VZV positive than among those who were VZV negative (OR 5.74, 95% CI 1.891–17.43).

Discussion

Our study showed that laboratory-confirmed mpox was reported across various age groups and populations but was more common among persons who were young adult, male, and mostly urban or semi-urban dwellers. The demographic characteristics of the mpox-positive participants in our study are similar to those of the 2017–2019 mpox outbreak in Nigeria, which also predominantly affected young adult urban dwellers. Most cases of mpox during the 2022 outbreak in Europe and North America were among young adult urban dwellers, mostly GBMSM (*6*,*26*). In contrast, only 7.4% of the mpox participants in our study self-reported themselves as GBMSM; MPXV is probably not currently spreading within that particular social group in Nigeria. Another possibility is that cases of mpox in that group have either been overlooked or not accurately reported because GBMSM may avoid seeking clinical assessment because of laws in Nigeria that criminalize same-sex relationships.

The types of exposure settings reported in our study suggest human-to-human and zoonotic transmissions of MPXV during the 2022 outbreak in Nigeria. We identified independent epidemiologic risk factors for mpox positivity among study participants as having had close contact with a person with confirmed mpox and being in an adult age group. Specific risk factors for mpox among adults were ≥1 markers of risky sexual behaviors (e.g., multiple sex partners and condomless casual sex), and both sexual and nonsexual close contact with a person with suspected mpox. Among children, independent risk factors for mpox positivity were close contact with a person with confirmed mpox and contact with wild/domestic animals. Besides nonsexual physical contact, it might be postulated that mpox in Nigeria is also partly transmitted via risky sexual behavior among adults who subsequently transmit it to children through close contact. Various studies conducted outside Africa during the 2022 outbreak also identified risk factors for being mpox positive as having had multiple sex partners and other markers of risky sexual behavior (*9*,*11*,*12*,*14*). Similarly, since 2023, a cluster of clade I strain mpox cases in the DRC was linked to sexual contact, including among GBMSM (*21*).

Studies conducted mainly outside Africa suggest that ≈80% of mpox patients during the 2022 outbreak had sexual encounters before their diagnosis (*4*,*8*), and other studies conducted outside Africa have

Table 4. Epidemiologic risk factors for PCR-confirmed mpox among children (<18 y) during mpox outbreak, Nigeria 2022*

	No. (%)			Univariate analysis		Multivariate analysis	
Variables	Total	Mpox-pos	Mpox-neg	cOR (95% CI)	p value†	aOR (95% CI)	p value†
Sex at birth							
F	30 (41.1)	9 (34.6)	21 (44.7)	Referent		Referent	
M	43 (58.9)	17 (65.4)	26 (55.3)	1.53 (0.57, 4.11)	0.403	1.56 (0.46, 5.27)	0.477
Age group							
0–9 y	42 (57.5)	15 (57.7)	27 (57.4)	1.01 (0.38, 2.66)	0.984	2.03 (0.59, 7.05)	0.264
10–1 y	31 (42.5)	11 (42.3)	20 (42.6)	Referent		Referent	
Close contact confirmed							
Yes	13 (17.8)	7 (26.9)	6 (12.8)	2.52 (0.74, 8.51)	0.13‡	4.76 (1.14, 19.87)	**0.032**
No	60 (82.2)	19 (73.1)	41 (87.2)	Referent		Referent	
Animal exposure§							
Yes	7 (9.6)	5 (19.2)	2 (4.3)	5.36 (0.96, 29.91)	0.05‡	9.97 (1.27, 78.34)	**0.029**
No	66 (90.4)	21 (80.8)	45 (95.7)	Referent		Referent	
Place residence					0.632		
Rural	12 (16.4)	5 (19.2)	7 (14.9)	1.36 (0.35, 4.81)			
Urban/semi-urban	61 (83.6)	21 (80.8)	40 (85.1)	Referent			
VZV status¶					**0.001**		
Positive	24 (37.5)	15 (62.5)	9 (22.5)	5.74 (1.89, 17.43)			
Negative	40 (62.5)	9 (37.5)	31 (77.5)	Referent			

*Boldface indicates statistical significance. aOR, adjusted odds ratio; cOR, crude odds ratio; VZV, varicella zoster virus.
†p values determined by χ^2 tests except as indicated.
‡Fisher exact test.
§The 5 mpox-pos children with animal exposures did not report associated contact with a human with suspected mpox.
¶Some VZV status data were missing.

shown prior sexual activity to be associated with mpox infection among GBMSM and among heterosexual adults (*27*,*28*). The role of sexual contact and sexual behavior in the transmission of mpox was first proposed during the 2017–2019 mpox outbreak in Nigeria (*16*,*17*). A single-center study conducted during the 2022 outbreak in Nigeria reported mpox among linked heterosexual partners, suggesting a relationship between prior sexual contact and mpox infection in Nigeria (*29*). Our study, which was conducted on a national scale in Nigeria, corroborates the prior observations and supports a role of sexual activity in transmission of the MPXV among adults during the 2022 mpox outbreak in Nigeria.

With regard to animal exposure being independently associated with mpox positivity among children and not adults, it is plausible but not confirmatory that zoonotic transmission of MPXV in Nigeria is more common among children than adults. However, the large confidence interval of the OR related to animal exposure suggests uncertainty of that finding.

In our study, 18% of participants with available HIV test results had positive results, and odds of being mpox positive were 5 times higher among PLHIV than among those without HIV. During the 2022 global outbreak, 30%–50% of mpox-positive persons were PLHIV (*30*); various studies, including reports from Nigeria, have shown that those with advanced HIV have more severe disease and higher death rates than their HIV-negative counterparts (*31*). A review of 86 confirmed mpox cases during the 2017–2019 mpox outbreak showed that persons with mpox were »7 times more likely to be living with HIV than were those without mpox (*32*). Because of missing HIV test data, we cannot make definitive conclusions regarding HIV as an independent risk factor for mpox in Nigeria during the 2022 mpox outbreak. Even so, HIV and mpox are both sexually transmitted infections, which makes it plausible that risky sexual behavior might be a common factor for acquisition and further transmission of mpox.

Approximately half of the mpox-negative participants in our study were VZV positive, and »36% of mpox-positive participants also had a VZV-positive test result. We previously reported VZV co-infection to be independently associated with severe mpox during the 2022 mpox in Nigeria (*23*). The high prevalence of VZV co-infection among mpox-positive and mpox-negative participants reflects the endemicity of chickenpox, herpes zoster infection, or both in Nigeria and underscores that those VZV-related conditions are the main differential diagnoses for mpox in Nigeria. Of note, VZV co-infection was associated with higher odds of mpox among children but lower odds among adults. The reasons for the contrasting findings are not obvious from our study data. Because we did not distinguish chickenpox from reactivated herpes zoster virus infection in all participants, we could not classify the prevalence of those VZV-related conditions in relation to age, if any. Furthermore, we did not include VZV in the multivariate analysis because of a substantial amount of missing data, and as such, we could not confirm whether our findings were truly reflective of an age-related difference in the associations between VZV and mpox infections or if they resulted from the effects of another confounder. On the basis of the high rates of VZV-mpox co-infections observed from prior studies of mainly the clade I virus (*33*,*34*), it has been proposed but not confirmed that a breach in the skin caused by VZV lesions could increase the likelihood of transmission of MPXV and that MPXV may directly trigger VZV reactivation, resulting in herpes zoster virus infection (*34*,*35*).

The major limitations of our study are associated with recruitment of hospital-associated cases only, which could have led to underascertainment of mild mpox-positive cases and mpox-negative suspected cases in the community and missing data related to VZV and HIV co-infections among some participants, which precluded inclusion of these variables for multivariate analysis. The predominance of moderate to severe cases could also bias our study toward HIV-positive participants, given that they are more likely to have severe illness and thus need to seek care at or get admitted into healthcare facilities. We did not determine virus clades in our study, but prior epidemiologic data suggest that the 2022 mpox outbreak in Nigeria probably resulted from the MPXV clade IIb strain (*36*,*37*).

In conclusion, our study reveals that mpox primarily affects adults in Nigeria, often associated with sexual transmission, and that among children affected by mpox, the prominent drivers are animal contact and VZV infection. Our findings emphasize the value of addressing both sexual and nonsexual transmission routes in public health efforts to control the spread of mpox in Nigeria.

Additional members of the NIDS study group Nigeria who are co-authors and contributed data: Chiedozie James Maduka (Federal Medical Centre, Umahia, Abia State, Nigeria), Aliyu Mamman Na'uzo (Federal Medical Centre, Kebbi State, Nigeria), Sampson Omagbemi Owhin (Federal Medical Center Owo, Ondo, Nigeria), Mohammed Asara Abdullahi (Ahmadu Bello University Teaching Hospital Shika Zaria, Nigeria), Aisha Habiba Sadauki (Baze

University Hospital, Abuja), Okonofua Martha (Irrua Specialist Teaching Hospital, Irrua, Edo State), Rosemary Audu and Ehimario Igumbor (Nigerian Institute of Medical Research, Lagos, Nigeria), Idotenyin Enyi (Ministry of Health, Delta State), Mohammed Yahaya (Usmanu Danfodiyo University Sokoto Nigeria), Chiemezie Amaku (Bingham University Teaching Hospital, Jos, Plateau State), Emeka Sampson (State Ministry of Health, Abakaliki, Ebonyi, Nigeria), Nathan Shehu (West African Center for Emerging Infectious Diseases, Jos University Teaching Hospital, Jos, Plateau State, Nigeria), Ogochukwu Chinedum Okoye and John Ohaju-Obodo (Delta State University, Abraka, Delta State, Nigeria), Olumuyiwa Elijah Ariyo (Federal Teaching Hospital Ido-Ekiti, Ekiti State, Nigeria), Eshan Henshaw (University of Calabar Teaching Hospital, Calabar, Cross Rivers State, Nigeria), Iorhen Ephraim Akase (College of Medicine, University of Lagos/ Lagos University Teaching Hospital, Lagos, Nigeria), Garba Iliyasu (College of Health Sciences. Bayero University Kano, Kano State, Nigeria), Adefolarin Opawoye (Lagos University Teaching Hospital, Lagos, Nigeria), Ubong Aniefio Udoh (Faculty of Medicine, University of Calabar, Calabar, Nigeria), Mahmoud Magaji Ado (Rasheed Shekoni Specialist Hospital and The Infectious Disease Centre, Dutse, Jigawa State, Nigeria), Ayanfe Omololu (King Fahad Specialist Hospital, Buraydah, Saudi Arabia), Ajayi David Bamidele (State Hospital Abeokuta Ogun state, Nigeria), and Adebola Olayinka (World Health Organization, Abuja, Nigeria).

Acknowledgments

We appreciate all healthcare workers in the various mpox treatment centers in Nigeria who participated in case management and the public health response during the 2022 mpox outbreak in Nigeria.

About the Author

Dr. Ogoina is an infectious diseases physician at the Niger Delta University Teaching Hospital and a professor of medicine and infectious diseases at the Niger Delta University, both in Bayelsa State, Nigeria, as well as president of the Nigerian Infectious Diseases Society. His research interests include HIV/AIDS and related opportunistic infections, healthcare-associated infections, antimicrobial use and resistance, infection prevention and control, and epidemic-prone infectious diseases.

References

1. Happi C, Adetifa I, Mbala P, Njouom R, Nakoune E, Happi A, et al. Urgent need for a non-discriminatory and non-stigmatizing nomenclature for monkeypox virus. PLoS Biol. 2022;20:e3001769. https://doi.org/10.1371/journal.pbio.3001769
2. Mitjà O, Ogoina D, Titanji BK, Galvan C, Muyembe JJ, Marks M, et al. Monkeypox. Lancet. 2023;401:60–74. https://doi.org/10.1016/S0140-6736(22)02075-X
3. World Health Organization. 2022–24 Mpox (monkeypox) outbreak: global trends 2023 [cited 2023 Apr 10]. https://worldhealthorg.shinyapps.io/mpx_global
4 Sharma A, Prasad H, Kaeley N, Bondalapati A, Edara L, Kumar YA. Monkeypox epidemiology, clinical presentation, and transmission: a systematic review. Int J Emerg Med. 2023;16:20. https://doi.org/10.1186/s12245-023-00491-3
5. Bragazzi NL, Kong JD, Mahroum N, Tsigalou C, Khamisy-Farah R, Converti M, et al. Epidemiological trends and clinical features of the ongoing monkeypox epidemic: a preliminary pooled data analysis and literature review. J Med Virol. 2023;95:e27931. https://doi.org/10.1002/jmv.27931
6. Thornhill JP, Barkati S, Walmsley S, Rockstroh J, Antinori A, Harrison LB, et al.; SHARE-net Clinical Group. Monkeypox virus infection in humans across 16 countries—April–June 2022. N Engl J Med. 2022;387:679–91. https://doi.org/10.1056/NEJMoa2207323
7. Hennessee I, Shelus V, McArdle CE, Wolf M, Schatzman S, Carpenter A, et al.; California Department of Public Health Monkeypox Pediatric Working Group. CDC Monkeypox Pediatric Working Group; CDC Monkeypox Pediatric Working Group. Epidemiologic and clinical features of children and adolescents aged <18 years with monkeypox—United States, May 17–September 24, 2022. MMWR Morb Mortal Wkly Rep. 2022;71:1407–11. https://doi.org/10.15585/mmwr.mm7144a4
8. Riser AP, Hanley A, Cima M, Lewis L, Saadeh K, Alarcón J, et al. Epidemiologic and clinical features of mpox-associated deaths—United States, May 10, 2022–March 7, 2023. MMWR Morb Mortal Wkly Rep. 2023;72:404–10. https://doi.org/10.15585/mmwr.mm7215a5
9. Moretti M, Heymans B, Yin N, Kaur S, Libois A, Quoilin S, et al. Diagnostic approach to monkeypox outbreak, a case-control study. Int J STD AIDS. 2023;34:338–45. https://doi.org/10.1177/09564624231152789
10. De la Herrán-Arita AK, González-Galindo C, Inzunza-Leyva GK, Valdez-Flores MA, Norzagaray-Valenzuela CD, Camacho-Zamora A, et al. Clinical predictors of monkeypox diagnosis: a case-control study in a nonendemic region during the 2022 outbreak. Microorganisms. 2023;11:2287. https://doi.org/10.3390/microorganisms11092287
11. Rimmer S, Barnacle J, Gibani MM, Wu MS, Dissanayake O, Mehta R, et al. The clinical presentation of monkeypox: a retrospective case-control study of patients with possible or probable monkeypox in a West London cohort. Int J Infect Dis. 2023;126:48–53. https://doi.org/10.1016/j.ijid.2022.11.020
12. Núñez I, Ceballos-Liceaga SE, de la Torre A, García-Rodríguez G, López-Martínez I, Sierra-Madero J, et al. Predictors of laboratory-confirmed mpox in people with mpox-like illness. Clin Microbiol Infect. 2023;29:1567–72. https://doi.org/10.1016/j.cmi.2023.07.016
13. Oeser P, Napierala H, Schuster A, Herrmann WJ. Risk factors for monkeypox infection—a cross-sectional study. Dtsch Arztebl Int. 2023;120:65–6. https://doi.org/10.3238/arztebl.m2022.0365
14. Zucker R, Lavie G, Wolff-Sagy Y, Gur-Arieh N, Markovits H, Abu-Ahmad W, et al. Risk assessment of human mpox infections: retrospective cohort study. Clin Microbiol Infect. 2023;29:1070–4. https://doi.org/10.1016/j.cmi.2023.04.022

15. Yinka-Ogunleye A, Aruna O, Dalhat M, Ogoina D, McCollum A, Disu Y, et al.; CDC Monkeypox Outbreak Team. Outbreak of human monkeypox in Nigeria in 2017-18: a clinical and epidemiological report. Lancet Infect Dis. 2019;19:872–9. https://doi.org/10.1016/S1473-3099(19)30294-4
16. Ogoina D, Yinka-Ogunleye A. Sexual history of human monkeypox patients seen at a tertiary hospital in Bayelsa, Nigeria. Int J STD AIDS. 2022;33:928–32. https://doi.org/10.1177/09564624221119335
17. Ogoina D, Izibewule JH, Ogunleye A, Ederiane E, Anebonam U, Neni A, et al. The 2017 human monkeypox outbreak in Nigeria - report of outbreak experience and response in the Niger Delta University Teaching Hospital, Bayelsa State, Nigeria. PLoS One. 2019;14:e0214229. https://doi.org/10.1371/journal.pone.0214229
18. Ogoina D, Iroezindu M, James HI, Oladokun R, Yinka-Ogunleye A, Wakama P, et al. Clinical course and outcome of human monkeypox in Nigeria. Clin Infect Dis. 2020;71:e210–4. https://doi.org/10.1093/cid/ciaa143
19. Mmerem JI, Umenzekwe CC, Johnson SM, Onukak AE, Chika-Igwenyi NM, Chukwu SK, et al. Mpox and chickenpox co-infection: case series from southern Nigeria. J Infect Dis. 2024;229(Supplement_2):S260–4. https://doi.org/10.1093/infdis/jiad556
20. World Health Organization. Multi-country outbreak of mpox, external situation report #32–30 April 2024 [cited 2024 May 4]. https://www.who.int/publications/m/item/multi-country-outbreak-of-mpox--external-situation-report-32--30-april-2024
21. Kibungu EM, Vakaniaki EH, Kinganda-Lusamaki E, Kalonji-Mukendi T, Pukuta E, Hoff NA, et al.; International Mpox Research Consortium. Clade I–associated mpox cases associated with sexual contact, the Democratic Republic of the Congo. Emerg Infect Dis. 2024;30:172–6. https://doi.org/10.3201/eid3001.231164
22. Nigeria Centre for Disease Control. National monkeypox public health response guidelines, Nigeria [cited 2024 Aug 2]. https://ncdc.gov.ng/themes/common/docs/protocols/96_1577798337.pdf
23. Ogoina D, Dalhat MM, Denue BA, Okowa M, Chika-Igwenyi NM, Yusuff HA, et al.; Nigerian Infectious Diseases Society Mpox Study Group. Clinical characteristics and predictors of human mpox outcome during the 2022 outbreak in Nigeria: a cohort study. Lancet Infect Dis. 2023;23:1418–28. https://doi.org/10.1016/S1473-3099(23)00427-9
24. Ogoina D, Damon I, Nakoune E. Clinical review of human mpox. Clin Microbiol Infect. 2023;29:1493–501. https://doi.org/10.1016/j.cmi.2023.09.004
25. Mitjà O, Alemany A, Marks M, Lezama Mora JI, Rodríguez-Aldama JC, Torres Silva MS, et al. SHARE-NET writing group. Mpox in people with advanced HIV infection: a global case series. Lancet. 2023;401:939–49. https://doi.org/10.1016/S0140-6736(23)00273-8
26. Vivancos R, Anderson C, Blomquist P, Balasegaram S, Bell A, Bishop L, et al.; UKHSA Monkeypox Incident Management Team. Monkeypox Incident Management Team. Community transmission of monkeypox in the United Kingdom, April to May 2022. Euro Surveill. 2022;27:2200422. https://doi.org/10.2807/1560-7917.ES.2022.27.22.2200422
27. Sharpe JD, Charniga K, Byrd KM, Stefanos R, Lewis L, Watson J, et al. Possible exposures among mpox patients without reported male-to-male sexual contact—six U.S. jurisdictions, November 1–December 14, 2022. MMWR Morb Mortal Wkly Rep. 2023;72:944–8. https://doi.org/10.15585/mmwr.mm7235a2
28. Girometti N, Byrne R, Bracchi M, Heskin J, McOwan A, Tittle V, et al. Demographic and clinical characteristics of confirmed human monkeypox virus cases in individuals attending a sexual health centre in London, UK: an observational analysis. Lancet Infect Dis. 2022;22:1321–8. https://doi.org/10.1016/S1473-3099(22)00411-X
29. Ogoina D, James HI. Mpox among linked heterosexual casual partners in Bayelsa, Nigeria. N Engl J Med. 2023;388:2101–4. https://doi.org/10.1056/NEJMc2300866
30. Ortiz-Saavedra B, Montes-Madariaga ES, Cabanillas-Ramirez C, Alva N, Ricardo-Martínez A, León-Figueroa DA, et al. Epidemiologic situation of HIV and monkeypox coinfection: a systematic review. Vaccines (Basel). 2023;11:246. https://doi.org/10.3390/vaccines11020246
31. Girometti N, Ogoina D, Tan DHS, Pozniak A, Klein MB. Intersecting HIV and mpox epidemics: more questions than answers. J Int AIDS Soc. 2022;25:e26043. https://doi.org/10.1002/jia2.26043
32. Yinka-Ogunleye A, Dalhat M, Akinpelu A, Aruna O, Garba F, Ahmad A, et al. Mpox (monkeypox) risk and mortality associated with HIV infection: a national case-control study in Nigeria. BMJ Glob Health. 2023;8:e013126. https://doi.org/10.1136/bmjgh-2023-013126
33. Hughes CM, Liu L, Davidson WB, Radford KW, Wilkins K, Monroe B, et al. A tale of two viruses: coinfections of monkeypox and varicella zoster virus in the Democratic Republic of Congo. Am J Trop Med Hyg. 2020;104:604–11. https://doi.org/10.4269/ajtmh.20-0589
34. Hoff NA, Morier DS, Kisalu NK, Johnston SC, Doshi RH, Hensley LE, et al. Varicella coinfection in patients with active monkeypox in the Democratic Republic of the Congo. EcoHealth. 2017;14:564–74. https://doi.org/10.1007/s10393-017-1266-5
35. MacNeil A, Reynolds MG, Carroll DS, Karem K, Braden Z, Lash R, et al. Monkeypox or varicella? Lessons from a rash outbreak investigation in the Republic of the Congo. Am J Trop Med Hyg. 2009;80:503–7. https://doi.org/10.4269/ajtmh.2009.80.503
36. Faye O, Pratt CB, Faye M, Fall G, Chitty JA, Diagne MM, et al. Genomic characterisation of human monkeypox virus in Nigeria. Lancet Infect Dis. 2018;18:246. https://doi.org/10.1016/S1473-3099(18)30043-4
37. Ndodo N, Ashcroft J, Lewandowski K, Yinka-Ogunleye A, Chukwu C, Ahmad A, et al. Distinct monkeypox virus lineages co-circulating in humans before 2022. Nat Med. 2023;29:2317–24. https://doi.org/10.1038/s41591-023-02456-8

Address for correspondence: Dimie Ogoina, Infectious Diseases Unit, Niger Delta University and Niger Delta University Teaching Hospital, PMB 100, Bayelsa, Nigeria; email: dimieogoina@gmail.com

Infection Rates and Symptomatic Proportion of SARS-CoV-2 and Influenza in Pediatric Population, China, 2023

Chao Shi,[1] Yuhe Zhang,[1] Sheng Ye,[1] Jiyang Zhou, Fuyu Zhu, Yumeng Gao, Yan Wang, Bingbing Cong, Shuyu Deng, You Li, Bing Lu, Xin Wang

We conducted a longitudinal cohort study of SARS-CoV-2 and influenza rates in childcare centers and schools in Wuxi, China, collecting 1,760 environmental samples and 9,214 throat swabs from 593 students (regardless of symptoms) in weekly collections during February–June 2023. We estimated a cumulative infection rate of 124.8 (74 episodes)/1,000 persons for SARS-CoV-2 and 128.2 (76 episodes)/1,000 persons for influenza. The highest SARS-CoV-2 infection rate was in persons 18 years of age, and for influenza, in children 4 years of age. The asymptomatic proportion of SARS-CoV-2 was 59.6% and 66.7% for influenza; SARS-CoV-2 symptomatic proportion was lower in 16–18-year-olds than in 4–6-year-olds. Only samples from frequently touched surface tested positive for SARS-CoV-2 (4/1,052) and influenza (1/1,052). We found asynchronous circulation patterns of SARS-CoV-2 and influenza, similar to trends in national sentinel surveillance. The results support vaccination among pediatric populations and other interventions, such as environmental disinfection in educational settings.

SARS-CoV-2 and influenza have caused substantial health threats. SARS-CoV-2 had caused >0.7 billion reported cases and 6.9 million deaths globally by May 2023, when the World Health Organization (WHO) declared the end of the Public Health Emergency of International Concern for COVID-19 (*1*,*2*). After several large waves during 2020–2022, SARS-CoV-2 continued to circulate at lower levels in 2 subsequent waves in November 2022–February 2023 and April–June 2023, according to the WHO Global Influenza Surveillance and Response System (*3*). Seasonal influenza causes annual epidemics, leading to an annual average of 0.3–0.6 million deaths globally (*4*). Although seasonal influenza declined substantially during the early phase of the COVID-19 pandemic, a resurgence of influenza was seen in December 2021 and afterward; activity gradually increased in 2 waves during December 2022–May 2023 (*3*).

In China, influenza epidemics primarily associated with influenza virus A(H3N2) were observed during April–December 2022, followed by a major SARS-CoV-2 epidemic during December 2022–February 2023 (*5*). The changes observed after nonpharmaceutical intervention (NPI) requirements were eased might reflect shifts in population-level immunity for SARS-CoV-2 and influenza, as well as changes in characteristics associated with Omicron variant predominance, which raises new questions on the infection extent and age-dependent risk profiles for SARS-CoV-2 and influenza.

Young children and students are commonly considered a priority group for prevention and control of seasonal respiratory viral infections, either because of their high susceptibility to severe outcomes or their role in virus transmission (*6*–*8*). However, the extent of influenza infections among pediatric populations and in educational settings remains unclear because of lack of data, as do the infection rate and age distribution of SARS-CoV-2 after the period of Omicron predominance (*9*–*15*). Reviews conducted before the Omicron period of predominance found low SARS-CoV-2 transmission among pediatric populations and in educational settings, yet many of those data were collected while NPIs were in place (*10*,*11*,*13*). New data quantifying infection rates and variations

Author affiliations: Nanjing Medical University, Nanjing, China (C. Shi, Y. Zhang, S. Ye, F. Zhu, B. Cong, S. Deng, Y. Li, B. Lu, X. Wang); Wuxi Centre for Disease Control and Prevention, Wuxi, China (C. Shi, J. Zhou, Y. Gao, Y. Wang, B. Lu); The University of Edinburgh, Edinburgh, Scotland, UK (Y. Li, X. Wang)

DOI: https://doi.org/10.3201/eid3009.240065

[1]These authors contributed equally to this article.

between age groups are necessary to develop and refine vaccination and control strategies for SARS-CoV-2 and influenza. Furthermore, comparing SARS-CoV-2 with influenza could offer insights for delineating between-virus heterogeneities in transmission, epidemic trajectories, and responses to control measures. Previous studies comparing SARS-CoV-2 and influenza have focused on clinical symptoms and severe outcomes, such as hospitalization and death (*16*–*18*), rather than comparing infection risk profiles of the 2 viruses in the same pediatric population.

Accurately estimating the incidence of respiratory viral infections is challenging because infections are usually partially observed in surveillance of active infections. Symptomatic infections are not fully captured because of lack of systematic testing, and mild and asymptomatic infections are particularly underrepresented because testing has primarily focused on symptomatic persons and those with severe illness. Estimating infection risk profile across subgroups and settings is further complicated by variations in the probability of developing symptoms and severe illness. Although seroprevalence indicates the extent of recent infections, distinguishing between seropositivity caused by natural infections or vaccination becomes difficult after widespread vaccination (*9*). Longitudinal cohort studies with prospective and intense virological testing could provide valuable information in this context. Few longitudinal cohort studies have quantified infection rates of SARS-CoV-2 and seasonal influenza among pediatric populations, and particularly after the Omicron wave and widespread vaccination (*11*,*14*,*15*,*19*–*21*).

Schools and childcare centers are primary settings for daily activities and interactions of the pediatric population, making them key settings for the spread of respiratory viruses within that group. We conducted a prospective and longitudinal cohort study in educational settings in Wuxi, China, investigating infection rates and age-dependent risk profiles of SARS-CoV-2 and influenza among the pediatric population. We report data over a full school term, spanning February–June 2023, corresponding to a period of increased influenza and SARS-CoV-2 activity in China (*22*).

Methods

Study Design and Participants

We conducted this cohort study in the city of Wuxi in Jiangsu Province, China. Wuxi spans an area of >4,500 km^2, including 5 districts, 2 county-level cities, and the Economic Development Zone. Wuxi had a resident population of 7.5 million in 2022, of which ≈1 million persons 4–18 years of age were enrolled in childcare centers and primary and secondary schools.

We conducted the study during a spring/summer school term during February–June 2023. We used a multistage sampling scheme, and first selected 2 childcare centers, 2 primary schools, 2 junior secondary schools, and a high school in rural and urban settings (Appendix Table 1, https://wwwnc.cdc.gov/EID/article/30/9/24-0065-App1.pdf). Assuming a 12%–18% attack rate of SARS-CoV-2 and influenza and a 5% loss to follow-up, we aimed to enroll a total of 595 persons and on average 85 persons per school (*23*,*24*). Assuming a lower attack rate of 5%, the sample size is sufficient to detect a difference of 9.5% or more between groups with 80% power and 5% level of significance. Given the required sample size, we randomly selected 4 classes in each childcare center and 2 classes in each school, and all students in the selected classes were invited to participate in this study. The study received ethics approval from Wuxi Center for Disease Control and Prevention (approval no. 202302). Informed consent or parental permission was obtained for all participants. We conducted analyses anonymously.

Data Collection and Follow-up

Follow-up was conducted weekly for SARS-CoV-2 and influenza infections, regardless of symptoms. Trained school doctors in each institution collected throat swab samples each week, except during the national holiday on May 1 and at the end of June, when semester exams and summer break gradually began across the institutions. School doctors interviewed persons who tested positive for SARS-CoV-2 or influenza, or the parents of children in childcare centers and primary schools, to collect information on respiratory symptoms during the week after the positive test using a predesigned questionnaire (Appendix Table 2). Information on participants' sex, age, and COVID-19 and influenza vaccination history were collected using questionnaires and by linking with the local vaccination registry.

We collected environmental samples on the day of respiratory sample collection each week in each school. We collected swab samples from frequently touched surfaces (e.g., handrails, floors) and surfaces of infrequent touch (e.g., lights and ceilings) for viral detection (Appendix).

Laboratory Methods

Respiratory specimens and environmental samples were placed in viral transport medium and

transported at 2–8°C to district Center for Disease Control and Prevention laboratories within 6 hours. They were stored at −80°C until nucleic acid extraction. We extracted viral RNA using nucleic acid diagnostic kits (Sansure Biotech [https://www.sansureglobal.com] for SARS-CoV-2; Jiangsu Bioperfectus [https://www.bioperfectus.com] for influenza). We tested each sample for SARS-CoV-2 and influenza virus within 48 hours of its receipt using real-time reverse transcription PCR (RT-PCR) and the nucleic acid test kit.

Definitions

SARS-CoV-2 and influenza infections were confirmed when throat swabs tested positive on real-time RT-PCR, regardless of symptoms. Multiple positive test results of throat swabs collected from one person within 28 days were considered 1 episode (*14*). We defined a symptomatic SARS-CoV-2 or influenza episode as a person reporting ≥1 symptom, including fever (body temperature ≥38°C), respiratory infection symptoms (cough, sore throat, congested nose, runny nose, or sneezing), or other symptoms (fatigue or vomiting).

Statistical Analysis

We excluded participants who did not meet the eligibility criteria on sample collection and testing (Appendix). We estimated cumulative infection rates and 95% CIs of SARS-CoV-2 and influenza infections by dividing the number of infection episodes by the number of participants using a Poisson distribution. We used the logistic regression model to investigate factors of infections and symptomatic infections. To depict epidemic dynamics of SARS-CoV-2 and influenza, we estimated weekly virus positivity among participants and environmental positivity using the number of positive test results dividing the number of tests each week, in comparison to the weekly influenza and SARS-CoV-2 positivity in influenza-like illnesses (ILI) using country-level sentinel surveillance data (*22*). To account for variations in the infection rate of the viruses across different types of educational institutions, we calculated the relative intensity of the virus using the number of positive tests each week dividing the total positive test results obtained throughout the study period (*25*). We compared proportions with χ^2 test or Fisher exact tests, as appropriate. We conducted analyses using R version 4.2.3 (The R Project for Statistical Computing, https://www.r-project.org). We considered a 2-sided p value <0.05 to be statistically significant.

Results

Study Participants

We enrolled 666 participants and excluded 73 participants that did not meet the eligibility criteria, yielding 593 (89.0%) participants included in the analysis. During the 18-week study period, we sampled and tested a total of 9,214 throat swabs, and each participant had 15.5 (95% CI 15.4–15.7) RT-PCR tests on average (Figure 1). We collected, on average, 15.3–16.1 respiratory samples across the educational settings and age groups (Appendix Table 4).

Infection Rates and Age-Dependent Risk Profiles

We identified 74 episodes of SARS-CoV-2 infections, yielding a cumulative rate of 124.8 (95% CI 98.0–156.7)/1,000 persons. SARS-CoV-2 infection rates varied significantly between types of educational settings, urban/rural settings, and age groups (Table 1; Figure 2). By types of educational settings, the rate ranged from 40.5 (95% CI 16.3–83.4)/1,000 persons in primary schools to 256.1 (95% CI 158.5–391.5)/1,000 persons in high schools. The infection rate per 1,000 persons was 153.6 (95% CI 115.1–200.9) in urban settings and 84.7 (95% CI 52.4–129.4) in rural settings. The infection rate was highest among persons 18 years of age and lowest in those 7–12 years of age (Figure 2). We found no statistically significant associations between SARS-CoV-2 infection and sex or vaccination history (Table 1).

We identified 76 influenza episodes, yielding a cumulative rate of 128.2 (95% CI 101.0–160.4)/1,000 persons (Table 1). Although the overall infection rate of influenza was similar to that for SARS-CoV-2, the influenza infection rate was higher than SARS-CoV-2 in childcare centers and among children 4–6 years of age (Table 1). Influenza infection rates were associated with types of educational settings, urban or rural settings, and age groups, and the infection rate was highest in childcare centers (219.7/1,000 persons), and lowest in primary schools (23.1/1,000 persons). The infection rate per 1,000 persons was 176.8 (95% CI 135.2–227.1) in urban settings and 60.5 (95% CI 33.9–99.8) in rural settings. By single year of age, the highest influenza infection rate was seen in children 4 years of age (Figure 2). We found no significant association between influenza infection risk and sex. Only 0.5% of the participants had received influenza vaccines in the 2 years before this study, and influenza vaccination history was not assessed in this study.

A total of 6 (8.1%) of the participants infected with SARS-CoV-2 and 5 (6.6%) participants infected with influenza tested positive in 2–3 consecutive weeks. Of

those 11 participants, 9 (82%) were 14–15 years of age and 2 were 4–6 years of age.

Circulation Patterns

The study period was from the 9th week through the 26th week of 2023. SARS-CoV-2 infections were sporadically detected during the 13th–15th week in secondary schools; subsequently, infections were identified continuously each week from the 18th through the 26th week (Figure 3, panels A, B). SARS-CoV-2 positivity reached its peak in the 22nd week. The SARS-CoV-2 circulation dynamic varied across types of educational settings; a clearly defined peak and a longer duration of circulation was seen in secondary schools, whereas plateaus and more flattened infection curves were seen in childcare centers and primary schools (Figure 3, panels A, C).

Influenza virus was circulating before SARS-CoV-2 and was detected continuously from the 9th week through the 16th week, reaching its peak in the 14th week (Figure 3, panel B). Sporadic infections were identified during weeks 20–23. Variations in the influenza circulation pattern were found between types of educational settings; influenza infections

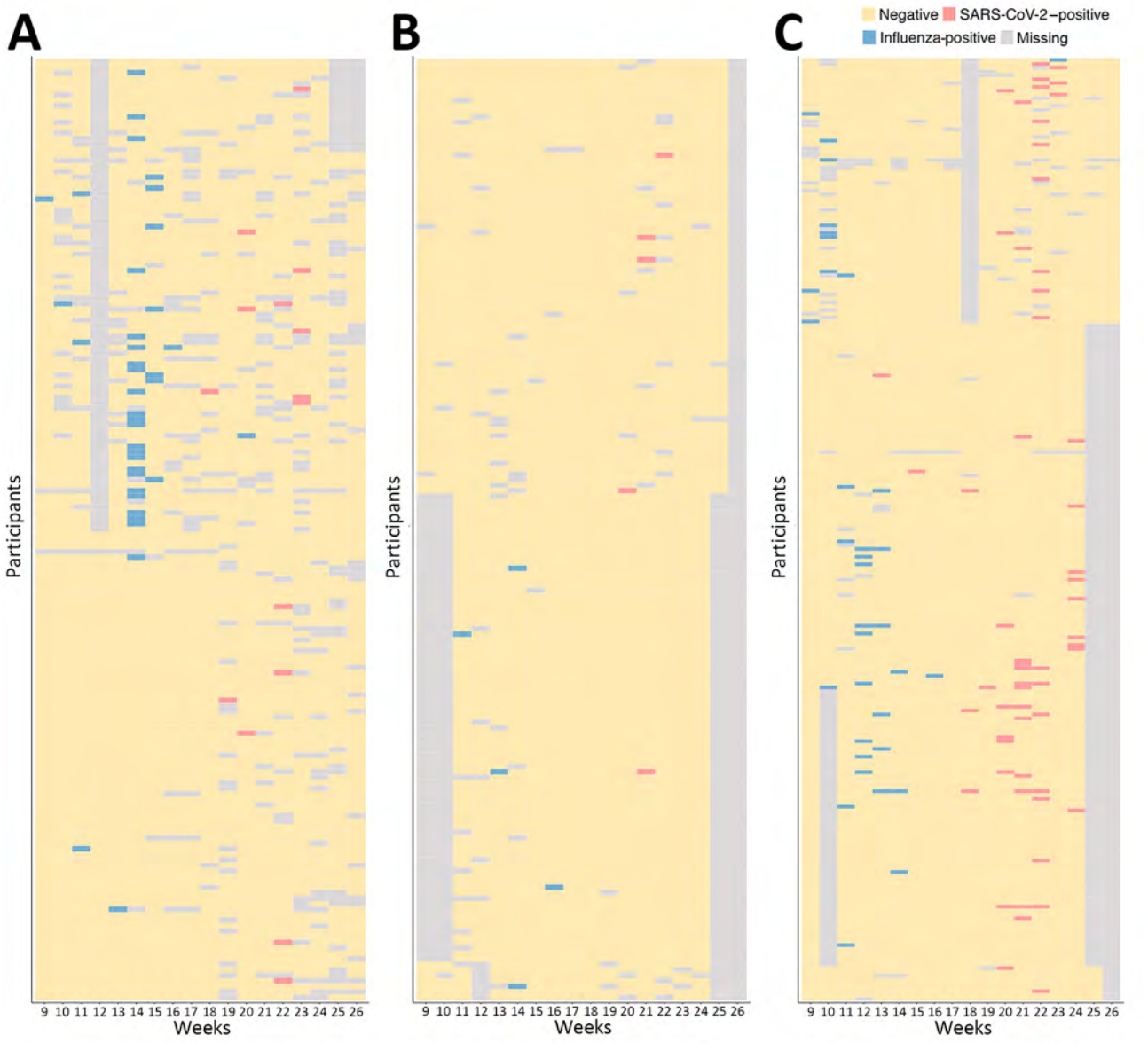

Figure 1. Longitudinal reverse-transcription PCR results of 593 participants by type of educational setting in study of infection rates, symptomatic proportion, and age-dependent risk profiles of SARS-CoV-2 and influenza in pediatric population, China, 2023. A) Childcare centers; B) primary schools; C) secondary schools (both junior secondary schools and high school). Each row shows longitudinal test results of 1 participant. Data are missing if no sample was tested.

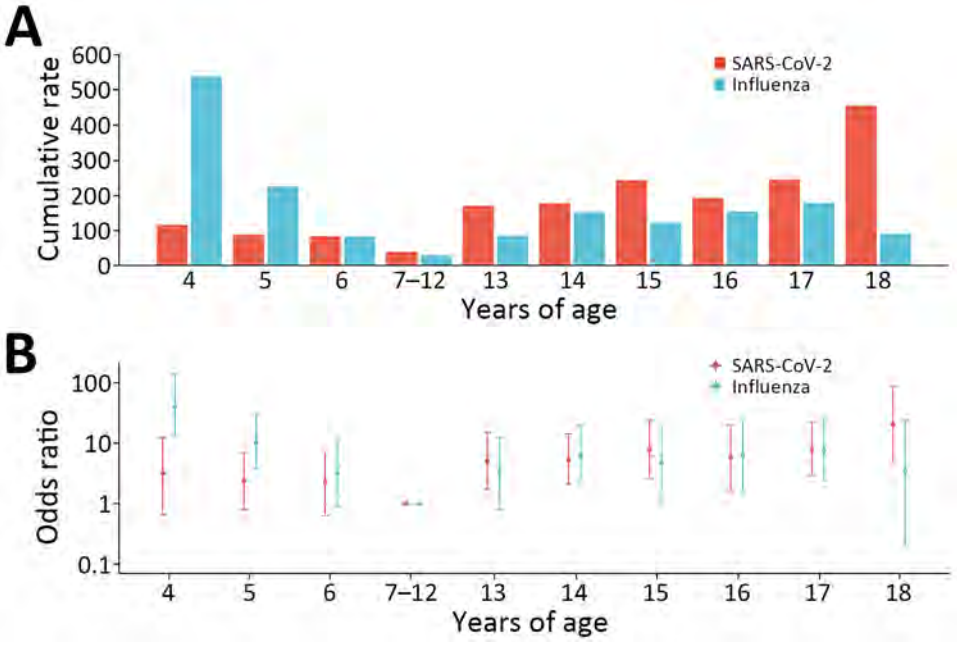

Figure 2. Infection rates and risk for SARS-CoV-2 and influenza infections by narrower age groups in study of infection rates, symptomatic proportion, and age-dependent risk profiles of SARS-CoV-2 and influenza in pediatric population, China, 2023. A) Cumulative infection rates per 1,000 persons; B) odds ratios (log scale) by age. Error bars indicate 95% CIs.

peaked sharply in childcare centers and more flattened infection curves were seen in secondary schools (Figure 3, panels C, D).

The dynamic of SARS-CoV-2 and influenza positivity generally mirrored that of SARS-CoV-2 and influenza positivity in ILI in the national sentinel surveillance, with some small differences. For instance, the SARS-CoV-2 epidemic peaked in the 22nd week in our study, whereas it peaked in the 21st week at the national level (Figure 3, panel B). Similarly, the influenza epidemic peaked in the 14th week in our study, whereas it peaked during weeks 10–12 at the national level. Moreover, the ILI–influenza positivity at the national level began to increase before the start of the school term.

Symptomatic Proportion and Symptoms

We collected symptom data for 47 (63.5%) of SARS-CoV-2 episodes and 39 (51.3%) of influenza episodes. Of those, 19 (40.4%) SARS-CoV-2 and 13 (33.3%) influenza episodes were symptomatic. The odds of SARS-CoV-2 symptomatic infection was significantly lower (odds ratio 0.1 [95% CI 0.0–0.8]) among persons 16–18 years of age than for those 4–6 years of age (Table 2). Cough (13/19) was the most frequently reported symptom for SARS-CoV-2, followed by runny nose (9/19) and congested nose (7/19). No participants with symptomatic SARS-CoV-2 infections reported seeking medical care.

The most reported symptoms for influenza were cough (7/13), fever (6/13), and runny nose (6/13) (Table 2). For SARS-CoV-2 and influenza, fever was reported only by participants in childcare centers and primary schools, not in secondary schools (Appendix Table 5). Only 2 participants >16 years of age infected with influenza reported symptom data. In total, 20% of participants with symptomatic influenza infections reported seeking medical care.

Environmental Samples

We collected and tested a total of 1,052 environmental samples from frequently touched surfaces and 708 samples from infrequently touched surfaces. All of the positive samples (4/1,052) were collected from frequently touched surfaces during weeks 20–21, corresponding to the period of high SARS-CoV-2–positivity among the participants. In contrast, a lower proportion (1/1,052) of environmental samples collected from frequently touched surfaces tested positive for influenza in the 11th week (Figure 3, panel B).

Discussion

This prospective longitudinal cohort study investigated infection rates, symptomatic proportion, environmental virus positivity, and circulation patterns of SARS-CoV-2 and influenza among pediatric populations in educational settings. Approximately 85% of participants were fully vaccinated with a primary SARS-CoV-2 vaccine, but none received a booster dose before this study; few received influenza vaccination during the 2022–23 influenza season. We estimated, approximately, an overall infection rate of 125 and 128 per 1,000 persons for SARS-CoV-2 and influenza; nearly 60% of participants infected with

SARS-CoV-2 and two thirds of participants infected with influenza were asymptomatic. We found different age-dependent infection risk profiles between SARS-CoV-2 and influenza. The highest SARS-CoV-2 infection rate was in persons 18 years of age, and the highest influenza infection rate was in children 4 years of age. A higher risk for symptomatic SARS-CoV-2 infections was seen in the younger group. The 2 viruses were only detected on frequently touched surfaces. We found asynchronous circulation patterns between SARS-CoV-2 and influenza, similar to trends shown in national-level sentinel surveillance data.

Using a longitudinal design and weekly virological testing regardless of symptoms, this study captured asymptomatic and mild infections, offering insights into transmission characteristics of SARS-CoV-2 across age subgroups in comparison with those of influenza. Aligning with previous SARS-CoV-2 systematic reviews that synthesized cohort and contact-tracing studies and a household cohort study from South Africa in which longitudinal virologic testing was conducted, our results of the age-varying SARS-CoV-2 infection risk indicate a higher extent of transmission among secondary school students than younger groups (*11*,*14*,*20*). In contrast to transmission of SARS-CoV-2, our findings suggest a higher extent of influenza transmission in young children than in older groups, consistent with an influenza cohort study in South Africa (*15*). That contrasting age-dependent infection risk profile between SARS-CoV-2 and influenza could be a consequence of varying age-dependent susceptibility and infectiousness between the 2 viruses. Contact tracing and cohort studies suggested higher susceptibility and infectiousness for SARS-CoV-2 in older children (>10 years) than in younger groups, which differs from influenza (*15*,*26*–*30*). A study in Nicaragua showed that persons 10–17 years of age shed SARS-CoV-2 longer than younger children (*26*). Studies in England and South Korea found higher secondary attack rates of SARS-CoV-2 among contacts >10 years of age than among younger children (*27*,*28*). In contrast, a higher secondary attack rate of influenza among younger children was found in studies in the United States and Mongolia (*29*,*30*). The South Africa influenza cohort study showed a higher risk for onward influenza transmission from index case-patients <5 years of age than index case-patients 5–18 years of age (*15*). The variations in influenza infection rates found among

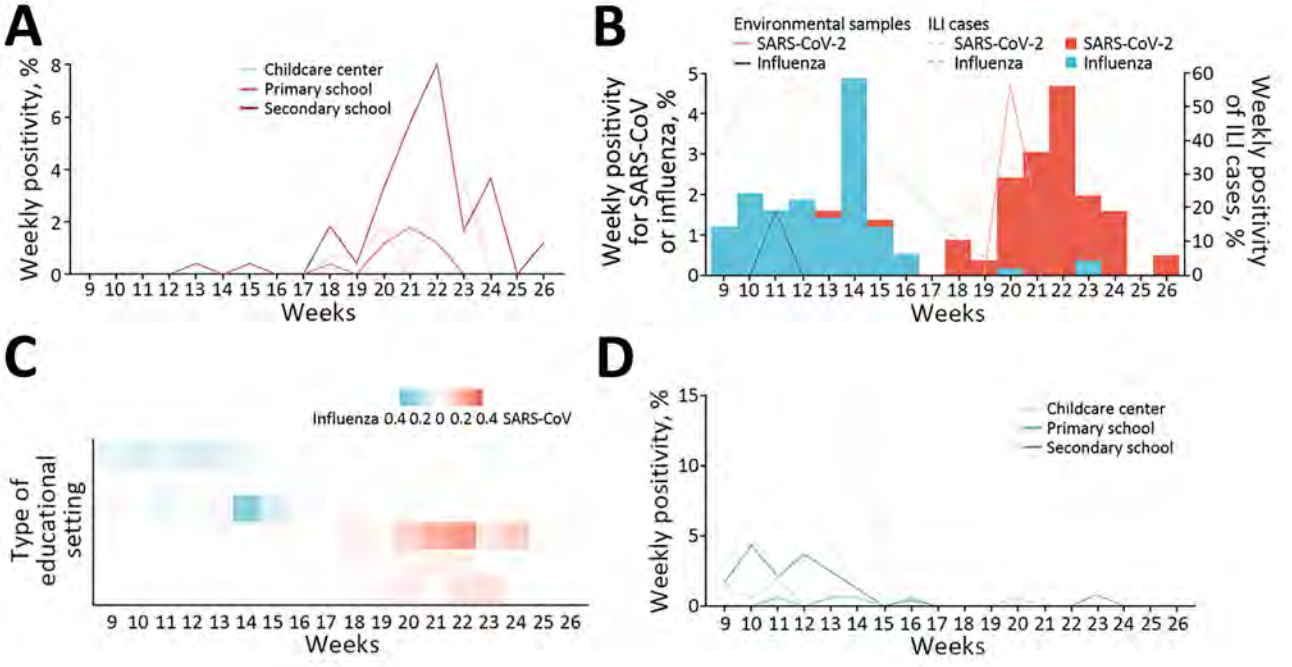

Figure 3. Circulation of SARS-CoV-2 and influenza during the spring/summer school term, February–June 2023, in study of infection rates, symptomatic proportion, and age-dependent risk profiles of SARS-CoV-2 and influenza in pediatric population, China, 2023. The term secondary schools refers to both junior secondary schools and high school. A) Weekly SARS-CoV-2 positivity by type of educational setting. B) Weekly SARS-CoV-2 and influenza positivity among study participants (bars) and from environmental sources (solid lines) and cases of ILI (dotted lines). Scales for the y-axes differ substantially to underscore patterns but do not permit direct comparisons. C) Relative intensity of SARS-CoV-2 and influenza by setting (bottom to top, childcare centers, primary schools, and secondary schools). D) Weekly influenza positivity by type of educational setting. ILI, influenza-like illness.

Table 1. Cumulative infection rates of SARS-CoV-2 and influenza and factors of infections among 593 participants in study of infection rates, symptomatic proportion, and age-dependent risk profiles of SARS-CoV-2 and influenza in pediatric population, China, 2023*

Characteristic	No. participants	SARS-CoV-2, n = 74		Influenza, n = 76		p value for SARS-CoV-2 vs. influenza
		Cumulative rates/ 1,000 persons (95% CI)†	Univariate OR (95% CI)	Cumulative rates/ 1,000 persons (95% CI)†	Univariate OR (95% CI)‡	
Overall	593	124.8 (98.0–156.7)	NA	128.2 (101.0–160.4)	NA	0.93
Sex						
F	311	115.8 (81.1–160.3)	Referent	112.5 (78.4–156.5)	Referent	>0.99
M	282	134.8 (95.4–185.0)	1.2 (0.8–2.0)	145.4 (104.3–197.2)	1.4 (0.9–2.3)	0.81
Age group, y§						
4–6	166	90.4 (50.6–149.0)	2.5 (1.0–6.6)	222.9 (156.9–307.2)	10.0 (4.2–29.8)	0.002
7–12	180	38.9 (15.6–80.1)	Referent	27.8 (9.0–64.8)	Referent	0.77
13–15	165	187.9 (127.7–266.7)	5.7 (2.6–14.5)	127.3 (78.8–194.5)	5.1 (2.0–15.6)	0.17
16–18	82	256.1 (158.5–391.5)	8.5 (3.6–22.5)	158.5 (84.4–271.1)	6.6 (2.4–21.2)	0.18
Type of educational setting						
Childcare center	173	86.7 (48.5–143.0)	2.3 (0.9–6.0)	219.7 (155.4–301.5)	11.9 (4.6–40.4)	0.001
Primary school	173	40.5 (16.3–83.4)	Referent	23.1 (6.3–59.2)	Referent	0.54
Junior secondary school	165	187.9 (127.7–266.7)	5.5 (2.5–13.9)	127.3 (78.8–194.5)	6.2 (2.3–21.5)	0.17
High school	82	256.1 (158.5–391.5)	8.2 (3.5–21.6)	158.5 (84.4–271.1)	8.0 (2.7–29.0)	0.18
Urban						
Y	345	153.6 (115.1–200.9)	2.0 (1.2–3.4)	176.8 (135.2–227.1)	3.3 (1.9–6.2)	0.47
N	248	84.7 (52.4–129.4)	Referent	60.5 (33.9–99.8)	Referent	0.39
COVID-19 vaccination history						
Unvaccinated	68	147.1 (70.5–270.4)	Referent	NA	NA	NA
1 dose	19	105.3 (12.7–380.2)	0.7 (0.1–2.9)	NA	NA	NA
2 doses	506	122.5 (93.9–157.1)	0.8 (0.4–1.8)	NA	NA	NA

*ORs were estimated using logistic regression model. NA, not applicable; NE, not estimated; OR, odds ratio.
†Cumulative rate and 95% CI indicate the number of episodes dividing the number of participants using Poisson distribution.
‡Influenza vaccination coverage was <1% and thus not included in the analysis for influenza.
§The age grouping generally corresponded to different types of educational settings. Most children in childcare centers, primary schools, junior secondary schools, and high schools were 4–6, 7–12, 13–15, and 16–18 years of age.

children 4 and 6 years of age (Figure 2) indicate that age might influence the spread of influenza within childcare centers. We reported infection rates by educational setting because contact patterns could be strongly influenced by social settings. Our results are generally consistent with a prior US study showing that primary school students tend to have fewer distinct contacts than those in junior secondary schools and high schools (*31*). The infection rates in different educational settings could inform school-based intervention strategies.

A recent meta-analysis found asymptomatic proportions associated with the Omicron variant varied widely from 14% to 57% for all age groups across studies (*32*). However, few studies have reported data for pediatric populations or by granular age groups. Our results (54% for persons 7–15 years of age) are similar to a seroprevalence study in the United States showing that 49% of Omicron infections were symptomatic among children 5–15 years of age; that study found higher symptomatic proportion for Delta infections (*33*). We found a lower probability of symptomatic SARS-CoV-2 infection in persons 16–18 years of age than among young children, which might be partly explained by the gradual development and maturation of human immunity from birth to young adulthood, providing protection against symptomatic infection and more severe illness (*34*). Few studies have reported asymptomatic influenza infections for the pediatric population. Our estimates of symptomatic influenza infections (35% [95% CI 20%–53%] for children 4–15 years of age) appeared slightly lower than that seen in the South Africa influenza cohort study (51% for children 5–12 years of age) (*15*).

A systematic review of studies conducted before the Omicron wave found that fever and cough were the most prevalent symptoms of SARS-CoV-2 and influenza infections among children with a median age of 5–8 years, broadly similar to the symptoms we observed (*16*). Of note, fever was reported only by students in childcare centers and primary schools (those 4–12 years of age) in our study, not by older students (Appendix Table 5). Those findings could indicate possible varying symptom profiles (e.g., fever) across age groups, and the inclusion of older and young children might explain why fever was not the most prevalent symptom in our study.

Only the samples collected from frequently touched surfaces when virus activity was high tested positive for SARS-CoV-2 (4/1,052) and influenza (1/1,052). This finding is consistent with a Hong Kong study conducted in childcare centers

and primary schools (*35*). The results suggest that contact by infected persons is a primary cause of environmental contamination in educational settings. Strengthening environmental disinfection could reduce SARS-CoV-2 and influenza transmission in educational settings.

Our results and the data collected by the WHO Global Influenza Surveillance and Response System have shown asynchronous circulation patterns of SARS-CoV-2 and influenza (*3*), which might indicate negative viral interference between the 2 viruses (*36*). Similar results have been indicated by population-level and individual-level epidemiologic data (*37*,*38*) and the low codetection rates of SARS-CoV-2 and influenza in a recent meta-analysis (*39*). A recent model of airway epithelium suggests that SARS-CoV-2 replication could be inhibited by antiviral responses triggered by influenza infections (*40*).

COVID-19 vaccines could prevent infections, thereby reducing virus spread. However, real-life observational data suggest a decline in vaccine effectiveness after 2 doses against infection with the Omicron variant, as well as waning protection over time among children and adolescents (*41*). In total, 80% of participants had received their last SARS-CoV-2 vaccine dose 12 months before, which might explain the lack of significant effect for SARS-CoV-2 vaccination in our study.

The first limitation of our study is that, although no widespread control measures were implemented, some participants might have adopted precautionary behaviors in response to test results, which might have reduced virus spread. Second, variations in the infection rates were observed between schools of the same type, possibly because of differences in virus transmission between the communities where the schools were located. Age-related estimates, which were derived using a generalized linear mixed meta-regression model accounting for between-school variations, were generally comparable to the main analysis, except for the wider CIs of the influenza infection rate for children 4–6 years of age (Appendix Table 6). Nevertheless, the generalizability of our estimates could be limited by the small number of schools included in this study. Third, symptoms of the infections were self-reported; symptom data was lacking among 43% of the infected persons and could cause biases to the estimates of symptomatic proportions (Appendix Table 4). We acknowledge that the estimation of influenza symptomatic proportion for persons 16–18 years of age is not feasible because of the sparce data. Moreover, we did not consider subtypes of SARS-CoV-2 or influenza virus because of lack of data. We reported data collected from students during a school term after a major SARS-CoV-2 epidemic across the country in late 2022 and early 2023; no participants received a booster SARS-CoV-2 vaccine dose before this study, and influenza vaccination coverage was low. We acknowledge that our findings might be context-dependent, influenced by the population's immunity level related to infection history and vaccination, as well as the implementation of NPIs. Future studies are needed to investigate possible long-term interactions between influenza and SARS-CoV-2.

Overall, we found different age-dependent infection risk profiles between SARS-CoV-2 and

Table 2. Proportion of symptomatic SARS-CoV-2 and influenza infections, factors of symptomatic infections, and frequency of symptoms in study of infection rates, symptomatic proportion, and age-dependent risk profiles of SARS-CoV-2 and influenza in pediatric population, China, 2023*

	SARS-CoV-2		Influenza	
Characteristic	Symptomatic episodes, n = 47	Univariate OR (95% CI)	Symptomatic episodes, n = 39	Univariate OR† (95% CI)
Overall	19/47 (40.4%)	NA	13/39 (33.3%)	NA
Age group, y				
4–6	4/7 (57.1%)	Referent	11/34 (32.4%)	Referent
7–15	13/24 (54.2%)	0.9 (0.1–4.9)	2/3 (66.7%)	1.8 (0.4–9.6)
16–18	2/16 (12.5%)	0.1 (0.0–0.8)	0/2 (0.0%)	NE
Received ≥2 doses of COVID-19 vaccine	39/47 (83.0%)	0.3 (0.1–1.6)	NA	NA
Symptom				
Fever	2/19 (10.5%)	NA	6/13 (46.2%)	NA
Cough	13/19 (68.4%)	NA	7/13 (53.8%)	NA
Sore throat	3/19 (15.8%)	NA	0/13 (0.0%)	NA
Congested nose	7/19 (36.8%)	NA	1/13 (7.7%)	NA
Runny nose	9/19 (47.4%)	NA	6/13 (46.2%)	NA
Fatigue	1/19 (5.3%)	NA	0/13 (0.0%)	NA
Vomiting	1/19 (5.3%)	NA	0/13 (0.0%)	NA
Sneezing	0/19 (0.0%)	NA	0/13 (0.0%)	NA
Medical attendance	0/19 (0.0%)	NA	3/13 (23.1%)	NA

*NA, not applicable; NE, not estimated; OR, odds ratio (estimated using logistic regression model).
†Influenza vaccination coverage was <5% and thus not included in the analysis for influenza.

influenza. The highest SARS-CoV-2 infection rate was in persons 18 years of age, and for influenza, in children 4 years of age. A higher proportion of symptomatic SARS-CoV-2 infections was seen in young children than in older groups. Our findings can inform both vaccination strategies and other interventions, such as mask wearing, environmental disinfection, and handwashing in educational settings for the control of SARS-CoV-2 and influenza.

The research was supported by Projects of Wuxi Municipal Bureau on Science and Technology (No. Y20212042), Top Talent Support Program for young and middle-aged people of Wuxi Health Committee (No. BJ2023095), Wuxi Medical Development Disciplines (No. FZXK2021010), and Jiangsu Provincial Department of Science and Technology COVID-19 Emergency Project (No. BE2023603).

X.W. reports personal fees from Pfizer and grants from GlaxoSmithKline outside the submitted work. Y.L. reported grants from the World Health Organization, Wellcome Trust, GlaxoSmithKline, and Pfizer outside the submitted work. All other authors declared that they have no competing interests.

X.W. conceived the study with inputs from B.L., C.S., and Y.L. C.S. and B.L. led the data collection with intellectual inputs from Y.L. and X.W. and inputs from J.Z., Y.G., and Y.W. Y.Z. led the collection of national sentinel surveillance data and the formal analysis and wrote the draft, with substantial contributions from S.Y., X.W., C.S., B.L., and Y.L. and additional intellectual inputs from F.Z., B.C., and S.D. All authors read and approved the final version of the protocol for publication.

About the Author

Mr. Shi is an associate professor at Nanjing Medical University and an associate director of Wuxi Centre for Disease Control and Prevention. His primary research interests include the control and prevention of acute infectious diseases.

References

1. World Health Organization. Number of COVID-19 cases and deaths reported to WHO. 2023 [cited 2023 Dec 20]. https://covid19.who.int/data
2. Contreras S, Iftekhar EN, Priesemann V. From emergency response to long-term management: the many faces of the endemic state of COVID-19. Lancet Reg Health Eur. 2023;30:100664. https://doi.org/10.1016/j.lanepe.2023.100664
3. World Health Organization. FluNet. 2023 [cited 2023 Dec 20]. https://www.who.int/tools/flunet
4. Iuliano AD, Roguski KM, Chang HH, Muscatello DJ, Palekar R, Tempia S, et al.; Global Seasonal Influenza-associated Mortality Collaborator Network. Estimates of global seasonal influenza-associated respiratory mortality: a modelling study. Lancet. 2018;391:1285–300. https://doi.org/10.1016/S0140-6736(17)33293-2
5. Chinese Center for Disease Control and Prevention. Weekly influenza report. 2023 [cited 2023 Dec 27]. https://ivdc.chinacdc.cn/cnic/zyzx/lgzb
6. Wang X, Li Y, O'Brien KL, Madhi SA, Widdowson MA, Byass P, et al.; Respiratory Virus Global Epidemiology Network. Global burden of respiratory infections associated with seasonal influenza in children under 5 years in 2018: a systematic review and modelling study. Lancet Glob Health. 2020;8:e497–510. https://doi.org/10.1016/S2214-109X(19)30545-5
7. McAllister DA, Liu L, Shi T, Chu Y, Reed C, Burrows J, et al. Global, regional, and national estimates of pneumonia morbidity and mortality in children younger than 5 years between 2000 and 2015: a systematic analysis. Lancet Glob Health. 2019;7:e47–57. https://doi.org/10.1016/S2214-109X(18)30408-X
8. Jackson C, Vynnycky E, Hawker J, Olowokure B, Mangtani P. School closures and influenza: systematic review of epidemiological studies. BMJ Open. 2013;3:e002149. https://doi.org/10.1136/bmjopen-2012-002149
9. Naeimi R, Sepidarkish M, Mollalo A, Parsa H, Mahjour S, Safarpour F, et al. SARS-CoV-2 seroprevalence in children worldwide: a systematic review and meta-analysis. EClinicalMedicine. 2023;56:101786. https://doi.org/10.1016/j.eclinm.2022.101786
10. Silverberg SL, Zhang BY, Li SNJ, Burgert C, Shulha HP, Kitchin V, et al. Child transmission of SARS-CoV-2: a systematic review and meta-analysis. BMC Pediatr. 2022;22:172. https://doi.org/10.1186/s12887-022-03175-8
11. Viner RM, Mytton OT, Bonell C, Melendez-Torres GJ, Ward J, Hudson L, et al. Susceptibility to SARS-CoV-2 infection among children and adolescents compared with adults: a systematic review and meta-analysis. JAMA Pediatr. 2021;175:143–56. https://doi.org/10.1001/jamapediatrics.2020.4573
12. Viner R, Waddington C, Mytton O, Booy R, Cruz J, Ward J, et al. Transmission of SARS-CoV-2 by children and young people in households and schools: a meta-analysis of population-based and contact-tracing studies. J Infect. 2022;84:361–82. https://doi.org/10.1016/j.jinf.2021.12.026
13 Vardavas C, Nikitara K, Mathioudakis AG, Hilton Boon M, Phalkey R, Leonardi-Bee J, et al. Transmission of SARS-CoV-2 in educational settings in 2020: a review. BMJ Open. 2022;12:e058308. https://doi.org/10.1136/bmjopen-2021-058308
14. Cohen C, Kleynhans J, von Gottberg A, McMorrow ML, Wolter N, Bhiman JN, et al.; PHIRST-C Group. SARS-CoV-2 incidence, transmission, and reinfection in a rural and an urban setting: results of the PHIRST-C cohort study, South Africa, 2020–21. Lancet Infect Dis. 2022;22:821–34. https://doi.org/10.1016/S1473-3099(22)00069-X
15. Cohen C, Kleynhans J, Moyes J, McMorrow ML, Treurnicht FK, Hellferscee O, et al.; PHIRST group. Asymptomatic transmission and high community burden of seasonal influenza in an urban and a rural community in South Africa, 2017–18 (PHIRST): a population cohort study. Lancet Glob Health. 2021;9:e863–74. https://doi.org/10.1016/S2214-109X(21)00141-8
16. Lee B, Ashcroft T, Agyei-Manu E, Farfan de los Godos E, Leow A, Krishan P, et al.; Usher Network for COVID-19 Evidence Reviews (UNCOVER) group. Clinical features of COVID-19 for integration of COVID-19 into influenza

surveillance: a systematic review. J Glob Health. 2022;12:05012. https://doi.org/10.7189/jogh.12.05012
17. Song X, Delaney M, Shah RK, Campos JM, Wessel DL, DeBiasi RL. Comparison of clinical features of COVID-19 vs seasonal influenza A and B in US children. JAMA Netw Open. 2020;3:e2020495. https://doi.org/10.1001/jamanetworkopen.2020.20495
18. Piroth L, Cottenet J, Mariet AS, Bonniaud P, Blot M, Tubert-Bitter P, et al. Comparison of the characteristics, morbidity, and mortality of COVID-19 and seasonal influenza: a nationwide, population-based retrospective cohort study. Lancet Respir Med. 2021;9:251–9. https://doi.org/10.1016/S2213-2600(20)30527-0
19. Wiedenmann M, Ipekci AM, Araujo-Chaveron L, Prajapati N, Lam YT, Alam MI, et al. SARS-CoV-2 variants of concern in children and adolescents with COVID-19: a systematic review. BMJ Open. 2023;13:e072280. https://doi.org/10.1136/bmjopen-2023-072280
20. Irfan O, Li J, Tang K, Wang Z, Bhutta ZA. Risk of infection and transmission of SARS-CoV-2 among children and adolescents in households, communities and educational settings: a systematic review and meta-analysis. J Glob Health. 2021;11:05013. https://doi.org/10.7189/jogh.11.05013
21. Leung NH, Xu C, Ip DK, Cowling BJ. Review article: the fraction of influenza virus infections that are asymptomatic: a systematic review and meta-analysis. Epidemiology. 2015;26:862–72. https://doi.org/10.1097/EDE.0000000000000340
22. Chinese Center for Disease Control and Prevention. National situation of SARS-CoV-2 infection. 2023 [cited 2023 Dec 25]. https://www.chinacdc.cn/jkzt/crb/zl/szkb_11803/jszl_13141
23. Shope TR, Chedid K, Hashikawa AN, Martin ET, Sieber MA, Des Ruisseau G, et al. Incidence and transmission of SARS-CoV-2 in US child care centers after COVID-19 vaccines. JAMA Netw Open. 2023;6:e2339355. https://doi.org/10.1001/jamanetworkopen.2023.39355
24. Tsang TK, Huang X, Fong MW, Wang C, Lau EHY, Wu P, et al. Effects of school-based preventive measures on COVID-19 incidence, Hong Kong, 2022. Emerg Infect Dis. 2023;29:1850–4. https://doi.org/10.3201/eid2909.221897
25. Li Y, Hodgson D, Wang X, Atkins KE, Feikin DR, Nair H. Respiratory syncytial virus seasonality and prevention strategy planning for passive immunisation of infants in low-income and middle-income countries: a modelling study. Lancet Infect Dis. 2021;21:1303–12. https://doi.org/10.1016/S1473-3099(20)30703-9
26. Maier HE, Plazaola M, Lopez R, Sanchez N, Saborio S, Ojeda S, et al. SARS-CoV-2 infection-induced immunity and the duration of viral shedding: results from a Nicaraguan household cohort study. Influenza Other Respir Viruses. 2023;17:e13074. https://doi.org/10.1111/irv.13074
27. Miller E, Waight PA, Andrews NJ, McOwat K, Brown KE, Höschler K, et al. Transmission of SARS-CoV-2 in the household setting: a prospective cohort study in children and adults in England. J Infect. 2021;83:483–9. https://doi.org/10.1016/j.jinf.2021.07.037
28. Park YJ, Choe YJ, Park O, Park SY, Kim YM, Kim J, et al.; COVID-19 National Emergency Response Center, Epidemiology and Case Management Team. Contact tracing during coronavirus disease outbreak, South Korea, 2020. Emerg Infect Dis. 2020;26:2465–8. https://doi.org/10.3201/eid2610.201315
29. Rolfes MA, Talbot HK, McLean HQ, Stockwell MS, Ellingson KD, Lutrick K, et al. Household transmission of influenza A viruses in 2021–2022. JAMA. 2023;329:482–9. https://doi.org/10.1001/jama.2023.0064
30. Nukiwa-Souma N, Burmaa A, Kamigaki T, Od I, Bayasgalan N, Darmaa B, et al. Influenza transmission in a community during a seasonal influenza A(H3N2) outbreak (2010–2011) in Mongolia: a community-based prospective cohort study. PLoS One. 2012;7:e33046. https://doi.org/10.1371/journal.pone.0033046
31. Guclu H, Read J, Vukotich CJ Jr, Galloway DD, Gao H, Rainey JJ, et al. Social contact networks and mixing among students in K-12 schools in Pittsburgh, PA. PLoS One. 2016;11:e0151139. https://doi.org/10.1371/journal.pone.0151139
32. Shang W, Kang L, Cao G, Wang Y, Gao P, Liu J, et al. Percentage of asymptomatic infections among SARS-CoV-2 Omicron variant-positive individuals: a systematic review and meta-analysis. Vaccines (Basel). 2022;10:1049. https://doi.org/10.3390/vaccines10071049
33. Fowlkes AL, Yoon SK, Lutrick K, Gwynn L, Burns J, Grant L, et al. Effectiveness of 2-dose BNT162b2 (Pfizer BioNTech) mRNA vaccine in preventing SARS-CoV-2 infection among children aged 5–11 years and adolescents aged 12–15 years—PROTECT Cohort, July 2021–February 2022. MMWR Morb Mortal Wkly Rep. 2022;71:422–8. https://doi.org/10.15585/mmwr.mm7111e1
34. Simon AK, Hollander GA, McMichael A. Evolution of the immune system in humans from infancy to old age. Proc Biol Sci. 2015;282:20143085. PubMed https://doi.org/10.1098/rspb.2014.3085
35. Fong MW, Leung NHL, Xiao J, Chu DKW, Cheng SMS, So HC, et al. Presence of influenza virus on touch surfaces in kindergartens and primary schools. J Infect Dis. 2020;222:1329–33. https://doi.org/10.1093/infdis/jiaa114
36. Piret J, Boivin G. Viral interference between respiratory viruses. Emerg Infect Dis. 2022;28:273–81. https://doi.org/10.3201/eid2802.211727
37. Lampros A, Talla C, Diarra M, Tall B, Sagne S, Diallo MK, et al. Shifting patterns of influenza circulation during the COVID-19 pandemic, Senegal. Emerg Infect Dis. 2023;29:1808–17. https://doi.org/10.3201/eid2909.230307
38. Stowe J, Tessier E, Zhao H, Guy R, Muller-Pebody B, Zambon M, et al. Interactions between SARS-CoV-2 and influenza, and the impact of coinfection on disease severity: a test-negative design. Int J Epidemiol. 2021;50:1124–33. https://doi.org/10.1093/ije/dyab081
39. Yan X, Li K, Lei Z, Luo J, Wang Q, Wei S. Prevalence and associated outcomes of coinfection between SARS-CoV-2 and influenza: a systematic review and meta-analysis. Int J Infect Dis. 2023;136:29–36. https://doi.org/10.1016/j.ijid.2023.08.021
40. Dee K, Schultz V, Haney J, Bissett LA, Magill C, Murcia PR. Influenza A and respiratory syncytial virus trigger a cellular response that blocks severe acute respiratory syndrome virus 2 infection in the respiratory tract. J Infect Dis. 2023;227:1396–406. https://doi.org/10.1093/infdis/jiac494
41. Piechotta V, Siemens W, Thielemann I, Toews M, Koch J, Vygen-Bonnet S, et al. Safety and effectiveness of vaccines against COVID-19 in children aged 5–11 years: a systematic review and meta-analysis. Lancet Child Adolesc Health. 2023;7:379–91. https://doi.org/10.1016/S2352-4642(23)00078-0

Address for correspondence: Xin Wang or Bing Lu, Nanjing Medical University, 101 Longmian Ave, Nanjing 211166, China; email: xin.wang@njmu.edu.cn or wxcdclub1966@163.com

Formation of Single-Species and Multispecies Biofilm by Isolates from Septic Transfusion Reactions in Platelet Bag Model

Cheryl Anne Hapip, Erin Fischer, Tamar Perla Feldman, Bethany L. Brown

During 2018–2021, eight septic transfusion reactions occurred from transfusion of platelet units contaminated with *Acinetobacter* spp., *Staphylococcus saprophyticus*, *Leclercia adecarboxylata*, or a combination of those environmental organisms. Whether biofilm formation contributed to evasion of bacterial risk mitigations, including bacterial culture, point-of-care testing, or pathogen-reduction technology, is unclear. We designed a 12-well plate-based method to evaluate environmental determinants of single-species and multispecies biofilm formation in platelets. We evaluated bacteria isolated from septic transfusion reactions for biofilm formation by using crystal violet staining and enumeration of adherent bacteria. Most combinations of bacteria had enhanced biofilm production compared with single bacteria. Combinations involving *L. adecarboxylata* had increased crystal violet biofilm production and adherent bacteria. This study demonstrates that transfusion-relevant bacteria can produce biofilms well together. More work is needed to clarify the effect of biofilms on platelet bacterial risk control strategies, but US Food and Drug Administration–recommended strategies remain acceptable.

Septic transfusion reactions (STRs) from bacterial contamination of platelets are a persistent cause of transfusion-associated deaths. Bacterial risk mitigation strategies are aimed at collection mitigations (e.g., taking donor's temperature, asking screening questions, and disinfecting skin at venipuncture site), pathogen reduction before storage, and detecting bacterial growth by culture and point-of-care rapid tests (*1*). Despite implementation of US Food and Drug Administration (FDA) guidance on bacterial risk control strategies by blood collection establishments and transfusion services, 8 STRs occurred during 2018–2021 from contaminated platelets units involving *Acinetobacter* spp. alone or in combination with *Staphylococcus saprophyticus*, *Leclercia adecarboxylata*, or both (Table) (*2*–*5*). FDA has communicated heightened awareness around single-species and multispecies contamination of platelet units and noted that the units involved in recent STRs either passed bacterial testing or were pathogen-reduced (*2*,*4*–*6*). Those observations raise the possibility that some bacteria may evade risk mitigations because of the route and timing of contamination or through survival strategies like biofilm production. Genetically related organisms have been isolated in culture bottles (e.g., BacT/ALERT; bioMérieux, https://www.biomerieux.com), on the outside of bags, at a collection set manufacturing facility, and in blood centers, and whole-genome sequencing (WGS) by the Centers for Disease Control and Prevention (CDC) suggests an environmental source of contamination (*3*–*5*).

Biofilms pose an ongoing challenge to infection control in healthcare settings by protecting bacteria against physical, mechanical, and biochemical methods of cleaning and disinfection, and by shielding bacteria from natural defense and treatments (*7*–*9*). Biofilms are complex structures consisting of single or polymicrobial bacteria and thrive on surfaces with moisture and nutrients. Biofilms initiate detachment of bacterial cells or cluster aggregates, produce endotoxins, have heightened evasion from immune surveillance, and form a protective barrier.

Acinetobacter spp., *S. saprophyticus,* and *L. adecarboxylata* can form biofilms (*10*,*11*), although synergistic growth enhancement and relevance of these monomicrobial or polymicrobial biofilms to platelets for transfusion is unknown (*4*,*10*,*12*–*14*). Biofilm-mediated

Author affiliation: American Red Cross, Rockville, Maryland, USA

DOI: https://doi.org/10.3201/eid3009.240372

Table. *Acinetobacter* spp. bacteria–related and polymicrobial septic transfusion reactions, United States, May 2018–July 2021*

Year and month	Location (outcome)	Risk mitigation (result)	Bacterial species
2018 May	Northern California	Pathogen-reduction technology	A–S†
2018 May	Utah (fatality)	Aerobic culture (neg)	A
2018 Oct	Connecticut‡	Aerobic culture (neg), rapid antigen test (neg)	A–S
2018 Oct	Connecticut‡	Aerobic culture (neg), rapid antigen test (neg)	A–S
2020 Jun	North and South Carolina (fatality)	Pathogen-reduction technology	A–S–L
2020 Jun	Central Ohio, Pennsylvania, New Jersey	Aerobic culture (neg), anaerobic culture (neg)	A§
2021 Jul	Ohio (fatality)	Pathogen-reduction technology	A–S–L†
2021 Jul	Virginia	Pathogen-reduction technology	S–L

*A, *Acinetobacter* spp.; L, *Leclercia adecarboxylata*; neg, negative; S, *Staphylococcus saprophyticus*.
†Clinical isolates used in the experiments.
‡Two separate reactions from a double platelet.
§Case was excluded from *Acinetobacter* spp. cluster investigation by Centers for Disease Control and Prevention and US Food and Drug Administration based on whole-genome sequencing data (*5*,*36*).

Acinetobacter spp. are opportunistic gram-negative pathogens, and infections by those pathogens are an increasingly relevant cause of medical device-related infections, likely because of their ability to rapidly generate resistant factors and tolerate harsh environments (*12*,*15*–*19*).

Environmental conditions, such as blood bag plastics and presence of platelets, may affect biofilm formation and, subsequently, bacterial risk mitigations. Previous laboratory studies have shown robust adhesion of *S. epidermidis* to the internal surface of platelet storage bags in the presence of plasma factors and platelets (*20*–*22*). Further, bacteria exhibit different traits between planktonic and sessile states because bacterial attachment to a surface causes a rapid change in gene expression levels; this mechanism may be important for platelet bag surfaces and other surfaces throughout the supply chain (*9*). Another study conducted using a non–FDA-approved pathogen-reduction technology (Mirasol; TerumoBCT, https://www.terumobct.com) demonstrated that platelet products inoculated with planktonic *S. epidermidis* had ≈1 log fewer bacteria after pathogen reduction than those inoculated with sessile cells, highlighting the potential importance of biofilms formation in platelets (*23*).

Acinetobacter spp., *S. saprophyticus*, and *L. adecarboxylata* behavior in coculture and the relevance to platelets for transfusion remains unknown. Preliminary investigations conducted at the American Red Cross Microbiology Laboratory demonstrated the effect of platelets on biofilm matrix production for single and combinations of transfusion-relevant biofilm-producing bacteria (*24*). Our study aimed to address gaps in knowledge by developing a plate-based biofilm evaluation model with platelet-relevant variables using isolates from recent STRs to investigate biofilm formation in contaminated platelets.

Materials and Methods

Platelet Products

All platelet donors for this study provided informed consent before collection. We collected platelet units on the Amicus apheresis collection system (Fresenius Kabi, https://www.fresenius-kabi.com) and stored in 65% platelet additive solution (PAS III) (35% plasma). We rested platelets for 2 hours, then agitated them in a platelet incubator overnight at 20°C–24°C. We conducted all experiments with 3–4 independent biologic replicates and performed each biologic replicate with a unique donor collected on a separate day. We tested biologic replicates in technical duplicates (Figure 1).

Transfusion-Relevant Bacterial Isolates

We obtained bacterial strains of *Acinetobacter* spp. (A), *S. saprophyticus* (S), and *L. adecarboxylata* (L) from the pathogen-reduced apheresis platelet units involved in the Northern California (May 2018) and the Ohio (July 2021) clinical STR cases (Table). We used a biofilm-producing *S. epidermidis* isolate (ATCC 35984) for the positive control.

Plastic Platelet Bag Material

We created 15-mm round coupons from Amicus platelet bags (Fresenius Kabi) by using a Cameo 4 instrument (Silhouette, https://www.silhouetteamerica.com). We sterilized the coupons by submerging them in freshly prepared 5% bleach for 5 minutes and then in 70% sterile alcohol for 15 minutes. We aseptically transferred the coupons and washed them in sterile distilled water 3 times to remove excess alcohol (*20*,*22*). We placed the coupons in a sterile 12-well plate (interior side up), which we allowed to air dry in a biosafety cabinet.

Development of 12-Well Microplate Model to Evaluate Bacterial Biofilms on Platelet Bag Plastics

To standardize testing of environmental variables on biofilm formation in platelet products, we

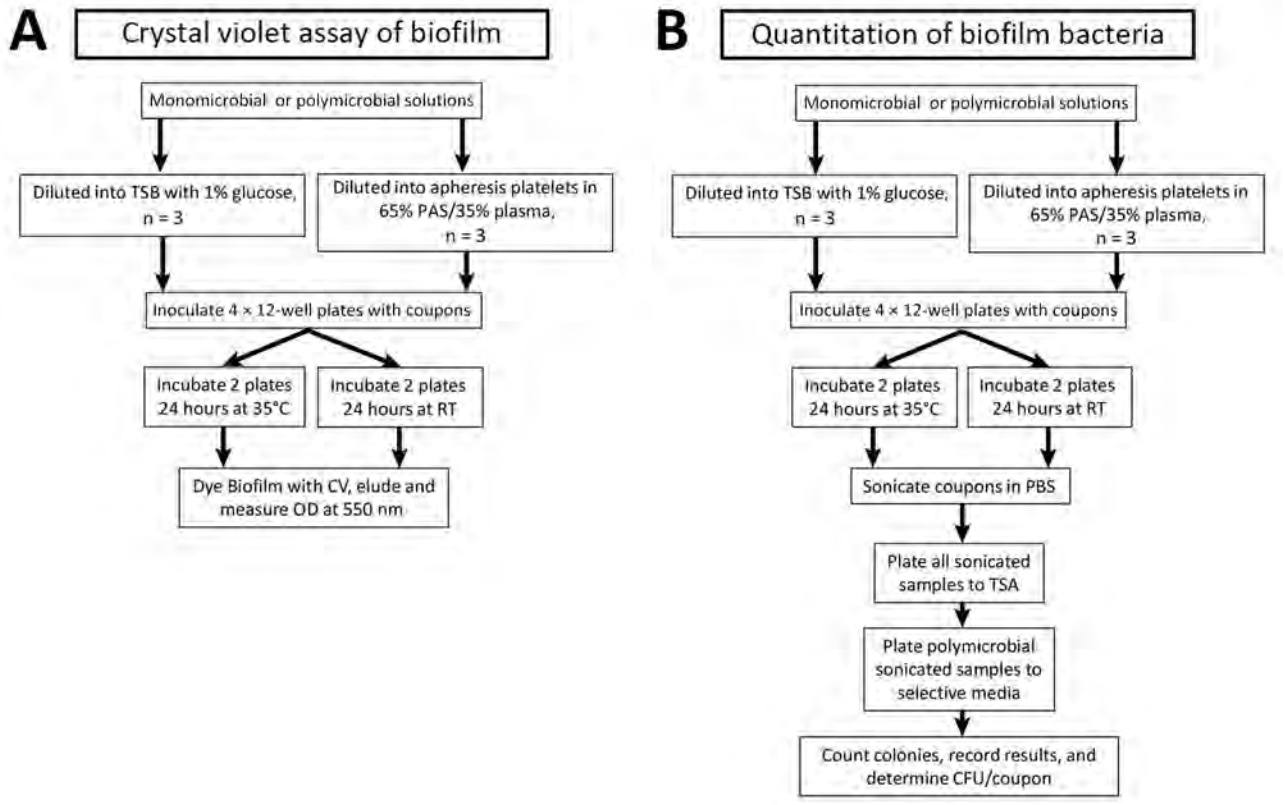

Figure 1. Overview of procedural steps taken to evaluate monomicrobial and polymicrobial biofilms grown on platelet bag coupons in different media (apheresis platelets vs. TSB–glucose) and at 22°C vs. 35°C. A) Study methodology for measuring biofilm production through crystal violet assay. B) Methods for determining CFU per coupon and comparative species composition of polymicrobial biofilms. CV, crystal violet; OD, optical density; PAS, platelet additive solution; RT, room temperature; TSA, tryptic soy agar; TSB, tryptic soy broth.

developed a multiwell plate assay that enabled simultaneous evaluation of single and pairwise combinations of bacteria grown on platelet bag plastics. We placed sterilized coupons cut from the platelet storage bags in plate wells before inoculation by using nontreated, sterile 12-well cell culture plates (Wuxi NEST Biotechnology, https://www.nestscientificusa.com). After 24 hours of bacterial growth, we removed the coupons from the plate, washed them, and used them to characterize the adherent biofilm. We used this simplified method to screen for effects of environmental variables on the quantity of viable adherent bacteria, biofilm matrix production, patterns in species composition, and spatial organization on the platelet bag plastic.

Inoculation and Controls

We transferred bacteria from frozen aliquots onto tryptic soy agar (TSA) plates, streaked them for isolation, and incubated them for 24 hours at 35°C. We added isolated colonies to tryptic soy broth (TSB) and incubated them overnight. We performed dilutions in TSB to obtain a 600-nm optical density (OD) corresponding to a concentration of ≈3×10^8 CFU/mL. A 1:100 dilution of the broth in either apheresis platelets or TSB with glucose (TSBG) gave a final inoculation concentration of ≈3×10^6 CFU/mL. We mixed equal volumes from the single bacterial inoculation tubes to prepare L–S, L–A, A–S, and L–A–S inoculation tubes. We added 1.5 mL from each inoculation tube to each labeled well containing a single coupon for a starting count of ≈4.5×10^6 CFU/well. We set up negative control wells with uninoculated growth medium (platelet or TSBG) with and without coupons. We prepared 2 duplicate sets of plates and incubated them for 24 hours (1 at room temperature and 1 at 35°C).

Control Checks for Inoculation Suspension Counts, Platelet Toxicity, and Sterility

We confirmed the population counts of the L, A, S, and positive control inoculation suspensions by serially diluting in sterile phosphate-buffered saline (PBS) pH 7.4 and plating the –3 and –4 dilutions by using the spread plate method (100 μL). We kept the inoculation suspension tubes at room temperature for 24 hours and replated them to check for platelet

toxicity. We defined platelet toxicity as a countable decrease in bacterial growth.

After 24 hours of incubation, we plated 100 μL from the negative wells onto TSA plates and incubated them at 36°C for 48 hours. We defined sterility as no growth on the TSA plates.

In Vitro Biofilm Assessment by Crystal Violet Staining Assay

We used crystal violet staining assay as a proxy to indicate the biomass of secreting material with these combinations of clinical isolates from STRs. After 24 hours, we carefully removed the starting inoculum from each well. We gently washed the coupons 2 times with 2 mL PBS. We fixed the coupon biofilms by allowing them to dry on a block heater set at 45°C–50°C for 1 hour. We stained the wells with 1 mL of 0.05% aqueous crystal violet for 15 minutes at room temperature (*22*,*24*). We removed the stain and gently washed the coupons 2 times with 2 mL sterile water (*25*). During the final wash, were removed the coupons and transferred them to new 12-well plates. We used 2 mL 30% (vol/vol) acetic acid to elute the bound crystal violet on the coupon and measured optical density at 550 nm (OD_{550}). We performed each assay with duplicate wells for each bacterium (or combination). We subtracted the baseline readings from the coupons containing TSBG and apheresis platelets without bacteria from the readings at OD_{550}.

Quantitation of Bacteria within Biofilm

We measured CFUs to quantify the bacteria present in the biofilms formed from these isolates and determine if they grow well together for those cocultured. We washed the wells in PBS and transferred the coupons to sterile Eppendorf tubes containing PBS. We vortexed these tubes thoroughly for 1 minute, placed them in a floating foam rack, and sonicated them at 40 kHz for 30 minutes by using the Branson 5800 Sonicator (Emerson, https://www.emerson.com), (*20*,*21*). After sonication, we thoroughly vortexed the tubes for 1 minute and serially diluted the solution in PBS. We plated dilutions onto TSA in duplicate and the selective and differential media (eosin methylene blue), Leeds, and MSA (mannitol salt agar) plates. We counted colonies on the TSA plates to determine the CFUs per coupon, and we counted the differential plates to determine percentage distribution of bacteria on the mixed coupons.

We quantitated the effect of sonication on the viability of each bacterium by measuring the CFU per milliliter of a 3×10^6 CFU/mL PBS suspension (by serial dilution) before sonication and after sonication. A decrease in CFU/mL would indicate loss of viability; we noted no loss in viability.

Microscopic Examination

We washed coupons with biofilm and fixed them with heat by placing the 12-well plates on a block heater set at 45°C–50°C for 1 hour. We Gram-stained the coupons by using a kit (Hardy Diagnostics, https://hardydiagnostics.com) according to the manufacturer's instructions. We first sonicated duplicate coupons and then the Gram-stained coupons to show efficacy of sonication. We visualized stained coupons by using light microscopic examination with a BX5 series microscope (Olympus, https://www.olympus-global.com) under the 10× objective (100× total magnification) and 60× objective (600× total magnification). We captured images by using Stream Motion Software (Olympus).

Statistical Analyses

Analyses included 3–4 biologic replicates per condition (Figure 1). Each biologic replicate represented a unique platelet donor tested in an independent experiment. We performed statistical analysis and visualization by using Excel version 2405 (Microsoft, https://www.microsoft.com) and Prism version 10 (GraphPad, https://www.graphpad.com). We identified statistical differences by using 2-way analysis of variance (ANOVA) or by application of a mixed effects model. We considered a p value of ≤ 0.05 as significant. We used Šídák's multiple comparison test to test the effect of a condition on an individual bacterial species when ANOVA or a mixed-effects model yielded statistically significant results. We used a threshold of $p \leq 0.05$ to determine significance of the adjusted p value (p_{adj}), which we determined by using multiple comparison testing.

Results

Effect of Growth Medium on Biofilm Formation on Platelet Bag Plastic

We investigated the effect of growth medium on bacterial burden and biofilm matrix production on storage bag plastic for all single and pairwise combinations of A, S, and L. By using our multiwell plate assay, we grew bacteria at 35°C in TSBG liquid medium or in apheresis platelets in PAS III (APH PLTs) from 3 unique donors. We found that all bacterial monoculture or coculture combinations in TSBG or APH PLTs resulted in viable bacteria adhered to the platelet storage bag plastic (Figure 2, panel A). The choice of growth medium had a differential effect depending on the bacterial species (or combination). Total

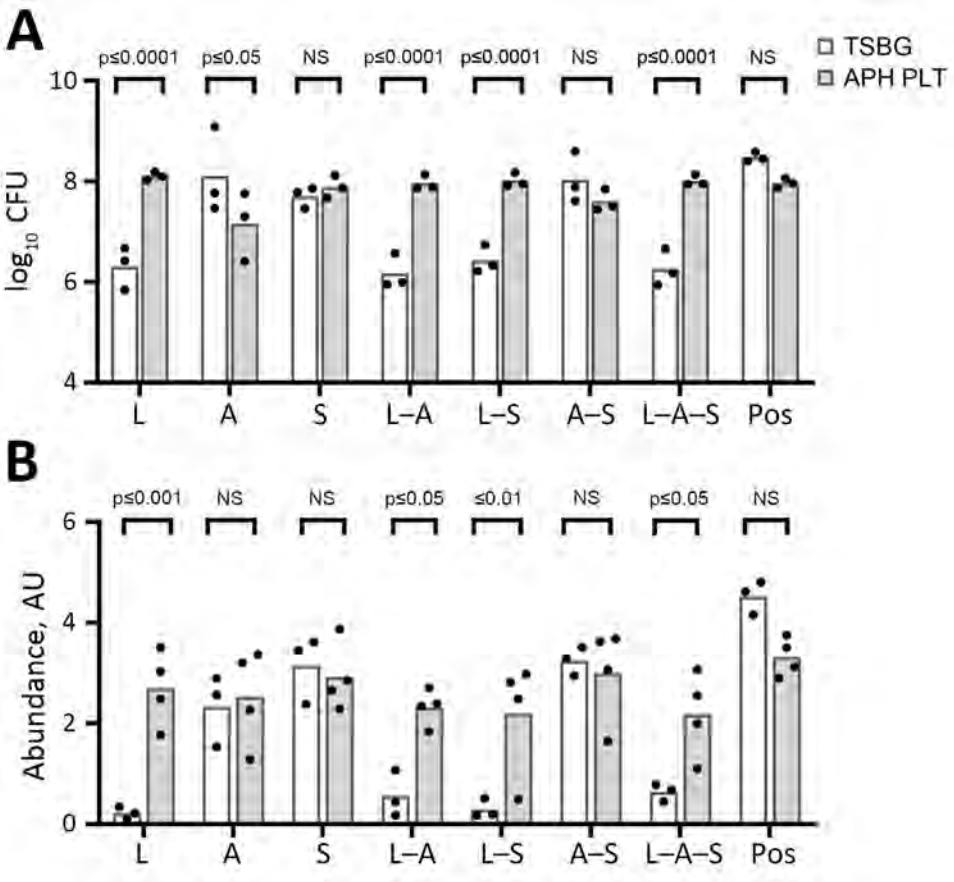

Figure 2. Effects of different growth media (TSBG) versus APH PLT for most bacteria on biofilm CFU recovery (A) and CV biofilm formation (B) on platelet bag coupons after 24 hours of incubation at 35°C. Baseline readings of TSBG and APH PLT without bacteria were subtracted from the readings at OD_{550}. *Leclercia adecarboxylata* and the polymicrobial biofilms containing *L. adecarboxylata* showed a significant ($p \leq 0.05$) increase in CFU within the biofilm and CV biomass when grown in APH PLT compared with TSBG. *Acinetobacter* spp. recovered from the biofilm was significantly decreased when grown in APH PLT. Each dot represents an individual biologic replicate inoculated with the corresponding monomicrobial or polymicrobial bacterial species. A, *Acinetobacter* spp.; APH PLT, apheresis platelets; AU, absorbance unit; CV, crystal violet; L, *L. adecarboxylata*; NS, not significant; OD, optical density; pos, positive control (*Staphylococcus epidermidis*); S, *S. saprophyticus*; TSBG, tryptic soy broth–glucose.

CFU counts of adherent bacteria were higher when L (p_{adj}<0.0001), L–S (p_{adj}<0.0001), and L–A–S (p_{adj} = 0.0058) were grown in APH PLTs compared with TSBG. In contrast, growth in APH PLTs appeared to diminish the number of bacteria adhered to the plastic coupon in monoculture of *Acinetobacter* alone by a log (p_{adj} = 0.0283). In a separate set of experiments, we used a crystal violet staining assay to quantify the production of biofilm matrix on the platelet storage bag coupon when bacteria were grown in TSBG compared with APH PLTs (Figure 2, panel B). Growth in APH PLTs resulted in a mean 12-fold increase in crystal violet staining of platelet plastic in cultures inoculated with *L. adecarboxylata* alone (p_{adj} = 0.0002) and mean 4.1-fold, 7.5-fold, and 3.4-fold increases when *L. adecarboxylata* was cultured in combination with *Acinetobacter* spp. (p_{adj} = 0.0123), *S. saprophyticus* (p_{adj} = 0.0056), or both *Acinetobacter* spp. and *S. saprophyticus* (p_{adj} = 0.038).

Limited Effect of Temperature on Biofilm Formation by STR Isolates

Many environmental bacteria thrive at 22°C, which is the temperature for conventional platelet storage. Therefore, we evaluated biofilm formation in APH PLTs at 22°C. Apart from *Acinetobacter* spp. alone, we did not detect a significant effect of growth in APH PLTs at 22°C on the number of STR bacteria adhered to the platelet plastic coupons compared with 35°C (Figure 3, panel A). When *Acinetobacter* spp. was cultured alone at 22°C, we found a mean log increase of 0.75 compared with growth at 35°C (p_{adj} = 0.0228). Although few significant differences were found in biofilm matrix production at 22°C compared with 35°C, we did observe a trend toward a decrease of bound crystal violet in biofilm matrix or biomass at room temperature (Figure 3, panel B).

L. adecarboxylata Compared with Other STR Bacteria in Multispecies Biofilms

To better understand the composition of multispecies biofilms, we used selective and differential media to quantify the contribution of each species to the overall number of viable, adherent bacteria on the platelet bag coupons (Figure 4). The inoculum for cocultures of bacteria in APH PLTs was composed of equal proportions of either pairs or all 3 of the STR-relevant bacterial species. Regardless of incubation

temperature, we found that *L. adecarboxylata* made up the highest percentage of the total CFUs on the platelet bag coupon when grown in combination with *Acinetobacter* spp., *S. saprophyticus*, or both. The population of *S. saprophyticus* was limited in the multispecies biofilms compared with *Acinetobacter* spp. and *L. adecarboxylata*. When all 3 species were cultured together, *S. saprophyticus* made up no more than 2% of the total CFU counts of bacteria adhered to the plastic coupon.

When grown in APH PLT or PAS III in 22°C conditions, the doubling rate for *S. saprophyticus* isolate is ≈169 minutes in the first 24 hours (Erin Fischer, American Red Cross unpub. data). This slower doubling rate, in comparison to *L. adecarboxylata* at 113 minutes and *Acinetobacter* spp. at 88 minutes, could contribute to the low total CFU percentage in the mixed biofilm. However, even the faster doubling rate of *Acinetobacter* spp. does not outcompete *L. adecarboxylata* in a polymicrobial biofilm incubated at either 22°C or 35°C (Figure 4).

Efficacy of Sonication

Disruption and bacterial enumeration of *Staphylococcus* spp. forming biofilms by sonication has received variable results (*26*). We incubated duplicate coupons in *S. saprophyticus*–inoculated APH PLT following our quantitation of biofilm bacteria study design (Figure 1). We Gram-stained coupons before the sonication stage and Gram-stained duplicate coupons after sonication (Figure 5). We examined the accumulation of platelets and gram-positive cocci on the coupon (Figure 5, panel A) and noted no evidence of platelets or cocci on the surface of the coupon after sonication (Figure 5, panel B), demonstrating that the sonication procedure was effective at removing the biofilm and bacteria from platelet coupons.

Discussion

In an investigation of the STRs that occurred during May–October 2018, CDC and FDA demonstrated that a subset of *Acinetobacter* spp. isolates from patients in 3 different states belonged to a novel taxon of *A. calcoaceticus–baumannii* complex (*3*). Later, Kracalik et al. (*4*) and Villa et al. (*5*) provided an update to the collaborative CDC and FDA investigations to include WGS data that suggested a common environmental source of bacteria upstream of blood manufacturing (*4*,*5*). Kracalik et al. (*4*) recommended additional

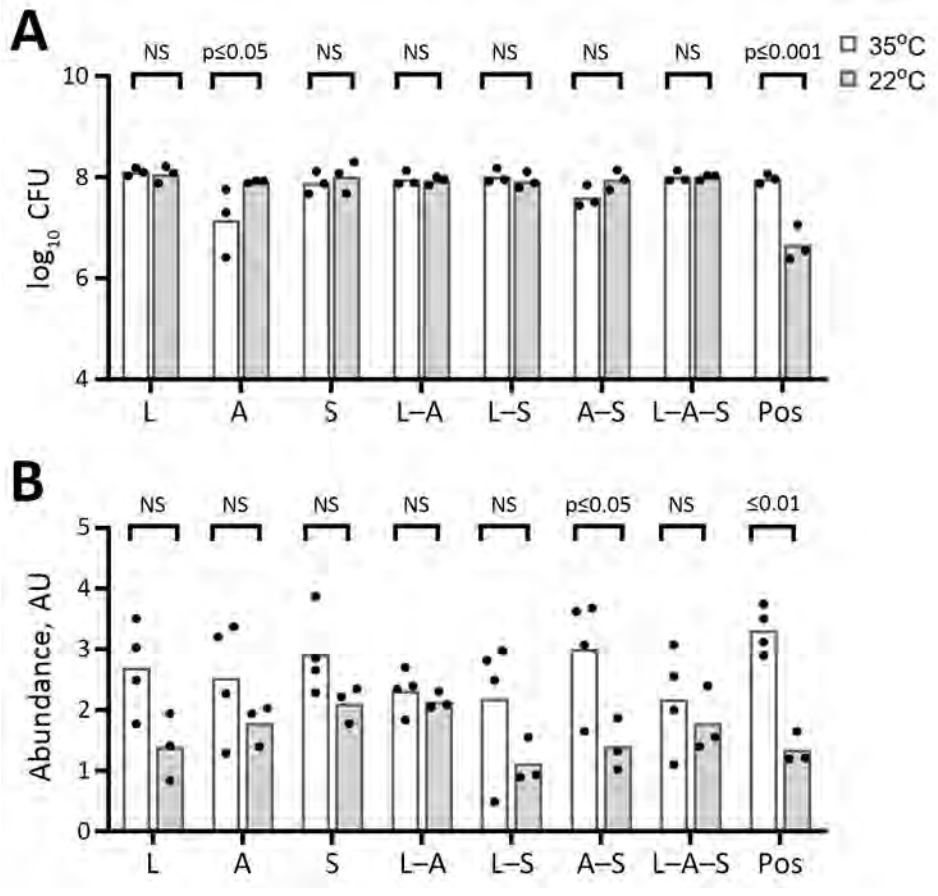

Figure 3. Effects of different incubation temperatures (22°C vs. 35°C) on biofilm CFU recovered (A) and CV biofilm formation (B) on platelet bag coupons after 24 hours of incubation in APH PLT. Baseline readings of TSBG and APH PLT with no bacteria were subtracted from the readings at OD_{550}. Incubation temperature showed no significant effect on quantitative monomicrobial or polymicrobial bacterial growth in APH PLTs, except for *Acinetobacter* spp. alone, which was lower at 35°C. There was a trend of decreased bound CV at room temperature for all bacteria, but only the *Acinetobacter* spp./*S. saprophyticus* combination showed statistically significant reduction between 35°C and 22°C. Each dot represents an individual biologic replicate inoculated with the corresponding monomicrobial or polymicrobial bacterial species. A, *Acinetobacter spp.*; APH PLT, apheresis platelets; AU, absorbance unit; CV, crystal violet; L, *Leclercia adecarboxylata*; NS, not significant; OD, optical density; pos, positive control (*Staphylococcus epidermidis*); S, *S. saprophyticus*; TSBG, tryptic soy broth–glucose.

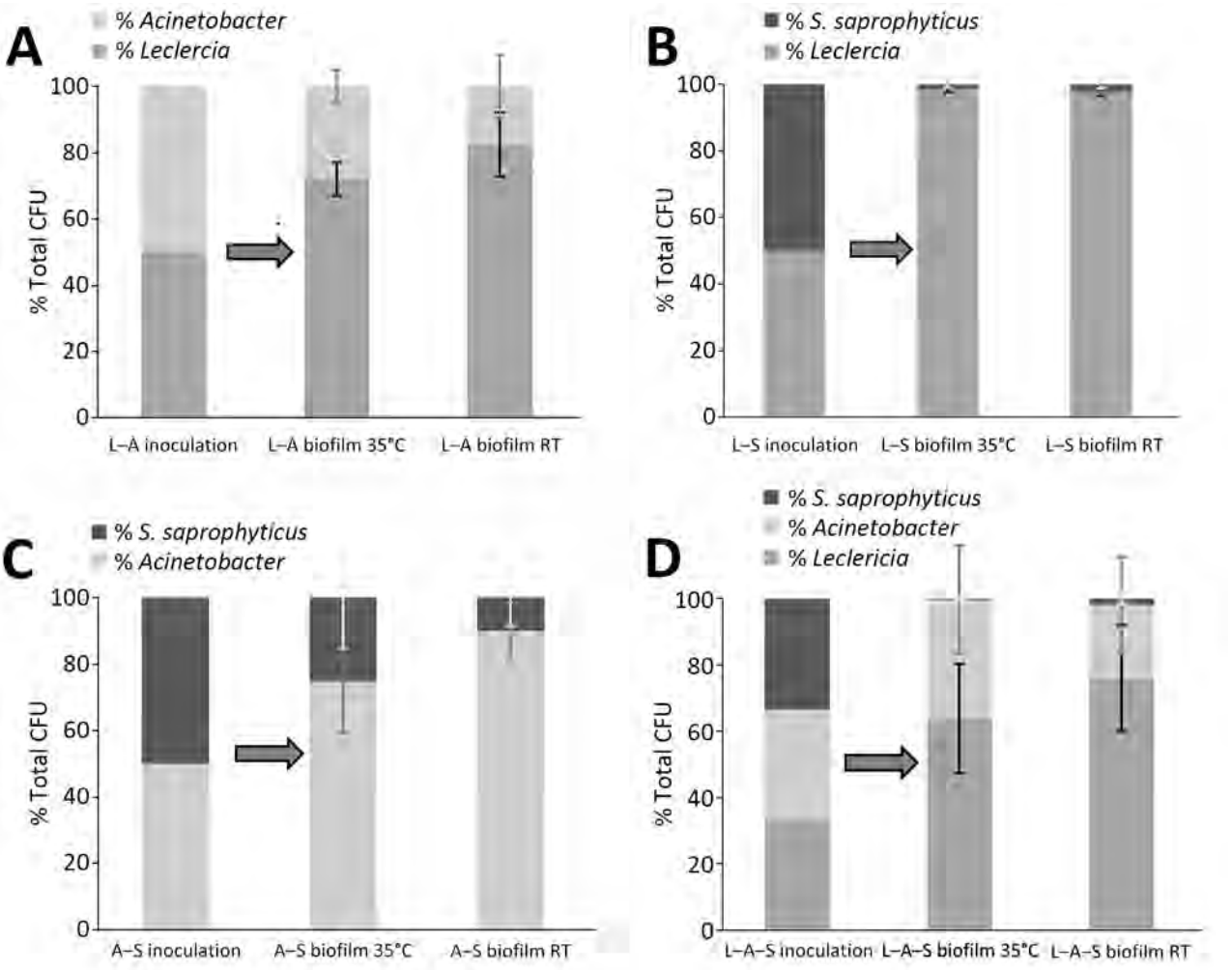

Figure 4. Average total CFU (n = 3) percentage comparison for 4 combinations of *Leclercia adecarboxylata*, *Acinetobacter* spp., and *Staphylococcus saprophyticus* mixed in equal parts and incubated together. Each bacterial species was measured in each polymicrobial biofilm after 24-hour incubation in apheresis platelets at both 35°C and room temperature. A) *L. adecarboxylata* and *Acinetobacter* spp.; B) *L. adecarboxylata* and *S. saprophyticus*; C) *Acinetobacter* spp. and *S. saprophyticus;* D) all 3 species incubated together. Even with a longer doubling time, *L. adecarboxylata* outcompeted *Acinetobacter* spp. in CFU percentage, whereas *S. saprophyticus* only accounts for 2% CFU in L–A–S polymicrobial biofilm grown at room temperature. Error bars represent SDs of the replicates. A, *Acinetobacter spp.*; L, *L. adecarboxylata*; RT, room temperature; S, *S. saprophyticus*.

studies to elucidate the effects of biofilm development on platelet bacterial risk control strategies.

Our goal was to investigate biofilm formation in platelet products by using specific isolates of *Acinetobacter* spp., *S. saprophyticus*, and *L. adecarboxylata* implicated in the 2018–2021 STR cases. Our study demonstrates that transfusion-relevant bacteria can produce biofilms well in monoculture and coculture combinations and that environmental conditions, such as growth medium and plastics, affect biofilms.

Our data showed a limited effect of temperature on biofilm formation by the STR isolates and that growth medium had a more significant effect on growth. As expected, biomass in APH PLTs was significantly higher than in TSBG. We observed a mean 12-fold increase in crystal violet staining of platelet plastic in cultures inoculated with *L. adecarboxylata* alone and mean 4.1-fold and 7.5-fold increases when *L. adecarboxylata* was cultured in combination with *Acinetobacter* spp. or *S. saprophyticus*. *L. adecarboxylata* also showed a significant increase in CFUs within the biofilm when grown in APH PLT compared with TSBG. Conversely, *Acinetobacter* spp. recovered from the biofilm significantly decreased when grown in APH PLT. Of note, our data also demonstrated that *L. adecarboxylata* outcompetes both *S. saprophyticus* and *Acinetobacter* spp. in a polymicrobial biofilm incubated in APH PLTs at either 22°C or 35°C.

Biofilm formation and composition changes with the environment, as previously shown (*27*,*28*). Our results are in line with previous reports that the platelet storage environment affects bacterial growth (*21*,*29*). Other research has shown that growing bacteria in the presence of platelets induces changes in expression of genes associated with biofilm maturation (*30*). Gene expression is controlled by many external and internal factors, such as 2-component or multicomponent signal transduction systems, quorum-sensing, small RNA, and secondary messengers such as cAMP; those systems monitor the environment and regulate the production of exopolysaccharides, fibrins, lipoproteins, and surface-associated proteins (pili and flagella), which together make up the biofilm biomass. Although our study does not address gene expression, the recent publication of WGS results for the STR isolates by CDC and FDA will enable future studies to address the role of specific genes in evasion of bacterial risk control strategies. The effect of platelets on expression of bacterial virulence factors remains poorly understood for bacteria that are classically associated with platelet contamination. Whether platelets and other variables in the platelet storage environment promote biofilm formation universally is an open question that warrants further exploration.

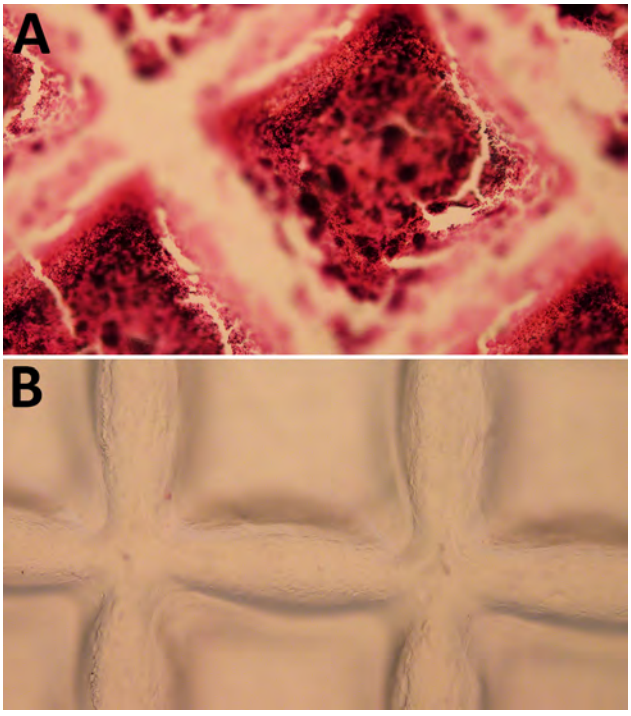

Figure 5. Gram-stained platelet bag coupons incubated with *Staphylococcus saprophyticus* in APH PLT before sonication and Gram-stained duplicate coupons after sonication. A) Accumulation of platelets and gram-positive cocci on the coupon. B) Visual analysis after sonication showing no evidence of platelets or cocci on the surface of the coupon, indicating that the sonication procedure effectively removed the biofilm and bacteria. The grid pattern observed on the coupon reflects the texture of the inner surface of Amicus (Fresenius Kabi, https://www.fresenius-kabi.com) platelet bags. APH PLT, apheresis platelets.

One limitations of our study is that the assays used were plate-based; therefore, we did not consider the effect of gas exchange and agitation in the platelet storage environment. To stain the biofilms, we used crystal violet, which is a basic aniline dye that binds to negatively charged peptidoglycan, DNA, extracellular protein, and polysaccharides. Bacterial gene expression in platelets is changed during growth in platelets compared with TSBG (*21*), and this change would most likely result in biofilm composition variations with differences in crystal violet–bound negatively charged molecules. Variation in biofilm production and composition also poses a challenge for selecting a bacterial strain that does not produce biofilm under all conditions tested in this study. Other research has demonstrated that strains thought to be biofilm-negative will produce biofilm under platelet storage conditions (*29*). Improved genotypic characterization of STR isolates could provide an avenue for engineering a biofilm-negative strain in future studies. Further, we did not conduct confocal microscopic examination, which limits our view of the formation, development, morphology, and structure of the biofilms.

Previous studies have proposed that some biofilm-forming bacteria may evade detection by bacterial culture or pathogen reduction and that planktonic versus sessile cells can affect efficacy (*4*,*23*,*31*). Phylogenetic evidence presented by the CDC and FDA investigation demonstrates genetic relatedness between the STR strains and isolates collected at the platelet collection set manufacturing site, strongly supporting the hypothesis that these bacteria were initially introduced into blood collection establishments from an upstream source. Of note, related strains also have been isolated from the hospital and blood bank environment, and some studies have noted microscopic bag leaks and variability in cocultured isolates implicated in these *Acinetobacter*-related STR (*32*). The relative contribution of limit of detection and low bacterial load, presence of inactivated pathogens, and biofilm formation or other evasion strategies to the failure of bacterial risk mitigation strategies is unknown. If biofilm formation causes evasion of bacterial testing or pathogen reduction, several questions remain for further investigation, including whether biofilms protect bacteria from the psoralen or UV light penetration needed for inactivation, whether viable but nonculturable cells found in some

bacterial biofilms are immune to the pathogen-reduction process, and whether certain parts of the platelet bag are more susceptible to biofilm formation than others.

In future studies on the relevance of biofilms in platelets for transfusion, using the correct genetic background when studying bacteria will be key. Researchers might consider reviewing the World Health Organization repository for platelet STR strains, particularly with the novel *A. calcoaceticus–baumannii* clusters identified in these recent STR cases and subsequent CDC and FDA investigations (*33*). Some species demonstrate that biofilm phenotypes differ between laboratory-adapted reference strains and clinical isolates, but whether this phylogenetic distinction translates to phenotypic differences is unknown (*34*). It may also be of interest to investigate bacterial contamination of indwelling catheters used to infuse blood products and to better understand bacterial load that may cause STRs given that, in some cases, co-components of platelets involved in STRs have been transfused without implication (*5*).

The FDA bacterial risk mitigation strategies remain acceptable, and more work is needed to understand the gaps in information regarding the 2018–2021 *Acinetobacter*-related STRs in the United States (*5*,*35*). Given the emerging medical device–related biofilm risks, a need exists to clarify the effects of biofilms on bacterial risk mitigation strategies and for innovative technologies to manage the complexities presented by biofilms (*9*).

These studies were conducted at and funded by the American Red Cross.

About the Author

Ms. Hapip is a microbiologist and project manager at the American Red Cross. Her primary research interests include bacterial physiology in blood products and pathogen-reduction systems and platelet metabolism.

References

1. Food and Drug Administration. Important information for blood establishments and transfusion services regarding bacterial contamination of platelets for transfusion. 2021 Dec 2 [cited 2024 Dec 15]. https://www.fda.gov/vaccines-blood-biologics/safety-availability-biologics/important-information-blood-establishments-and-transfusion-services-regarding-bacterial
2. Fridey JL, Stramer SL, Nambiar A, Moayeri M, Bakkour S, Langelier C, et al. Sepsis from an apheresis platelet contaminated with *Acinetobacter calcoaceticus/baumannii* complex bacteria and *Staphylococcus saprophyticus* after pathogen reduction. Transfusion. 2020;60:1960–9. https://doi.org/10.1111/trf.15951
3. Jones SA, Jones JM, Leung V, Nakashima AK, Oakeson KF, Smith AR, et al. Sepsis attributed to bacterial contamination of platelets associated with a potential common source—multiple states, 2018. MMWR Morb Mortal Wkly Rep. 2019;68:519–23. https://doi.org/10.15585/mmwr.mm6823a2
4. Kracalik I, Kent AG, Villa CH, Gable P, Annambhotla P, McAllister G, et al. Posttransfusion sepsis attributable to bacterial contamination in platelet collection set manufacturing facility, United States. Emerg Infect Dis. 2023;29:1979–89. https://doi.org/10.3201/eid2910.230869
5. Villa CH, Illoh O, Kracalik I, Basavaraju SV, Eder AF. Posttransfusion sepsis attributable to bacterial contamination in platelet collection set manufacturing, United States. Transfusion. 2023;63:2351–7. https://doi.org/10.1111/trf.17589
6. Food and Drug Administration. Important information for blood establishments and transfusion services regarding bacterial contamination of platelets for transfusion. 2022 Dec 22 [cited 2023 Dec 15]. https://www.fda.gov/vaccines-blood-biologics/safety-availability-biologics/important-information-blood-establishments-and-transfusion-services-regarding-bacterial
7. Ledwoch K, Dancer SJ, Otter JA, Kerr K, Roposte D, Rushton L, et al. Beware biofilm! Dry biofilms containing bacterial pathogens on multiple healthcare surfaces; a multi-centre study. J Hosp Infect. 2018;100:e47–56. https://doi.org/10.1016/j.jhin.2018.06.028
8. Moris V, Lam M, Amoureux L, Magallon A, Guilloteau A, Maldiney T, et al. What is the best technic to dislodge *Staphylococcus epidermidis* biofilm on medical implants? BMC Microbiol. 2022;22:192. https://doi.org/10.1186/s12866-022-02606-x
9. Sharma S, Mohler J, Mahajan SD, Schwartz SA, Bruggemann L, Aalinkeel R. Microbial biofilm: a review on formation, infection, antibiotic resistance, control measures, and innovative treatment. Microorganisms. 2023;11:1614. https://doi.org/10.3390/microorganisms11061614
10. Didouh N, Khadidja M, Campos C, Sampaio-Maia B, Boumediene MB, Araujo R. Assessment of biofilm, enzyme production and antibiotic susceptibility of bacteria from milk pre- and post-pasteurization pipelines in Algeria. Int J Food Microbiol. 2023;407:110389. https://doi.org/10.1016/j.ijfoodmicro.2023.110389
11. Zeighami H, Valadkhani F, Shapouri R, Samadi E, Haghi F. Virulence characteristics of multidrug resistant biofilm forming *Acinetobacter baumannii* isolated from intensive care unit patients. BMC Infect Dis. 2019;19:629. https://doi.org/10.1186/s12879-019-4272-0
12. Gedefie A, Demsis W, Ashagrie M, Kassa Y, Tesfaye M, Tilahun M, et al. *Acinetobacter baumannii* biofilm formation and its role in disease pathogenesis: a review. Infect Drug Resist. 2021;14:3711–9. https://doi.org/10.2147/IDR.S332051
13. Kerantzas CA, Merwede J, Snyder EL, Hendrickson JE, Tormey CA, Kazmierczak BI, et al. Assessment of polymicrobial interactions in bacterial isolates from transfused platelet units associated with sepsis. Transfusion. 2022;62:2458–63. https://doi.org/10.1111/trf.17136
14. Lawal OU, Barata M, Fraqueza MJ, Worning P, Bartels MD, Goncalves L, et al. *Staphylococcus saprophyticus* from clinical and environmental origins have distinct biofilm composition. Front Microbiol. 2021;12:663768. https://doi.org/10.3389/fmicb.2021.663768
15. Colquhoun JM, Rather PN. Insights into mechanisms of biofilm formation in *Acinetobacter baumannii* and implications for uropathogenesis. Front Cell Infect Microbiol. 2020;10:253. https://doi.org/10.3389/fcimb.2020.00253

16. Gottesman T, Fedorowsky R, Yerushalmi R, Lellouche J, Nutman A. An outbreak of carbapenem-resistant *Acinetobacter baumannii* in a COVID-19 dedicated hospital. Infect Prev Pract. 2021;3:100113. https://doi.org/10.1016/j.infpip.2021.100113
17. Perez S, Innes GK, Walters MS, Mehr J, Arias J, Greeley R, et al. Increase in hospital-acquired carbapenem-resistant *Acinetobacter baumannii* infection and colonization in an acute care hospital during a surge in COVID-19 admissions—New Jersey, February–July 2020. MMWR Morb Mortal Wkly Rep. 2020;69:1827–31. https://doi.org/10.15585/mmwr.mm6948e1
18. Upmanyu K, Haq QMR, Singh R. Factors mediating *Acinetobacter baumannii* biofilm formation: opportunities for developing therapeutics. Curr Res Microb Sci. 2022;3:100131. https://doi.org/10.1016/j.crmicr.2022.100131
19. Wong D, Nielsen TB, Bonomo RA, Pantapalangkoor P, Luna B, Spellberg B. Clinical and pathophysiological overview of *Acinetobacter* infections: a century of challenges. Clin Microbiol Rev. 2017;30:409–47. https://doi.org/10.1128/CMR.00058-16
20. Hadjesfandiari N, Schubert P, Fallah Toosi S, Chen Z, Culibrk B, Ramirez-Arcos S, et al. Effect of texture of platelet bags on bacterial and platelet adhesion. Transfusion. 2016;56:2808–18. https://doi.org/10.1111/trf.13756
21. Loza-Correa M, Kalab M, Yi QL, Eltringham-Smith LJ, Sheffield WP, Ramirez-Arcos S. Comparison of bacterial attachment to platelet bags with and without preconditioning with plasma. Vox Sang. 2017;112:401–7. https://doi.org/10.1111/vox.12513
22. Wilson-Nieuwenhuis JST, Dempsey-Hibbert N, Liauw CM, Whitehead KA. Surface modification of platelet concentrate bags to reduce biofilm formation and transfusion sepsis. Colloids Surf B Biointerfaces. 2017;160:126–35. https://doi.org/10.1016/j.colsurfb.2017.09.019
23. Taha M, Culibrk B, Kalab M, Schubert P, Yi QL, Goodrich R, et al. Efficiency of riboflavin and ultraviolet light treatment against high levels of biofilm-derived *Staphylococcus epidermidis* in buffy coat platelet concentrates. Vox Sang. 2017;112:408–16. https://doi.org/10.1111/vox.12519
24. Hapip CA, Brown BL. The role of biofilms in the blood center environment. American Association for Advancement of Blood and Biotherapies. 2022 [cited 2022 Oct 21]. https://aabb.confex.com/aabb/2022/meetingapp.cgi/Paper/10736
25. Allkja J, Bjarnsholt T, Coenye T, Cos P, Fallarero A, Harrison JJ, et al. Minimum information guideline for spectrophotometric and fluorometric methods to assess biofilm formation in microplates. Biofilm. 2019;2:100010. https://doi.org/10.1016/j.bioflm.2019.100010
26. Sandbakken ET, Witsø E, Sporsheim B, Egeberg KW, Foss OA, Hoang L, et al. Highly variable effect of sonication to dislodge biofilm-embedded *Staphylococcus epidermidis* directly quantified by epifluorescence microscopy: an in vitro model study. J Orthop Surg Res. 2020;15:522. https://doi.org/10.1186/s13018-020-02052-3
27. Ahmad I, Nadeem A, Mushtaq F, Zlatkov N, Shahzad M, Zavialov AV, et al. Csu pili dependent biofilm formation and virulence of *Acinetobacter baumannii*. NPJ Biofilms Microbiomes. 2023;9:101. https://doi.org/10.1038/s41522-023-00465-6
28. Nyanasegran PK, Nathan S, Firdaus-Raih M, Muhammad NAN, Ng CL. Biofilm signaling, composition and regulation in *Burkholderia pseudomallei*. J Microbiol Biotechnol. 2023;33:15–27. https://doi.org/10.4014/jmb.2207.07032
29. Ali H, Greco-Stewart VS, Jacobs MR, Yomtovian RA, Rood IGH, de Korte D, et al. Characterization of the growth dynamics and biofilm formation of *Staphylococcus epidermidis* strains isolated from contaminated platelet units. J Med Microbiol. 2014;63:884–91. https://doi.org/10.1099/jmm.0.071449-0
30. Loza-Correa M, Yousuf B, Ramirez-Arcos S. *Staphylococcus epidermidis* undergoes global changes in gene expression during biofilm maturation in platelet concentrates. Transfusion. 2021;61:2146–58. https://doi.org/10.1111/trf.16418
31. Greco-Stewart VS, Brown EE, Parr C, Kalab M, Jacobs MR, Yomtovian RA, et al. *Serratia marcescens* strains implicated in adverse transfusion reactions form biofilms in platelet concentrates and demonstrate reduced detection by automated culture. Vox Sang. 2012;102:212–20. https://doi.org/10.1111/j.1423-0410.2011.01550.x
32. Fadeyi EA, Wagner SJ, Goldberg C, Lu T, Young P, Bringmann PW, et al. Fatal sepsis associated with a storage container leak permitting platelet contamination with environmental bacteria after pathogen reduction. Transfusion. 2021;61:641–8. https://doi.org/10.1111/trf.16210
33. Spindler-Raffel E, Benjamin RJ, McDonald CP, Ramirez-Arcos S, Aplin K, Bekeredjian-Ding I, et al.; ISBT Working Party Transfusion-Transmitted Infectious Diseases (WP-TTID), Subgroup on Bacteria. Enlargement of the WHO international repository for platelet transfusion-relevant bacteria reference strains. Vox Sang. 2017;112:713–22. https://doi.org/10.1111/vox.12548
34. Fux CA, Uehlinger D, Bodmer T, Droz S, Zellweger C, Mühlemann K. Dynamics of hemodialysis catheter colonization by coagulase-negative staphylococci. Infect Control Hosp Epidemiol. 2005;26:567–74. https://doi.org/10.1086/502586
35. Food and Drug Administration. Bacterial risk control strategies for blood collection establishments and transfusion services to enhance the safety and availability of platelets for transfusion. 2020 Dec [cited 2023 Dec 15]. https://www.fda.gov/regulatory-information/search-fda-guidance-documents/bacterial-risk-control-strategies-blood-collection-establishments-and-transfusion-services-enhance
36. Kracalik I, Sapiano MRP, Wild RC, Chavez Ortiz J, Stewart P, Berger JJ, et al. Supplemental findings of the 2021 National Blood Collection and Utilization Survey. Transfusion. 2023;63(Suppl 4):S19–42. https://doi.org/10.1111/trf.17509

Address for correspondence: Bethany L Brown, American Red Cross, Holland Lab for the Biomedical Sciences, 15601 Crabbs Branch Way, Rockville, MD 20855, USA; email: bethany.brown2@redcross.org

Role of Direct Sexual Contact in Human Transmission of Monkeypox Virus, Italy

Giuseppe Sberna, Gabriella Rozera, Claudia Minosse, Licia Bordi, Valentina Mazzotta, Alessandra D'Abramo, Enrico Girardi, Andrea Antinori, Fabrizio Maggi, Eleonora Lalle

The 2022 global mpox outbreak was driven by human-to-human transmission, but modes of transmission by sexual relationship versus sexual contact remain unclear. We evaluated sexual transmission of mpox by using monkeypox virus (MPXV) G2R-mRNA as a marker of ongoing viral replication through in vitro experiments. We analyzed clinical samples of 15 MPXV-positive patients in Italy from different biological regions by using the setup method. The presence of MPXV DNA, MPXV G2R-mRNA, or both in all analyzed lesion swab samples, independent of viral load, confirmed a higher infectivity risk from skin lesions. Positivity for MPXV G2R-mRNA in nasopharyngeal swabs was associated with high MPXV load, whereas positive results for MPXV G2R-mRNA were obtained only in the 2 semen samples with the lowest MPXV loads. Our results suggest that close or skin-to-skin contact during sexual intercourse is the main route of sexual transmission and that semen is a minor driver of infection, regardless of MPXV load.

Monkeypox virus (MPXV) is the etiologic agent of zoonotic mpox disease. Although the virus was first discovered in colonies of monkeys kept for research in 1958, MPXV is mainly transmitted to humans through physical contact with wild infected animals (i.e., squirrels, rats, and mice), with contaminated materials, or with an infectious person (*1*). The first human case of mpox was recorded in 1970 in the Democratic Republic of the Congo; the virus is endemic in central and west Africa, where outbreaks are regularly reported (*1*).

Before 2022, sporadic mpox cases had been described outside Africa, mainly linked to travel. However, during May–June 2022, the emergence and rapid spread of mpox in >50 countries where the disease was not endemic, led the World Health Organization (WHO) to declare the mpox outbreak a public health emergency of international concern (*2*). The outbreak, caused mostly by the clade IIb variant of the virus, was driven by human-to-human transmission via close contact with infected persons; most cases were described among men who had sex with men. In several studies, viral DNA has been identified and isolated in the semen of infected persons for weeks after they acquired the infection, supporting the hypothesis of sexual transmission (*2*–*4*). Viral DNA was also detected in biologic samples such as saliva, nasopharyngeal swabs (NPS), blood, and urine, thus not always implying the infectivity of the biologic sample (*5*). Now, new in vivo and in vitro models able to mimic aspects of viral biology, such as infectivity, can be developed (*6*).

Cell culture is considered the standard for virus isolation. Nevertheless, several factors, such as suboptimal sensitivity, eventual long storage of the samples, or the presence of antibodies against the virus in the clinical samples, can contribute to the failure of this procedure, resulting in the inability to establish real viability and infectivity. To improve knowledge about the route of transmission of this infection, finding an alternative method able to overcome problems associated with viral isolation and verify the infective capacity of MPXV in different biological regions is essential.

Considering that MPXV replication strategy is based on a cascade of 3 gene classes (early, intermediate, and late) (*7*,*8*), in this study, we explored the possibility of using an early transcript as a marker of ongoing viral replication. G2R is a crucial gene transcribed during the early phase of infection and can interact with the viral RNA polymerase during the intermediate and late phases of viral replication, thus affecting the fidelity of the transcription process (*8*). Therefore, we selected G2R as a surrogate marker of ongoing replication, because the presence of the

Author affiliation: National Institute for Infectious Diseases, Lazzaro Spallanzani, Rome, Italy

DOI: https://doi.org/10.3201/eid3009.240075

G2R-mRNA transcript discriminates between actively replicating and nonreplicating samples, providing an indirect indication of the possible transmission mode.

We conducted a preliminary experiment using Vero E6 cells infected in vitro with MPXV to assess the effectiveness of the developed method for detecting and measuring G2R-mRNA levels. We then analyzed clinical specimens that tested positive for MPXV DNA.

Methods

Ethics Statement

This study was conducted in accordance with the Declaration of Helsinki and with protocol code no. 40z, Register of Non-Covid Trials 2022. The study was approved by the Ethical Committee of the Lazzaro Spallanzani Institute MpoxCohort protocol "Studio di coorte osservazionale monocentrica su soggetti che afferiscono per sospetto clinico o epidemiologico di malattia del vaiolo delle scimmie (mpox)."

In Vitro Experiments

We maintained Vero E6 cells in modified eagle medium supplemented with 10% heat-inactivated fetal calf serum (FCS) at 37°C in a humidified atmosphere of 5% CO_2 and exposed to MPXV isolate hMpxv/Italy/un-INMI-Pt2/2022, clade/lineage IIb B.1 (GISAID accession no. EPI_ISL_13251120 [https://www.gisaid.org]; GenBank accession no. ON745215.1) for 1 hour and 30 minutes at 37°C at a multiplicity of infection of 0.01. At the end of the adsorption period, we washed and incubated cells at 37°C; at 30 minutes and 1, 2, 3, 4, 6, 24, and 48 hours postinfection (hpi), we harvested, inactivated, and tested cells and supernatants for MPXV DNA and G2R-mRNA presence by digital droplet PCR (ddPCR).

Clinical Samples

During May–September 2022, a total of 29 samples (7 nasopharyngeal swab, 10 skin lesion swab, 8 semen, and 4 urine samples) were collected for diagnostic purposes from 15 patients admitted to the National Institute for Infectious Diseases (INMI) Lazzaro Spallanzani in Rome, Italy. Patients had a positive diagnosis of mpox within 7 days of symptom onset. We retrospectively analyzed those samples.

MPXV DNA and G2R-mRNA Quantification

To establish the presence of viral DNA, we first analyzed samples from different anatomic sites of patients with an mpox diagnosis by a commercial MPXV real-time PCR kit (Jiangsu BioPerfectus Technologies Co., Ltd., http://www.bioperfectus.com) on the ELITe InGenius instrument (ELITechGroup SAS, https://www.elitechgroup.com), obtaining a semiquantitative measure by cycle threshold (Ct) value. We further analyzed biological samples that tested positive for MPXV DNA by real-time PCR and cell supernatants from the in vitro experiments by using ddPCR to obtain quantitative results expressed as copies per milliliter. In brief, we extracted 140 μL of supernatant from infected cells and biologic samples by using the QIAamp Viral DNA Mini Kit (QIAGEN, https://www.qiagen.com) according to the manufacturer's instructions. We quantified MPXV DNA by using the QX200 AutoDG Digital Droplet PCR system (Bio-Rad Laboratories, https://www.bio-rad.com), as previously described (*9*).

To perform G2R-mRNA quantification, we extracted total RNA by using the RNeasy Mini Kit (QIAGEN) according to the manufacturer's instructions. To selectively degrade any traces of DNA, we treated RNA extracted with DNase (TURBO DNase Kit; Thermo Fisher Scientific, https://www.thermofisher.com). We then reverse transcribed 10 μL of RNA per sample according to the instructions of the SuperScript IV First-Strand cDNA Synthesis reaction kit (Thermo Fisher) by using 50 μmol OLigo d(T)20 as primers to select mRNA. We performed quantification by using the Bio-Rad QX200 AutoDG ddPCR system, targeting the early gene, G2R-mRNA (*10*). To confirm the absence of MPXV DNA fragments, all RNA-extracted samples underwent MPXV DNA PCR after treatment with DNase.

Statistical Analysis

We performed linear regression analysis by using GraphPad Prism version 9 (https://www.graphpad.com). We expressed results as correlation coefficients (r).

Results

In Vitro Cell Culture Experiments

To establish if G2R-mRNA could be considered a surrogate marker of ongoing MPXV replication, we tested for its presence in vitro in infected Vero E6 cells. Cell-associated G2R-mRNA was detected at low levels until 30 minutes postinfection, when it started to increase, showing a peak at 1 hpi (Figure 1). This result was expected because the G2R gene is early transcribed during viral infection. After 1 hpi, we observed a slight increase in cell-associated G2R-mRNAs throughout the infection until 24 hpi; levels remained stable thereafter. All RNA samples treated with DNase were negative for MPXV DNA, confirming

the absence of MPXV DNA fragments and the strength of the setup method (data not shown).

MPXV DNA levels released in the supernatant steadily increased at each timepoint, peaking at 24 hpi. We observed substantially lower levels of DNA released in the supernatants for mRNA cell-associated DNA, starting at 30 minutes postinfection and continuing throughout the observation period.

MPXV DNA and G2R-mRNA in Clinical Specimens

MPXV DNA and G2R-mRNA were present in NPS, skin lesion swabs, urine, and semen samples (Table 1). All samples were positive for MPXV DNA by diagnostic real-time PCR (mean Ct 27.3, range 13.3–37.7), except for all urine and 2 semen samples that showed negative results (Ct >45.0). We performed absolute quantification of positive MPXV DNA samples by ddPCR, and linear regression analysis found a highly negative correlation (r = −0.99) between the Ct values and the amount of MPXV DNA (Figure 2).

G2R-mRNA was detectable in all skin lesions (r = 0.71) 4 of 7 NPS samples (r = 0.64), showing a good correlation with MPXV DNA in both matrices. Of note, we observed low positivity for G2R-mRNA presence in only 2 of 8 semen samples; therefore, we could not correlate those results with DNA levels. Nevertheless, we emphasize that semen samples with the highest DNA copy numbers tested negative for G2R-mRNA, which is different from what we observed in other matrices (Table).

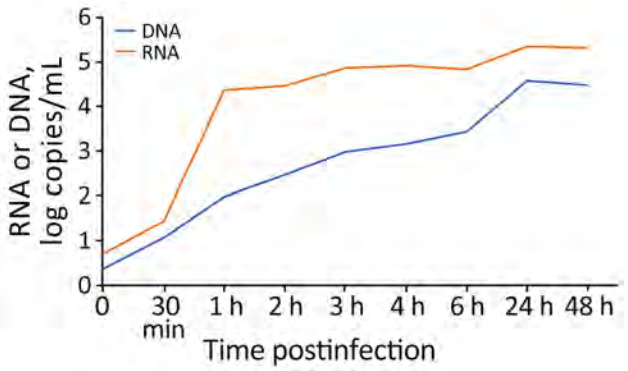

Figure 1. In vitro kinetics of MPXV infection in Vero E6 cell line in study of role of direct sexual contact in human transmission of MPXV, Italy. Cell-associated G2R-mRNA, a surrogate marker of ongoing replication, was detected at low levels until 30 minutes postinfection, when it started to increase, showing a peak at 1 hour postinfection. After 1 hour, a slight increase was observed until 24 hours; levels remained stable thereafter. MPXV DNA levels released in the supernatant steadily increased at each time point, peaking at 24 hours postinfection. MPXV, monkeypox virus.

Table. Molecular results of analyzed samples in study of role of direct sexual contact in human transmission of MPXV, Italy*

Sample type	Patient no.	MPXV DNA Ct	MPXV DNA ddPCR, copies/µL	G2R-mRNA ddPCR, copies/µL
Semen	1	24.5	3,576	ND
	2	34.5	2.2	2.4
	4	ND	NT	NT
	5	ND	NT	NT
	6	27.9	145.2	ND
	8	28.7	98.8	ND
	11	34.3	12.4	6.0
	12	37.7	ND	ND
Skin lesion swab				
Penis	1	22.2	1,216	7.2
Cutaneous	2	13.2	4,000,000	504
Penis	3	24.3	4,296	3.6
Scapula	5	35.4	2.1	2.8
Anal	9	35.6	1,552	4.8
Cutaneous	10	15.5	380,000	608
Anal	10	20.0	49,060	79.6
Pubis	13	15.9	521,000	16.4
Neck	13	17.7	117,600	10.8
Back	15	23.0	8,188	4.4
Nasopharyngeal swab	1	21.2	22,080	13.2
	2	31.1	48	1.2
	4	27.8	520	1.6
	5	37.5	4.9	ND
	6	28.5	164.4	10
	7	37.2	1.0	ND
	14	33.3	6.9	ND
Urine	1	ND	NT	NT
	2	ND	NT	NT
	5	ND	NT	NT
	6	ND	NT	NT

*Ct, cycle threshold; ddPCR, digital droplet PCR; MPXV, monkeypox virus; ND, not detected; NT, not tested.

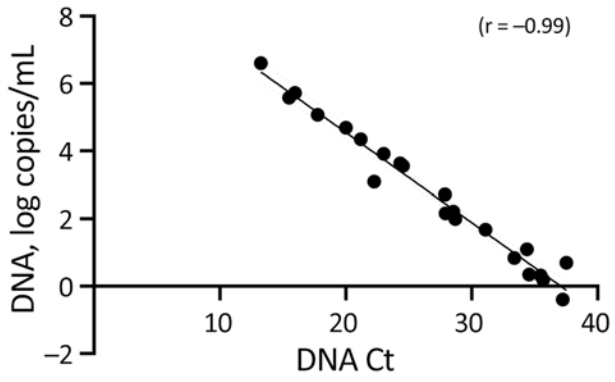

Figure 2. Linear regression analysis of Ct values and MPXV DNA levels in clinical specimens from study of role of direct sexual contact in human transmission of MPXV, Italy. Results show highly negative correlation (r = −0.99) between Ct values and the amount of MPXV DNA. Ct, cycle threshold; MPXV, monkeypox virus.

Discussion

During January 1, 2022–February 2024, more than 94,000 laboratory-confirmed cases of mpox, including 181 deaths, were reported to WHO from 117 member states across all 6 WHO regions (*11*). Cases and sustained chains of transmission have been reported concurrently in nonendemic and endemic countries in widely disparate geographic areas and have involved mainly, but not exclusively, men who have sex with men. Although close physical contact with lesions on the skin or mucosal surfaces of mpox-symptomatic persons represents the main factor for human-to-human transmission in this outbreak (*12*), recent studies suggest that sexual activity could represent an important route of disease transmission (*2*,*13*). Lesions on the genitalia, perianal, and inguinal areas of infected persons that tested positive for MPXV DNA (*4*,*14*), as well as the high prevalence of positivity in semen samples from mpox cases (*9*,*15*), have been considered further evidence supporting the sexual transmission route. A correlation between the amount of viral load and infectious virus titer has already been described for lesion and NPS swab samples (*16*); on the contrary, difficulties in viral isolation were found for semen samples, even when the viral load was high (*17*). That evidence opens the issue concerning the difference between sexual and sexual contact transmissions. To overcome problems associated with viral isolation and to verify the real infectious capacity of MPXV in different biological regions, we first evaluated the possibility of using MPXV G2R-mRNA as a marker of ongoing viral replication through in vitro experiments. The presence of high levels of G2R-mRNA during the early phase of infection (within 1 hour), associated with low levels of MPXV DNA, confirms that this method reflects the replication strategy of MPXV, because G2R is an early gene. Therefore, we applied the same method in vivo to analyze clinical samples from different biological regions of MPXV-positive patients.

Our results showed the presence of either MPXV DNA or MPXV G2R-mRNA in all analyzed lesion swab samples, independent of MPXV DNA load, thus confirming a higher infectivity risk from skin lesions. As far as NPS samples are concerned, the presence of MPXV G2R-mRNA was associated with a high MPXV DNA load, indicating higher infectivity in NPS samples with low Ct values (*16*). When analyzing semen samples, we obtained positive results for MPXV G2R-mRNA in only the 2 samples with the lowest MPXV DNA level, suggesting that this biologic fluid could represent a minor route in the context of sexual transmission, regardless of viral load. A possible explanation for the other 6 semen samples showing high MPXV DNA levels in the absence of viral replication (i.e., negative MPXV G2R-mRNA) could be a passive diffusion from skin lesions on the genitals or hands (*18*). In fact, when analyzing data coming from patient 1, we observed a lesion on the penis with a high viral load (Ct 22.2) and a clear positivity for the presence of G2R-mRNA, indicating active replication in that site. Nevertheless, semen from the same patient showed a high viral load (Ct 24.5), in the absence of active replication (negative G2R-mRNA), with negative urine samples, suggesting possible contamination of semen from a lesion on the penis.

In conclusion, the use of MPXV G2R-mRNA as a marker of replication enables discrimination between infected and contaminated samples, overcoming the problems related to viral isolation and providing an explanation for the difficulty encountered in isolating the virus from semen samples even with a high viral load (*17*). Despite the limited number of tested samples, our data support the evidence that sexual contact is the main route of sexual transmission, whereas semen samples can represent a minor driver of infection, independent of MPXV DNA load. This evidence is crucial to enable development of proper interventions and to provide valuable support for decision-making regarding protective measures for mpox patients and their close contacts.

This research was funded by Ministero della Salute: Ricerca Corrente—Linea 1.

Author contributions: G.S., molecular testing, analysis of results, writing; G.R., C.M., molecular testing; V.M., A.A., A.D.A., enrolling patients and editing; F.M., E.G., review and editing; E.L., L.B., conceptualization, writing, review,

and editing. The authors declare that they have no known competing financial interests or personal relationships that could have appeared to influence the work reported in this article.

About the Author

Dr. Sberna is a research scientist at the National Institute for Infectious Diseases Lazzaro Spallanzani, Rome, Italy. His primary research interests are HIV, viral infections, respiratory viruses, and chronic and emerging acute infections.

References

1. World Health Organization. Mpox (monkeypox). 2023 April 18 [cited 2023 Nov 20]. https://www.who.int/news-room/fact-sheets/detail/monkeypox
2. Thornhill JP, Barkati S, Walmsley S, Rockstroh J, Antinori A, Harrison LB, et al.; SHARE-net Clinical Group. Monkeypox virus infection in humans across 16 countries—April–June 2022. N Engl J Med. 2022;387:679–91. https://doi.org/10.1056/NEJMoa2207323
3. World Health Organization. Mpox (monkeypox) outbreak 2022—global. 2022 [cited 2023 Nov 20]. https://www.who.int/emergencies/situations/monkeypox-oubreak-2022
4. Antinori A, Mazzotta V, Vita S, Carletti F, Tacconi D, Lapini LE, et al.; INMI Monkeypox Group. Epidemiological, clinical and virological characteristics of four cases of monkeypox support transmission through sexual contact, Italy, May 2022. Euro Surveill. 2022;27:2200421. https://doi.org/10.2807/1560-7917.ES.2022.27.22.2200421
5. Lapa D, Carletti F, Mazzotta V, Matusali G, Pinnetti C, Meschi S, et al.; INMI Monkeypox Study Group. Monkeypox virus isolation from a semen sample collected in the early phase of infection in a patient with prolonged seminal viral shedding. Lancet Infect Dis. 2022;22:1267–9. https://doi.org/10.1016/S1473-3099(22)00513-8
6. Rosa RB, Ferreira de Castro E, Vieira da Silva M, Paiva Ferreira DC, Jardim ACG, Santos IA, et al. In vitro and in vivo models for monkeypox. iScience. 2023;26:105702. https://doi.org/10.1016/j.isci.2022.105702
7. Arndt WD, White SD, Johnson BP, Huynh T, Liao J, Harrington H, et al. Monkeypox virus induces the synthesis of less dsRNA than vaccinia virus, and is more resistant to the anti-poxvirus drug, IBT, than vaccinia virus. Virology. 2016;497:125–35. https://doi.org/10.1016/j.virol.2016.07.016
8. Condit RC, Xiang Y, Lewis JI. Mutation of vaccinia virus gene G2R causes suppression of gene A18R ts mutants: implications for control of transcription. Virology. 1996;220:10–9. https://doi.org/10.1006/viro.1996.0280
9. Colavita F, Mazzotta V, Rozera G, Abbate I, Carletti F, Pinnetti C, et al. Kinetics of viral DNA in body fluids and antibody response in patients with acute monkeypox virus infection. iScience. 2023;26:106102. https://doi.org/10.1016/j.isci.2023.106102
10. Meis RJ, Condit RC. Genetic and molecular biological characterization of a vaccinia virus gene which renders the virus dependent on isatin-beta-thiosemicarbazone (IBT). Virology. 1991;182:442–54. https://doi.org/10.1016/0042-6822(91)90585-Y
11. World Health Organization. 2022–23 mpox (monkeypox) outbreak: global trends 2022. 2024 February [cited 2024 Apr 24]. https://worldhealthorg.shinyapps.io/mpx_global
12. Tiecco G, Degli Antoni M, Storti S, Tomasoni LR, Castelli F, Quiros-Roldan E. Monkeypox, a literature review: what is new and where does this concerning virus come from? Viruses. 2022;14:1894. https://doi.org/10.3390/v14091894
13. Sah R, Abdelaal A, Reda A, Katamesh BE, Manirambona E, Abdelmonem H, et al. Monkeypox and its possible sexual transmission: where are we now with its evidence? Pathogens. 2022;11:924. https://doi.org/10.3390/pathogens11080924
14. Mahase E. Monkeypox: gay and bisexual men with high exposure risk will be offered vaccine in England. BMJ. 2022;377:o1542. https://doi.org/10.1136/bmj.o1542
15. Reda A, Abdelaal A, Brakat AM, Lashin BI, Abouelkheir M, Abdelazeem B, et al. Monkeypox viral detection in semen specimens of confirmed cases: a systematic review and meta-analysis. J Med Virol. 2023;95:e28250. https://doi.org/10.1002/jmv.28250
16. Paran N, Yahalom-Ronen Y, Shifman O, Lazar S, Ben-Ami R, Yakubovsky M, et al. Monkeypox DNA levels correlate with virus infectivity in clinical samples, Israel, 2022. Euro Surveill. 2022;27:2200636. https://doi.org/10.2807/1560-7917.ES.2022.27.35.2200636
17. Noe S, Zange S, Seilmaier M, Antwerpen MH, Fenzl T, Schneider J, et al. Clinical and virological features of first human monkeypox cases in Germany. Infection. 2023;51:265–70. https://doi.org/10.1007/s15010-022-01874-z
18. Reda A, Sah R, Rodriguez-Morales AJ, Shah J. Viral replication and infectivity of monkeypox through semen. Lancet Infect Dis. 2022;22:1531–2. https://doi.org/10.1016/S1473-3099(22)00611-9

Address for correspondence: Licia Bordi, Laboratory of Virology, National Institute for Infectious Diseases, Lazzaro Spallanzani IRCCS, Via Portuense 292, Rome 00149, Italy; email: licia.bordi@inmi.it

Molecular Epidemiology of Western Equine Encephalitis Virus, South America, 2023–2024

Aline Scarpellini Campos, Ana Claúdia Franco, Fernanda M. Godinho, Rosana Huff, Darlan S. Candido, Jader da Cruz Cardoso, Xinyi Hua, Ingra M. Claro, Paola Morais, Carolina Franceschina, Thales de Lima Bermann, Franciellen Machado dos Santos, Milena Bauermann, Tainá Machado Selayaran, Amanda Pellenz Ruivo, Cristiane Santin, Juciane Bonella, Carla Rodenbusch, José Carlos Ferreira, Scott C. Weaver, Vilar Ricardo Gewehr, Gabriel Luz Wallau, William M. de Souza,[1] Richard Steiner Salvato[1]

Western equine encephalitis virus (WEEV) is a mosquitoborne virus that reemerged in December 2023 in Argentina and Uruguay, causing a major outbreak. We investigated the outbreak using epidemiologic, entomological, and genomic analyses, focusing on WEEV circulation near the Argentina–Uruguay border in Rio Grande do Sul state, Brazil. During November 2023–April 2024, the outbreak in Argentina and Uruguay resulted in 217 human cases, 12 of which were fatal, and 2,548 equine cases. We determined cases on the basis of laboratory and clinical epidemiologic criteria. We characterized 3 fatal equine cases caused by a novel WEEV lineage identified through a nearly complete coding sequence analysis, which we propose as lineage C. Our findings highlight the importance of continued surveillance and equine vaccination to control future WEEV outbreaks in South America.

Western equine encephalitis virus (WEEV) is a mosquitoborne alphavirus that causes central nervous system (CNS) infection in humans and equids in the United States, Canada, and the southern cone of South America (*1*). WEEV is transmitted in enzootic and epizootic transmission cycles mainly by *Culex* and *Aedes* mosquitoes among birds and lagomorphs, which can lead to sporadic spillover to equids and humans (*2*,*3*). In humans, western equine encephalitis (WEE) infections are usually mild or asymptomatic, causing fever, headache, and myalgia (*4*). However, some patients experience encephalitis, which can be fatal in 5%–15% of cases (*5*). In equids, WEEV infection can cause neurologic disease (blindness, staggering, and seizures) with high case-fatality rates, often leading to death within days. As of July 2024, no specific treatments or vaccines are available to treat or prevent WEEV infection in humans; inactivated vaccines effectively prevent the disease in equids (*6*).

The largest WEEV outbreaks, which caused tens of thousands of equine and >3,000 human cases, were reported in the 1930s–1940s. However, <700 confirmed cases were reported in the United States after the 1960s, and none has been reported during the past 25 years (*1*,*4*). Similarly, major outbreaks occurred in South America during the 1970s and 1980s, followed by isolated cases in Argentina in 1996 and Uruguay in 2009 (*1*,*7*,*8*). In December 2023, a large WEEV reemergence began with a major outbreak in Argentina and Uruguay. In this study, we contextualize the WEEV outbreak in Argentina and Uruguay and investigate active WEEV circulation in Rio Grande do Sul, Brazil, a state bordering those countries.

Author affiliations: Secretaria de Saúde do Estado do Rio Grande do Sul, Porto Alegre, Brazil (A.S. Campos, F.M. Godinho, R. Huff, J. da Cruz Cardoso, P. Morais, C. Franceschina, F. Machado dos Santos, M. Bauermann, T.M. Selayaran, A.P. Ruivo, R.S. Salvato); Universidade Federal do Rio Grande do Sul, Porto Alegre (A.C. Franco, T. de L. Bermann, R.S. Salvato); Imperial College London, London, UK (D.S. Candido); University of Kentucky, Lexington, Kentucky, USA (X. Hua, I.M. Claro, W.M. de Souza); Secretaria de Agricultura do Estado do Rio Grande do Sul, Porto Alegre (C. Santin, J. Bonella, C. Rodenbusch, J.C. Ferreira, V.R. Gewehr); University of Texas Medical Branch, Galveston, Texas, USA (S.C. Weaver); Fundação Oswaldo Cruz, Recife, Brazil (G.L. Wallau); Bernhard Nocht Institute for Tropical Medicine, Hamburg, Germany (G.L. Wallau)

DOI: http://doi.org/10.3201/eid3009.240530

[1]These senior authors contributed equally to this article.

Materials and Methods

Epidemiologic Data

We obtained epidemiologic data of WEEV cases in equids and humans in Argentina and Uruguay from the Pan American Health Organization (*9*). The dataset included demographic and clinical characteristics and the aggregate number of human WEE cases in Argentina per epidemiologic week from epidemiologic week 43 (October 22–28) in 2023 to epidemiologic week 23 (June 2–8) in 2024. The equine WEE cases included laboratory-confirmed and suspected cases based on clinical or epidemiologic criteria.

Equine Samples

We performed molecular screening in brain tissue samples from fatal horse cases, which were submitted to the Center for Health Surveillance of Rio Grande do Sul State during January 1, 2023–April 10, 2024. All samples were stored at −80°C until testing (Appendix Table 1, https://wwwnc.cdc.gov/EID/article/30/9/24-0530-App1.pdf).

Entomologic Surveillance

We carried out entomologic surveillance in the Uruguaiana municipality in Rio Grande do Sul, focusing on 2 nearby horse breeding farms with a recent history of neurologic equine disease; we later confirmed 1 WEEV-positive case. We deployed 8 CDC light traps (John W. Hock Co., https://www.johnwhock.com) and 4 Biogents BG-Pro traps (Biogents, https://biogents.com) positioned at a height of 1.5 m above ground level, placed near horses and vegetation. We conducted mosquito sampling during 2 time periods at each site: a 24-hour period starting at 6 P.M. and a 12-hour period of 6 P.M.–6 A.M. We flash-froze captured mosquitoes, stored them in liquid nitrogen, and transported for storage at −80°C at the Rio Grande do Sul State Center for Health Surveillance in Porto Alegre. We identified mosquito species morphologically using standard keys (*10*,*11*). We pooled mosquitoes by species and date, ≤10 mosquitoes per pool. We amplified the cytochrome oxidase I gene by PCR and sequenced for the molecular identification of mosquito pools, following previously described methods (*12*) (Appendix Table 2).

PCR Testing for Viruses

We immersed brain tissue fragments (≈2 g/cm^3) in 800 μL of TRIzol reagent (ThermoFisher Scientific, https://www.thermofisher.com) and subjected to disruption using a Precellys 24 Touch (Thomas Scientific, https://www.thomassci.com). We immediately centrifuged the mixture to isolate the supernatant, from which we extracted viral RNA using the Extracta Kit Fast–DNA and RNA Viral (Loccus, https://www.loccus.com.br) according to the manufacturer's instructions. We homogenized the mosquito pool samples with 800 μL of phosphate-buffered saline and extracted RNA using Extracta Kit Fast–DNA and RNA Viral. We tested all extracted RNA by quantitative real-time reverse transcription PCR (rRT-PCR) targeting WEEV using the TaqMan RNA to-CT 1-Step Kit (ThermoFisher Scientific), as previously described (*13*). We performed reactions on a CFX Opus 96 Real-Time PCR System (Bio-Rad Laboratories, https://www.bio-rad.com). In addition, we screened the samples using rRT-PCR targeting eastern equine encephalitis (*13*), West Nile, St. Louis encephalitis (*14*), Mayaro, and Oropouche viruses (*15*) (Appendix Table 3). We also tested equine brain tissue samples for rabies viruses (*16*).

WEEV Genome Sequencing and Assembly

We conducted WEEV genome sequencing on 3 horse brain samples that tested positive by rRT-PCR. We achieved a near-complete genome using the hybrid–capture-based metagenomic approach enabled by Illumina Viral Surveillance Panel and RNA Prep with Enrichment kit (Illumina, https://www.illumina.com), according to the manufacturer's instructions. We sequenced VSP-enriched libraries on an Illumina MiSeq platform and processed the generated raw FASTQ files through the ViralFlow 1.0 pipeline (*17*) for assembly, using the 1971 Oregon WEEV strain 71V-1658 (GenBank accession no. NC_003908.1), as a reference genome.

Phylogenetic Analysis

We generated 3 novel WEEV genomes with >98% coverage and aligned them with WEEV strains with complete coding sequences that were available in the GenBank database as of June 10, 2024. We performed multiple sequence alignment (MSA) using MAFFT version 7.450 (https://mafft.cbrc.jp/alignment/software) as previously described (*18*) and conducted manual adjustment using Geneious Prime 2023.0.4 (https://www.geneious.com). We screened the dataset for recombination events using all available methods in RDP version 4 (https://rdp4.software.informer.com) (*19*). We generated a maximum-likelihood (ML) phylogeny tree using IQ-TREE version 2 (http://www.iqtree.org) under a general time-reversible plus invariable plus gamma model determined by ModelFinder (*20*,*21*). We used the ultrafast-bootstrap approach

with 1,000 replicates to determine the statistical support for nodes in the ML phylogeny (*22*). We estimated regressed root-to-tip genetic divergence against sampling dates to examine the temporal signal and identify sequences with low data quality of our datasets, such as assembly errors, sample contamination, data annotation errors, sequencing, and alignment errors (*23*). We identified no obvious outliers. We estimated the dated phylogenetic tree using BEAST version 1.10.4 (http://beast.community) under a general time-reversible plus invariable plus gamma model (*24*), an uncorrelated log-normal relaxed molecular clock (UCLD) model with an exponential rate distribution as previously described (*1*), and a Skygrid tree prior (*25*) with 102 grids with one grid every 2 years since the root of the tree. We used BEAGLE (http://beagle-lib.googlecode.com) to enhance computation speed (*26*). Last, we ran the evolutionary analyses independently in triplicate for 500 million steps, sampling parameters and trees every 50,000 steps. We generated maximum clade credibility summary trees using TreeAnnotator version 1.10.69 (https://beast.community/treeannotator) and visualized the phylogenetic tree by using Figtree version 1.4.2 (http://tree.bio.ed.ac.uk/software/figtree).

Results

During November 18, 2023–April 6, 2024, a major WEE outbreak occurred in Argentina and Uruguay, causing 112 human and 127 equine cases, all laboratory-confirmed (Figure 1, panel A). On the basis of clinical and epidemiologic criteria, Argentina also reported 68 suspected human cases and 1,481 suspected equine cases, and Uruguay documented 37 suspected human cases and 940 suspected equine cases. The WEE outbreak began in northeastern Argentina, spreading to central regions and Uruguay. In Argentina, 47 confirmed equine cases were reported across 17 of 23 provinces, peaking in epidemiologic week 49 of 2023 and declining sharply by epidemiologic week 8 of 2024. A total of 107 human WEE cases, including 12 fatal cases, were identified in 8 provinces of Argentina; 63/107 (58.9%) were concentrated in Buenos Aires Province, mirroring the highest equine case burden of 14/47 (29.8%) (Figure 1, panel A). The human outbreak peaked between epidemiologic week 51 of 2023 and epidemiologic week 3 of 2024; during that period, 58/107 (54.2%) of cases occurred. Available data show that the human WEE case-patients were predominantly male (male-to-female ratio 6.6:1), and 76/106 (71.7%) were ≥50 years of age. The most common symptoms were fever (82%), headache (76%),

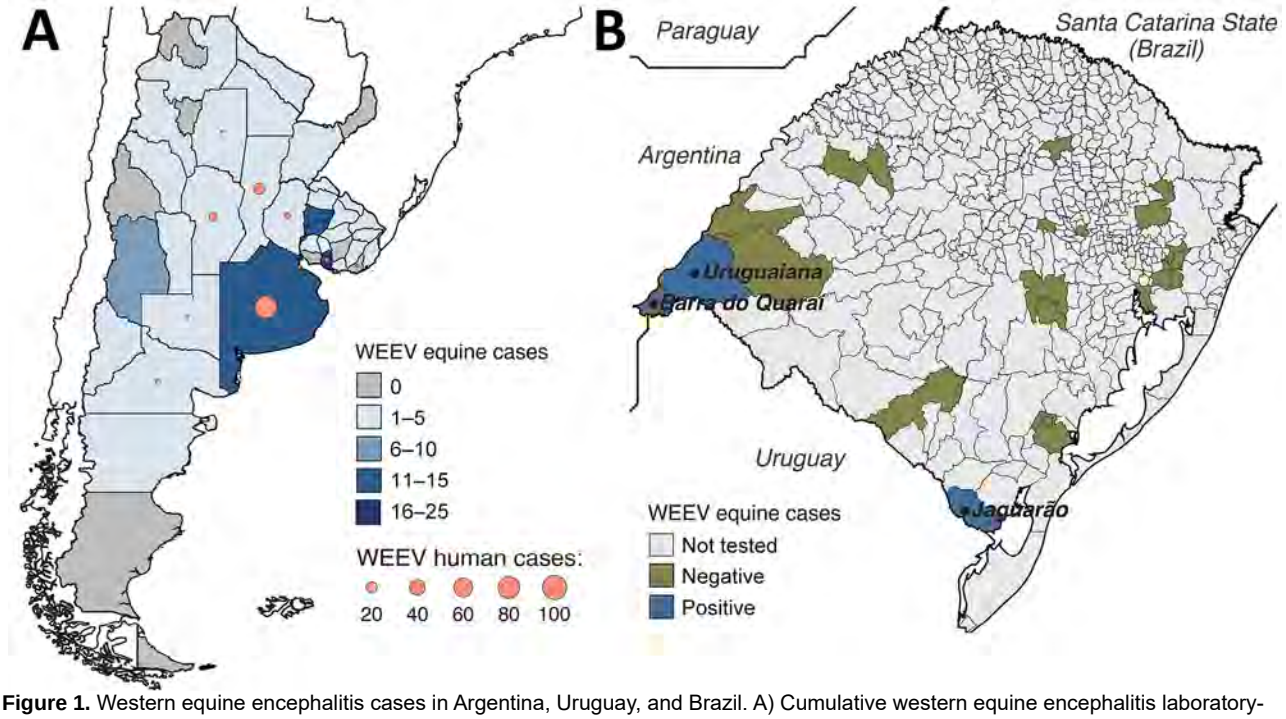

Figure 1. Western equine encephalitis cases in Argentina, Uruguay, and Brazil. A) Cumulative western equine encephalitis laboratory-confirmed cases in Argentina and Uruguay reported to the Pan American Health Organization (PAHO) during October 2023–June 2024 (*9*). B) Locations of deaths among horses in Rio Grande do Sul state, Brazil, that tested positive (blue) and negative (yellow) for WEEV by rT-PCR during December 2023–April 2024. The cases were identified by our molecular epidemiology study in Barra do Quaraí on December 21, 2023 (EQ1090), in Uruguaiana on December 28, 2023 (EQ1122), and in Jaguarão on January 30, 2024 (EQ237). WEEV, western equine encephalitis virus.

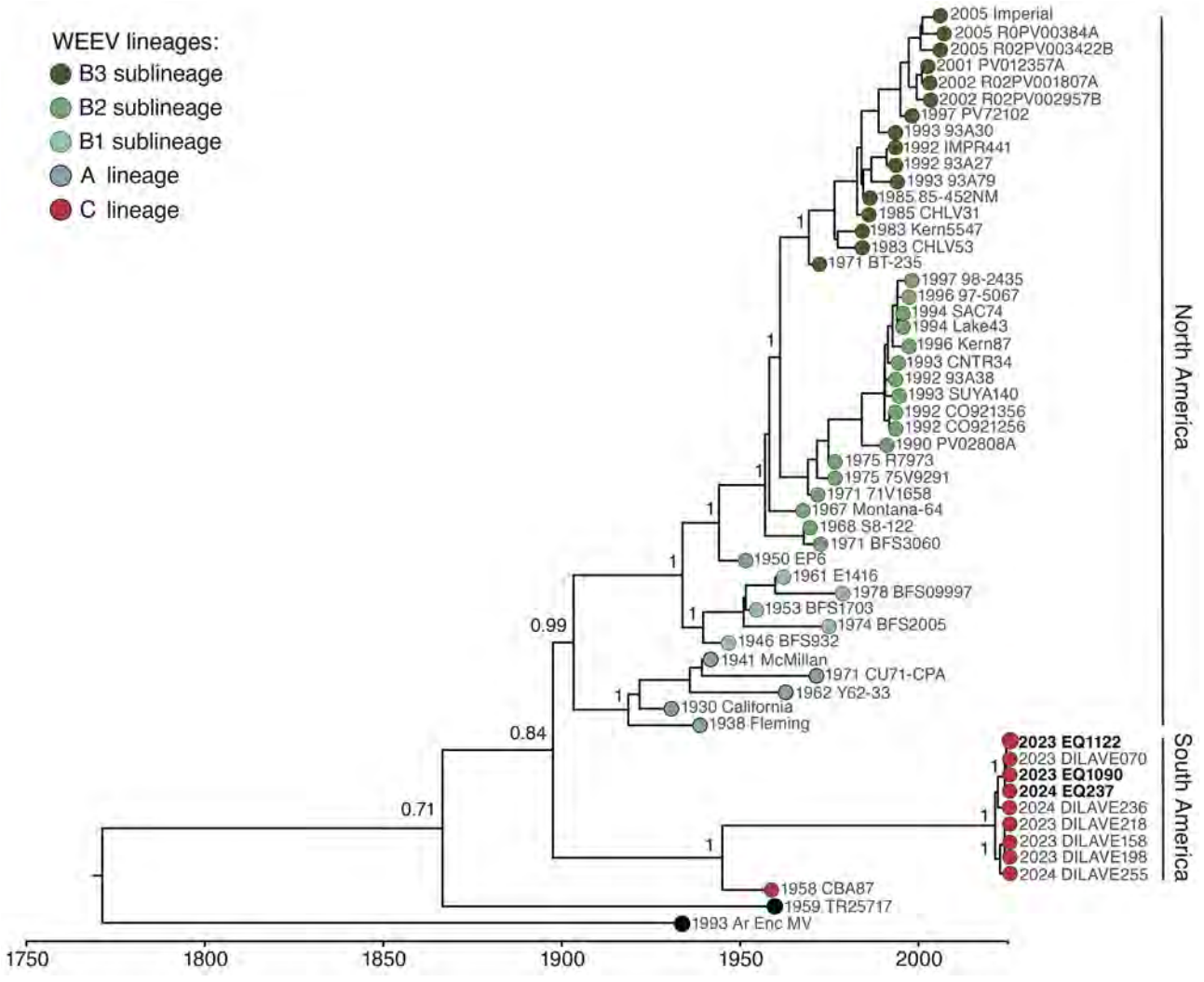

Figure 2. Maximum-likelihood phylogenetic tree of 3 new WEEV strains from Rio Grande do Sul state, Brazil (bold text), and reference sequences. Tip colors indicate WEEV lineage. We used an uncorrelated log-normal relaxed molecular clock model with an exponential rate distribution for generating the time-rooted tree. Posterior probability scores appear next to key well-supported nodes. Dates at key nodes are the estimated dates of divergence from a common ancestor, with Bayesian credible intervals. WEEV, western equine encephalitis virus.

and mental confusion (63%). Uruguay exhibited a similar pattern; the equine outbreak preceded human cases. The largest proportion of confirmed equine cases (28.8%, 23/80) occurred in San José Department, which also reported 3/5 confirmed human cases (Figure 1, panel A). No WEEV cases were reported in Argentina and Uruguay between epidemiologic week 15 of 2023 (April 7–14) and epidemiologic week 24 of 2024 (June 11–17).

During December 2023–April 2024, we conducted a molecular diagnostic and entomologic study to investigate the presence of WEEV in Rio Grande do Sul state, Brazil. In the entomologic surveillance, we captured 971 mosquitoes across 7 genera that were combined into 117 pools for further analysis (Appendix Table 2). The most prevalent genus was *Culex*, constituting 664/971 (68.4%) mosquitoes. All mosquito pools tested negative for WEEV, eastern equine encephalitis, West Nile, St. Louis encephalitis, Mayaro, and Oropouche viruses.

During January 1, 2023–April 10, 2024, we received brain samples from 31 fatal horse cases from 22/497 (4.4%) municipalities in Rio Grande do Sul. We tested 31 horse brain tissue samples by rRT-PCR and detected WEEV RNA in 3 (9.7%) with cycle threshold (Ct) values of 26–27 (Figure 1, panel B; Appendix Table 1). All 3 horses exhibited signs of neurologic disease (i.e., paralysis and incoordination) and none was vaccinated against WEEV. One horse was 2 months of age and died on December 21, 2023, in

Barra do Quaraí municipality; the second was 2 years of age and died December 28 in Uruguaiana municipality. Those municipalities are located on the Brazil border with Argentina and Uruguay. The third case was a 5-month-old horse that died on January 30, 2024, in Jaguarão municipality, on the Brazil–Uruguay border. In addition, those 3 fatal horse cases were positive for rabies virus by rRT-PCR; the etiologic cause of death remained inconclusive for the other 22 fatal horse cases (Appendix Table 1).

Next, we used Illumina sequencing to generate the nearly complete (≥98%) coding sequences for 3 WEEV strains with a mean depth of coverage of 606-fold/nt. We submitted sequences to GenBank (accession nos. PP544260, PP669617, and PP66961). The maximum-likelihood phylogenetic analysis showed that 3 WEEV strains circulating in the Rio Grande do Sul state in 2024 clustered together in a well-supported clade (posterior probability = 1) with 6 genome sequences of WEEV obtained from equine cases in Uruguay during the outbreak of 2023–2024 (Figure 2). That clade represents a novel WEEV lineage closely related to the 1958 CBA87 strain from Argentina, which we proposed as the C lineage (Figure 2). We confirmed that our genomic dataset had a strong temporal signal based on regression of genetic divergence from root-to-tip against sample collection dates (R_2 = 0.7763) (Figure 3, panel A). Those novel WEEV strains from Brazil shared 94.9–97.6% nucleotide identity with the 1958 CBA87 strain (Appendix Table 2). The time to the most recent common ancestor (tMRCA) for WEEV strains associated with the 2023–2024 outbreak in Brazil was estimated to be early 2019 (95% Bayesian credible interval early 2012 to mid-2022) with a mean evolutionary rate of 2.6 × 10^{-4} substitutions/nucleotide/year (UCLD, mean 2.6 × 10^{-4}, median: 2.6 × 10^{-4}; 95% height posterior density 1.8 × 10^{-4} – 3.5 × 10^{-4} substitutions/nucleotide/year). Using Skygrid reconstruction with a grid with an interval of 2 years based on tMRCA for all WEEV, we found an effective population size that has been decreasing between the late 1960s and 1980s (Figure 3, panel B). We found no evidence of recombination in WEEV strains of the C lineage.

Discussion

We contextualized the major WEE outbreak in South America in 2023–2024 and identified a new WEEV lineage associated with this outbreak from 3 fatal horse cases from Rio Grande do Sul, Brazil. The new lineage forms a distinct clade evolving independently for many decades from those circulating in North America (*1*,*4*,*27*). Our findings strongly suggest that WEEV has been circulating in South America since 2009 with cases likely unreported. We hypothesize 2 complementary explanations for the lack of reported WEE cases from April 2009–November 2023 in South America: limited enzootic circulation of the WEEV between vectors and resident/migratory birds, or a lack of WEEV surveillance, particularly in rural or remote areas, where cases might go undetected. The WEE outbreak in South America appears to have ended in April 2024, when the last case was reported. This cessation of cases may be due to the increased or mandatory immunization of horses against WEE in Argentina, Uruguay, and Brazil. Widespread equine

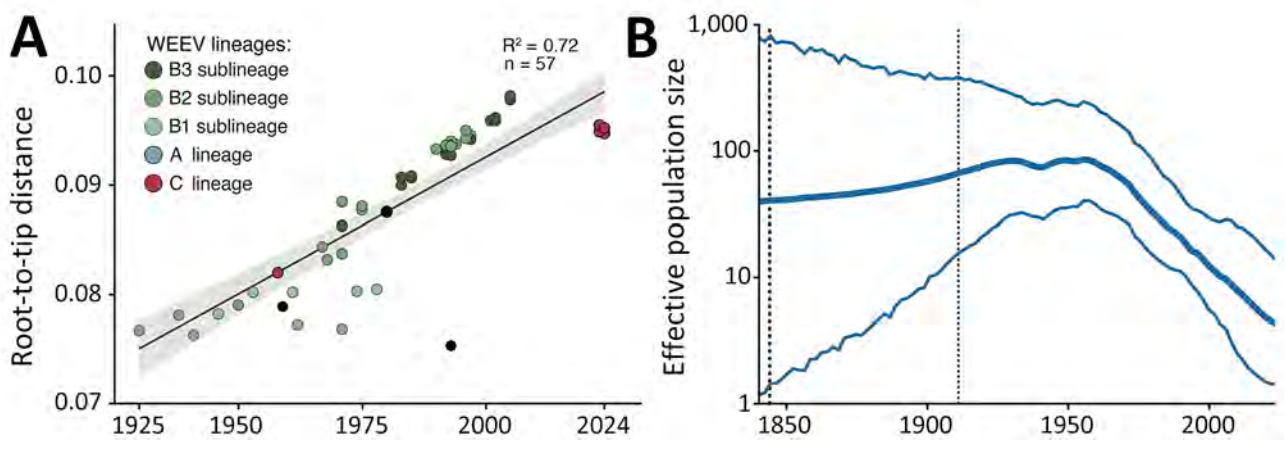

Figure 3. Phylogenetic analysis of WEEV strains from Rio Grande do Sul state, Brazil, and reference sequences. A) Regression of sequence sampling dates against root-to-tip genetic distances in a maximum likelihood phylogeny of the WEEV strains. Sequences are colored according to geographic source. Line indicates the correlation; shading indicates 95% CIs. B) Effective population size of WEEV through time using the Skygrid model. Thin blue lines represent 95% Bayesian credibility interval, and the thick blue line represents the posterior median. Vertical dotted lines indicate the best estimates for the time of the root of the tree (left) and the upper highest posterior density (right). WEEV, western equine encephalitis virus.

immunization in the region may contribute to suppressing WEEV re-emergence in the near future.

Some experimental murine model studies indicate reduced virulence of recent WEEV isolates (B3 strains) compared with earlier isolates (A, B1, B2 strains), which could explain decreased human and equine cases in North America (*1*,*4*,*28*). Alternatively, the lack of reported WEE cases in North America since 1999 may a result of WEEV's silent or underreported circulation, because WEEV continued to be detected in mosquitoes during 2004–2007 (*29*). In contrast, the large numbers of neurologic and fatal cases in humans and equids in Argentina, Brazil, and Uruguay in 2023–2024 suggest that contemporary WEEV strains circulating in South America might be more virulent than those currently circulating in North America. Further research is needed to elucidate the virulence determinants that might explain this apparent difference between WEEV lineages from South and North America.

The first limitation of our study is that we focused on identifying active WEEV infections using molecular methods only in fatal horse cases. Horses with mild signs of disease should also be tested. Also, age-stratified serologic studies are needed to determine the extent of previous WEEV exposure in the equine and human populations, and patterns of past infections. Second, we did not detect WEEV RNA in any mosquitoes, which may be explained by the generally low (e.g., <1%) arbovirus infection rates observed in mosquitoes, even during outbreaks, and including WEEV. For instance, 0.02% (55/271,889) of mosquitoes captured in California, USA, during 2004–2013 were positive for WEEV by rRT-PCR (*29*). Also, our entomologic investigation showed that *Culex* spp. were the most abundant mosquito species in the region; further studies with an emphasis on *Culex* spp. mosquitoes, as well as the *Aedes albifasciatus* mosquito, a previously incriminated WEEV vector (*3*,*30*), are needed to better understand the transmission dynamics of WEEV in South America. Third, we were unable to determine whether ecologic drivers were associated with the current outbreaks, but further studies should investigate climate factors, anthropogenic changes, and migratory bird routes and activity (*31*).

In conclusion, our study identified active WEEV circulation in Rio Grande do Sul, Brazil, and a novel viral lineage associated with fatal cases in horses. These findings highlight the critical need for continuous laboratory diagnosis and surveillance for WEEV in both horses and humans, as well as ecologic studies using a One Health approach to better understand the transmission dynamics and ecologic drivers contributing to WEEV re-emergence in South America. Finally, horse immunization should be considered to mitigate the effect on animal health.

This article was preprinted at https://www.medrxiv.org/content/10.1101/2024.04.15.24305848v1.

This study was supported by Fundação de Amparo à Pesquisa do Estado do Rio Grande do Sul and the Fundação Oswaldo Cruz (grant no. 23/2551-0000510-7). R.S.S was supported by National Council for Scientific and Technological Development (CNPq) and Fundação de Amparo à Pesquisa do Estado do Rio Grande do Sul (grant no. 07/2022). G.L.W. had support from a CNPq–1D productivity research fellowship (307209/2023-7). W.M.dS. was supported by Burroughs Wellcome Fund (grant no. 1022448), and Wellcome Trust–Digital Technology Development award (Climate Sensitive Infectious Disease Modelling; 226075/Z/22/Z). S.C.W. was supported by National Institutes of Health (grant nos. AI12094, U01AI151801, and AI121452).

About the Author

Dr. Campos is a public health specialist at the State Health Surveillance Center of Rio Grande do Sul, Brazil. Her research interests include surveillance, investigation, and countermeasures of zoonotic and vectorborne diseases.

References

1. Bergren NA, Auguste AJ, Forrester NL, Negi SS, Braun WA, Weaver SC. Western equine encephalitis virus: evolutionary analysis of a declining alphavirus based on complete genome sequences. J Virol. 2014;88:9260–7. https://doi.org/10.1128/JVI.01463-14
2. Calisher CH, Monath TP, Mitchell CJ, Sabattini MS, Cropp CB, Kerschner J, et al. Arbovirus investigations in Argentina, 1977–1980. Am J Trop Med Hyg. 1985;34:956–65. https://doi.org/10.4269/ajtmh.1985.34.956
3. Avilés G, Sabattini MS, Mitchell CJ. Transmission of western equine encephalomyelitis virus by Argentine *Aedes albifasciatus* (Diptera: Culicidae). J Med Entomol. 1992;29:850–3. https://doi.org/10.1093/jmedent/29.5.850
4. Bergren NA, Haller S, Rossi SL, Seymour RL, Huang J, Miller AL, et al. "Submergence" of Western equine encephalitis virus: evidence of positive selection argues against genetic drift and fitness reductions. PLoS Pathog. 2020;16:e1008102. https://doi.org/10.1371/journal.ppat.1008102
5. Cohen R, O'Connor RE, Townsend TE, Webb PA, McKey RW. Western equine encephalomyelitis; clinical observations in infants and children. J Pediatr. 1953;43:26–34. https://doi.org/10.1016/S0022-3476(53)80084-3
6. Bartelloni PJ, McKinney RW, Calia FM, Ramsburg HH, Cole FE Jr. Inactivated western equine encephalomyelitis vaccine propagated in chick embryo cell culture. Am J Trop Med Hyg. 1971;20:146–9. https://doi.org/10.4269/ajtmh.1971.20.146

7. Avilés G, Bianchi TI, Daffner JF, Sabattini MS. Post-epizootic activity of Western equine encephalitis virus in Argentina [in Spanish]. Rev Argent Microbiol. 1993;25:88–99.
8. Delfraro A, Burgueño A, Morel N, González G, García A, Morelli J, et al. Fatal human case of Western equine encephalitis, Uruguay. Emerg Infect Dis. 2011;17:952–4. https://doi.org/10.3201/eid1705.101068
9. Pan American Health Organization. Western equine encephalitis in the Region of the Americas [in Spanish]. 2024 [cited 27 Jul 2024]. https://shiny.paho-phe.org/encephalitis
10. Consoli RAGB, Lourenço de Oliveira R. Main mosquitoes of health importance in Brazil [in Portuguese]. 2nd edition. Rio de Janeiro: FIOCRUZ; 1998.
11. Forattini OP. Medical culicidology. Vol 2. Identification, biology, epidemiology. Sao Paulo: University of Sao Paulo; 2002.
12. Muñoz-Gamba AS, Laiton-Donato K, Perdomo-Balaguera E, Castro LR, Usme-Ciro JA, Parra-Henao G. Molecular characterization of mosquitoes (Diptera: Culicidae) from the Colombian rainforest. Rev Inst Med Trop São Paulo. 2021;63:e24. https://doi.org/10.1590/s1678-9946202163024
13. Lambert AJ, Martin DA, Lanciotti RS. Detection of North American eastern and western equine encephalitis viruses by nucleic acid amplification assays. J Clin Microbiol. 2003;41:379–85. https://doi.org/10.1128/JCM.41.1.379-385.2003
14. Lanciotti RS, Kerst AJ. Nucleic acid sequence-based amplification assays for rapid detection of West Nile and St. Louis encephalitis viruses. J Clin Microbiol. 2001;39:4506–13. https://doi.org/10.1128/JCM.39.12.4506-4513.2001
15. Naveca FG, Nascimento VAD, Souza VC, Nunes BTD, Rodrigues DSG, Vasconcelos PFDC. Multiplexed reverse transcription real-time polymerase chain reaction for simultaneous detection of Mayaro, Oropouche, and Oropouche-like viruses. Mem Inst Oswaldo Cruz. 2017;112:510–3. https://doi.org/10.1590/0074-02760160062
16. Wadhwa A, Wilkins K, Gao J, Condori Condori RE, Gigante CM, Zhao H, et al. A pan-lyssavirus Taqman real-time RT-PCR assay for the detection of highly variable rabies virus and other lyssaviruses. PLoS Negl Trop Dis. 2017;11:e0005258. https://doi.org/10.1371/journal.pntd.0005258
17. Dezordi FZ, Neto AMDS, Campos TL, Jeronimo PMC, Aksenen CF, Almeida SP, et al.; Fiocruz COVID-19 Genomic Surveillance Network. ViralFlow: a versatile automated workflow for SARS-CoV-2 genome assembly, lineage assignment, mutations and intrahost variant detection. Viruses. 2022;14:217. https://doi.org/10.3390/v14020217
18. Katoh K, Standley DM. MAFFT multiple sequence alignment software version 7: improvements in performance and usability. Mol Biol Evol. 2013;30:772–80. https://doi.org/10.1093/molbev/mst010
19. Martin DP, Murrell B, Golden M, Khoosal A, Muhire B. RDP4: detection and analysis of recombination patterns in virus genomes. Virus Evol. 2015;1:vev003. https://doi.org/10.1093/ve/vev003
20. Minh BQ, Schmidt HA, Chernomor O, Schrempf D, Woodhams MD, von Haeseler A, Lanfear R. IQ-TREE 2: new models and efficient methods for phylogenetic inference in the genomic era. Mol Biol Evol. 2020;37:1530–4.
21. Kalyaanamoorthy S, Minh BQ, Wong TKF, von Haeseler A, Jermiin LS. ModelFinder: fast model selection for accurate phylogenetic estimates. Nat Methods. 2017;14:587–9. https://doi.org/10.1038/nmeth.4285
22. Hoang DT, Chernomor O, von Haeseler A, Minh BQ, Vinh LS. UFBoot2: improving the ultrafast bootstrap approximation. Mol Biol Evol. 2018;35:518–22. https://doi.org/10.1093/molbev/msx281
23. Rambaut A, Lam TT, Max Carvalho L, Pybus OG. Exploring the temporal structure of heterochronous sequences using TempEst (formerly Path-O-Gen). Virus Evol. 2016;2:vew007. https://doi.org/10.1093/ve/vew007
24. Suchard MA, Lemey P, Baele G, Ayres DL, Drummond AJ, Rambaut A. Bayesian phylogenetic and phylodynamic data integration using BEAST 1.10. Virus Evol. 2018;4:vey016. https://doi.org/10.1093/ve/vey016
25. Gill MS, Lemey P, Faria NR, Rambaut A, Shapiro B, Suchard MA. Improving Bayesian population dynamics inference: a coalescent-based model for multiple loci. Mol Biol Evol. 2013;30:713–24. https://doi.org/10.1093/molbev/mss265
26. Ayres DL, Darling A, Zwickl DJ, Beerli P, Holder MT, Lewis PO, et al. BEAGLE: an application programming interface and high-performance computing library for statistical phylogenetics. Syst Biol. 2012;61:170–3. https://doi.org/10.1093/sysbio/syr100
27. Weaver SC, Kang W, Shirako Y, Rumenapf T, Strauss EG, Strauss JH. Recombinational history and molecular evolution of western equine encephalomyelitis complex alphaviruses. J Virol. 1997;71:613–23. https://doi.org/10.1128/jvi.71.1.613-623.1997
28. Mossel EC, Ledermann JP, Phillips AT, Borland EM, Powers AM, Olson KE. Molecular determinants of mouse neurovirulence and mosquito infection for Western equine encephalitis virus. PLoS One. 2013;8:e60427. https://doi.org/10.1371/journal.pone.0060427
29. Brault AC, Fang Y, Reisen WK. Multiplex qRT-PCR for the detection of western equine encephalomyelitis, St. Louis encephalitis, and West Nile viral RNA in mosquito pools (Diptera: Culicidae). J Med Entomol. 2015;52:491–9. https://doi.org/10.1093/jme/tjv021
30. Cardoso J, Corseuil E, Barata JMS. Culicinae (Diptera, Culicidae) occurring in the state of Rio Grande do Sul, Brasil [in Portuguese]. Revista Brasileira de Entomologia. 2005;49:275–87. https://doi.org/10.1590/S0085-56262005000200013
31. de Souza WM, Weaver SC. Effects of climate change and human activities on vector-borne diseases. Nat Rev Microbiol. 2024. https://doi.org/10.1038/s41579-024-01026-0

Address for correspondence: William M. de Souza, University of Kentucky, Microbiology, Immunology and Molecular Genetics, 760 Press Ave, Lexington, KY 40508, USA; email: wmdesouza@uky.edu; and Richard Steiner Salvato, Secretaria de Saude do Estado do Rio Grande do Sul, Porto Alegre, Rio Grande do Sul, Brazil; email: richardssalvato@gmail.com

Medical Costs of Nontuberculous Mycobacterial Pulmonary Disease, South Korea, 2015–2019

Shihwan Chang,[1] Sol Kim,[1] Young Ae Kang, Moo Suk Park, Hojoon Sohn,[2] Youngmok Park[2]

Nontuberculous mycobacterial pulmonary disease (NTM-PD) prevalence is a rising public health concern. We assessed the long-term healthcare systems perspective of costs incurred by 147 NTM-PD patients at a tertiary hospital in South Korea. Median cumulative total medical cost in managing NTM-PD patients was US $5,044 (interquartile range US $3,586–$9,680) over 49.7 months (interquartile range 33.0–68.2 months) of follow-up. The major cost drivers were diagnostic testing and medication, accounting for 59.6% of total costs. Higher costs were associated with hospitalization for *Mycobacterium abscessus* infection and pulmonary comorbidities. Of the total medical care costs, 50.2% were patient co-payments resulting from limited national health insurance coverage. As South Korea faces significant problems of poverty during old age and increasing NTM-PD prevalence, the financial and socio-economic burden of NTM-PD may become a major public health concern that should be considered with regard to adequate strategies for NTM-PD patients.

Nontuberculous mycobacteria pulmonary disease (NTM-PD) is a chronic respiratory condition of growing concern. Its management is often complicated by multiple biological, clinical, healthcare-associated, and patient factors. Increased NTM infection can be attributed to the widespread presence of NTM in the environment, multiple transmission routes, and insufficient preventive measures (*1*). Diagnosing NTM-PD alone does not require immediate treatment (*2*), often resulting in a period of medical observation before treatment initiation. Eradication of NTM is further challenged by lengthy treatment, lack of effective treatment regimens, antimicrobial resistance, adverse reactions to treatment, and low adherence to therapeutic guidelines (*2*–*5*). Unfavorable treatment outcomes and frequent recurrence necessitate continued observation even after treatment completion (*6*,*7*). By increasing the NTM-PD disease burden (*1*,*3*,*8*,*9*), such issues pose considerable financial strain for healthcare systems and patients.

Among earlier studies evaluating the NTM-PD burden, only a few reviewed the costs associated with NTM-PD (*10*,*11*). A 2017 study in Germany reported a nearly 4-fold increase in the mean direct medical expenditure for patients with NTM-PD compared with those who had never had NTM-PD (*12*). A 2020 study in Canada estimated that NTM-PD management required an annual mean cost of US $11,541 (*13*). Regardless of between-country differences in costs associated with NTM-PD, evidence suggests that NTM-PD poses a substantial cost burden from the healthcare provider perspective (*14*).

To better elucidate the cost burdens associated with NTM-PD, we analyzed the medical costs incurred by patients with NTM-PD in South Korea. Furthermore, we aimed to determine the distribution of costs over the follow-up period and the effects of causative NTM species or pulmonary comorbidities on the costs. Our study was approved by the Institutional Review Board of Severance Hospital (4-2021-1663), with an informed consent waiver considering its retrospective design.

Methods

We retrospectively reviewed electronic health records (EHRs) and institution billing records (IBRs) of patients who had NTM-PD during 2015–2019 in Severance Hospital, a tertiary referral hospital in South Korea. We restricted the review of medical cost

Author affiliations: Yonsei University College of Medicine, Seoul, South Korea (S. Chang, S. Kim, Y.A. Kang, M.S. Park, Y. Park), Severance Hospital, Seoul (S. Chang, S. Kim, Y.A. Kang, M.S. Park, Y. Park), Seoul National University College of Medicine, Seoul (H. Sohn), Seoul National University Institute of Health Policy and Management, Seoul (H. Sohn)

DOI: https://doi.org/10.3201/eid3009.231448

[1]These first authors contributed equally to this article.

[2]These authors were co–principal investigators.

data to patients who had initiated and completed ≥12 months of NTM-PD treatment before February 2022 (Figure 1). We did not analyze costs incurred by healthcare services provided by or prescribed from institutions other than Severance Hospital.

We extracted patient-level data from the EHR on clinical history, laboratory and imaging tests, prescribed treatment regimens, treatment outcomes, and fee-for-service costs for all relevant medical procedures and care services used by the included patients leading up to February 28, 2022. For costs that could not be ascertained from the IBRs (e.g., medications or health services prescribed from Severance Hospital but received from elsewhere), we referenced the Korean Health Insurance Review and Assessment Service catalog for unit cost/prices (as of January 2019) to calculate estimated total medical costs (*15*). We based the definition of direct medical out-of-pocket costs on patient co-payment amount assessed for each health service used, estimated by the cost ceilings for each item defined by the National Health Insurance Service (NHIS, https://www.nhis.or.kr) (Appendix Table 1, https://wwwnc.cdc.gov/EID/article/30/9/23-1448-App1.pdf).

To categorize hospital visits related to NTM-PD management, we divided the follow-up period into 4 periods: prediagnostic, pretreatment, treatment, and post-treatment (Figure 2). We defined the treatment period as the first uninterrupted NTM-PD treatment documented in the EHR.

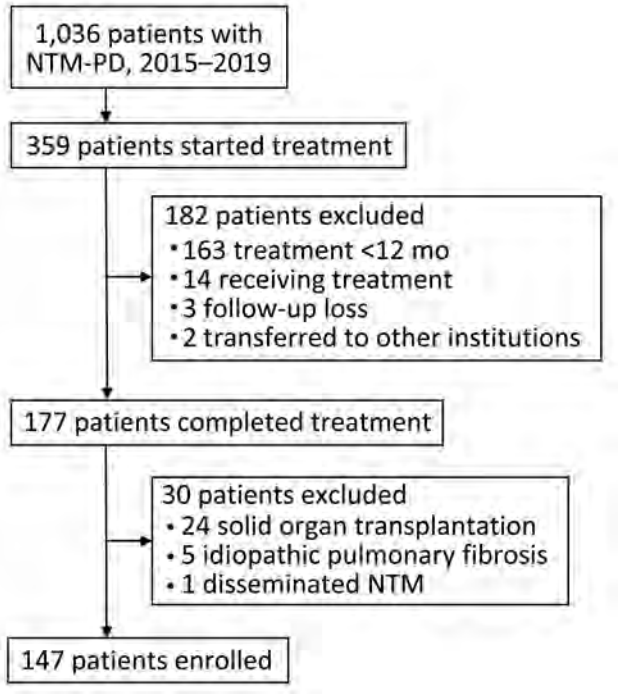

Figure 1. Patient selection for study of medical costs of nontuberculous mycobacterial pulmonary disease, South Korea, 2015–2019. NTM, nontuberculous mycobacteria; PD, pulmonary disease.

All costs were assessed from the healthcare system perspective, which includes costs associated with patient co-payments (Table 1). Cumulative per-patient cost was defined as the total costs incurred at all NTM-PD–related visits over the entire follow-up period. Cost assessments were further categorically based on each period of follow-up, type of visit, and medical services. Subgroup analyses were based on NTM species, presence of pulmonary comorbidities, and type of services received (hospital admission, surgical treatment, and management of treatment complications).

All costs were assessed as 2019 United States dollars (US $), based on the mean exchange rate for South Korean won and US $ (1,165.69 won/US $1) and adjusted for the medical consumer price index and a 3% discount rate for costs incurred before 2019 (*16*,*17*). For all statistical analyses, we used SPSS Statistics 23 (IBM, https://www.ibm.com) and a 2-tailed significance level of 0.05.

Results

Patient Selection and Baseline Characteristics

Of the 1,036 patients with NTM-PD and IBRs for 2015–2019, we included 147 in the final analysis (Figure 1). Median participant age was 61.0 years (interquartile range [IQR] 54.0–66.0 years), 100 (68.0%) participants were female and 47 (32%) were male, and 5 (3.4%) participants had previously received treatment for NTM-PD (Table 2).

From the index date, the median follow-up duration of our cohort was 49.7 months (IQR 33.0–68.2 months) and median treatment duration was 14.8 months (IQR 13.3–18.4 months). Over the entire follow-up period, 71 (48.3%) patients were admitted for NTM-PD ≥1 time.

Overall Per-Patient Medical Costs

The median per-patient cumulative total cost for NTM-PD treatment was US $5,044 (IQR $3,586–$9,680), or US $1,319 annually (Table 3; Appendix Table 2). Patients incurred a median out-of-pocket cost of US $2,535, which accounted for 50.2% of the total cost. For outpatient visits, patients with NTM-PD incurred a median total cost of US $3,863 (IQR $2,969–$5,333), or US $965 annually per patient. The 71 patients admitted for NTM-PD were hospitalized for a median of 9 days (IQR 3–30 days), incurring a median

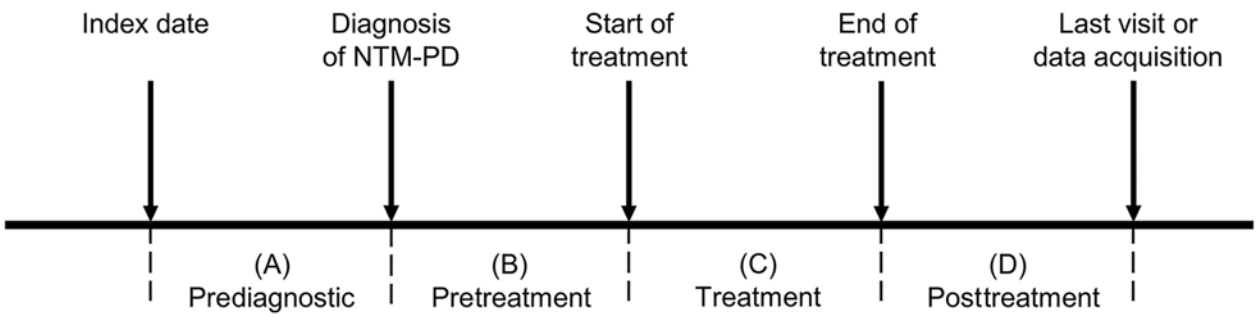

Figure 2. Diagnostic and treatment timeline for study of medical costs of nontuberculous mycobacterial pulmonary disease, South Korea, 2015–2019. The index date was defined as the date of the first pulmonology visit in which the physician initially evaluated the patient for NTM-PD. NTM, nontuberculous mycobacteria; PD, pulmonary disease.

total admission cost of US $5,620 (IQR $1,296–$9,186), or US $1,146 annually (Appendix Table 3).

Patients with any history of hospitalization for NTM-PD–related treatment (median US $9,429) incurred a median total cost 2.5 times greater than those without (median US $3,773) (Appendix Table 4). However, costs for outpatient visits did not differ between both groups, suggesting that hospitalization costs were the main driver of increased medical cost for this patient group.

The median cumulative cost during the overall follow-up period was US $5,470 (IQR $3,613–$9,914) (Table 4; Figure 3; Appendix Table 5). The median per-patient cost was highest during the treatment period (US $2,108), followed by the pretreatment (US $616) and post-treatment (US $451) periods. Costs per patient were lowest for the prediagnostic period (US $425). Medical costs sharply increased approximately 6 months before treatment initiation, peaking during the first 3 months. Costs gradually decreased approximately 1 year after treatment initiation (Appendix Figure 1).

By types of medical services, costs for diagnostic tests shared the highest cumulative (59.6%, US $3,006), outpatient (59.1%, US $2,282), and admission (54.3%, US $1,590) costs over the entire follow-up period (Table 3). Diagnostic tests consistently accounted for the highest costs in any follow-up period (Table 4, Figure 3). Medication costs accounted for the second largest proportion of the cumulative costs for the entire follow-up period (23.7%, US $1,197) and for those incurred only during treatment (38.6%, US $814) but not in all other periods.

Subgroup Analyses and Patient-Level Cost Drivers

When comparing costs by the 2 major NTM species, the overall duration of follow-up was longer for the 112 patients treated for *M. avium* complex (MAC) infection (median 51.4 months) than for the 15 treated for *M. abscessus* infection (median 33.1 months);

Table 1. Definitions of visits related to NTM-PD and assessment costs based on category and relevance of treatment used in study of medical costs of NTM-PD, South Korea, 2015–2019*

Variable	Examples
Category	
Medications	All medications, all fees for drug administration (i.e., intravenous access) and dispensing
Diagnostic tests	Acid fast bacilli smear/cultures, NTM identification, NTM drug-susceptibility tests, laboratory tests using patient specimen (i.e., complete blood count, blood chemistry, urinalysis), imaging studies (e.g., computed tomography, radiography), pulmonary function tests, induced sputum, invasive procedures (e.g., bronchoscopy, radiologic intervention)
Clinical services	Doctors' fees for admission, outpatient visits, and consultation; hospital fees; meals during admission; fees for documentation
Relevance to NTM-PD	
Direct	Antibiotics for NTM-PD treatment, acid fast bacilli smear/cultures, NTM identification, NTM drug-susceptibility tests, laboratory studies for diagnosis and treatment of NTM, surgical management of NTM
Indirect	Medications for symptom control (i.e., cough, sputum, hemoptysis); medications for management of adverse events associated with NTM management; antibiotics and medications for management of pulmonary comorbidities; laboratory studies for all NTM-PD-related visits, unless categorized as direct-related; medical expenses for all NTM-PD-related visits
Unrelated	Costs of management of nonpulmonary comorbidities (i.e., hypertension, diabetes mellitus)

*NTM-PD-related visits were defined as all visits to the pulmonology department and nonpulmonology visits, including outpatient referrals for management of adverse events during NTM-PD treatment, consultations during admissions for NTM-PD management, and visits for surgical management of NTM-PD. Non-NTM-PD–related visits defined as all nonpulmonology visits that do not fit the criteria for an NTM-PD-related visit (i.e., visits for hypertension). NTM, nontuberculous mycobacteria; PD, pulmonary disease.

p = 0.006). All 15 patients with *M. abscessus* infection had been admitted for NTM-PD treatment, experiencing ≥2 hospitalizations that resulted in total stays of 33 days (IQR 28–62 days). Nearly 40.2% of patients with MAC infection were admitted for a median duration of 5 days (IQR 2–10 days) (Appendix Table 6). Likewise, median medical costs incurred by patients with *M. abscessus* infection (US $19,190) were higher than those incurred by patients with MAC infection (US $4,557; p<0.001) (Table 5; Appendix Tables 7, 8); the main driver of the cost difference between the groups was admission costs.

Regarding patient-level factors, the number of outpatient and admission visits, total length of stay, and death associated with *M. abscessus* infection (compared with MAC infection) were associated with increased total medical care costs for NTM-PD (Appendix Table 9). Multiple linear regression results revealed that the number of admissions and *M. abscessus* infections (compared with MAC infections) were positively associated with the total medical cost (i.e., more admissions and *M. abscessus* infections increased costs), whereas culture conversion was associated with decreased total cost (Table 6).

Table 2. Baseline characteristics of participants in study of medical costs of nontuberculous mycobacterial pulmonary disease, South Korea, 2015–2019*

Variable	Total, n = 147
Age at diagnosis, y, median (IQR)	61.0 (54.0–66.0)
Female	100 (68.0)
Comorbidity	
History of tuberculosis	29 (19.7)
History of NTM treatment	5 (3.4)
Bronchiectasis	36 (24.5)
Chronic obstructive pulmonary disease	21 (14.3)
Asthma	11 (7.5)
Lung cancer	3 (2.0)
History of thoracic operation	12 (8.2)
Hypertension	10 (6.8)
Diabetes mellitus	6 (4.1)
Other malignancy	17 (11.6)
Causative species	
M. avium complex	112 (76.2)
M. abscessus	15 (10.2)
M. kansasii	10 (6.8)
M. fortuitum	2 (1.4)
Other†	8 (5.4)
Duration, mo, median (IQR)	
Total duration of follow-up	49.7 (33.0–68.2)
Prediagnostic	0.2 (0.0–2.2)
Pretreatment	3.5 (1.9–8.2)
Treatment	14.8 (13.3–18.4)
Post-treatment	19.5 (9.6–35.6)
No. outpatient visits, median (IQR)	23.0 (18.0–33.0)
No. admissions, n = 71, median (IQR)	1.0 (1.0–2.0)
Length of stay per admission, d, median (IQR)	6.0 (2.0–15.5)
Total length of stay, d, median (IQR)	9.0 (3.0–30.0)
Treatment outcome	
Culture conversion	115 (78.2)
Microbiologic cure	101 (68.7)
Retreatment for recurrence	13 (8.8)
All-cause mortality	6 (4.1)

*Data are presented as no. (%) patients except as indicated. NTM, nontuberculous mycobacteria.
†Includes mixed infections.

Out-of-Pocket Costs

Patients incurred a median out-of-pocket cost of US $2,535 (Table 3), accounting for 50.2% of the cumulative cost. The co-payment for outpatient visits and admissions was 55% (median US $2,124) and 26.6% (median US $1,494) of the cumulative costs for the respective visits. Similar to the patterns observed for cumulative costs, out-of-pocket costs over the follow-up period indicated that the highest co-payment was observed for the treatment period (US $1,029), followed by the pretreatment (US $359) and post-treatment (US $287) periods (Table 4; Figure 3).

Discussion

Our report of comprehensive and detailed NTM-PD medical care costs in South Korea indicates that each patient with NTM-PD incurred a total cost of US $5,044 over a median follow-up period of 49.7 months, which translates to a median annual cost of US $1,319. Restricting analysis to the 87 patients with complete follow-up data brings the total median cost slightly higher, to US $5,470. Our analyses revealed that most NTM-PD–associated medical services were not fully covered through the Korean NHIS, resulting in a median out-of-pocket cost accounting for 50.2% (US $2,535) of the total care costs. Most (66.4%) of the total NTM-PD medical costs were incurred between 6 months before and 1 year after treatment initiation. The largest share of the total medical costs during the entire follow-up period was costs associated with diagnostic tests. Medical costs were higher for patients with *M. abscessus* infection and those with pulmonary comorbidities because of more frequent hospital visits and more extended hospitalizations.

In earlier studies evaluating medical costs of pulmonary infections in South Korea, medical costs for NTM-PD were considerably higher than those for asthma (US $267, reported in 2017) and drug-susceptible tuberculosis (US $754, reported in 2022) and were comparable to the costs for treating and managing tuberculosis-destroyed lungs (US $1,838, reported in 2019) (*18*–*20*). Furthermore, a recent 2023 study conducted by our team using the NHIS database reported that patients with NTM infection incurred at least 1.5 times higher annual medical costs than the healthy control population (a total annual medical cost of US $2,279.99 vs. US $1,496.26) (*21*). In

Table 3. Cost analysis of the treatment of nontuberculous mycobacterial pulmonary disease, South Korea, 2015–2019*

Variable	Median costs (interquartile range)			
	Cumulative†	Out-of-pocket	Annual‡	Per visit§
All visits, n = 147				
Total	5,044 (3,586–9,680)	2,535 (1,779–4,087)	1,319 (845–2,478)	NA
Nonbenefit	115 (13–431)	115 (13–497)	28 (3–109)	NA
Medication	1,197 (656–2,728)	362 (214–872)	296 (178–676)	NA
Diagnostic tests	3,006 (2,134–4,511)	1,536 (1,152–2,332)	701(536– 1,199)	NA
Clinical services	616 (416–1,749)	426 (312–839)	140 (106–481)	NA
Outpatient visits, n = 147				
Total	3,863 (2,969–5,333)	2,124 (1,476–2,702)	965 (753–1,370)	163 (134–198)
Nonbenefit	35 (7–115)	35 (7–115)	8 (2–32)	1 (0–5)
Medication	1,050 (584–1,904)	347 (178–664)	247 (159–466)	40 (27–70)
Diagnostic tests	2,282 (1,806–2,997)	1,317 (991–1,772)	598 (433–753)	99 (78–121)
Clinical services	448 (347–597)	368 (272–474)	110 (87–137)	19 (17–20)
Admissions, n = 71				
Total	5,620 (1,296–9,186)	1,494 (506–3,340)	1,146 (291–2,983)	3,493 (1,011–6,141)
Nonbenefit	326 (107–887)	326 (107–887)	65 (24–224)	212 (103–452)
Medication	464 (31–1,773)	94 (11–412)	110 (8–442)	275 (26–900)
Diagnostic tests	1,590 (734–4,405)	498 (233–1,785)	317 (182–1,269)	1,243 (653–2,045)
Clinical services	1,470 (289–4,118)	348 (72–1,000)	359 (66–1,382)	1,111 (200–2,634)

*Currency in US $, rounded to the nearest dollar. NA, not applicable.
†All costs pertaining to each category of visit.
‡Cumulative cost divided by the duration of total follow-up in years.
§Cumulative cost for outpatients divided by the number of outpatient visits.
¶Cumulative cost of admission divided by the number of admissions.

addition, patients with NTM-PD incurred large copayments or direct out-of-pocket costs for medical services not covered through the NHIS. Those costs comprised >50% of the total medical costs, suggesting that long-term disease burden directly translates to a considerable cost burden for patients with NTM-PD compared with other chronic respiratory conditions (*22*,*23*).

We report the long-term costs associated with NTM-PD and the cost drivers by different phases of disease management, types of medical services, and parts of the medical costs borne by patients. Costs start to increase approximately 6 months before treatment initiation, peak during the first quarter of treatment, and then decrease after approximately 1 year of treatment (Appendix Figure 1). That period, which roughly coincides with the pretreatment and treatment periods (Table 2), accounts for 66.4% of the total cost (Appendix Figure 2). A combination of factors may explain the cost concentration observed throughout that period, when intensive laboratory studies are needed to decide when to initiate treatment and monitor treatment outcomes as well as treatment and management of associated adverse events. Previous studies have demonstrated that the economic burden is greater during the early follow-up phases. In a recent study that compared healthcare expenditures among patients with NTM infection and matched controls, medical costs were the highest 6 months before NTM-PD diagnosis (*21*). Similar studies conducted in Germany and the United States reported that annual overall healthcare costs were highest during the first year after NTM-PD diagnosis (*12*,*24*). Another study conducted in Canada demonstrated that costs attributable to NTM-PD during the acute-care phase (i.e., the first

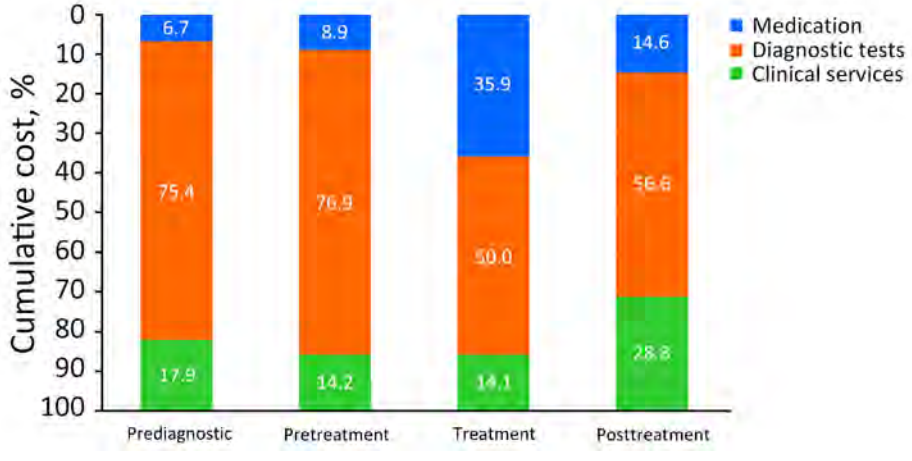

Figure 3. Cost proportion analysis by follow-up period, in study of medical costs of nontuberculous mycobacterial pulmonary disease, South Korea, 2015–2019. Cumulative cost was analyzed by each follow-up period. Numbers within bars represent the percentage of each cost category.

Table 4. Cumulative cost for each category and proportions of out-of-pocket cost in study of medical costs of nontuberculous mycobacterial pulmonary disease, South Korea, 2015–2019*

Period	Median cost, US$ (IQR)	% Out-of-pocket
Overall follow-up		
Total	5,470 (3,613–9,914)	47.4
Medication	1,171 (550–2,509)	29.6
Diagnostic tests	3,093 (2,134–4,597)	49.9
Clinical services	633 (435–1,749)	75.7
Prediagnostic		
Total	425 (255–1,052)	60.2
Medication	10 (0–77)	30.0
Diagnostic tests	393 (231–766)	56.2
Clinical services	44 (24–99)	86.4
Pretreatment		
Total	616 (399–1,079)	58.3
Medication	18 (0–74)	33.3
Diagnostic tests	497 (279–864)	60.0
Clinical services	65 (40–111)	78.5
Treatment		
Total	2,108 (1,660–3,590)	48.8
Medication	814 (512–1,362)	31.0
Diagnostic tests	1,051 (837–1,726)	56.7
Clinical services	209 (180–303)	84.7
Posttreatment		
Total	451 (138–1,363)	63.6
Medication	7 (0–220)	28.6
Diagnostic tests	295 (94–902)	51.2
Clinical services	89 (42–229)	60.7

*Data are for 87 patients with data for all 4 periods of follow-up.

150 days after the first hospital visit associated with NTM-PD) were greater than those associated with subsequent care phases (*13*).

Earlier studies have identified hospitalization costs as the main cost driver of NTM-PD management (*12*,*13*,*24*). Among our study population, 71 (48.3%) patients were admitted for NTM-PD–related issues throughout the follow-up period. Admission costs accounted for ≈59.6% of the total costs incurred by those patients, consistent with earlier findings reporting hospitalization costs accounting for as much as 69% of the total medical costs for NTM-PD (*14*). In our study, the main cost drivers for hospital admissions (54.3%) and the entire NTM-PD management (59.6%) were diagnostic tests (Table 3). The second largest cost driver, medication costs (23.7% of the total cost), was concentrated in the treatment period (38.4% of the costs during treatment) (Table 3; Appendix Figure 2). Our estimates were higher than those in France (6%), Germany (9%–21.8%), and the United Kingdom (12%) but lower than those in Canada (6%–70%), which may reflect differences in clinical practice and patient characteristics across countries (*11*,*12*,*14*). Furthermore, a relatively lower proportion of medication costs for managing NTM-PD in South Korea may be attributed to the government-negotiated drug costs for those approved for reimbursement schemes by the NHIS, which are generally lower than the market prices in other high-income settings (*25*).

Clinically challenging patient subgroups, such as those with *M. abscessus* infections (*2*,*26*) or comorbidities, probably require more healthcare resources and incur more costs for disease management (*10*,*11*). Our study directly assessed the increased costs and cost drivers associated with managing more difficult subgroups of patients with NTM-PD in South Korea. Patients with the *M. abscessus* subtype incurred costs 4.2 times higher than those infected with MAC, which was almost exclusively because of the increased costs associated with longer and more frequent hospitalizations for patients with *M. abscessus* infection (Table 5; Appendix Table 6). Moreover, patients with pulmonary comorbidities bore ≥67.4% more costs to treat and manage NTM-PD than those without comorbidities (Appendix Tables 10–12). NTM-PD patients with pulmonary comorbidities incurred approximately twice as much medication cost and a 50% increase in diagnostic test costs. When comparing the cost driver by types of clinical visits, we found that most of the increased medical costs were attributable to hospitalization costs.

Our cost estimates of NTM-PD management in South Korea were considerably lower than those in Germany and Canada. In 2011, Leber et al. estimated an annual cost of approximately CA $6,000 required to treat NTM-PD in Canada (*11*). In 2017, researchers in Germany compared the healthcare costs of patients with NTM-PD with those of uninfected controls and reported an attributable direct annual cost associated with NTM-PD of €9,093.20 (*12*). Our estimate of US $1,319 as the annual cost of managing NTM-PD is substantially lower in absolute terms; the large difference in medical costs for NTM-PD may be attributable to lower fee-for-service costs for medical care in South Korea than in Germany or Canada. According to a 2021 health report of the Organisation for Economic Cooperation and Development (OECD, https://www.oecd.org), per-capita healthcare expenditure in Korea (US $3,406) is approximately half of that in Canada (US $5,370) and Germany (US $6,518); however, healthcare use (e.g., annual consultations per person) far exceeds (17.2 in 2019 for South Korea) that of Germany (9.8) and Canada (6.6) (*23*). Those discrepancies may result from considerable differences in medical fee schedules across those countries. If medical service fees in South Korea are equivalent to those of Canada and Germany, costs associated with NTM-PD management in South Korea would be equivalent to, if not higher than, those of Canada and Germany.

Although our study did not assess patient perspective costs, we were able to assess patient co-pay-

Table 5. Analysis of cumulative cost based on causative species in study of medical costs of nontuberculous mycobacterial pulmonary disease, South Korea, 2015–2019*

Variable	Costs, median (interquartile range)		
	Mycobacterium avium complex, n = 112	*M. abscessus*, n = 15	p value
All visits			
Total	4,557 (3,334–7,086)	19,190 (9,914–26,219)	<0.001
Medication	1,069 (614–1,799)	2,767 (2,441–4,225)	<0.001
Diagnostic tests	2,830 (2,078–4,055)	5,726 (3,334–11,190)	<0.001
Clinical services	541 (377–930)	6,093 (4,263–11,972)	<0.001
Outpatient visits			
Total	3,859 (2,960–5,124)	3,300 (3,016–4,278)	0.492
Medication	976 (543–1,645)	983 (738–1,466)	0.823
Diagnostic tests	2,292 (1,805–3,060)	1,863 (1,650–2,480)	0.110
Clinical services	444 (347–564)	506 (318–643)	0.399
Admissions†			
Total	1,710 (933–7,747)	14,197 (6,711–22,521)	<0.001
Medication	61 (20–516)	1,784 (1,456–3,153)	<0.001
Diagnostic tests	998 (653–4,793)	3,093 (1,590–9,867)	0.024
Clinical services	556 (147–1,863)	5,639 (3,847–11,439)	<0.001

*Currency in US $, rounded to the nearest dollar.
†*M. avium* complex n = 45.

ment costs associated with all medical services used through NTM-PD management. Patients incurring higher medical costs experienced higher co-payment and out-of-pocket costs for their illness management. Except for patients with *M. abscessus* infection, patients in our cohort paid approximately more than half of the cumulative total medical care costs incurred during their disease management at our institution alone, which represents a much larger share (in terms of co-payment) of medical costs relative to the general South Korea population average (30%) and ≥3 times the share of costs reported from Canada (15%) and Germany (13%) (*23*).

Given the limited scope of our data, we were not able to ascertain cost burdens associated with nonmedical direct and indirect costs. As such, the direct patient out-of-pocket medical care costs assessed represent only ≈2% of the South Korea Gross Domestic Product per capita. However, South Korea faces substantial problems with poverty during old age, which affects 43.8% of the elderly population according to the OECD. That proportion is the highest in the OECD rankings and 3 times greater than the OECD average of 13.5% (*27*). NTM-PD patients in our study and South Korea in general are elderly (*8*,*21*,*28*). Given those considerations, we suspect that NTM-PD may impose major socio-economic burdens on the patients, which may be much more significant for particular subgroups (e.g., those with multiple hospitalizations or *M. abscessus* infections and those who remain culture positive despite treatment). More research is needed to better understand the socio-economic consequences of NTM-PD (including the level of catastrophic costs experienced by the patient and their household because of NTM-PD) and guide the development of relevant policy measures.

Among the interpretation and generalizability limitations of our study, our study cohort was derived from a single institution. Thus, our cost estimates may not fully represent the general medical costs of NTM-PD management across South Korea. It is

Table 6. Multiple linear regression analysis of factors driving cumulative cost in study of medical costs of nontuberculous mycobacterial pulmonary disease, South Korea, 2015–2019*

Model no., variable(s)	B	SE	β	t	p value	R^2	Adjusted R^2
1						0.616	0.610
No. admissions	6058.547	627.484	0.785	9.655	<0.001		
2						0.739	0.730
No. admissions	5503.292	532.913	0.713	10.327	<0.001		
Causative species: MAC = 0, *M. abscessus* = 1	7921.642	1530.022	0.358	5.177	<0.001		
3						0.758	0.746
No. admissions	5379.334	520.642	0.697	10.332	<0.001		
Causative species: MAC = 0, *M. abscessus* = 1	7445.211	1502.260	0.336	4.956	<0.001		
Culture conversion	−3082.792	1455.967	−0.142	−2.117	0.039		

*N = 147 patients. Variables include age, sex, history of tuberculosis, history of nontuberculous mycobacteria treatment, bronchiectasis, asthma, chronic obstructive pulmonary disease, lung cancer, causative species (MAC vs. *M. abscessus*), total follow-up duration, treatment duration, number of outpatient visits, number of admissions, culture conversion, microbiologic cure, retreatment for recurrence, and death from any cause. MAC, *Mycobacterium avium* complex; NA, not applicable.

possible that NTM-PD patients included in our sample may have sought care for NTM-PD at other institutions before and during follow-up visits to Severance Hospital, which may result in higher healthcare systems perspective per-patient costs. However, annual per-patient NTM management costs reported from an earlier study in South Korea that used the national health insurance claims database (healthcare systems perspective) (US $1,197.75/y) were equivalent to (or slightly lower than) our cost estimates (US $1,319/y) (*21*). Although we are not able to directly compare the 2 studies by using patient-level data, similarities in the cost estimates suggest that many NTM patients may be managed at a single institution and that our estimates closely represent those of general NTM patients in South Korea. Although it is difficult to ascertain and attribute differences in NTM-PD medical costs attributed to patients in South Korea compared with those in other countries, similarities in the overall trends (key cost drivers by types of healthcare use and types of diseases) suggest that the magnitude of our estimates largely represents differences in clinical practices and medical service costs across other countries with similar estimates. Second, we were limited in assessing any additional NTM-PD–related costs that patients and the healthcare systems may have incurred, such as nonmedical costs and productivity loss. Therefore, our cost estimates may underestimate true costs for NTM-PD management. Data from patient cost survey studies (to ascertain short- and long-term patient costs) and large panel data comprising multi-institutional cohorts with medical insurance claims information may provide a complete disease and financial burden of NTM-PD. Last, although we compared the costs associated with NTM-PD with those associated with other respiratory conditions, lack of an adequate control group with no history of NTM-PD limited our assessment of the relative disease and financial burden of NTM-PD.

In conclusion, our comprehensive, long-term assessment of medical costs associated with NTM-PD management demonstrates that NTM-PD poses a substantial disease burden on and financial costs to healthcare services and patients. Our findings suggest that the cost burden is considerably higher for patients with *M. abscessus* infection or pulmonary comorbidities, which is attributable to the longer duration of disease management and more frequent and longer hospitalization required. In addition, unlike patients with other respiratory infection–related illnesses, patients with NTM-PD bear much larger direct out-of-pocket costs that account for approximately 50% of direct medical costs. Although additional evidence from more complete data sources may be needed to fully ascertain long-term disease burden and costs, our study findings provide initial evidence that can be used for developing policies to support patients with NTM-PD and alleviate financial burdens during their disease management.

The data that support the findings of this study are available from the corresponding author (Y.P.) upon reasonable request.

This research was supported by the "Korea Disease Control and Prevention Agency (KDCA)" research project (project #20211111777-00).

Authors have no conflicts of interest to declare.

Authors met the criteria for authorship recommended by the International Committee of Medical Journal Editors, were fully responsible for all content, and were involved in all stages of manuscript development. Study conception and design: Y.A.K., H.S., Y.P.; data collection: S.C., S.K.; Y.A.K., M.S.P., and Y.P; and data interpretation: S.C., Y.A.K., H.S., and Y.P.

About the Author

Dr. Chang is a clinical fellow of pulmonary and critical care medicine at Severance Hospital of Yonsei University in Seoul. His primary research interests include respiratory infections.

References

1. Jeon D. Infection source and epidemiology of nontuberculous mycobacterial lung disease. Tuberc Respir Dis (Seoul). 2019;82:94–101. https://doi.org/10.4046/trd.2018.0026
2. Daley CL, Iaccarino JM, Lange C, Cambau E, Wallace RJ Jr, Andrejak C, et al. Treatment of nontuberculous mycobacterial pulmonary disease: an official ATS/ERS/ESCMID/IDSA clinical practice guideline. Clin Infect Dis. 2020;71:e1–36. https://doi.org/10.1093/cid/ciaa241
3. Stout JE, Koh WJ, Yew WW. Update on pulmonary disease due to non-tuberculous mycobacteria. Int J Infect Dis. 2016;45:123–34. https://doi.org/10.1016/j.ijid.2016.03.006
4. Griffith DE, Aksamit TR. Managing *Mycobacterium avium* complex lung disease with a little help from my friend. Chest. 2021;159:1372–81. https://doi.org/10.1016/j.chest.2020.10.031
5. Adjemian J, Prevots DR, Gallagher J, Heap K, Gupta R, Griffith D. Lack of adherence to evidence-based treatment guidelines for nontuberculous mycobacterial lung disease. Ann Am Thorac Soc. 2014;11:9–16. https://doi.org/10.1513/AnnalsATS.201304-085OC
6. Pasipanodya JG, Ogbonna D, Deshpande D, Srivastava S, Gumbo T. Meta-analyses and the evidence base for microbial outcomes in the treatment of pulmonary *Mycobacterium avium-intracellulare* complex disease. J Antimicrob Chemother. 2017;72(suppl_2):i3–19. https://doi.org/10.1093/jac/dkx311

7. Pasipanodya JG, Ogbonna D, Ferro BE, Magombedze G, Srivastava S, Deshpande D, et al. Systematic review and meta-analyses of the effect of chemotherapy on pulmonary *Mycobacterium abscessus* outcomes and disease recurrence. Antimicrob Agents Chemother. 2017;61:e01206-17. https://doi.org/10.1128/AAC.01206-17
8. Lee H, Myung W, Koh WJ, Moon SM, Jhun BW. Epidemiology of nontuberculous mycobacterial infection, South Korea, 2007–2016. Emerg Infect Dis. 2019;25:569–72. https://doi.org/10.3201/eid2503.181597
9. Winthrop KL, Marras TK, Adjemian J, Zhang H, Wang P, Zhang Q. Incidence and prevalence of nontuberculous mycobacterial lung disease in a large U.S. managed care health plan, 2008–2015. Ann Am Thorac Soc. 2020;17:178–85. https://doi.org/10.1513/AnnalsATS.201804-236OC
10. Ballarino GJ, Olivier KN, Claypool RJ, Holland SM, Prevots DR. Pulmonary nontuberculous mycobacterial infections: antibiotic treatment and associated costs. Respir Med. 2009;103:1448–55. https://doi.org/10.1016/j.rmed.2009.04.026
11. Leber A, Marras TK. The cost of medical management of pulmonary nontuberculous mycobacterial disease in Ontario, Canada. Eur Respir J. 2011;37:1158–65. https://doi.org/10.1183/09031936.00055010
12. Diel R, Jacob J, Lampenius N, Loebinger M, Nienhaus A, Rabe KF, et al. Burden of non-tuberculous mycobacterial pulmonary disease in Germany. Eur Respir J. 2017;49:1602109. https://doi.org/10.1183/13993003.02109-2016
13. Ramsay LC, Shing E, Wang J, Marras TK, Kwong JC, Brode SK, et al. Costs associated with nontuberculous mycobacteria infection, Ontario, Canada, 2001–2012. Emerg Infect Dis. 2020;26:2097–107. https://doi.org/10.3201/eid2609.190524
14. Goring SM, Wilson JB, Risebrough NR, Gallagher J, Carroll S, Heap KJ, et al. The cost of *Mycobacterium avium* complex lung disease in Canada, France, Germany, and the United Kingdom: a nationally representative observational study. BMC Health Serv Res. 2018;18:700. https://doi.org/10.1186/s12913-018-3489-8
15. Health Insurance Review and Assessment Service. Reimbursed drugs and price ceilings [cited 2022 May 12]. https://www.hira.or.kr/bbsDummy.do?pgmid=HIRAA030014050000
16. US Internal Revenue Service. Yearly average currency exchange rates [cited 2024 Feb 1]. https://www.irs.gov/individuals/international-taxpayers/yearly-average-currency-exchange-rates
17. Korean Statistical Information Service. Annual consumer price index by expenditure category [cited 2024 Feb 1]. https://kosis.kr/statHtml/statHtml.do?orgId=101&tblId=DT_1J22135&vw_cd=MT_ETITLE&list_id=P2_6&scrId=&language=en&seqNo=&lang_mode=en&obj_var_id=&itm_id=&conn_path=MT_ETITLE&path=%252Feng%252FstatisticsList%252FstatisticsListIndex.do
18. Lee YJ, Kwon SH, Hong SH, Nam JH, Song HJ, Lee JS, et al. Health care utilization and direct costs in mild, moderate, and severe adult asthma: a descriptive study using the 2014 South Korean Health Insurance Database. Clin Ther. 2017;39:527–36. https://doi.org/10.1016/j.clinthera.2017.01.025
19. Lee S, Kim MJ, Lee SH, Kim HY, Kim HS, Oh IH. Comparison of disability-adjusted life years (DALYs) and economic burden on people with drug-susceptible tuberculosis and multidrug-resistant tuberculosis in Korea. Front Public Health. 2022;10:848370. https://doi.org/10.3389/fpubh.2022.848370
20. Lee HY, Han DJ, Kim KJ, Kim TH, Oh YM, Rhee CK. Clinical characteristics and economic burden of tuberculous-destroyed lung in Korea: a National Health Insurance Service-National Sample Cohort-Based Study. J Thorac Dis. 2019;11:2324–31. https://doi.org/10.21037/jtd.2019.06.14
21. Lee SW, Chang S, Park Y, Kim S, Sohn H, Kang YA. Healthcare use and medical cost before and after diagnosis of nontuberculous mycobacterial infection in Korea: The National Health Insurance Service-National Sample Cohort Study. Ther Adv Respir Dis. 2023;17:17534666221148660. https://doi.org/10.1177/17534666221148660
22. Ruger JP, Kim HJ. Out-of-pocket healthcare spending by the poor and chronically ill in the Republic of Korea. Am J Public Health. 2007;97:804–11. https://doi.org/10.2105/AJPH.2005.080184
23. Organization for Economic Cooperation and Development. Health at a glance 2021 [cited 2024 Jul 22]. https://www.oecd-ilibrary.org
24. Marras TK, Mirsaeidi M, Chou E, Eagle G, Zhang R, Leuchars M, et al. Health care utilization and expenditures following diagnosis of nontuberculous mycobacterial lung disease in the United States. J Manag Care Spec Pharm. 2018;24:964–74. https://doi.org/10.18553/jmcp.2018.18122
25. Chung WJ, Kim HJ. Interest groups' influence over drug pricing policy reform in South Korea. Yonsei Med J. 2005;46:321–30. https://doi.org/10.3349/ymj.2005.46.3.321
26. Griffith DE, Daley CL. Treatment of *Mycobacterium abscessus* pulmonary disease. Chest. 2022;161:64–75. https://doi.org/10.1016/j.chest.2021.07.035
27. Kang J, Park J, Cho J. Inclusive aging in Korea: eradicating senior poverty. Int J Environ Res Public Health. 2022;19:2121. https://doi.org/10.3390/ijerph19042121
28. Park JH, Shin S, Kim TS, Park H. Clinically refined epidemiology of nontuberculous mycobacterial pulmonary disease in South Korea: overestimation when relying only on diagnostic codes. BMC Pulm Med. 2022;22:195. https://doi.org/10.1186/s12890-022-01993-1

Address for correspondence: Youngmok Park, Division of Pulmonary and Critical Care Medicine, Department of Internal Medicine, Yonsei University College of Medicine, Severance Hospital, 50-1 Yonsei-ro, Seodaemun–gu, 03722 Seoul, South Korea; email: 0mokfv@yuhs.ac

Ecologic, Geoclimatic, and Genomic Factors Modulating Plague Epidemics in Primary Natural Focus, Brazil

Matheus F. Bezerra, Diego L.R.S. Fernandes, Igor V. Rocha, João L.L.P. Pitta, Natan D.A. Freitas, André L.S. Oliveira, Ricardo J.P.S. Guimarães, Elainne C.S. Gomes, Cecília Siliansky de Andreazzi, Marise Sobreira, Antonio M. Rezende, Pedro Cordeiro-Estrela, Alzira M.P. Almeida

Plague is a deadly zoonosis that still poses a threat in many regions of the world. We combined epidemiologic, host, and vector surveillance data collected during 1961–1980 from the Araripe Plateau focus in northeastern Brazil with ecologic, geoclimatic, and *Yersinia pestis* genomic information to elucidate how these factors interplay in plague activity. We identified well-delimited plague hotspots showing elevated plague risk in low-altitude areas near the foothills of the plateau's concave sectors. Those locations exhibited distinct precipitation and vegetation coverage patterns compared with the surrounding areas. We noted a seasonal effect on plague activity, and human cases linearly correlated with precipitation and rodent and flea *Y. pestis* positivity rates. Genomic characterization of *Y. pestis* strains revealed a foundational strain capable of evolving into distinct genetic variants, each linked to temporally and spatially constrained plague outbreaks. These data could identify risk areas and improve surveillance in other plague foci within the Caatinga biome.

Plague is a deadly bacterial disease caused by *Yersinia pestis* and is implicated in major pandemics throughout the course of human history. Despite the decline in global incidence, plague outbreaks still occur in regions where the bacterium maintains a sylvatic cycle (*1*,*2*). In addition, plague resurgence has been reported after long periods of quiescence, making active animal surveillance in its natural foci critical to prevent outbreaks in human populations (*3*).

Plague incidence typically undergoes accentuated variations over time (*2*). Evidence from studies performed in central Asia and North America demonstrate that such variations are triggered by the combined effect of geoclimatic and ecologic factors. Temperature, precipitation, landscape, vegetation, soil composition, and host–vector densities and diversity have been reported to interplay in a trophic web that leads to plague dissemination in both wild fauna and humans (*3*–*5*). However, information regarding the role the geoclimatic and ecologic aspects in the modulation of plague systems in foci of Brazil is lacking.

The current demarcation of plague focal areas in Brazil lacks granularity and encompasses extensive regions solely based on geologic formations with reported plague cases (*6*). Thus, identification of specific geoclimatic and environmental patterns indicating hotspots for increased plague risk could provide valuable information for implementing more assertive and targeted animal surveillance.

Author affiliations: Instituto Aggeu Magalhães, Fiocruz, Brazil (M.F. Bezerra, D.L.R.S Fernandes, I.V. Rocha, J.L.L.P. Pitta, E.C.S. Gomes, M. Sobreira, A.M. Rezende, A.M.P. Almeida); Laboratório de Mamíferos, Pós Graduação em Ciências Biológicas (Zoologia), Universidade Federal da Paraíba, João Pessoa, Brazil (N.D.A. Freitas, P. Cordeiro-Estrela); Núcleo de Geoprocessamento, Instituto Aggeu Magalhães, Fiocruz (A.L.S. Oliveira); Laboratório de Geoprocessamento, Instituto Evandro Chagas, Belém, Brazil (R.J.P.S. Guimarães); Laboratório de Biologia e Parasitologia de Mamíferos Silvestres Reservatórios, Instituto Oswaldo Cruz, Fiocruz, Rio de Janeiro, Brazil (C.S. de Andreazzi); Universidad Complutense de Madrid, Madrid, Spain (C.S. de Andreazzi); International Platform for Science, Technology and Innovation in Health, PICTIS, Ílhavo, Portugal (C.S. de Andreazzi); Group of Biotechnology Applied to Pathogens, René Rachou Institute, Fiocruz (A.M. Rezende)

DOI: https://doi.org/10.3201/eid3009.240468

The Araripe Plateau (Chapada do Araripe) constitutes a geologic landmark situated along the border of Pernambuco, Ceará, and Piauí states of Brazil. Although the region is in the core of the semiarid biome known as Caatinga, the plateau is topped by savanna, and its slopes have lush forest vegetation because of orographic precipitation and a permeable tabletop (*7*,*8*). The Araripe Plateau was considered the epicenter of plague in Brazil until 1980, when the last confirmed human case in the region was notified (*9*).

We took advantage of the geographically well-delimited features of the Araripe Plateau and the robust amount of data obtained from the Pilot Plague Program (*10*) regarding human and animal surveillance to perform a case study of a plague focus in Brazil through a One Health perspective. By combining 20 years of epidemiologic data with ecologic, geoclimatic, and *Y. pestis* genomic variables, we aimed to unravel the intricate dynamics of plague in a natural focus in Brazil.

Methods

Data Collection

In brief, we retrieved information on *Y. pestis* reservoirs, vector surveillance, and notification of human plague cases from the national Brazilian Plague Reference Service (https://www.cpqam.fiocruz.br/sr/peste) document repository. We obtained metadata from the Fiocruz *Y. pestis* collection of the World Data Centre for Microorganisms (https://www.wdcm.org; collection no. 1040) and the CONCEPAS database (http://cyp.fiocruz.br). We collected demographic and climatic variables from multiple public databases (Appendix 1 Figure 1, https://wwwnc.cdc.gov/EID/article/30/9/24-0468-App1.pdf).

Geospatial Analysis

We collected coordinates from human cases where public health conducted site visits. To identify plague risk hotspots, we calculated the kernel density estimation (KDE) and space-time scan (SaTScan, https://www.satscan.org) statistics. We interpolated rainfall data from meteorologic stations by using inverse weighted distance and used the normalized difference vegetation index (NDVI) as a proxy for vegetation coverage (Appendix 1).

Laboratory Testing for Plague

Human plague diagnosis was performed through a combination of clinical and epidemiologic assessment and laboratory testing, such as culturing bubo aspirates or blood cultures. Rodent diagnoses were made by direct microscopy observation of spleen imprints and blood smears, followed by conventional bacteriology. Fleas also were tested via bacterial culturing (Appendix 1).

Statistical Analysis and Ecologic Networks

We calculated linear regression, nonlinear correlations, principal component analysis (PCA) and receiver operating characteristic curves by using GraphPad Prism version 10.1 (GraphPad, https://www.graphpad.com). We analyzed the fundamental properties of each host–vector plague network by using the bipartite package in R (The R Project for Statistical Computing, https://www.r-project.org). We considered $p<0.05$ statistically significant.

Whole-Genome Sequencing and Bioinformatic Analysis

We performed DNA extraction by using the DNeasy Blood & Tissue Kit (QIAGEN, https://www.qiagen.com). We conducted genomic library preparation using the Nextera XT Library Preparation Protocol (Illumina, https://www.illumina.com) and used the MiSeq sequencer and 600-cycle version 3 cartridge (Illumina) for sequencing. We assembled genomes by using VelvetOptimiser and annotated by using the Prokka pipeline, as previously described (*11*). We conducted core single-nucleotide variant (SNV) calling by using Snippy (https://github.com/tseemann/snippy) and used IQ-TREE2 (http://www.iqtree.org) to perform phylogenetic analyses based on the core SNV. We then visualized results by using the iTOL (https://itol.embl.de) platform.

Results

Spatiotemporal Features of Plague Outbreaks in the Araripe Plateau Region

During 1961–1980 in the Araripe Plateau focus, 551 human plague cases were reported; 292 were in the state of Pernambuco, 240 in the state of Ceará, and only 1 in the state of Piauí (Appendix 1 Figure 2, panels A, B). However, we excluded 18 cases in Pernambuco from the spatial analysis because case locations were unknown.

Human plague cases were concentrated mostly at the foothills of the Araripe Plateau, in regions of lower altitude, but close to the plateau's slope (Figure 1). KDE analysis concentrated the plague risk more intensely in 3 areas of lower altitude in the municipalities of Exu, Bodocó, and Araripina, and those areas

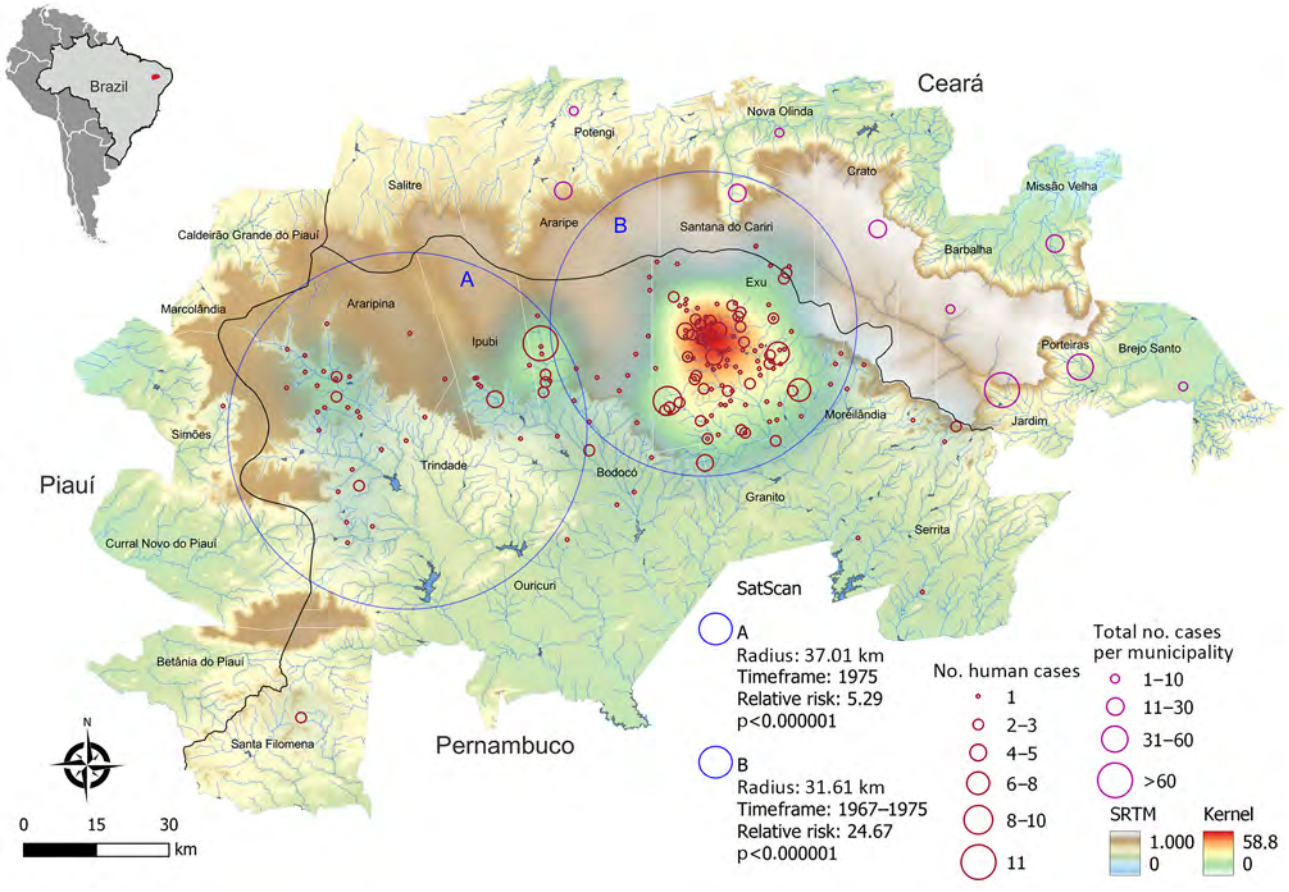

Figure 1. Spatial distribution and risk analysis of human plague cases in a study of ecologic, geoclimatic, and genomic factors modulating plague epidemics in primary natural focus, Brazil. Background colors show the altimetry (m) from SRTM. The black line shows the tri-state boundaries between Pernambuco, Ceará, and Piauí. Red circles identify plague risk areas by application of KDE in human cases in Pernambuco. Blue circles A and B indicate plague risk clusters calculated by SaTScan for 1975 (A) and 1967–1975 (B). Pink circles indicate spatial distribution of human plague cases by number of occurrences per municipality in Ceará. Inset map shows Brazil with the Araripe Plateau focus in red. KDE, kernel density estimation; SaTScan, space-time scan (https://www.satscan.org) statistics; SRMT, Shuttle Radar Topography Mission (https://www.earthdata.nasa.gov).

are closed in by concave cliffs (Figure 1). Conversely, only a few cases were reported on the top of the plateau. To overcome bias of heterogeneous population density, we performed a SaTScan analysis using the census tracts as geographic areas, which confirmed the findings from the KDE analysis. Furthermore, the estimated relative risk for the population living within the radius of 2 areas were much higher than for the surrounding areas; 5.29-fold higher in area A and 24.67-fold higher in area B (Figure 1). The year-by-year dynamics of plague cases in the region was clearly visible (Video, https://wwwnc.cdc.gov/EID/article/30/9/24-0468-V1.htm).

Effect of Eco-Epidemiologic and Climatic Variables on the Dynamics of Human Plague Cases

By analyzing precipitation levels and data from 40,972 rodents and 39,150 fleas tested for *Y. pestis* in the Araripe Plateau region during 1966–1980, we were able to assess the seasonal and annual effect of those variables on the number of human cases. Overall, the years with higher rodent and flea *Y. pestis* positivity rates overlapped the years with more human cases (Figure 2, panels B, D, F, H, J). In addition, using rodent capture success as a proxy for animal abundance, we found that years with more human cases and *Y. pestis*–positive animals also had reduced rodent abundance, indicating that *Y. pestis* circulation had a major effect on the rodent population. Of note, the annual dynamics of average pluviosity (rainfall amount) showed a 1-year delay effect when compared with human cases until 1976 (Figure 3, panel A), after which plague became quiescent in the region. Thus, we considered the pluviosity from the previous year in further analyses.

Next, we evaluated the seasonal aspects of those variables by measuring the average monthly rates for several additional variables during 1966–1980. Along with the human cases, rodent and flea *Y. pestis* positivity rates, flea index (number of fleas per host), and rodent abundance all showed a strong seasonal component, peaking during the end of winter and beginning of spring (August–October) (Figure 2). We noted that rainfall occurred mostly in the first semester, peaking during late summer and early fall (February–April) (Figure 3, panel B).

The occurrence of human cases was proportionally related to rodent (R^2 = 0.94) and flea (R^2 = 0.93) *Y. pestis* positivity rates, and human cases related more moderately (R^2 = 0.65) to the previous year's pluviosity (Figure 4, panel A). We also ran those

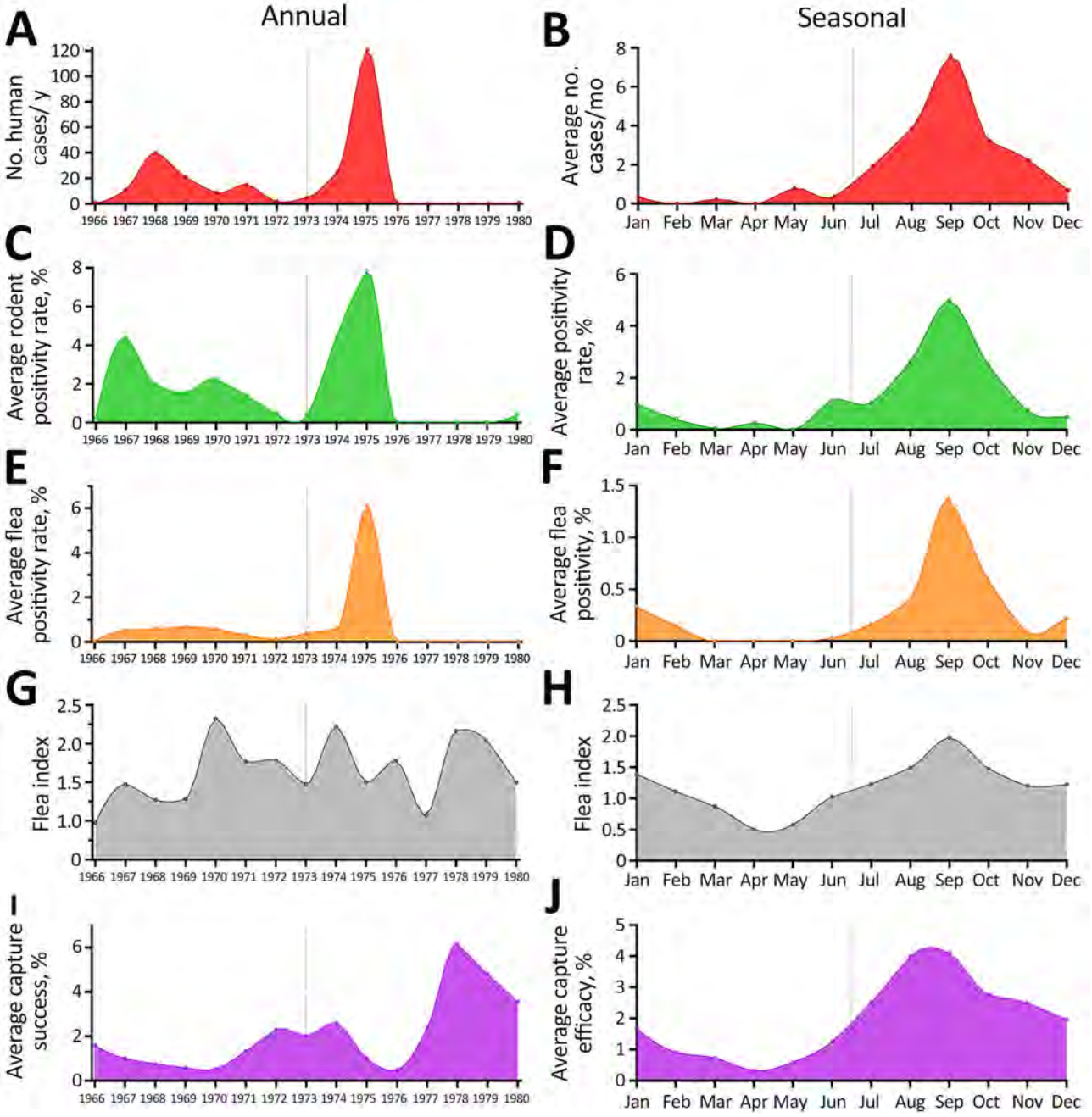

Figure 2. Annual (left column) and seasonal (right column) dynamics of plague occurrence and flea and rodent capture and abundance rates in a study of ecologic, geoclimatic, and genomic factors modulating plague epidemics in primary natural focus, Brazil. A, B) Human cases; C, D) rodent positivity; E, F) flea positivity; G, H) flea index (number of fleas per host); I, J) rodent capture success. Vertical lines provide midpoints for comparison between measured indices.

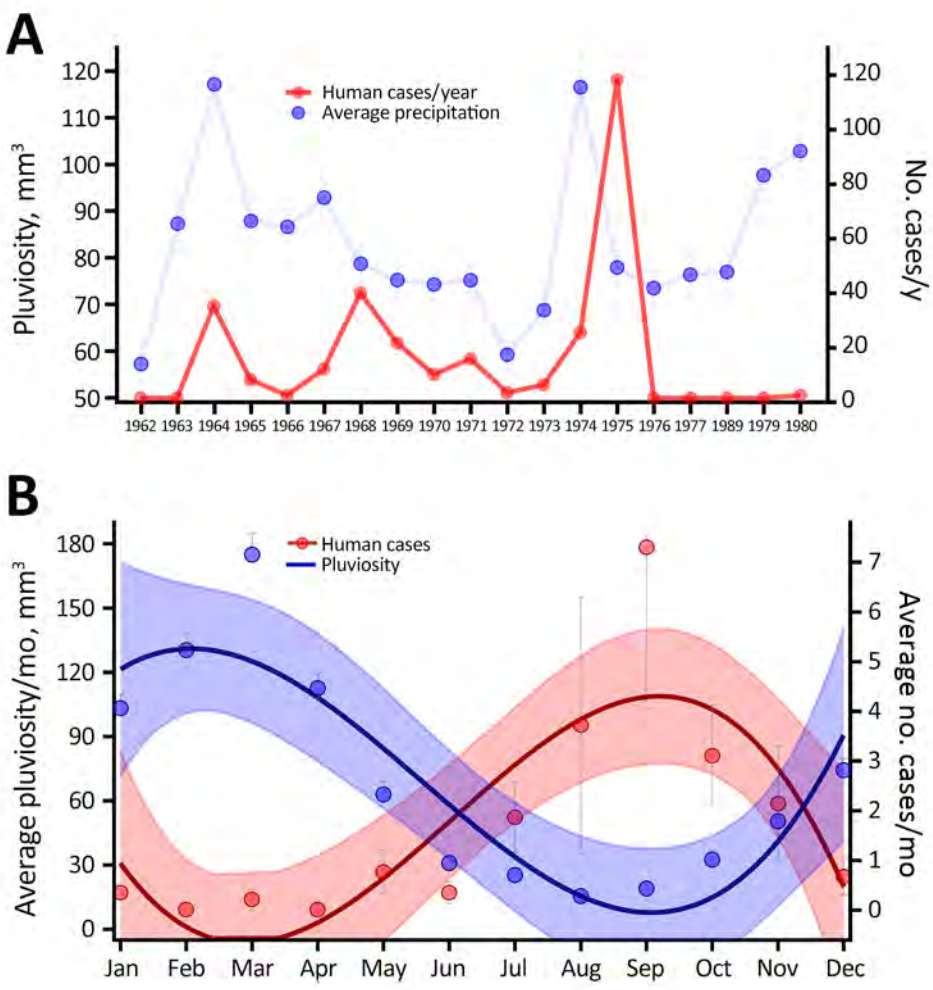

Figure 3. Effects of climatic variables on human cases in a study of ecologic, geoclimatic, and genomic factors modulating plague epidemics in primary natural focus, Brazil. A) Yearly average pluviosity (rainfall amount); B) monthly average pluviosity. Dots indicate averages; whiskers indicate upper and lower limits. Average pluviosity (mm^3) was measured in municipalities in the state of Pernambuco in the Araripe Plateau region during 1962–1980. The curves in panel B represent the third order polynomial interpolation of cases and pluviosity averages; shaded areas indicate 95% CIs.

variables in a multivariable regression model; however, rodent and flea positivity were also mutually dependent and therefore redundant ($R^2 = 0.94$) (Appendix 1 Figure 2, panels C, D). For that reason, the model was better explained by a single variable linear regression. Linear regression of flea index showed no impact of this variable on human cases or rodent infection. By comparing monthly averages during 1966–1980, we found that the rodent abundance (capture success), flea index, and rodent and flea *Y. pestis* positivity rates had a stark linear proportionality with human cases at a seasonal level (Figure 4, panel B). Of note, although the effect of rodent and flea *Y. pestis* positivity rates on human cases showed a linear pattern, rodent abundance had a negative exponential correlation with plague activity in humans, and *Y. pestis* positivity in animal hosts and vectors (Figure 5).

The PCA of multiple eco-epidemiologic and climatic features revealed that distinct years clustered together according to the intensity of human cases, suggesting a synergic effect among those variables. Of note, 1975, which had the highest number of human cases, showed unique eco-climatic features. Those features included lower abundance of *Necromys lasiurus* mice; distinct ecologic network parameters, such as host–vector robustness and modularity; high precipitation (considering a 1-year lagged effect); and higher *Y. pestis*–positivity rates in rodents and vectors (Figure 6; Appendix 1 Figure 2, panel E). We designated years as epidemic or low-activity according to the PCA analysis.

Spatiotemporal Dynamic of Human Plague Cases by Rainfall and Vegetation Coverage

On the basis of our preliminary findings that human plague cases correlated with the average pluviosity from the previous years in the Araripe Plateau region (Figure 3, panel A), we expanded our analysis to evaluate whether that effect would also demonstrate a spatial pattern. By interpolating pluviometry data from meteorologic stations in the region, we observed

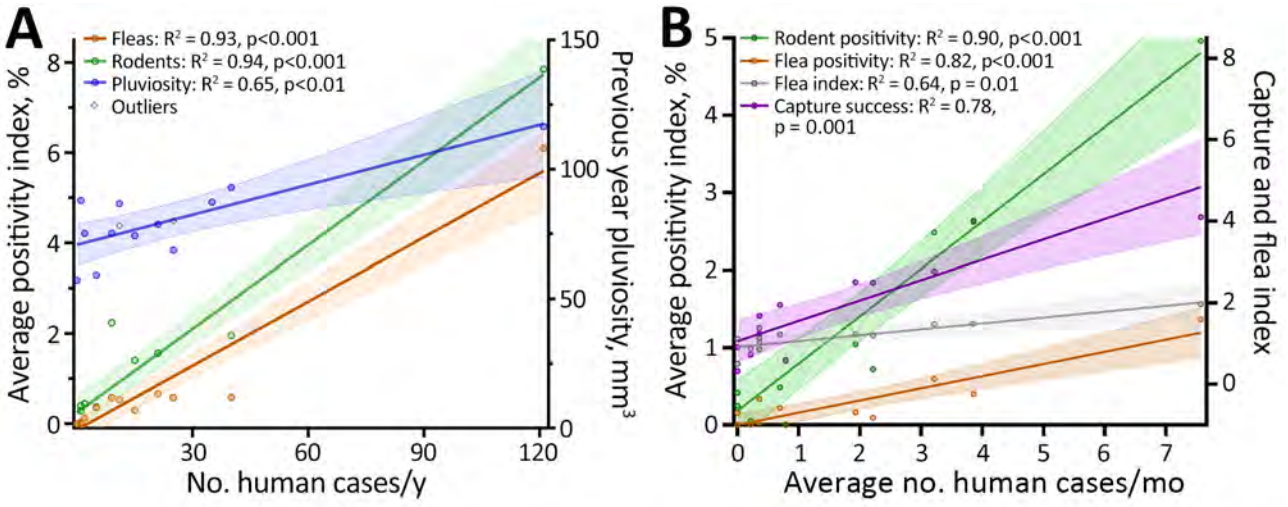

Figure 4. Linear regression of human cases, rodent and flea positivity, and pluviosity (rainfall amount) in a study of ecologic, geoclimatic, and genomic factors modulating plague epidemics in primary natural focus, Brazil. Annual (A) and monthly (B) average number of human cases compared with *Yersinia pestis* positivity among rodents and fleas and average pluviosity are shown. The previous year pluviosity data only included years from the plague outbreaks, 1966–1976. Solid lines indicate averages, shaded areas indicate 95% CIs, and dots indicate outliers.

a marked overlap between clusters of plague cases and rainfall volume during the study period (Figure 7, panel A). Similar to the plague cases, rain was more intense in lower altitude areas neighboring the elevated plateau. Next, we also investigated the spatial distribution of rainfall in the years that anticipated major outbreaks (1967 and 1974) or epidemiologic silence (1972) and observed a 1-year delay in spatial overlap between rainfall and plague cases (Appendix 1 Figure 3).

Considering the semiarid climate in the region, we hypothesized that one of the mechanisms through which rainfall could modulate plague would be effects on the availability of vegetation as a food source for wild rodents. NDVI data showed that vegetation was concentrated in the slopes of the Araripe Plateau, overlapping the main rainfall and plague case areas (Figure 7, panel B).

Ecologic Aspects of Plague in Araripe Plateau and Ecologic Networks

N. lasiurus mice were the most representative rodent species during the study period. Nevertheless, *N. lasiurus* mice representation varied through time and was greatly reduced in epidemic years (Figure 8, panel A). Moreover, reduction of *N. lasiurus* mice populations had a dramatic effect on the overall capture success rate. Of note, after the abrupt shift from a major plague outbreak in 1975 to quiescence, the wild rodent population quickly reestablished.

Among flea vector species, the most common in captured rodents was *Polygenis* spp. fleas, which were the predominant and almost exclusive species in wild rodents, including *N. lasiurus* mice. On the other hand, *Xenopsylla* spp. fleas were mostly found in the synanthropic *Rattus rattus* rats. Less commonly,

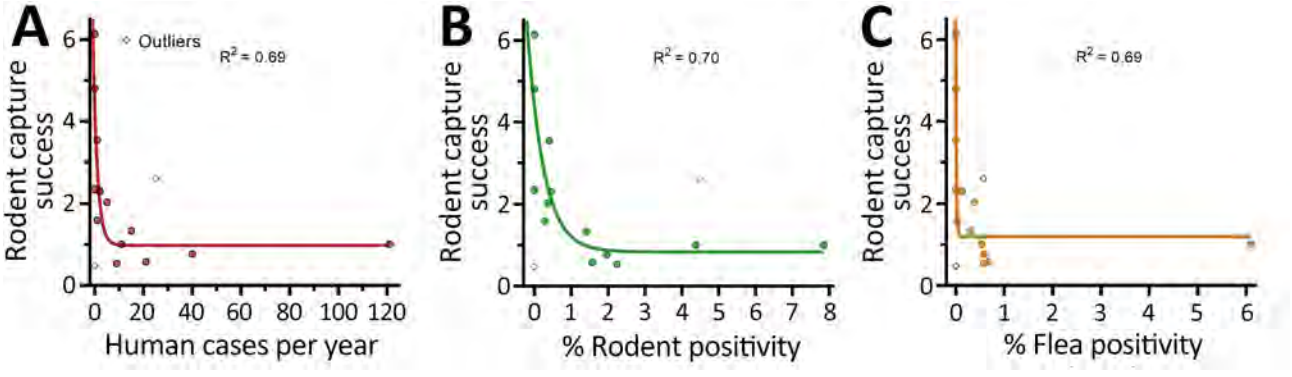

Figure 5. Exponential correlation between rodent capture success and human and animal *Yersinia pestis* positivity in a study of ecologic, geoclimatic, and genomic factors modulating plague epidemics in primary natural focus, Brazil. A) Human cases; B) rodent positivity; C) flea positivity. Capture success serves as a proxy for rodent abundance.

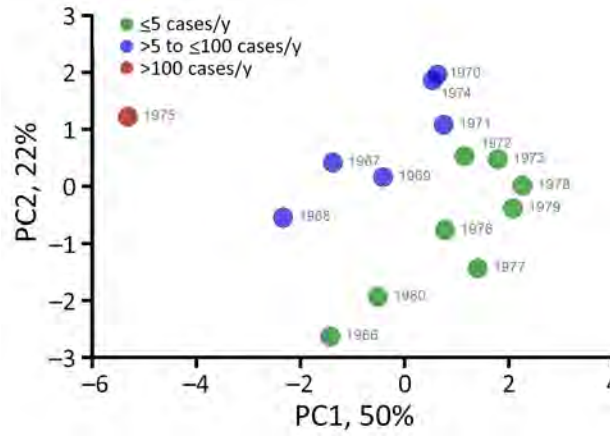

Figure 6. Year-based principal component analysis in a study of ecologic, geoclimatic, and genomic factors modulating plague epidemics in primary natural focus, Brazil. PC based on eco-epidemiologic and climatic features. The weight of each included variable is provided in Appendix 1 Figure 2, panel E (https://wwwnc.cdc.gov/EID/30/9/24-0468-App1.pdf). PC, principal component.

Adorapsylla spp. and *Ctenocephalides* spp. fleas were also identified (Figure 8, panel B). Because the method of flea species classification changed over time, we referred to fleas only at the genus level.

The structural properties of the host–vector network exhibited significantly higher robustness in epidemic years than low-activity epidemiologic years (Figure 6), and effects were seen in both small mammal (Mann-Whitney p = 0.014) and flea (Mann-Whitney p = 0.029) groups (Figure 9). Modularity (quantitative modularity) and nestedness (weighted nested overlap and decreasing fill [NODF]) values surpassed those predicted by null models, and appeared similar across epidemiologic years as the connectance, a term used to describe the ratio of observed ecological interactions to the total potential for such interactions. By sorting years according to their epidemiologic status, we observed distinct patterns of biologic interactions between small mammals and flea species (Figure 10, panel A). We also calculated annual values for the ecologic network metrics (Appendix 1 Figure 4, panel A).

Using only epidemiologic variables, 11 of 14 plague years (1977 singularity resulted in an invalid value) were correctly classified by the linear discriminant analysis; 1969 and 1975 were misclassified as not epidemic, and 1976 was misclassified as epidemic. When using 5 different network variable combinations with epidemiologic variables, we found the correct classification of those 14 years was obtained by adding only modularity and nestedness. Those findings showed that the network variables increased the correct discrimination by 21.43% compared with the eco-epidemiologic variables alone. We summarized probabilities of classification for all models by using epidemiologic and network variables, and found that, in terms of predictive probability, 1969 and 1976 were less prone to correct prediction by different models (Appendix 1 Figure 4, panel B).

Monthly-Based Eco-Epidemiologic Surveillance Parameters as Predictors of Human Plague Risk

To estimate how data from animal surveillance can provide informative alerts of risk for human plague, we next analyzed monthly data. The receiver operating characteristic curve analysis revealed that 0.86% rodent positivity and 0.34% flea positivity are the optimal cutoff values of risk for human cases. We found that rodent and flea *Y. pestis* positivity rates were strong predictors of plague activity in humans in the same month: for fleas, area under the curve was 0.77, sensitivity was 66.7% and specificity was 88.3%; for rodents, area under the curve was 0.86, sensitivity was 83.3%, and specificity was 81.8%. The other ecologic variables, such as capture success and flea index, on the other hand, were poor predictors (Figure 11).

Genomic Features from *Y. pestis* Isolates

We analyzed 913 *Y. pestis* isolates from human cases, animal reservoirs, and vectors, including 439 isolates from Brazil and 474 from elsewhere. The core genome analysis resulted in a conserved sequence that was equivalent to 46% of the CO92 reference strain (GenBank accession no. GCA_000009065.1). The core SNV contained a total of 1,867 SNV sites that diverged from the CO92 genome.

The core SNV approach identified discernible patterns of geographic distribution of *Y. pestis* lineages at the global level. Strains from Brazil were a relatively homogeneous genetic group, assigned within the 1.ORI phylogenetic population (Figure 12). Isolates from Brazil constituted a monophyletic clade that derived directly from strains from South America and North America, which in turn branched from strains from Yunnan and Southeast Asia. That genetic connection sheds light on the historical dissemination of *Y. pestis* in Brazil. Among *Y. pestis* genomes from the NextStrain dataset (https://nextstrain.org), strains from the same geographic plague foci grouped together within the phylogenetic tree (Figure 12).

The plague spikes in Brazil during 1966–1972 were constituted by a basal occurrence of the main, undifferentiated, genetic group that we termed Araripe ancestor (Figure 12), which derived some transitory groups that were unsuccessful in replacing the basal lineage over time. One of those

genetic groups, group D, was isolated in August 1969 and quickly expanded, representing 76% (28/37) of *Y. pestis* isolates during October 1969–March 1970, when the cases in the region ceased. In the second semester of 1970, when plague started to disseminate again, we did not identify any group D strains, and we assigned the new isolates to the Araripe ancestor group.

The *Y. pestis* strains isolated during the 1974–1975 outbreak formed a monophyletic and discernible clade, group E (Figure 12). Of note, the only 2 isolates during the quiescent year of 1973 were group E, which was uncommon in previous years. After 1973, however, that clade promptly replaced the previous strains circulating in the region, which overlapped with an unprecedented upsurge of plague cases (Figure 13). In addition, the lineage replacement caused by group E strains was observed temporally and spatially (Figure 14). We noted the apomorphic mutations that defined each of those derived groups, along with their predicted effects on protein function (Appendix 2 Table 1, https://wwwnc.cdc.gov/EID/article/30/9/24-0468-App2.xlsx).

Discussion

We aimed to dissect plague epidemics that occurred in the Araripe Plateau focus of Brazil. By combining epidemiologic, ecologic, climatic, and genomic information, we were able to learn relevant aspects of the intricate spatiotemporal dynamics of plague in the region. Analysis from the temporal series showed that eco-epidemiologic and climatic factors had a stark and linear influence on the risk for human plague. Monthly rodent and flea positivity rates strongly

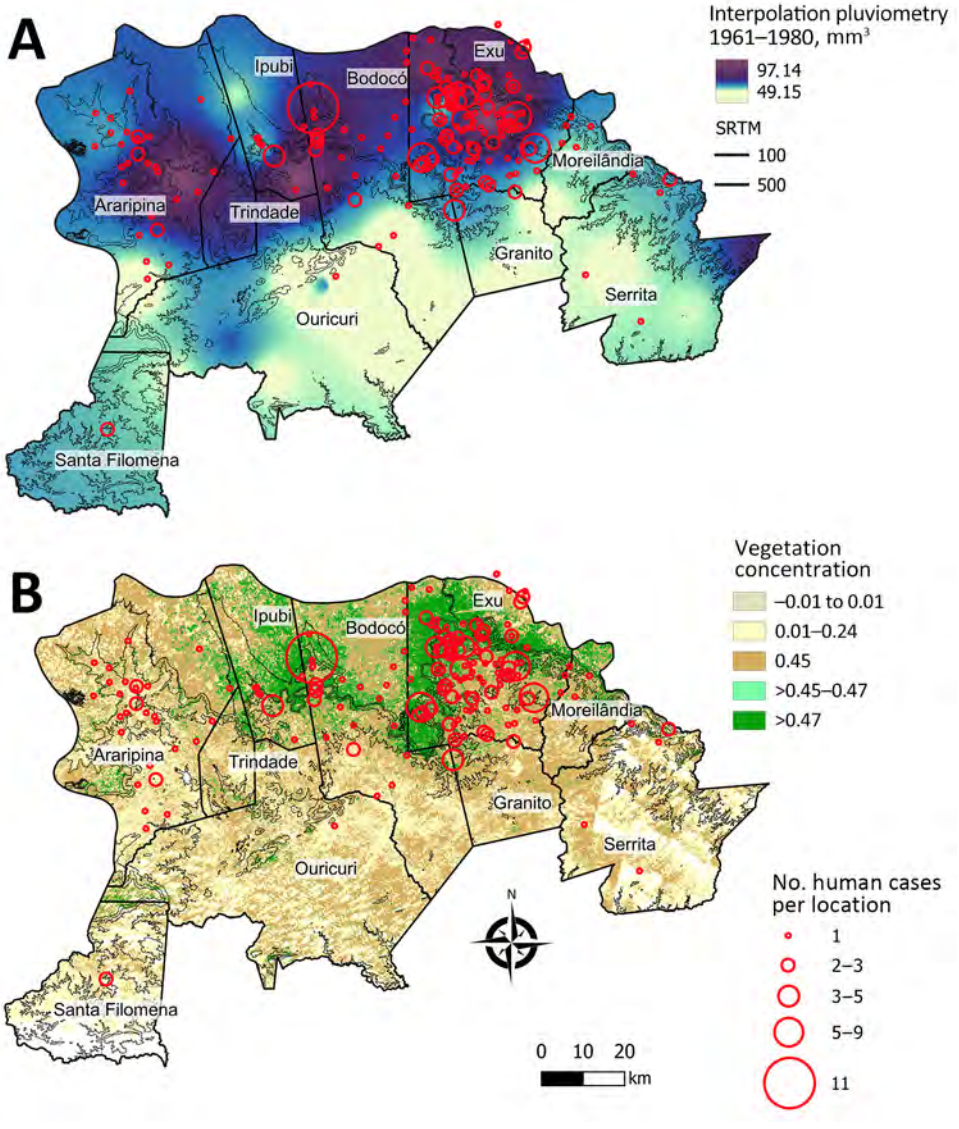

Figure 7. Spatial distribution of rainfall (pluviometry) and vegetation coverage in a study of ecologic, geoclimatic, and genomic factors modulating plague epidemics in primary natural focus, Brazil. A) Locations of human cases and interpolation of average pluviometry (1961–1980) in the Araripe Plateau municipalities of Pernambuco state. B) Locations of human cases and normalized difference vegetation index model showing vegetation concentrated in the slopes of the Araripe Plateau, overlapping the main rainfall and plague case areas. Images obtained by the Landsat 4 satellite in 1984.

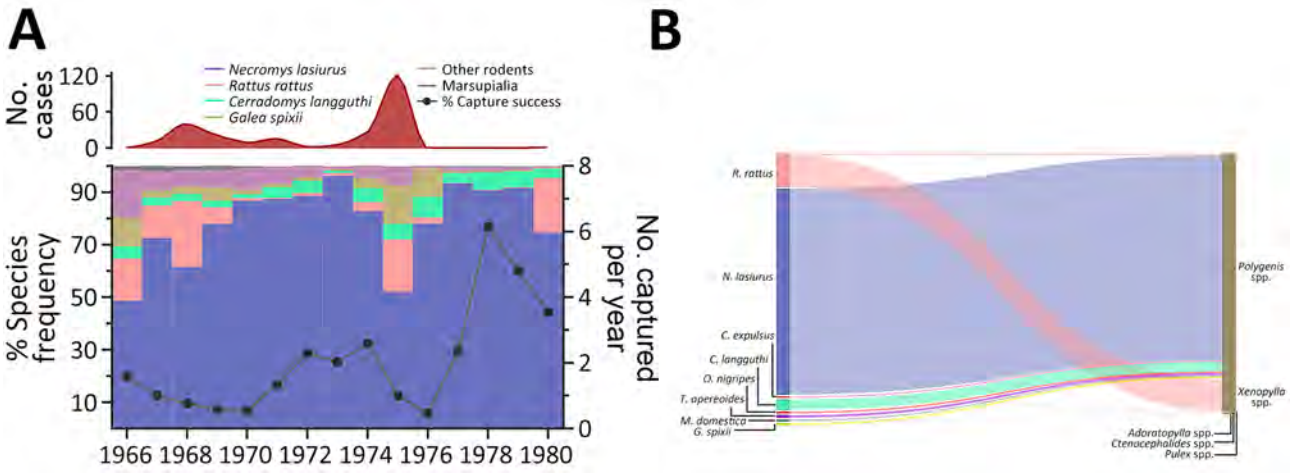

Figure 8. Diversity of rodent and flea species during distinct epidemiologic scenarios of plague in a study of ecologic, geoclimatic, and genomic factors modulating plague epidemics in primary natural focus, Brazil. A) Frequency of each rodent species on capture traps per year (left axis), yearly capture success (right axis) and human plague cases (red curve on top). B) Sankey diagram representing the distribution of rodents and other small mammal hosts according to the flea species and frequency.

indicated the risk for human cases and cutoff values were <1% positivity, meaning any basal detection of *Y. pestis* bacteria in wildlife signaled a risk for human plague cases. Although these indicators have high sensitivity and specificity, detecting early-stage risk requires a large number of sampled animals. Those findings support previous studies suggesting that serosurveys in sentinel species, such as dogs, are more efficient and require fewer tests (*12*).

Human plague in the Araripe Plateau region typically started at the end of the rainy season and peaked in the driest months, August–September. Our results showed that rainfall affected plague dynamics in this semiarid region by modulating the wild rodent and flea abundance. Sylvatic rodent and flea populations expand after the rainy season until the peak of the dry season, and once food and water sources become scarce, rodents carrying vector fleas

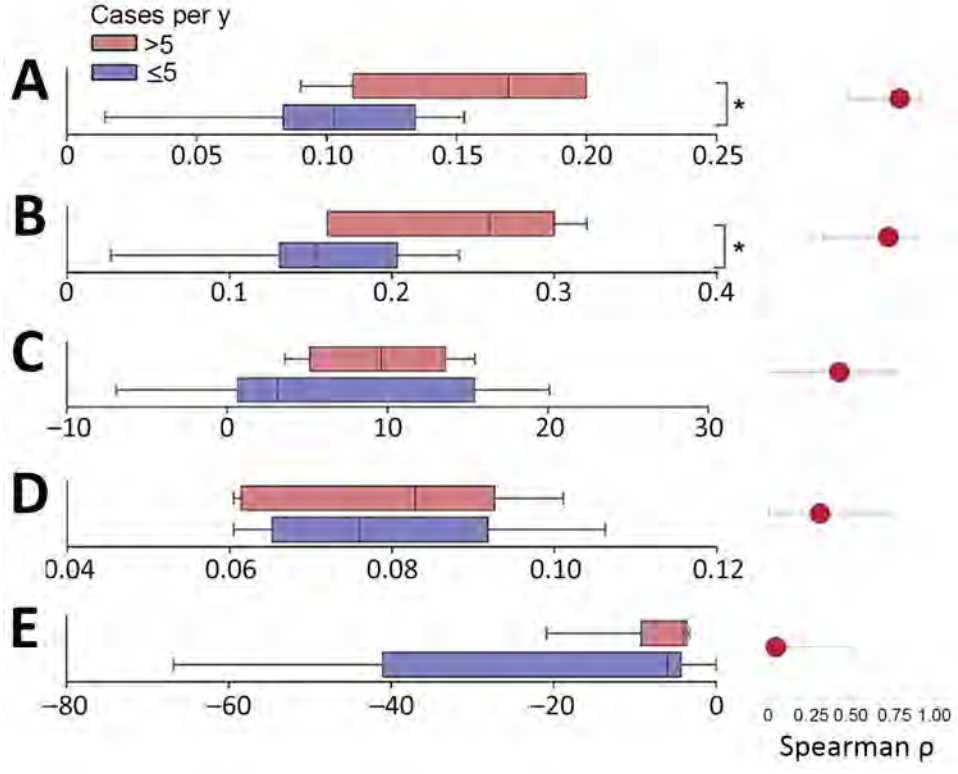

Figure 9. Comparison between ecologic networks parameters in a study of ecologic, geoclimatic, and genomic factors modulating plague epidemics in primary natural focus, Brazil. Graphs compare nonepidemic years (cases ≤5) with epidemic years (cases >5). A) Host robustness; B) vector robustness; C) modularity; D) connectance, which is used to characterize community-wide specialization; E) nestedness based on overlap and decreasing fill. Cutoff value for epidemic status was defined according to the cluster at the principal component analysis. Mann-Whitney test was used to compare groups. Asterisks (*) indicate statistically significant difference ($p<0.05$). The lower and upper error bars correspond to the first and third quartiles (the 25th and 75th percentiles). Vertical lines within boxes represent medians.

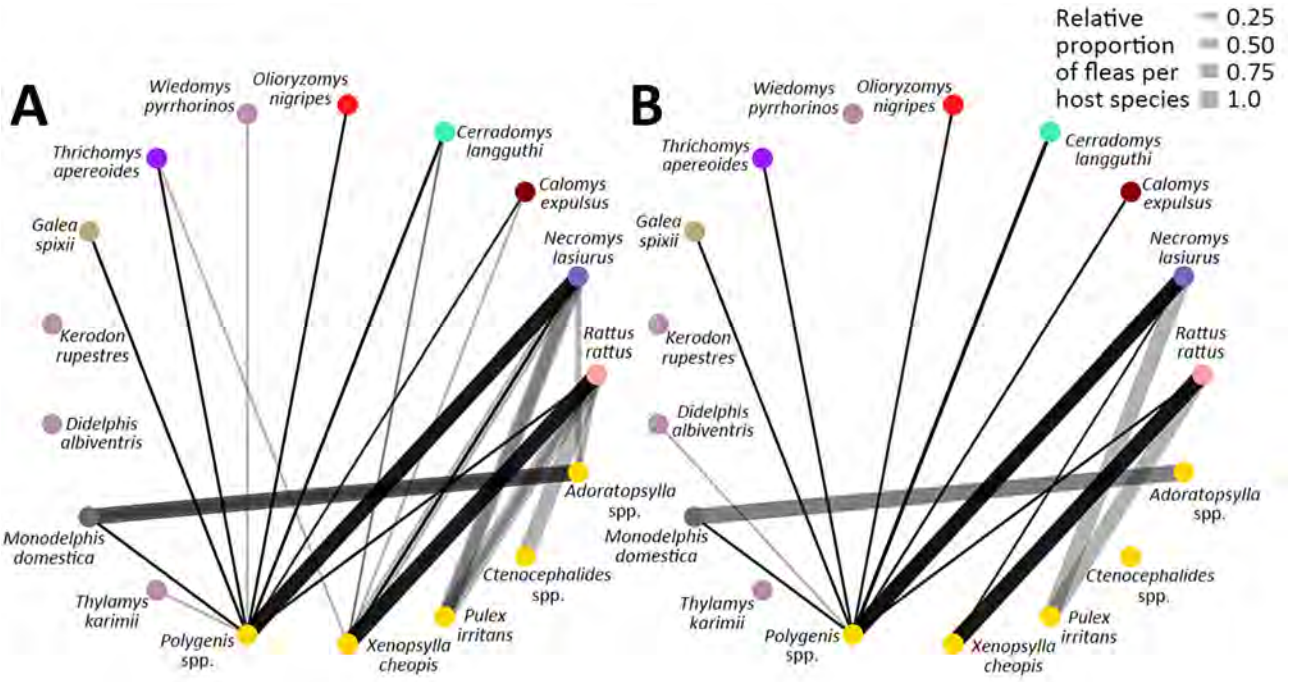

Figure 10. Potential *Yersinia pestis* transmission networks in a study of ecologic, geoclimatic, and genomic factors modulating plague epidemics in primary natural focus, Brazil. A) Epidemic years, ≥5 human cases; B) nonepidemic years, <5 human cases. Transmission networks were based on biologic interactions between host and vector species. Weight of links represent relative proportion of flea species per small mammal.

are attracted to human domestic perimeters by the grain crops grown there. Those events overlap the quick dissemination of plague in the rodent communities, leading to rodent dieoffs and the search for new hosts by the fleas.

Precipitation patterns have been implicated in plague risk in distinct ecosystems (*4*,*13*–*15*). Our findings suggest that rainfall could set the ground conditions for plague dissemination in the following year. Similarly, studies from other plague systems also reported a lagged effect of precipitation on plague risk (*15*–*17*). Of note, the plague epidemic described here overlapped with a period of cool and negative Pacific decadal oscillation teleconnection that lasted until 1976 (*18*–*20*), which is supported by previous studies performed in other ecosystems (*17*).

Geospatial analysis revealed that locations at lower altitudes and closer to the concave sectors from the plateau were at higher risk for plague occurrence. We hypothesized that those locations provided specific conditions that led to the dissemination of plague in wildlife and, eventually,

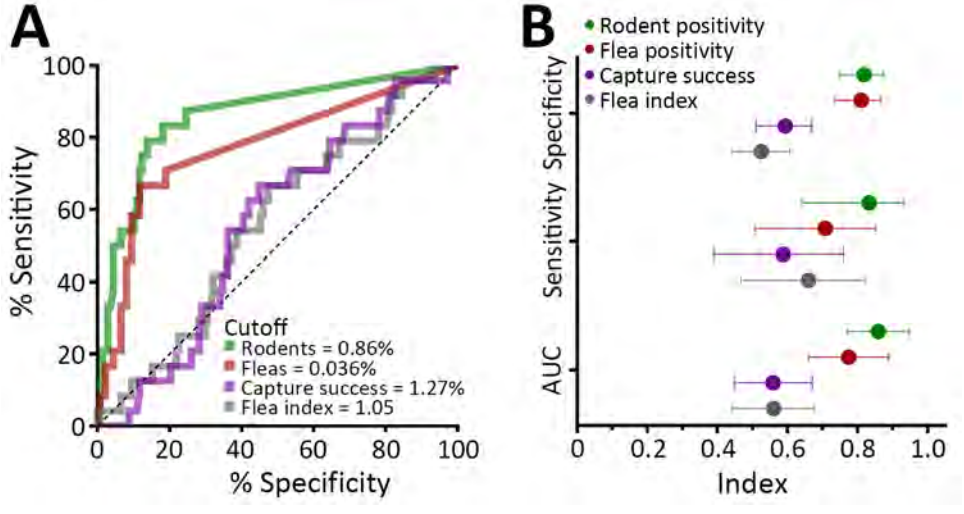

Figure 11. Human risk prediction in a study of ecologic, geoclimatic, and genomic factors modulating plague epidemics in primary natural focus, Brazil. Prediction used ecologic variables at a monthly level. A) Receiver operating characteristic curves and cutoff values of the ecologic variables for the prediction of >2 human cases within the same month. B) Sensitivity, specificity, and AUC for each variable. Error bars indicate 95% CIs. AUC, area under the curve.

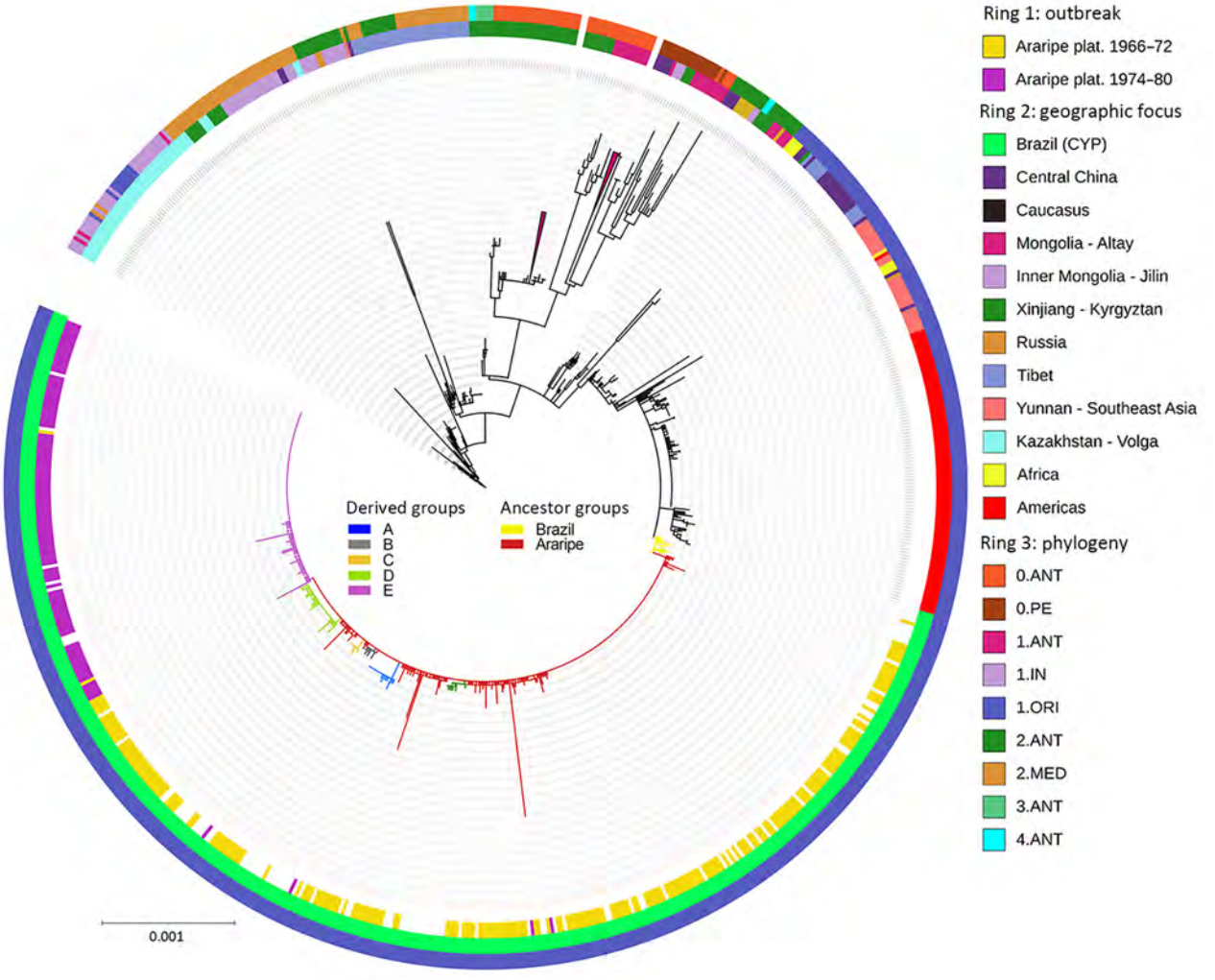

Figure 12. Genomic characterization of *Yersinia pestis* strains in a study of ecologic, geoclimatic, and genomic factors modulating plague epidemics in primary natural focus, Brazil. Phylogenetic tree was based on the 1,867 single-nucleotide variants identified in the core genome from 913 strains isolated in the Araripe Plateau and included in the analysis. The rings contain metadata regarding the epidemiologic features from the Araripe Plateau outbreaks (ring 1), the attributed geographic foci (ring 2), and genetic group provided in the NextStrain dataset (https://nextstrain.org) (ring 3). Brazil branches are colored according to their genetic subgroups. Scale bar indicates nucleotide substitutions per site.

in humans. That hypothesis was further supported by the marked spatial overlap between plague hotspots with increased rainfall and vegetation coverage areas. Of note, although the top of the plateau has savanna-like vegetation, the concave slopes are described to encompass unique characteristics,

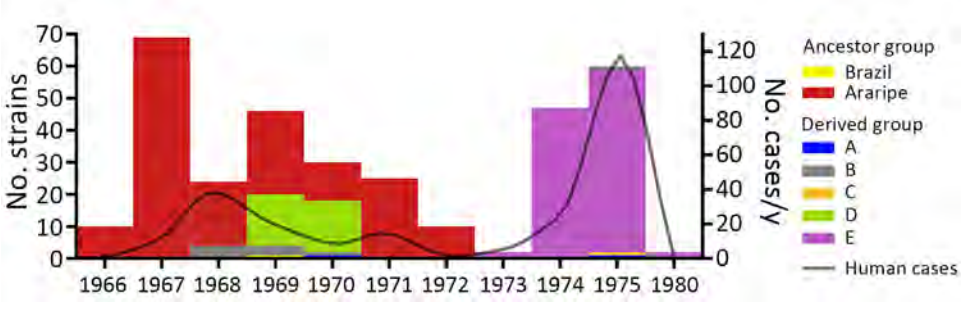

Figure 13. Temporal distribution of *Yersinia pestis* strains in a study of ecologic, geoclimatic, and genomic factors modulating plague epidemics in primary natural focus, Brazil. The graph shows genomic characterization of *Y. pestis* strains from this study compared with the number of human plague cases per year. Scales for the y-axes differ substantially to underscore patterns, but do not permit direct comparisons.

including forest vegetation and increased water availability due to orographic rain (*7*,*21*). Those findings support the trophic cascade hypothesis and underscore the influence of climate factors, such as water availability, vegetation coverage, and host–vector abundance, on *Y. pestis* dissemination. Similar patterns have been observed in other systems, indicating a broader ecologic context where climate is implicated in the spread of plague (*14*,*17*,*22*). Identifying well-defined hotspots with conditions optimal for plague outbreaks is crucial for maximizing an assertive epidemiologic surveillance of this neglected yet reemerging disease, especially in resource-constrained settings.

The scarcity of satellite-derived data throughout the period studied restricted our access to variables essential for modeling the suitability of plague resurgence. Moreover, the abrupt disappearance of plague

Figure 14. Spatial distribution of *Yersinia pestis* strains in a study of ecologic, geoclimatic, and genomic factors modulating plague epidemics in primary natural focus, Brazil. The sequence strains from the Araripe Plateau are shown during various timeframes: A) August 1966–October 1969; B) November 1969–March 1970; C) April 1970–May 1973; and D) June 1973–December 1980. Detailed spatiotemporal dynamics of *Y. pestis* lineages in the Araripe Plateau are available at https://microreact.org/project/fNz1zKcNyCTmKQrtke33Gm-yersinia-pestis-strains-in-the-araripe-plateau-brazil.

after a massive rodent dieoff in 1975 potentially could be attributed to the depletion of sensitive hosts or vectors and the expansion of resistant ones (*22*,*23*). Consequently, further research encompassing later timeframes and integrating satellite-derived climatic, topographic, and land-use data, alongside assessments of host–vector suitability for *Y. pestis* infection, is imperative for accurately modeling potential scenarios of plague resurgence.

Beyond its effects on human health, sylvatic plague raises major conservation concerns. Our findings show that plague activity correlated with substantial declines in abundance of *N. lasiurus* mice. The drastic effect on wild rodent abundance has been reported to cascade through the ecosystem, affecting prey–predator balance and consequently, biodiversity and ecosystem stability (*24*). Furthermore, plague can disturb ecologic systems by directly infecting a wide range of mammal species (*25*,*26*). In this study, the presence of generalist species with extensive interactions contributed substantially to the network's robustness during epidemic years; however, a sharp population decline in those species impacts most of their interaction partners, rendering generalist species surveillance crucial (*27*,*28*). We found the potential for plague maintenance via multiple species interactions, akin to patch dynamics (*29*), is especially evident during epidemic years. Such periods exhibited greater stability in maintaining transmission pathways despite local species extinctions, which was evidenced by higher network robustness in epidemic years.

The amalgamation of phylogenetic and spatiotemporal characteristics in *Y. pestis* isolates from the Araripe focus highlighted the incidence of a foundational ancestral strain. That strain exhibited the capability to evolve into distinct genetic groups, each linked to temporally and spatially constrained outbreaks. Of note, the large outbreak of 1974–1975 was observed in immediate succession to the displacement of previously prevalent *Y. pestis* strains by a singular clade. The expansion of specific *Y. pestis* clades temporarily overlapped with 2 atypical years, 1969 and 1976, in the eco-epidemiologic linear model. Phylogroup D appeared in 1969, and 1976 marked the aftermath of the largest plague outbreak period in the region; strains from that outbreak were genetically characterized by displacement of prior lineages by phylogroup E.

The results from this study rely on records generated during epidemiologic surveillance of human and animal plague. The first limitation of this study is the lack of case-level data in the state of Ceará in the northern range of the Araripe Plateau, which limited most data analysis to the southern part in Pernambuco state. The second limitation is that, although plague surveillance in rodents and fleas was uninterrupted during the study period, outbreaks in specific sites might have biased the rodent capture effort toward specific locations. Finally, because satellite images were available only after the study period, a 4-year delay occurs between surveillance and NDVI representation.

In conclusion, this study identified well-delimited pockets of plague activity spanning areas just a few kilometers wide in the Araripe Plateau region of Brazil. Through the lens of One Health, we determined plague hotspots by using a specific combination of rainfall, vegetation, and landscape features. We also measured the impact of plague activity on wild rodent populations and spillover events in humans. Our research provides a holistic understanding of the ecologic implications of plague in an ecosystem of Brazil. Our findings from Araripe Plateau data could help refine plague risk areas and improve surveillance in other plague foci within the Caatinga biome.

Acknowledgments

We thank Cássia Docena and Gustavo Barbosa Lima and the Núcleo de Plataforma Tecnológica Fiocruz for the assistance during the whole-genome sequencing experiments. We are also thankful to the Coordenação de Coleções Biológicas and Coordenação de Vigilância em saúde e Laboratórios de Referência at Fiocruz for their support. In addition, we thank the Pathogen and Microbiome Institute at Northern Arizona University, Flagstaff, Arizona, USA, for supporting the sequencing of *Yersinia pestis* strains.

The spatial coordinates of meteorology stations, the NextStrain dataset metadata, the sequencing data of the newly sequenced strains and MicroReact input dataset with the Araripe Plateau strains are available in Appendix 2 Tables 3–6 and Appendix 3 (https://wwwnc.cdc.gov/EID/article/30/9/24-0468-App2.xlsx). Fiocruz-CYP strains are also deposited at World Data Centre for Microorganisms (https://www.wdcm.org; collection ID 1040). Individualized data on human cases and surveillance may be accessed upon request to the authors. Data from satellite images and precipitation were obtained from publicly available sources described in Appendix 1. The sequences used in the work are freely available in GenBank; accession numbers are provided in Appendix 2 Table 6.

This work was supported by the Inova Novos Talentos–Fiocruz/Fundação Oswaldo Cruz (grant no. VPPCB-008-FIO-18-2-73 to M.F.B.) and Inova PROEP (grant no. IAM-005-FIO-22-2-2-36 to M.S.).

Author contributions: M.F.B, D.L.S.R., and A.M.P.A. conceived the project; D.L.S.R., E.C.S.G., A.L.S.O, and R.J.P.S. performed the geoprocessing analysis; I.V.R. and M.S. performed the *Yersinia pestis* culture-related experiments and curated the Fiocruz-CYP collection data; I.V.R. performed the genomic sequencing; J.L.L.P.P. and A.M.R. performed the bioinformatic analysis; N.D.A.F., C.S.A., and P.C.E. performed the ecological networks analysis; M.F.B. and A.M.P.A. performed the epidemiological and animal surveillance analysis; A.M.P.A. and D.L.S.R. accessed the PPP documentary collection to acquire epidemiologic and animal surveillance data; A.M.P.A., M.S., and M.F.B. acquired the funding; M.F.B. wrote the original draft of the manuscript, and all authors revised and approved the submitted version.

About the Author

Dr. Bezerra is a biomedical technologist at the Plague National Reference Laboratory, Aggeu Magalhães Institute–Oswaldo Cruz Foundation–Recife, Brazil. His research interests include laboratory diagnosis, genomic surveillance, and epidemiology of plague and other zoonotic diseases.

References

1. Vallès X, Stenseth NC, Demeure C, Horby P, Mead PS, Cabanillas O, et al. Human plague: an old scourge that needs new answers. PLoS Negl Trop Dis. 2020;14:e0008251. https://doi.org/10.1371/journal.pntd.0008251
2. World Health Organization. Plague around the world in 2019. Wkly Epidemiol Rec. 2019;94:289–92.
3. Bramanti B, Stenseth NC, Walløe L, Lei X. Plague: a disease that changed the path of human civilization. Adv Exp Med Biol. 2016;918:1–26. https://doi.org/10.1007/978-94-024-0890-4_1
4. Xu L, Wang Q, Yang R, Ganbold D, Tsogbadrakh N, Dong K, et al. Climate-driven marmot-plague dynamics in Mongolia and China. Sci Rep. 2023;13:11906. https://doi.org/10.1038/s41598-023-38966-1
5. Carlson CJ, Bevins SN, Schmid BV. Plague risk in the western United States over seven decades of environmental change. Glob Change Biol. 2022;28:753–69. https://doi.org/10.1111/gcb.15966
6. Faria ACM, Almeida AMP, Lima Júnior FEF, Fonseca LX, Sobreira M, Nunes ML, et al. Plague [in Portuguese]. In: Werneck GL, editor. Health Surveillance Guide, 3rd edition [in Portuguese]. Brasília: Ministry of Health; 2023. p. 1077–90.
7. Guerra M, Silva MJSE. Palm swamps of the Araripe Plateau: subspaces of exception in the semiarid of the state of Ceará, Brazil. Ateliê Geográfico. 2020;14:51–66.
8. Menezes Silva MT, Falcão Sobrinho J, Bezerra de Souza E. Floristic composition in slope areas with different land uses in Chapada do Araripe–CE [in Portuguese]. Geosul. 2022;37:117–40. https://doi.org/10.5007/2177-5230.2022.e82020
9. Fernandes DLRDS, Gomes ECS, Bezerra MF, E Guimarães RJPS, de Almeida AMP. Spatiotemporal analysis of bubonic plague in Pernambuco, northeast of Brazil: case study in the municipality of Exu. PLoS One. 2021;16:e0249464. https://doi.org/10.1371/journal.pone.0249464
10. Baltazard M. The exemplary approach of a field epidemiologist M. Baltazard and the plague foyers of the Brazilian Northeast [in Portuguese]. Bull Soc Pathol Exot. 2004;97:87–117.
11. Pitta JLLP, Bezerra MF, Fernandes DLRDS, Block T, Novaes AS, Almeida AMP, et al. Genomic analysis of *Yersinia pestis* strains from Brazil: search for virulence factors and association with epidemiological data. Pathogens. 2023;12:991. https://doi.org/10.3390/pathogens12080991
12. Gage K. Plague surveillance. In: Dennis DT, Gage KL, Gratz NG, Poland JD, Tikhomirov E, editors. Plague manual: epidemiology, distribution, surveillance and control. Geneva: World Health Organization; 1999.
13. Yuan X, Yang L, Li H, Wang L. Spatiotemporal variations of plague risk in the Tibetan Plateau from 1954–2016. Biology (Basel). 2022;11:304. https://doi.org/10.3390/biology11020304
14. Xu L, Schmid BV, Liu J, Si X, Stenseth NC, Zhang Z. The trophic responses of two different rodent-vector-plague systems to climate change. Proc Biol Sci. 2015;282:20141846. https://doi.org/10.1098/rspb.2014.1846
15. Parmenter RR, Yadav EP, Parmenter CA, Ettestad P, Gage KL. Incidence of plague associated with increased winter-spring precipitation in New Mexico. Am J Trop Med Hyg. 1999;61:814–21. https://doi.org/10.4269/ajtmh.1999.61.814
16. Brown HE, Ettestad P, Reynolds PJ, Brown TL, Hatton ES, Holmes JL, et al. Climatic predictors of the intra- and inter-annual distributions of plague cases in New Mexico based on 29 years of animal-based surveillance data. Am J Trop Med Hyg. 2010;82:95–102. https://doi.org/10.4269/ajtmh.2010.09-0247
17. Enscore RE, Biggerstaff BJ, Brown TL, Fulgham RE, Reynolds PJ, Engelthaler DM, et al. Modeling relationships between climate and the frequency of human plague cases in the southwestern United States, 1960–1997. Am J Trop Med Hyg. 2002;66:186–96. https://doi.org/10.4269/ajtmh.2002.66.186
18. Andreoli R, Kayano MT. ENSO-related rainfall anomalies in South America and associated circulation features during warm and cold Pacific decadal oscillation regimes. Int J Climatol. 2005;25:2017–30. https://doi.org/10.1002/joc.1222
19. Rolim LZR, Oliveira da Silva SM, de Souza Filho F. Analysis of precipitation dynamics at different timescales based on entropy theory: an application to the State of Ceará, Brazil. Stochastic Environ Res Risk Assess. 2022;36:2285–301. https://doi.org/10.1007/s00477-021-02112-y
20. Garreaud RD, Vuille M, Compagnucci R, Marengo J. Present-day South American climate. Palaeogeogr Palaeoclimatol Palaeoecol. 2009;281:180–95. https://doi.org/10.1016/j.palaeo.2007.10.032
21. Lima FJ, Corrêa ACB, Lima GG, Marçal MS, Paisani JC, Pontelli ME. Late quaternary geomorphological evolutionary dynamics of the Araripe sedimentary plateau, northeast of Brazil. J S Am Earth Sci. 2023;124:1–13.
22. Ben Ari T, Gershunov A, Gage KL, Snäll T, Ettestad P, Kausrud KL, et al. Human plague in the USA: the importance of regional and local climate. Biol Lett. 2008;4:737–40. https://doi.org/10.1098/rsbl.2008.0363
23. Andrianaivoarimanana V, Rajerison M, Jambou R. Exposure to *Yersinia pestis* increases resistance to plague in black rats and modulates transmission in Madagascar.

BMC Res Notes. 2018;11:898. https://doi.org/10.1186/s13104-018-3984-3
24. Biggins ED, Kosoy MY. Influence of introduced plague on North American mammals: implications from ecology of plague in Asia. J Mammal. 2001;82:906–16. https://doi.org/10.1644/1545-1542(2001)082<0906:IOIPON>2.0.CO;2
25. Eads DA, Livieri TM, Dobesh P, Hughes JP, Fly J, Redmond H, et al. Plague mitigation for prairie dog and black-footed ferret conservation: degree and duration of flea control with 0.005% fipronil grain bait. Curr Res Parasitol Vector Borne Dis. 2023;3:100124. https://doi.org/10.1016/j.crpvbd.2023.100124
26. Bevins SN, Chandler JC, Barrett N, Schmit BS, Wiscomb GW, Shriner SA. Plague exposure in mammalian wildlife across the western United States. Vector Borne Zoonotic Dis. 2021;21:667–74. https://doi.org/10.1089/vbz.2020.2765
27. Dallas T, Cornelius E. Co-extinction in a host-parasite network: identifying key hosts for network stability. Sci Rep. 2015;5:13185. https://doi.org/10.1038/srep13185
28. Reis Da Silva Fernandes DL, Filgueira Bezerra M, Sobreira Bezerra DA Silva M, Leal NC, DE Souza Reis CR, DE Almeida AMP. Rodent hosts and flea vectors in Brazilian plague foci: a review. Integr Zool. 2021;16:810–9. https://doi.org/10.1111/1749-4877.12480
29. Strona G, Lafferty KD. Environmental change makes robust ecological networks fragile. Nat Commun. 2016;7:12462. https://doi.org/10.1038/ncomms12462

Address for correspondence: Matheus Bezerra, Departamento de Microbiologia, Instituto Aggeu Magalhães, Brazil Av. Professor Moraes Rego–Campus UFPE, Fiocruz 50740-465, Brazil; email: matheus.bezerra@fiocruz.br

Use of Open-Source Epidemic Intelligence for Infectious Disease Outbreaks, Ukraine, 2022

Anjali Kannan, Rosalie Chen, Zubair Akhtar, Braidy Sutton, Ashley Quigley, Margaret J. Morris, C. Raina MacIntyre

Formal infectious disease surveillance in Ukraine has been disrupted by Russia's 2022 invasion, leading to challenges with tracking and containing epidemics. To analyze the effects of the war on infectious disease epidemiology, we used open-source data from EPIWATCH, an artificial intelligence early-warning system. We analyzed patterns of infectious diseases and syndromes before (November 1, 2021–February 23, 2022) and during (February 24–July 31, 2022) the conflict. We compared case numbers for the most frequently reported diseases with numbers from formal sources and found increases in overall infectious disease reports and in case numbers of cholera, botulism, tuberculosis, HIV/AIDS, rabies, and salmonellosis during compared with before the invasion. During the conflict, although open-source intelligence captured case numbers for epidemics, such data (except for diphtheria) were unavailable/underestimated by formal surveillance. In the absence of formal surveillance during military conflicts, open-source data provide epidemic intelligence useful for infectious disease control.

On February 24, 2022, Russia forces launched an armed attack against Ukraine (*1*), escalating the ongoing Russo-Ukrainian conflict that began in 2014 when Russia annexed Crimea and resulting in one of Europe's biggest threats to peace and security since the Cold War (*2*). The healthcare sector in Ukraine has been heavily affected, and 18 months into the recent conflict, ≈10,000 civilians had died (*3*). Such conflict situations increase the risk for epidemics (*4*), and the disruption or cessation of public health surveillance creates challenges for tracking them. Rapid epidemic intelligence using open-source data may be an alternative form of surveillance for infectious disease outbreaks during times of conflict.

Author affiliation: University of New South Wales, Kensington, Sydney, New South Wales, Australia

DOI: https://doi.org/10.3201/eid3009.240082

Before 2022, the healthcare system in Ukraine had already experienced major stressors, including 8 years of conflict in the eastern part of the country, followed by the COVID-19 pandemic (*1*). Several weeks before Russia invaded, the fourth COVID-19 wave in Ukraine peaked, further decreasing numbers of available healthcare staff and increasing stress on hospitals (*1*). As of February 20, 2022, only 34.5% of the Ukraine population had received 2 doses of COVID-19 vaccine and only 2% of the eligible population had received a booster (*5*).

Other vaccine-preventable diseases were also highly prevalent in Ukraine before the invasion, and some of the lowest vaccine coverage rates in Europe were in Ukraine (*5*). For example, vaccine-derived poliomyelitis reemerged in 2021, after previous cases in 2015 and 2016 (*6*,*7*). A polio vaccination campaign targeting 140,000 children was implemented shortly after the outbreak but was paused as the conflict began (*6*). Similarly, a large measles epidemic affected Ukraine during 2017–2019, in part because of low vaccination coverage, which was the lowest in Europe in 2016 (31%) (*5*). Although reported cases decreased substantially in 2020 (264 cases) and 2021 (16 cases), recent shortages in measles vaccines pose a threat (*8*).

Compared with rates for most other countries in Europe, rates of tuberculosis (TB) in Ukraine are higher, and a substantial proportion of infections are multidrug resistant (*5*). Before the recent conflict, the COVID-19 pandemic had also significantly affected TB diagnosis and treatment centers, thus hindering TB control (*9*).

In 2019, the second largest HIV/AIDS epidemic in eastern Europe and central Asia was in Ukraine; ≈1.0% of the Ukraine population were reported to be living with the infection (*10*,*11*). Drivers of the epidemic included risky drug injection practices and disruption of treatment centers because of

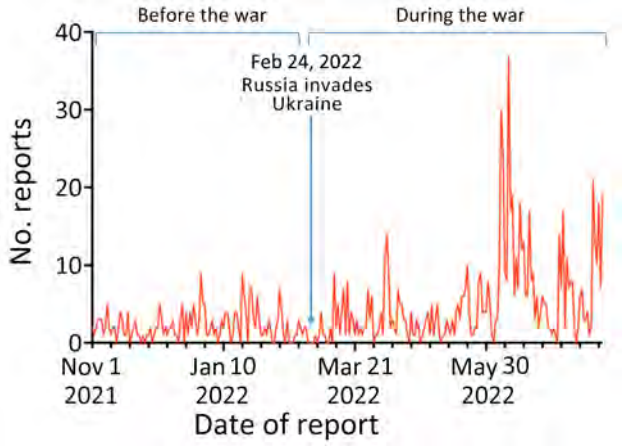

Figure 1. Daily EPIWATCH (https://www.epiwatch.org) reports of outbreaks in Ukraine before and during Russia's invasion, November 1, 2021–July 31, 2022.

conflict, which could further exacerbate the HIV/AIDS burden in Ukraine (*6*).

The ongoing conflict, escalated by the invasion, has resulted in the destruction of healthcare infrastructure in Ukraine (*12*). In the 11 months after Russia invaded, 707 attacks on the Ukraine healthcare system were reported (*12*). Disruption of vaccination programs, limited testing capacity, displacement, and overcrowding can increase the risk for reemergence of vaccine-preventable infections such as polio, COVID-19, influenza, measles, TB, and pertussis (*6*). In addition, water supplies in cities such as Mariupol are not safe to drink because of damaged sewage systems and raw sewage leakage into nearby rivers and streams, yet many people still drink contaminated water (*4*). Risk for various infectious diseases is further increased by lack of regular housing and shelter, reduced caloric intake, and poor hygiene and sanitation.

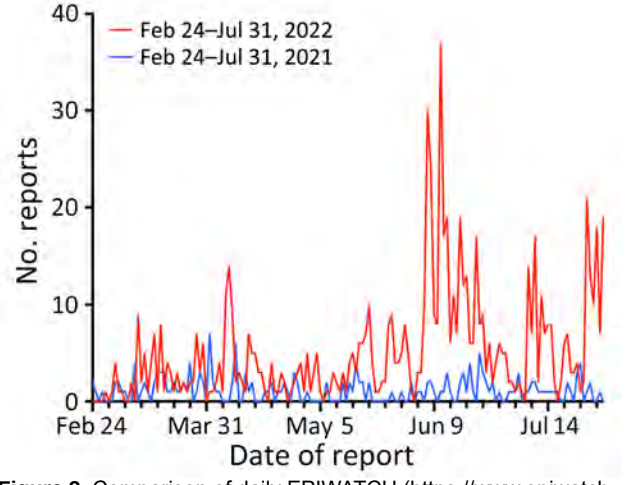

Figure 2. Comparison of daily EPIWATCH (https://www.epiwatch.org) reports of outbreaks in Ukraine during Russia's invasion (February 24, 2022–July 31, 2022) and in the same period of the previous year (February 24, 2021–July 31, 2021).

After February 2022, formal surveillance for most infectious diseases ceased, and reporting of notifiable infectious diseases has since been minimal. Open-source data can help overcome the lack of formal disease surveillance by harnessing information from open sources such as news media, medical organizations, and social media. Use of artificial intelligence (AI) can generate early warning signals from open-source data and provide epidemiologic information regarding infectious diseases in the absence of formal surveillance in a war zone (*13*).

To analyze patterns of infectious diseases and syndromes before (November 1, 2021–February 23, 2022) and during (February 24–July 31, 2022) the invasion (hereafter called the conflict), we used EPIWATCH (https://www.epiwatch.org), an open-source AI-based epidemic early warning system that has been operating since 2016. EPIWATCH collects open-source data, which are then processed by 2 AI systems to generate epidemic signals (*13*); the system has the proven capacity to capture early warning signals for infectious diseases (*14*–*16*). Because our study involved analysis of open-source published data that was anonymous, ethics approval was not required.

Methods

To enable comparison of periods before and during the conflict, we gathered open-source data from EPIWATCH for Ukraine for 2 periods before (November 1, 2021–February 23, 2022, and February–July 2021) and during (February 24–July 31, 2022 the conflict. EPIWATCH collects outbreak reports on specific infectious diseases and clinical syndromes, including undiagnosed syndromes such as severe acute respiratory infection, pneumonia, rash and fever, and encephalitis.

The before-conflict period served as a baseline for comparing disease reports from the during-conflict period. To capture a relevant snapshot of epidemics in Ukraine around the time the conflict began, which could influence epidemics occurring during the conflict, we selected the 3 months before the conflict as a baseline for the immediate before-conflict period. To account for seasonal variations of disease incidence, we also collected data for the same period during the previous year (February 24–July 31, 2021) as a second comparator.

EPIWATCH searches for ≈200 specific disease and syndrome terms in 46 languages, and ≈70% of all intelligence gathered is from non-English sources

(*17*). EPIWATCH gathered data for all areas within the internationally recognized borders of Ukraine in the Ukrainian and Russian languages (because Russian is spoken in some parts of Ukraine). The Russian language had already been in use in EPIWATCH since September 2019. After Russia invaded Ukraine on February 24, 2022, the EPIWATCH team added the Ukrainian language to the EPIWATCH search engine. To reduce ascertainment bias caused by adding a new language, identical EPIWATCH search terms were applied retrospectively in the Ukrainian language by using the Google search engine for the 2 before-conflict control periods in 2021–2022; those terms were added to the dataset to compare trends before and during the conflict. Because the retrospective search used the same search terms and search engine (Google) for prospective data collection, the results should be comparable.

We downloaded EPIWATCH outbreak report data for Ukraine for the periods of interest, combined with retrospective data in the Ukrainian language, and screened the data for eligibility. Inclusion criteria for the final analysis were reports focusing on infectious diseases and syndromes among humans; zoonotic diseases (diseases circulating among animals that can be transmitted to humans); and having data regarding confirmed, probable, or suspected cases. We excluded reports not meeting those criteria.

To conduct descriptive epidemiologic analysis of outbreak reports, we used Microsoft Excel (https://www.microsoft.com). We extracted data on diseases, syndromes, populations affected, and location and time and analyzed the data by reporting periods. We compared numbers of reports from the before- and during-conflict periods as well as from the previous year and constructed graphs by using Prism (GraphPad, https://www.graphpad.com).

We next extracted case numbers from the reports. We extracted from EPIWATCH reports the number of cases of the 8 most reported diseases and created a line list for further analysis. We included cases in the line list only if reports had definitive numbers. If case numbers were vague or cumulative, we excluded them. We also removed duplicate case numbers. Then, we searched for formal case numbers published by organizations engaged in formal surveillance (e.g., the World Health Organization and the European Centre for Disease Control and Prevention). We then compared during-conflict case numbers from EPIWATCH with case numbers of the same diseases published by formal surveillance during the same period, when available.

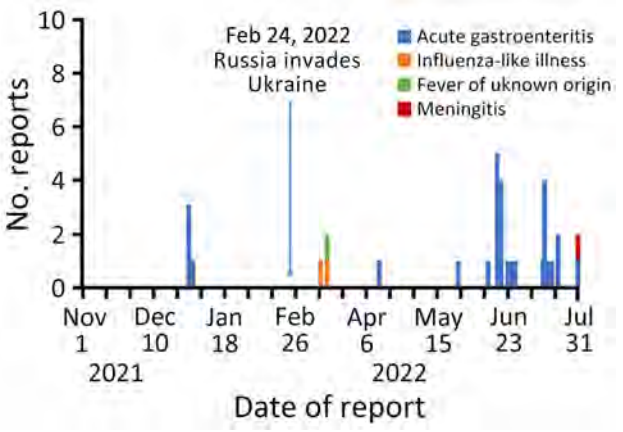

Figure 3. Number of reports of clinical syndromes per day before and during Russia's invasion, Ukraine, November 1, 2021—July 31, 2022.

Results

We identified 805 outbreak reports in EPIWATCH during February 24, 2022–July 31, 2022, for an average of 5 reports per day. In comparison, 259 reports were collected in the 3 months before the conflict (November 1, 2021–February 23, 2022), an average of 2 reports per day (Figure 1). Reports initially peaked (n = 14) on April 7, 2022, largely regarding a diphtheria outbreak in the Ternopil Oblast of western Ukraine. The largest peak was in June, when 37 reports were attributed to an outbreak of cholera in Mariupol in eastern Ukraine. For the same period in the previous year, we found 180 reports, indicating a 447% increase during the conflict (Figure 2).

Before the invasion, there were a total of 4 reports of clinical syndromes, all of which were acute gastroenteritis (Figure 3). After the invasion, syndromic reports increased; acute gastroenteritis (87.1% of reports) was the most common, followed by influenza-like illness (6.5%), fever of unknown origin (3.2%), and meningitis (3.2%).

According to individual reports from June 2022 of acute gastroenteritis, many illnesses were identified as dysentery or suspected cholera. Among other reports of acute gastroenteritis, a report from May 26, 2022, cited an outbreak of unknown cause resulting in acute gastroenteritis signs/symptoms among 17 internally displaced persons in the Lviv region. In addition, starting on July 20, 2022, an outbreak affecting 91 persons within 1 week was reported in the Odessa region. A report of meningitis recorded on July 31, 2022, mentioned an overall increase in viral/bacterial meningitis cases in Ukraine since before the conflict.

Before the conflict, the most frequently reported outbreaks were COVID-19, influenza, and

poliomyelitis, accounting for 70% of the total reports during that period (Table 1). In the during-conflict period, the most frequently reported diseases were COVID-19 (increased from 106 to 187 reports), cholera (from 0 to 157 reports), botulism (from 22 to 122 reports), TB (from 11 to 75 reports), HIV/AIDS (from 6 to 61 reports), rabies (from 12 to 40 reports), salmonellosis (from 4 to 39 reports), and diphtheria (from 2 to 29 reports) (Table 2). Only cholera was not reported before the conflict.

Table 1. Numbers of daily reports of disease outbreaks before and during Russia's invasion, by disease, Ukraine, November 1, 2021–July 31, 2022*

Disease	No. reports	
	Before conflict	During conflict
COVID-19	106	187
Cholera	0	157
Botulism	22	122
Tuberculosis	11	75
HIV/AIDS	6	61
Rabies	12	40
Salmonellosis	4	39
Diphtheria	2	29
Poliomyelitis	37	19
Varicella	1	15
Rotavirus infection	9	15
Malaria	8	13
Influenza	39	10
Measles	1	9
Leptospirosis	1	8
SARS-CoV-1 infection	3	8
Other†	2	7
Hepatitis A	0	6
Escherichia coli infection	2	5
Hepatitis, unspecified	0	4
Hepatitis C	1	4
Lyme disease	0	3
Encephalitis	0	3
Tularemia	1	3
Staphylococcus infection	2	3
Anthrax, unspecified	0	2
Mpox	0	2
Shigellosis	0	2
Smallpox	0	2
Meningococcal	2	2
CCHF	0	1
Newcastle disease	0	1
Q fever	0	1
Tetanus	0	1
Yersiniosis	0	1
Typhoid fever	1	1
Dirofilariasis	2	1
Avian influenza, unspecified	4	1
Brucellosis	1	0
Influenza A(H1N1)	3	0
Influenza A(H3N2)	11	0
Influenza A(H5N1)	1	0
Influenza B	1	0
Listeriosis	5	0
Pneumonia of unknown origin	1	0
Rubella	1	0
Trichinellosis	1	0

*Data are reports of outbreaks, not case numbers. CCHF, Crimean-Congo hemorrhagic fever.
†Reports containing information about diseases that were deemed by EPIWATCH analysts to not fit in any of the existing disease/syndrome

Frequency of reporting decreased for poliomyelitis (from 37 to 19 reports), influenza-unspecified (from 39 to 10 reports), and influenza A(H3N2) (0 reports) during the conflict (Table 1).

With regard to our comparison of case numbers from EPIWATCH and from formal surveillance, most diseases were not reported by formal surveillance, except for botulism, TB, and diphtheria (Table 3). For botulism, the number of cases identified through EPIWATCH (32 cases) was lower than that identified through formal surveillance (51 cases) (*22*). For TB, the only statistic found by formal surveillance was for the Rivne Oblast for the first quarter of 2022 (113 cases), whereas EPIWATCH was able to collect case number data for the entire reporting period and across more locations (5,647 cases) (*23*). Both EPIWATCH and formal surveillance identified 2 cases of diphtheria (*22*).

Discussion

The ongoing escalation of the conflict in Ukraine is one of the world's fastest growing humanitarian crises and has disrupted health systems and reduced outbreak detection and response capabilities in the country (*24*). We have demonstrated the value of using open-source epidemic intelligence to gain information about unfolding epidemics and public health priorities in a conflict zone where formal surveillance is reduced or lacking. We were able to identify new epidemics that occurred during the conflict, such as cholera, botulism, and human cases of rabies (which were presumably exacerbated by an increased number of displaced domestic dogs). The increases in cholera and gastroenteritis reflect declining hygiene and sanitation during the conflict, including lack of access to safe drinking water and toilets and subsequent improper disposal of fecal waste (*25*). The increase may also be exacerbated by improper handling and disposal of dead bodies (*26*), such as burial in shallow graves, which increases the risk for transmission of some diseases (*26*,*27*). We also identified increased HIV/AIDS and TB cases. HIV clinics were shut down during the conflict (*4*), most likely affecting testing and surveillance. In addition, medications such as antiretroviral drugs have become scarce or been misused, which may increase the risk for drug-resistant HIV and may subsequently limit treatment options and further increase transmission (*6*). Overall, the disruption of transportation networks during the conflict has decreased access to medical supplies and treatment for infectious diseases (*4*). Lack of access to testing and treatments has also resulted in loss of continuity of care, poorer outcomes, and increased community transmission (*6*).

Table 2. Case numbers for the most frequently reported diseases seasonally and before and during Russia's invasion, by period, Ukraine

Disease	Seasonal, February 24–July 31, 2021	Before invasion, November 1, 2021–February 23, 2022	During invasion, February 24–July 31, 2022
COVID-19	279,671	599,695	7,338
Cholera	0	0	10,015
Botulism	9	11	32
Tuberculosis	5,851	4,799	5,647
HIV + AIDS	3,717	3,255	4,333
Rabies			
Human	0	2	13
Animal	0	11	20
Salmonellosis	109	0	57
Diphtheria	0	7	2

Using EPIWATCH, we were able to extract more complete case data for the 8 most reported infectious diseases compared with formal surveillance. During the conflict, formal reporting of infectious diseases such as COVID-19 notably decreased, most likely because of lack of testing. The collapse of formal surveillance systems in Ukraine during the conflict resulted from a variety of factors (e.g., high levels of displacement, attacks on healthcare facilities, lack of routine data collection, limited testing and treatment, reduced diagnostic capabilities, and changes in disease testing policies) (*28*). After the invasion, case numbers from the Ukraine government or other formal surveillance sources for many diseases either ceased to be reported or were not up to date. Some formal surveillance systems continued to report cases of botulism, TB, and diphtheria, but even for those, we showed that numbers are probably underestimated.

Weak or absent formal surveillance during wartime hampers timely and targeted interventions such as vaccination programs (*29*). Solely relying on formal surveillance may result in missed early warning signals from other sources, heightening the risk that diseases will spread internationally, particularly if refugees migrate to other countries. In that context, open-source epidemic intelligence can provide early warnings of epidemics.

Among the limitations of our study, open-source data are not subject to validation compared with formal surveillance data. However, EPIWATCH uses 3 AI subsystems to improve data quality and exclude irrelevant material (*30*). All data are then further curated by human analysts, who follow standardized operating procedures. EPIWATCH provides reports of outbreaks, rather than case numbers; thus, monitoring report trends reflects signal strength, and case numbers extracted from reports may be less precise. However, for most diseases there was no formal surveillance or case reporting during the

Table 3. Comparison of cases extracted from outbreak reports collected by EPIWATCH and by formal surveillance during Russia's invasion for the 8 most frequently reported diseases, Ukraine, February 24–July 31, 2022*

Disease	No. cases obtained from EpiWatch	No. cases reported by government or other surveillance
COVID-19	7,338	COVID-19 surveillance in Ukraine ceased in February 2022 (*18*).
Cholera	10,015	None. The WHO situation report from June 22, 2022, mentions increased social media publications about the threat of cholera, and the report from June 29, 2022, mentions the detection of non-O1 *Vibrio cholerae* environmental samples; however, no case numbers were reported (*19*,*20*). In December 2022, WHO published a 2022 global situational summary report on cholera; however, it did not mention of cases of cholera in Ukraine (*21*).
Botulism	32	51 cases were reported by the WHO Health Cluster Ukraine in the first 6 months of 2022 (*22*).
Tuberculosis	5,647	113 cases were reported by the WHO Health Cluster Ukraine in the Rivne Oblast for the first quarter of 2022, with a last update on April 2022 (*23*).
HIV + AIDS	4,333	None. The cessation of HIV/AIDS surveillance has not officially been announced; no government or other reporting was found.
Rabies		None. The cessation of rabies surveillance has not officially been announced; no government or other reporting was found.
Human	13	
Animal	20	
Salmonellosis	57	None. The cessation of salmonellosis surveillance has not officially been announced; no government or other reporting was found.
Diphtheria	2	2 cases were reported by the WHO Health Cluster Ukraine, with last update in April 2022 (*22*).

*EPIWATCH (https://www.epiwatch.org) statistics are for total cases in the entire country and not specific oblasts. WHO, World Health Organization.

conflict, whereas we were able to extract case numbers from the open-source reports. Another limitation is ascertainment bias because media reporting may be increased in regions of Ukraine with larger populations. As a result, data from smaller regions were less frequently obtained, and thus, infectious diseases may be underestimated. Last, because we added the Ukrainian language in February 2022, ascertainment bias could have contributed to the observed increase in reports from that time. However, we accounted for that difference by using a control period in the previous year, for which we retrospectively collected data in the Ukrainian language. Historical open-source reports of outbreaks from Ukraine might have been removed or censored by 2022, which may have reduced the potential for data capture; however, there is no evidence to suggest this was the case. A longer control period may have been more informative of longer-term trends and is planned in a follow-up study.

Our study provides an overview of epidemic activity in Ukraine during the Russian escalation of the Russo-Ukrainian war in 2022, demonstrating that EPIWATCH was able to capture a breadth of data that was not captured by other formal sources. Open-source digital disease surveillance therefore provides a useful way to gather real-time health intelligence in a conflict zone when formal surveillance is absent or reduced. Using EPIWATCH and other open-source health intelligence systems can be valuable for real-time decision support in disaster contexts, including conflict or natural disasters.

Funding for EPIWATCH comes from the Balvi Filantropik. Fund, which supports A.K., R.C., Z.A., B.S., and A.Q. C.R.M. is supported by a National Health and Medical Research Council Investigator grant (no. 2016907).

C.R.M. and M.J.M. conceived the study; A.K., C.R.M., and M.J.M. designed the study methods; A.K. conducted the analysis with assistance from R.C., Z.A., and B.S. and oversight by A.Q. C.R.M. and M.J.M. supervised the analysis, provided guidance on analysis, reviewed the outputs of the analysis, and provided critical feedback. All authors contributed to the final manuscript.

About the Author

Ms. Kannan is a research officer at the National Centre for Immunisation Research and Surveillance, Australia, and is currently completing a master's degree in public health at the University of New South Wales. Her research interests are infectious disease epidemiology, health policy, and health emergencies.

References

1. Roborgh S, Coutts AP, Chellew P, Novykov V, Sullivan R. Conflict in Ukraine undermines an already challenged health system. Lancet. 2022;399:1365–7. https://doi.org/10.1016/S0140-6736(22)00485-8
2. Mankof J. Russia's War in Ukraine: Identity, History, and Conflict. Washington: Institute for National Strategic Studies; 2022.
3. United Nations Department of Operational Support. Ukraine: report documents mounting deaths, rights violations. New York: United Nations; 2023.
4. The Lancet Infectious Diseases. War and infectious diseases: brothers in arms. Lancet Infect Dis. 2022;22:563. https://doi.org/10.1016/S1473-3099(22)00235-3
5. Nijman RG, Bressan S, Brandenberger J, Kaur D, Keitel K, Maconochie IK, et al. Update on the coordinated efforts of looking after the health care needs of children and young people fleeing the conflict zone of Ukraine presenting to European Emergency Departments—a joint statement of the European Society for Emergency Paediatrics and the European Academy of Paediatrics. Front Pediatr. 2022;10:897803. https://doi.org/10.3389/fped.2022.897803
6. Essar MY, Matiashova L, Tsagkaris C, Vladychuk V, Head M. Infectious diseases amidst a humanitarian crisis in Ukraine: a rising concern. Ann Med Surg (Lond). 2022;78:103950. https://doi.org/10.1016/j.amsu.2022.103950
7. World Health Organization. Circulating vaccine-derived poliovirus type 2 (cVDPV2)—Ukraine. Geneva: The Organization; 2021.
8. Loboda A, Smiyan O, Popov S, Petrashenko V, Zaitsev I, Redko O, et al. Child health care system in Ukraine. Turk Pediatri Ars. 2020;55(Suppl 1):98–104.
9. Stone J. Ukraine war likely to cause disease outbreaks. 2022 Apr 4 [cited 2023 Dec 2]. https://www.medscape.com/viewarticle/971575
10. Joint United Nations Programme on HIV/AIDS. Global AIDS monitoring 2019: Ukraine [cited 2023 Nov 20]. https://www.unaids.org/sites/default/files/country/documents/UKR_2020_countryreport.pdf
11. Reyes-Urueña J, Marrone G, Noori T, Kuchukhidze G, Martsynovska V, Hetman L, et al.; EU/EEA HIV network. HIV diagnoses among people born in Ukraine reported by EU/EEA countries in 2022: impact on regional HIV trends and implications for healthcare planning. Euro Surveill. 2023;28:2300642. https://doi.org/10.2807/1560-7917.ES.2023.28.48.2300642
12. Vos CD, Gallina A, Kovtoniuk P, Poltavets U, Romy J, Rusnak D, et al. Destruction and devastation: one year of Russia's assault on Ukraine's health care system [cited 2023 Dec 2]. https://phr.org/our-work/resources/russias-assault-on-ukraines-health-care-system
13. MacIntyre CR, Lim S, Quigley A. Preventing the next pandemic: Use of artificial intelligence for epidemic monitoring and alerts. Cell Rep Med. 2022;3:100867. https://doi.org/10.1016/j.xcrm.2022.100867
14. Kpozehouen EB, Chen X, Zhu M, Macintyre CR. Using open-source intelligence to detect early signals of COVID-19 in China: descriptive study. JMIR Public Health Surveill. 2020;6:e18939. https://doi.org/10.2196/18939
15. Thamtono Y, Moa A, MacIntyre CR. Using open-source intelligence to identify early signals of COVID-19 in Indonesia. Western Pac Surveill Response J. 2021;12:40–5. https://doi.org/10.5365/wpsar.2020.11.2.010
16. Hutchinson D, Kunasekaran M, Quigley A, Moa A, MacIntyre CR. Could it be monkeypox? Use of an AI-based epidemic early warning system to monitor

rash and fever illness. Public Health. 2023;220:142–7. https://doi.org/10.1016/j.puhe.2023.05.010
17. MacIntyre CR, Chen X, Kunasekaran M, Quigley A, Lim S, Stone H, et al. Artificial intelligence in public health: the potential of epidemic early warning systems. J Int Med Res. 2023; 51:3000 6052311 59335. https://doi.org/10.1177/03000605231159335
18. Zoaib Habib T, Ennab F, Matiashova L, Nawaz FA, Volkova A, Trill V, et al. Double trouble: COVID-19 vaccine misinformation amidst conflict in Ukraine. Ann Med Surg (Lond). 2022;80:104127. https://doi.org/10.1016/j.amsu.2022.104127
19. World Health Organization Ukraine Country Office. War in Ukraine: situation report from WHO Ukraine country office, June 22, 2022 [cited 2023 Dec 4]. https://iris.who.int/bitstream/handle/10665/356991/WHO-EURO-2022-5319-45083-65130-eng.pdf
20. World Health Organization Ukraine Country Office. War in Ukraine: situation report from WHO Ukraine country office, June 29, 2022 [cited 2023 Dec 4]. https://iris.who.int/bitstream/handle/10665/358091/WHO-EURO-2022-5319-45083-65187-eng.pdf
21. World Health Organization. Cholera—global situation [cited 2023 Dec 4]. https://www.who.int/emergencies/disease-outbreak-news/item/2022-DON426
22. World Health Organization. Ukraine Public Health Situation Analysis (PHSA)—long-form (last update July 2022) [EN/UK] [cited 2024 Jul 29]. https://reliefweb.int/report/ukraine/ukraine-public-health-situation-analysis-phsa-long-form-last-update-july-2022-enuk
23. World Health Organization. Ukraine Public Health Situation Analysis (PHSA) —long-form (last update April 2022) [EN/UK] [cited 2024 Dec 4]. https://reliefweb.int/report/ukraine/ukraine-public-health-situation-analysis-phsa-long-form-last-update-april-2022
24. Schroeder A, Sherer PM. Ukraine war is becoming the fastest-growing humanitarian crisis since World War II [cited 2023 May 28]. https://www.directrelief.org/2022/03/ukraines-war-is-creating-the-fastest-growing-crisis-since-world-war-ii
25. World Health Organization. Compendium of WHO and other UN guidance on health and environment. Chapter 3: WASH [cited 2023 Dec 2]. https://cdn.who.int/media/docs/default-source/who-compendium-on-health-and-environment/who_compendium_chapter3_01092021.pdf
26. Healing T. Surveillance and control of communicable disease in conflicts and disasters. conflict and catastrophe medicine. Conflict and Catastrophe Medicine. 2009:197–222. https://doi.org/10.1007/978-1-84800-352-1_13
27. Hunder M. Cholera and other diseases could kill thousands in Ukraine's Mariupol—mayor [cited 2023 May 30]. https://www.reuters.com/world/europe/cholera-other-diseases-could-kill-thousands-ukraines-mariupol-mayor-2022-06-10
28. Beauté J, Kramarz P. Public health surveillance in countries hosting displaced people from Ukraine. Euro Surveill. 2022;27:2200430. https://doi.org/10.2807/1560-7917.ES.2022.27.22.2200430
29. Baaees MSO, Naiene JD, Al-Waleedi AA, Bin-Azoon NS, Khan MF, Mahmoud N, et al. Community-based surveillance in internally displaced people's camps and urban settings during a complex emergency in Yemen in 2020. Confl Health. 2021;15:54. https://doi.org/10.1186/s13031-021-00394-1
30. Raina MacIntyre C, Lim S, Gurdasani D, Miranda M, Metcalf D, Quigley A, et al. Early detection of emerging infectious diseases—implications for vaccine development. Vaccine. 2024;42:1826–30. https://doi.org/10.1016/j.vaccine.2023.05.069

Address for correspondence: Ashley Quigley, Biosecurity Program, The Kirby Institute, Faculty of Medicine, University of New South Wales, Level 6 Wallace Wurth Bldg, High St, Kensington, New South Wales 2052, Australia; email: ashley.quigley@unsw.edu.au

Autochthonous Leishmaniasis Caused by *Leishmania tropica*, Identified by Using Whole-Genome Sequencing, Sri Lanka

Hermali Silva,[1] Tiago R. Ferreira,[1] Kajan Muneeswaran, Sumudu R. Samarasinghe, Eliza V.C. Alves-Ferreira, Michael E. Grigg, Naduviladath V. Chandrasekharan, David L. Sacks, Nadira D. Karunaweera

Cutaneous leishmaniasis is atypical in Sri Lanka because *Leishmania donovani*, which typically causes visceral disease, is the causative agent. The origins of recently described hybrids between *L. donovani* and other *Leishmania* spp. usually responsible for cutaneous leishmaniasis remain unknown. Other endemic dermotropic *Leishmania* spp. have not been reported in Sri Lanka. Genome analysis of 27 clinical isolates from Sri Lanka and 32 Old World *Leishmania* spp. strains found 8 patient isolates clustered with *L. tropica* and 19 with *L. donovani*. The *L. tropica* isolates from Sri Lanka shared markers with strain *Lt*K26 reported decades ago in India, indicating they were not products of recent interspecies hybridization. Because *L. tropica* was isolated from patients with leishmaniasis in Sri Lanka, our findings indicate *L. donovani* is not the only cause of cutaneous leishmaniasis in Sri Lanka and potentially explains a haplotype that led to interspecies dermotropic *L. donovani* hybrids.

Leishmaniasis is a heterogeneous group of diseases caused by protozoan parasites of the genus *Leishmania*, transmitted by the bite of phlebotomine sand flies (*1*). The 3 typical clinical presentations of leishmaniasis affecting humans are visceral leishmaniasis (VL), cutaneous leishmaniasis (CL), and mucocutaneous leishmaniasis (MCL) (*1*). Those who are most affected are persons in Asia, Africa, and Latin America who suffer from poverty (*2*).

Author affiliations: University of Colombo, Colombo, Sri Lanka (H. Silva, K. Muneeswaran, S.R. Samarasinghe, N.V. Chandrasekharan, N.D. Karunaweera); Laboratory of Parasitic Diseases, National Institutes of Health, Bethesda, Maryland, USA (T.R. Ferreira, E.V.C. Alves-Ferreira, M.E. Grigg, D.L. Sacks)

DOI: https://doi.org/10.3201/eid3009.231238

Although *Leishmania donovani* causes VL in other countries in Asia and Africa, an atypical variant of the same species is almost exclusively associated with CL in Sri Lanka (*3*). Common symptoms of CL are papules, nodules, plaques, and ulcers. Leishmaniasis cases in Sri Lanka have increased over the past 2 decades, from 22 in 2001 to 3,389 in 2022 (https://www.epid.gov.lk). Over the past 2 decades, <10 cases of leishmaniasis have been VL in Sri Lanka; some cases have included severe chronic conditions preceding or occurring after the *Leishmania* infection (*4*). There are 2 primary hotspots in Sri Lanka, 1 in the southern province and 1 in the north-central province (*5*).

The genetic factors associated with disease phenotypes of leishmaniasis are not well understood. The A2 multigene family in *Leishmania* might be associated with either dermotropic or viscerotropic phenotypes (*6*). A2 gene variants encode stress-induced transmembrane proteins that are key for the parasite tropism to internal organs observed in visceralizing species (*6*). Abnormal changes in the number of chromosome copies that characterize extensive aneuploidy, usually harmful in most complex organisms, are frequent and highly tolerated in *Leishmania* parasites because they have a role in gene expression modulation (*7*,*8*).

The leishmaniasis disease profile worldwide is typically associated with the causative species of *Leishmania* (*9*). However, descriptions of emerging isolates and atypical phenotypes have made this association less clear (*6*,*10*). Recent genetic studies have shown that the *Leishmania* natural population structure is more complex than previously thought, partially because of the plasticity of the parasite genome and the occurrence of sexual reproduction (*11*).

[1]These authors contributed equally to this article.

Isolates from the same clade might carry relevant genetic features accounting for shifts in clinical phenotypes. For example, *L. donovani* isotype MON-37 (from the Montpellier typing system) is the known causative agent of CL in Sri Lanka, and MON-2 is the known causative agent of VL in India (*3*,*12*).

A more recent analysis of *L. donovani* clinical isolates from Sri Lanka reported interspecies genomic hybrids between *L. donovani* and 2 common cutaneous species, *L. major* from Africa and *L. tropica* from the Middle East (*13*). The evidence of hybridization and introgression history in the *Leishmania* population in Sri Lanka suggests genetic exchange might have played a role in the insurgence of dermotropic *L. donovani*. However, many epidemiologic aspects of this model are unclear. Most CL causing *L. donovani* isolates described to date do not display clear evidence of hybridization with dermotropic species, and the parental strains of possible hybrid parasites in Sri Lanka remain unknown. Currently, <20 high quality next-generation sequencing (NGS) datasets of *Leishmania* spp. isolated from patients in Sri Lanka are publicly available (*13*). Therefore, it is crucial to perform whole-genome sequencing (WGS) analysis on a wider range of clinical isolates to better understand the atypical pathogenesis of leishmaniasis in Sri Lanka.

We studied WGS results of 27 *Leishmania* clinical isolates from Sri Lanka and made multiple genetic comparisons by using 32 different Old World *Leishmania* strains, including 5 interspecies *L. donovani* hybrids previously reported in Sri Lanka. Among the genomes analyzed, we describe autochthonous *L. tropica* isolates in patients from Sri Lanka who, apart from 1 exception, did not have travel history outside the country.

This study has been approved by the Ethics Review Committee, Faculty of Medicine, University of Colombo, Sri Lanka (approval no. EC-16-080). Written, informed consent was obtained from the participants.

Methods

Leishmania Culture

We cultured *Leishmania* promastigotes from 27 lesion aspirates (26 CL and 1 MCL) in M199 culture medium supplemented with 10% heat-inactivated fetal bovine serum (Thermo Fisher Scientific, https://www.thermofisher.com) and 100 IU/ml of penicillin and 100mg/ml of streptomycin (Thermo Fisher Scientific). We incubated the cultures at 25 ± 1°C until the logarithmic phase promastigote count reached 10^7/mL and then harvested them.

Genomic DNA Isolation and Sequencing

We extracted DNA from the cultured *Leishmania* promastigotes by using a QIAamp DNA Mini Kit (QIAGEN, https://www.qiagen.com) and prepared libraries by using the Nextera XT DNA library preparation kit (Illumina, https://www.illumina.com) and the Nextera DNA Flex library preparation kit (Illumina), according to the manufacturer's instructions. Paired-end sequencing was conducted by Applied Biological Materials (British Columbia, Canada) by using the NextSeq (2×75bp) and HiSeq 4000 (2×150bp) platforms (Illumina).

WGS Data Analysis

We analyzed WGS data of 27 clinical isolates from this study and 32 *Leishmania* genomes of Old World species available from the National Center for Biotcechnology Information Sequence Read Archive (https://www.ncbi.nlm.nih.gov/sra) or the European Nucleotide Archive (https://ebi.ac.uk/ena). We detected genome-wide single-nucleotide polymorphisms (SNPs) in each sample after mapping high-quality reads to the reference strain, *L. tropica* L590 or *L. donovani* CL–Sri Lanka (genome available on TriTrypDB, https://tritrypdb.org). We extracted the consensus sequences of 7 different genetic markers to identify the clinical isolates at the species level. Phylogenetic analysis by NGS multilocus sequence typing (MLST) involved 59 genomes of nucleotide sequences with the indicated number of base pairs from the following genes: ribosomal RNA internal transcribed spacer (ITS; *L. donovani* CL–Sri Lanka CP029526:1015798–1016063), 265 bp; glucose-6-phosphate dehydrogenase (*G6PD*; LtrL590_34:26953–27953), 1,001 bp; glucose-6-phosphate isomerase (*GPI*; LtrL590_12:302579–303479), 901 bp; isocitrate dehydrogenase precursor (*ICD*; LTRL590_SCAF000112:124407–125407), 1,001 bp; phosphomannose isomerase (*PMI*; LtrL590_32:632360–633360), 1,001 bp; aspartate aminotransferase (*AST*; LtrL590_35:290874–291838), 965 bp; and inosine-guanine nucleoside hydrolase (*IGNH*; LtrL590_14:44174–44933), 760 bp (*14*). We extracted the ITS reference sequence from the *L. donovani* CL–Sri Lanka reference genome because the ITS sequence is not fully assembled in *L. tropica* L590. We conducted phylogenetic analysis with maximum-likelihood method and tamura-nei model by using NGS MLST sequences as input in MEGA X (*15*). We compiled the pileup of read alignments to each locus used for 3 representative *L. tropica* genomes (Appendix 1 Figure 1, https://wwwnc.cdc.gov/EID/article/30/9/23-1238-App1.pdf). We checked the aneuploidy profiles by inferring the chromosome copy values from

whole-genome analysis normalized read depth after we mapped to the *L. tropica* L590 reference genome v.57, found in TriTrypDB, and assuming that all samples are diploid.

To confirm the absence of species admixture in the new *L. tropica* from Sri Lanka, we studied the genomewide zygosity profiles and the population genetic structure by tracking SNP frequencies in all 59 WGS samples. After mapping, we used aligned reads to identify SNPs in heterozygosity (allele frequency 0.15–0.85) or in homozygosity (allele frequency >0.85) by using the PAINT software suite (*16*). We investigated the gene sequences of the A2 virulence factor (*L. donovani* CL–Sri Lanka CP029521:270000–320000) to identify any association with the phenotype of CL. We generated pseudo-sequences from 1,368,585 high-quality whole-genome linked SNPs that had information in ≥50% of the samples to build phylogenetic network trees in SplitsTree v.6.0.2.3 (https://software-ab.cs.uni-tuebingen.de/download/splitstree6/welcome.html) (*17*). We calculated hamming distances and used the neighbor-net method to generate a splits network. A total of 1,000 bootstrap split replicates were used for internode confirmation of the phylogenetic tree of the *L. tropica* genomes, with a minimum 50% cutoff.

Data Availability

Data supporting the conclusions of this article are within the article and Appendix files, including Sequence Read Archive accession numbers for all the genomic data used in this work (Appendix 2 Tables 1–3, https://wwwnc.cdc.gov/EID/article/30/9/23-1238-App2.xlsx). We deposited raw sequencing data in the National Center for Biotechnology Information BioProject archive (accession no. PRJNA904745).

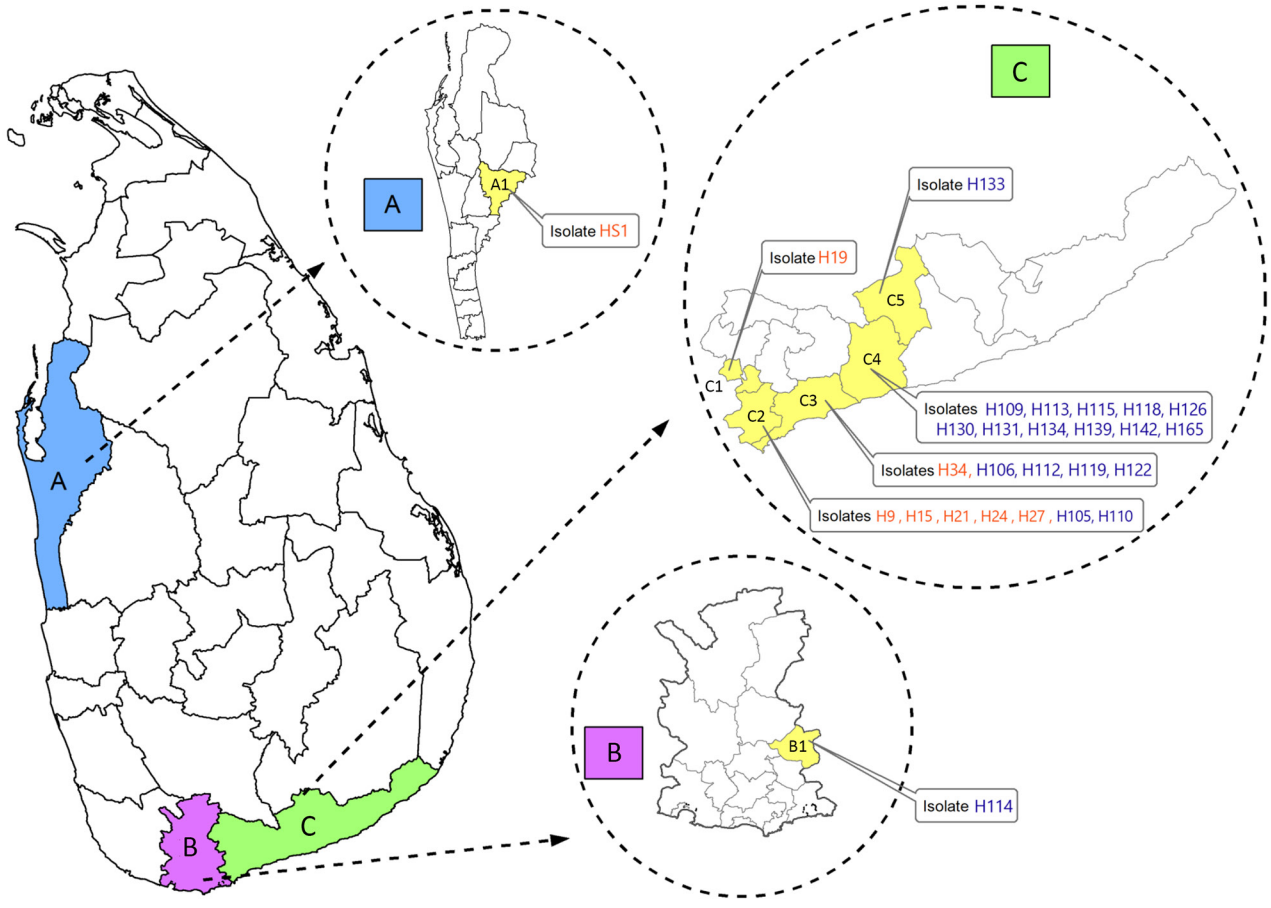

Figure 1. Geographic locations of patients with cutaneous or mucocutaneous leishmaniasis in Sri Lanka. The mucocutaneous leishmaniasis patient was from the Puttalam district (A), Anamaduwa subdistrict. The cutaneous leishmaniasis patients were from both the Matara (B) and Hambantota (C) districts. Isolates labeled in orange were identified as *Leishmania tropica*. Isolates labeled in blue were identified as *L. donovani*. A, Puttalam district; A1, Anamaduwa; B, Matara district; B1, Hakmana; C, Hambantota district; C1, Okewela; C2, Beliatta; C3, Tangalle; C4, Ambalantota; C5, Sooriyawewa.

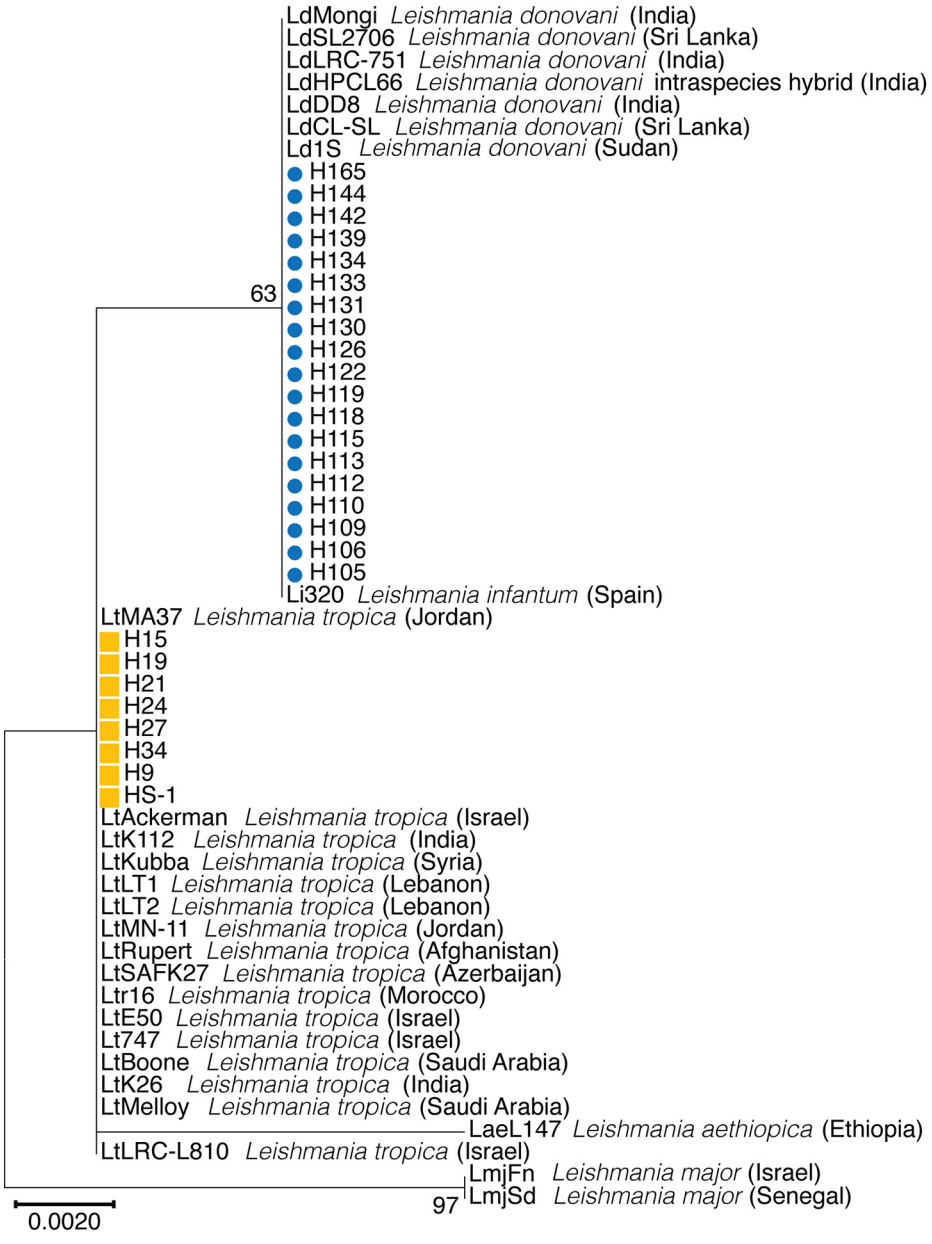

Figure 2. Phylogenetic analysis of *Leishmania* spp. clinical patient isolates from Sri Lanka and reference *Leishmania* spp. strains using sequences of the ribosomal RNA internal transcribed spacer (ITS). Sri Lanka isolates (H and HS) form 2 groups, 1 co-cluster with *L. donovani* (blue circles) and 1 with *L. tropica* (orange squares). Maximum-likelihood method and Tamura-nei models were performed for phylogenetic analysis using MEGA X (*15*). For each gene, the phylogenetic tree with the highest log likelihood (−429.25p for ITS) is presented from 1,000 bootstrap replicates. Bootstrap percentages >55% are shown for each branch. Scale bar represents the number of mutations per site.

Results

We recovered *Leishmania* clinical isolates from 27 patients in 3 administrative districts in Sri Lanka: Hambantota (n = 25), Matara (n = 1), and Puttalam (n = 1) (Figure 1). The CL patients were from the southern region and the MCL patient was from the north-western region of the country. Clinical manifestations of the CL lesions consisted of 8 papules, 3 plaques, and 15 ulcers. Eight of the ulcers were ulcerated nodules (Appendix 2 Table 4).

Species Variability among Clinical Isolates

NGS and MLST revealed that 19 genomes sequenced in this study belonged to the *L. donovani* complex and 8 to *L. tropica*. This finding was observed in every single locus investigated by MLST (Figure 2; Appendix 1 Figures 2, 3). Of note, the *ICD* gene sequence of the single MCL isolate, HS1, is more similar to *L. tropica* strains from the Middle East (including LtKubba from Syria, and LtLT1 and LtLT2 from Lebanon) than to isolates from Sri Lanka (Figure 2) (*8*,*18*).

Chromosome Copy Profiles

Genome-wide read depth analysis revealed highly conserved chromosome copy profiles among the 7 Sri Lanka *L. tropica* CL isolates (H9, H15, H19, H21, H24, H27, and H34), and a divergent pattern in the single

MCL isolate, HS1 (Figure 3, panels A, B). Polysomy of chromosome 31 (>3 copies) was seen in all samples. This polysomy was commonly observed in previous studies on *Leishmania* spp (*19*,*20*).

Trisomy (2.4–3.5 copies) of chromosomes 2, 21, and 31 and near-trisomy (2.2–2.4 copies) of chromosomes 5, 8, 10, and 13 were detected in *L. tropica* isolates from Sri Lanka except for HS1, which displayed trisomic chromosomes 6, 9, 11, 14, 19, 20, 30, 32, and 33 (Figure 3, panel B). In comparison, *L. donovani* clinical isolates from Sri Lanka displayed a more heterogenous distribution of chromosome copy values with varied karyotypes (Figure 3, panels A, B). Of the 3 previously reported *L. donovani*–*L. tropica* hybrids, SRR67 and SRR66 showed multiple near-trisomy matches with the *L. tropica* isolates from Sri Lanka on chromosomes 5, 8, 10, and 13. Of note, near-monosomy of chromosome 2 (1.2–1.4 copies) was detected in SRR64, SRR65, and SRR69 (Figure 3, panel B).

Genome-Wide Zygosity Profiles and Phylogenetic Network Analysis

The total number of SNPs per sample ranged from 117,729 (in LtMA37 WGS) to 2,059,343 (in SRR65 WGS) within the sample cohort after mapping reads to the *L. tropica* L590 reference genome (Figure 4 panel A). The 3 previously reported *L. donovani*–*L. tropica* hybrids showed low homozygosity (<0.12; SRR66–69). In contrast, most of the SNPs in the *L. donovani* isolates from Sri Lanka (H105–165) and in the intraspecies *L. donovani* hybrid LdHPCL66, identified in the Himachal Pradesh province of India, were homozygous (>0.98) (Figure 4, panel A) (*10*). Highly skewed heterozygosity was detected in most of the *L. tropica* genomes because they are genetically more similar to the *L. tropica* L590 reference genome than to *L. donovani*. For comparison, we also mapped reads to the *L. donovani* CL–Sri Lanka reference genome (Figure 4, panel B). As we expected for *L. donovani*–*L. tropica* progeny, both the genome-wide SNP frequencies and absolute numbers in the previously reported hybrids SRR66–69 were largely unaffected by the reference genome used for mapping (Figure 4). All *L. donovani* laboratory strains showed high ratios of homozygous SNPs.

We generated a network splits tree by using whole-genome SNPs for all the 59 *Leishmania* genomes, highlighting the separation between the *L. donovani* and *L.tropica* isolates from Sri Lanka, with

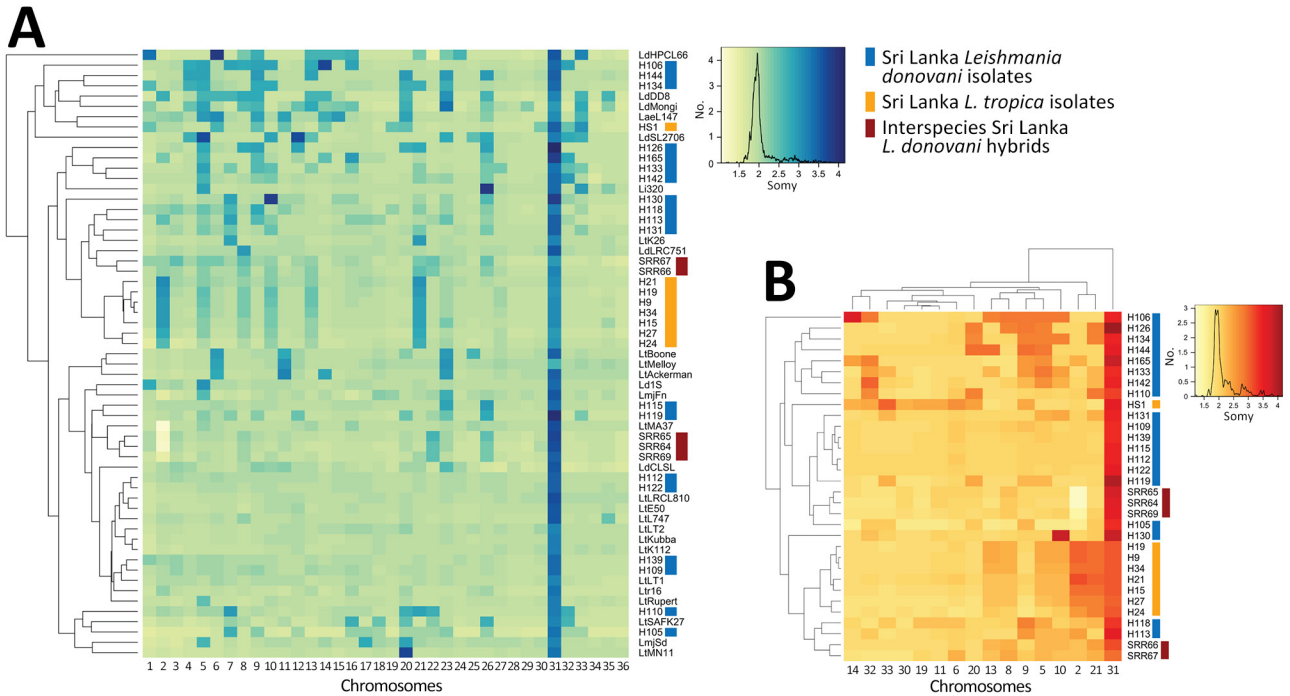

Figure 3. Highly conserved aneuploidy profiles within the cutaneous *Leishmania tropica* clade from Sri Lanka. A) Heat map visualization of *Leishmania* abnormal chromosome numbers in 27 patient isolates from Sri Lanka and 32 previously described strains or hybrids. *L. tropica* isolates from Sri Lanka are labeled with orange lines and *L. donovani* isolates from Sri Lanka are labeled with blue lines. B) Subset of the data shown in panel A highlighting only chromosomes that are polysomic in ≥1 isolate. Chromosome copy values were inferred from whole-genome analysis normalized read depth after mapping to the *L. tropica* L590 reference genome available on TriTrypDB (https://www.tritrypdb.org), with the assumption that all samples have a 2n DNA content. Somy, abnormal chromosome numbers.

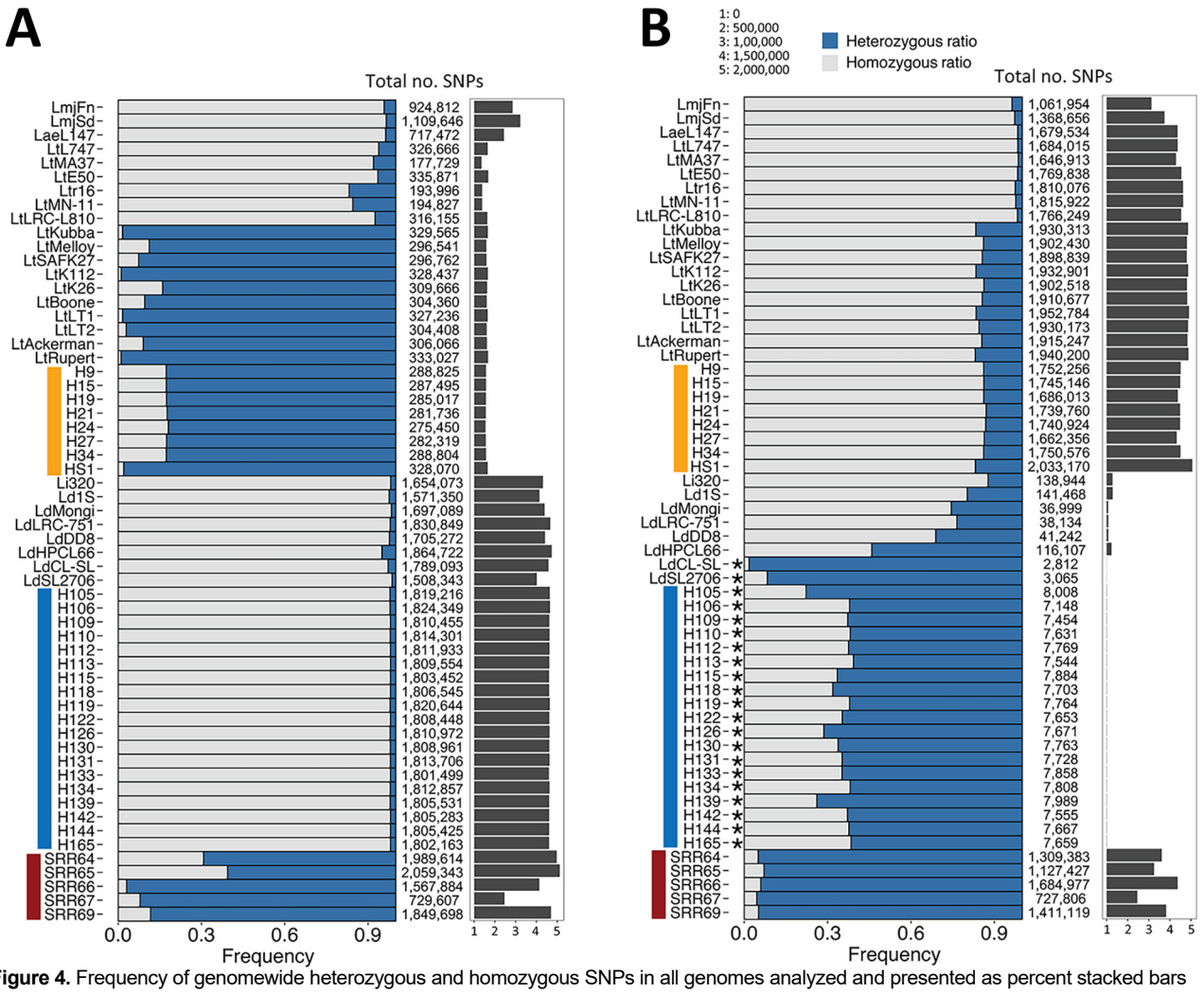

Figure 4. Frequency of genomewide heterozygous and homozygous SNPs in all genomes analyzed and presented as percent stacked bars after mapping sequencing reads from *Leishmania* spp. isolates from Sri Lanka. A) Mapped to *L. tropica* L590. B) Mapped to *L. donovani* cutaneous leishmaniasis reference genome. The total number of SNPs detected using the PAINT software suite (*16*) is shown to the right of the main plot. Vertical bars at left: blue, *L. donovani*; orange, *L. tropica*; red, interspecies hybrids. Asterisks (*) indicate the biased heterozygosity profiles of *L. donovani* genomes that are highly similar to the reference genome (LdCL-SL), resulting in a low number of SNPs SNP, single-nucleotide polymorphism. Asterisks (*) indicate the biased heterozygosity profiles of *L. donovani* genomes that are highly similar to the reference genome (LdCL-SL), resulting in a low number of SNPs.

the hybrids found in the middle point of the tree (Figure 5, panel A). A more detailed analysis by using only the data from the *L. tropica* genomes revealed 2 different subclusters of *L. tropica* in Sri Lanka. Although HS1 co-clusters with strains found in Syria (LtKubba) (*8*) and Lebanon (LtLT1 and LtLT2) (*18*) (Appendix 1 Figure 4, panels A, B), the other *L. tropica* from Sri Lanka form a discrete subgroup more genetically similar to the LtK26 strain from India (Figure 5, panel B). This finding corroborated the phylogenetic profile observed by the MLST analysis by using the *ICD* gene sequence (Appendix 1 Figure 3, panel C). Identification of *L. tropica* phylogenetic groups confirms worldwide *L. tropica* populations described by a previous comparative genomics study (*18*). We further expand on those findings by suggesting an additional population, consisting of LtK26 strain from India (*8*) and the H9–34 *L. tropica* from Sri Lanka.

Genomewide Genetic Variations and Shared Ancestries

From the list of SNPs identified by using the PAINT software suite (*16*), we selected the 1,354,425 homozygous alleles that were different between *L. tropica* K26 and *L. donovani* SL2706 as representatives of the 2 clades found in Sri Lanka. We tracked their inheritance in hybrids SRR66, SRR67, and SRR69 and in the 27 Sri Lanka isolates. *L. donovani*–*L. tropica*

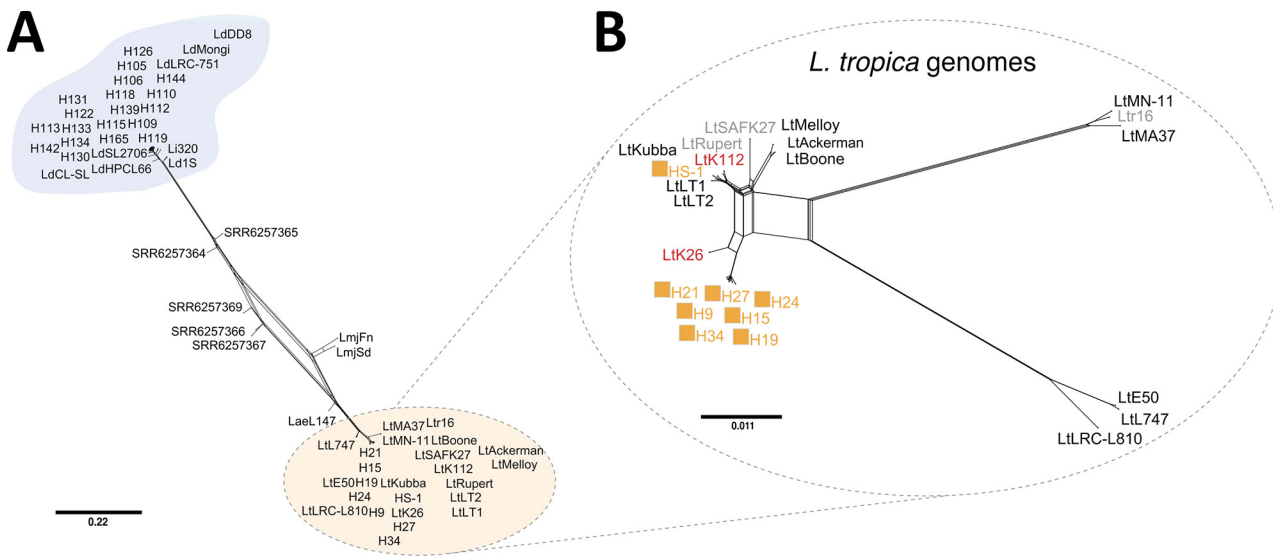

Figure 5. Phylogenetic network of all *Leishmania* isolates from Sri Lanka and Old World strains analyzed and visualized as a splits tree built using genomewide single-nucleotide polymorphisms in SplitsTree 6 (*17*). A) The cluster of the *L. donovani* complex is found at the top of the tree (blue) and the *L. tropica* are found at the bottom (orange). B) Phylogenetic network analysis of only the *L. tropica* genomes in our dataset. Orange squares, *L. tropica* isolates from Sri Lanka (HS1, H9–34); black font, Middle Eastern *L. tropica*; gray font, Azerbaijan (SAFK27) (*8*), Morocco (Ltr16) (*21*), and Afghanistan (Rupert) (*8*); red font, Indian *L. tropica* (K26 and K112) (*8*). Scale bar represents nucleotide substitutions per position.

markers were remarkably heterozygous across the whole genome of the SRR66–69 hybrids, suggesting they have undergone recent hybridization with biparental contribution from *L. donovani* and *L. tropica* in all 36 chromosomes (Figure 6, panel A). The number of SNPs shared with the *L. tropica* lineage from Sri

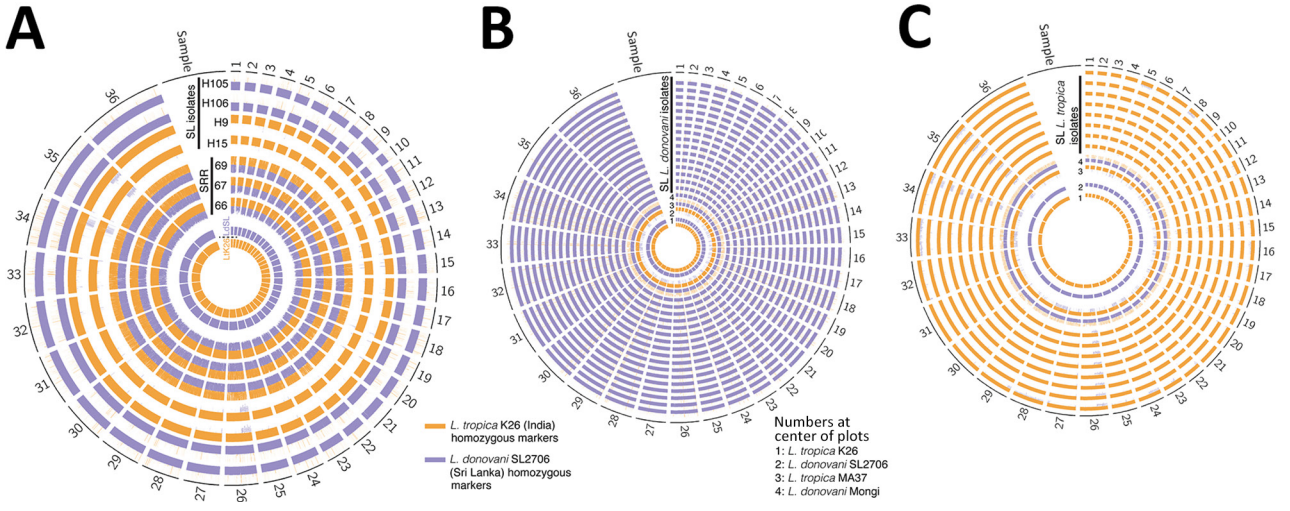

Figure 6. *Leishmania tropica* and *L. donovani* strains from the Indian subcontinent that share genetic markers with interspecies hybrids found in Sri Lanka. A) Circos plot (*22*) representation of the inheritance pattern of all genome-wide homozygous single-nucleotide polymorphism differences between strains *L. tropica* K26, found in India, and *L. donovani* SL2706, found in Sri Lanka. Each concentric circular track depicts parental allele contribution in the different genomes. Chromosomes are separated by white radial lines with chromosome numbers shown on the outermost circle. Representative genomes of the 2 species from Sri Lanka are shown, *L. tropica* (H9 and H15) and *L. donovani* (H105 and H106). *L. donovani* interspecies hybrids (SRR66–69) are examples of recent hybridization (*13*,*23*). Window size of 10 kb was used in the whole-genome sequencing analysis with the PAINT software suite (*17*) and reference genome LtrL590 available on TriTrypDB (https://www.tritrypdb.org). B) Circos plot (*22*) representing the allelic inheritance of LtK26 and LdSL2706 parental markers for the different *L. donovani* clinical isolates analyzed from Sri Lanka. C) Circos plot (*22*) representing the allelic inheritance of LtK26 and LdSL2706 parental markers for the different *L. tropica* clinical isolates analyzed from Sri Lanka. *L. donovani* Mongi (India) and *L. tropica* MA37 (Jordan) genomes are shown as references of nonmixed species genomes. SL, Sri Lanka.

Lanka was lower in the *L. donovani–L. major* hybrids (SRR64–65) (Appendix 1 Figure 5); only 31.5% of the heterozygous SNPs were explained by the tested *L. donovani–L. tropica* admixture compared with 70% in the *L. donovani–L. tropica* hybrids (SRR66–69). Visual inspection at the single-nucleotide level confirmed the extensive heterozygosity of *L. donovani–L. tropica* markers in the SRR66–69 hybrids for most of the sites analyzed, which was not as evident in the SRR64–65 hybrids (Figure 7; Appendix 1 Figure 6). The *L. donovani* (H105-H165) isolates from Sri Lanka showed low heterozygosity of selected parental markers and high similarity, and the *L. tropica* (HS1, H9-H34) isolates from Sri Lanka showed low heterozygosity of selected parental markers and high similarity to *L. tropica* from India lineages, evidence that these isolates have not experienced recent admixture of species (Figure 6, panels B, C).

A2 Gene Variations

L. donovani and the hybrids from Sri Lanka contain the full A2 gene sequences of all 4 annotated copies in the *L. donovani* CL–Sri Lanka reference genome on chromosome 22. Read depths in *L. tropica* isolates from Sri Lanka were virtually zero in those positions (Figure 8, panel A), except for HS1, which contained very low partial coverage of the A2 gene, indicating a truncated gene sequence. Of note, isolates H106, H109, and H119 causing plaque lesions in patients were the only isolates from Sri Lanka to carry A2 sequences that are highly similar to the *L. donovani* CL–Sri Lanka reference, which also induced a plaque lesion phenotype (Figure 8, panel B).

Discussion

This study identified an endemic *L. tropica* causing leishmaniasis in Sri Lanka. The 7 patients with CL caused by *L. tropica* had never traveled overseas, and 1 had not traveled outside their district of residence for 5 years. The CL patients had been living in their area of residence either since birth or for 20–60 years. Thus, it is likely that these are autochthonous cases of CL caused by *L. tropica*.

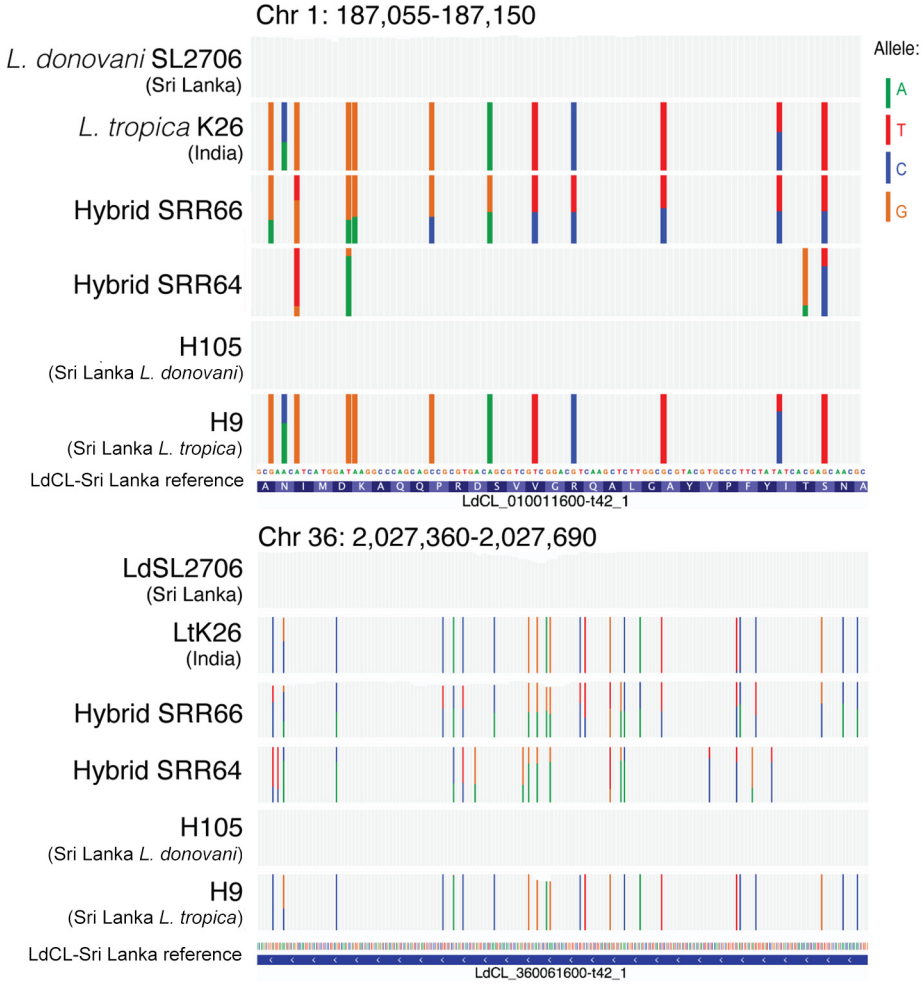

Figure 7. Representative nucleotide-level visualization of the inheritance of parental allelic markers on chromosomes 1 (upper panel) and 36 (lower panel) in *L. donovani–L. tropica* hybrid SRR66, *L. donovani–L. major* hybrid SRR64, and isolates from Sri Lanka (H105 and H9). Coverage plots highlighting single nucleotide polymorphisms were generated by using the integrative genomics viewer (https://igv.org), a match with the reference genome is represented as gray bars (*24*).

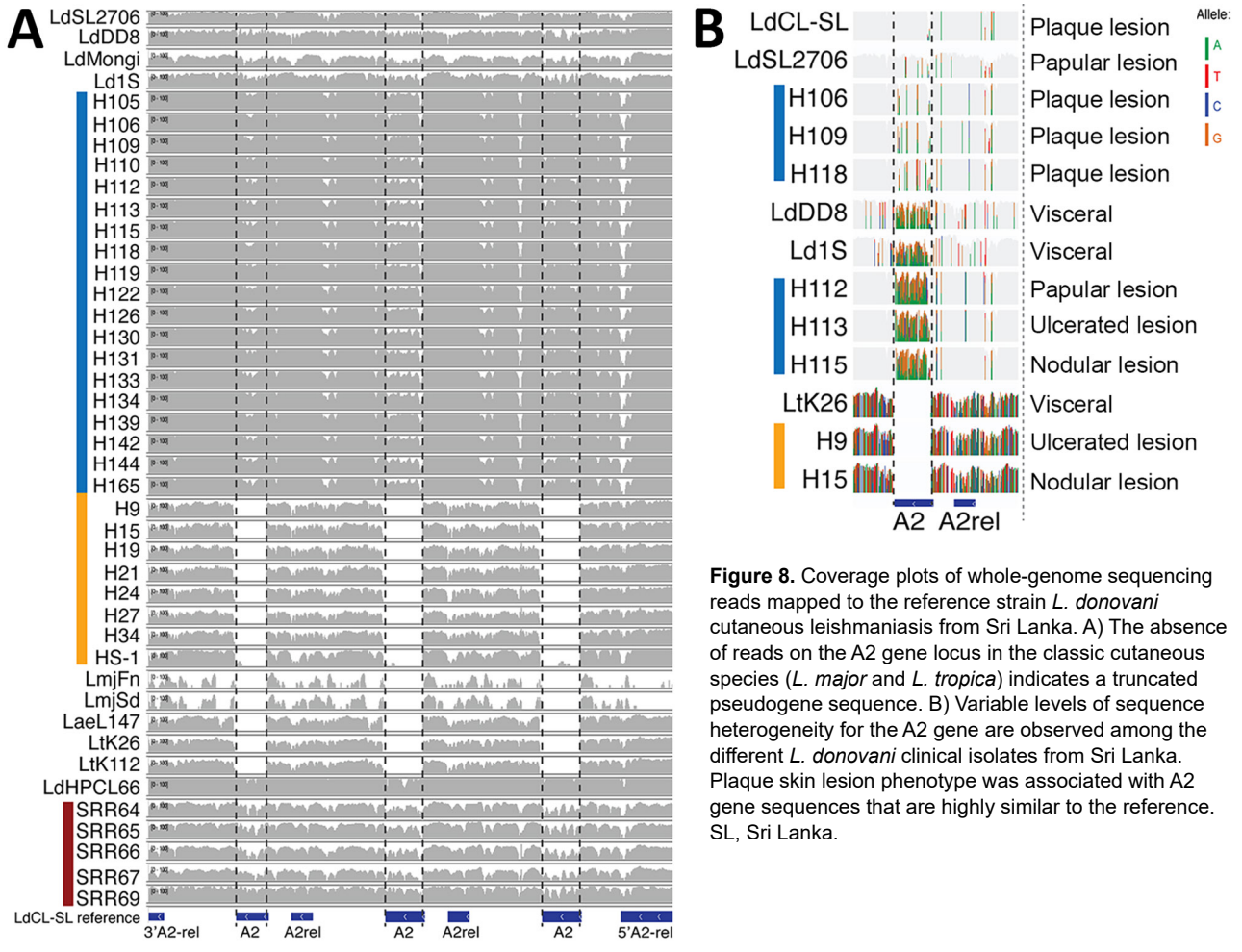

Figure 8. Coverage plots of whole-genome sequencing reads mapped to the reference strain *L. donovani* cutaneous leishmaniasis from Sri Lanka. A) The absence of reads on the A2 gene locus in the classic cutaneous species (*L. major* and *L. tropica*) indicates a truncated pseudogene sequence. B) Variable levels of sequence heterogeneity for the A2 gene are observed among the different *L. donovani* clinical isolates from Sri Lanka. Plaque skin lesion phenotype was associated with A2 gene sequences that are highly similar to the reference. SL, Sri Lanka.

This study identified MCL caused by the *L. tropica* isolate HS1 in Sri Lanka. The patient's upper lip, nose, and the perinasal regions were affected similar to previously reported cases of MCL caused by *L. tropica* (*25*,*26*). This MCL patient had traveled to Dubai and Iraq 8 years before the diagnosis and had no history of cutaneous leishmaniasis. The time elapsed since the first appearance of symptoms to diagnosis was ≈8 months (Appendix 2 Table 4). Those facts suggest that either the patient began experiencing symptoms 7 years after a possible exposure during overseas travel or they acquired the infection in Sri Lanka.

The 7 cutaneous *L. tropica* isolates from Sri Lanka (H9–H34) were collected in southern Sri Lanka and belong to a genetically conserved subgroup that only co-clustered with *L. tropica* LtK26 from India. In contrast, the MCL-associated HS1 strain was isolated from a different geographic area and displayed a divergent chromosome copy profile more similar to *L. tropica* strains from Syria (LtKubba) and Lebanon (LtLT1 and LtLT2) than to the other *L. tropica* isolates from Sri Lanka (Figure 3; Figure 5, panel B), and a divergent genomewide SNP profile. Thus, it is possible that the infection was acquired in the Gulf region, and the mucosal manifestations might have become apparent years after the primary exposure.

Chromosome aneuploidy was evident among the study samples and the pattern differed between the *L. tropica* and *L. donovani* isolates. Noninteger chromosome copy values observed in this study are commonly found in *Leishmania* because of mosaic aneuploidy occurring in cultured parasite populations (*19*). Recent studies have shown that clonal growth in both sand flies and in vitro culture can by itself lead to major changes in chromosome copy values and karyotype diversity even after just 1 passage through the insect vector (*20*,*27*). In fact, concerning chromosome copy values, the *L. donovani*–*L. tropica* hybrids were among the most homogeneous genomes in our analysis.

From the data on patients' residence and travel within Sri Lanka (Appendix 2 Table 4), it is evident that both *L. tropica* and *L. donovani* may not be

restricted to a single administrative area at the micro level. Considering that *L. tropica* is predominantly causing anthroponotic leishmaniasis and that the patients with CL have traveled to other districts, further studies in additional locations and with other potential vectors would benefit the current understanding of leishmaniasis spread and genetic variability in Sri Lanka. In addition, zoonotic transmission of *L. tropica* through reservoirs such as rock hyraxes has been reported in other countries, and studies are needed to assess potential animal reservoirs of these parasites in Sri Lanka (*28*). Currently, there are no data available to dismiss either scenario, and both may represent valid and relevant routes of infection in the country. In addition to *L. tropica* causing cutaneous disease, its potential to visceralize in humans is known (*29*–*31*). Even though CL is the current predominant phenotype of leishmaniasis in Sri Lanka, the presence of *L. tropica* and *L. donovani*, both with potential visceralizing properties, raises concerns.

Studies on A2 gene expression in old world *Leishmania* spp. suggest its useful in determining species-specific organ tropism (*32*). Even though the pathogenicity of leishmaniasis is not fully understood, the understanding of CL lesions is they progress from an initial papule to a nodule or a plaque which can ultimately ulcerate. Several virulence factors were studied in the sequenced samples to understand the variability in *Leishmania* pathogenesis leading to different phenotypes. Because primarily cutaneous parasite species have a truncated A2 pseudogene, A2 is a gene family that occurs in *L. donovani* but not in *L. tropica* (*6*), a result seen in our study samples as well. A2 is necessary in the pathology of leishmaniasis and is known to aid in visceralization of the infection and survival within the host (*33*–*35*). Our analysis of the A2 gene in different phenotypes of *L. donovani* revealed marked differences in the plaque phenotype when compared with papules, nodules, and ulcers. A study conducted in Pakistan found that the clinical appearance of CL is not solely dependent on *L. tropica* genetic variations (*36*). This possibility could not be investigated in our study because most of the *L. tropica*–induced CL cases were ulcerated.

We have found there are ≥5 different populations of *Leishmania* in Sri Lanka: SL1, SL2A, SL2B, SL3 (*13*), and *L. tropica* from Sri Lanka (SL4). Our study has shown *L. tropica* has caused both CL and MCL in Sri Lanka. Those findings suggest further studies on differences in clinical phenotypes, potential vector species, and reservoirs of *Leishmania* species in Sri Lanka would be beneficial. Revisiting diagnostic and research approaches might be necessary in consideration of this species variability. Analysis by PCR and restriction fragment length polymorphism represent the inexpensive and easy laboratory methods available for distinguishing between the 2 species (*37*).

In conclusion, although this large *Leishmania* WGS dataset provides valuable insights, further whole-genome studies might lead to better understanding of the *Leishmania* species infecting people in Sri Lanka and might shed light on the extent of genetic heterogeneity of infective clades circulating in the country. This discovery is a turning point in understanding the pathology of leishmaniasis in Sri Lanka and may contribute to the development of more efficient diagnostics and treatments for CL and MCL caused by *L. tropica*.

Acknowledgments

We thank the staff members of the study sites, the Department of Parasitology at the University of Colombo, and Hernan A. Lorenzi for support with programming code.

This study was financially supported by the University of Colombo (grant no. AP/3/2/2017/PG/31); the United States-Japan Cooperative Medical Sciences Program, National Institutes of Health, USA (award no. DAA3-19-65623); National Institute of Allergy and Infectious Diseases, National Institutes of Health (award no. U01AI136033); and in part by the Intramural Research Program, National Institute of Allergy and Infectious Diseases, National Institutes of Health.

Author contributions: study design and leadership, H.S., N.V.C., and N.D.K.; funding acquisition, H.S. and N.D.K.; study oversight and supervision, N.D.K., N.V.C., and D.L.S.; data and sample collection, H.S.; bioinformatics analysis, H.S., K.M., S.S., and T.R.F.; data processing and data visualization, T.R.F.; data interpretation and manuscript drafting, H.S. and T.R.F.; provision of bioinformatic scripts and pipelines, E.V.C.A.F. and M.E.G. All authors reviewed the manuscript.

About the Author

Dr. Silva is a senior lecturer in parasitology at the University of Colombo, Sri Lanka. Her research interests include epidemiology, pathogenesis, and treatment and drug resistance of human parasites.

References

1. Desjeux P. Leishmaniasis: current situation and new perspectives. Comp Immunol Microbiol Infect Dis. 2004;27:305–18. 10.1016/j.cimid.2004.03.004 https://doi.org/10.1016/j.cimid.2004.03.004
2. Alvar J, Yactayo S, Bern C. Leishmaniasis and poverty. Trends Parasitol. 2006;22:552–7. 10.1016/j.pt.2006.09.004 https://doi.org/10.1016/j.pt.2006.09.004

3. Karunaweera ND, Pratlong F, Siriwardane HVYD, Ihalamulla RL, Dedet JP. Sri Lankan cutaneous leishmaniasis is caused by *Leishmania donovani* zymodeme MON-37. Trans R Soc Trop Med Hyg. 2003;97:380–1. https://doi.org/10.1016/S0035-9203(03)90061-7
4. Siriwardana HVYD, Karunanayake P, Goonerathne L, Karunaweera ND. Emergence of visceral leishmaniasis in Sri Lanka: a newly established health threat. Pathog Glob Health. 2017;111:317–26. https://doi.org/10.1080/20477724.2017.1361564
5. Karunaweera ND, Senanayake S, Ginige S, Silva H, Manamperi N, Samaranayake N, et al. Spatiotemporal distribution of cutaneous leishmaniasis in Sri Lanka and future case burden estimates. PLoS Negl Trop Dis. 2021;15:e0009346. https://doi.org/10.1371/journal.pntd.0009346
6. Zhang WW, Ramasamy G, McCall LI, Haydock A, Ranasinghe S, Abeygunasekara P, et al. Genetic analysis of *Leishmania donovani* tropism using a naturally attenuated cutaneous strain. PLoS Pathog. 2014;10:e1004244. https://doi.org/10.1371/journal.ppat.1004244
7. Sterkers Y, Lachaud L, Crobu L, Bastien P, Pagès M. FISH analysis reveals aneuploidy and continual generation of chromosomal mosaicism in *Leishmania* major. Cell Microbiol. 2011;13:274–83. https://doi.org/10.1111/j.1462-5822.2010.01534.x
8. Iantorno SA, Durrant C, Khan A, Sanders MJ, Beverley SM, Warren WC, et al. Gene expression in *Leishmania* is regulated predominantly by gene dosage. MBio. 2017;8:1–20. https://doi.org/10.1128/mBio.01393-17
9. Burza S, Croft SL, Boelaert M. Leishmaniasis. Lancet. 2018;392:951–70. https://doi.org/10.1016/S0140-6736(18)31204-2
10. Lypaczewski P, Thakur L, Jain A, Kumari S, Paulini K, Matlashewski G, et al. An intraspecies *Leishmania donovani* hybrid from the Indian subcontinent is associated with an atypical phenotype of cutaneous disease. iScience. 2022;25:103802. https://doi.org/10.1016/j.isci.2022.103802
11. Inbar E, Shaik J, Iantorno SA, Romano A, Nzelu CO, Owens K, et al. Whole genome sequencing of experimental hybrids supports meiosis-like sexual recombination in *Leishmania*. PLoS Genet. 2019;15:e1008042. https://doi.org/10.1371/journal.pgen.1008042
12. Karunaweera ND. *Leishmania donovani* causing cutaneous leishmaniasis in Sri Lanka: a wolf in sheep's clothing? Trends Parasitol. 2009;25:458–63. https://doi.org/10.1016/j.pt.2009.07.002
13. Lypaczewski P, Matlashewski G. *Leishmania donovani* hybridisation and introgression in nature: a comparative genomic investigation. Lancet Microbe. 2021;2:e250–8. https://doi.org/10.1016/S2666-5247(21)00028-8
14. Zemanová E, Jirků M, Mauricio IL, Horák A, Miles MA, Lukeš J. The *Leishmania donovani* complex: genotypes of five metabolic enzymes (ICD, ME, MPI, G6PDH, and FH), new targets for multilocus sequence typing. Int J Parasitol. 2007;37:149–60. https://doi.org/10.1016/j.ijpara.2006.08.008
15. Kumar S, Stecher G, Li M, Knyaz C, Tamura K. MEGA X: Molecular evolutionary genetics analysis across computing platforms. Mol Biol Evol. 2018;35:1547–9. https://doi.org/10.1093/molbev/msy096
16. Shaik JS, Dobson DE, Sacks DL, Beverley SM. *Leishmania* sexual reproductive strategies as resolved through computational methods designed for aneuploid genomes. Genes (Basel). 2021;12:1–16. https://doi.org/10.3390/genes12020167
17. Huson DH, Bryant D. Application of phylogenetic networks in evolutionary studies. Mol Biol Evol. 2006;23:254–67. https://doi.org/10.1093/molbev/msj030
18. Salloum T, Moussa R, Rahy R, Al Deek J, Khalifeh I, El Hajj R, et al. Expanded genome-wide comparisons give novel insights into population structure and genetic heterogeneity of *Leishmania tropica* complex. PLoS Negl Trop Dis. 2020;14:e0008684. https://doi.org/10.1371/journal.pntd.0008684
19. Dumetz F, Imamura H, Sanders M, Seblova V, Myskova J, Pescher P, et al. Modulation of aneuploidy in *Leishmania donovani* during adaptation to different *in vitro* and *in vivo* environments and its impact on gene expression. MBio. 2017;8:1–14. https://doi.org/10.1128/mBio.00599-17
20. Ferreira TR, Inbar E, Shaik J, Jeffrey BM, Ghosh K, Dobson DE, et al. Self-Hybridization in *Leishmania major*. MBio. 2022;13:e0285822. https://doi.org/10.1128/mbio.02858-22
21. Bussotti G, Gouzelou E, Côrtes Boité M, Kherachi I, Harrat Z, Eddaikra N, et al. *Leishmania* genome dynamics during environmental adaptation reveal strain-specific differences in gene copy number variation, karyotype instability, and telomeric amplification. MBio. 2018;9:1–18. https://doi.org/10.1128/mBio.01399-18
22. Krzywinski M, Schein J, Birol I, Connors J, Gascoyne R, Horsman D, et al. Circos: an information aesthetic for comparative genomics. Genome Res. 2009;19:1639–45. https://doi.org/10.1101/gr.092759.109
23. Samarasinghe SR, Samaranayake N, Kariyawasam UL, Siriwardana YD, Imamura H, Karunaweera ND. Genomic insights into virulence mechanisms of *Leishmania donovani*: evidence from an atypical strain. BMC Genomics. 2018;19:843. https://doi.org/10.1186/s12864-018-5271-z
24. Robinson JT, Thorvaldsdóttir H, Winckler W, Guttman M, Lander ES, Getz G, et al. Integrative genomics viewer. Nat Biotechnol. 2011;29:24–6. https://doi.org/10.1038/nbt.1754
25. Shirian S, Oryan A, Hatam GR, Daneshbod Y. Three *Leishmania/L.* species—*L. infantum, L. major, L. tropica*—as causative agents of mucosal leishmaniasis in Iran. Pathog Glob Health. 2013;107:267–72. https://doi.org/10.1179/2047773213Y.0000000098
26. Shirian S, Oryan A, Hatam GR, Daneshbod K, Daneshbod Y. Molecular diagnosis and species identification of mucosal leishmaniasis in Iran and correlation with cytological findings. Acta Cytol. 2012;56:304–9. https://doi.org/10.1159/000337450
27. Bussotti G, Li B, Pescher P, Vojtkova B, Louradour I, Pruzinova K, et al. *Leishmania* allelic selection during experimental sand fly infection correlates with mutational signatures of oxidative DNA damage. Proc Natl Acad Sci U S A. 2023;120:e2220828120. https://doi.org/10.1073/pnas.2220828120
28. Waitz Y, Paz S, Meir D, Malkinson D. Effects of land use type, spatial patterns and host presence on *Leishmania tropica* vectors activity. Parasit Vectors. 2019;12:320. https://doi.org/10.1186/s13071-019-3562-0
29. Sohrabi Y, Havelková H, Kobets T, Šíma M, Volkova V, Grekov I, et al. Mapping the genes for susceptibility and response to *Leishmania tropica* in mouse. PLoS Negl Trop Dis. 2013;7:e2282. https://doi.org/10.1371/journal.pntd.0002282
30. Magill AJ, Grögl M, Gasser RA Jr, Sun W, Oster CN. Visceral infection caused by *Leishmania tropica* in veterans of Operation Desert Storm. N Engl J Med. 1993;328:1383–7. https://doi.org/10.1056/NEJM199305133281904
31. Sacks DL, Kenney RT, Kreutzer RD, Jaffe CL, Gupta AK, Sharma MC, et al. Indian kala-azar caused by *Leishmania tropica*. Lancet. 1995;345:959–61. https://doi.org/10.1016/S0140-6736(95)90703-3

32. Ghedin E, Zhang WW, Charest H, Sundar S, Kenney RT, Matlashewski G. Antibody response against a *Leishmania donovani* amastigote-stage-specific protein in patients with visceral leishmaniasis. Clin Diagn Lab Immunol. 1997;4:530–5. https://doi.org/10.1128/cdli.4.5.530-535.1997
33. Zhang WW, Matlashewski G. Characterization of the A2-A2rel gene cluster in *Leishmania donovani*: involvement of A2 in visceralization during infection. Mol Microbiol. 2001; 39:935–48. https://doi.org/10.1046/j.1365-2958.2001.02286.x
34. McCall LI, Matlashewski G. Localization and induction of the A2 virulence factor in *Leishmania*: evidence that A2 is a stress response protein. Mol Microbiol. 2010;77:518–30. https://doi.org/10.1111/j.1365-2958.2010.07229.x
35. Al-Khalaifah HS. Major molecular factors related to *Leishmania* pathogenicity. Front Immunol. 2022;13:847797. https://doi.org/10.3389/fimmu.2022.847797
36. Khan NH, Llewellyn MS, Schönian G, Sutherland CJ. Variability of cutaneous leishmaniasis lesions is not associated with genetic diversity of *Leishmania tropica* in Khyber Pakhtunkhwa province of Pakistan. Am J Trop Med Hyg. 2017;97:1489–97. https://doi.org/10.4269/ajtmh.16-0887
37. De Silva NL, De Silva VNH, Deerasinghe ATH, Rathnapala UL, Itoh M, Takagi H, et al. Development of a highly sensitive nested PCR and its application for the diagnosis of cutaneous leishmaniasis in Sri Lanka. Microorganisms. 2022;10:990. https://doi.org/10.3390/microorganisms10050990

Address for correspondence: Nadira D. Karunaweera, University of Colombo, 25, Kynsey Road, Colombo 08, Sri Lanka; email: nadira@parasit.cmb.ac.lk

Lower Microscopy Sensitivity with Decreasing Malaria Prevalence in the Urban Amazon Region, Brazil, 2018–2021

Priscila T. Rodrigues, Igor C. Johansen, Winni A. Ladeia, Fabiana D. Esquivel, Rodrigo M. Corder, Juliana Tonini, Priscila R. Calil, Anderson R.J. Fernandes, Pablo S. Fontoura, Carlos E. Cavasini, Joseph M. Vinetz, Marcia C. Castro, Marcelo U. Ferreira, on behalf of the Mâncio Lima Cohort Study Working Group[1]

Malaria is increasingly diagnosed in urban centers across the Amazon Basin. In this study, we combined repeated prevalence surveys over a 4-year period of a household-based random sample of 2,774 persons with parasite genotyping to investigate the epidemiology of malaria in Mâncio Lima, the main urban transmission hotspot in Amazonian Brazil. We found that most malarial infections were asymptomatic and undetected by point-of-care microscopy. Our findings indicate that as malaria transmission decreases, the detection threshold of microscopy rises, resulting in more missed infections despite similar parasite densities estimated by molecular methods. We identified genetically highly diverse populations of *Plasmodium vivax* and *P. falciparum* in the region; occasional shared lineages between urban and rural residents suggest cross-boundary propagation. The prevalence of low-density and asymptomatic infections poses a significant challenge for routine surveillance and the effectiveness of malaria control and elimination strategies in urbanized areas with readily accessible laboratory facilities.

Despite recent progress toward elimination, persisting malaria transmission in the Americas continues to pose a risk for infection to 120 million persons (*1*). The Amazon Basin, spanning 9 countries of South America, accounts for ≈90% of the 600,000 laboratory-confirmed cases recorded annually on the continent (*2*). The actual malaria burden may be significantly underestimated because point-of-care microscopy is not sensitive enough to detect the parasites in all low-density infections, most of which are asymptomatic, in the Amazon Basin (*3*–*5*).

Traditionally considered a rural disease, malaria is now emerging in rapidly growing urban centers across the Amazon Basin (*6*–*8*). After decades of massive rural-to-urban migration, 75% of the population in the Brazilian Amazon now resides in settlements classified as urban according to municipality law (https://censo2022.ibge.gov.br/panorama). This classification is adopted by the Brazilian Institute of Geography and Statistics, the country's census bureau. Urban health facilities, generally more accessible and better equipped than their rural counterparts, can provide prompt malaria diagnosis and treatment and prevent new infections (*9*). However, chronic asymptomatic and submicroscopic infections can escape detection and sustain transmission. The rapid, unplanned urbanization of this region may transform malaria into an urban disease in the Amazon Basin, with broad public health implications.

Author affiliations: Centro Nacional de Pesquisa em Energia e Materiais, Campinas, Brazil (P.T. Rodrigues); University of São Paulo, São Paulo, Brazil (P.T. Rodrigues, I.C. Johansen, W.A. Ladeia, F.D. Esquivel, R.M. Corder; J. Tonini, P.R. Calil, A.R.J. Fernandes, P.S. Fontoura, M.U. Ferreira); State University of Campinas, Campinas (I.C. Johansen); Universidade Federal do ABC, Santo André, Brazil (J. Tonini); Instituto Federal de Educação, Ciência e Tecnologia de Minas Gerais, Belo Horizonte, Brazil (A.R.J. Fernandes); Ministry of Health, Brasília, Brazil (P.S. Fontoura); Faculdade de Medicina de São José do Rio Preto, São José do Rio Preto, Brazil (C.E. Cavasini); Yale School of Medicine, New Haven, Connecticut, USA (J.M. Vinetz); Universidad Peruana Cayetano Heredia, Lima, Peru (J.M. Vinetz); Harvard T.H. Chan School of Public Health, Boston, Massachusetts, USA (M.C. Castro); Global Health and Tropical Medicine, NOVA University of Lisbon, Lisbon, Portugal (M.U. Ferreira); Institute of Hygiene and Tropical Medicine, NOVA University of Lisbon (M.U. Ferreira)

DOI: http://doi.org/10.3201/eid3009.240378

[1]Group members are listed at the end of this article.

In this study, we combined population-based prevalence data and parasite genotyping to examine the epidemiology of residual malaria in the main urban transmission hotspot of Brazil. We tested the hypothesis that, once introduced into receptive urbanized spaces, malaria parasites spread unnoticed among asymptomatic carriers, potentially causing outbreaks more frequently than parasite lineages restricted to remote rural villages.

The Institutional Review Board of the Institute of Biomedical Sciences, University of São Paulo, and the National Committee on Ethics in Research of the Ministry of Health of Brazil approved this study protocol (CAAE no. 6467416.6.0000.5467). We obtained written informed consent and assent from all study participants or their parents or guardians.

Methods

Study Site

The municipality or county of Mâncio Lima (Figure 1) (*7*) had an annual parasite incidence (number of laboratory-confirmed malaria cases per 1,000 persons per year) estimated at 422.8, the highest in Brazil, at the study onset in 2018. Half of the municipality's population lived in the town of Mâncio Lima (Appendix Figure 1, https://wwwnc.cdc.gov/EID/article/30/9/24-0378-App1.pdf), which accounted for 48% of the municipality's malaria cases in 2018. *Anopheles* (*Nyssorhynchus*) *darlingi*, the primary malaria vector, thrives in fish farming tanks and ponds that were opened across the town starting in the early 2000s (*10*).

Household Panel Survey

We analyzed biological specimens and data from a household-based random sample comprising 20% of the residents in the town of Mâncio Lima (*11*). Our analysis included repeated measurements on a cohort of residents in the same households to characterize temporal changes in the outcomes of interest (*12*). Study waves took place in April–May 2018 (wave 1), September–October 2018 (wave 2), May–June 2019 (wave 3), September–October 2019 (wave 4), October–November 2020 (wave 5), April–May 2021 (wave 6), and October–November 2021 (wave 7). Over the 4-year study period, the incidence of microscopy-confirmed malaria decreased markedly among urban residents (Figure 2).

We recorded sociodemographic and illness information and used a household-based wealth index as a proxy of socioeconomic status (Appendix). We collected finger-prick capillary blood samples from participants >3 months of age, regardless of any symptoms, for malaria diagnosis and parasite genotyping. We asked participants whether they had experienced any signs or symptoms that might have been caused by a malarial infection ≤7 days before the interview. We specifically asked those reporting any signs or symptoms whether they had fever, chills, or headache.

Figure 1. Location of the municipality of Mâncio Lima, Brazil, the study site for study of microscopy sensitivity and decreased malaria prevalence in the urban Amazon Region, Brazil, 2018–2021. Mâncio Lima (dark gray shading), population 19,294 in 2022, is situated in the upper Juruá Valley region (light gray shading) of the western Brazilian Amazon, adjacent to the border with Peru, covering an area of 5,453 km^2. Inset map shows location of study area in South America.

Laboratory Diagnosis of Malaria

We stained thick blood smears with Giemsa (Merck KGaA, https://www.emdgroup.com) and examined for malaria parasites under 1,000× magnification; a research microscopist who had >15 years of experience reviewed ≥200 fields. The protocols for slide staining and reading remained consistent throughout the study period. We also tested blood samples for malarial antigens, during waves 3 and 4, using the QuickProfile Pf/Pv (Lumiquick, https://lumiquick.com) rapid diagnostic test, and used them for DNA extraction followed by molecular diagnosis, during all study waves (Appendix).

We initially screened samples with a genus-specific PCR that targets a conserved sequence of the *cytb* gene of human-infecting malaria parasites (*13*) using a detection threshold of 0.2 amplicon copies/μL, equivalent to as few as 4 parasites/mL, assuming an average of 50 mitochondrial genome copies per blood-stage parasite. We further tested positive samples with separate species-specific quantitative TaqMan assays (ThermoFisher Scientific, https://www.thermofisher. com) that targeted mitochondrial genome sequences of *P. vivax* (84-bp domain of the *cox1* gene) or *P. falciparum* (90-bp domain spanning the 3′ end of the *cox1* gene and the nearby intergenic region) (*14*). Those techniques amplify circulating DNA from peripheral-blood parasites in addition to DNA released from dead parasites (*15*) sequestered in capillaries or accumulating in extravascular spaces of the bone marrow and spleen, providing an indirect estimate of the total parasite burden harbored by the host.

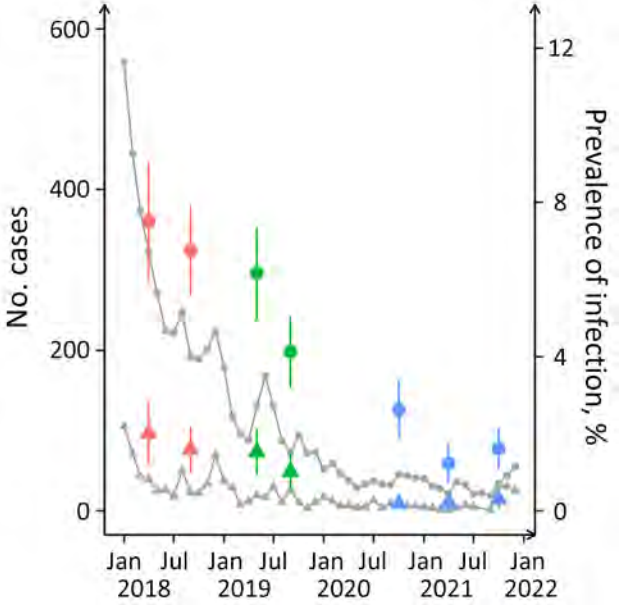

Figure 2. Monthly counts of microscopy-confirmed cases and percentages of infections diagnosed by PCR for *Plasmodium vivax* and *P. falciparum* in study of microscopy sensitivity and decreased malaria prevalence in the urban Amazon Region, Brazil, January 2018–December 2021. Circles indicate *Plasmodium vivax* and triangles *P. falciparum.* Red circles and triangles represent study waves 1 (April–May 2018) and 2 (September–October 2018); green, waves 3 (May–June 2019) and 4 (September–October 2019); blue, waves 5 (October–November 2020), 6 (April–May 2021), and 7 (October–November 2021). Error bars indicate 95% CIs for prevalence rates. Anonymized malaria case notifications were downloaded from the electronic database of the Ministry of Health of Brazil (http://200.214.130.44/sivep_malaria).

Parasite Sampling and Genotyping

To map the spread of parasite lineages across the region, we genotyped isolates collected during the panel study waves (Mâncio Lima sample set) along with 3 additional sample sets (Table 1; Appendix Figure 2). The Azul River/Nova Cintra set comprised samples obtained in April 2016 during cross-sectional surveys in riverine villages along Azul River, 6–8 hours by motorboat from the municipality of Mâncio Lima, and Nova Cintra on the Juruá River, municipality of Rodrigues Alves, in addition to samples collected in July 2018 and July 2019 along Azul River (*14*). The Vila Assis Brasil set included samples collected during cross-sectional surveys in August–September 2018, March 2019, and September–October 2019 in a periurban village 15 km away from Mâncio Lima by paved road (*16*). The health facility sample set consisted of isolates from symptomatic patients with microscopy-confirmed malaria who attended clinics in the municipalities of Mâncio Lima, Cruzeiro do Sul, and Rodrigues Alves during April 2018–April 2020; most of those samples were collected in 2019 (*11*). We inferred the likely sites of infection by considering patients' places of residence and history of recent travel.

We typed 6 microsatellite loci for each species: MS2, MS5, MS6, MS7, MS9, and MS15 for *P. vivax* (*17*) and polyα, TAA81, TAA42, TA87, TA109, and TA60 for *P. falciparum* (*18*) (Appendix Table 1). We defined haplotypes as unique combinations of alleles at each locus, considering only the most abundant allele when ≥2 alleles were detected in the same sample (Appendix). We calculated the expected heterozygosity as an estimate of genetic diversity and the standardized index of association as a measure of multilocus linkage disequilibrium with LIAN 3.7 software as previously described (*19*) (Appendix). We used the goeBURST algorithm implemented in PHYLOViZ (https://www.phyloviz.net) to identify clusters of genetically related haplotypes (*20*) that might be informative about parasite migration patterns (Appendix, Appendix Figure 3).

Table 1. *Plasmodium* spp. samples used for molecular genotyping in study of microscopy sensitivity and decreased malaria prevalence in the urban Amazon Region, Brazil, 2018–2021

Species and year	Sample collection site	Place of infection, urban/periurban or rural	Symptoms, Y/N	Microscopy, positive/negative	Total
P. vivax					
2016	Azul River and Nova Cintra	0/2	0/2	0/2	2
2018	Mâncio Lima	42/0	5/37	7/35	42
	Vila Assis Brasil	0/42	9/33	11/31	42
	Health facilities	2/1	3/0	3/0	3
	All sites, 2018	44/43	17/70	21/66	87
2019	Mâncio Lima	28/0	2/26	1/27	28
	Vila Assis Brasil	0/61	6/55	4/57	61
	Azul River	0/3	1/2	1/2	3
	Health facilities	14/33	47/0	47/0	47
	All sites, 2019	62/77	56/83	53/86	139
2020	Mâncio Lima	13/0	0/13	1/12	13
2021	Mâncio Lima	23/0	4/19	1/22	23
Total, all sites, 2016–2021		122/142	77/187	76/188	264
P. falciparum					
2018	Azul River	0/2	0/2	2/0	2
	Mâncio Lima	39/0	15/24	17/22	39
	Vila Assis Brasil	0/10	2/8	4/6	10
	Health facilities	3/0	3/0	3/0	3
	All sites, 2018	42/12	20/34	26/28	54
2019	Azul River	0/3	0/3	0/3	3
	Mâncio Lima	7/0	2/5	1/6	7
	Vila Assis Brasil	0/19	3/16	1/18	19
	Health facilities	13/36	49/0	49/0	49
	All sites, 2019	20/58	54/24	51/27	78
2020	Mâncio Lima	9/0	1/8	0/9	9
	Health facilities	2/0	2/0	2/0	2
	All sites, 2020	9/2	3/8	2/9	11
2021	Mâncio Lima	19/0	4/15	0/19	19
Total, all sites, 2018-21		92/70	81/81	79/83	162

Statistical Analysis

We entered data using the REDCap system (https://projectredcap.org/software) and analyzed using Stata 15.1 software (StataCorp LLC, https://www.stata.com). We defined statistical significance at the 5% level for 2-tailed tests. We calculated sensitivity, specificity, positive predictive value (PPV), negative predictive value (NPV), and accuracy, along with their 95% CIs, for microscopy and clinical signs and symptoms as predictors of infection detected by molecular methods (Appendix).

We used multivariable mixed-effects logistic regression models to identify correlates of malarial infection and disease while adjusting for potential confounders. We performed separate analyses for the following outcomes: TaqMan-confirmed *P. vivax,* regardless of any symptoms; TaqMan-confirmed *P. falciparum* infection, regardless of any symptoms; and clinical malaria (TaqMan-confirmed *P. vivax* or *P. falciparum* infection and reported fever, chills, or headache within the previous 7 days) (Appendix). We estimated odds ratios (ORs) with 95% CIs to quantify the influence of each predictor on the outcome. We also used logistic regression models (*21*) to describe the detectability of infection by microscopy as a continuous function of the number of species-specific amplicon copies per microliter measured by TaqMan.

Results

Prevalence of Submicroscopic and Asymptomatic Infection

We analyzed data from 2,774 residents in Mâncio Lima, ranging in age from 4 months to 103 years and distributed into 879 households, who underwent malaria parasite screening during ≥1 study wave. The number of participants varied from 1,093 in wave 1 to 2,043 in wave 7 (Appendix Table 2); 529 (19.1%) persons were screened at all time points, whereas 402 (14.5%) participated in a single study wave. Out of 11,730 specimens screened by PCR, 11,717 (99.9%) were also tested by microscopy.

PCR followed by TaqMan detected ≈10 times more infections than microscopy: out of 11,730 samples screened, 467 (4.0%) were positive for *Plasmodium vivax*, 104 (0.9%) for *P. falciparum,* and 54 (0.5%) for both species. Microscopy revealed 42 (0.4%) samples positive for *P. vivax*, 18 (0.2%) for *P. falciparum*, and 1 (0.01%) for both species, among 11,717 microscopically examined samples; we identified no other *Plasmodium* species (Table 2). None of the 54 mixed-species infections detected by TaqMan had been correctly identified by microscopy. Conversely, the only mixed-species infection diagnosed by microscopy

yielded a positive TaqMan result for *P. vivax* only (Appendix Table 3).

Compared with molecular methods, microscopy demonstrated a diagnostic sensitivity of 8.5% (95% CI 6.5%–11.1%), specificity of 99.9% (95% CI 99.9%–100.0%), PPV of 86.9% (95% CI 75.9%–93.3%), NPV of 95.1% (95% CI 95.0%–95.2%), and accuracy of 95.1% (95% CI 94.7%–95.5%) (Appendix, Appendix Tables 3, 4). The proportion of molecularly diagnosed malarial infections that were asymptomatic varied from 73.8% in wave 2 to 96.8% in wave 6, with a higher proportion of asymptomatic infections during the latest study waves (Table 2). When compared with PCR followed by Taqman, the overall diagnostic sensitivity of reported fever, chills, or headache was only 16.0% (95% CI 13.2%–19.1%); specificity was 90.8% (95% CI 90.3%–91.4%), PPV 8.9% (95% CI 7.53%–10.6%), NPV 95.1% (95% CI 94.9%–95.2%), and accuracy 86.8% (95% CI 86.2%–87.5%). Overall, we observed a higher prevalence of infection with *P. vivax* and *P. falciparum* and of clinical malaria among adolescent and adults from the poorest households in the town (Appendix Tables 2,5), as indicated by adjusted multiple logistic regression analysis incorporating >11,000 observations.

Table 2. Factors associated with *Plasmodium* spp. infection and clinical malaria, as revealed by mixed-effects multiple logistic regression analysis, in the urban population of Mâncio Lima, Brazil, 2018–2021*

	Outcome					
	P. vivax infection		*P. falciparum* infection		Clinical malaria	
Factor	OR (95% CI)	p value	OR (95% CI)	p value	OR (95% CI)	p value
Individual-level variables						
Age						
<10	Referent		Referent	Ref	1	Ref
10–19	3.35 (1.99–5.67)	<0.0001	2.48 (0.97–6.33)	0.057	3.49 (1.01–12.11)	0.048
20–29	4.00 (2.22–7.19)	<0.0001	3.57 (1.38–9.25)	0.009	6.24 (1.82–21.46)	0.004
30–39	3.39 (1.99–5.80)	<0.0001	2.29 (0.90–5.83)	0.082	4.34 (1.31–14.41)	0.017
40–49	3.40 (1.83–6.33)	<0.0001	3.35 (1.21–9.26)	0.020	6.97 (2.16–22.53)	0.001
50–59	2.71 (1.38–5.31)	0.004	3.11 (1.10–8.81)	0.032	4.98 (1.27–19.53)	0.021
≥60	3.94 (2.07–7.49)	<0.0001	3.74 (1.41–9.91)	0.008	8.56 (2.52–28.98)	0.001
Trend		0.003		0.011		<0.0001
Sex						
F	Referent		Referent		Referent	
M	1.04 (0.79–1.38)	0.767	1.72 (1.20–2.47)	0.003	0.72 (0.48–1.06)	0.095
Any past malaria						
No	Referent		Referent		Referent	
Yes	2.39 (1.70–3.34)	<0.0001	3.27 (1.93–5.52)	<0.0001	4.29 (2.58–7.12)	<0.0001
Bed net use past night						
No	Referent		Referent		Referent	
Yes, not treated	0.70 (0.48–1.02)	0.063	0.74 (0.40–1.34)	0.318	0.42 (0.23–0.76)	0.004
Yes, insecticide-treated	0.91 (0.67–1.23)	0.530	0.84 (0.52–1.37)	0.494	0.59 (0.35–1.00)	0.051
Household-level variables						
Wealth index quartile						
1, poorest	Referent		Referent		Referent	
2	0.60 (0.44–0.82)	0.001	0.53 (0.31–0.90)	0.019	0.52 (0.28–0.93)	0.028
3	0.46 (0.30–0.71)	<0.0001	0.63 (0.36–1.07)	0.092	0.52 (0.29–0.94)	0.029
4, wealthiest	0.39 (0.22–0.71)	0.002	0.51 (0.23–1.12)	0.094	0.39 (0.12–1.27)	0.118
Trend		<0.0001		0.064		0.018
Presence of eave gaps						
Yes	Referent		Referent		Referent	
No	0.71 (0.42–1.19)	0.194	0.47 (0.24–0.95)	0.034	0.11 (0.03–0.46)	0.002
Study wave number and dates						
1, Apr–May 2018	Referent		Referent		Referent	
2, Sep–Oct 2018	1.61 (1.05–2.49)	0.030	2.26 (1.17–4.34)	0.014	3.78 (1.91–4.50)	<0.0001
3, May–Jun 2019	1.50 (0.96–2.33)	0.073	2.29 (1.27–4.13)	0.006	2.15 (0.97–4.75)	0.058
4, Sep–Oct 2019	0.77 (0.48–1.25)	0.294	1.18 (0.56–2.49)	0.664	0.56 (0.20–1.60)	0.283
5, Oct–Nov 2020	0.54 (0.32–0.92)	0.025	0.68 (0.29–1.59)	0.378	0.48 (0.16–1.41)	0.183
6, Apr–May 2021	0.24 (0.13–0.42)	<0.0001	0.43 (0.17–1.05)	0.063	0.10 (0.01–0.83)	0.032
7, Oct–Nov 2021	0.26 (0.15–0.47)	<0.0001	0.34 (0.11–1.02)	0.053	0.56 (0.18–1.71)	0.308
No. observations†	11,676		11,615		11,569	

*Infection is defined as a positive genus-specific PCR result confirmed by species-specific TaqMan assay positive for *Plasmodium vivax* or *P. falciparum*, regardless of any symptoms. Clinical malaria is defined as a positive genus-specific PCR result confirmed by species-specific TaqMan assay positive for *P. vivax* or *P. falciparum*. in a study participant who reported symptoms (fever, chills, or headache) within the previous 7 days. Note that clinical malaria may be due to *P. vivax*, *P. falciparum*, or both species (mixed infections). OR, odds ratio.

†The numbers of observations differ among outcomes because some exposure categories were dropped from the analysis in order to allow logistic models for *P. falciparum* infection and clinical malaria to converge.

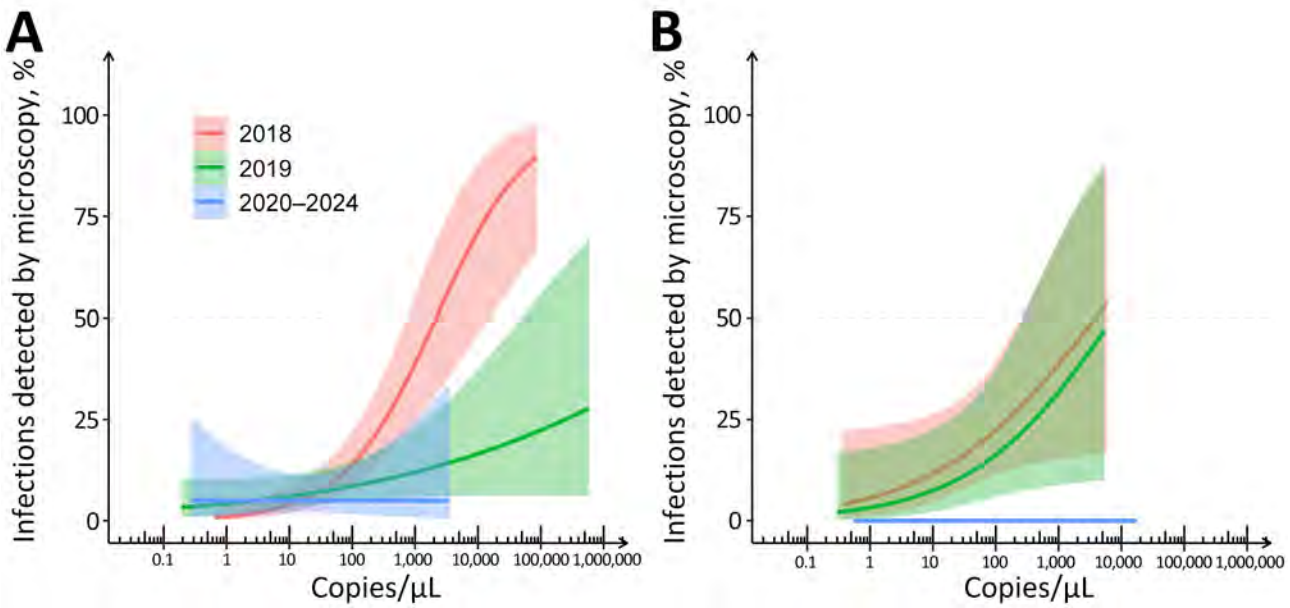

Figure 3. Proportion of TaqMan-detected single-species *Plasmodia vivax* (A) and *P. falciparum* (B) infections that were detected by microscopy according to parasite density (amplicon copies per microliter measured by species-specific TaqMan assays) in study of microscopy sensitivity and decreased malaria prevalence in the urban Amazon Region, Brazil, January 2018–December 2021. Lines represents the fitted logistic model trends; the shaded area indicates 95% CI for waves 1 and 2 (2018; red), waves 3 and 4 (2019; green) and waves 5–7 (2020–2021; blue). For this analysis, data from waves 1 and 2 (2018), 3 and 4 (2019), and 5–7 (2020–2021) were combined to achieve balanced sample sizes for fitting logistic models. CI could not be properly estimated for *P. falciparum* infections in waves 5–7 because of the small sample size (Appendix Table 2). The dashed horizontal line indicates 50% microscopic detectability at a given parasite density threshold, which for *P. vivax* infections in 2018 corresponds to 2,088 (95% CI 734–14,572) amplicon copies/µL.

Parasite Detectability over Time

The prevalence of malarial infection diagnosed by microscopy and molecular methods, either symptomatic or asymptomatic, significantly declined during the study period (Figure 2; Appendix Table 2). The later study waves exhibited an increased proportion of submicroscopic infections, which might be attributed to lower average parasite densities during periods of decreased transmission (*21*). However, TaqMan-quantified *P. vivax* densities remained consistent during 2018–2021 at an overall geometric mean of 19.0 amplicon copies/µL (Appendix Table 2). In contrast, *P. falciparum* densities (geometric mean 10.5 amplicon copies/µL) fluctuated more prominently, from 3.2 amplicon copies/µL in wave 6 to 86.3 amplicon copies/µL in wave 5, although the limited sample size prevented robust identification of temporal trends (Appendix Table 2).

The likelihood of detecting parasite by microscopy as a function of TaqMan-measured parasite density diminished with time. In 2018, we anticipated to identify 50% of *P. vivax* infections by microscopy at a density of 2,088 (95% CI 734–14,572) amplicon copies/µL or ≈42 parasites/µL (Figure 3, panel A). Nevertheless, most *P. vivax* infections above this threshold were undetected by microscopy in subsequent years, consistent with a decline in microscopy sensitivity. At a given TaqMan-measured average parasite density, the diagnostic sensitivity of peripheral-blood microscopy decreased during periods of lowest malaria prevalence. Despite the considerably smaller sample size, we noted a similar temporal trend in the microscopic diagnosis of *P. falciparum* infections (Figure 3, panel B). Those findings suggest that a higher proportion of infections are overlooked by peripheral-blood microscopy as malaria prevalence declines.

Parasite Lineages over Space and Time

During 2018–2021, we genotyped 122 *P. vivax* and 92 *P. falciparum* isolates collected in the town of Mâncio Lima, along with 142 *P. vivax* and 70 *P. falciparum* isolates from surrounding rural areas (Table 1; Appendix Figure 2). The parasites exhibited a high genetic diversity (average heterozygosity >0.8 for both species) that varied little over time in Mâncio Lima (Appendix Table 2). Both *P. vivax* and *P. falciparum* populations displayed substantial linkage disequilibrium (Appendix), consistent with the circulation of near-clonal parasite lineages across the region (*22*). Of interest, minimal spanning trees showed no clear

clustering based on infection sites in the Juruá Valley for *P. vivax* (Figure 4) and *P. falciparum* (Figure 5). Instead, parasite haplotypes from the town of Mâncio Lima and the rural surroundings were evenly distributed in the trees. We observed 1 instance for *P. vivax* and 6 instances for *P. falciparum* of haplotype sharing among parasites from the town and rural areas, indicating substantial connectivity between urban and rural populations.

We observed some evidence of temporal clustering of parasite lineages (Appendix). Parasites from both species circulating in the town of Mâncio Lima during 2019 formed clusters (Appendix Figure 4) that were enriched in lineages from symptomatic and patent infections (Appendix Figure 5). Similarly, clusters of patent and symptomatic *P. vivax* and *P. falciparum* infections were also observed in the analysis of the complete Juruá Valley dataset, combining data from urban and rural sites (Appendix Figure 6).

Discussion

In this extensive population-based study spanning 4 years, we found increasing proportions of asymptomatic and submicroscopic infections as the overall number of urban malaria cases decreased in the main transmission hotspot of Brazil. Of notable practical importance, the utility of microscopic diagnosis for detecting parasitemia diminished as malaria transmission decreased, which carries medical and public health implications. This challenge is not unique to our study site; microscopy has been demonstrated to overlook a higher proportion of *P. falciparum* infections in the areas of lowest malaria prevalence across sub-Saharan Africa (*23*). Molecular diagnosis may be necessary for identifying low-density malarial infections in low transmission settings, where microscopy-based parasite prevalence is <10% (*24*). However, new field-deployable tests for parasite DNA detection should undergo validation before widespread implementation in peripheral laboratories in the Amazon Basin (*5*). Furthermore, positive PCR results should be interpreted as indicative of either current or recent infection (*15*).

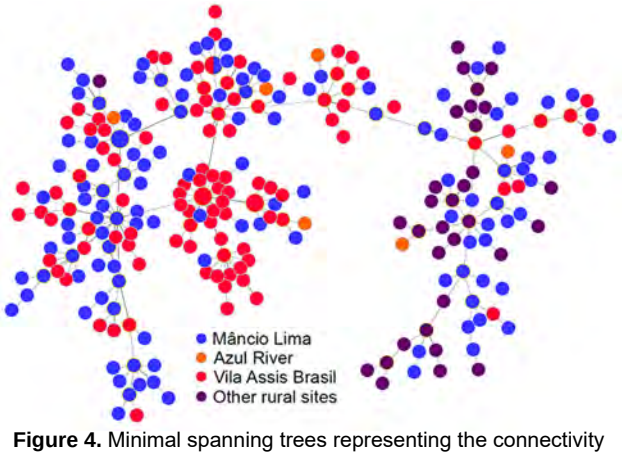

Figure 4. Minimal spanning trees representing the connectivity of *Plasmodium vivax* haplotypes from the Juruá Valley region of Brazil (264 isolates collected 2016–2021). Circles represent haplotypes with size linearly proportional to the number of isolates sharing them. Lines connect pairs of haplotypes with ≤5 allele mismatches and the overall network represents the most likely haplotype genealogy, ensuring that the summed distance of all links of the tree is the minimum possible. Haplotype colors indicate the likely site of infection (Appendix Figure 2). The circle with blue and red slices indicates a haplotype that was shared by 2 parasites from different (urban and rural) origins.

Few studies have identified changes in microscopy sensitivity with decreasing malaria transmission by repeatedly sampling the same population (*16*,*25*). Here, we provide evidence of rising microscopy detection thresholds, showing that a higher proportion of *P. vivax* and *P. falciparum* infections were missed at comparable parasite densities as malaria incidence diminished over time. Of note, molecular methods can detect circulating DNA released by dead trophozoites and schizonts that may have been concealed in capillaries and venules or extravascular territories (*15*). We speculate that, at lower transmission, fewer parasites accumulating in deep-organ blood vessels and extravascular spaces tend to circulate in the peripheral blood, where they can be identified by microscopy, perhaps indicative of parasites' adaptation to seasonal variation in vector abundance (*26*) or enhanced control measures (*27*). Temporal changes in *P. falciparum* sequestration patterns, particularly in regions with seasonal malaria transmission (*26*), can theoretically influence parasite detectability in the peripheral blood. However, additional longitudinal studies are required to validate this hypothesis.

Our findings demonstrate that parasite lineages spread across rural–urban boundaries, suggesting that rural areas with limited diagnosis and surveillance may serve as important sources for malaria reintroduction. Rural–urban mobility introduces malaria parasites into receptive, more densely populated urbanized spaces (*28*). The most mobile residents of Mâncio Lima are men 16–60 years of age who lack formal employment in the town and are often engaged in subsistence or commercial farming in periurban settlements (*29*). We found that closely related lineages of *P. vivax* and *P. falciparum* are shared among urban and rural residents, indicating the free circulation of malaria parasites across the rural–urban boundaries in the Juruá

Valley. Efficient parasite spreaders, such as forestgoers in Southeast Asia villages (*30*), can be selectively targeted for more intensive and effective malaria control interventions that cannot be readily delivered to the entire community, in this and similar endemic settings across the Amazon.

Brazil has an ambitious plan to achieve zero malaria by reducing cases from 150,000 in 2022 to <68,000 by 2025, eliminating *P. falciparum* malaria and associated deaths by 2030, eliminating cases and deaths by any species by 2035, and preventing malaria reintroduction from 2035 onward (*31*). However, elimination plans can be undermined by the establishment of malaria transmission in highly connected urbanized spaces that serve as both sinks and sources of parasite lineages. The large urban and periurban malaria outbreaks recorded in the Juruá Valley since the mid-2000s, when the region became the main transmission hotspot of Brazil, have been linked to the opening of fishponds for commercial aquaculture (*6*,*7*,*32*). By 2015, the Juruá Valley contributed 18% of the country's malaria burden (*33*). Although most infections diagnosed during our study were asymptomatic, parasite carriers are exposed to recurrent episodes of parasitemia, which lead to chronic anemia and other possible clinical and immunologic consequences (*34*). Of importance, the hidden parasite reservoir missed by routine surveillance substantially contributes to human-to-mosquito parasite transmission in similar low-endemicity settings (*4*,*21*,*35*,*36*).

The country's strategy for malaria surveillance and control comprises several actions: to provide prompt microscopy-based diagnosis and treatment after detection of isolated cases or clusters of cases; to detect additional cases, once an index case has been diagnosed; and to implement vector control measures in the vicinity of passively detected cases (*37*). Active surveillance around cases has gradually been implemented in Brazil since reactive case detection was demonstrated to be feasible and effective for malaria control in the Amazon (*38*), although molecular diagnosis is rarely used with this purpose.

The role of long-lasting insecticide-treated bed nets (LLINs) and indoor residual spraying in malaria control in Mâncio Lima is uncertain. Only 46% of the study participants reported using LLINs the previous night; <15% had their houses sprayed within the previous 12 months (Appendix Table 5). Larval source management is currently limited to periodically removing vegetation from the margins of fish farming tanks and emptying those no longer used for aquaculture. Alternatively, the periodic application of environmentally safe biolarvicides can drastically reduce anopheline larval density in fish tanks (*39*), but its feasibility for large-scale use remains to be determined.

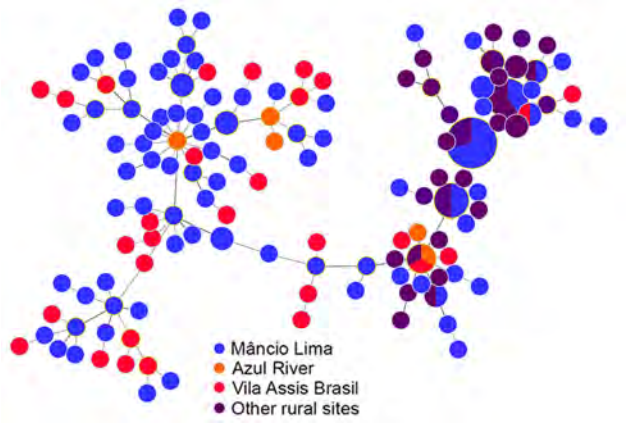

Figure 5. Minimal spanning trees representing the connectivity of *Plasmodium falciparum* haplotypes from the Juruá Valley region of Brazil (162 isolates collected 2018 –2021). Similar to Figure 4, circles represent haplotypes with size linearly proportional to the number of isolates sharing them and lines connect pairs of haplotypes with ≤5 allele mismatches. Haplotype colors indicate the likely site of infection (Appendix Figure 2, https://wwwnc.cdc.gov/EID/article/30/9/24-0378-App1.pdf). In 7 circles (haplotypes), slices of different colors indicate that the corresponding haplotypes were shared by parasites from different geographic origins.

The primary strength of this study lies in its household panel design (*12*), which enabled us to examine temporal trends of malarial infection and disease at the community level and to identify changes in the sensitivity of diagnostic microscopy over 4 years. The first limitation of this study is that only 61 microscopy-positive infections and 100 clinical malaria episodes were diagnosed during 7 study waves, despite screening a large population, as expected under low transmission. Second, we defined clinical malaria on the basis of perceived signs and symptoms, rather than fever measured at the time of interviews. We argue that perceived symptoms, although not highly specific and prone to recall bias, are the key drivers of healthcare seeking and define which infections will be identified by passive surveillance and eventually treated. Third, microsatellite genotyping provides a relatively limited view of genetic variation and connectivity among local parasites, compared with targeted amplicon sequencing (*40*) or whole-genome analysis (*41*). However, our results are broadly consistent with genome-wide analyses that showed recent ancestry sharing between urban and rural near-clonal lineages of *P. vivax* across Juruá Valley (*22*).

In conclusion, our research illustrates how parasite lineages can spread across rural–urban boundaries and

cause predominantly asymptomatic infections that are increasingly missed by microscopy as the overall malaria incidence drops. The presence of an undetected urban malaria reservoir may require more effort toward regional control and elimination strategies.

The Mâncio Lima Cohort Study Group comprised the following investigators in 2018–2022: Alexandre S. Nogueira, Anderson R.J. Fernandes, Andreea-Beatrice Rusu, Fabiana D. Esquivel, Igor C. Johansen, Jaques N. de Carvalho, Juliana Tonini, Lais C. Salla, Marcelo U. Ferreira, Maria José Menezes, Pablo S. Fontoura, Priscila R. Calil, Priscila T. Rodrigues, Rodrigo M. Corder, Thaís C. de Oliveira, Vanessa C. Nicolete, and Winni A. Ladeia (University of São Paulo, São Paulo, Brazil); Rodrigo M. de Souza and Amanda O.S. Fernandes (Federal University of Acre, Cruzeiro do Sul, Brazil); Paulo E.M. Ribolla (State University of São Paulo, Botucatu, Brazil); Carlos E. Cavasini (Faculdade de Medicina de São José do Rio Preto, São José do Rio Preto, Brazil); Joseph M. Vinetz (Yale School of Medicine, New Haven, Connecticut, USA); and Marcia C. Castro (Harvard T.H. Chan School of Public Health, Boston, USA).

Acknowledgments

We thank the 2,774 participants in the Mâncio Lima Urban Cohort Study. We thank Ajucilene (Joice) G. Mota, Francisco Melo, and their team at the Health Secretary of Mâncio Lima for their overall logistic support; Juliana C. Belizário, Bárbara Prado C. Silva, Vanessa C. Nicolete, Amanda O. S. Fernandes, and Isabel Giacomini for fieldwork; Jaques N. de Carvalho for laboratory support, and Maria José Menezes for administrative support.

This work was supported by the Fundação de Amparo à Pesquisa do Estado de São Paulo (FAPESP), Brazil (2016/18740–9 to M.U.F.), the National Institutes of Health (grant U19 AI089681 to J.M.V.), and the Fundação para a Ciência e Tecnologia, Portugal (institutional GHTM project, UID/04413/2020). FAPESP provided scholarships to P.T.R., I.C.J., W.A.L., F.D.E., and P.S.F; the Conselho Nacional de Desenvolvimento Científico e Tecnológico (CNPq), Brazil, provided scholarships to R.M.C. and M.U.F.; and the Coordenação de Aperfeiçoamento de Pessoal de Nível Superior provided a scholarship to W.A.L. The funders had no role in study design, data collection and interpretation, or in the decision to submit the work for publication.

Author contributions: P.T.R., I.C.J., J.M.V., M.C.C. and M.U.F. contributed to the study design and implementation; P.T.R., I.C.J., W.A.L., J.T., R.M.C., A.R.J.F., P.S.F. C.E.C., and M.U.F contributed to field data collection; P.T.R., W.A.L., F.D.E., J.T., and P.R.C. contributed to methods and laboratory analyses; I.C.J, R.M.C., A.R.J.F., M.C.C., and M.U.F. contributed to data management, formal analysis, and visualization; J.M.V. and M.U.F. contributed to project management. All authors contributed to the writing and reviewed and approved the final manuscript. All authors had full access to all the data in the study and had final responsibility for the decision to submit for publication.

About the Author

Dr. Rodrigues is a staff researcher at the Brazilian Center for Research in Energy and Materials in Campinas, Brazil. Her research interests have recently shifted from malaria diagnosis and molecular epidemiology to the development of robust and efficient microbial cell factories.

References

1. World Health Organization. World malaria report 2022. Geneva: The Organization; 2022.
2. Ferreira MU, Castro MC. Malaria situation in Latin America and the Caribbean: residual and resurgent transmission and challenges for control and elimination. Methods Mol Biol. 2019;2013:57–70. https://doi.org/10.1007/978-1-4939-9550-9_4
3. Bousema T, Okell L, Felger I, Drakeley C. Asymptomatic malaria infections: detectability, transmissibility and public health relevance. Nat Rev Microbiol. 2014;12:833–40. https://doi.org/10.1038/nrmicro3364
4. Ferreira MU, Corder RM, Johansen IC, Kattenberg JH, Moreno M, Rosas-Aguirre A, et al. Relative contribution of low-density and asymptomatic infections to *Plasmodium vivax* transmission in the Amazon: pooled analysis of individual participant data from population-based cross-sectional surveys. Lancet Reg Health Am. 2022;9:100169. https://doi.org/10.1016/j.lana.2021.100169
5. Torres K, Ferreira MU, Castro MC, Escalante AA, Conn JE, Villasis E, et al. Malaria resilience in South America: epidemiology, vector biology, and immunology insights from the Amazonian International Center of Excellence in Malaria Research Network in Peru and Brazil. Am J Trop Med Hyg. 2022;107(Suppl):168–81. https://doi.org/10.4269/ajtmh.22-0127
6. Costa KM, de Almeida WA, Magalhães IB, Montoya R, Moura MS, de Lacerda MV. Malaria in Cruzeiro do Sul (Western Brazilian Amazon): analysis of the historical series from 1998 to 2008 [in Portuguese]. Rev Panam Salud Publica. 2010;28:353–60. https://doi.org/10.1590/s1020-49892010001100005
7. Olson SH, Gangnon R, Silveira GA, Patz JA. Deforestation and malaria in Mâncio Lima County, Brazil. Emerg Infect Dis. 2010;16:1108–15. https://doi.org/10.3201/eid1607.091785
8. Salla LC, Rodrigues PT, Corder RM, Johansen IC, Ladeia-Andrade S, Ferreira MU. Molecular evidence of sustained urban malaria transmission in Amazonian Brazil, 2014–2015. Epidemiol Infect. 2020;148:e47. https://doi.org/10.1017/S0950268820000515
9. Wilson ML, Krogstad DJ, Arinaitwe E, Arevalo-Herrera M, Chery L, Ferreira MU, et al. Urban malaria: understanding

its epidemiology, ecology, and transmission across seven diverse ICEMR network sites. Am J Trop Med Hyg. 2015;93(Suppl):110–23. https://doi.org/10.4269/ajtmh.14-0834
10. dos Reis IC, Codeço CT, Degener CM, Keppeler EC, Muniz MM, de Oliveira FG, et al. Contribution of fish farming ponds to the production of immature *Anopheles* spp. in a malaria-endemic Amazonian town. Malar J. 2015;14:452. https://doi.org/10.1186/s12936-015-0947-1
11. Johansen IC, Rodrigues PT, Tonini J, Vinetz J, Castro MC, Ferreira MU. Cohort profile: the Mâncio Lima cohort study of urban malaria in Amazonian Brazil. BMJ Open. 2021;11:e048073. https://doi.org/10.1136/bmjopen-2020-048073
12. Lipps O. Panel surveys: advantages and disadvantages compared with repeated cross-sectional surveys. FORS guide no. 14, version 1.0. Lausanne: Swiss Centre of Expertise in the Social Sciences FORS; 2021. https://doi.org/10.24449/FG-2021-00014
13. Putaporntip C, Buppan P, Jongwutiwes S. Improved performance with saliva and urine as alternative DNA sources for malaria diagnosis by mitochondrial DNA-based PCR assays. Clin Microbiol Infect. 2011;17:1484–91. https://doi.org/10.1111/j.1469-0691.2011.03507.x
14. Barros LB, Calil PR, Rodrigues PT, Tonini J, Fontoura PS, Sato PM, et al. Clinically silent *Plasmodium vivax* infections in native Amazonians of northwestern Brazil: acquired immunity or low parasite virulence? Mem Inst Oswaldo Cruz. 2022;117:e220175. https://doi.org/10.1590/0074-02760220175
15. Vafa Homann M, Emami SN, Yman V, Stenström C, Sondén K, Ramström H, et al. Detection of malaria parasites after treatment in travelers: a 12-months longitudinal study and statistical modelling analysis. EBioMedicine. 2017;25:66–72. https://doi.org/10.1016/j.ebiom.2017.10.003
16. Fontoura PS, Macedo EG, Calil PR, Corder RM, Rodrigues PT, Tonini J, et al. Changing clinical epidemiology of *Plasmodium vivax* malaria as transmission decreases: Population-based prospective panel survey in the Brazilian Amazon. J Infect Dis. 2024;229:947–58. https://doi.org/10.1093/infdis/jiad456
17. Karunaweera ND, Ferreira MU, Hartl DL, Wirth DF. Fourteen polymorphic microsatellite DNA markers for the human malaria parasite *Plasmodium vivax*. Mol Ecol Notes. 2007;7:172–5. https://doi.org/10.1111/j.1471-8286.2006.01534.x
18. Anderson TJ, Su XZ, Bockarie M, Lagog M, Day KP. Twelve microsatellite markers for characterization of *Plasmodium falciparum* from finger-prick blood samples. Parasitology. 1999;119:113–25. https://doi.org/10.1017/S0031182099004552
19. Hudson RR. Analytical results concerning linkage disequilibrium in models with genetic transformation and conjugation. J Evol Biol. 1994;7:535–48. https://doi.org/10.1046/j.1420-9101.1994.7050535.x
20. Francisco AP, Bugalho M, Ramirez M, Carriço JA. Global optimal eBURST analysis of multilocus typing data using a graphic matroid approach. BMC Bioinformatics. 2009;10:152. https://doi.org/10.1186/1471-2105-10-152
21. Slater HC, Ross A, Felger I, Hofmann NE, Robinson L, Cook J, et al. The temporal dynamics and infectiousness of subpatent *Plasmodium falciparum* infections in relation to parasite density. Nat Commun. 2019;10:1433. https://doi.org/10.1038/s41467-019-09441-1
22. de Oliveira TC, Corder RM, Early A, Rodrigues PT, Ladeia-Andrade S, Alves JMP, et al. Population genomics reveals the expansion of highly inbred *Plasmodium vivax* lineages in the main malaria hotspot of Brazil. PLoS Negl Trop Dis. 2020;14:e0008808. https://doi.org/10.1371/journal.pntd.0008808
23. Whittaker C, Slater H, Nash R, Bousema T, Drakeley C, Ghani AC, et al. Global patterns of submicroscopic *Plasmodium falciparum* malaria infection: insights from a systematic review and meta-analysis of population surveys. Lancet Microbe. 2021;2:e366–74. https://doi.org/10.1016/S2666-5247(21)00055-0
24. World Health Organization. WHO Evidence Review Group on Malaria Diagnosis in Low Transmission Settings. Malaria Policy Advisory Committee Meeting Report, Session 10. 2014 [cited 2024 Jul 30]. https://www.who.int/docs/default-source/malaria/mpac-documentation/mpac-mar2014-diagnosis-low-transmission-settings-report.pdf?sfvrsn=5694f918_2.
25. Barbosa S, Gozze AB, Lima NF, Batista CL, Bastos MS, Nicolete VC, et al. Epidemiology of disappearing *Plasmodium vivax* malaria: a case study in rural Amazonia. PLoS Negl Trop Dis. 2014;8:e3109. https://doi.org/10.1371/journal.pntd.0003109
26. Andrade CM, Fleckenstein H, Thomson-Luque R, Doumbo S, Lima NF, Anderson C, et al. Increased circulation time of *Plasmodium falciparum* underlies persistent asymptomatic infection in the dry season. Nat Med. 2020;26:1929–40. https://doi.org/10.1038/s41591-020-1084-0
27. Björkman A, Morris U. Why asymptomatic *Plasmodium falciparum* infections are common in low-transmission settings. Trends Parasitol. 2020;36:898–905. https://doi.org/10.1016/j.pt.2020.07.008
28. Martens P, Hall L. Malaria on the move: human population movement and malaria transmission. Emerg Infect Dis. 2000;6:103–9. https://doi.org/10.3201/eid0602.000202
29. Johansen IC, Rodrigues PT, Ferreira MU. Human mobility and urban malaria risk in the main transmission hotspot of Amazonian Brazil. PLoS One. 2020;15:e0242357. https://doi.org/10.1371/journal.pone.0242357
30. Tripura R, von Seidlein L, Sovannaroth S, Peto TJ, Callery JJ, Sokha M, et al. Antimalarial chemoprophylaxis for forest goers in southeast Asia: an open-label, individually randomised controlled trial. Lancet Infect Dis. 2023;23:81–90. https://doi.org/10.1016/S1473-3099(22)00492-3
31. Ministry of Health of Brazil. Eliminate Malaria Brazil: national plan for the elimination of malaria [in Portuguese]. 2022 [cited 2024 Jul 30]. https://www.gov.br/saude/pt-br/centrais-de-conteudo/publicacoes/svsa/malaria/politicas-de-saude/elimina-malaria-brasil-plano-nacional-de-eliminacao-da-malaria
32. Johansen IC, Ferreira MU. Unintended consequences of 'development' in the Amazon: commercial aquaculture and malaria in Mâncio Lima, Brazil. In: Ioris AAR, editor. Environment and development: challenges, policies and practices. London; Palgrave Macmillan: 2021. p. 387–410. https://doi.org/10.1007/978-3-030-55416-3_14
33. Ferreira MU, Castro MC. Challenges for malaria elimination in Brazil. Malar J. 2016;15:284. https://doi.org/10.1186/s12936-016-1335-1
34. Chen I, Clarke SE, Gosling R, Hamainza B, Killeen G, Magill A, et al. "Asymptomatic" malaria: a chronic and debilitating infection that should be treated. PLoS Med. 2016;13:e1001942. https://doi.org/10.1371/journal.pmed.1001942
35. Tadesse FG, Slater HC, Chali W, Teelen K, Lanke K, Belachew M, et al. The relative contribution of symptomatic and asymptomatic *Plasmodium vivax* and *Plasmodium falciparum* infections to the infectious reservoir in a

low-endemic setting in Ethiopia. Clin Infect Dis. 2018; 66:1883–91. https://doi.org/10.1093/cid/cix1123
36. Almeida GG, Costa PAC, Araujo MDS, Gomes GR, Carvalho AF, Figueiredo MM, et al. Asymptomatic *Plasmodium vivax* malaria in the Brazilian Amazon: submicroscopic parasitemic blood infects *Nyssorhynchus darlingi*. PLoS Negl Trop Dis. 2021;15:e0009077. https://doi.org/10.1371/journal.pntd.0009077
37. Pan American Health Organization. Stratification of malaria based on risk of transmission and elimination of foci. Washington; The Organization: 2019 [cited 2024 Jul 30]. https://www3.paho.org/hq/index.php?option=com_docman&view=download&slug=malaria-technical-advisory-group-session-8-2019&Itemid=270&lang=en
38. Fontoura PS, Finco BF, Lima NF, de Carvalho JF Jr, Vinetz JM, Castro MC, et al. Reactive case detection for *Plasmodium vivax* malaria elimination in rural Amazonia. PLoS Negl Trop Dis. 2016;10:e0005221. https://doi.org/10.1371/journal.pntd.0005221
39. Fontoura PS, Silva MF, da Costa AS, Ribeiro FS, Ferreira MS, Ladeia-Andrade S, et al. Monthly biological larviciding associated with a tenfold decrease in larval density in fish farming ponds and reduced community-wide malaria incidence in northwestern Brazil. Parasit Vectors. 2021;14:445. https://doi.org/10.1186/s13071-021-04964-3
40. Holzschuh A, Lerch A, Gerlovina I, Fakih BS, Al-Mafazy AH, Reaves EJ, et al. Multiplexed ddPCR-amplicon sequencing reveals isolated *Plasmodium falciparum* populations amenable to local elimination in Zanzibar, Tanzania. Nat Commun. 2023;14:3699. https://doi.org/10.1038/s41467-023-39417-1
41. Schaffner SF, Badiane A, Khorgade A, Ndiop M, Gomis J, Wong W, et al. Malaria surveillance reveals parasite relatedness, signatures of selection, and correlates of transmission across Senegal. Nat Commun. 2023;14:7268. https://doi.org/10.1038/s41467-023-43087-4

Address for correspondence: Marcelo U. Ferreira, Institute of Biomedical Sciences, University of São Paulo, Av. Prof. Lineu Prestes 1374, 05508-900 São Paulo, Brazil; email: muferrei@usp.br or muferrei@ihmt.unl.pt

Effects of Rotavirus Vaccination Coverage among Infants on Hospital Admission for Gastroenteritis across All Age Groups, Japan, 2011–2019

Kenji Kishimoto, Susumu Kunisawa, Kiyohide Fushimi, Yuichi Imanaka

We assessed the effect of rotavirus vaccination coverage on the number of inpatients with gastroenteritis of all ages in Japan. We identified patients admitted with all-cause gastroenteritis during 2011–2019 using data from the Diagnosis Procedure Combination system in Japan. We used generalized estimating equations with a Poisson distribution, using hospital codes as a cluster variable to estimate the impact of rotavirus vaccination coverage by prefecture on monthly numbers of inpatients with all-cause gastroenteritis. We analyzed 294,108 hospitalizations across 569 hospitals. Higher rotavirus vaccination coverage was associated with reduced gastroenteritis hospitalizations compared with the reference category of vaccination coverage <40% (e.g., for coverage ≥80%, adjusted incidence rate ratio was 0.87 [95% CI 0.83–0.90]). Our results show that achieving higher rotavirus vaccination coverage among infants could benefit the entire population by reducing overall hospitalizations for gastroenteritis for all age groups.

Gastroenteritis is one of the most common infectious diseases, characterized by rapid onset of diarrhea with or without nausea, vomiting, fever, and abdominal pain (*1*,*2*). Enteric viruses and bacteria are major causes of gastroenteritis (*3*,*4*), although causes of hospitalizations related to gastroenteritis are often unidentified (*5*). Gastroenteritis affects persons of all ages and is a leading cause of death worldwide (*6*,*7*); younger children, the elderly, and immunocompromised patients in particular are at risk of severe gastroenteritis (*8*–*11*). Gastroenteritis-related hospitalizations and outpatient visits continue to be significant burdens on health systems (*3*,*12*,*13*).

Rotavirus is a leading cause of gastroenteritis and diarrhea, including fatal illnesses, in both young children and persons of all ages (*6*). A recent systematic review and meta-analysis reported that the pooled rotavirus prevalence was 7.6% (95% CI 6.2%–9.2%) among persons ≥5 years of age with diarrhea (*14*). Rotavirus infection is estimated to cause >200,000 deaths annually in children <5 years of age (*15*). Oral live-attenuated rotavirus vaccines for infants have been implemented worldwide since 2006. The World Health Organization in 2009 recommended routine immunization for all infants to prevent rotavirus disease (*16*).

In Japan, the rotavirus vaccine was introduced in 2011 to be administered to infants 2–8 months of age. Rotavirus vaccination coverage in Japan gradually increased from 30% in 2012 to 78% in 2019; however, disparity among prefectures in coverage rates remains relatively high (≈30% in 2019) (*17*). Implementation of rotavirus vaccines has substantially reduced hospitalizations from rotavirus and all-cause acute gastroenteritis in infants and younger children both in Japan and in other countries (*18*–*20*). Of note, population-based surveillance for rotavirus gastroenteritis hospitalizations after introduction of rotavirus vaccination identified a reduction in age-specific hospitalization rates among children ineligible for rotavirus vaccination because they were above the upper age limit (*21*). Furthermore, a large study analyzing saved bacterial cultures from fecal samples reported an almost 50% decline in rotavirus prevalence among adults during the peak rotavirus season after the

Author affiliations: Graduate School of Medicine, Kyoto University, Kyoto, Japan (K. Kishimoto, S. Kunisawa, Y. Imanaka) Tokyo Medical and Dental University Graduate School of Medicine, Tokyo, Japan (K. Fushimi); Centre for Health Security, Graduate School of Medicine, Kyoto University, Kyoto (Y. Imanaka);

DOI: https://doi.org/10.3201/eid3009.240259

vaccine was introduced (*22*). Those studies suggest that rotavirus vaccination for infants might indirectly protect older children and adults from rotavirus.

The long-term impacts of rotavirus vaccination on the entire population have not been fully clarified. Given that gastroenteritis constitutes a significant health concern for person in all age groups, analyzing the effects of rotavirus vaccination on older age groups is warranted. Several recent studies investigating long-term trends after rotavirus vaccine introduction have shown the potential indirect protection of rotavirus vaccination against gastroenteritis (*23*,*24*). However, those findings of indirect protection in adults lack consistency, and to date, associations between increases in vaccination coverage and indirect impact from vaccination on gastroenteritis remain unclear. We aimed to assess the effect of rotavirus vaccination coverage on the number of all-age hospital inpatients with gastroenteritis in Japan. We also aimed to describe trends in the numbers of inpatients at high risk of severe gastroenteritis as a foundation for better understanding the public health impacts of infant rotavirus vaccination.

This study was approved by the Ethics Committee, Graduate School of Medicine, Kyoto University (approval no. R0135). Research was conducted in accordance with the Ethical Guidelines for Medical and Health Research Involving Human Subjects of the Ministry of Health, Labour, and Welfare, Japan.

Methods

Data Source

We used the Diagnosis Procedure Combination (DPC) administrative claims database, which is a case-mix classification system used in Japan for reimbursing acute care hospitals under the public medical insurance scheme (25). DPC administrative claims data include information on hospital codes, patient demographics, admission and discharge dates, admission routes, outcomes, primary and secondary diagnoses (based on codes from the International Classification of Diseases 10th Revision [ICD-10]), comorbidities, complications, and claims for medical services (*25*). We extracted DPC administrative claims data from the database of the DPC Study Group, comprising voluntarily participating hospitals, which account for >50% of all acute inpatients in Japan (*26*). We obtained data on rotavirus vaccination coverage by prefecture and year as actual measured values from a previous review of rotavirus vaccination in Japan (*17*).

Study Population and Definitions

We used data from hospitals that had continuously provided DPC data to the DPC Study Group during 2011–2019 to select the study population. We included in the study all hospitalization data that stated a primary diagnosis, diagnosis causing admission, or the most medically resource-intensive diagnosis of all-cause gastroenteritis during January 2011–December 2019. We used date of discharge, rather than date of admission, to determine the number of monthly inpatients because DPC data were generated after discharge. Gastroenteritis was defined by ICD-10 codes A08.x–A09.x. We categorized included patients into 4 age groups: <5, 5–19, 20–59, and ≥60 years. We defined patients as age-ineligible for rotavirus vaccination if they were age ≥1 year in 2011, ≥2 years in 2012, ≥3 years in 2013, ≥4 years in 2014, ≥5 years in 2015, ≥6 years in 2016, ≥7 years in 2017, ≥8 years in 2018, and ≥9 years in 2019. We obtained information on underlying conditions and medications of patients from the database. We defined underlying conditions at admission by ICD-10 codes C00.0-C97 for cancer and B20.x-B24 for HIV and defined immunocompromised patients as those with cancer or HIV or who had received steroids or immunosuppressants. We defined the rotavirus epidemic season as February–April, on the basis of data from previous studies (*27*,*28*).

Statistical Analysis

Our primary outcome of interest was the monthly number of inpatients with all-cause gastroenteritis. We presented the results of time-series of monthly gastroenteritis hospitalizations in total, by age group, and among immunocompromised patients. We also presented annual gastroenteritis hospitalizations during the rotavirus epidemic season in total, by age group, and among immunocompromised patients. We estimated the impact of RV vaccination coverage on the basis of monthly number of gastroenteritis hospitalizations generalized estimating equations (GEE) (*29*–*31*) using a log-link function and Poisson distribution. We performed primary analyses using the GEE model for overall patients, the age-ineligible population, and immunocompromised patients. We further performed prespecified secondary analyses on data only from rotavirus-epidemic seasons. In our analyses, we did not account for repeated admission of the same patient, because we assumed that disease duration is short and recurrence rare among patients with gastroenteritis.

Because the numbers of gastroenteritis hospitalizations had a serial correlation within each hospital because of local characteristics and were therefore not

independent, we designated hospital codes as cluster variables in the GEE models. We used an exchangeable correlation structure in the GEE model. We considered monthly gastroenteritis inpatients by hospital as a dependent variable and rotavirus vaccination coverage by prefecture as an independent variable. We included age groups, years, and months as covariates in the adjusted model. We treated rotavirus vaccination coverage by prefecture and year as categorical variables (based on incremental 10% increases in coverage), because we assumed that the relationship between coverage and the primary outcome was nonlinear. We considered coverage <40% to be the reference category because annual mean coverage reached as high as 30% in 2012, the second year of the study period. We also treated the 4 age groups and 12 month–defined groups as categorical variables. We calculated incidence rate ratios (IRRs) and 95% CIs from the GEE model. We considered p values <0.05 statistically significant; all tests were 2-tailed. We conducted statistical analyses using Stata/SE version 16.1 (StataCorp LLC, https://www.stata.com).

Results

We analyzed 294,108 hospitalizations for gastroenteritis from 569 hospitals in all 47 prefectures in Japan during 2011–2019. Among patient characteristics, median age was 41 years (interquartile range [IQR] 9–73 years), and the highest number (38.3%) of patients was in the ≥60-year age group. The proportion of immunocompromised patients was 12.94% (Table 1).

Table 1. Characteristics of gastroenteritis patients in study of effects of rotavirus vaccination coverage among infants on hospital admission for gastroenteritis across all age groups, Japan, 2011–2019*

Characteristic	Value
Overall no. patients	294,108
Median age, y (IQR)	41 (9–73)
Age group, y	
<5	51,501 (17.5)
5–19	47,570 (16.2)
20–59	82,392 (28.0)
≥60	112,645 (38.3)
Immunocompromised patients	38,058 (12.9)
Underlying conditions	
Cancer	23,948 (8.1)
HIV infection	120 (0.04)
Medication	
Steroids	17,276 (5.9)
Immunosuppressants	3,459 (1.2)
Median stay, d (IQR)	5 (3–9)

*Values are no. (%) patients except as indicated. IQR, interquartile range

Time-Series of Gastroenteritis Hospitalizations

Annual mean rotavirus vaccination coverage in Japan increased from 30% in 2012 to 78% in 2019 (Figure 1, panel A) (*17*). Monthly numbers of gastroenteritis inpatients showed seasonality, peaking in winter (November–January). We observed epidemic peaks in December 2012 and December 2016. We found no obvious secular trends in overall gastroenteritis hospitalizations (Figure 1, panel A). We observed a trend of decreasing gastroenteritis hospitalizations among children <5 years of age in the first half of the study period (Figure 1, panel B), but numbers remained relatively stable among older children and adolescents (Figure 1, panel C) and young adults (Figure 1, panel D). We observed a secular trend of increased hospitalizations among adults ≥60 years of age (Figure 1, panel E) and among immunocompromised patients (Figure 1, panel F). Secular trends in the annual numbers of gastroenteritis hospitalizations during rotavirus epidemic seasons varied (Figure 2). We observed a

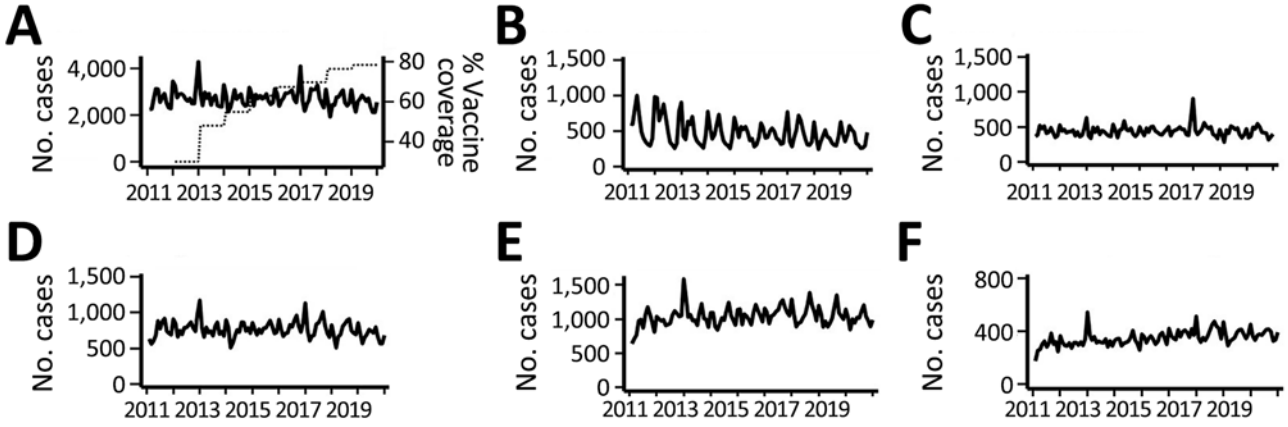

Figure 1. Time trends in gastroenteritis hospitalizations among different study populations in study of effects of rotavirus vaccination coverage among infants on hospital admission for gastroenteritis across all age groups, Japan, 2011–2019. A) Monthly numbers of gastroenteritis inpatients in the overall population, compared with annual mean rotavirus vaccination coverage. B–F) Monthly numbers of gastroenteritis hospitalizations among different study populations: B) young children <5 years of age; C) older children and adolescents 5–19 years of age; D) adults 20–59 years of age; E) older adults ≥60 years of age; F) immunocompromised persons.

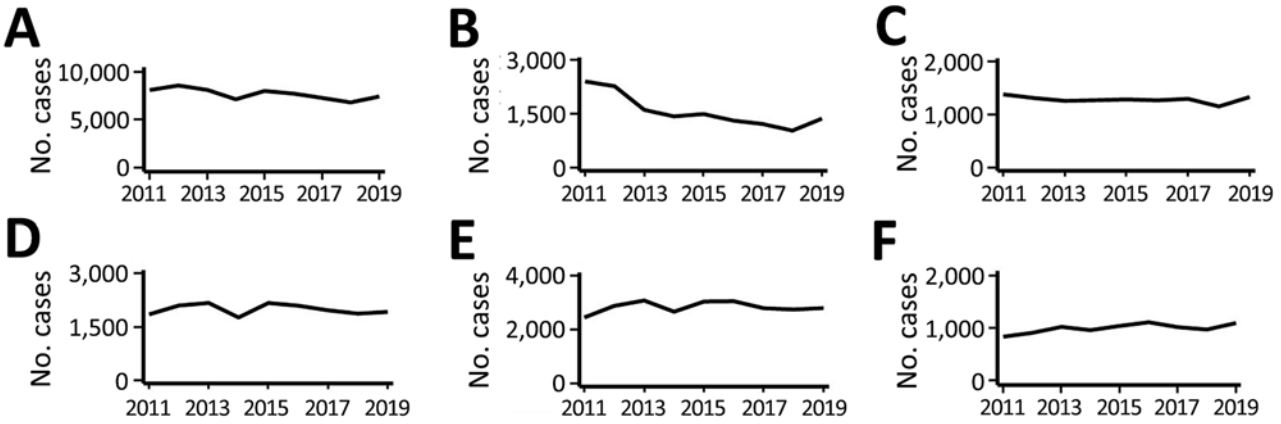

Figure 2. Annual numbers of gastroenteritis hospitalizations during the rotavirus vaccination epidemic season among different study populations in study of effects of rotavirus vaccination coverage among infants on hospital admission for gastroenteritis across all age groups, Japan, 2011–2019. A) Overall population; B) young children <5 years of age; C) older children and adolescents 5–19 years of age; D) adults 20–59 years of age; E) older adults ≥60 years of age; F) immunocompromised persons.

decreasing trend in hospitalizations during rotavirus -epidemic seasons in young children (Figure 2, panel B) and an increasing trend in older adults (Figure 2, panel E) and immunocompromised patients (Figure 2, panel F).

Association of Vaccination Coverage with Monthly Numbers of Gastroenteritis Inpatients

Among the overall patient population (N = 294,108), higher rotavirus vaccination coverage was associated with reduced monthly gastroenteritis hospitalizations compared with the reference category of <40% coverage. The IRR for gastroenteritis hospitalization was 0.87 (95% CI 0.83–0.90) for vaccination coverage of ≥80% after adjusting for age group, year, and month (Table 2; Figure 3, panel A). In the age-ineligible population for rotavirus vaccination (n = 247,156), the IRR for gastroenteritis hospitalization was also lower for vaccination coverage of ≥80% (adjusted IRR 0.90, 95% CI, 0.87–0.94), and the association between coverage and decreased monthly gastroenteritis hospitalizations was not consistently observed when coverage was <80%. (Figure 3, panel B). However, rotavirus vaccination coverage was not associated with changes in monthly gastroenteritis hospitalizations among immunocompromised patients (Figure 3, panel C). Secondary analyses restricted to rotavirus epidemic seasons also revealed associations between vaccination coverage and monthly gastroenteritis hospitalizations (Table 3). IRRs for gastroenteritis hospitalization gradually decreased with increasing vaccination coverage in the overall population (Figure 3, panel D). We found no vaccination coverage–related reduction in IRRs among the population age-ineligible for vaccination (Figure 3, panel E) or immunocompromised patients (Figure 3, panel F).

Discussion

Our study demonstrated the effect of rotavirus vaccination coverage on all-age gastroenteritis hospitalizations in Japan. Overall, we found that higher rotavirus vaccination coverage among infants was associated with lower monthly gastroenteritis hospitalizations for all age groups. We found a decreasing trend in

Table 2. Generalized estimating equations analyses to estimate the impact of rotavirus vaccination coverage on monthly number of gastroenteritis hospitalizations across all age groups, Japan, 2011–2019*

Vaccination coverage, %	IRR (95% CI)					
	Overall, N = 294,108		Age-ineligible for vaccination, n = 247,156		Immunocompromised, n = 38,058	
	Crude	Adjusted†	Crude	Adjusted†	Crude	Adjusted†
<40	Referent		Referent		Referent	
40–49	0.96 (0.95–0.97)	0.94 (0.93–0.95)	0.97 (0.96–0.98)	0.95 (0.94–0.97)	1.01 (0.97–1.04)	0.99 (0.95–1.03)
50–59	0.97 (0.96–0.98)	0.94 (0.93–0.96)	1.01 (0.99–1.02)	0.98 (0.96–1.00)	1.04 (1.01–1.08)	1.03 (0.98–1.07)
60–69	0.98 (0.97–0.99)	0.94 (0.92–0.96)	1.02 (1.00–1.03)	0.99 (0.96–1.01)	1.03 (1.00–1.07)	1.01 (0.95–1.07)
70–79	0.97 (0.96–0.98)	0.91 (0.89–0.94)	1.00 (0.99–1.01)	0.96 (0.93–0.99)	1.05 (1.02–1.09)	1.02 (0.95–1.09)
≥80	0.94 (0.92–0.95)	0.87 (0.83–0.90)	0.95 (0.93–0.96)	0.90 (0.87–0.94)	1.06 (1.02–1.11)	1.02 (0.93–1.12)

*IRR, incidence rate ratio.
†Adjusted for age group, year, and month.

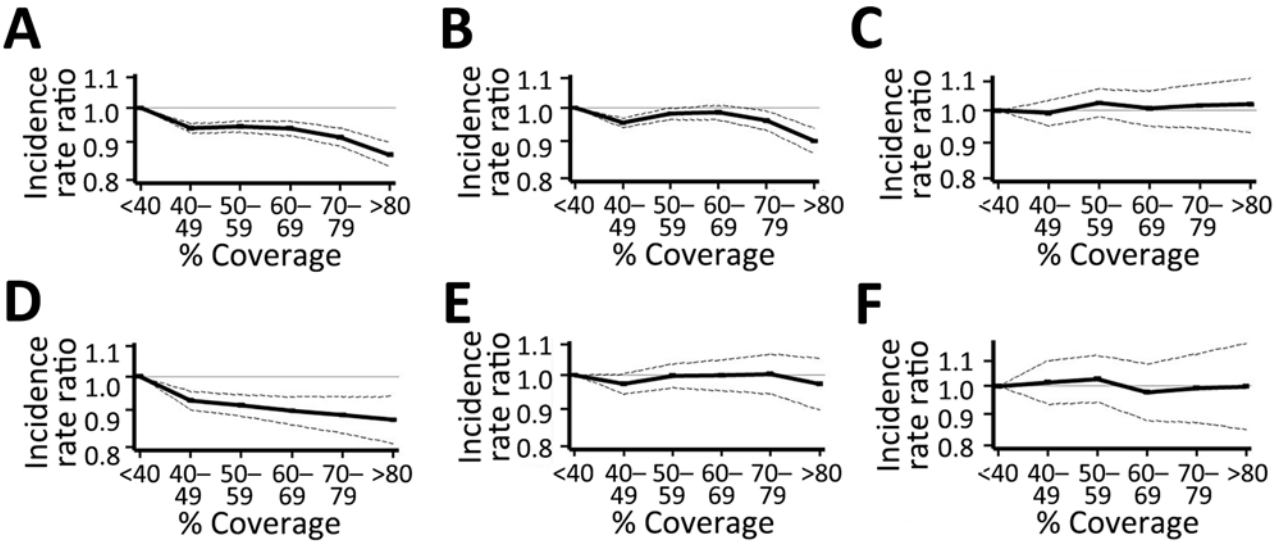

Figure 3. Association between vaccination coverage percentages and gastroenteritis hospitalization from generalized estimating equations analyses in study of effects of rotavirus vaccination coverage among infants on hospital admission for gastroenteritis across all age groups, Japan, 2011–2019. A–C) Annual associations for the overall population (A), the vaccination age-ineligible population (B), and immunocompromised persons (C). D–F) Associations during rotavirus epidemic seasons, February–April, for the overall population (D), vaccination age-ineligible population (E), and immunocompromised persons (F). Dashed lines indicate 95% CIs; gray horizontal lines indicate an incidence rate ratio of 1.0.

IRRs for gastroenteritis hospitalizations as vaccination coverage increased in the overall population. Those results highlight the impact of coverage levels in understanding the effect of rotavirus vaccination on the entire population. The magnitude of this effect seems to be relatively small, however, with a point estimate of ≈0.9 for IRRs. We also showed trends in gastroenteritis hospitalizations among immunocompromised patients, who are at risk of severe gastroenteritis, after rotavirus vaccination introduction. Of note, rotavirus vaccination coverage was not associated with changes in monthly gastroenteritis hospitalizations among immunocompromised patients. Our results suggest that higher rotavirus vaccination coverage among infants has little effect on reducing gastroenteritis hospitalization in immunocompromised patients.

The findings of this study provide meaningful insights into the indirect protective benefits of rotavirus vaccination. Previous studies have suggested that infant rotavirus vaccination affords indirect protection against rotavirus in unvaccinated persons (*21*–*24*). Moreover, a multihospital discharge database study showed a lower gastroenteritis hospitalization rate among members of households in which a child had received the rotavirus vaccine (*32*). Infant rotavirus vaccination may contribute to reducing rotavirus transmission among unvaccinated persons by decreasing the probability of vaccine recipients becoming infected and likelihood of secondary transmission (*21*,*22*,*32*). In addition, the cumulative increase in rotavirus vaccine recipients might potentially lead to a reduction in rotavirus transmission in the entire

Table 3. Generalized estimating equations analyses, restricted to data from rotavirus epidemic seasons (February–April), to estimate the impact of rotavirus vaccination coverage on the monthly number of gastroenteritis hospitalizations across all age groups, Japan, 2011–2019*

Vaccination coverage, %	IRR (95% CI)					
	Overall, n = 69,025		Age-ineligible for vaccination, n = 56,605		Immunocompromised, n = 8,878	
	Crude	Adjusted†	Crude	Adjusted†	Crude	Adjusted†
<40	Referent		Referent		Referent	
40–49	0.93 (0.91–0.95)	0.93 (0.90–0.95)	0.96 (0.93–0.98)	0.97 (0.94–1.00)	1.03 (0.95–1.11)	1.01 (0.94–1.10)
50–59	0.92 (0.90–0.94)	0.91 (0.88–0.95)	0.98 (0.95–1.00)	1.00 (0.96–1.04)	1.05 (0.98–1.12)	1.03 (0.94–1.12)
60–69	0.91 (0.89–0.93)	0.90 (0.86–0.94)	0.96 (0.93–0.98)	1.00 (0.95–1.05)	1.01 (0.95–1.07)	0.98 (0.88–1.09)
70–79	0.90 (0.88–0.92)	0.89 (0.84–0.94)	0.94 (0.92–0.97)	1.00 (0.94–1.07)	1.03 (0.97–1.10)	0.99 (0.87–1.13)
≥80	0.89 (0.86–0.92)	0.87 (0.81–0.94)	0.90 (0.86–0.93)	0.97 (0.90–1.05)	1.04 (0.95–1.14)	1.00 (0.85–1.17)

*IRR, incidence rate ratio.
†Adjusted for age group, year, and month.

population. The burden of rotavirus infection in adults compared with children is not well understood (*33*). Recent reports have highlighted the substantial magnitude of rotavirus in adults with gastroenteritis (*6*). Furthermore, several large studies have shown reductions in adult hospitalization after vaccination introduction (*23*,*24*), although the most affected age group varied among different cohorts, and findings in relation to indirect protection are inconsistent for adults. Taken together, those findings might provide supporting evidence for routine rotavirus immunization of infants and additional clues for understanding disease transmission.

Among major strengths of this study were use of 9-year longitudinal data from >500 hospitals and use of rotavirus vaccination coverage data at the regional level. Several studies of pneumococcal conjugate vaccine have investigated the association between vaccination coverage and indirect protection in the unvaccinated population (*34*,*35*). A recent study in Spain found an association between reductions in rotavirus gastroenteritis hospitalizations and regional rotavirus vaccination coverage in children <5 years of age (*36*). Those studies suggested that use of vaccination coverage data can provide valuable insights into understanding regional variations in vaccination coverage and associations between vaccination coverage and indirect protection. An additional strength of this study was its description of the postvaccination trends in hospitalizations for gastroenteritis among immunocompromised patients.

Among our study's limitations was an inherent problem with the diagnostic coding of gastroenteritis. Previous studies have shown the relatively low sensitivity in diagnosing gastroenteritis using ICD codes, both in children and adults (*37*,*38*). Possible misclassification of the diagnosis might have resulted in underestimation of the incidence rate of gastroenteritis. The effect of this limitation appears to be mitigated, however, because it is likely that any misclassification occurred equally across different levels of vaccination coverage. Another limitation was that we did not investigate the effect of vaccination coverage on rotavirus gastroenteritis hospitalization. We presumed that an analysis restricted only to patients with the diagnosis of rotavirus gastroenteritis would result in further underestimation of incidence because patients with gastroenteritis are typically not routinely tested for rotavirus in clinical settings (*39*,*40*). Instead, we performed secondary analyses with a restriction to the rotavirus epidemic season, which demonstrated results consistent with those of the primary analysis.

Another notable limitation of this study was that rotavirus vaccination coverage was obtained at an aggregate level. Heterogeneity in the distribution of vaccination coverage within the prefecture may lead to confounding for the observed association. Thus, to avoid the ecologic fallacy (*41*), our results should be interpreted with caution. In addition, we lacked information on socioeconomic status, which could affect both childhood vaccination coverage (*42*,*43*) and hospitalization rates. Although we used hospital codes as a cluster variable in the GEE models, results do not account for unmeasured confounding factors. The study population selected from hospitals in the DPC Study Group might have introduced selection bias, another potential limitation. The effect of this bias seems to be limited, however, given the broad coverage of the DPC Study Group database in acute inpatient care in Japan (*25*).

In conclusion, our study assessed the effects of infant rotavirus vaccination coverage on the number of all-age gastroenteritis hospitalizations in Japan and found higher rotavirus vaccination coverage was associated with a decline in gastroenteritis hospitalization in the overall population. However, the effect size was relatively small. Our study also found gastroenteritis hospitalizations among immunocompromised patients were not affected after rotavirus vaccination introduction. Our findings shed light on the importance of rotavirus vaccination coverage and suggest that, by reducing gastroenteritis hospitalizations, rotavirus vaccination among infants might benefit the entire population.

This study was supported by grants from the Ministry of Health, Labour and Welfare, Japan (grant nos. 22AA2003 and 23HA2002 to Y.I.) and the Japan Society for the Promotion of Science (grant no. 23H00448 to Y.I.).

Author contributions: K.K.: conceptualization, formal analysis, investigation, methodology, writing (original draft); S.K.: data curation, methodology, writing (review and editing); K.F.: resources, writing (review and editing); Y.I.: funding acquisition, project administration, resources, supervision, writing (review and editing).

References

1. Bányai K, Estes MK, Martella V, Parashar UD. Viral gastroenteritis. Lancet. 2018;392:175–86. https://doi.org/10.1016/S0140-6736(18)31128-0
2. Hartman S, Brown E, Loomis E, Russell HA. Gastroenteritis in children. Am Fam Physician. 2019;99:159–65.
3. Bresee JS, Marcus R, Venezia RA, Keene WE, Morse D, Thanassi M, et al.; US Acute Gastroenteritis Etiology Study Team. The etiology of severe acute gastroenteritis among adults visiting emergency departments in the United States.

J Infect Dis. 2012;205:1374–81. https://doi.org/10.1093/infdis/jis206
4. Cardemil CV, Balachandran N, Kambhampati A, Grytdal S, Dahl RM, Rodriguez-Barradas MC, et al. Incidence, etiology, and severity of acute gastroenteritis among prospectively enrolled patients in 4 Veterans Affairs hospitals and outpatient centers, 2016–2018. Clin Infect Dis. 2021;73:e2729–38. https://doi.org/10.1093/cid/ciaa806
5. Lopman BA, Hall AJ, Curns AT, Parashar UD. Increasing rates of gastroenteritis hospital discharges in US adults and the contribution of norovirus, 1996–2007. Clin Infect Dis. 2011;52:466–74. https://doi.org/10.1093/cid/ciq163
6. Troeger C, Blacker BF, Khalil IA, Rao PC, Cao S, Zimsen SRM, et al.; GBD 2016 Diarrhoeal Disease Collaborators. Estimates of the global, regional, and national morbidity, mortality, and aetiologies of diarrhoea in 195 countries: a systematic analysis for the Global Burden of Disease Study 2016. Lancet Infect Dis. 2018;18:1211–28. https://doi.org/10.1016/S1473-3099(18)30362-1
7. Vos T, Lim SS, Abbafati C, Abbas KM, Abbasi M, Abbasifard M, et al.; GBD 2019 Diseases and Injuries Collaborators. Global burden of 369 diseases and injuries in 204 countries and territories, 1990-2019: a systematic analysis for the Global Burden of Disease Study 2019. Lancet. 2020;396:1204–22. https://doi.org/10.1016/S0140-6736(20)30925-9
8. Tate JE, Burton AH, Boschi-Pinto C, Steele AD, Duque J, Parashar UD; World Health Organization–Coordinated Rotavirus Surveillance Network. 2008 estimate of worldwide rotavirus-associated mortality in children younger than 5 years before the introduction of universal rotavirus vaccination programmes: a systematic review and meta-analysis. Lancet Infect Dis. 2012;12:136–41. https://doi.org/10.1016/S1473-3099(11)70253-5
9. Chen Y, Liu BC, Glass K, Kirk MD. High incidence of hospitalisation due to infectious gastroenteritis in older people associated with poor self-rated health. BMJ Open. 2015;5:e010161. https://doi.org/10.1136/bmjopen-2015-010161
10. Schmidt-Hieber M, Bierwirth J, Buchheidt D, Cornely OA, Hentrich M, Maschmeyer G, et al.; AGIHO Working Group. Diagnosis and management of gastrointestinal complications in adult cancer patients: 2017 updated evidence-based guidelines of the Infectious Diseases Working Party (AGIHO) of the German Society of Hematology and Medical Oncology (DGHO). Ann Hematol. 2018;97:31–49. https://doi.org/10.1007/s00277-017-3183-7
11. Balachandran N, Cates J, Kambhampati AK, Marconi VC, Whitmire A, Morales E, et al. Risk factors for acute gastroenteritis among patients hospitalized in 5 Veterans Affairs medical centers, 2016–2019. Open Forum Infect Dis. 2022;9:ofac339. https://doi.org/10.1093/ofid/ofac339
12. van Dongen JAP, Rouers EDM, Schuurman R, Bonten MJM, Bruijning-Verhagen P; RIVAR Study Group. Acute gastroenteritis disease burden in infants with medical risk conditions in the Netherlands. Pediatr Infect Dis J. 2021;40:300–5. https://doi.org/10.1097/INF.0000000000003002
13. Moon RC, Bleak TC, Rosenthal NA, Couturier B, Hemmert R, Timbrook TT, et al. Epidemiology and economic burden of acute infectious gastroenteritis among adults treated in outpatient settings in US health systems. Am J Gastroenterol. 2023;118:1069–79. https://doi.org/10.14309/ajg.0000000000002186
14. Arakaki L, Tollefson D, Kharono B, Drain PK. Prevalence of rotavirus among older children and adults with diarrhea: a systematic review and meta-analysis. Vaccine. 2021;39:4577–90. https://doi.org/10.1016/j.vaccine.2021.06.073
15. Tate JE, Burton AH, Boschi-Pinto C, Parashar UD; World Health Organization–Coordinated Global Rotavirus Surveillance Network. Global, regional, and national estimates of rotavirus mortality in children <5 years of age, 2000–2013. Clin Infect Dis. 2016;62(Suppl 2):S96–105. https://doi.org/10.1093/cid/civ1013
16. World Health Organization. Rotavirus vaccines: an update. Wkly Epidemiol Rec. 2009;84:533–40.
17. Tsugawa T, Akane Y, Honjo S, Kondo K, Kawasaki Y. Rotavirus vaccination in Japan: efficacy and safety of vaccines, changes in genotype, and surveillance efforts. J Infect Chemother. 2021;27:940–8. https://doi.org/10.1016/j.jiac.2021.04.002
18. Kobayashi M, Adachi N, Miyazaki M, Tatsumi M. Decline of rotavirus-coded hospitalizations in children under 5 years: a report from Japan where rotavirus vaccines are self-financed. Vaccine. 2018;36:2727–32. https://doi.org/10.1016/j.vaccine.2017.10.033
19. Aliabadi N, Antoni S, Mwenda JM, Weldegebriel G, Biey JNM, Cheikh D, et al. Global impact of rotavirus vaccine introduction on rotavirus hospitalisations among children under 5 years of age, 2008-16: findings from the Global Rotavirus Surveillance Network. Lancet Glob Health. 2019;7:e893–903. https://doi.org/10.1016/S2214-109X (19)30207-4
20. Mwenda JM, Hallowell BD, Parashar U, Shaba K, Biey JN, Weldegebriel GG, et al. Impact of rotavirus vaccine introduction on rotavirus hospitalizations among children under 5 years of age—World Health Organization African Region, 2008–2018. Clin Infect Dis. 2021;73:1605–8. https://doi.org/10.1093/cid/ciab520
21. Payne DC, Staat MA, Edwards KM, Szilagyi PG, Weinberg GA, Hall CB, et al.; New Vaccine Surveillance Network (NVSN). Direct and indirect effects of rotavirus vaccination upon childhood hospitalizations in 3 US Counties, 2006–2009. Clin Infect Dis. 2011;53:245–53. https://doi.org/10.1093/cid/cir307
22. Anderson EJ, Shippee DB, Weinrobe MH, Davila MD, Katz BZ, Reddy S, et al. Indirect protection of adults from rotavirus by pediatric rotavirus vaccination. Clin Infect Dis. 2013;56:755–60. https://doi.org/10.1093/cid/cis1010
23. Wilson SE, Rosella LC, Wang J, Renaud A, Le Saux N, Crowcroft NS, et al. Equity and impact: Ontario's infant rotavirus immunization program five years following implementation. A population-based cohort study. Vaccine. 2019;37:2408–14. https://doi.org/10.1016/j.vaccine.2019.01.061
24. Baker JM, Tate JE, Steiner CA, Haber MJ, Parashar UD, Lopman BA. Longer-term direct and indirect effects of infant rotavirus vaccination across all ages in the United States in 2000–2013: analysis of a large hospital discharge data set. Clin Infect Dis. 2019;68:976–83. https://doi.org/10.1093/cid/ciy580
25. Hayashida K, Murakami G, Matsuda S, Fushimi K. History and profile of diagnosis procedure combination (DPC): development of a real data collection system for acute inpatient care in Japan. J Epidemiol. 2021;31:1–11. https://doi.org/10.2188/jea.JE20200288
26. Yasunaga H. Real world data in Japan: Chapter II. The diagnosis procedure combination database. Ann Clin Epidemiolol. 2019;1:76–79.
27. Suzuki H, Sakai T, Tanabe N, Okabe N. Peak rotavirus activity shifted from winter to early spring in Japan. Pediatr Infect Dis J. 2005;24:257–60. https://doi.org/10.1097/01.inf.0000154327.00232.4d
28. Tajiri H, Takeuchi Y, Takano T, Ohura T, Inui A, Yamamoto K, et al. The burden of rotavirus gastroenteritis

and hospital-acquired rotavirus gastroenteritis among children aged less than 6 years in Japan: a retrospective, multicenter epidemiological survey. BMC Pediatr. 2013;13:83. https://doi.org/10.1186/1471-2431-13-83
29. Liang KY, Zeger SL. Longitudinal data analysis using generalized linear models. Biometrika. 1986;73:13–22. https://doi.org/10.1093/biomet/73.1.13
30. Yarnell CJ, Fu L, Manuel D, Tanuseputro P, Stukel T, Pinto R, et al. Association between immigrant status and end-of-life care in Ontario, Canada. JAMA. 2017;318:1479–88. https://doi.org/10.1001/jama.2017.14418
31. Insaf TZ, Sommerhalter KM, Jaff TA, Farr SL, Downing KF, Zaidi AN, et al. Access to cardiac surgery centers for cardiac and non-cardiac hospitalizations in adolescents and adults with congenital heart defects—a descriptive case series study. Am Heart J. 2021;236:22–36. https://doi.org/10.1016/j.ahj.2021.02.018
32. Cortese MM, Dahl RM, Curns AT, Parashar UD. Protection against gastroenteritis in US households with children who received rotavirus vaccine. J Infect Dis. 2015;211:558–62. https://doi.org/10.1093/infdis/jiu503
33. Karakusevic A, Devaney P, Enstone A, Kanibir N, Hartwig S, Carias CDS. The burden of rotavirus-associated acute gastroenteritis in the elderly: assessment of the epidemiology in the context of universal childhood vaccination programs. Expert Rev Vaccines. 2022;21:929–40. https://doi.org/10.1080/14760584.2022.2066524
34. Chan J, Gidding HF, Blyth CC, Fathima P, Jayasinghe S, McIntyre PB, et al. Levels of pneumococcal conjugate vaccine coverage and indirect protection against invasive pneumococcal disease and pneumonia hospitalisations in Australia: An observational study. PLoS Med. 2021; 18:e1003733. https://doi.org/10.1371/journal.pmed.1003733
35. Oyewole OR, Lang P, Albrich WC, Wissel K, Leib SL, Casanova C, et al. The impact of pneumococcal conjugate vaccine (PCV) coverage heterogeneities on the changing epidemiology of invasive pneumococcal disease in Switzerland, 2005–2019. Microorganisms. 2021;9:1078. https://doi.org/10.3390/microorganisms9051078
36. Ruiz-Contreras J, Alfayate-Miguelez S, Carazo-Gallego B, Onís E, Díaz-Munilla L, Mendizabal M, et al. Rotavirus gastroenteritis hospitalizations in provinces with different vaccination coverage rates in Spain, 2013–2018. BMC Infect Dis. 2021;21:1138. https://doi.org/10.1186/s12879-021-06841-x
37. Hsu VP, Staat MA, Roberts N, Thieman C, Bernstein DI, Bresee J, et al. Use of active surveillance to validate international classification of diseases code estimates of rotavirus hospitalizations in children. Pediatrics. 2005;115:78–82. https://doi.org/10.1542/peds.2004-0860
38. Pindyck T, Hall AJ, Tate JE, Cardemil CV, Kambhampati AK, Wikswo ME, et al. Validation of acute gastroenteritis–related International Classification of Diseases, Clinical Modification Codes in pediatric and adult US populations. Clin Infect Dis. 2020;70:2423–7. https://doi.org/10.1093/cid/ciz846
39. Patel MM, Tate JE, Selvarangan R, Daskalaki I, Jackson MA, Curns AT, et al. Routine laboratory testing data for surveillance of rotavirus hospitalizations to evaluate the impact of vaccination. Pediatr Infect Dis J. 2007;26:914–9. https://doi.org/10.1097/INF.0b013e31812e52fd
40. Cardemil CV, O'Leary ST, Beaty BL, Ivey K, Lindley MC, Kempe A, et al. Primary care physician knowledge, attitudes, and diagnostic testing practices for norovirus and acute gastroenteritis. PLoS One. 2020;15:e0227890. https://doi.org/10.1371/journal.pone.0227890
41. Wakefield J. Ecologic studies revisited. Annu Rev Public Health. 2008;29:75–90. https://doi.org/10.1146/annurev.publhealth.29.020907.090821
42. Pearce A, Law C, Elliman D, Cole TJ, Bedford H; Millennium Cohort Study Child Health Group. Factors associated with uptake of measles, mumps, and rubella vaccine (MMR) and use of single antigen vaccines in a contemporary UK cohort: prospective cohort study. BMJ. 2008;336:754–7. https://doi.org/10.1136/bmj.39489.590671.25
43. Kuroda H, Goto A, Kawakami C, Yamamoto K, Ito S, Kamijima M, et al.; Japan Environment and Children's Study (JECS) Group. Association between a single mother family and childhood undervaccination, and mediating effect of household income: a nationwide, prospective birth cohort from the Japan Environment and Children's Study (JECS). BMC Public Health. 2022;22:117. https://doi.org/10.1186/s12889-022-12511-7

Address for correspondence: Yuichi Imanaka, Department of Healthcare Economics and Quality Management, Graduate School of Medicine, Kyoto University, Yoshida Konoe-cho, Sakyo-ku, Kyoto 606-8501, Japan; email: imanaka-y@umin.net

Emergence of Extensively Drug-Resistant *Neisseria gonorrhoeae*, France, 2023

François Caméléna, Manel Mérimèche, Julie Brousseau, Mary Mainardis, Pascale Verger, Caroll Le Risbé, Elise Brottet, Alexandra Thabuis, Cécile Bébéar, Jean-Michel Molina, Florence Lot, Emilie Chazelle,[1] Béatrice Berçot[1]

Since 2022, Europe has had 4 cases of extensively drug-resistant *Neisseria gonorrhoeae*, sequence type 16406, that is resistant to ceftriaxone and highly resistant to azithromycin. We report 2 new cases from France in 2023 involving strains genetically related to the 4 cases from Europe as well as isolates from Cambodia.

Neisseria gonorrhoeae, the causative agent of gonorrhea, remains a persistent global public health concern. *N. gonorrhoeae* is classified by the World Health Organization as a priority pathogen because of the emergence of multidrug-resistant isolates and rapid increases in antimicrobial drug resistance rates. Because of the frequency of resistance to cefixime, azithromycin, and fluoroquinolones, ceftriaxone is the recommended first-line treatment of *N. gonorrhoeae* (*1*). Four cases of extensively drug-resistant (XDR) *N. gonorrhoeae*, containing the *penA-60* allele and the A2059G mutation of 23S rRNA, belonging to sequence type 16406 have been reported in Austria, the United Kingdom, and France since 2022 (*2*–*4*). The enhanced gonococcal surveillance program in Cambodia identified 3 similar isolates during 2021–2022 (*5*). We report 2 new cases of XDR *N. gonorrhoeae* in France from 2023. Both patients gave consent for the publication of this report.

The Cases

The patient in case 1 is a 40-year-old man living in the Rhône-Alpes region. He sought care in July 2023 for reported urethritis that occurred 15 days after unprotected sexual contact with a person living in Cambodia. The patient did not receive treatment in Cambodia before returning to France, and he had no sexual relations after his return. Laboratory testing of urethral samples was positive for gonococcal DNA and negative for *Chlamydia trachomatis*. *N. gonorrhoeae* was identified by using culture and designated as F95. The patient was treated with an intramuscular dose of ceftriaxone (1 g) during the visit. He attended a follow-up consultation with his general practitioner in September, during which control samples from his urethra, anus, and throat were collected. No *N. gonorrhoeae* DNA was detected from those samples; however, the patient still reported urethritis. Repeat laboratory testing was positive for *C. trachomatis*, and the patient was treated.

The patient in case 2 is a 60-year-old man living with a partner in the Rhône-Alpes region. The patient sought care for reports of urethritis in August 2023. Symptom onset occurred 1 week after the patient had sexual contact with a sex worker in France. The patient had no documented travel to Asia. Laboratory testing of urine samples by using culture and PCR were positive for *N. gonorrhoeae*, designated F96, and *C. trachomatis*. In September, the patient was treated with ceftriaxone (1 g) for the *N. gonorrhoeae* infection and azithromycin (1 g) for the *C. trachomatis* infection. At a follow-up consultation a

Author affiliations: Saint Louis–Lariboisière University Hospitals, Paris, France (F. Caméléna, M. Mérimèche, J. Brousseau, M. Mainardis, J.-M. Molina, B. Berçot); French National Reference Center for bacterial STI, Paris (F. Caméléna, M. Mérimèche, J. Brousseau, M. Mainardis, B. Berçot); Paris Cité University, Paris (F. Caméléna, M. Mérimèche, J. Brousseau, J.-M. Molina, B. Berçot); Biogroup Oriade Noviale, Saint Martin d'Hères, France (P. Verger, C. Le Risbé); National Public Health Agency, Lyon, France (E. Brottet, A. Thabuis); National Reference Centre for Bacterial Sexually Transmitted Infections, Bordeaux, France (C. Bébéar); University Bordeaux, Bordeaux (C. Bébéar); Santé publique France, Saint-Maurice, France (F. Lot, E. Chazelle).

DOI: https://doi.org/10.3201/eid3009.240557

[1]These authors contributed equally to this article.

few weeks later, the patient reported no symptoms. Control samples from his urethra, anus, and throat were tested by using PCR and were negative for *N. gonorrhoeae* and *C. trachomatis*.

The 2 *N. gonorrhoeae* isolates, F95 and F96, were sent to the national reference center for sexually transmitted infections in Paris for confirmation and genomic analysis. We conducted phenotypic antimicrobial drug susceptibility testing and found that both isolates were XDR (*6*). The isolates demonstrated resistance to penicillin G, cefixime, ceftriaxone, ciprofloxacin, azithromycin, tetracycline, and doxycycline; both isolates were susceptible to ertapenem and aminoglycosides (Table). We conducted whole-genome sequencing by using an Illumina MiSeq (Illumina, https://www.illumina.com) system (300 cycles, 2 × 150 bp). We performed bioinformatic analysis as previously described (*4*). The sequences obtained are available from the European Nucleotide Archive and GenBank (accession no. PRJNA1082518).

We aligned the genomes of F95 and F96 with ceftriaxone-resistant strains previously isolated in France (WHOY [F89], F90, F91, and F92), Japan (WHOX), and the United States (LRRBGS-1327). We also aligned the F95 and F96 genomes with strains highly resistant to azithromycin and resistant to ceftriaxone recently found in the United Kingdom (WHOQ and H22-494), Austria (AT158), France (F93 and F94), Cambodia (22R655558T, 22R655567T, and 22R655494S), and Australia (A2735 and A2543) (*2*–*5*,*7*–*12*). We used ParSNP v.1.2 (https://github.com/marbl/parsnp) to correct the alignments for recombination. We then constructed a maximum-likelihood phylogeny for core-genome comparisons. We visualized the comparisons by using iTol (https://itol.embl.de), as previously described (*4*, *7*). The whole-genome sequencing analysis revealed that isolates F95 and F96 belonged to sequence type 16406. The F95 and F96 strains were assigned to sequence type 22862 by using *N. gonorrhoeae* multiantigen sequence typing (*porB* 822, *tbpB* 294) and 5793 by using *N. gonorrhoeae* sequence typing for antimicrobial resistance (profile no. 60.001_89_13_1_7_3_1).

Our molecular analysis of isolates F95 and F96 revealed several mutations associated with antimicrobial resistance (Table). Both isolates contained the mosaic allele *penA-60.001*, which encodes a penicillin binding protein 2 with amino-acid substitutions (A311V, T4835) that impair the binding of extended-spectrum cephalosporins (ESCs). This impairment renders the isolates resistant to ESCs. F95 and F96 contain the A39T mutation in the *MtrR* repressor gene, without promoter deletions, which causes an overexpression of the MtrCDE efflux pump and an increase in the MIC of ESCs. The isolates produced TEM-135 penicillinase with a M182T substitution known to increase the stability of the enzyme, which typically proceeds additional mutations that extend the range of resistance to ESCs. In addition, F95 and F96 carried the A2059G mutation in the 4 alleles of the 23S rRNA-encoding gene, conferring high levels of resistance to azithromycin (*6*). The quinolone resistance-determining regions of F95 and F96 contained S91F and D95A substitutions in *GyrA* (a subcomponent of DNA gyrase), and an S87R substitution in *ParC* (a component of topo-isomerase IV). Those substitutions are responsible for high level resistance to ciprofloxacin. Finally, both strains contained the *tet(M)* gene and a V57M amino-acid substitution in the *rpsJ* gene (encoding the S10 ribosomal protein), conferring a high level of tetracycline resistance.

The F95 isolate had no single-nucleotide polymorphism relative to the F96 isolate. Both isolates clustered with other XDR *N. gonorrhoeae* isolates that contained the *penA-60.001* allele and the A2059G mutation in 23S rRNA, indicating a common evolutionary origin (Figure). F95 and F96 were closely related to the recently reported azithromycin-

Table. MICs and molecular resistance mechanisms of extremely drug-resistant *Neisseria gonorrhoeae* strains F95 and F96, recovered from 2 patients in France, 2023*

Antimicrobial	F95 MIC, mg/L	F96 MIC, mg/L	EUCAST interpretation	Molecular mechanism(s) of resistance
Penicillin	>32	>32	R	$bla_{TEM-135}$
Cefixime	1	1	R	*penA* 60.001 (mosaic; A311V; T483S); *mtrR*, A39T; *ponA*, L421P; *porB* structure, porB1a
Ceftriaxone	0.25	0.25	R	
Cefotaxime	0.5	0.5	R	
Ertapenem	0.032	0.016	NA	NA
Azithromycin	>256	>256	R (high-level)	23S rRNA, A2059G; *mtrR*, A39T
Tetracycline	32	32	R (high-level)	*tetM*; *rpsJ*, V57M; *mtrR*, A39T
Doxycycline	16	16	R	
Ciprofloxacin	2	4	R	*gyrA*, S91F and D95A; *parC*, S87R
Spectinomycin	16	16	S	NA
Gentamicin	8	8	NA	NA
Rifampin	0.125	0.064	NA	NA

*MIC testing done using ETEST (bioMérieux, https://www.biomerieux.com). EUCAST, European Committee on Antimicrobial Susceptibility testing; NA, not applicable because of a lack of breakpoints for interpretation; R, resistant; S, susceptible.

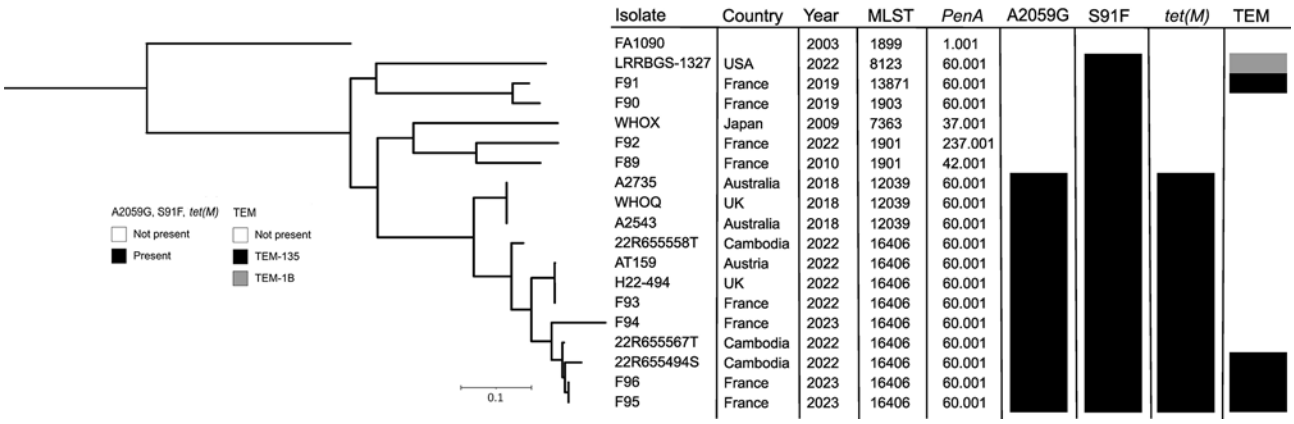

Isolate	Country	Year	MLST	*PenA*	A2059G	S91F	*tet(M)*	TEM
FA1090		2003	1899	1.001				
LRRBGS-1327	USA	2022	8123	60.001				
F91	France	2019	13871	60.001				
F90	France	2019	1903	60.001				
WHOX	Japan	2009	7363	37.001				
F92	France	2022	1901	237.001				
F89	France	2010	1901	42.001				
A2735	Australia	2018	12039	60.001				
WHOQ	UK	2018	12039	60.001				
A2543	Australia	2018	12039	60.001				
22R655558T	Cambodia	2022	16406	60.001				
AT159	Austria	2022	16406	60.001				
H22-494	UK	2022	16406	60.001				
F93	France	2022	16406	60.001				
F94	France	2023	16406	60.001				
22R655567T	Cambodia	2022	16406	60.001				
22R655494S	Cambodia	2022	16406	60.001				
F96	France	2023	16406	60.001				
F95	France	2023	16406	60.001				

Figure. Phylogenetic tree of 19 *Neisseria gonorrhoeae* isolates, including 2 from patients in France, compared on the basis of their main resistance determinants. The phylogenetic tree was built from 10,907 total core single-nucleotide polymorphism positions. The F95 and F96 isolates from 2 patients in France were compared with ceftriaxone-resistant and extensively drug-resistant *N. gonorrhoeae* isolates from Europe, Australia, Cambodia, Japan, and the United States. The tree is rooted on *N. gonorrheae* FA1090, a laboratory reference strain. Scale bar indicates the branch length corresponding to genetic change.

resistant and ceftriaxone-resistant 22R655567T XDR isolates from Cambodia, only differing by 113 single-nucleotide polymorphisms. On the phylogenetic tree, the F95 and F96 isolates belonged to the same lineage as the XDR isolates from Cambodia. This lineage is further divided into multiple sublineages: the A2543 XDR clone, which has been reported to be spreading internationally (*4*,*11*); the sublineage including AT159, H22-494, and F93; the sublineage F94; the sublineage 22R655558T; and the sublineage including F95, F96, 22R655567T, and 22R655494S (Figure) (*2*–*5*,*10*).

The patients in both cases were successfully treated with 1 g ceftriaxone, which suggests that EUCAST breakpoints (https://www.eucast.org) for ceftriaxone resistance (MIC >0.125 mg/L) might be too low for genital infections (*13*). In case 2, the patient likely contracted XDR *N. gonorrhoeae* infection through sexual contact with a sex worker. However, no additional information was obtained about the sex worker, and our investigation did not establish a link to case 1. The XDR *N. gonorrhoeae* isolates also contained the *tetM* gene, which confers resistance to tetracycline and doxycycline. Several public health departments in California, USA, recommend the use of doxycycline postexposure prophylaxis in men who have sex with men, and the indirect selection of *N. gonorrhoeae* containing *tet(M)* because of the use of doxycycline postexposure prophylaxis is possible (*14*,*15*).

Conclusions

We report 2 cases of XDR *N. gonorrhoeae* strains from France. These strains are highly resistant to azithromycin, resistant to ceftriaxone, and genetically related to isolates from Cambodia. Our findings raise concerns about the spread of XDR *N. gonorrhoeae* in Southeast Asia. The emergence and spread of XDR *N. gonorrhoeae* isolates suggest the need to reconsider current recommendations for the first-line treatment of gonococcal infections. Novel and effective therapies against these XDR isolates are required, as is the need for international collaboration to monitor antimicrobial resistance.

Acknowledgments

We thank Monica Lahra and her team for access to the genomes of *N. gonorrhoeae* strains isolated in Cambodia. We also thank the general practitioner and the patients for agreeing to the publication of this case report.

This study received financial support from the French National Public Health Agency (Saint-Maurice, France) via the French reference center for bacterial sexually transmitted infections.

About the Author

Dr. Caméléna is a clinical microbiologist at the French national reference center for bacterial sexually transmitted infections in Paris, France. His main research interests are the epidemiology, genetics, and pathogenicity of *N. gonorrhoeae*.

References

1. Unemo M, Lahra MM, Escher M, Eremin S, Cole MJ, Galarza P, et al. WHO global antimicrobial resistance surveillance for *Neisseria gonorrhoeae* 2017–18: a retrospective observational study. Lancet Microbe. 2021;2:e627–36. https://doi.org/10.1016/S2666-5247(21)00171-3

2. Pleininger S, Indra A, Golparian D, Heger F, Schindler S, Jacobsson S, et al. Extensively drug-resistant (XDR) *Neisseria gonorrhoeae* causing possible gonorrhoea treatment failure with ceftriaxone plus azithromycin in Austria, April 2022. Euro Surveill. 2022;27:1–5. https://doi.org/10.2807/1560-7917.ES.2022.27.24.2200455
3. Day M, Pitt R, Mody N, Saunders J, Rai R, Nori A, et al. Detection of 10 cases of ceftriaxone-resistant *Neisseria gonorrhoeae* in the United Kingdom, December 2021 to June 2022. Euro Surveill. 2022;27:2200803. https://doi.org/10.2807/1560-7917.ES.2022.27.46.2200803
4. Maubaret C, Caméléna F, Mrimèche M, Braille A, Liberge M, Mainardis M, et al. Two cases of extensively drug-resistant (XDR) *Neisseria gonorrhoeae* infection combining ceftriaxone-resistance and high-level azithromycin resistance, France, November 2022 and May 2023. Euro Surveill. 2023;28:1–5. https://doi.org/10.2807/1560-7917.ES.2023.28.37.2300456
5. Ouk V, Pham CD, Wi T, van Hal SJ, Lahra MM; EGASP Cambodia working group. The enhanced gonococcal surveillance programme, Cambodia. Lancet Infect Dis. 2023; 23:e332–3. https://doi.org/10.1016/S1473-3099(23)00479-6
6. Unemo M, Shafer WM. Antimicrobial resistance in *Neisseria gonorrhoeae* in the 21st century: past, evolution, and future. Clin Microbiol Rev. 2014;27:587–613. https://doi.org/10.1128/CMR.00010-14
7. Poncin T, Merimeche M, Braille A, Mainardis M, Bebear C, Jacquier H, et al. Two cases of multidrug-resistant *Neisseria gonorrhoeae* related to travel in south-eastern Asia, France, June 2019. Euro Surveill. 2019;24:1–4. https://doi.org/10.2807/1560-7917.ES.2019.24.36.1900528
8. Poncin T, Fouere S, Braille A, Camelena F, Agsous M, Bebear C, et al. Multidrug-resistant *Neisseria gonorrhoeae* failing treatment with ceftriaxone and doxycycline in France, November 2017. Euro Surveill. 2018;23:2–4. https://doi.org/10.2807/1560-7917.ES.2018.23.21.1800264
9. Unemo M, Golparian D, Nicholas R, Ohnishi M, Gallay A, Sednaoui P. High-level cefixime- and ceftriaxone-resistant *Neisseria gonorrhoeae* in France: novel *penA* mosaic allele in a successful international clone causes treatment failure. Antimicrob Agents Chemother. 2012;56:1273–80. https://doi.org/10.1128/AAC.05760-11
10. Jennison AV, Whiley D, Lahra MM, Graham RM, Cole MJ, Hughes G, et al. Genetic relatedness of ceftriaxone-resistant and high-level azithromycin resistant *Neisseria gonorrhoeae* cases, United Kingdom and Australia, February to April 2018. Euro Surveill. 2019;24:1–4. https://doi.org/10.2807/1560-7917.ES.2019.24.8.1900118
11. Ohnishi M, Golparian D, Shimuta K, Saika T, Hoshina S, Iwasaku K, et al. Is *Neisseria gonorrhoeae* initiating a future era of untreatable gonorrhea?: Detailed characterization of the first strain with high-level resistance to ceftriaxone. Antimicrob Agents Chemother. 2011;55:3538–45. https://doi.org/10.1128/AAC.00325-11
12. Reimche JL, Pham CD, Joseph SJ, Hutton S, Cartee JC, Ruan Y, et al. Novel strain of multidrug non-susceptible *Neisseria gonorrhoeae* in the USA. Lancet Infect Dis. 2024;24:e149–51. https://doi.org/10.1016/S1473-3099(23)00785-5
13. Unemo M, Golparian D, Oxelbark J, Kong FYS, Brown D, Louie A, et al. Pharmacodynamic evaluation of ceftriaxone single-dose therapy (0.125–1g) to eradicate ceftriaxone-susceptible and ceftriaxone-resistant *Neisseria gonorrhoeae* strains in a hollow fibre. J Antimicrob Chemother. 2024;00:1–8.
14. Vanbaelen T, Manoharan-Basil SS, Kenyon C. Doxycycline postexposure prophylaxis could induce cross-resistance to other classes of antimicrobials in *Neisseria gonorrhoeae*: an in silico analysis. Sex Transm Dis. 2023;50:490–3. https://doi.org/10.1097/OLQ.0000000000001810
15. Mortimer TD, Grad YH. A genomic perspective on the near-term impact of doxycycline post-exposure prophylaxis on *Neisseria gonorrhoeae* antimicrobial resistance. Clin Infect Dis. 2023;77:788–91. https://doi.org/10.1093/cid/ciad279

Address for correspondence: Beatrice Berçot, Saint-Louis Hospital, APHP, 1 avenue Claude Vellefaux, 75010 Paris, France; email: beatrice.bercot@aphp.fr

Avian and Human Influenza A Virus Receptors in Bovine Mammary Gland

Charlotte Kristensen, Henrik E. Jensen, Ramona Trebbien, Richard J. Webby, Lars E. Larsen

An outbreak of influenza A (H5N1) virus was detected in dairy cows in the United States. We detected influenza A virus sialic acid -α2,3/α2,6-galactose host receptors in bovine mammary glands by lectin histochemistry. Our results provide a rationale for the high levels of H5N1 virus in milk from infected cows.

Influenza A virus (IAV) is a negative, single-stranded RNA virus. Viral evolution has enabled some IAVs to cross species barriers and to be established in humans and various mammals (*1*). Cattle are susceptible to infection with influenza C and D viruses but have been regarded as almost resistant to infection with IAV (*2*). An unexpected highly pathogenic avian influenza (HPAI) virus H5N1 (clade 2.3.4.4b) was detected in dairy cattle in Texas, USA, and has spread to 131 herds in 12 different states in the United States (*3*,*4*). Although extremely high levels of virus in milk from infected cows (*5*) were unexpected, previous studies and a report from Friedrich-Loeffler Institute (FLI; Insel Riems, Germany) (*6*) have shown that the inoculation of IAVs into the mammary glands of cows and goats results in productive viral infection (*2*).

Hemagglutinin (HA) binds to sialic acids (SA) terminally attached to glycans, enabling viral endocytosis and membrane fusion. Hemagglutinins of human- and swine-adapted IAVs frequently prefer SAs linked to galactose (Gal) in an α2,6 linkage (SA-α2,6, human receptor), whereas avian IAVs prefer an α2,3 linkage (SA-α2,3, avian receptor) (*7*). Furthermore, IAVs adapted to chickens generally prefer SA-α2,3-Gal with a β1,4 linkage to N-acetylgalactosamine (GalNac; SA-α2,3-Gal-β1,4-GalNac, referred to as chicken receptor), whereas IAVs isolated from ducks favor SA-α2,3-Gal with a β1,3 linkage to N-acetylglucosamine (GlcNac; SA-α2,3-Gal-β1,3-GlcNac, referred to as duck receptor) (*7*).

To investigate IAV receptor expression on the surface of epithelial cells, in situ techniques, such as lectin histochemistry, are useful (*8*). A limitation of using lectins is that they provide information only about the terminal end of the host receptors; a complete quantification of the receptors is not possible. Three studies have reported the IAV receptors in the bovine respiratory tract by using lectins (*9*–*11*), but studies describing the IAV receptor distribution in other bovine tissues are sparse. The aim of this study was to investigate the in situ expression of IAV receptors in the bovine mammary glands by lectin histochemistry.

The Study

We included 2 archived bovine mammary glands obtained from the same lactating dairy cow (4 years of age) of a Danish Holstein breed and included mammary glands from 8 cows of different breeds and ages obtained from a slaughterhouse in Denmark (Table). The tissues were formalin-fixed, paraffin-embedded, and cut into 4–5 μm sections.

We detected the human receptor SA-α2,6 using biotinylated *Sambucus nigra* lectin (SNA) (B-1305-2; Vector Laboratories, https://vectorlabs.com). We detected the chicken receptor SA-α2,3-Gal-β1,4 using biotinylated *Maackia amurensis* lectin I (MAA-I) (B-1315-2; Vector Laboratories) and the duck receptor (SA-α2,3-Gal-β1,3) biotinylated MAA-II (B-1265-1; Vector Laboratories) as previously described (*13*). We semiquantified the staining on the surface of the epithelial cells as the percentage of positive surface area in 2 images from each slide (Figure 1, panels D, E;

Author affiliations: University of Copenhagen, Frederiksberg, Denmark (C. Kristensen, H.E. Jensen, L.E. Larsen); Statens Serum Institut, Copenhagen, Denmark (R. Trebbien); St. Jude Children's Research Hospital, Memphis, Tennessee, USA (R.J. Webby)

DOI: http://doi.org/10.3201/eid3009.240696

Table. The average percentage of epithelial staining of the human and duck influenza A virus receptors in the alveoli and ducts in 9 cows with different breeds, ages, and parity status*

Breed	Age, y	Parity	Lactation†	% SNA		% MAA-II, alveoli‡
				Alveoli	Ducts	
Jersey	6	4	Late	53	18	37
Danish Holstein	4	2	Late	57	3	47
	7	5	Late	40	21	46
	6	4	Early/mid	47	4	44
	5	2	Late	58	24	61
	6	4	Early/mid	51	10	49
	5	3	Early/mid	55	1	51
	4	3	Late	52	32	48
Unknown	Unknown	Unknown	Early/mid	59	6	47
Average	5	3	NA	54	13	48

*MAA-II, duck receptor; NA, not applicable; SNA, human receptor.
†All images were obtained from active alveoli of the mammary glands and the staining is therefore not representative for the whole section of cows in late lactation. The lactation period was determined by investigating the luminal size of the alveoli and the amount of connective tissue (*12*).
‡The staining did not exceed the amount of staining observed with the neuraminidase treatment, suggesting a nonspecific staining in the ducts.

Figure 2, panels D, E) and reported the average (*13*). We applied 2 negative controls. To investigate potential background staining (blind), we added no lectins; to investigate the amount of nonspecific binding, we applied a neuraminidase pretreatment before each lectin, as previously reported (*13*). We included a confirmed IAV-negative pig lung as a positive control.

In the mammary gland, the human receptor (detected by SNA) and the duck receptor (detected by MAA-II) were widely distributed in the alveoli, but less so in the ducts, whereas we detected no positive staining of the chicken receptor by MAA-I (Table; Figures 1, 2; Appendix Tables, https://wwwnc.cdc.gov/EID/article/30/9/24-0696-App1.pdf), except for 1 cow expressing the chicken receptor in a lactiferous duct. Both human and duck receptors were primarily expressed in the active alveoli and less expressed in less active alveoli (Figure 1,2). We found a significant negative correlation between the percentage of SNA staining in the alveoli and the parity status of the cows but not with the MAA-II lectin staining (Figure 3).

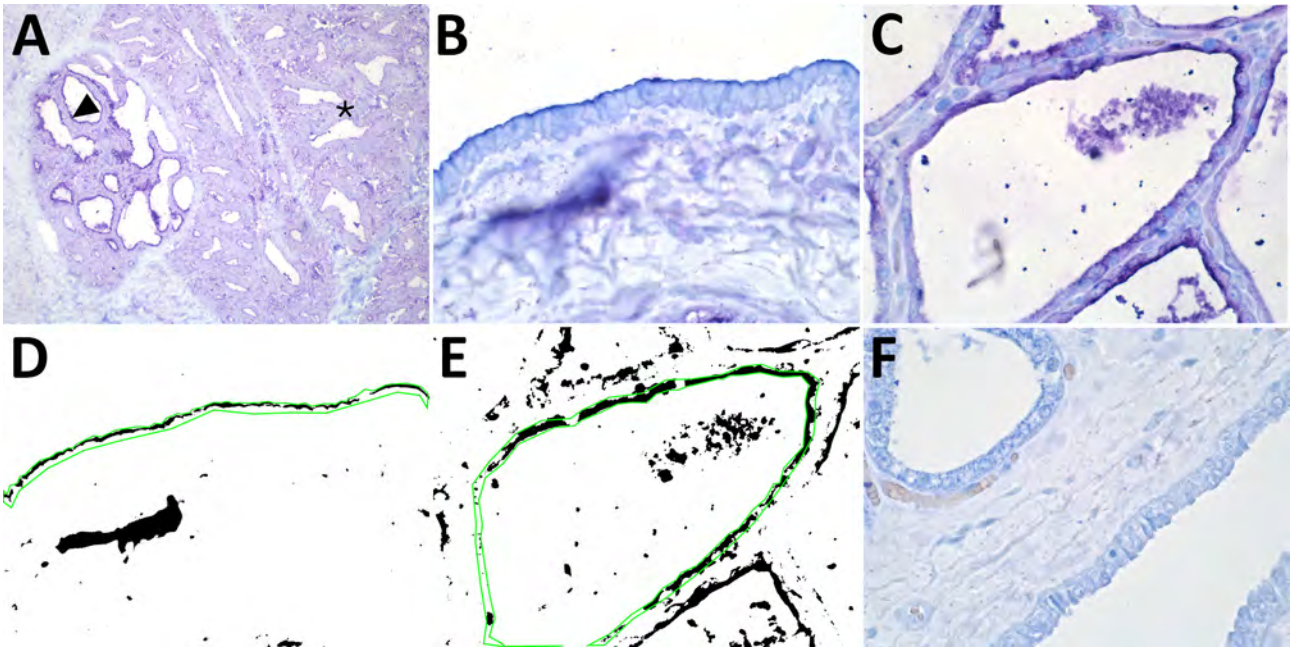

Figure 1. Results of staining showing wide expression of the human receptor for influenza A virus (designated SNA) in the bovine mammary gland. A) An example of the SNA staining of a mammary gland from a cow in late lactation. Arrowhead indicates expression of the human receptor in the active alveoli. Asterisks indicate less staining in the less active alveoli. Original magnification ×10. B, C) SNA staining of a duct (B) and (C) an alveolus in a 7-year-old cow. Original magnification ×60. D, E) Positive staining obtained from the image analysis. Green line shows the region of interest. Original magnification ×60. F) A neuraminidase pretreatment negative control showed markedly reduced staining of the SNA lectin. Original magnification ×60. The staining was visualized using Vector Blue (Vector Laboratories, https://vectorlabs.com).

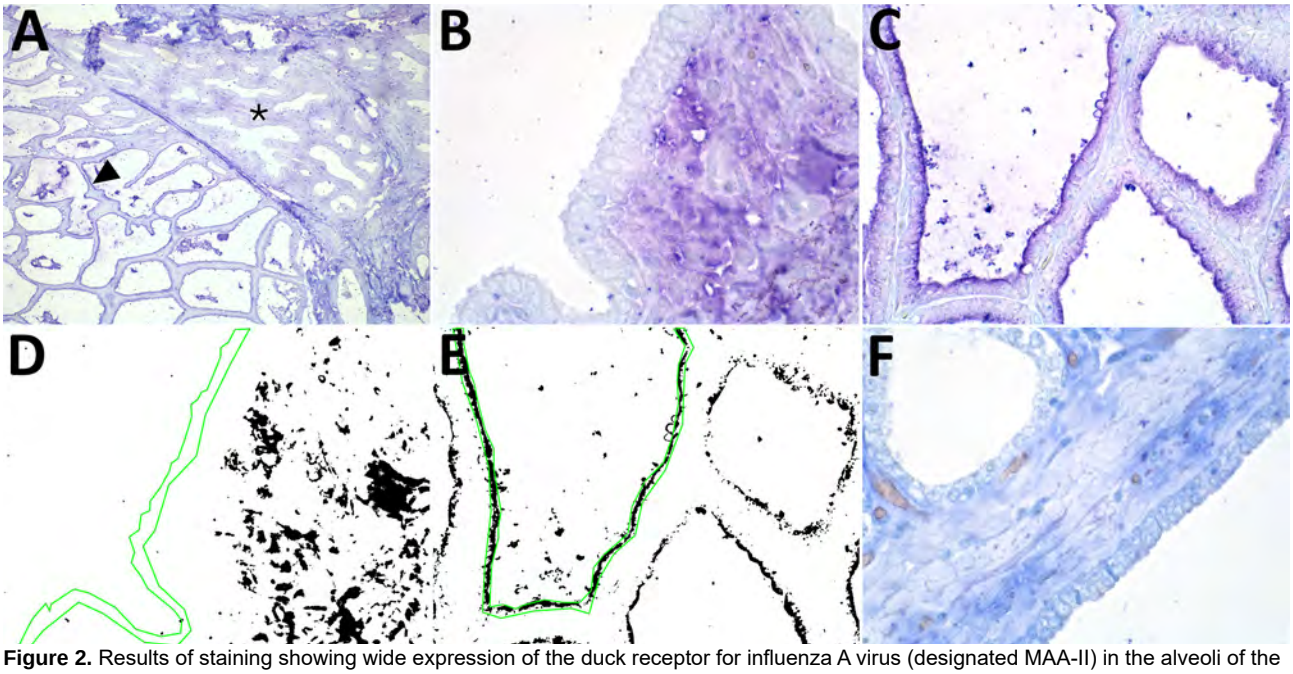

Figure 2. Results of staining showing wide expression of the duck receptor for influenza A virus (designated MAA-II) in the alveoli of the bovine mammary gland. A) An example of the MAA-II staining of a mammary gland from a cow in late lactation. Arrowhead indicates expression of the duck receptor in active alveoli. Asterisks indicate less staining in the less active alveoli. Original magnification ×10. B, C) MAA-II staining of a duct (B) and an alveolus (C) in a 3-year-old cow. Original magnification ×60. D, E) Positive staining obtained from the image analysis. Green line shows the region of interest. Original magnification ×60. F) A neuraminidase pretreatment negative control showed markedly reduced staining of the MAA-II lectin in the alveolus but some nonspecific staining in the duct epithelium. The staining was visualized using Vector Blue (Vector Laboratories, https://vectorlabs.com). Original magnification ×60.

We detected nonspecific staining (positive staining after neuraminidase pretreatment) in the endothelial cells with the SNA and MAA-I lectins, in the bovine erythrocytes with the MAA-I lectin, and in the ducts of the MAA-II lectin, but observed no nonspecific staining elsewhere (Appendix Figure, https://wwwnc.cdc.gov/EID/article/30/9/24-0696-App1.pdf). The positive controls of the pig lung corresponded to previous findings (*13*) (Appendix Figure).

Our investigation evaluated the expression of IAV receptors in situ in the mammary gland of cattle, which typically has been considered less susceptible to IAV infection (*2*). Of note was the finding that both the human receptors (SA-α2,6) and the duck receptors (SA-α2,3-Gal-β1,3) were highly expressed in the active alveoli in mammary glands but lower expressed in the less active alveoli, which could indicate that cows peaking in lactation are more susceptible for infection. The findings of the 2 receptors are in agreement with 2 novel studies investigating the IAV receptors in the bovine mammary gland of 2–3 cows (*11*; M.R. Carrasco et al., unpub. data, https://doi.org/10.1101/2024.05.24.595667). The transmission routes and the pathogenesis of H5N1 in cows remain unclear, but the virus remains infectious after 1 hour on the milking equipment (V.L. Sage et al., unpub. data, https://doi.org/10.1101/2024.05.22.24307745); the US Department of Agriculture has

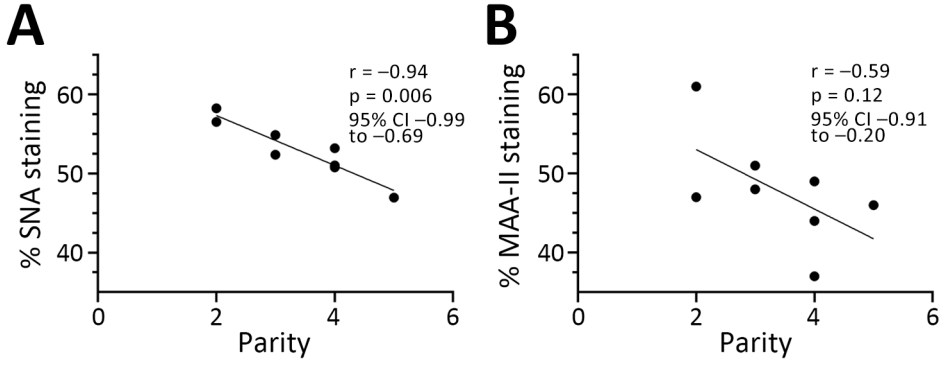

Figure 3. Pearson correlation coefficient showing a significant negative correlation between the percentage of SNA staining (bovine receptor) in the alveoli and the parity status of the cows (A) but not for MAA-II staining (duck receptor) (B). Original magnification ×60. Statistics and graphs made using GraphPad Prism version 10.2.3 (GraphPad Software, www.graphpad.com).

reported that only some udder quarters may be involved in infection, suggesting an ascending infection as a possible transmission route. Of interest, the human and duck receptors were less expressed in the ducts of the mammary gland, making an ascending mammary gland infection using those receptors more challenging. An investigation of the receptor binding preference of A/Texas/37/2024 showed that an I199T mutation of the hemagglutinin protein increased the receptor binding breadth to a higher number of conformations of the avian receptor, including hybrid N-glycans, compared with previous H5N1 viruses (M.R. Good et al., unpub. data, https://doi.org/10.1101/2024.06.22.600211); those hybrid N-glycans might not be detected by the lectins used in our study (*14*). M.R. Carrasco, et al. (unpub. data) showed limited binding of older AIV strains and a mouse-adapted human influenza strain (PR8) in the mammary gland of cows, whereas the preliminary report from FLI (*6*) showed that genotypes from Europe of the clade 2.3.4.4b H5 HPAI viruses could also replicate in the mammary glands of cows. Thus, more studies are needed to investigate the susceptibility of cows to different IAV strains and variants.

The SNA lectin detects both of the 2 most common sialic acids, N-acetylneuraminic acid (Neu5Ac) and N-glycolylneuraminic acid (Neu5Gc) (*14*). Neu5Ac is mainly the preferred SA for IAVs, except for equine IAVs, which have a higher preference for Neu5Gc (*7*). Cattle express both Neu5Ac and Neu5Gc in their tissues, but the amount of Neu5Ac in bovine milk is 30 times higher than for Neu5Gc (*15*), which indicates that the SNA staining detected in our study was caused by staining of Neu5Ac. However, further studies such as mass spectrometry, which gives detailed information about the IAV receptors (e.g., sialic acid type, length, branching), are needed to confirm the cause of SNA staining and also to accomplish a comprehensive quantification of the distribution of receptors in bovine tissues (*8*).

Conclusions

The expression of the duck receptor in the mammary gland of cows fits with the observed widespread infections among cattle in the United States with HPAI H5N1. The co-expression of both human and avian receptors in the mammary glands indicates susceptibility to other IAVs than those from avian origin, which is worrying from a zoonotic perspective. The presence of the IAV receptors, however, does not provide evidence that cattle are susceptible to all IAVs; other host factors (*1*) probably play a role for successful replication.

This article was preprinted at https://www.biorxiv.org/content/10.1101/2024.05.03.592326v1.

Acknowledgments

We thank Elisabeth Wairimu Petersen and Betina Gjedsted Andersen for practical laboratory help.

This work was supported by the Novo Nordisk Foundation (FluZooMark: NNF19OC0056326).

About the Author

Dr. Kristensen is a postdoctoral researcher at the University of Copenhagen in the virology and pathology research fields. Her primary focus is zoonotic influenza A viruses.

References

1. Yoon S-W, Webby RJ, Webster RG. Evolution and ecology of influenza A viruses. In: Compans R, Oldstone M, editors. Influenza pathogenesis and control. Vol. I. Current topics in microbiology and immunology. Cham (Switzerland); Springer; 2014. p 359–75. https://doi.org/10.1007/82_2014_396
2. Sreenivasan CC, Thomas M, Kaushik RS, Wang D, Li F. Influenza A in bovine species: a narrative literature review. Viruses. 2019;11:561. https://doi.org/10.3390/v11060561
3. Centers for Disease Control and Prevention. H5N1 bird flu: current situation summary. [cited 2024 Jun 28]. https://www.cdc.gov/flu/avianflu/avian-flu-summary.htm
4. Ly H. Highly pathogenic avian influenza H5N1 virus infections of dairy cattle and livestock handlers in the United States of America. Virulence. 2024;15:2343931. https://doi.org/10.1080/21505594.2024.2343931
5. World Health Organization. Joint FAO/WHO/WOAH preliminary assessment of recent influenza A(H5N1) viruses. 23 April 2024 [cited 2024 Jun 24]. https://www.who.int/publications/m/item/joint-fao-who-woah-preliminary-assessment-of-recent-influenza-a(h5n1)-viruses
6. Friedrich-Loeffler-Institut. Rapid risk assessment for highly pathogenic avian influenza H5 (HPAI H5) clade 2.3.4.4b. 2024 [cited 2024 Jul 15]. https://www.openagrar.de/servlets/MCRFileNodeServlet/openagrar_derivate_00060240/FLI-Risikoeinschaetzung_HPAI_H5_2024-07-05_en.pdf
7. Zhao C, Pu J. Influence of host sialic acid receptors structure on the host specificity of influenza viruses. Viruses. 2022;14:2141. https://doi.org/10.3390/v14102141
8. Varki NM, Varki A. Diversity in cell surface sialic acid presentations: implications for biology and disease. Lab Invest. 2007;87:851–7. https://doi.org/10.1038/labinvest.3700656
9. Thontiravong A, Rung-ruangkijkrai T, Kitikoon P, Oraveerakul K, Poovorawan Y. Influenza A virus receptor identification in the respiratory tract of quail, pig, cow and swamp buffalo. Thai J Vet Med. 2011;41:15. https://doi.org/10.56808/2985-1130.2322
10. Uprety T, Sreenivasan CC, Bhattarai S, Wang D, Kaushik RS, Li F. Isolation and development of bovine primary respiratory cells as model to study influenza D virus infection. Virology. 2021;559:89–99. https://doi.org/10.1016/j.virol.2021.04.003

11. Nelli RK, Harm TA, Siepker C, Groeltz-Thrush JM, Jones B, Twu NC, et al. Sialic acid receptor specificity in mammary gland of dairy cattle infected with highly pathogenic avian influenza A(H5N1) virus. Emerg Infect Dis. 2024;30:1361–73. https://doi.org/10.3201/eid3007.240689
12. Hurley WL, Loor JJ. Mammary gland: growth, development and involution. In: Fuquay JW, Fox PF, McSweeney PLH, editors. Encyclopedia of dairy sciences. 2nd ed. Vol. 3. San Diego: Academic Press; 2011. p. 338–345.
13. Kristensen C, Larsen LE, Trebbien R, Jensen HE. The avian influenza A virus receptor SA-α2,3-Gal is expressed in the porcine nasal mucosa sustaining the pig as a mixing vessel for new influenza viruses. Virus Res. 2024;340:199304. https://doi.org/10.1016/j.virusres.2023.199304
14. Bojar D, Meche L, Meng G, Eng W, Smith DF, Cummings RD, et al. A useful guide to lectin binding: machine-learning directed annotation of 57 unique lectin specificities. ACS Chem Biol. 2022;17:2993–3012. https://doi.org/10.1021/acschembio.1c00689
15. Spichtig V, Michaud J, Austin S. Determination of sialic acids in milks and milk-based products. Anal Biochem. 2010;405:28–40. https://doi.org/10.1016/j.ab.2010.06.010

Address for correspondence: Charlotte Kristensen, University of Copenhagen, Stigbøjlen 4, 1870 Frederiksberg C, Denmark; email: chark@sund.ku.dk

Cocirculation of Genetically Distinct Highly Pathogenic Avian Influenza H5N5 and H5N1 Viruses in Crows, Hokkaido, Japan

Yik Lim Hew, Takahiro Hiono, Isabella Monne, Kei Nabeshima, Saki Sakuma, Asuka Kumagai, Shunya Okamura, Kosuke Soda, Hiroshi Ito, Mana Esaki, Kosuke Okuya, Makoto Ozawa, Toshiyo Yabuta, Hiroki Takakuwa, Linh Bao Nguyen, Norikazu Isoda, Kohtaro Miyazawa, Manabu Onuma, Yoshihiro Sakoda

We isolated highly pathogenic avian influenza (HPAI) H5N5 and H5N1 viruses from crows in Hokkaido, Japan, during winter 2023–24. They shared genetic similarity with HPAI H5N5 viruses from northern Europe but differed from those in Asia. Continuous monitoring and rapid information sharing between countries are needed to prevent HPAI virus transmission.

H5 highly pathogenic avian influenza viruses (HPAIVs) of the A/goose/Guangdong/1/1996 lineage have diversified into multiple clades, threatening wild birds and poultry worldwide. Clade 2.3.4.4b HPAIVs have been consistently isolated in Asia and Europe since 2016 (*1*–*3*) and expanded further to North America in late 2021 (*4*). The global circulation of H5 HPAIVs over a relatively short time highlights the pivotal role of migratory birds in virus dissemination (*5*). H5 HPAIVs in clade 2.3.4.4 frequently acquire the neuraminidase (NA) gene from locally circulating low pathogenicity avian influenza viruses (LPAIVs), which often infect waterfowl, leading to the generation of novel H5Nx reassortant viruses, such as H5N2, H5N6, and H5N8 (*6*).

Author affiliations: Hokkaido University, Sapporo, Japan (Y.L. Hew, T. Hiono, L.B. Nguyen, N. Isoda, Y. Sakoda); Istituto Zooprofilattico Sperimentale delle Venezie, Padova, Italy (I. Monne); National Institute for Environmental Studies, Tsukuba, Japan (K. Nabeshima, M. Onuma); National Agriculture and Food Research Organization, Tsukuba (S. Sakuma, A. Kumagai, K. Miyazawa); Tottori University, Tottori, Japan (S. Okamura, K. Soda, H. Ito); Kagoshima University, Kagoshima, Japan (M. Esaki, K. Okuya, M. Ozawa); Kyoto Sangyo University, Kyoto, Japan (T. Yabuta, H. Takakuwa)

DOI: https://doi.org/10.3201/eid3009.240356

During the winter seasons 2021–22 and 2022–23, Hokkaido, located in the northernmost part of Japan, experienced HPAIV outbreaks driven by bird migration that substantially affected poultry and other resident birds. Those viruses clustered in the group 2 (G2) d subgroup within clade 2.3.4.4.b, which has multiple subgroups, G2a–e, and shared a common ancestor with HPAIVs detected in Europe in late 2020 (*7*). HPAIV subgroup G2d might have undergone intercontinental transmission from Europe to Japan (*8*,*9*). During winter 2023–24, H5N5 HPAIVs were detected in a crow flock in Hokkaido, and further monitoring revealed cocirculation of 2 distinct viruses in the crow population. We investigated the genetic origin and antigenicity of H5N5 HPAIVs isolated in Hokkaido.

The Study

We conducted passive surveillance of HPAIV infections in wild birds in a public garden in Sapporo, the prefectural capital of Hokkaido, Japan; ≈2,000 crows flock together during winter and are observed by garden staff. We isolated viruses from tracheal and cloacal swab samples collected from dead crows in the garden by inoculating 10-day-old embryonated eggs; we confirmed results by using reverse transcription PCR (Appendix, https://wwwnc.cdc.gov/EID/article/30/9/24-0356-App1.pdf). On November 23 and 24, 2023, we isolated H5N1 HPAIVs from 2 dead large-billed crows (*Corvus macrorhynchos*), designated as A/large-billed crow/Hokkaido/B067/2023 (H5N1) and A/large-billed crow/Hokkaido/B068/2023 (H5N1). The hemagglutinin (HA) gene sequences from those 2 H5N1 HPAIVs indicated they clustered with the G2d subgroup of HPAIVs found in Hokkaido during the winter seasons 2021–22 and

2022–23. In contrast, HA genes of 3 H5 HPAIVs isolated from dead crows on January 8–11, 2024, were closely related to the G2a subgroup of H5N5 HPAIVs found in northern Europe and North America. Subsequent whole-genome sequencing analysis of the 3 G2a HPAIVs confirmed their subtype was H5N5; we named them A/large-billed crow/Hokkaido/B073/2024 (H5N5), A/large-billed crow/Hokkaido/B074/2024 (H5N5), and A/crow/Hokkaido/B075/2024 (H5N5) (Table 1).

We phylogenetically analyzed virus isolates along with reference sequences obtained from GISAID (https://www.gisaid.org); the HA genes of H5N5 HPAIVs isolated in Hokkaido diverged considerably from HPAIVs isolated in Japan during winter 2020–21 (*10*), forming a distinct branch within the G2a subgroup (Figure). In addition, the other gene segments of H5N5 HPAIVs from Hokkaido were genetically distant from those in HPAIV strains isolated in Japan during winter 2021–22 (Appendix Figures 1–6). BLAST (https://blast.ncbi.nlm.nih.gov) analysis of sequences from GISAID revealed that all 8 gene segments of H5N5 HPAIVs from Hokkaido were very close (genetic similarity >99%) to H5N5 HPAIVs detected in northern Europe since 2022, in contrast to those from North America (Table 2), suggesting a low possibility of virus transmission from North America. H5N5 HPAIVs from Hokkaido shared a common ancestor with H5N5 HPAIV from Europe assigned the genotype EA-2021-I by the European Food Safety Authority (*11*). Parent strains of H5N5 HPAIVs from Europe, represented by A/swan/Rostov/2299-2/2020 (H5N5), were proposed to originate in western Russia during autumn 2020. Those viruses underwent genetic evolution via reassortment events involving H5N8 HPAIVs circulating in Europe since 2018 (*12*) and the N5 NA gene derived from concurrently circulating LPAIVs (*13*). H5N5 HPAIVs reported in northern Europe during 2022–2023 exhibited specific genetic differences compared with H5N5 HPAIVs detected in Europe during autumn 2020, particularly in the N5 NA gene. Those differences included a 66-bp nucleotide deletion within the N5 NA gene, which we also observed in the H5N5 HPAIVs from Hokkaido. Truncation of the NA stalk has been attributed to the adaptation of those viruses from wild birds to *Galliformes* spp. birds (*14*). However, most H5N5 HPAIV infections in Europe were detected in wild birds, and no cases have been detected in *Galliformes* spp. birds since 2022 (*15*). Further investigation is needed to

Table 1. H5 viruses isolated in Hokkaido and Kumamoto, Japan, in winter 2023–24 in study of cocirculation of genetically distinct highly pathogenic avian influenza H5N5 and H5N1 viruses in crows*

Virus name	Subgroup	Date†	City/town	Latitude	Longitude	Accession no.
A/large-billed crow/Hokkaido/B067/2023 (H5N1)	G2d	2023 Nov 23	Sapporo	43°03′50″N	141°20′35″E	EPI_ISL_18591747
A/large-billed crow/Hokkaido/B068/2023 (H5N1)	G2d	2023 Nov 24	Sapporo	43°03′50″N	141°20′35″E	EPI_ISL_18594618
A/large-billed crow/Hokkaido/0112F066T/2023 (H5N5)	G2a	2023 Dec 19	Erimo	42°00′59″N	143°08′53″E	EPI_ISL_18837770
A/large-billed crow/Hokkaido/0112F066C/2023 (H5N5)	G2a	2023 Dec 19	Erimo	42°00′59″N	143°08′53″E	EPI_ISL_18838019
A/large-billed crow/Hokkaido/B073/2024 (H5N5)	G2a	2024 Jan 8	Sapporo	43°03′50″N	141°20′35″E	EPI_ISL_18792212
A/large-billed crow/Hokkaido/B074/2024 (H5N5)	G2a	2024 Jan 9	Sapporo	43°03′50″N	141°20′35″E	EPI_ISL_18830859
A/crow/Hokkaido/B075/2024 (H5N5)	G2a	2024 Jan 11	Sapporo	43°03′50″N	141°20′35″E	EPI_ISL_18830860
A/large-billed crow/Hokkaido/B076/2024 (H5N1)	G2d	2024 Jan 12	Sapporo	43°03′50″N	141°20′35″E	EPI_ISL_18830861
A/large-billed crow/Hokkaido/B078/2024 (H5N1)	G2d	2024 Jan 17	Sapporo	43°03′50″N	141°20′35″E	EPI_ISL_18876661
A/carrion crow/Hokkaido/B079/2024 (H5N1)	G2d	2024 Jan 18	Sapporo	43°03′50″N	141°20′35″E	EPI_ISL_18876662
A/large-billed crow/Hokkaido/B080/2024 (H5N1)	G2d	2024 Jan 22	Sapporo	43°03′50″N	141°20′35″E	EPI_ISL_18932042
A/carrion crow/Hokkaido/B081/2024 (H5N1)	G2d	2024 Jan 26	Sapporo	43°03′50″N	141°20′35″E	EPI_ISL_18876663
A/large-billed crow/Hokkaido/B104/2024 (H5N5)	G2a	2024 Feb 20	Sapporo	43°03′50″N	141°20′35″E	EPI_ISL_19033207
A/large-billed crow/Hokkaido/B120/2024 (H5N5)	G2a	2024 Mar 16	Sapporo	43°03′50″N	141°20′35″E	EPI_ISL_19055087
A/large-billed crow/Hokkaido/B157/2024 (H5N5)	G2a	2024 Apr 30	Sapporo	43°03′50″N	141°20′35″E	EPI_ISL_19174744
A/peregrine falcon/Kumamoto/4301C001/2024 (H5N5)	G2d	2024 Jan 16	Kumamoto	32°56′07″N	130°33′45″E	EPI_ISL_18876660

*Accession numbers are from GISAID (https://www.gisaid.org).
†Date of sample collection.

clarify whether NA stalk truncation affects pathogenesis of H5N5 HPAIVs.

During winter 2023–24, we confirmed H5N5 HPAIV infections in wild birds, especially in crows, in Erimo (December 19, 2023, in south-central Hokkaido) and in Kushiro (January 18, 2024, in eastern Hokkaido); we also confirmed infection in a peregrine falcon (*Falco peregrinus*) in Tamana, Kumamoto

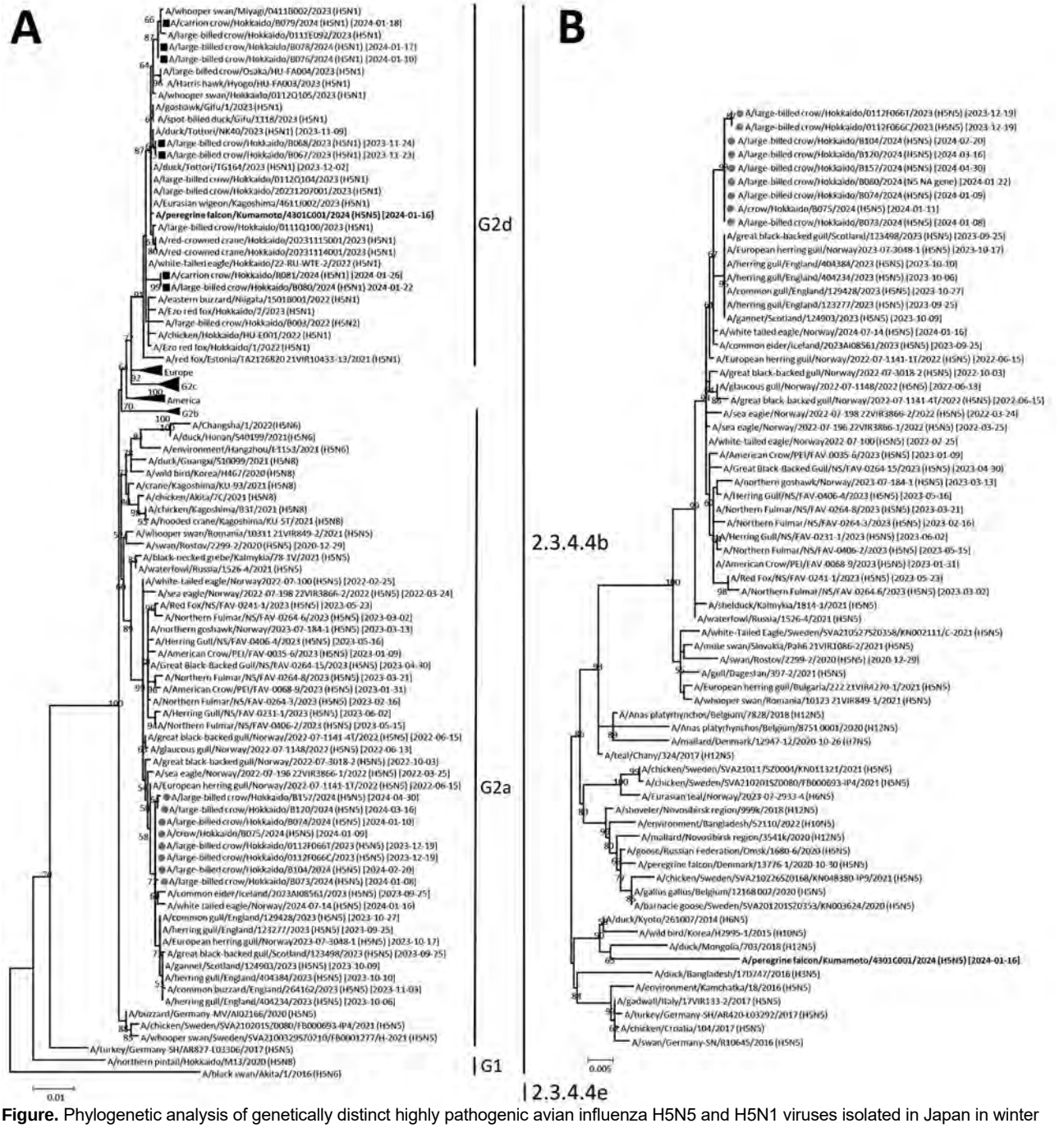

Figure. Phylogenetic analysis of genetically distinct highly pathogenic avian influenza H5N5 and H5N1 viruses isolated in Japan in winter 2023–24. H5 hemagglutinin (A) and N5 neuraminidase (B) gene segments of H5N5 highly pathogenic avian influenza viruses (HPAIVs) isolated in winter 2023–24 were compared with reference strains within clade 2.3.4.4b obtained from GISAID (https://www.gisaid.org). Squares indicate H5N1 and circles indicate H5N5 HPAIVs isolated from crows in Hokkaido in winter 2023–24. Bold text indicates the H5N5 HPAIV isolated from a peregrine falcon in Kumamato in the southern part of Japan in winter 2023–24. Trees were constructed by using the maximum-likelihood method and MEGA 7 software (https://www.megasoftware.net). Bootstrap values (>50%) from 1,000 replicates are indicated on nodes. Isolated viruses belonging to subgroups G1, G2a, and G2d and clade 2.3.4.4b are indicated. Dates after strain names indicate sample collection dates for HPAIV-infected animals. Scale bar indicates number of nucleotide substitutions per site.

Table 2. BLAST search results of H5N5 HPAIVs isolated in Japan in winter 2023–24 in study of cocirculation of genetically distinct H5N5 and H5N1 HPAIVs in crows, Hokkaido, Japan*

Virus name	Gene	Most homologous strain	Homology, %	Accession no.
A/large-billed crow/Hokkaido/B073/2024 (H5N5)†	PB2	A/Common eider/Iceland/2023AI08561/2023 (H5N5)	99.7	EPI2791002
	PB1	A/Common eider/ Iceland/2023AI08561/2023 (H5N5)	99.8	EPI2791003
	PA	A/Common eider/ Iceland/2023AI08561/2023 (H5N5)	99.7	EPI2791001
	HA	A/Common gull/England/129428/2023 (H5N5)	99.8	EPI2815885
	NP	A/Herring gull/England/404384/2023 (H5N5)	99.9	EPI2815894
	NA	A/Herring gull/England/404384/2023 (H5N5)	99.5	EPI2815900
	M	A/Herring gull/England/404384/2023 (H5N5)	99.9	EPI2815896
	NS	A/Herring gull/England/404384/2023 (H5N5)	99.9	EPI2815895
A/peregrine falcon/Kumamoto/4301C001/ 2024 (H5N5)‡	PB2	A/large-billed crow/Hokkaido/20231207001/2023 (H5N1)	99.9	EPI2898966
	PB1	A/large-billed crow/Hokkaido/20231207001/2023 (H5N1)	99.9	EPI2898967
	PA	A/large-billed crow/Hokkaido/0111Q100/2023 (H5N1)	99.8	EPI2841124
	HA	A/large-billed crow/Hokkaido/20231207001/2023 (H5N1)	99.9	EPI2898969
	NP	A/large-billed crow/Hokkaido/0112Q104/2023 (H5N1)	99.7	EPI2815894
	NA	A/Duck/Hokkaido/W24/ 2020 (H6N5)	99.1	EPI1896526
	M	A/large-billed crow/Hokkaido/20231207001/2023 (H5N1)	100	EPI2815896
	NS	A/large-billed crow/Hokkaido/20231207001/2023 (H5N1)	99.9	EPI2898973

*Gene segment sequences of 2 H5N5 HPAIVs were compared with those of other H5 virus sequences by using BLAST (https://blast.ncbi.nlm.nih.gov). Accession numbers are from GISAID (https://www.gisaid.org). HA, hemagglutinin; HPAIV, highly pathogenic avian influenza virus; M, matrix protein; NA, neuraminidase; NP, nucleoprotein; NS, nonstructural protein; PA, polymerase acidic; PB1, polymerase basic 1; PB2, polymerase basic 2.
†H5N5 HPAIV isolated in Hokkaido in winter 2023–24.
‡H5N5 HPAIV isolated in Kumamoto Prefecture in winter 2023–24.

Table 3. Cross-hemagglutination inhibition assay titers of H5 HPAIVs in study of cocirculation of genetically distinct H5N5 and H5N1 HPAIVs in crows, Hokkaido, Japan*

Tested virus	Subtype	Clade	Subgroup	Titers using antiserum against indicated H5 viruses							
				Cr/Hok/ B003/22	Ck/Hok/ E001/22	Ew/Hok/ Q71/22	WTE/Hok/ R22/22	Dk/VN/ HU16-DD3/23	Mdk/ DRC/ KAF1/17	Ck/Kum/ 1-7/14	Bs/Aki/1/ 16
Cr/Hok/ B073/24†	H5N5	2.3.4.4b	G2a	640	160	40	640	320	640	320	320
Cr/Hok/ B003/22	H5N2	2.3.4.4b	G2d	**640**	640	80	320	640	1,280	640	160
Ck/Hok/ E001/22	H5N1	2.3.4.4b	G2d	320	**640**	160	320	640	1,280	640	80
Ew/Hok/ Q71/22	H5N1	2.3.4.4b	G2b	320	640	**320**	160	640	1,280	320	160
WTE/Hok /R22/22	H5N1	2.3.4.4b	G2d	640	640	160	**320**	640	2,560	640	80
Dk/VN/ HU16-DD3/23	H5N1	2.3.4.4b	G2c	640	320	80	640	**640**	320	320	80
Ck/Hok/ B102/23	H5N1	2.3.4.4b	G2c	640	320	80	320	1,280	160	160	40
Mdk/ DRC/ KAF1/17	H5N8	2.3.4.4b	NA	640	640	80	160	640	**1,280**	640	80
Fox/Hok/ 1/22	H5N1	2.3.4.4b	G2d	640	320	160	640	640	640	320	160
Cr/Hok/ B067/23	H5N1	2.3.4.4b	G2d	160	160	80	320	640	320	80	40
Np/Hok/ M13/20	H5N8	2.3.4.4b	G1	640	640	20	160	640	2,560	640	40
Ck/Kum/ 1–7/14	H5N8	2.3.4.4c	NA	320	640	40	20	160	640	**640**	80
Bs/Akita/ 1/16	H5N6	2.3.4.4e	NA	160	320	20	80	160	320	160	**640**

*Antiserum against H5 virus isolates was used to test antigenicity of different H5Nx HPAIVs. Bold values indicate homologous titers.
Each abbreviated name is defined as follows: Cr/Hok/B073/24 (H5N5), A/large-billed crow/Hokkaido/B073/2024 (H5N5); Cr/Hok/B003/22, A/large-billed crow/Hokkaido/B003/2022 (H5N2); Ck/Hok/E001/22, A/chicken/Hokkaido/HU-E001/2022 (H5N1); Ew/Hok/Q71/22, A/Eurasian wigeon/Hokkaido/Q71/2022 (H5N1); WTE/Hok/R22/22, A/white-tailed eagle/Hokkaido/22-RU-WTE-2/2022 (H5N1); Dk/VN/HU-16-DD3/23, A/duck/Vietnam/HU16-DD3/2023 (H5N1); Ck/Hok/B102/23, A/chicken/Hokkaido/HU-B102/2023 (H5N1); Mdk/DRC/KAF1/17, A/Muscovy duck/DR Congo/KAF1/2017 (H5N8); Fox/Hok/1/22, A/Ezo red fox/Hokkaido/1/2022 (H5N1); Cr/Hok/B067/23, A/large-billed crow/Hokkaido/B067/2023 (H5N1); Np/Hok/M13/20, A/northern pintail/Hokkaido/M13/2020 (H5N1); Ck/Kum/1–7/14, A/chicken/Kumamoto/1–7/2014 (H5N8); Bs/Akita/1/16, A/black swan/Akita/1/2016 (H5N6). HPAIV, highly pathogenic avian influenza virus; NA, not applicable.
†H5N5 virus isolated in Hokkaido in winter 2023–24.

Prefecture, Kyushu Island, on January 16, 2024. We classified the isolate from Tamana, A/peregrine falcon/Kumamoto/4301C001/2024 (H5N5), into the G2d subgroup according to its HA gene sequence, whereas its NA gene sequence was similar to that of LPAIVs isolated in East Asia (Table 2). Although this combination had not been observed in Japan, reassortment events between the HPAIV H5N1 G2d subgroup and LPAIVs have been documented (*9*). We detected H5N5 HPAIVs in Hokkaido in January 2024; a total of 85 crows were found dead in the Sapporo garden, 80 of which we diagnosed as HPAIV positive by the end of April. No HPAIVs were detected in birds within the garden after April 2024. The continuous detection of H5N5 HPAIVs in the Sapporo garden during January–April without unusual deaths of birds other than crows and multiple isolations of H5N5 HPAIVs in other areas of Hokkaido suggest the potential for widespread dissemination of H5N5 HPAIVs within the Hokkaido region.

H5N1 G2d HPAIVs persisted in crows residing in the Sapporo garden even after the introduction of H5N5 G2a viruses, indicating concurrent circulation of genetically distinct viruses within a single crow population. Indeed, the average nanopore sequencing coverage for A/large-billed crow/Hokkaido/B080/2024 (H5N1) was 5497.4 reads for the N1 NA gene (G2d subgroup) and 1943.7 reads for the N5 NA gene (G2a subgroup) (Appendix Table 1). This observation suggests single hosts were co-infected with 2 viruses and reassortment occurred between viruses originating from geographically distant areas. Antigenic characterization of H5N5 HPAIVs suggested that the antigenicity of A/large-billed crow/Hokkaido/B073/2024 (H5N5) was close (2–4-fold differences in hemagglutination inhibition titers) to that of other H5 HPAIVs in the G2d subgroup (Table 3) despite their genetic diversity (Appendix Table 2).

Conclusions

We found that H5N5 HPAIVs consisting of unique gene constellations were likely introduced into Japan through a step-by-step bird migration through northern Eurasia. We confirmed the cocirculation of 2 genetically distinct viruses in a single flock of crows. The presence of H5N5 HPAIV infections in waterfowl in Japan is relatively unknown, and the lack of reports from neighboring countries on the presence of H5N5 HPAIVs from Europe has hampered the reconstruction of this genotype's spread to eastern Asia. Continuous monitoring and rapid information sharing between countries are needed to determine the global dynamics of HPAIVs and prevent their spread.

Acknowledgments

We thank Mayumi Endo and Fumihito Takaya for their technical assistance; Japan Ministry of the Environment and Hokkaido Prefecture for their kind cooperation, and the authors and laboratories that identified and submitted the sequences to the GISAID's EpiFlu database that were used in this study. All GISAID data submitters can be contacted directly via the GISAID website (https://www.gisaid.org).

This work was supported by the Japan Agency for Medical Research and Development (grant no. JP223fa627005). This work was also partially supported by the Japan International Cooperation Agency within the framework of the Science and Technology Research Partnership for Sustainable Development (grant no. JP23jm0110019); Japan Science and Technology Agency's Support for Pioneering Research Initiated by the Next Generation (grant no. JPMJSP2119); the research project on Regulatory Research Projects for Food Safety, Animal Health, and Plant Protection (grant no. JPJ008617.23812859) funded by the Ministry of Agriculture, Forestry, and Fisheries of Japan; the Doctoral Program for World-Leading Innovative and Smart Education, powered by the Japan Ministry of Education, Culture, Sports, Science and Technology; and the WISE Grant-in-Aid for graduate students, Program for One Health Frontier of the Graduate School of Excellence, Hokkaido University (grant no. PH36210001).

About the Author

Mr. Hew is a PhD candidate at Hokkaido University, Sapporo, Japan. His primary research focuses on the molecular diagnosis and epidemiology of avian influenza viruses.

References

1. WHO/OIE/FAO H5N1 Evolution Working Group. Toward a unified nomenclature system for highly pathogenic avian influenza virus (H5N1). Emerg Infect Dis. 2008;14:e1. https://doi.org/10.3201/eid1407.071681
2. Lycett SJ, Duchatel F, Digard P. A brief history of bird flu. Phil Trans R Soc Lond B Biol Sci. 2019;374:20180257. https://doi.org/10.1098/rstb.2018.0257
3. Pohlmann A, King J, Fusaro A, Zecchin B, Banyard AC, Brown IH, et al. Has epizootic become enzootic? Evidence for a fundamental change in the infection dynamics of highly pathogenic avian influenza in Europe, 2021. mBio. 2022;13:e0060922. https://doi.org/10.1128/mbio.00609-22
4. Kandeil A, Patton C, Jones JC, Jeevan T, Harrington WN, Trifkovic S, et al. Rapid evolution of A(H5N1) influenza viruses after intercontinental spread to North America. Nat Commun. 2023;14:3082. https://doi.org/10.1038/s41467-023-38415-7
5. Global Consortium for H5N8 and Related Influenza Viruses. Role for migratory wild birds in the global spread of avian

influenza H5N8. Science. 2016;354:213–7. https://doi.org/10.1126/science.aaf8852
6. de Vries E, Guo H, Dai M, Rottier PJM, van Kuppeveld FJM, de Haan CAM. Rapid emergence of highly pathogenic avian influenza subtypes from a subtype H5N1 hemagglutinin variant. Emerg Infect Dis. 2015;21:842–6. https://doi.org/10.3201/eid2105.141927
7. Baek YG, Lee YN, Lee DH, Shin JI, Lee JH, Chung DH, et al. Multiple reassortants of H5N8 clade 2.3.4.4b highly pathogenic avian influenza viruses detected in South Korea during the winter of 2020–2021. Viruses. 2021;13:490. https://doi.org/10.3390/v13030490
8. Isoda N, Onuma M, Hiono T, Sobolev I, Lim HY, Nabeshima K, et al. Detection of new H5N1 high pathogenicity avian influenza viruses in winter 2021–2022 in the Far East, which are genetically close to those in Europe. Viruses. 2022;14:2168. https://doi.org/10.3390/v14102168
9. Hew LY, Isoda N, Takaya F, Ogasawara K, Kobayashi D, Huynh LT, et al. Continuous introduction of H5 high pathogenicity avian influenza viruses in Hokkaido, Japan: characterization of viruses isolated in winter 2022–2023 and early winter 2023–2024. Transbound Emerg Dis. 2024;2024:1–18. https://doi.org/10.1155/2024/1199876
10. Sakuma S, Uchida Y, Kajita M, Tanikawa T, Mine J, Tsunekuni R, et al. First outbreak of an H5N8 highly pathogenic avian influenza virus on a chicken farm in Japan in 2020. Viruses. 2021;13:489. https://doi.org/10.3390/v13030489
11. European Food Safety Authority; European Centre for Disease Prevention and Control; European Union Reference Laboratory for Avian Influenza; Fusaro A, Gonzales JL, Kuiken T, Mirinavičiūtė G, Niqueux É, Ståhl K, et al. Avian influenza overview December 2023–March 2024. EFSA J. 2024;22:e8754. https://doi.org/10.2903/j.efsa.2024.8754
12. Świętoń E, Fusaro A, Shittu I, Niemczuk K, Zecchin B, Joannis T, et al. Sub-Saharan Africa and Eurasia ancestry of reassortant highly pathogenic avian influenza A(H5N8) virus, Europe, December 2019. Emerg Infect Dis. 2020;26:1557–61. https://doi.org/10.3201/eid2607.200165
13. Zinyakov N, Andriyasov A, Zhestkov P, Kozlov A, Nikonova Z, Ovchinnikova E, et al. Analysis of avian influenza (H5N5) viruses isolated in the southwestern European part of the Russian Federation in 2020–2021. Viruses. 2022;14:2725. https://doi.org/10.3390/v14122725
14. Hoffmann TW, Munier S, Larcher T, Soubieux D, Ledevin M, Esnault E, et al. Length variations in the NA stalk of an H7N1 influenza virus have opposite effects on viral excretion in chickens and ducks. J Virol. 2012;86:584–8. https://doi.org/10.1128/JVI.05474-11
15. European Union Reference Laboratory. EURL avian flu data portal [cited 2024 Mar 7]. https://eurlaidata.izsvenezie.it

Address for correspondence: Takahiro Hiono, One Health Research Center, Hokkaido University, North 18, West 9, Kita-ku, Sapporo, Hokkaido 060-0818, Japan; email: hiono@vetmed.hokudai.ac.jp

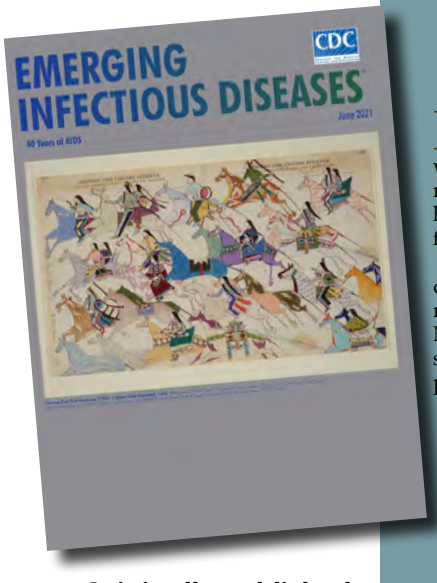

Originally published in June 2021

etymologia revisited

Enterocytozoon bieneusi

['entərə ˌsaitə'ʒu:ən biə'nəusɪ]

From the Greek *en'tĕr-ō-sī'tōn* (intestine), *kútos* (vessel, cell), and *zō'on* (animal), and the surname Bieneus, in memory of the first infected patient whose case was reported in Haiti during 1985. *Enterocytozoon bieneusi*, a member of the wide-ranging phylum Microsporidia, is the only species of this genus known to infect humans. Microsporidia are unicellular intracellular parasites closely related to fungi, although the nature of the relationship is not clear.

E. bieneusi, a spore-forming, obligate intracellular eukaryote, was discovered during the HIV/AIDS pandemic and is the main species responsible for intestinal microsporidiosis, a lethal disease before widespread use of antiretroviral therapies. More than 500 genotypes are described, which are divided into different host-specific or zoonotic groups. This pathogen is an emerging issue in solid organ transplantation, especially in renal transplant recipients.

Sources

1. Desportes I, Le Charpentier Y, Galian A, Bernard F, Cochand-Priollet B, Lavergne A, et al. Occurrence of a new microsporidan: *Enterocytozoon bieneusi* n.g., n. sp., in the enterocytes of a human patient with AIDS. J Protozool. 1985;32:250–4. https://doi.org/10.1111/j.1550-7408.1985.tb03046.x
2. Didier ES, Weiss LM. Microsporidiosis: not just in AIDS patients. Curr Opin Infect Dis. 2011;24:490–5. https://doi.org/10.1097/QCO.0b013e32834aa152
3. Han B, Weiss LM. Microsporidia: obligate intracellular pathogens within the fungal kingdom. Microbiol Spectr. 2017;5:97–113. https://doi.org/10.1128/microbiolspec.FUNK-0018-2016
4. Moniot M, Nourrisson C, Faure C, Delbac F, Favennec L, Dalle F, et al. Assessment of a multiplex PCR for the simultaneous diagnosis of intestinal cryptosporidiosis and microsporidiosis: epidemiologic report from a French prospective study. J Mol Diagn. 2021;23:417–23. https://doi.org/10.1016/j.jmoldx.2020.12.005

https//wwwnc.cdc.gov/eid/article/27/6/et2706_article

Mosquitoes as Vectors of *Mycobacterium ulcerans* Based on Analysis of Notifications of Alphavirus Infection and Buruli Ulcer, Victoria, Australia

Andrew H. Buultjens, Ee Laine Tay, Aidan Yuen, N. Deborah Friedman, Timothy P. Stinear, Paul D.R. Johnson

Alphavirus infections are transmitted by mosquitoes, but the mode of transmission for *Mycobacterium ulcerans*, which causes Buruli ulcer, is contested. Using notification data for Victoria, Australia, during 2017–2022, adjusted for incubation period, we show close alignment between alphavirus and Buruli ulcer seasons, supporting the hypothesis of mosquito transmission of *M. ulcerans*.

Victoria, Australia, has been experiencing an intensifying outbreak of Buruli ulcer (*1*). The mode of transmission for *Mycobacterium ulcerans*, which causes Buruli ulcer, has been contested. The first evidence that mosquitoes might transmit the causative organism, *Mycobacterium ulcerans*, to humans was published in 2007 (*2*,*3*). Contemporaneous research also reported that native possums were a key environmental reservoir, shed *M. ulcerans* in their excreta, and frequently suffer from Buruli ulcer themselves. Combining those facts, we proposed that mosquitoes transmit *M. ulcerans* from possums to humans and likely between possums (*4*).

Further reports from Victoria published in April 2009 (*5*) and December 2021 (*6*) considered correlations between patterns of annual notified cases of Ross River and Barmah Forest viruses (alphavirus infections) and Buruli ulcer. A positive correlation would be expected if Buruli ulcer were mosquito transmitted, as has been established for alphavirus infections. The 2009 report (*5*) identified a partial correlation between annual notifications of alphavirus infections and Buruli ulcer during 2002–2008, consistent with the mosquitoborne transmission hypothesis. However, the 2021 report (*6*) indicated no ongoing statistical association in annual notifications since 2008 using linear statistical methods and concluded that factors other than mosquitoes were likely behind the change in Buruli ulcer incidence in Victoria. We hypothesized that a new analysis of notification data during a period of higher Buruli ulcer incidence using a nonlinear statistical approach applied this time to monthly instead of annual notifications would help to resolve the question of transmission vectors so that we could focus and intensify our Buruli ulcer prevention efforts at a public health level.

Separate ethics approval was not required because notification data in this study were collected and used under the legislative authority of the Public and Wellbeing Act of 2008, and we used only aggregated, deidentified data. Data were summated by month and accessed with permission and assistance from senior epidemiologists at the Victoria Department of Health.

The Study

Victoria, the smallest of Australia's mainland states, has a temperate southern hemisphere climate with distinct seasons. Officially, summer in Victoria is defined as December–February, autumn as March–May, winter as July–August, and spring as September–November.

Buruli ulcer was initially made legally notifiable to the Department of Health in Victoria in January

Author affiliations: Doherty Institute, University of Melbourne, Melbourne, Victoria, Australia (A.H. Buultjens, T.P. Stinear); Victoria Department of Health, Melbourne (E.L. Tay, A. Yuen, N.D. Friedman); Austin Health, Heidelberg, Victoria, Australia (P.D.R. Johnson); University of Melbourne, Melbourne (P.D.R. Johnson)

DOI: https://doi.org/10.3201/eid3009.231073

2004, but notifications have markedly increased only in more recent years. The surveillance definition for Buruli ulcer in Victoria has been updated recently (*7*). Cases of alphavirus infection, classified according to national surveillance definitions, have been nationally notifiable for many years. In collaboration with colleagues at the Victoria Department of Health, we analyzed all notification data from Victoria for cases of both Buruli ulcer and alphavirus infection (Ross River virus and Barmah Forest virus infections combined) by month for the 6 calendar years 2017–2022 (Appendix, https://wwwnc.cdc.gov/EID/article/30/9/23-1073-App1.pdf). We assumed month of notification to be the same as month of diagnosis.

During 2017–2022, Victoria had 3,839 notified alphavirus infection cases. Notifications were strongly clustered by season (summer and autumn) and month. For Buruli ulcer, there were 1,761 notifications over the 6-year study period, also strongly clustered by month and season but peaking during winter and spring (Figure 1, panel A). The incubation period for Buruli ulcer has previously been calculated using interview information from case-patients who had only short exposures in Buruli ulcer–endemic areas. Two published estimates indicated medians of 4.5 and 5 months (*8*). To estimate and graphically illustrate the time offset between months of inferred transmission and notification, we assumed incubation period plus time to diagnosis/notification of 5 months for Buruli ulcer and 1 month for alphavirus infections (Figure 1, panel B).

In addition, to test for confirmation bias, we reexamined the data using an observer-independent signal processing technique, cross-correlation, to analyze the relationship between the notification distributions. In the alphavirus time-series, the first 3 months of 2017 were identified as outliers using z-scores; therefore, we excluded those 3 timepoints from both datasets. The censored data series then underwent logarithmic transformation and smoothing to amplify the cyclic signal within the data. We displayed and analyzed data using Prism 10.0 (GraphPad, https://www.graphpad.com) or R (The R Project for Statistical Computing, https://www.r-project.org). The overlaid transformed series revealed an almost antiphase relationship between the Buruli ulcer and alphavirus signals, indicating the presence of similar but temporally offset cyclic patterns (Figure 2, panel A).

We used the correlate function in the NumPy Python library (*9*) to identify the time-shift factor in months that optimized the correlation between the 2 signals. The algorithm identified –5 months as the optimal time shift. To test for statistical robustness, we performed the same cross-correlation analysis on 1,000 randomly reshuffled instances of the Buruli ulcer notification series. The resulting distribution from these iterations centered around 0, well separated from the optimal shift of –5 months (Figure 2, panel B). When we adjusted the Buruli ulcer notifications by that assumption-independent −5 months, we observed a close sinusoidal alignment with alphavirus notifications (Figure 2, panel C).

Our results showed that inferred transmission of alphavirus infections and Buruli ulcer simultaneously reach their maximums during December–May (summer and autumn) and minimums during June–November (winter and spring) every year during the 6-year study period. The accepted explanation in temperate Victoria for variation by season in alphavirus infection notifications is that warmer weather

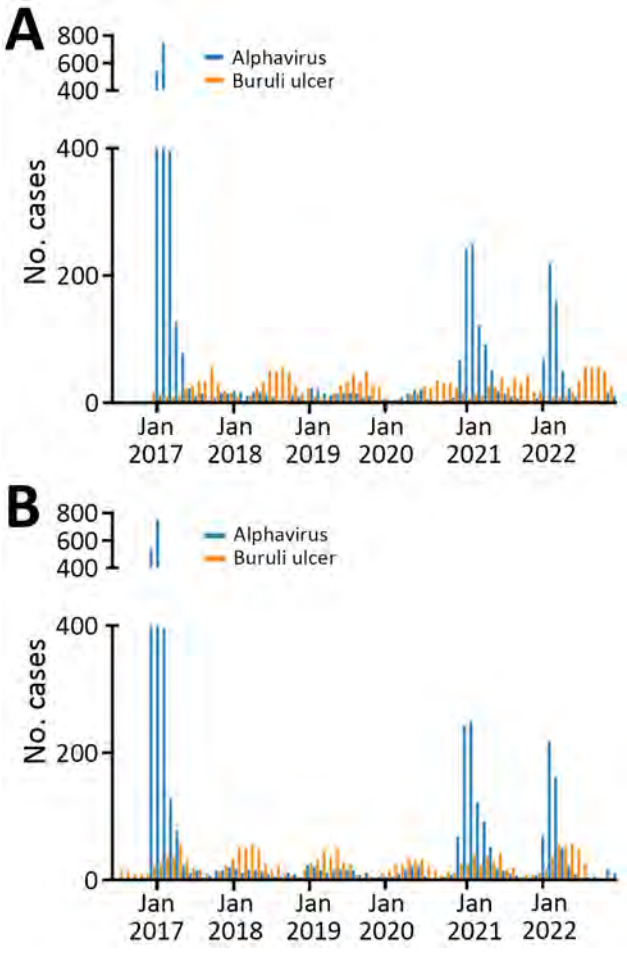

Figure 1. Alphavirus infection and Buruli ulcer notifications in Victoria, Australia, 2017–2022. A) Unadjusted month and year of notification. B) Month and year of notification manually adjusted for the known median Buruli ulcer incubation period of 5 months.

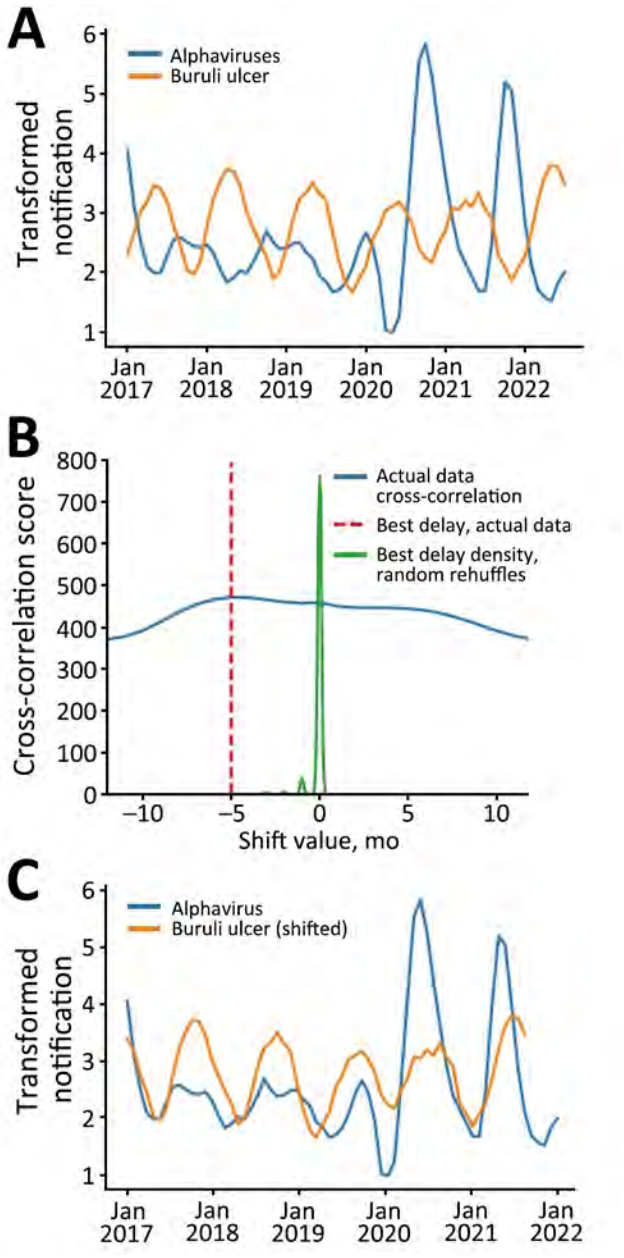

Figure 2. Analysis of temporally adjusted Buruli ulcer and alphavirus notifications in Victoria, Australia, 2017–2022. A) Notifications over time (no delay). Plot of the 2 datasets (outliers censored) was log transformed and smoothed by month and year. B) Optimal shift and cross-correlation analysis. Algorithmically determined cross correlation (blue line) and optimal curve shift of –5 months (vertical red dashed line) that best aligned the 2 log transformed curves shown in panel A. In green is a density curve that depicts the outcomes of 1,000 random data shuffles, serving as a visual indicator of how the observed –5 months curve shift diverges from random chance expectations. C) Notifications over time shifted to incorporate the Buruli ulcer incubation period of 5 months. Cross-correlation aligned smoothed log-transformed notification curves show synchronous inferred transmission peaks and troughs for both alphavirus infection and Buruli ulcer.

provides necessary climatic conditions for increased prevalence of mosquito vectors. Even though animal reservoirs of alphaviruses are present throughout the year, transmission to humans falls to almost 0 during colder months. A recently published detailed quantitative observational study showed that *M. ulcerans* in possum excreta, and, by inference, in possums as wildlife reservoirs, is similarly present in the environment throughout the year (*10*). Hence, the previous paradigm of Buruli ulcer transmission by direct exposure to a stably contaminated environment does not fit well with the periodic notification patterns we observed.

Our study addressed and offers evidence to resolve the question of correlation between alphavirus infection and Buruli ulcer notifications, but a wealth of other published research much more directly establishes a central role for mosquitoes in the transmission of Buruli ulcer in Victoria. That research includes evidence that human Buruli ulcer risk closely correlates with the proportion of mosquitoes PCR positive for *M. ulcerans* trapped in 7 towns on the Bellarine peninsula in Victoria during the mid-2000s (*11*). A survey of mosquitoes performed 15 years later on the Mornington peninsula in Victoria, on the opposite side of Port Phillip Bay from the original studies, demonstrated that 5.1/1,000 mosquitoes trapped there during 2016–2021 carried *M. ulcerans*. The more recent study also presented genomic evidence that *M. ulcerans* strains in mosquitoes were indistinguishable from the human and possum Buruli ulcer outbreak strains. In addition, the mosquito species most closely linked to Buruli ulcer transmission, *Aedes notoscriptus*, feeds on both humans and possums; some individual trapped mosquitoes simultaneously contained both human and possum blood (*12*).

We have attempted to investigate alternative models of transmission that would explain the anatomic distribution of Buruli ulcer lesions we observed in Victoria (*13*), including variation in human skin temperature (*14*), and the hypothesis that outdoor exposure in Buruli ulcer–endemic areas leads to skin contamination with *M. ulcerans* (*15*). There was no support from those studies for an alternative model.

Conclusions

We conducted an analysis of statewide notifications of alphavirus infections and Buruli ulcer in Victoria, Australia, adjusted for incubation period. Our findings support other published evidence that Buruli ulcer is transmitted during the mosquito season by mosquitoes in this temperate region.

About the Author

Dr. Buultjens is a postdoctoral fellow in the Stinear Group at the Peter Doherty Institute for Infection and Immunity, University of Melbourne, Victoria, Australia. He focuses on the evolution and spread of clinically significant bacterial pathogens such as *Mycobacterium ulcerans*, *Legionella pneumophila*, and *Enterococcus faecium* and on microbial genomics.

References

1. Loftus MJ, Tay EL, Globan M, Lavender CJ, Crouch SR, Johnson PDR, et al. Epidemiology of Buruli ulcer infections, Victoria, Australia, 2011–2016. Emerg Infect Dis. 2018;24:1988–97. https://doi.org/10.3201/eid2411.171593
2. Johnson PDR, Azuolas J, Lavender CJ, Wishart E, Stinear TP, Hayman JA, et al. *Mycobacterium ulcerans* in mosquitoes captured during outbreak of Buruli ulcer, southeastern Australia. Emerg Infect Dis. 2007;13:1653–60. https://doi.org/10.3201/eid1311.061369
3. Quek TY, Athan E, Henry MJ, Pasco JA, Redden-Hoare J, Hughes A, et al. Risk factors for *Mycobacterium ulcerans* infection, southeastern Australia. Emerg Infect Dis. 2007;13:1661–6. https://doi.org/10.3201/eid1311.061206
4. Fyfe JA, Lavender CJ, Handasyde KA, Legione AR, O'Brien CR, Stinear TP, et al. A major role for mammals in the ecology of *Mycobacterium ulcerans*. PLoS Negl Trop Dis. 2010;4:e791. https://doi.org/10.1371/journal.pntd.0000791
5. Johnson PDR, Lavender CJ. Correlation between Buruli ulcer and vector-borne notifiable diseases, Victoria, Australia. Emerg Infect Dis. 2009;15:614–5. https://doi.org/10.3201/eid1504.081162
6. Linke JA, Athan E, Friedman ND. Correlation between Buruli ulcer incidence and vectorborne diseases, southeastern Australia, 2000–2020. Emerg Infect Dis. 2021;27:3191–2. https://doi.org/10.3201/eid2712.203182
7. Betts JM, Tay EL, Johnson PDR, Lavender CJ, Gibney KB, O'Brien DP, et al. Buruli ulcer: a new case definition for Victoria. Commun Dis Intell (2018). 2020:44.
8. Loftus MJ, Trubiano JA, Tay EL, Lavender CJ, Globan M, Fyfe JAM, et al. The incubation period of Buruli ulcer (*Mycobacterium ulcerans* infection) in Victoria, Australia remains similar despite changing geographic distribution of disease. PLoS Negl Trop Dis. 2018;12:e0006323. https://doi.org/10.1371/journal.pntd.0006323
9. NumPy. numpy.correlate [cited 2023 Jul 22]. https://numpy.org/doc/stable/reference/generated/numpy.correlate.html
10. Vandelannoote K, Buultjens AH, Porter JL, Velink A, Wallace JR, Blasdell KR, et al. Statistical modeling based on structured surveys of Australian native possum excreta harboring *Mycobacterium ulcerans* predicts Buruli ulcer occurrence in humans. eLife. 2023;12:e84983. https://doi.org/10.7554/eLife.84983
11. Lavender CJ, Fyfe JA, Azuolas J, Brown K, Evans RN, Ray LR, et al. Risk of Buruli ulcer and detection of *Mycobacterium ulcerans* in mosquitoes in southeastern Australia. PLoS Negl Trop Dis. 2011;5:e1305. https://doi.org/10.1371/journal.pntd.0001305
12. Mee PT, Buultjens AH, Oliver J, Brown K, Crowder JC, Porter JL, et al. Mosquitoes provide a transmission route between possums and humans for Buruli ulcer in southeastern Australia. Nat Microbiol. 2024;9:377–89. https://doi.org/10.1038/s41564-023-01553-1
13. Yerramilli A, Tay EL, Stewardson AJ, Kelley PG, Bishop E, Jenkin GA, et al. The location of Australian Buruli ulcer lesions—implications for unravelling disease transmission. PLoS Negl Trop Dis. 2017;11:e0005800. https://doi.org/10.1371/journal.pntd.0005800
14. Sexton-Oates NK, Stewardson AJ, Yerramilli A, Johnson PDR. Does skin surface temperature variation account for Buruli ulcer lesion distribution? PLoS Negl Trop Dis. 2020;14:e0007732. https://doi.org/10.1371/journal.pntd.0007732
15. Velink A, Porter JL, Stinear TP, Johnson PDR. Mycobacterium ulcerans not detected by PCR on human skin in Buruli ulcer endemic areas of south eastern Australia. PLoS Negl Trop Dis. 2023;17:e0011272. https://doi.org/10.1371/journal.pntd.0011272

Address for correspondence: Paul D.R. Johnson, Department of Infectious Diseases and Immunology, Austin Hospital, Studley Road, Heidelberg, VIC 3084, Australia; email: paul.johnson@austin.org.au

Fatal Case of *Naegleria fowleri* Primary Amebic Meningoencephalitis from Indoor Surfing Center, Taiwan, 2023

Hsin-Yi Wei, Yi-Wen Lai, Shu-Ying Li, Yen-I Lee, Meng-Kai Hu, Da-Der Ji, Chia-ping Su

We investigated a fatal case of primary amoebic meningoencephalitis from an indoor surfing center in Taiwan. The case was detected through encephalitis syndromic surveillance. Of 56 environmental specimens, 1 was positive for *Naegleria fowleri* ameba. This report emphasizes the risk for *N. fowleri* infection from inadequately disinfected recreational waters, even indoors.

Primary amoebic meningoencephalitis (PAM) is a rare but fatal disease caused by *Naegleria fowleri*, a single-cell, free-living ameba. *N. fowleri* amebae usually live in natural waters, but occasionally can be found in swimming pools, surf parks, and other recreational waters that have not been adequately disinfected (*1*). We report a case of PAM in Taiwan from an indoor recreational water facility.

The Study

A 30-year-old woman visited an indoor surfing center in northern Taiwan in July 2023. Five days after her visit, she started experiencing neurologic symptoms, including headache and stiffness in her shoulders and neck. Fever and generalized tonic-clonic seizures then occurred, and she was admitted to the hospital. Her condition deteriorated rapidly, and she died 3 days later. The hospital reported the case to the Taiwan Centers for Disease Control (TCDC) as encephalitis with an unknown cause.

In 2010, TCDC implemented encephalitis syndromic surveillance to identify the causative agents responsible for cases of unexplained encephalitis (*2*). Surveillance involves screening for 41 pathogens by using multiplex quantitative reverse transcription PCR (qRT-PCR) (*2*). In this case, *N. fowleri* was the only pathogen detected from the patient. After next-generation sequencing analyses, the TCDC reference laboratory assembled the complete 49,558-bp *N. fowleri* mitochondrial sequence from the patient (*3*) and submitted the sequence to GenBank (accession no. OR459835).

The investigation team and the local public health authority (LPHA) went to the surfing center to conduct an environmental investigation and took various water and biofilm samples to test for *N. fowleri* (Table; Appendix, https://wwwnc/cdc.gov/EID/article/30/9/23-1604-App1.pdf). TCDC classified this work as a public health investigation; thus, it was not subject to institutional review board approval.

The surfing facility includes a swimming pool, spa pool, wave pool, dining area, and shower rooms on the first floor (Figure 1). A waterslide, gym, and billiards are on the second floor, and a basketball court is on the third floor. The basement is equipped with a water filtration system that has a chlorination function and can only be accessed by ladder (Figure 2, panel A). The water supply is municipal tap water. The water for the wave pool is extracted from the swimming pool, not directly from the municipal water source. The facility drains water from the pools every 2–3 months for thorough pool cleaning. Staff members add chlorine powder after the facility closes each day to maintain the chlorine level in the pool, but they do not add chlorine to the wave pool. Staff conduct water quality tests every day but do not keep records of results.

Before this fatal case occurred, the pool had not been completely drained and refilled for >2 months.

Author affiliations: Taiwan Centers for Disease Control, Ministry of Health and Welfare, Taipei, Taiwan (H.-Y. Wei, Y.-W. Lai, S.-Y. Li, Y.-I. Lee, M.-K. Hu); National Yang Ming Chiao Tung University, Taipei (D.-D. Ji); New Taipei Municipal Tucheng Hospital and National Tsing Hua University, Hsinchu, Taiwan (C.-p. Su)

DOI: https://doi.org/10.3201/eid3009.231604

However, before the investigation team took samples, most of the water had been drained from the pools and the pools had been cleaned.

After the onsite investigation, water quality testing of collected specimens revealed the following: chlorine content was 0.87 parts per million (ppm) in the swimming pool and 0.06 ppm in the spa pool; pH value was 7.4 in the swimming pool and unavailable in the spa pool (Figure 1). The normal residual chlorine standard for swimming pools is 1–3 ppm; thus, the test results for the collected specimens revealed the chlorine content was insufficient.

We collected a total of 30 water samples and 26 biofilm swab samples, which we submitted for qRT-PCR testing (Table). Among those specimens, 55 from the pool were negative, but 1 specimen from stagnant water beneath the basement ladder was positive for *N. fowleri* (Figure 2). That water might have been seepage from pipes associated with the pump motor, but further investigation showed that the positive specimen was not associated with pool water. Because employees access the basement daily to operate the filtration system, we could not rule out the possibility of pool contamination from staff shoes or feet.

The surf center had several design deficiencies, such as overlapping pathways connecting each facility. The staircase leading from the swimming pool to the second-floor water slide is used by visitors to general activity areas, such as the gym or basketball court. The facility did not provide a footbath for swimmers to use before entering the pool, and the pool had no drainage ditch along its edges. Such design deficiencies might increase the risk for external contamination to be introduced to the swimming pool.

Table. Environmental samples collected and qRT-PCR results in an investigation of a fatal case of *Naegleria fowleri* primary amebic meningoencephalitis from indoor surfing center, Taiwan, 2023*

Sample collection site	No. samples	Results
Water samples		
Swimming pool	5	Negative
Spa pool	5	Negative
Reservoir of surf pool	13	Negative
Two inflatable outdoor swimming pools	6	Negative
Stagnant water under basement ladder	1	Positive, Ct 33.55
Biofilm samples		
Water inlet of swimming pool	1	Negative
Main drains of swimming pool	2	Negative
Connection outlet of swimming and spa pools	1	Negative
Water outlets of spa pool	2	Negative
Water inlet of spa pool	1	Negative
Main drain of spa pool	1	Negative
Showerheads of spa pool	1	Negative
Surf ramp	5	Negative
Reservoir of surf pool	12	Negative

*Ct, cycle threshold; qRT-PCR, quantitative reverse transcription PCR.

The LPHA traced 12 employees and 630 customers by telephone, but none reported symptoms during the surveillance period. The surfing center suspended operations for comprehensive cleanup and disinfection. The facility addressed deficiencies and completed renovations before it reopened. The staff members were instructed to maintain free chlorine levels at 1–3 ppm and a pH of 7.2–7.8.

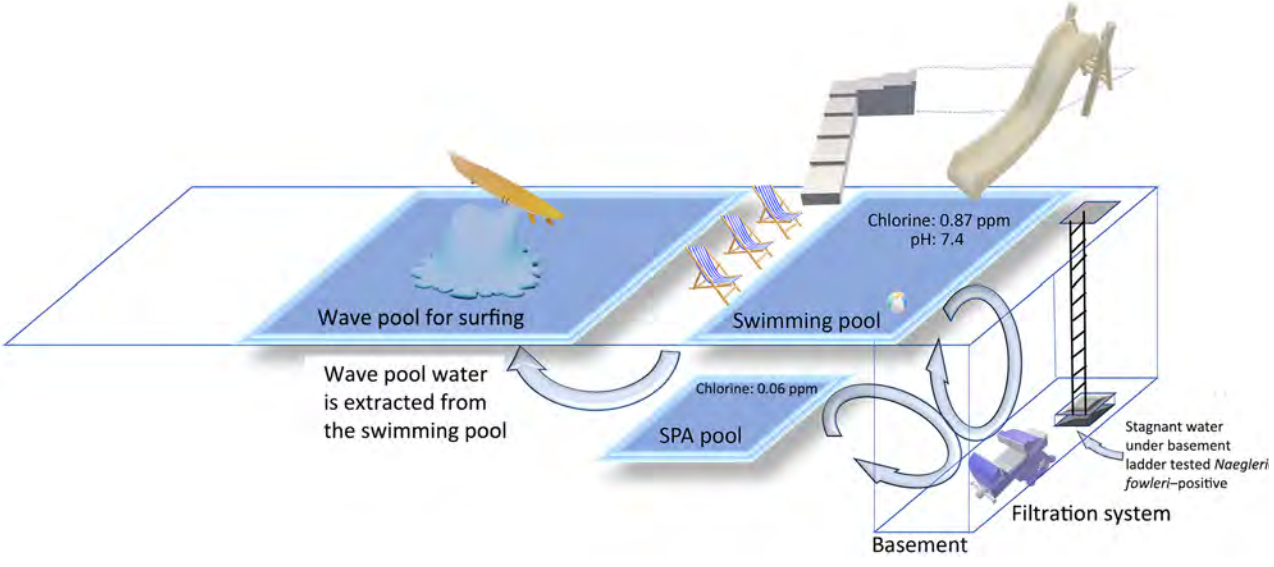

Figure 1. Illustration of 3 pools and basement mechanical area in an investigation of a fatal case of *Naegleria fowleri* primary amebic meningoencephalitis from indoor surfing center, Taiwan, 2023. Chlorine levels for pools are shown. Water for the wave pool was extracted from the swimming pool, and no additional chlorine was added to the wave pool. ppm, parts per million.

Figure 2. Basement mechanical area in an investigation of a fatal case of *Naegleria fowleri* primary amebic meningoencephalitis from indoor surfing center, Taiwan, 2023. A) The opening to the basement with ladder visible to right of opening; B) stagnant water beneath the basement ladder; C) depression under basement ladder after water was drained.

Conclusions

PAM cases are rare. In the United States, 0–5 cases were diagnosed annually during 2013–2022 (*1*). In some instances, *N. fowleri* has been found in underchlorinated recreational waters. However, the event we describe occurred in an indoor water body that was entirely supplied by municipal tapwater. Although we found 1 positive environmental sample, the nucleic acid within the specimen was insufficient for sequencing and could not be used to prove a connection between the case and the *N. fowleri* in the environment.

The negative results from other samples might be related to the fact that most of the pool water had been drained and the pool had been cleaned before we conducted environmental sampling. The stagnant water that yielded *N. fowleri*–positive qRT-PCR results was collected from the damp, unpainted basement (Figure 2). That water might have been seepage from pipes, but the ameba could have originated from cracks in the floor or walls or from dirt on the shoes of staff members going into the basement. Unfortunately, we did not gather other environmental specimens from the basement, nor did we sample the shoe soles of staff members working in the basement. Consequently, the origin of *N. fowleri* and its transmission pathways in this case remained unknown.

Activities known to pose a higher risk for *N. fowleri* infection include diving and jumping into water. For beginner surfers, maintaining balance on the water can be difficult, and falling into the waves frequently enables water to flow into the nose. In 2018, a man in New Jersey, USA, also died from PAM after visiting a surf resort (*4*). We recommend that persons playing in recreational waters avoid letting water enter the nasal cavity.

Chlorine decay might be more challenging to address in wave pools for surfing because such levels can be higher in turbulent water surging at high speeds (*5*,*6*). However, current guidance on chlorine maintenance specific to wave pools is relatively lacking. In the surfing center we investigated, the water in the wave pool is extracted from the swimming pool. The staff adds chlorine powder to the swimming pool but not to the wave pool. Therefore, chlorine concentration could be even lower in the wave pool than in the swimming pool, which already had insufficient chlorine levels. Because we did not isolate the free-living ameba from the positive sample, we could not conduct a chlorination sensitivity test.

In conclusion, insufficient levels of residual chlorine can pose a risk for PAM, even in indoor water facilities. Indoor facilities should emphasize water quality and sanitation. Facility owners should maintain daily disinfection practices and LPHA should conduct inspections to ensure water quality in recreational facilities.

Acknowledgments

We thank the staff of the Center for Diagnostics and Vaccine Development and the Taipei Regional Control Center of the Taiwan Centers for Disease Control, as well as partners at Department of Health, New Taipei City Government, for their dedicated outbreak investigation, meticulous data collection, and efforts that made this study possible.

About the Author

Dr. Wei is a medical officer in the Centers for Disease Control, Ministry of Health and Welfare, Taiwan. Her primary research interest is infectious disease epidemiology.

References

1. Centers for Disease Control and Prevention. Frequently asked questions about *Naegleria fowleri*, commonly known as the "brain-eating ameba" [cited 2023 Oct 6]. https://www.cdc.gov/parasites/naegleria/general.html
2. Taiwan Centers for Disease Control. Abstract of technology project: detection of important emerging and re-emerging infectious pathogens and its applications [cited 2024 Jul 29]. https://www.cdc.gov.tw/En/Professional/ProgramResultInfo/ppxd4Xu5zcYwcLHniXKk6w
3. Lin YC, Li MS, Chang JC, Huang SE, Tseng CP, Wu FT, et al. Application of next-generation sequencing in public health—detection of *Naegleria fowleri* by using metagenomic sequencing. Taiwan Epidemiology Bulletin. In press 2024.
4. Miko S, Cope JR, Hlavsa MC, Ali IKM, Brown TW, Collins JP, et al. A case of primary amebic meningoencephalitis associated with surfing at an artificial surf venue: environmental investigation. ACS ES T Water. 2023;3:1126–33. https://doi.org/10.1021/acsestwater.2c00592
5. Nono D, Odirile PT, Basupi I, Parida BP. Assessment of probable causes of chlorine decay in water distribution systems of Gaborone city, Botswana. Water SA. 2019;45:190–8. https://doi.org/10.4314/wsa.v45i2.05
6. Jamwal P, Mohan Kumar MS. Effect of flow velocity on chlorine decay in water distribution network: a pilot loop study. Curr Sci. 2016;111:1349–54. https://doi.org/10.18520/cs/v111/i8/1349-1354

Address for correspondence: Chia-ping Su, New Taipei Municipal Tucheng Hospital, No. 6, Section 2, Jincheng Road, Tucheng District, New Taipei City 236, Taiwan; email: sigbird@gmail.com

Epidemiology of Lyme Disease Diagnoses among Older Adults, United States, 2016–2019[1]

Amy M. Schwartz, Christina A. Nelson, Alison F. Hinckley

We used Medicare data to identify >88,000 adults ≥65 years of age diagnosed and treated for Lyme disease during 2016–2019 in the United States. Most diagnoses occurred among residents of high-incidence states, in summer, and among men. Incidence of diagnoses was substantially higher than that reported through public health surveillance.

Lyme disease (LD) is the most reported vector-borne disease in the United States (*1*). In separate efforts designed to better measure the burden of disease in the United States, we used employer-sponsored insurance claims data to quantify LD diagnoses (*2*,*3*). However, those data lacked information on persons ≥65 years of age, a group commonly affected by LD (*2*,*3*). In this complementary effort we used similar methods to analyze Medicare fee-for-service (FFS) data to describe LD diagnoses among beneficiaries ≥65 years of age.

The Study

We examined Medicare FFS claims data and Part D drug event data (Appendix, https://wwwnc.cdc.gov/EID/article/30/9/24-0454-App1.pdf) to identify LD diagnoses. We restricted the analyzed population to Medicare FFS beneficiaries ≥65 years of age who participated in Parts A, B, and D for at least 12 months of a calendar year or until their month of death during 2016–2019.

Aligning with previously described methods (*2*), we defined LD diagnosis as an International Classification of Diseases, 10th Revision, Clinical Modification code for LD combined with a drug claim for an antibiotic indicated for LD (Appendix) within 30 days of the LD code and prescribed for ≥7 days. We defined an inpatient LD diagnosis as hospitalization with a primary code for LD or a primary code for a known manifestation or plausible co-infection of LD plus a secondary code (A69.2x) for LD (Appendix) (*2*,*3*).

We compared the restricted Medicare FFS study population with 2019 US Census estimation data for persons ≥65 years of age to ensure the 2 groups were similar with respect to sex, age, race, ethnicity, and region (*4*). We grouped states into incidence regions based on previous definitions (*3*).

We compared LD diagnoses identified in the Medicare FFS data to confirmed and probable cases among persons ≥65 years of age reported through national LD surveillance (*5*). State and local health departments investigate and tabulate LD surveillance cases and classify them according to the Council of State and Territorial Epidemiologists (https://www.cste.org) case definition in effect during the reporting year (*5*). We used SAS 9.4 and SAS Enterprise Guide 7.1 (SAS Institute Inc, https://www.sas.com/en_us) for analyses. The Centers for Disease Control and Prevention deemed this activity not research.

Census Population and Medicare FFS Restricted Population

After restricting by enrollment criteria, we found that the Medicare FFS population had a median 17,872,466 person-years and the Census population had a median 51,561,372 persons during the study period (Appendix Figure 1). Compared with the Census population, the Medicare FFS population was slightly older (median age 74 years vs. 73 years), included more women (median 59.3% vs. 55.6%) (Appendix Figure 2),

Author affiliations: Centers for Disease Control and Prevention, Fort Collins, Colorado, USA (A.M. Schwartz, C.A. Nelson, A.F. Hinckley); University of Iowa, Iowa City, Iowa, USA (A.M. Schwartz)

DOI: http://doi.org/10.3201/eid3009.240454

[1]Preliminary results from this study were presented at the International Conference on Emerging Infectious Diseases; August 7–10, 2022, Atlanta, Georgia, USA.

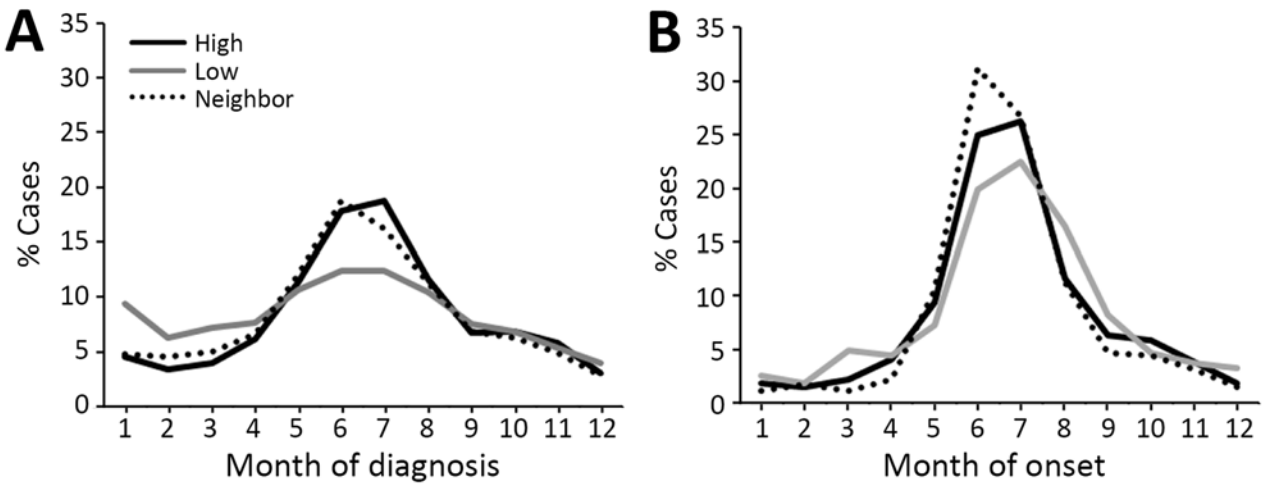

Figure 1. Analysis of Lyme disease among older adults, United States, 2016–2019. A) Percentage of Lyme disease diagnoses by month according to Medicare fee-for-service data. B) Percentage of Lyme disease cases by month of onset from US surveillance data.

and featured a larger percentage of White/non-Hispanic persons (83.8% vs. 76.8%). The Medicare FFS population had a larger percentage of beneficiaries from states neighboring high-incidence states (median 28.0%) compared with the Census population (26.5%) and a lower percentage of beneficiaries from low-incidence states (47.5% vs. 51.4%). The characteristics of the Medicare FFS population remained stable during the study period.

Characteristics of LD Diagnoses

We identified 88,485 LD diagnoses among Medicare FFS beneficiaries during 2016–2019, noting an average incidence of 123.5 diagnoses/100,000 person-years. We calculated a total of 34,183 LD cases reported through surveillance during 2016–2019, and an average incidence of 16.6 cases/100,000 persons (Appendix Figure 3).

Geographic Distribution

Approximately 82% of LD diagnoses were among residents of high-incidence states (Table). The median incidence of LD diagnoses was 346.9/100,000 person-years among residents of high-incidence states, 35.3/100,000 person-years among residents of states or jurisdictions neighboring high-incidence states, and 29.4/100,000 person-years among residents of low-incidence states. In comparison, 93% of LD surveillance cases were among residents of high-incidence states. The median incidence of those cases was 57.1/100,000 persons among residents of high-incidence states, 3.6/100,000 persons among residents of states or jurisdictions neighboring high-incidence states, and 0.6/100,000 persons among residents of low-incidence states.

Seasonality

Most (57.8%) LD diagnoses occurred during May–August, but most (72.6%) LD surveillance cases had onset during the summer months (Table; Appendix Figure 4). Compared with Medicare data, the peak in surveillance cases was more prominent for all regions. In addition, a larger proportion of LD diagnoses occurred in winter months among residents of low-incidence areas (Figure 1).

Sex Distribution

Most (56.1%) LD diagnoses occurred among men; slightly more (60.4%) men were represented in surveillance cases. The median annual incidence of LD diagnoses among male Medicare beneficiaries was 134.3 diagnoses/100,000 person-years (range 131.6–160.5 diagnoses/100,000 person-years); median annual incidence of LD diagnoses among female beneficiaries was 109.5 diagnoses/100,000 person-years (range 103.3–125.7 diagnoses/100,000 person-years). In comparison, according to surveillance data, median annual incidence among men was 19.6 cases/100,000 persons (range 17.8–22.5/100,000 persons), and median annual incidence among women was 13.2 cases/100,000 persons (range 12.3–14.9/100,000 persons).

Age and Sex by Region

In high-incidence states, men had the highest incidence of LD for all age groups in both Medicare and surveillance data (Figure 2). In neighboring states, according to Medicare data, women had a slightly

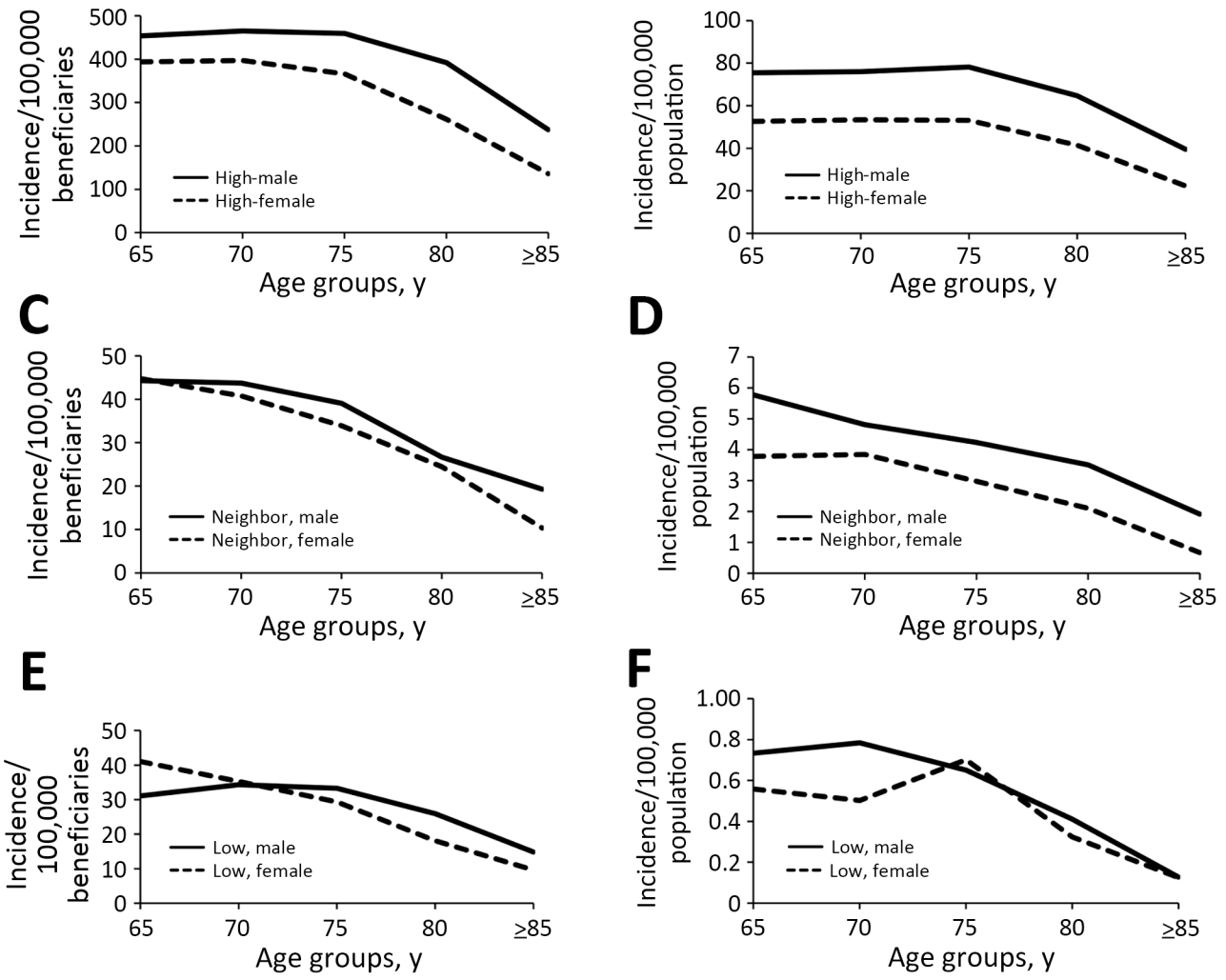

Figure 2. Lyme disease incidence for older adults, United States, 2016–2019. Results according to age group, sex, and geographic category of Lyme disease endemicity based on Medicare fee-for-service beneficiary data (A, C, F) and from US surveillance data (B, D, F). A, B) Disease incidence for men and women in high-incidence states. C, D) Disease incidence for men and women in neighboring states. E, F) Disease incidence for men and women in low-incidence states. Incidence calculated as diagnoses/100,000 beneficiaries in Medicare fee-for-service plans or cases/100,000 population among each subcategory. Scales for each y-axis differ substantially to underscore overall age-related incidence patterns but do not permit direct comparison of the magnitude of Lyme disease between systems or geographic categories.

higher incidence than men in only 1 age group (65–69 years), whereas according to surveillance data men had a higher incidence of LD across all age groups. In low-incidence states, according to Medicare data, women had a slightly higher incidence than men in 1 age group (65–69 years); in surveillance data,

Table. Characteristics of Lyme disease diagnoses according to Medicare fee-for-service claims data versus cases identified by national surveillance in a population of persons ≥65 years of age, United States, 2016–2019*

	High-incidence states		Neighboring states		Low-incidence states	
Characteristic	Medicare	Surveillance	Medicare	Surveillance	Medicare	Surveillance
Person-years	72,298	NA	5,958	NA	10,009	NA
Diagnoses or cases, no.	72,455	31,879	5,978	1,714	10,052	590
Diagnoses or cases, %	81.9	93.3	6.7	5.0	11.3	1.7
Incidence among men	422.9	71.0	38.3	4.6	30.1	0.6
Incidence among women	321.3	46.6	33.4	3.0	29.2	0.5
Occurring in May–August, %	59.5	72.2	58.2	79.9	45.8	66.2
Median incidence, 2016–2019	346.9	57.1	35.3	3.6	29.4	0.6
(range)	(337.2–417.8)	(52.9–65.6)	(27.9–36.6)	(2.4–5.3)	(27.7–31.6)	(0.5–0.6)

*Incidence calculated as diagnoses/100,000 person-years in Medicare fee-for-service or cases/100,000 population among each surveillance subcategory. NA, not applicable.

women had a higher incidence than men in a single age group (75–79 years).

Conclusions

Among persons ≥65 years of age, epidemiologic trends for sex, age, and region are similar for Medicare diagnoses and cases identified through public health surveillance. Nevertheless, overall diagnoses per person-year are ≈7-fold higher than for LD incidence in surveillance data. Those findings align with findings reported in our previous claims analysis (*3*). Seasonality of LD differed somewhat by region when comparing Medicare FFS and surveillance data: high-incidence states and neighboring states exhibited similar patterns for diagnoses and surveillance cases, but low-incidence states demonstrated a more muted peak for LD diagnoses in summer. Those findings also aligned with past claims analyses (*2*,*3*).

Some differences exist between this study and previous claims analyses (*2*,*3*). Within the Medicare population, men had a higher incidence of LD compared with women in all age groups in the high-incidence and neighboring states. In past claims analyses, male incidence was higher in children (both regions) and older adults (high-incidence states). Overdiagnosis of LD has been previously reported (*6*–*9*) and may contribute to some of those differences.

We used methods similar to past claims analyses to identify LD diagnoses (*2*,*3*); those stated limitations also apply here. However, the source from which our present data are derived is different from past analyses, and its representativeness is a strength. Nearly all adults ≥65 years of age enroll in either the Medicare FFS program or the Medicare Advantage program, making Medicare FFS a reliable and consistent, though still incomplete, source of data for most US citizens in this age group. We noted some differences between the Medicare FFS population and the Census population regarding race, ethnicity, and sex, but differences were small and did not fluctuate over the study period.

In conclusion, we found that LD diagnoses identified from the Medicare FFS databases exhibit similar patterns to those of surveillance data, and that most diagnoses occur among residents of high-incidence states, in summer months, and among male beneficiaries. These findings, combined with data gathered in similar analyses, add insight into LD patterns that are unique to this older population in the United States.

About the Author

Ms. Schwartz is an epidemiologist and is currently pursuing a PhD at University of Iowa, Iowa City, Iowa, USA. Her primary research interests are the epidemiology and prevention of vector-borne infections.

References

1. Schwartz AM, Hinckley AF, Mead PS, Hook SA, Kugeler KJ. Surveillance for Lyme disease—United States, 2008–2015. MMWR Surveill Summ. 2017;66:1–12. https://doi.org/10.15585/mmwr.ss6622a1
2. Nelson CA, Saha S, Kugeler KJ, Delorey MJ, Shankar MB, Hinckley AF, et al. Incidence of clinician-diagnosed Lyme disease, United States, 2005–2010. Emerg Infect Dis. 2015;21:1625–31. https://doi.org/10.3201/eid2109.150417
3. Schwartz AM, Kugeler KJ, Nelson CA, Marx GE, Hinckley AF. Use of commercial claims data for evaluating trends in Lyme disease diagnoses, United States, 2010–2018. Emerg Infect Dis. 2021;27:499–507. https://doi.org/10.3201/eid2702.202728
4. US Census Bureau. 2019 Census demographic profile summary file. 2020 [cited 2021 Dec 7]. https://www.census.gov/newsroom/press-kits/2020/population-estimates-detailed.html
5. Centers for Disease Control and Prevention. National Notifiable Diseases System: Lyme disease (*Borrelia burgdorferi*) [cited 2022 Dec 19]. https://ndc.services.cdc.gov/conditions/lyme-disease
6. Kobayashi T, Higgins Y, Samuels R, Moaven A, Sanyal A, Yenokyan G, et al. Misdiagnosis of Lyme disease with unnecessary antimicrobial treatment characterizes patients referred to an academic infectious diseases clinic. Open Forum Inf Dis. 2019;6:ofz299. https://doi.org/10.1093/ofid/ofz299
7. Kobayashi T, Higgins Y, Melia MT, Auwaerter PG. Mistaken identity: many diagnoses are frequently misattributed to Lyme disease. Am J Med. 2022;135:503–511.e5. https://doi.org/10.1016/j.amjmed.2021.10.040
8. Rose CDFP, Fawcett PT, Gibney KM, Doughty RA. The overdiagnosis of Lyme disease in children residing in an endemic area. Clin Pediatr (Phila). 1994;33:663–8. https://doi.org/10.1177/000992289403301105
9. Sigal LH. Summary of the first 100 patients seen at a Lyme disease referral center. Am J Med. 1990;88:577–81. https://doi.org/10.1016/0002-9343(90)90520-N

Address for correspondence: Alison F. Hinckley, Centers for Disease Control and Prevention, 3156 Rampart Rd, Fort Collins, CO, 80521, USA; email: cue0@cdc.gov

Zoonotic *Mansonella ozzardi* in Raccoons, Costa Rica, 2019–2022

Joban Quesada, Paula Alfaro-Segura, Alberto Solano-Barquero, Karen Vega, Ernesto Rojas-Sánchez, Mauricio Jiménez, Alicia Rojas

Mansonella ozzardi, a filarioid parasite, causes human mansonellosis in the Americas. We identified raccoons (*Procyon lotor*) as wildlife reservoirs of *M. ozzardi* in Costa Rica. Noting the sympatry of free-ranging raccoons and humans, we conclude that mansonellosis is a considerable public health risk in the region.

Mansonella ozzardi is a nematode belonging to the family Onchocercidae and the etiologic agent of human mansonellosis in the Caribbean and Central and South America (*1*). *M. ozzardi* adult worms infect subcutaneous tissues of humans and release their microfilariae into the blood, which can be ingested by biting midges or ceratopogonids that, once infected, can then transmit the parasite (*2*). Human mansonellosis is usually asymptomatic, but researchers have reported fever, joint pain, headache, lower-limb chills, cutaneous rashes, and keratitis (*2*). Although humans are known to be the only natural, definitive hosts of the parasite, a study submitting patas monkeys (*Erythrocebus patas*) to experimental infection with *M. ozzardi* (*3*) suggested the possible presence of wild reservoirs.

Raccoons act as reservoirs for an assortment of zoonotic pathogens, including *Baylisascaris procyonis*. Procyonids have expanded their geographic range into urban areas because of forest fragmentation and loss of their sylvatic habitat (*4*), leading to increased contact with humans. The only *Mansonella* spp. reported in raccoons were *Mansonella llewellyni* parasites, detected in blood samples from the United States (*5*).

Author affiliations: University of Costa Rica, San José, Costa Rica (J. Quesada, P. Alfaro-Segura, A. Solano-Barquero, A. Rojas); National University of Costa Rica Hospital for Minor and Wild Species, Heredia, Costa Rica (K. Vega, E. Rojas-Sánchez, M. Jiménez)

DOI: http://doi.org/10.3201/eid3009.231415

The Study

We analyzed the internal transcribed spacer 1 (ITS1) and 12S loci of circulating microfilariae collected from blood samples of raccoons in Manuel Antonio National Park (Quepos, province of Puntarenas) and surrounding areas in Costa Rica. Raccoons were captured for routine health evaluation during 2019–2022. Wildlife specialists captured raccoons by using Tomahawk traps in areas where local persons and park rangers reported a high frequency of raccoons. Researchers then sedated the raccoons and collected blood samples. Sample collection, procedures, and analyses were approved under permits R-CM-UNA-005–2021-OT-CONAGEBIO and SINAC-PNI-ACOPAC-021–2019. Laboratory technicians stored the blood at 4°C prior to subsequent analysis. Raccoons were released once they fully recovered from the anesthesia.

We performed microscopic assessment of all blood samples by using the Knott modified technique (Appendix, https://wwwnc.cdc.gov/EID/article/30/9/23-1415-App1.pdf). We then extracted DNA from blood samples by using the DNeasy Blood and Tissue Kit (QIAGEN, https://www.qiagen.com), according to the manufacturer's instructions. We then amplified mitochondrial 12S rRNA by using 12S.C345.F and 12S.C345R primers (*6*) and amplified the nuclear ITS1 loci with rDNA2 and rDNA158S primers (*7*). All reactions included *Toxocara canis* DNA as a positive control and a nontemplate control with PCR-grade water. We examined obtained amplicons on 1.5% agarose gels, purified positive reactions with Exo-SAP, and sequenced in both directions according to the Sanger method using the ABI 3730xl System (Macrogen Inc., https://dna.macrogen.com).

We used MEGA 7.0 software (https://www.megasoftware.net) to inspect and trim ITS1 sequences and aligned our sequences with other *Mansonella* spp.

sequences available in GenBank by using the MUSCLE algorithm. We constructed a Bayesian inference tree by using the BEAST package (https://beast.community) and drew a Templeton Crandall-Sing haplotype network. Finally, we calculated Nei's genetic distance for the ITS1 sequences (Appendix).

We observed microfilariae in 23.5% (4/17) of the raccoon blood samples in concentrations ranging 200–800 microfilariae/mL (Table). We noted the morphology of the observed microfilariae to be compatible with *M. ozzardi* original descriptions: 180–190 μm long and 3–4 μm wide; no sheath; tail elongated and slender without nuclei (Appendix) (*8*).

DNA could be isolated from 17 blood samples. In molecular analyses, 3 of 4 raccoons scoring positive at Knott's test also demonstrated positive PCR tests, and 4 of 7 raccoons that tested negative at Knott's test drew positive results by ITS-1 and 12S PCRs. Five of the 17 blood samples tested positive in the ITS1 PCR, and 4 of the 17 samples tested positive in the 12S PCR (Table). ITS1 sequences obtained from our analyses were 397–441-bp long and 97.0%–99.1% similar, with 100% of coverage with *M. ozzardi* isolated from humans in Brazil (GenBank accession no. MN432519). The 12S sequences were 107–151-bp long and 97.1%–99.1% similar to *M. ozzardi* from Brazil (GenBank accession no. LT623914.1). We deposited our new sequences into GenBank (accession nos. OR636492–6 for ITS1 and OR700019–22 for 12S).

Mansonella spp. clustered according to the nominal species in the ITS1 phylogenetic tree. Moreover, the *M. ozzardi* sequences we generated clustered in a separate clade in the BI tree, haplotype network and Nei's genetic distance principal component analysis. The haplotype network revealed 6 *M. ozzardi* haplotypes: 1 from Costa Rica, 2 from Japan, 2 from Brazil, and 1 from Argentina (Figure).

M. ozzardi is a filarioid nematode affecting humans in the Americas. Human mansonellosis is not completely harmless, and ocular impairment has been reported in humans from Panama (*9*). The lack of specific symptoms associated with mansonellosis usually leads to underdiagnosed infections and inadequate treatment (*10*). Accurate and prompt detection of the disease is therefore critical to avoid complications.

In our study, as in prior reports, PCR provided higher sensitivity compared with microscopic methods because molecular tools target DNA sequences rather than whole parasitic structures (*11*,*12*). Our results were as expected except for 1 sample determined to be positive by Knott's test and negative in PCRs, possibly due to a prolonged period at room temperature that might have affected DNA quality. We attempted amplification of larger fragments of other genes but failed due to the presence of fragmented DNA.

Our findings suggest that raccoons are potential definitive hosts of *M. ozzardi*. Confirming the role of these procyonids in the life cycle of this worm, however, requires investigation into the anatomic location of adult worms inside the animals, the reservoir capacity of raccoons, and the feeding preference of intermediate hosts to raccoons. The *Simulium sanguineum* black fly, found in Panama, is the only simulid species reported thus far in Central America to act as intermediate host of *M. ozzardi*, but this simulid has not been reported in Costa Rica (*13*). Nevertheless, other *Simulium* spp. flies have been detected in this country, suggesting a need for more research to track infection status of such species and to determine the potential intermediate hosts used by *M. ozzardi* in Costa Rica.

Sympatry of raccoons and humans in densely populated regions has become a public health problem that can increase pathogen spillover to humans (*14*). Costa Rica is not the only country facing the expansion of raccoon populations into urban areas, largely due to human invasion of wildlife habitats resulting in ecosystem fragmentation. Several countries in Europe have reported a rise in the number and geographic range of racoons into human-inhabited environments.

Table. Molecular and microscopic findings of *Mansonella ozzardi* in raccoons (*Procyon lotor*) from Manuel Antonio National Park and surroundings, Costa Rica, 2019–2022*

Sample identification	Sex of host	ITS1 loci results	12S rRNA gene results	Knott's test results, microfilariae/mL
1P	F	Negative	Negative	200
2CP	F	LQS	97% ID, 95% QC†	600
MP11	M	99.02% ID, 100% QC‡	99.02% ID, 100% QC†	Negative
MP12	M	99.1% ID, 100% QC‡	LQS	Negative
MP14	M	97.02% ID, 100% QC‡	LQS	800
MP16	M	Negative	98.68% ID, 100% QC†	400
MP17	M	97.37% ID, 100% QC‡	97.52% ID, 100% QC†	Negative
MP18	M	98.27% ID, 100% QC‡	LQS	Negative

*ID, percentage of identity; ITS, internal transcribed tracer; LQS, low-quality sequence; QC, query coverage.
†When compared with 12S sequence from Brazil (GenBank accession no. LT623914).
‡When compared with ITS1 sequence from Brazil (GenBank accession no. MN432519).

This expansion may increase pathogen spillover and the transmission of perilous diseases or parasites, such as *M. ozzardi*, to both domestic animals and humans (*15*). In Costa Rica, raccoons are reservoirs and carriers of such pathogens as *Salmonella* (*14*) and *B. procyonis*, one of the causing agents of visceral larva migrans (*4*). The encroachment of raccoons into urban areas thus represents a patent zoonotic risk (*4*,*14*).

Conclusions

Because our findings implicate raccoons as potential reservoirs of the *M. ozzardi* parasite, and given the

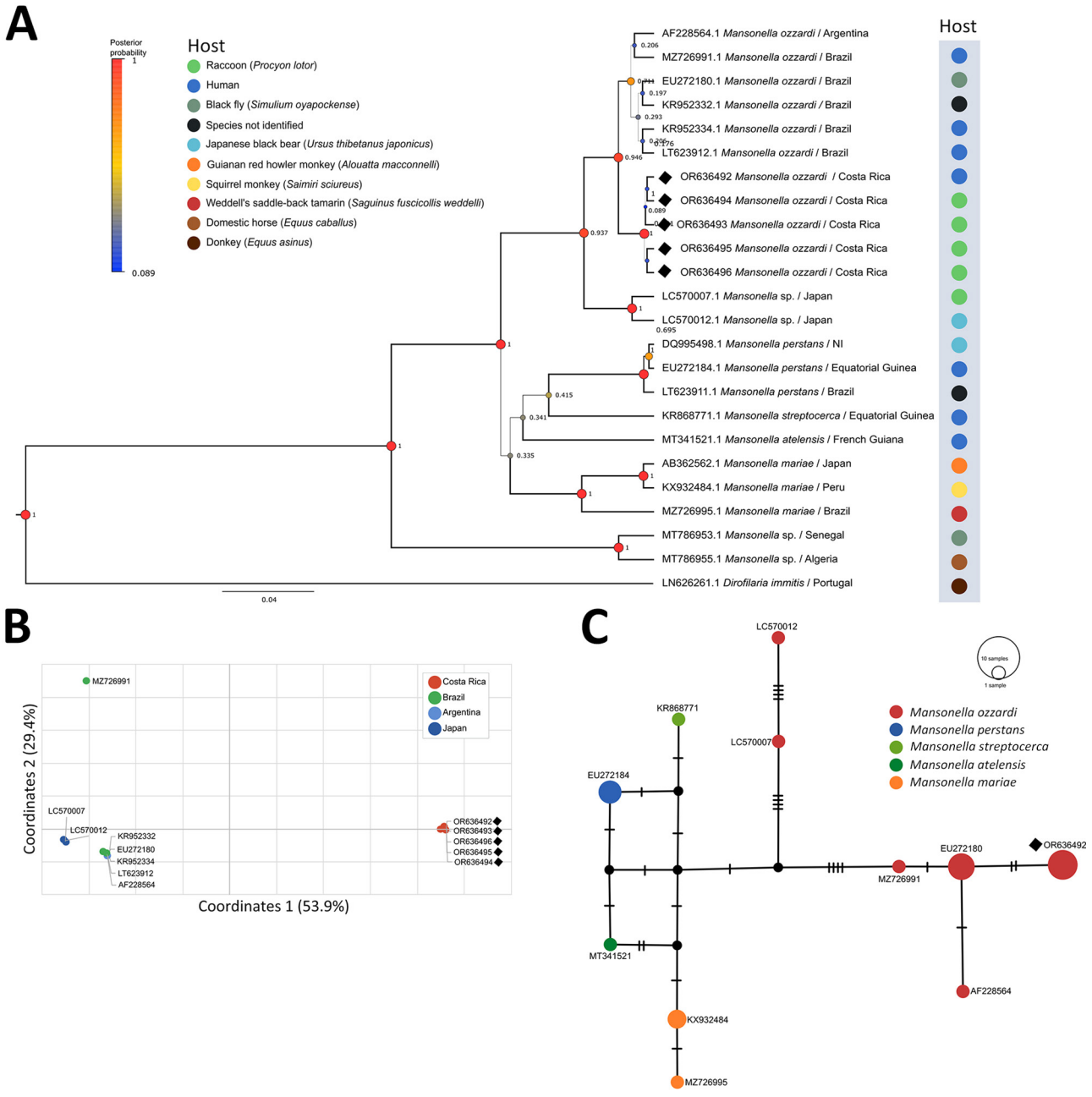

Figure. Phylogenetic and haplotypic analysis of *Mansonella ozzardi* ITS1 sequences obtained from racoons (*Procyon lotor*) in Costa Rica, 2019–2022 (black diamonds). A) Bayesian inference phylogenetic tree of *Mansonella* spp. based on the Hasegawa-Kishino-Yano with gamma distribution model. Line thickness and node size are proportional to posterior probability values. B) Principal component analysis of Nei's genetic distance of *M. ozzardi* sequences from different geographic locations. C) Templeton Crandall Sing haplotype network of *Mansonella* spp. sequences. Black circles indicate hypothetical haplotypes; hatchmarks indicate mutational steps between haplotypes. GenBank accession numbers are shown for all sequences.

scarcity of information on intermediate hosts, we recommend active surveillance of *M. ozzardi* infections in humans. Our findings also support the need for histopathological studies to determine the location of adult *M. ozzardi* parasites in infected procyonids and further investigation into possible intermediate hosts and their feeding preferences to *P. lotor*. Such investigations will be crucial to providing a full understanding of the lifecycle of *M. ozzardi* in Costa Rica.

About the Author

Mr. Quesada is a microbiology student and a research assistant at the Centro de Investigación en Enfermedades Tropicales in the University of Costa Rica. His interests include tropical medicine, protozoa, and helminth parasites of human and veterinary importance and flaviviruses associated with ticks.

References

1. Shelley AJ, Coscarón S. Simuliid blackflies (Diptera: Simuliidae) and ceratopogonid midges (Diptera: Ceratopogonidae) as vectors of *Mansonella ozzardi* (Nematoda: Onchocercidae) in northern Argentina. Mem Inst Oswaldo Cruz. 2001;96:451–8. https://doi.org/10.1590/S0074-02762001000400003
2. Lima NF, Veggiani Aybar CA, Dantur Juri MJ, Ferreira MU. *Mansonella ozzardi*: a neglected New World filarial nematode. Pathog Glob Health. 2016;110:97–107. https://doi.org/10.1080/20477724.2016.1190544
3. Orihel TC, Lowrie RC Jr, Eberhard ML, Raccurt C, Kozek WJ, Tidwell MA, et al. Susceptibility of laboratory primates to infection with *Mansonella ozzardi* from man. Am J Trop Med Hyg. 1981;30:790–4. https://doi.org/10.4269/ajtmh.1981.30.790
4. Baldi M, Alvarado G, Smith S, Santoro M, Bolaños N, Jiménez C, et al. *Baylisascaris procyonis* parasites in raccoons, Costa Rica, 2014. Emerg Infect Dis. 2016;22:1502–3. https://doi.org/10.3201/eid2208.151627
5. Rabinowitz AR, Patton S, Major V. Microfilariae of *Tetrapetalonema llewellyni* in raccoons of Cades Cove, Great Smoky Mountains National Park, Tennessee, USA. J Wildl Dis. 1985;21:449–50. https://doi.org/10.7589/0090-3558-21.4.449
6. Chan AHE, Chaisiri K, Morand S, Saralamba N, Thaenkham U. Evaluation and utility of mitochondrial ribosomal genes for molecular systematics of parasitic nematodes. Parasit Vectors. 2020;13:364. https://doi.org/10.1186/s13071-020-04242-8
7. Rojas A, Dvir E, Farkas R, Sarma K, Borthakur S, Jabbar A, et al. Phylogenetic analysis of *Spirocerca lupi* and *Spirocerca vulpis* reveal high genetic diversity and intra-individual variation. Parasit Vectors. 2018;11:639. https://doi.org/10.1186/s13071-018-3202-0
8. Ash LR, Orihel TC. Parasites: a guide to laboratory procedures and identification. Chicago: American Society of Clinical Pathologists Press; 1987.
9. Vianna LM, Martins M, Cohen MJ, Cohen JM, Belfort R Jr. *Mansonella ozzardi* corneal lesions in the Amazon: a cross-sectional study. BMJ Open. 2012;2:e001266. https://doi.org/10.1136/bmjopen-2012-001266
10. Dahmer KJ, Palma-Cuero M, Ciuoderis K, Patiño C, Roitman S, Li Z, et al. Molecular surveillance detects high prevalence of the neglected parasite *Mansonella ozzardi* in the Colombian Amazon. J Infect Dis. 2023;228:1441–51. https://doi.org/10.1093/infdis/jiad331
11. Morales-Hojas R, Post RJ, Shelley AJ, Maia-Herzog M, Coscarón S, Cheke RA. Characterisation of nuclear ribosomal DNA sequences from *Onchocerca volvulus* and *Mansonella ozzardi* (Nematoda: Filarioidea) and development of a PCR-based method for their detection in skin biopsies. Int J Parasitol. 2001;31:169–77. https://doi.org/10.1016/S0020-7519(00)00156-9
12. Adami YL, Rodrigues G, Alves MC, Moraes MA, Banic DM, Maia-Herzog M. New records of *Mansonella ozzardi*: a parasite that is spreading from the state of Amazonas to previously uninfected areas of the state of Acre in the Purus River region. Mem Inst Oswaldo Cruz. 2014;109:87–92. https://doi.org/10.1590/0074-0276130243
13. Petersen JL, Bawden MP, Wignall FS, Latorre CR, Johnson CM, Miranda CR. *Mansonella ozzardi* in Darién (Panama) [in Spanish]. Rev Med Panama. 1984;9:236–46.
14. Baldi M, Barquero Calvo E, Hutter SE, Walzer C. Salmonellosis detection and evidence of antibiotic resistance in an urban raccoon population in a highly populated area, Costa Rica. Zoonoses Public Health. 2019;66:852–60. https://doi.org/10.1111/zph.12635
15. Beltrán-Beck B, García FJ, Gortázar C. Raccoons in Europe: disease hazards due to the establishment of an invasive species. Eur J Wildl Res. 2012;58(1):5–15. https://doi.org/10.1007/s10344-011-0600-4

Address for correspondence: Alicia Rojas, Faculty of Microbiology, University of Costa Rica, Sede Rodrigo Facio Brenes, Montes de Oca, San José 11501-2060, Costa Rica; email: anaalicia.rojas@ucr.ac.cr

Autochthonous Human Babesiosis Caused by *Babesia venatorum*, the Netherlands

Niekie Spoorenberg,[1] Clara F. Köhler,[1] Evelien Vermeulen,[1] Suzanne Jurriaans, Marion Cornelissen, Kristina E.M. Persson, Iris van Doorn, Hein Sprong, Joppe W. Hovius, Rens Zonneveld

Severe babesiosis with 9.8% parasitemia was diagnosed in a patient in the Netherlands who had previously undergone splenectomy. We confirmed *Babesia venatorum* using PCR and sequencing. *B. venatorum* was also the most prevalent species in *Ixodes ricinus* ticks collected around the patient's home. Our findings warrant awareness for severe babesiosis in similar patients.

Human babesiosis is a tickborne disease caused by protozoans that infect red blood cells. Immunocompromised persons and those who have undergone splenectomies are at risk for severe illness (*1*). Most confirmed cases of babesiosis in Europe have been in such patients and have most frequently been *Babesia divergens* infections (*1*). In the Netherlands, DNA of *Babesia* species have previously been reported in *Ixodes ricinus* ticks, blood of animals, and in several human samples (*2*–*4*). However, reports of autochthonous human babesiosis in the Netherlands are lacking. We report a case of autochthonous human babesiosis in the Netherlands, as well as data on *Babesia* DNA in ticks collected near the patient's home. Handling of data and patient samples was performed according to the highest ethics standards. Informed consent was received from the patient.

Author affiliations: Amsterdam University Medical Center, University of Amsterdam, Amsterdam, the Netherlands (N. Spoorenberg, E. Vermeulen, S. Jurriaans, M. Cornelissen, I. van Doorn, J.W. Hovius, R. Zonneveld); Amsterdam Institute for Immunology & Infectious Diseases, Amsterdam (N. Spoorenberg, S. Jurriaans, M. Cornelissen, J.W. Hovius, R. Zonneveld); Centre for Infectious Disease Control, National Institute for Public Health and the Environment (RIVM), Bilthoven, the Netherlands (C.F. Köhler, H. Sprong); Lund University, Lund, Sweden (K.E.M. Persson); Skåne University Hospital, Lund (K.E.M. Persson)

DOI: https://doi.org/10.3201/eid3009.240556

The Study

In September 2023, a 69-year-old man was admitted to the hospital with fever (38°C), malaise, macroscopic hematuria, and laboratory results indicative of acute hemolysis. His medical history reported Hodgkin disease stage 3A in 1977, which went into remission after splenectomy and mantle field radiotherapy, and a diffuse large B-cell lymphoma in 2015, also in remission after being treated with 6 cycles of chemotherapy treatment. Several months before this hospitalization, chronic inflammatory demyelinating polyneuropathy had been diagnosed, and he was treated with immunoglobulins, plasma exchange, and dexamethasone pulse therapy.

At the hospital, microscopy on peripheral blood smears revealed red blood cell inclusion bodies. The patient did not report recent travel to malaria-endemic areas but recalled a tick bite that occurred 2 months before near his home. Additional microscopy showed parasites with morphologic features that resembled *Babesia* spp.; 9.8% of red blood cells were infected (Figure 1). Immediately after admission, a red blood cell exchange transfusion and intravenous treatment with clindamycin and quinine reduced parasitemia to <1%. Treatment was switched to oral azithromycin and atovaquone. After 14 days, parasites were no longer detectable with microscopy. *Babesia* DNA remained detectable despite treatment until 4 months after admission. After proguanil was added to the treatment regimen, *Babesia* DNA disappeared the next week. Oral treatment was discontinued approximately 6 weeks later. No relapse of babesiosis has occurred, despite reinitiation of immunosuppressive drugs (Figure 2).

We visualized parasites using fluorescence microscopy on acridine-stained blood in quantitative buffy coat capillaries and conventional microscopy

[1]These authors contributed equally to this article.

on Giemsa-stained thick and thin smears (Figure 1). Results of histidine-rich protein 2 and aldolase antigen testing (Biozek, https://www.biozek.com) and malaria loop-mediated isothermal amplification (Meridian Bioscience, https://www.meridianbioscience.com) were negative. A *Plasmodium* 18S ribosomal DNA PCR with known cross-reactivity with *Babesia* spp. was positive (*5*). Sanger sequencing of the ≈125 bp PCR amplicon revealed 100% homology with both *B. divergens* and *B. venatorum*. *Babesia* 18S ribosomal RNA (628 bp) amplification and sequencing showed 100% homology with *B. venatorum* (Figure 3, panel A) but not with *B. divergens*. Mitochondrial cytochrome oxidase subunit I (COI) amplification and sequencing showed 100% homology with *B. venatorum* from animals and ticks in the Netherlands (*3*). Species-specific PCRs for 4 *Babesia* spp. further confirmed the presence of *B. venatorum* DNA. A crude merozoite extract–based *B. divergens* ELISA showed optical densities slightly above the cutoff (*6*). Low titers might have resulted from continued plasmapheresis or poor cross-reactivity of antibodies against *B. venatorum* with *B. divergens* antigens.

To assess current and local risk of acquiring babesiosis, we collected questing ticks in 3 areas within 2–3.5 km of the patient's home using blanket dragging (*7*). We selected the areas on the basis of the presence of (wild) ungulates, which are amplifying hosts of *Babesia* sensu stricto (*3*). Roe deer were present in all areas. In addition, areas 1 and 2 were grazed by fallow deer (*Dama dama*), domestic cattle (*Bos taurus*), and Konik horses (*Equus caballus ferus*). Of note, in area 1, a small herd of European bison (*Bison bonasus*) was introduced in 2007.

We collected a total of 2,786 *I. ricinus* ticks. Ticks were tested in pools because prevalence of *Babesia* DNA in ticks in the Netherlands is very low (*3*). If a pool was positive, only 1 tick was considered positive in that pool. Overall, 25 (0.9%) ticks were infected with *Babesia* s.s. based on amplification of mitochondrial COI (Table). From those *Babesia*-positive ticks, we amplified DNA with *Babesia* species–specific PCRs, which were positive for *B. venatorum* (n = 20), *B. capreoli* (n = 4), and the European variant of *B. odocoilei* (n = 1). Phylogenetic analysis demonstrated that the *B. venatorum* COI sequence from the patient clustered with *B. venatorum* sequences from ticks collected near the patient's home (Figure 3, panel B). We calculated that 0.7% of ticks were infected with *B. venatorum*. The estimated incidence of tick bites in humans is 1.1 million/year, so human exposure to *B. venatorum* is ≈7,920 persons per year (*8*).

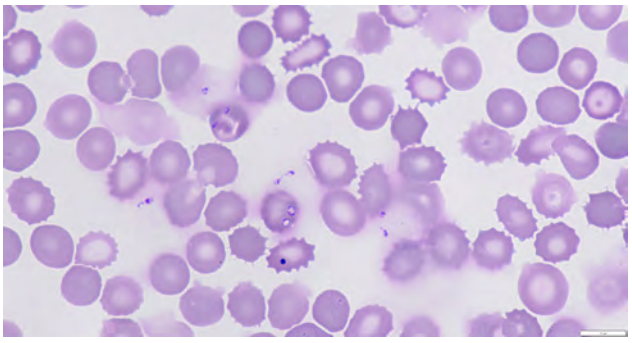

Figure 1. *Babesia venatorum* parasites in blood of patient with autochthonous human babesiosis, the Netherlands. Giemsa-stained thin smear from blood of patient before start of treatment and visualized with light microscopy (original magnification ×1,250) shows and pleomorphic amoeboid and vacuolar asexual stages of *Babesia* spp., positioned within and outside red blood cells, which is typically observed in human babesiosis. Of note, 1 dark blue–stained Howell-Jolly body is observed.

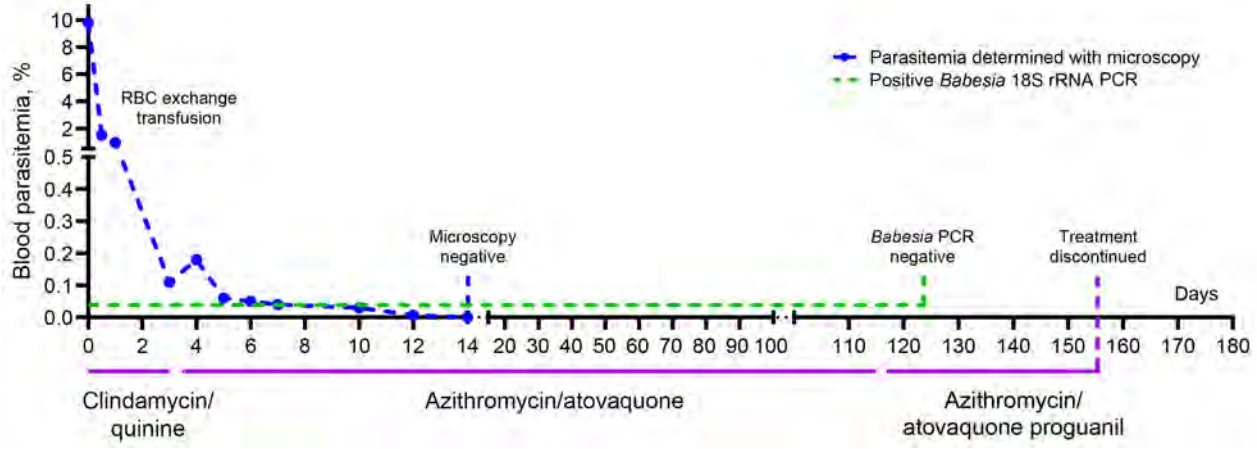

Figure 2. Clinical evolution of illness and treatment in case-patient with autochthonous human babesiosis caused by *Babesia venatorum*, the Netherlands. RBC, red blood cell.

Conclusions

This case of autochthonous human babesiosis concerned life-threatening disease in a highly susceptible patient who had a rare medical history of diffuse large B-cell lymphoma years after Hodgkin disease. He was presumably infected with *B. venatorum* after a tick bite. The clinical course was favorable after prompt therapy, and parasites were undetectable

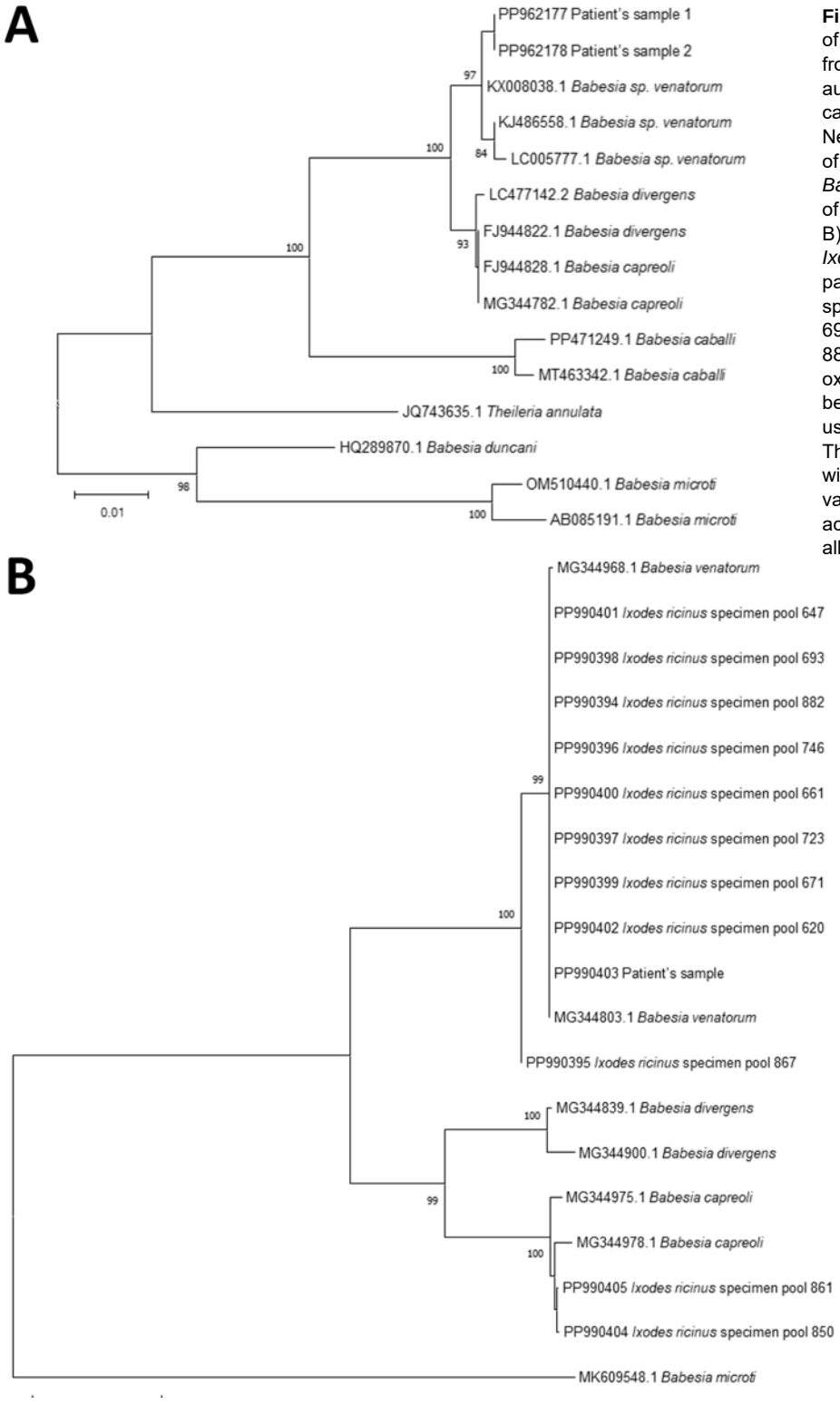

Figure 3. Phylogenetic analysis of *Babesia* sequences obtained from patient samples in study of autochthonous human babesiosis caused by *Babesia venatorum*, the Netherlands. A) Neighbor-joining tree of the phylogenetic relationship of *Babesia* species based on sequences of a fragment of 18S ribosomal RNA. B) *Babesia* sequences isolated from *Ixodes ricinus* ticks collected near the patient's residence (*Ixodes ricinus* specimen pool 620, 647, 661, 671, 693, 723, 746, 850, 861, 867, and 882), of a fragment of cytochrome oxidase subunit 1. The distance between sequences was calculated using the Kimura 2-parameter model. The bootstrap test was performed with 500 replicates. Bootstrap values >70 are displayed. GenBank accession numbers are provided for all sequences.

Table. *Babesia* sensu stricto species found in nymphal and adult *Ixodes ricinus* ticks in study of autochthonous human babesiosis caused by *Babesia venatorum*, the Netherlands*

Area	No. ticks tested	No. positive results (% total collected)			
		Babesia s.s.	*B. capreoli*	*B. odocoilei*	*B. venatorum*
1	982	4 (0.5)	None	None	4 (0.4)
2	1,126	10 (0.9)	4 (0.4)	1 (0.1)	5 (0.4)
3	678	11 (1.6)	None	None	11 (1.6)
Total	2,786	25 (0.9)	4 (0.1)	1 (0.04)	20 (0.7)

*Ticks were collected in 3 natural areas near the patient's residence. *Babesia* s.s. were identified to the species level by species-specific PCRs.

after 2 weeks. Persistent *Babesia* DNA disappeared after adding proguanil to the treatment regimen. Of all *Babesia* DNA found in local ticks, *B. venatorum* was most prevalent, indicating a higher chance of exposure to this species. This finding is notable because, in Europe, most described human babesiosis has been caused by *B. divergens*, much less frequently by *B. venatorum* or *B. microti* (*1*).

In the Netherlands, DNA of ≥8 *Babesia* spp. have been found in animals and ticks but not in humans (*2*–*4*). Positive serologic results in studies among blood donors and persons with increased tick bite exposure indicate that self-limiting and unnoticed infections might occur in the general population in Europe (*9*,*10*). However, further investigations in such populations did not report *Babesia* DNA as evidence for human babesiosis (*11*,*12*). Scarcity of cases might also be explained by lack of awareness and underdiagnosis or misdiagnosis. Indeed, in several published cases, diagnosis was delayed or made postmortem (*13*). The morphologic overlap between *Babesia* and *Plasmodium* spp. in microscopy is high, making sensitive and specific testing for malaria imperative to prevent misdiagnosis and associated treatment delays. Last, underdiagnosis might also be the result of the high proportion of human babesiosis that could occur after unnoticed bites from nymphal ticks.

Different *Babesia* spp. are specific to different animal reservoirs. Therefore, determining infecting *Babesia* spp. can help assign surveillance among ticks and specific animals. A previous study conducted in the Netherlands during 2000–2019 found a widespread occurrence of *B. venatorum* DNA in 0.8% of 25,849 sampled *I. ricinus* ticks (*3*). *B. venatorum* was present in 46% (n = 290) of sampled roe deer (*Capreolus capreolus*) and to a much lesser extent in sheep (*Ovis aries*). Roe deer are highly present in the areas investigated for this case report, and the patient had observed many around his home. Tick densities could have increased in recent decades and changes in wildlife management could have contributed to spread of *Babesia*-infected ticks (*14*). Those changes might have driven wildlife infected with *B. venatorum* into areas where the parasite was formerly absent. Unfortunately, we were not able to sample local ungulates to investigate *Babesia* spp. prevalence. Finally, climate change might affect spatial and temporal tick distribution and increase the risk for and prevalence of human babesiosis, which warrants further surveillance studies (*15*). Although it remains unclear which factors have driven this occurrence of human babesiosis, awareness among clinicians is warranted, especially for susceptible patients.

Acknowledgments

We thank Kimberly de Vries, Myrna Bouman, Leonie van Boetzelaer-Wittich, Ellen Wentink, Danielle Oude Velthuis, Carla Wassenaar, Chris van der Meer, and Leny Nieuwendijk for extensive microscopic analysis of all blood samples of the patient. The authors also thank Ankje de Vries, Manoj Fonville, Anna Rombouts, Amber van den Bron, Corine Nellestijn, Fion Brouwer, and Sophie van Tol for conducting fieldwork and Fokla Zorgdrager, Manoj Fonville, and Anne Wattimena for excellent detection and typing of *Babesia* spp. in the patient and in ticks. Finally, the authors thank Dieuwertje Hoornstra for delivering insights on unpublished prospective data on evidence of babesiosis in patients in the Netherlands and Gary Wormser for treatment advice.

About the Author

Dr. Spoorenberg is an infectious diseases specialist at the Amsterdam University Medical Center, including in the Multidisciplinary Lyme Borreliosis Center. Her primary research interests are centered around clinical management of infectious diseases.

References

1. Bajer A, Beck A, Beck R, Behnke JM, Dwużnik-Szarek D, Eichenberger RM, et al. Babesiosis in southeastern, central and northeastern Europe: an emerging and re-emerging tick-borne disease of humans and animals. Microorganisms. 2022;10:945. https://doi.org/10.3390/microorganisms10050945
2. Wielinga PR, Fonville M, Sprong H, Gaasenbeek C, Borgsteede F, van der Giessen JW. Persistent detection of Babesia EU1 and Babesia microti in *Ixodes ricinus* in the Netherlands during a 5-year surveillance: 2003–2007. Vector Borne Zoonotic Dis. 2009;9:119–22. https://doi.org/10.1089/vbz.2008.0047

3. Azagi T, Jaarsma RI, Docters van Leeuwen A, Fonville M, Maas M, Franssen FFJ, et al. Circulation of *Babesia* species and their exposure to humans through *Ixodes ricinus*. Pathogens. 2021;10:386. https://doi.org/10.3390/pathogens10040386
4. Jahfari S, Hofhuis A, Fonville M, van der Giessen J, van Pelt W, Sprong H. Molecular detection of tick-borne pathogens in humans with tick bites and erythema migrans, in the Netherlands. PLoS Negl Trop Dis. 2016;10:e0005042. https://doi.org/10.1371/journal.pntd.0005042
5. van Vugt M, Wetsteyn JC, Haverkort M, Kolader M, Verhaar N, Spanjaard L, et al. New England souvenirs. J Travel Med. 2011;18:425–6. https://doi.org/10.1111/j.1708-8305.2011.00562.x
6. Tijani MK, Svenson J, Adlerborn P, Danielsson L, Teleka A, Ljungqvist Lovmar M, et al. How to detect antibodies against *Babesia divergens* in human blood samples. Open Forum Infect Dis. 2024;11:ofae028.
7. Kohler CF, Sprong H, Fonville M, Esser H, De Boer WF, Van der Spek V, et al. Sand lizards (*Lacerta agilis*) decrease nymphal infection prevalence for tick-borne pathogens *Borrelia burgdorferi* sensu lato and *Anaplasma phagocytophilum* in a coastal dune ecosystem. J Appl Ecol. 2023;60:1115–26. https://doi.org/10.1111/1365-2664.14379
8. Hofhuis A, Harms M, van den Wijngaard C, Sprong H, van Pelt W. Continuing increase of tick bites and Lyme disease between 1994 and 2009. Ticks Tick Borne Dis. 2015;6:69–74. https://doi.org/10.1016/j.ttbdis.2014.09.006
9. Lempereur L, Shiels B, Heyman P, Moreau E, Saegerman C, Losson B, et al. A retrospective serological survey on human babesiosis in Belgium. Clin Microbiol Infect. 2015;21:96.e1–7. https://doi.org/10.1016/j.cmi.2014.07.004
10. Svensson J, Hunfeld KP, Persson KEM. High seroprevalence of *Babesia* antibodies among *Borrelia burgdorferi*-infected humans in Sweden. Ticks Tick Borne Dis. 2019;10:186–90. https://doi.org/10.1016/j.ttbdis.2018.10.007
11. Bloch EM, Siller A, Tonnetti L, Drews SJ, Spencer BR, Hedges D, et al. Molecular screening of blood donors for *Babesia* in Tyrol, Austria. Transfus Med Hemother. 2023;50:330–3. https://doi.org/10.1159/000528793
12. Hoornstra D, Harms MG, Gauw SA, Wagemakers A, Azagi T, Kremer K, et al. Ticking on Pandora's box: a prospective case-control study into 'other' tick-borne diseases. BMC Infect Dis. 2021;21:501. https://doi.org/10.1186/s12879-021-06190-9
13. Bläckberg J, Lazarevic VL, Hunfeld KP, Persson KEM. Low-virulent *Babesia venatorum* infection masquerading as hemophagocytic syndrome. Ann Hematol. 2018;97:731–3. https://doi.org/10.1007/s00277-017-3220-6
14. Sprong H, Hofhuis A, Gassner F, Takken W, Jacobs F, van Vliet AJ, et al. Circumstantial evidence for an increase in the total number and activity of *Borrelia*-infected *Ixodes ricinus* in the Netherlands. Parasit Vectors. 2012;5:294. https://doi.org/10.1186/1756-3305-5-294
15. Drews SJ, Kjemtrup AM, Krause PJ, Lambert G, Leiby DA, Lewin A, et al. Transfusion-transmitted *Babesia* spp.: a changing landscape of epidemiology, regulation, and risk mitigation. J Clin Microbiol. 2023;61:e0126822. https://doi.org/10.1128/jcm.01268-22

Address for correspondence: Rens Zonneveld, Department of Medical Microbiology and Infection Prevention, Amsterdam UMC, Meibergdreef 9, 1105 AZ, Amsterdam, the Netherlands; email: r.zonneveld@amsterdamumc.nl

Participatory, Virologic, and Wastewater Surveillance Data to Assess Underestimation of COVID-19 Incidence, Germany, 2020–2024

Anna Loenenbach,[1] Ann-Sophie Lehfeld,[1] Peter Puetz,[1] Barbara Biere,[1]
Susan Abunijela, Silke Buda, Michaela Diercke, Ralf Dürrwald, Timo Greiner, Walter Haas,
Maria Helmrich, Kerstin Prahm, Jakob Schumacher, Marianne Wedde, Udo Buchholz

Using participatory, virologic, and wastewater surveillance systems, we estimated when and to what extent reported data of adult COVID-19 cases underestimated COVID-19 incidence in Germany. We also examined how case underestimation evolved over time. Our findings highlight how community-based surveillance systems can complement official notification systems for respiratory disease dynamics.

To monitor COVID-19 epidemic spread, the World Health Organization tracked worldwide incidence by relying on notification data of laboratory-confirmed cases (*1*). In Germany, public health and social measures (PHSM), such as lockdowns and testing policies, were linked to COVID-19 incidence measured by the country's routine notifiable disease surveillance system, particularly in the first 1.5 years of the pandemic.

We examined how sensitively the national notifiable disease surveillance system reflected the true COVID-19 incidence in Germany. Our intent was to date and quantify changes in underestimation of national notifiable disease surveillance–derived COVID-19 incidence by relating it to participatory, virologic, and wastewater surveillance systems and to identify PHSM that contributed to changes in surveillance sensitivity.

The Study

Our indicator of interest was adult COVID-19 notification incidence in Germany, hereafter GNS-I (German notification system incidence), during 2020–2024. In the notification system, SARS-CoV-2–positive test results were notified to local health authorities, including samples taken from physician practices, citizen testing sites, and systematic testing in workplaces and schools. The system only reported PCR-positive cases; thus, non–PCR-confirmed citizen self-tests were not included in GNS-I data.

We used 2 comparison indicators to estimate COVID-19 incidence: GrippeWeb virologic positivity rate incidence (GW-VPR-I) and GrippeWeb self-reported positivity incidence (GW-SR-I) (Table). GW-VPR-I is incidence among adults calculated through combined data from the GrippeWeb participatory surveillance system (*1*) and from virologic sentinel surveillance in primary care settings (*2*), as described previously (*3*). GW-SR-I is self-reported laboratory or self-testing results from GrippeWeb.

Each week, ≈8,000 GrippeWeb participants in Germany self-report symptoms related to any kind of acute respiratory illness (ARI), which includes any illness with sore throat, cough, or fever. Participants also report potential test results. ARI are dichotomized into influenza-like illness (ILI; i.e., fever with sore throat or cough) and non-ILI. GrippeWeb provides ARI, ILI, and non-ILI incidence rates in the general population (*1*). The National Influenza Centre conducts virologic surveillance in cooperation with ≈140 practices (general and pediatric practices) that submit nasal or throat swab samples from ARI patients (*4*). Samples are analyzed by real-time PCR for different respiratory pathogens, including SARS-CoV-2.

Authors affiliation: Robert Koch Institute, Berlin, Germany

DOI: https://doi.org/10.3201/eid3009.240640

[1]These first authors contributed equally to this article.

Table. List of surveillance systems and indicators used for participatory, virologic, and wastewater surveillance data to assess underestimation of COVID-19 incidence, Germany, 2020–2024*

Abbreviations	Definition	Description and formulas
Surveillance systems		
GNS	German notification system	Mandatory notification system for infectious diseases according to German Infection Protection Act
GW	GrippeWeb	Participatory ILI and non-ILI online surveillance system for the general population, which began in 2011
VSS	Virological surveillance system	Established in primary care practices
WWS	Wastewater surveillance system	Monitors aggregated SARS-CoV-2 viral load in wastewater and began during calendar week 22 2022
Indicator		
GNS-I	German notification system incidence†	COVID-19 incidence reference indicator using data from GNS
GW-VPR-I	GrippeWeb and virologic positivity rate incidence†	COVID-19 incidence comparison indicator using data from GrippeWeb and VSS Formula: Weekly GW-VPR-I = GW ILI incidence × VSS SARS-CoV-2 positivity rate among ILI patients + GW non-ILI incidence × VSS SARS-CoV-2 positivity rate among non-ILI patients
GW-SR-I	GrippeWeb self-reported testing results†	COVID-19 incidence comparison indicator using GrippeWeb self-reported pathogen detection results for self-tested or laboratory-confirmed positive tests; data collection started in calendar week 27, 2022 Formula: COVID-19 incidence measured by GW-SR-I = weekly number of adult GW participants with any acute respiratory infection and a positive COVID-19 test ÷ weekly number of all reports of adults (ill or not ill)
SC2-VL-WW	Aggregated SARS-CoV-2 viral load in wastewater	COVID-19 comparison indicator using WWS system and expressed as the number of SARS-CoV-2 gene fragments per liter in wastewater
UEF	Underestimation factor	Two underestimation factors were calculated as an indicator to estimate the sensitivity of GNS-derived COVID-19 incidence with the help of GW and VSS surveillance data Formulas: $UEF_{GW\text{-}VPR\text{-}I}$ = COVID-19 incidence measured by GW-VPR-I ÷ COVID-19 incidence measured by GNS-I $UEF_{GW\text{-}SR\text{-}I}$ = COVID-19 incidence measured by GW-SR-I ÷ COVID-19 incidence measured by GNS-I

*ILI, influenza-like illness.
†COVID-19 incidence indicator.

To compare GNS-I with GW-VPR-I, we used incidence from calendar week (CW) 40 of 2020 through CW 4 of 2024 (CW40/2020–CW04/2024). To compare GNS-I with GW-SR-I, we included CW27/2022 (beginning of collection of self-reported SARS-CoV-2 detections in GrippeWeb) through CW04/2024. We smoothed GW-VPR-I and GW-SR-I data by using the locally estimated scatterplot smoothing (LOESS) method (*5*).

Beginning in CW22/2022, SARS-CoV-2 was monitored weekly by wastewater surveillance (WWS) in ≤153 wastewater treatment plants (*6*). Data were aggregated as SARS-CoV-2 viral load in wastewater (SC2-VL-WW). We also used LOESS to smooth weekly mean SC2-VL-WW data.

We used an underestimation factor (UEF) to express sensitivity of GNS-I by GW-VPR-I ($UEF_{GW\text{-}VPR\text{-}I}$) and GW-SR-I ($UEF_{GW\text{-}SR\text{-}I}$), which we calculated as the weekly ratio of smoothed GW-VPR-I and GW-SR-I relative to nonsmoothed GNS-I (Table; Figure). In addition, we gathered information on dates of pandemic related PHSM.

In general, measured COVID-19 incidence by GNS-I, GW-VPR-I, and GW-SR-I, as well as SC2-VL-WW, all agreed in timing of COVID-19 waves (Figure, panel A). GW-VPR-I was similar to the GNS-I until ≈CW17/2022, after which the 2 curves diverged. From CW27/2022, GW-SR-I aligned with GW-VPR-I. SC2-VL-WW confirmed the course of GW-VPR-I and GW-SR-I, which indicated that COVID-19 waves that peaked during CW26/2022, CW38/2022, and CW50/2022 were substantially stronger than suggested by GNS-I.

We identified 4 major sensitivity phases of GNS-I and estimated a segmented linear regression to specify 3 breakpoints (*7*,*8*). We calculated a common piecewise trendline of the smoothed $UEF_{GW\text{-}VPR\text{-}I}$ and $UEF_{GW\text{-}SR\text{-}I}$ data (Figure, panel B). During phase 1, CW40/2020–CW10/2022, the linear trend of $UEF_{GW\text{-}VPR\text{-}I}$ varied ≈1.1–1.5, indicating close agreement between GNS-I and GW-VPR-I. Two COVID-19 waves, driven by Omicron BA.1, peaking in CW05/2022, and BA.2, peaking in CW11/2022, were still well captured by GNS-I. During that time, many workplaces, hospitals, nursing homes, kindergartens, and schools tested regularly for SARS-CoV-2. However, during CW10/2022–CW17/2022, regular testing at workplaces and

schools was gradually discontinued. Until the end of phase 2 (CW49/2022), smoothed GW-VPR-I and GW-SR-I slowly increased to ≈2.8 ($UEF_{GW\text{-}VPR\text{-}I}$ was 2.7; $UEF_{GW\text{-}SR\text{-}I}$ was 2.9).

At the end of 2022, no-cost testing ceased for all citizens, after which we noted a steep increase of both smoothed UEFs during phase 3 (CW49/2022–CW28/2023): $UEF_{GW\text{-}VPR\text{-}I}$ increased from ≈2.7 to 110.1 and $UEF_{GW\text{-}SR\text{-}I}$ increased from 2.9 to 81.6 (Figure, panel B). SC2-VL-WW showed similar trends during that period, but GNS-I data barely captured the phase 3 waves.

Through a trend change in both UEFs, we identified a fourth phase starting around CW28/2023 that was not accompanied by PHSM changes. Smoothed $UEF_{GW\text{-}VPR\text{-}I}$ peaked around CW32/2023, then decreased to ≈30.3; $UEF_{GW\text{-}SR\text{-}I}$ peaked around CW28/2023, after which it fluctuated between ≈50–70. SC2-VL-WW followed the steady rise of the 2 GrippeWeb indicators and peaked in CW50/2023. GNS-I remained low in phase 4.

One limitation of our study is the incongruence among the indicators; GNS-I includes data for illnesses and asymptomatic infections, whereas GW-VPR-I and GW-SR-I only estimate illness incidence. However, because the information on presence or absence of symptoms is not always available in GNS-I data, deriving a pure COVID-19 incidence from GNS-I is not possible. Another limitation is that WWS provides viral load per liter from all population age groups, and neither incidence nor prevalence data are collected; whether the shedding properties of variants differ enough to substantially modify the viral load detected in wastewater is unknown. Last, the association of sensitivity phases and PHSM is only descriptive and ecologic in nature.

Conclusions

Assessing the timing and degree of COVID-19 underestimation is crucial for interpretating notification system data. Until the first half of 2022, serosurveys among blood donors in Germany estimated

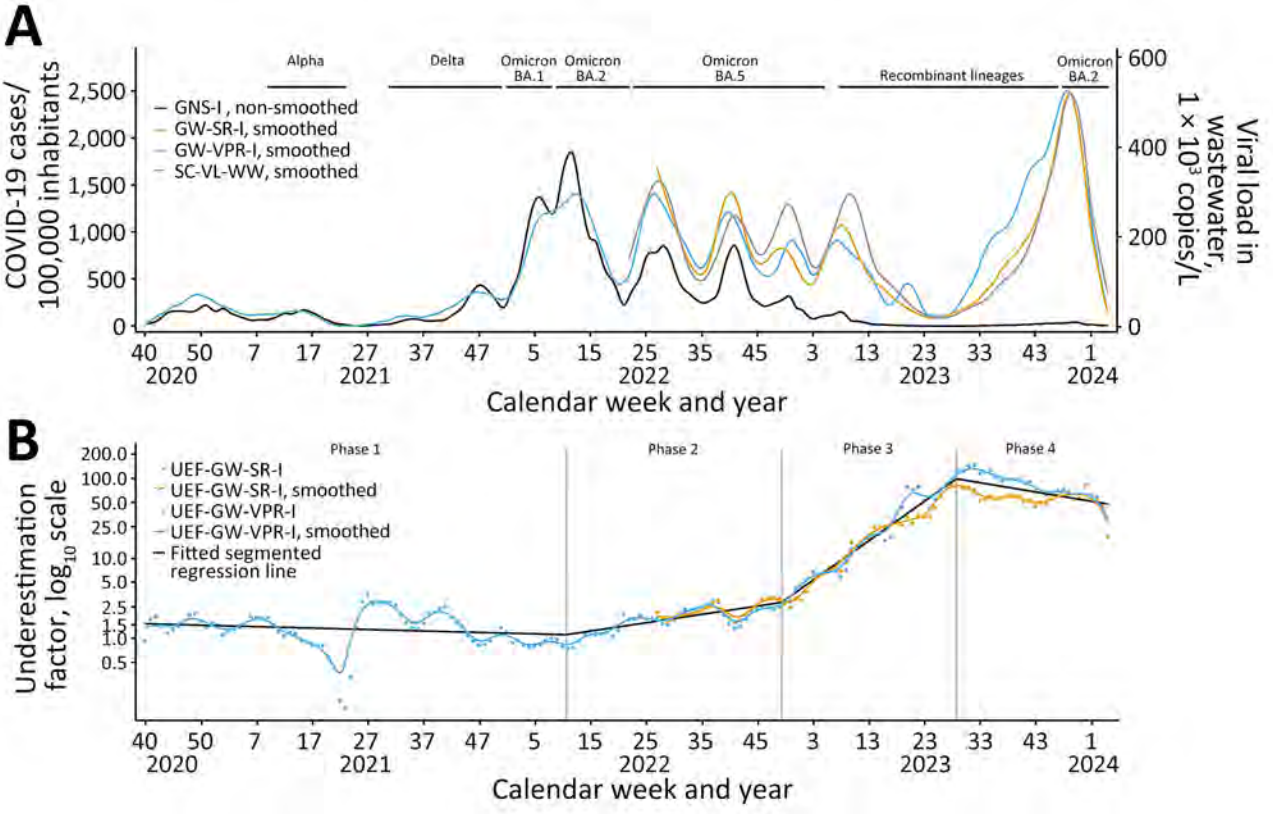

Figure. Incidence and underestimation factors in a study of participatory, virologic, and wastewater surveillance data to assess underestimation of COVID-19 incidence, Germany, 2020–2024. A) Smoothed and unsmoothed surveillance data on COVID-19 incidence (cases/100,000 adult population) compared with wastewater viral load. SARS-CoV-2 variant phases in Germany are labeled. B) Two different UEFs plus common piecewise trendline of smoothed UEF and timeframes for phases calendar week 40 of 2020 through calendar week 4 of 2024. Vertical lines mark the breakpoints between COVID-19 phases with different degrees of underestimation. GNS-I, incidence from German notification system; GW-SR-I, GrippeWeb self-reported incidence; GW-VPR-I, GrippeWeb and virologic positivity rate incidence; SC2-VL-WW, aggregated SARS-CoV-2 viral load in wastewater; UEF, underestimation factor.

the degree of underestimation at ≈1.5 of GNS-I, comparing well with the common piecewise trendline of $UEF_{GW\text{-}VPR\text{-}I}$ in the same timeframe ($UEF_{GW\text{-}SR\text{-}I}$ started from CW27/2022) (*9*). Other than cross-sectional serosurveys (*9*–*11*), approaches to estimate underestimation included analysis of fatality rates and death tolls (*12*,*13*), and a multiplier model that used reported laboratory-confirmed data as a starting point (*14*). However, none of those approaches compared weekly notification rates and, thus, cannot pinpoint sensitivity breakpoints. We compared weekly national notifiable COVID-19 incidence to 2 independent indicators estimating population-level incidence, and our findings are supported by WWS results.

We identified 2 major sensitivity breakpoints, demonstrating that PHSM introductions or cessations might have directly affected the changing sensitivity of notification data. Ending systematic testing in workplaces and schools (first breakpoint) and ending no-cost testing (second breakpoint) likely contributed to the decrease of national notifiable disease surveillance system sensitivity. The close agreement between WWS and GrippeWeb-derived incidence indicators suggests that SARS-CoV-2 wastewater data are useful for indicating trends in infection waves.

Although population-level immunity could influence the probability of persons testing COVID-19–positive to some degree, immunity mainly protects against severe disease but does not necessarily prevent infection or illness. For example, the high estimated COVID-19 incidence at the end of 2023 had weekly incidences of ≥2% (Figure).

As Germany transitioned from the pandemic to endemic phase and implemented a stepwise reduction in testing, GNS-I became less capable of reflecting actual COVID-19 incidence. Our study results stress the value of additional community-based and wastewater surveillance systems to complement official notification systems (*15*). Community-based surveillance can describe the epidemiologic situation, particularly when PHSM, such as testing policies, are lifted and testing access decreases. Thus, systems like GrippeWeb (and wastewater surveillance) will be increasingly crucial, especially for respiratory diseases of epidemic and pandemic potential.

Acknowledgments

We thank all participants who contributed to GrippeWeb, primary care sentinel physicians participating in the virologic sentinel, local health authorities for notification data, and wastewater facilities for providing data.

We thank all staff members of the acute respiratory infections team at the Respiratory Infections Unit at Robert Koch Institute, as well as all staff members at the National Influenza Centre. We thank Romy Kerber for providing detailed information on the different SARS-CoV-2 variant phases in Germany. We also thank the Federal Ministry of Health for funding wastewater surveillance by the project Abwassermonitoring für die epidemiologische Lagebewertung (AMELAG) until the end of 2024. Finally, we are indebted to Ulrike Braun, Marcus Lukas, and all wastewater treatment plants, laboratories, universities, and state authorities involved in the AMELAG project.

Data and code can be accessed at https://github.com/peterpuetz2020/extent_of_underestimation.

Author contributions: A.L., B.B., A.S.L., P.P., and U.B. conceptualized and designed the study; A.L., A.S.L., P.P., B.B., S.A., S.B., M.D., R.D., T.G., M.H., K.P., J.S., M.W., and U.B. performed data collection; A.L., A.S.L., P.P., M.H., and U.B. performed data analysis; A.L., A.S.L., P.P., B.B., S.A., S.B., M.D., R.D., T.G., W.H., M.H., K.P., J.S., M.W., and U.B. performed data interpretation; A.L. and U.B. prepared the original manuscript draft; A.L., A.S.L., P.P., M.H., and U.B. performed data analysis; A.L., A.S.L., P.P., B.B., S.A., S.B., M.D., R.D., T.G., W.H., M.H., K.P., J.S., M.W., and U.B. reviewed and revised the manuscript; and U.B. supervised the project.

About the Author

Dr. Loenenbach is a senior scientist at the Robert Koch Institute, Berlin, Germany. Her research interests include investigation of infectious disease outbreaks, general field epidemiology, and epidemiology of infectious respiratory diseases.

References

1. Bayer C, Remschmidt C, an der Heiden M, Tolksdorf K, Herzhoff M, Kaersten S, et al. Internet-based syndromic monitoring of acute respiratory illness in the general population of Germany, weeks 35/2011 to 34/2012. Euro Surveill. 2014;19:20684. https://doi.org/10.2807/1560-7917.ES2014.19.4.20684
2. Goerlitz L, Tolksdorf K, Buchholz U, Prahm K, Preuß U, An der Heiden M, et al. Monitoring of COVID-19 by extending existing surveillance for acute respiratory infections [in German]. Bundesgesundheitsblatt Gesundheitsforschung Gesundheitsschutz. 2021;64:395–402. https://doi.org/10.1007/s00103-021-03303-2
3. Buchholz U, Lehfeld AS, Tolksdorf K, Cai W, Reiche J, Biere B, et al. Respiratory infections in children and adolescents in Germany during the COVID-19 pandemic. J Health Monit. 2023;8:20–38.
4. Oh DY, Buda S, Biere B, Reiche J, Schlosser F, Duwe S, et al. Trends in respiratory virus circulation following COVID-19-targeted nonpharmaceutical interventions in Germany, January–September 2020: analysis of national

surveillance data. Lancet Reg Health Eur. 2021;6:100112. https://doi.org/10.1016/j.lanepe.2021.100112
5. Cleveland WS, Devlin SJ. Locally weighted regression: an approach to regression analysis by local fitting. J Am Stat Assoc. 1988;83:596–610. https://doi.org/10.1080/01621459.1988.10478639
6. Robert Koch Institute (RKI). Wastewater-based surveillance on SARS-CoV-2. AMELAG weekly report 2024 Feb 21 [cited 2024 Feb 23]. https://www.rki.de/EN/Content/Institute/DepartmentsUnits/InfDiseaseEpidem/Div32/WastewaterSurveillance/Report.html
7. Muggeo VM. Estimating regression models with unknown break-points. Stat Med. 2003;22:3055–71. https://doi.org/10.1002/sim.1545
8. Muggeo VM. Segmented: an R package to fit regression models with broken-line relationships. R News. 2008;8:20–5.
9. Bartig S, Beese F, Wachtler B, Grabka MM, Mercuri E, Schmid L, et al. Socioeconomic differences in SARS-CoV-2 infection and vaccination in Germany: a seroepidemiological study after one year of COVID-19 vaccination campaign. Int J Public Health. 2023;68:1606152. https://doi.org/10.3389/ijph.2023.1606152
10. Offergeld R, Preußel K, Zeiler T, Aurich K, Baumann-Baretti BI, Ciesek S, et al. Monitoring the SARS-CoV-2 pandemic: prevalence of antibodies in a large, repetitive cross-sectional study of blood donors in Germany—results from the SeBluCo Study 2020–2022. Pathogens. 2023;12:551. https://doi.org/10.3390/pathogens12040551
11. Skowronski DM, Kaweski SE, Irvine MA, Kim S, Chuang ESY, Sabaiduc S, et al. Serial cross-sectional estimation of vaccine-and infection-induced SARS-CoV-2 seroprevalence in British Columbia, Canada. CMAJ. 2022;194:E1599–609. https://doi.org/10.1503/cmaj.221335
12. McKenzie L, Shoukat A, Wong KO, Itahashi K, Yasuda E, Demarsh A, et al. Inferring the true number of SARS-CoV-2 infections in Japan. J Infect Chemother. 2022;28:1519–22. https://doi.org/10.1016/j.jiac.2022.08.002
13. Noh J, Danuser G. Estimation of the fraction of COVID-19 infected people in U.S. states and countries worldwide. PLoS One. 2021;16:e0246772. https://doi.org/10.1371/journal.pone.0246772
14. Reese H, Iuliano AD, Patel NN, Garg S, Kim L, Silk BJ, et al. Estimated incidence of coronavirus disease 2019 (COVID-19) illness and hospitalization—United States, February–September 2020. Clin Infect Dis. 2021;72:e1010–7. https://doi.org/10.1093/cid/ciaa1780
15. World Health Organization (WHO). Crafting the mosaic framework for resilient surveillance for respiratory viruses of epidemic and pandemic potential. Geneva: The Organization; 2023 [cited 2023 Dec 30]. https://www.who.int/publications/i/item/9789240070288

Address for correspondence: Udo Buchholz, Robert Koch Institute, Department for Infectious Disease Epidemiology, Seestraße 10, Berlin 13353, Germany; email: buchholzu@rki.de

etymologia revisited

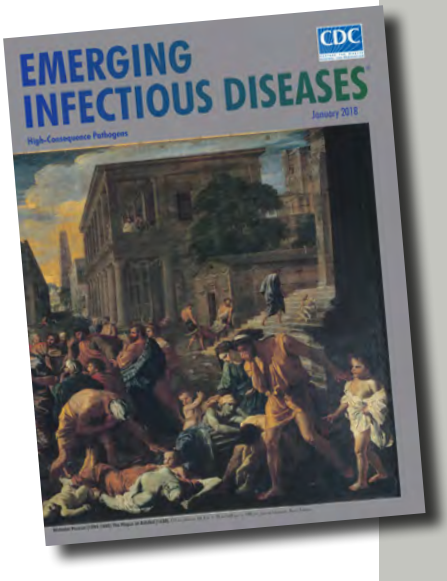

Originally published in January 2018

Plague

[plāg]

Plague (from the Latin *plaga*, "stroke" or "wound") infections are believed to have been common since at least 3000 BCE. Plague is caused by the ancestor of current *Yersinia* (named for Swiss bacteriologist Alexandre Yersin, who first isolated the bacterium) *pestis* strains. However, this ancestral *Y. pestis* lacked the critical *Yersinia* murine toxin (*ymt*) gene that enables vectorborne transmission. After acquiring this gene (sometime during 1600–950 BCE), which encodes a phospholipase D that protects the bacterium inside the flea gut, *Y. pestis* evolved the ability to cause pandemics of bubonic plague. The first recoded of these, the Justinian Plague, began in 541 ACE and eventually killed more than 25 million persons.

References:

1. Alexandre Yersin BW. Etymologia: yersinia. Emerg Infect Dis. 2010;16:496.
2. Centers for Disease Control and Prevention. History of plague [cited 2017 Oct 19]. https://www.cdc.gov/plague/history/index.html.
3. Rasmussen S, Allentoft ME, Nielsen K, Orlando L, Sikora M, Sjögren K-G, et al. Early divergent strains of Yersinia pestis in Eurasia 5,000 years ago. Cell. 2015;163:571–82.

https://wwwnc.cdc.gov/eid/article/24/1/et-2401_article

Retrospective Seroprevalence of Orthopoxvirus Antibodies among Key Populations, Kenya

Kristi Loeb,[1] Kieran A. Milner,[1] Candice Lemaille, Brielle Martens, Derek Stein, Julie Lajoie, Souradet Y. Shaw, Anne W. Rimoin, Placide Mbala-Kingebeni, Nicole A. Hoff, Ryan S. Noyce, Keith R. Fowke, Joshua Kimani, Lyle McKinnon, Jason Kindrachuk

We identified a cluster of mpox exposures among key populations in Kenya through retrospective serologic screening. We identified strong seropositivity among sex workers and gay, bisexual, and other men who have sex with men. These findings demonstrate the need for increased mpox surveillance among mpox-endemic and mpox-endemic–adjacent regions in Africa.

Mpox (formerly monkeypox) is a zoonotic viral disease caused by monkeypox virus (MPXV) that saw rapid geographic expansion resulting in a global epidemic in 2022 (*1*). MPXV consists of 2 distinct clades (clades I and clade II); clade I infections are associated with greater disease severity (*1*,*2*). Clade II MPXV is subdivided into 2 subclades (clades IIa and IIb); clade IIb is linked to the global epidemic (*3*,*4*). Although zoonosis has been the primary driver of human infections and outbreaks have occurred primarily in tropical forest regions within mpox-endemic countries, during the 2022 epidemic, >90% of infections were linked to secondary transmission, mainly through close, intimate (often sexual) contact. Historically, mpox has primarily affected younger populations; however, most of those mpox cases were associated with clade I (*3*). The average age of clade IIb mpox case-patients during the 2022 epidemic was >30 years; most were male (98.7%) and identified as gay, bisexual, and other men who have sex with men (GBMSM) (84%) (*4*). During the 2022 epidemic, common clinical characteristics for mpox included fever, physical asthenia or lethargy, lymphadenopathy, and rash; atypical lesion location also was noted.

MPXV reemerged in Nigeria in 2017 and resulted in ongoing endemic circulation. In contrast to historic mpox, disease has been more prevalent in urban regions and among adults (*5*). Human-to-human transmission and a high proportion of genital ulcers also were noted. More recently, transmission of clade I MPXV associated with intimate contact has been reported in the Democratic Republic of the Congo (DRC), including geographic expansion and cases in multiple large urban areas (*6*).

MPXV genome sequencing demonstrated linkages between reemergence in Nigeria and global expansion in 2022 (*7*,*8*). Given the reemergence of mpox in Nigeria with sustained nonzoonotic transmission, ongoing global circulation, rapid expansion in DRC, and acquisition associated with intimate contact, an urgent need exists for expanded mpox surveillance in Africa, particularly among key populations at increased risk for infection. Given the paucity of mpox surveillance data and the role of Nairobi (capital city of Kenya) as a major economic and transit center in Africa, we undertook retrospective orthopoxvirus (OPXV) serologic screening that focused on key populations.

Author affiliations: University of Manitoba, Winnipeg, Manitoba, Canada (K. Loeb, K.A. Milner, C. Lemaille, B. Martens, D. Stein, J. Lajoie, S.Y. Shaw, K.R. Fowke, J. Kimani, L. McKinnon, J. Kindrachuk); Cadham Provincial Laboratory, Winnipeg (D. Stein); University of Nairobi, Nairobi, Kenya (J. Lajoie, K.R. Fowke, J. Kimani, L. McKinnon); University of California–Los Angeles, Los Angeles, California, USA (N.A. Hoff, A.W. Rimoin); Institut National de Recherche Biomédicale, Kinshasa, Democratic Republic of the Congo (P. Mbala-Kingebeni); University of Alberta, Edmonton, Alberta, Canada (R.S. Noyce)

DOI: https://doi.org/10.3201/eid3009.240510

[1]These first authors contributed equally to this article.

The Study

We used historic serum samples from male and female sex workers (n = 656) enrolled at the Sex Workers Outreach Program (SWOP) in Nairobi, Kenya (*9*). We assayed samples for IgG seropositivity by using a modified ELISA assay with UV-inactivated vaccinia virus (VACV). We screened samples by using a 1:50 dilution (*10*). We collected samples during 2013–2018; age range of participants was 19–69 years at sample acquisition (Table). Female sex workers accounted for 72.3% (474/656) of our sample population, followed by other (non–sex workers or nonidentified; 18.4% [122/656]) and GBMSM (9.3% [61/656]). We defined seropositivity on the basis of absorbance values >3 SDs above baseline. Most (76.7% [503/656]) samples were provided by persons 20–55 years of age; we found the highest percentage of seropositive samples among participants 20–39 years of age (37.4% [37/99]) and 40–55 years of age (36.4% [36/99]) among all seropositive samples tested. We detected 89% seropositivity among persons living with HIV; however, HIV positivity was high (85.8% [563/676]) among the sample population (Figure; Appendix Figure, https://wwwnc.cdc.gov/EID/article/30/9/24-0510-App1.pdf).

We next selected 111 samples from the ELISA screen for subsequent analysis by the OPXV IgG Panel (Meso Scale Discovery, https://www.mesoscale.com), which includes 5 MPXV antigens: A29, A35, B6, E8, and M1 and their corresponding VACV orthologs. We tested samples by using 1:500 dilutions. Cross-reactivities for the assay range from 198% (MPXV A35R and VACV A33R) to 43.4% (MPXV E8L and VACV D9L), and lower limits of quantitation ranged from 0.021 to 0.058 AU/mL. We selected 86 samples that met seropositive criteria from the ELISAs (>3 SDs above baseline) and 25 seronegative or borderline samples. We blinded samples during testing and repeated sampling on a subset of blinded samples for validation. Average age for participants from whom samples were taken was 49 years (range 29–74 years); samples were from female sex workers, GBMSM, and non–sex workers. We detected OPXV seropositivity across all age groups in our sample cohort, and had strong signals (≥10,000 AU/mL) within all age groups, including persons born after cessation of the global smallpox vaccination program (*11*). OPXV-positive samples included 5 samples from persons in the 20–39-year age group, with calculated concentrations of >1,000 AU/mL. Our data suggest MPXV exposure among groups already at increased risk for infection in Kenya.

Conclusions

The reemergence of clade II MPXV in Nigeria in 2017, followed in 2022 by the rapid global expansion of clade II MPXV across non–mpox-endemic regions

Table. Demographic data for all participants in a retrospective study of seroprevalence of orthopoxvirus antibodies among key populations, Nairobi, Kenya, 2013–2018*

Characteristic	Human orthopoxvirus seropositivity		Total (%)
	Positive	Negative	
Age group, y			
≤19	0	1 (0.2)	1 (0.2)
20–39	37 (37.4)	188 (33.8)	225 (34.3)
40–55	36 (36.4)	242 (43.4)	278 (42.4)
56–65	8 (8.1)	60 (10.8)	68 (10.4)
>65	2 (2.0)	5 (0.9)	7 (1.1)
Unknown	16 (16.2)	61 (11.0)	77 (11.7)
Total	99	557	656
Sample collection year			
2013	1 (1.0)	7 (1.3)	8 (1.2)
2014	5 (5.1)	55 (9.9)	60 (9.1)
2015	3 (3.0)	15 (2.7)	18 (2.7)
2016	3 (3.0)	13 (2.3)	16 (2.4)
2017	61 (61.6)	277 (49.7)	338 (51.5)
2018	26 (26.3)	190 (34.1)	216 (32.9)
Total	99	557	656
HIV status			
Negative	11 (11.1)	82 (14.7)	93 (14.2)
Positive	88 (88.9)	475 (85.3)	563 (85.8)
Total	99	557	656
Key population			
Female sex worker	63 (63.6)	411 (73.8)	474 (72.3)
GBMSM	15 (15.2)	46 (8.3)	61 (9.3)
Non–sex worker	21 (21.2)	100 (17.9)	121 (18.4)
Total	99	557	656

*Participants were enrolled at the Sex Workers Outreach Program (SWOP) in Nairobi, Kenya. Values are no. (%). Seropositivity determined by ELISA using UV-inactivated vaccinia virus. GBMSM, gay, bisexual, and other men who have sex with men.

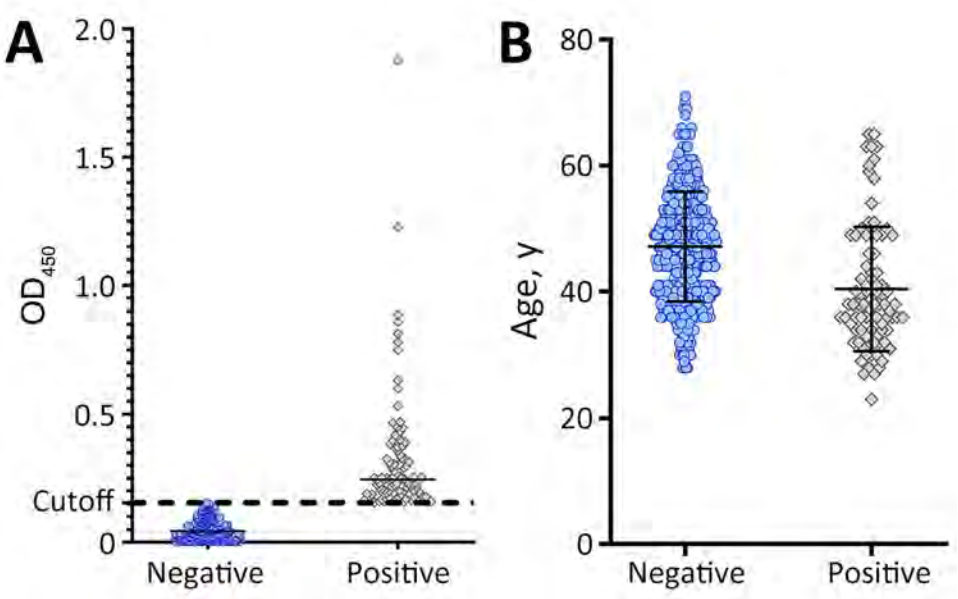

Figure. Retrospective assessment of orthopoxvirus antibody seropositivity among key populations, Nairobi, Kenya, 2013–2018. Orthopoxvirus seropositivity was assessed in banked samples acquired from 792 sex workers. A) Seropositivity was determined by ELISA using UV-inactivated vaccinia virus. Cutoff line indicates baseline seropositivity. Positives were determined as 3 SDs above the cutoff. Horizontal bar indicates median. B) Age distribution across all seropositive and seronegative samples. Horizontal bars indicate median with upper quartile above, lower quartile below. OD_{450}, optical density at 450 nm.

and the continued expansion of the current clade I outbreak in DRC, highlight the need for ongoing mpox surveillance. Given the geographic proximity and expansive shared borders of multiple countries in East Africa with DRC, frequent movement of persons across those regions, and the role of Nairobi as a commercial and tourism center, expanded mpox surveillance is needed urgently.

Although MPXV transmission between humans has historically occurred through close contact with infected persons (*2*,*10*–*12*), transmission during the global mpox epidemic was strongly linked to close, intimate (including sexual) contact. Transmission through close and sexual contacts have been observed during the ongoing mpox outbreak in DRC.

Given the risk for further expansion of MPXV in Africa, we screened for indications of historic mpox exposures in key populations at increased risk for infection in Kenya. Our data suggest that unreported MPXV exposures have occurred within key populations. The smallpox vaccination campaign in Kenya ended in 1972 (although vaccinations may have occurred later), and only importation-related cases were reported after 1970 (*11*). Thus, seropositivity against VACV and MPXV in persons ≤52 years of age in our sample population is strongly indicative of environmental exposure to an orthopoxvirus independent of variola virus. Although camelpox virus has been reported among camels in northern Kenya, few human orthopoxvirus infections have been reported in the region and zoonosis is rare (*12*). Camelpox cannot be discounted given antigenic similarities to other human orthopoxviruses; however, the clustering of seropositivity among key populations in our study suggests an alternative virus source. No other orthopoxviruses are known to infect humans in Kenya; thus, our serologic data suggest potential MPXV exposure.

Our findings highlight the need for expanded and sustained mpox surveillance that includes non–mpox-endemic regions close to areas with active mpox outbreaks. In addition, stigmatization and fear of repercussions or persecution encountered by sex workers and GBMSM communities may have also limited the historical identification of mpox in non–mpox-endemic regions of sub-Saharan Africa.

One limitation of our study stems from the antigenic similarity among human orthopoxviruses. The MPXV antigens we used in this study have VACV orthologs, and the seropositivity we detected cannot definitively identify prior mpox nor differentiate MPXV clades. However, given the seropositivity among persons within key populations linked to sex work and dense sexual networks, including persons born after the global smallpox vaccination program ended, our data support expanded mpox surveillance in regions proximal to mpox-endemic areas.

In summary, our data suggest that mpox introduction among sex workers in Kenya probably occurred before identification of MPXV reemergence in Nigeria, the 2022 epidemic, and the ongoing outbreak in DRC. The source of these exposures could have included undiagnosed mpox circulation and introduction from either Central or West Africa,

considering the lack of clade-specific determination through serologic screening. Thus, a definitive need exists to establish enhanced surveillance for groups at elevated risk for MPXV infection in Kenya and surrounding regions.

Acknowledgment

We are grateful to the Sex Worker Outreach Program participants for their continued partnership on this and other investigations.

This work was supported by the International Mpox Research Consortium through funding from the Canadian Institutes of Health Research and International Development Research Centre (grant no. 202209MRR-489062-MPX-CDAA-168421), the US Department of Defense, Defense Threat Reduction Agency, Monkeypox Threat Reduction Network (grant no. HDTRA1-21-1-0040), and the US Department of Agriculture Non-Assistance Cooperative Agreement (grant no. 20230048).

About the Author

Ms. Loeb is a MSc student at the University of Manitoba. Her research interests include emerging infectious diseases and public health. Mr. Milner is a medical student and is completing a BSc in Medicine program at the University of Manitoba. His research interests include infectious diseases and clinical medicine.

References

1. Weaver JR, Isaacs SN. Monkeypox virus and insights into its immunomodulatory proteins. Immunol Rev. 2008;225:96–113. https://doi.org/10.1111/j.1600-065X.2008.00691.x
2. McCollum AM, Damon IK. Human monkeypox. Clin Infect Dis. 2014;58:260–7. https://doi.org/10.1093/cid/cit703
3. Jezek Z, Szczeniowski M, Paluku KM, Mutombo M. Human monkeypox: clinical features of 282 patients. J Infect Dis. 1987;156:293–8. https://doi.org/10.1093/infdis/156.2.293
4. World Health Organization. Mpox (monkeypox) outbreak: global trends [cited 2024 April 10]. https://worldhealthorg.shinyapps.io/mpx_global
5. Yinka-Ogunleye A, Aruna O, Dalhat M, Ogoina D, McCollum A, Disu Y, et al.; CDC Monkeypox Outbreak Team. Outbreak of human monkeypox in Nigeria in 2017–18: a clinical and epidemiological report. Lancet Infect Dis. 2019;19:872–9. https://doi.org/10.1016/S1473-3099(19)30294-4
6. Kibungu EM, Vakaniaki EH, Kinganda-Lusamaki E, Kalonji-Mukendi T, Pukuta E, Hoff NA, et al.; International Mpox Research Consortium. Clade I–associated mpox cases associated with sexual contact, the Democratic Republic of the Congo. Emerg Infect Dis. 2024;30:172–6. https://doi.org/10.3201/eid3001.231164
7. Gigante CM, Korber B, Seabolt MH, Wilkins K, Davidson W, Rao AK, et al. Multiple lineages of monkeypox virus detected in the United States, 2021–2022. Science. 2022;378:560–5. https://doi.org/10.1126/science.add4153
8. Ndodo N, Ashcroft J, Lewandowski K, Yinka-Ogunleye A, Chukwu C, Ahmad A, et al. Distinct monkeypox virus lineages co-circulating in humans before 2022. Nat Med. 2023;29:2317–24. https://doi.org/10.1038/s41591-023-02456-8
9. Omollo K, Lajoie J, Oyugi J, Wessels JM, Mwaengo D, Kimani J, et al. Differential elevation of inflammation and $CD4^+$ T cell activation in Kenyan female sex workers and non-sex workers using depot-medroxyprogesterone acetate. Front Immunol. 2021;11:598307. https://doi.org/10.3389/fimmu.2020.598307
10. Sejvar JJ, Chowdary Y, Schomogyi M, Stevens J, Patel J, Karem K, et al. Human monkeypox infection: a family cluster in the midwestern United States. J Infect Dis. 2004;190:1833–40. https://doi.org/10.1086/425039
11. Fenner F, Henderson DA, Arita I, Jezek Z, Ladnyi ID. Smallpox and its eradication. Geneva: World Health Organization; 1988. p. 963–4 [cited 2024 Apr 10]. https://iris.who.int/handle/10665/39485
12. Balamurugan V, Venkatesan G, Bhanuprakash V, Singh RK. Camelpox, an emerging orthopox viral disease. Indian J Virol. 2013;24:295–305. https://doi.org/10.1007/s13337-013-0145-0

Address for correspondence: Jason Kindrachuk, University of Manitoba, Department of Medical Microbiology and Infectious Diseases, 523-745 Bannatyne Ave, Winnipeg, MB R3E 0J9, Canada; email: jason.kindrachuk@umanitoba.ca

Non-HIV and Immunocompetent Patient with COVID-19 and Severe *Pneumocystis jirovecii* Pneumonia Co-Infection

Songsong Yu, Tiecheng Yang

Pneumocystis jirovecii pneumonia is an opportunistic infection that affects HIV-infected and immunocompromised persons and rarely affects immunocompetent patients. However, after the advent of the COVID-19 pandemic, some COVID-19 patients without immunocompromise or HIV were infected with *P. jirovecii*. Clinical manifestations were atypical, easily misdiagnosed, and rapidly progressive, and the prognosis was poor.

Pneumocystis jirovecii pneumonia (PJP) is an opportunistic infection that usually affects immunocompromised patients, most commonly those with HIV infection (*1*). PJP in immunocompetent persons is extremely rare (*2*), particularly among middle-aged persons. Currently, the number of non-HIV patients with PJP is rapidly increasing because of organ transplantation, improvements in diagnosis and treatment of autoimmune diseases, and use of immunosuppressive drugs (including corticosteroids or immunomodulatory monoclonal antibodies). The mortality rate for patients with PJP but not HIV is significantly higher than for those with HIV (up to 30%) (*3*).

Since 2019, COVID-19 infection has become a threat to human health, damaging the epithelial barrier of the airway and inducing abnormal immune responses, which in turn leads to deregulation of the immune system. Therefore, ≈19% of patients with COVID-19 experience pulmonary coinfections (*4*). We report the case of an immunocompetent woman in China who was co-infected with COVID-19 and *P. jirovecii*.

The Case

On June 25, 2023, a 52-year-old woman visited the emergency department of Beijing Shijitan Hospital, Capital Medical University (Beijing, China), with an 8-day history of fever (maximum 39.5°C) accompanied by weakness and anorexia and a 5-day history of cough with expectoration. Until 5 days before admission, she had not experienced coughing, expectoration, chills, vomiting, sore throat, or shortness of breath. Results of influenza A/B virus antigen and COVID-19 testing were negative. Laboratory findings were peripheral leukocyte count 5.25 × 10^9 cells/L (85.5% neutrophils, 8.9% lymphocytes) and C-reactive protein level 118.03 mg/L. Chest computed tomography (CT) scan indicated blurred bronchial vascular bundles in bilateral lungs with multiple tree-in-bud signs, multiple ground-glass shadows, and subpleural consolidation (Figure 1). After receiving intravenous moxifloxacin (0.4 g/d for 3 days), the patient still had high fever, and chest CT scan showed substantially increased bilateral tree-in-bud signs, ground-glass shadows, and subpleural consolidation in lungs (Figure 2). She had no relevant medical history.

At admission, physical examination revealed rough breathing sounds. Peripheral leukocyte count was 4.35 × 10^9 cells/L (89.1% neutrophils, 8.9% lymphocytes, 1.6% monocytes), and C-reactive protein level was 199.96 mg/L. Serum alanine aminotransferase was 61 U/L, aspartate aminotransferase 65 U/L, lactate dehydrogenase 283 U/L, albumin 33.6 g/L, and plasma D-dimer 2,902 ng/mL. Arterial blood gas indicated a pH of 7.46, partial pressure of CO_2 (pCo_2) 35 mm Hg, and partial pressure of O_2 (pO_2) 78 mm Hg (fraction of inspired O_2 [FiO_2] 29%). Results were negative for serum mycobacterium tuberculosis antibody, Epstein-Barr virus capsid IgM, cytomegalovirus IgM, galactomannan and 1,3-β-d-glucan, serum IgE, antinuclear antibody, antineutrophilic cytoplasmic antibody, and tumor markers. Blood and sputum culture results were unremarkable.

Author affiliation: Beijing Shijitan Hospital, Capital Medical University, Beijing, China

DOI: https://doi.org/10.3201/eid3009.240615

After admission, the patient received moxifloxacin and piperacillin/tazobactam, but her fever remained (maximum 40.7°C), accompanied by loss of appetite, aggravated weakness, and shortness of breath after activity. On hospitalization day 7, arterial blood gas indicated pH 7.45, pCO_2 46 mm Hg, and pO_2 59 mm Hg (FiO_2 41%). Chest CT scan showed bilateral blurred bronchovascular bundles, interlobular thickening, and subpleural small-band ground-glass changes in the lungs with increased bilateral pleural effusion (Figure 3).

Culture of bronchalveolar lavage fluid (BALF) from the basal segment of the lower left lung revealed no bacteria and fungi. However, metagenomic next-generation sequencing (mNGS) of BALF detected *P. jirovecii* (222 sequences), *Candida albicans* (2,393 sequences), and SARS-CoV-2 (37 sequences). Peripheral T-lymphocyte subsets included 80/μL CD4+ and 196/μL CD8+ T cells. The diagnosis was COVID-19 with severe *P. jirovecii* co-infection.

On hospital day 8, antimicrobial treatment comprised oral sulfamethoxazole/trimethoprim (0.8 g/160 mg every 8 h), intravenous caspofungin (70 mg on the first day, then 50 mg/d), and prednisone acetate (40 mg every 12 h for 5 days, 40 mg/d for 5 days, then 20 mg/d for 11 days). Concomitant treatments were intravenous human immunoglobulin, nutritional support, and noninvasive ventilator transnasal high-flow oxygen therapy. On day 2 after treatment, the patient's fever abated; on day 3, shortness of breath resolved. On day 17, arterial blood gas indicated pH of 7.46, pCO_2 40 mm Hg, and pO_2 127 mm Hg (FiO_2 29%). Chest CT scan indicated that all lung lesions were absorbed bilaterally (Figure 4), and peripheral T-lymphocyte subsets comprised 561/μL CD4+ and 514/μL CD8+ T cells.

Conclusions

Patients with COVID-19 who are older, have comorbidities, and are unvaccinated are susceptible to opportunistic infections such as aspergillus, candidiasis, and tuberculosis (*5*). Only a few cases have been reported in which immunosuppressed patients with moderate-to-severe COVID-19 pneumonia were co-infected with *P. jirovecii (5*). The prevalence of *P. jirovecii* infection in non-HIV patients (37 cases/1,000 patients) was significantly higher during the COVID-19 pandemic than before (13.1 cases/1,000 patients) (*6*). Moreover, before the pandemic, the mortality rate for non-HIV patients infected with PJP was higher (≈35%–50%) (*7*).

The prevalence of *P. jirovecii* colonization in immunocompetent persons varies. J.S. Kang found that 34.3% of patients with PJP had a history of COVID-19 and that 25.7% did not have underlying immunosuppressive conditions (*6*). The JiroCOVID study found

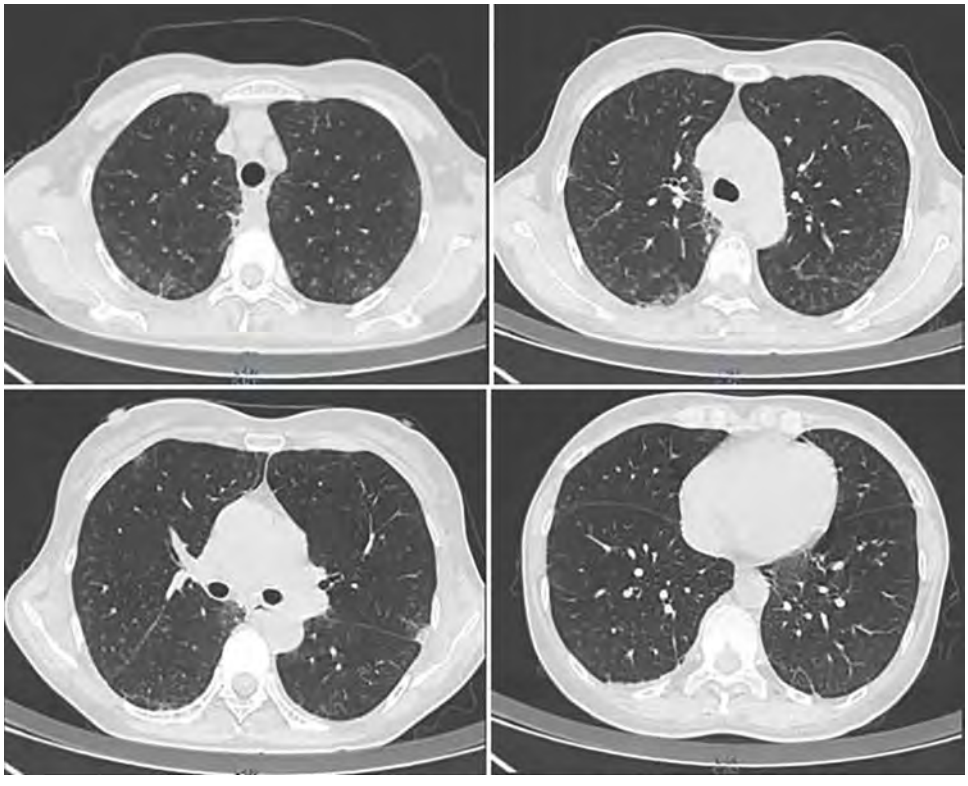

Figure 1. Chest computed tomography scans of immunocompetent patient in China who was co-infected with COVID-19 and non-HIV severe *Pneumocystis jirovecii* pneumonia, performed on June 22, 2023. Images show bronchial vascular bundles blurred in bilateral lungs with multiple tree-in-bud signs, multiple ground-glass shadows, and bilateral subpleural consolidation.

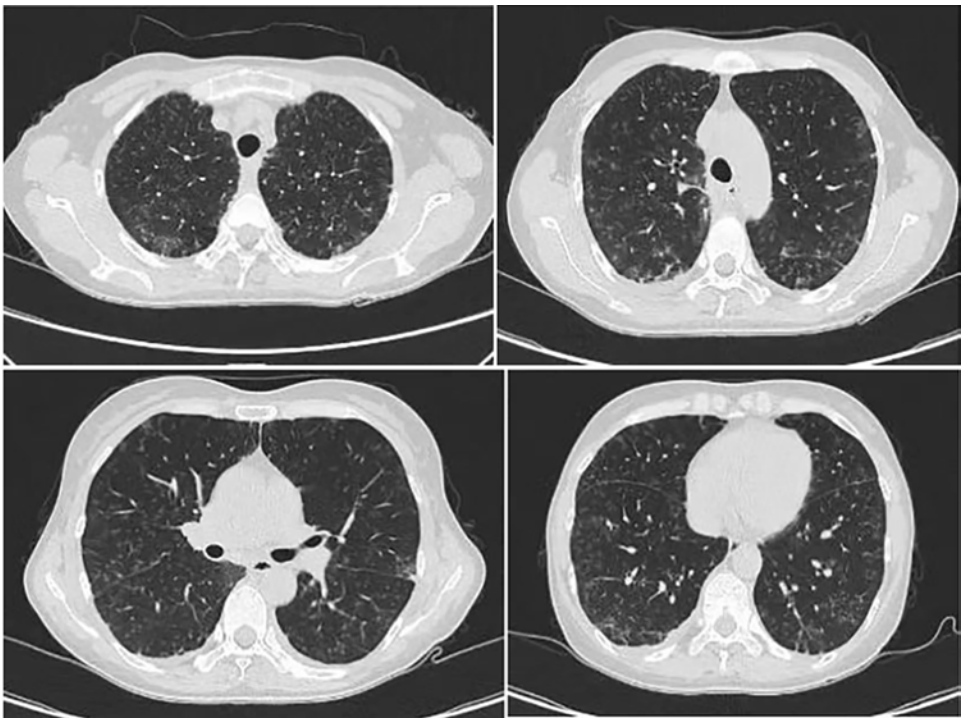

Figure 2. Chest computed tomography scans of immunocompetent patient in China who was co-infected with COVID-19 and non-HIV severe *Pneumocystis jirovecii* pneumonia, performed on June 25, 2023. Images show multiple tree-in-bud signs, ground-glass shadows, and substantially increased bilateral subpleural consolidation in the lungs.

that the prevalence of *P. jirovecii* colonization and infection was extremely low in immunocompetent patients, only 1.7% (*8*). Gentile et al. found that all but 1 patient with COVID-19 had no underlying immunosuppressive conditions or other risk factors for PJP infection (*9*). Thus, *P. jirovecii* infection is easily overlooked in patients without immunocompromise.

After patients are infected with COVID-19, the virus attacks the lymphocyte immune system, resulting in decreased CD4+ and CD8+ T-cell counts. The probability of opportunistic infection greatly increases when the $CD4^+$ T-cell count is <200/μL (*3*). COVID-19 damages the epithelial barrier and induces an abnormal immune response resulting from immune system dysregulation (*6*). Unlike the patients reported by Gentile et al., who received treatment with corticosteroids for COVID-19 pneumonia, the patient we report had no other risk factors.

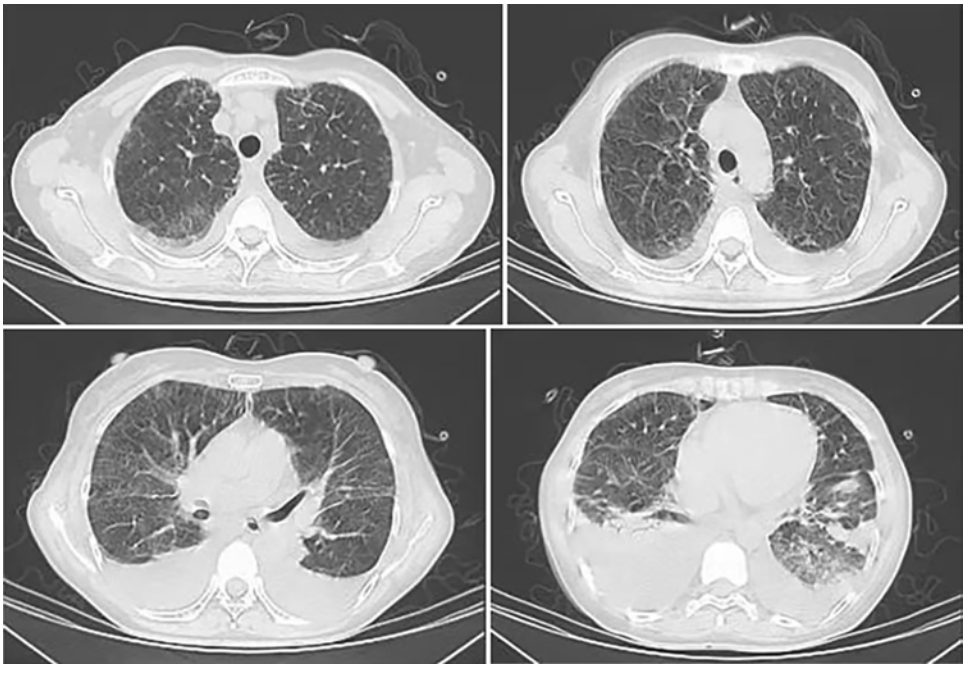

Figure 3. Chest computed tomography scans of immunocompetent patient in China who was co-infected with COVID-19 and non-HIV severe *Pneumocystis jirovecii* pneumonia, performed on June 30, 2023. Images show blurred bronchovascular bundles, interlobular thickening, and subpleural small-band of ground-glass changes in bilateral lungs, with increased bilateral pleural effusion.

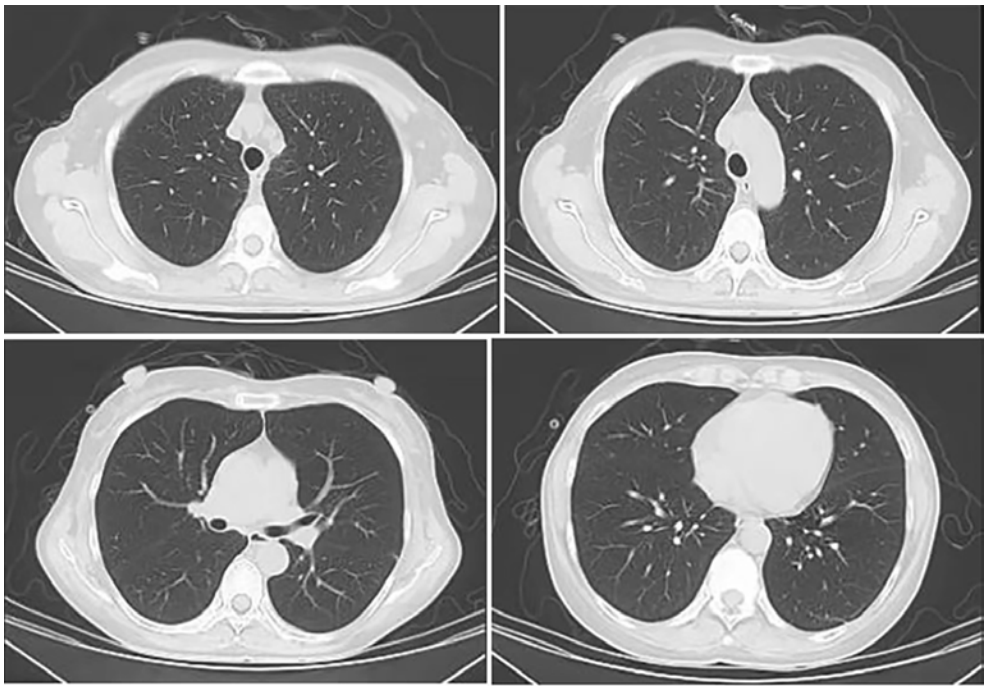

Figure 4. Chest computed tomography scans of immunocompetent patient in China who was co-infected with COVID-19 and non-HIV severe *Pneumocystis jirovecii* pneumonia, performed on July 17, 2023. All lung lesions were absorbed bilaterally.

In China, only 4 patients with COVID-19 have been reported to be co-infected with PJP, including 2 patients with HIV infection and 2 older patients with chronic pulmonary diseases (*10*,*11*). COVID-19 co-infection with PJP has not been reported among patients who were immunocompetent and had no comorbidities. Although tests for COVID-19 returned negative results several times for the patient we report, we found SARS-CoV-2 RNA in BALF. Meanwhile, the peripheral T-cell count decreased to 80/μL, suggesting that the immune system was attacked by COVID-19. Therefore, for patients with atypical imaging manifestations, clinicians should search for opportunistic pathogens.

P. jirovecii is a fungus for which rates of colonization in the respiratory tract are low and is difficult to grow in vitro; therefore, it is difficult to detect through sputum cultures. β-d-glucan testing is considered an assistive method for diagnosis; sensitivity is 94% for HIV patients and 86% for non-HIV patients, and specificity is 83% for both groups of patients (*12*). Detection of *P. jirovecii* in BALF is considered the standard for PJP diagnosis.

Although *Candida* was detected in BALF from this patient, according to the 2016 guidelines of the Infectious Diseases Society of America, *Candida* isolated from the respiratory tract is primarily considered colonization (*13*). Therefore, we considered *Candida* colonization a possibility.

In the patient we report, the clinical manifestations of the disease in the early stages were atypical and could be easily misdiagnosed. Furthermore, SARS-CoV-2 tests conducted on nasopharyngeal swab samples and by sputum cultures yielded negative results. Fortunately, BALF testing using mNGS provided timely evidence for clinical diagnosis and treatment.

For patients with COVID-19 who are immunocompetent and not HIV infected but show persistently high fever and atypical viral or bacterial pneumonia on chest CT scan, clinicians should be highly vigilant of the possibility of PJP. Aggressive BALF and mNGS testing may help achieve a definitive diagnosis.

About the Author

Dr. Yu is a chief physician in the emergency department of Beijing Shijitan Hospital, Capital Medical University, who is mainly skilledin the diagnosis and treatment of acute critically ill patients.

References

1. Huang X, Weng L, Yi L, Li M, Feng YY, Tian Y, et al. Clinical features of acute respiratory failure due to pneumocystis pneumonia in non-HIV immunocompromised patient [in Chinese]. Zhonghua Yi Xue Za Zhi. 2016;96:3057–61.
2. Jeican II, Inişca P, Gheban D, Tăbăran F, Aluaş M, Trombitas V, et al. COVID-19 and *Pneumocystis jirovecii* pulmonary coinfection—the first case confirmed through autopsy. Medicina (Kaunas). 2021;57:302. https://doi.org/10.3390/medicina57040302

3. Gingerich AD, Norris KA, Mousa JJ. Pneumocystis pneumonia: immunity, vaccines, and treatments. Pathogens. 2021;10:236. https://doi.org/10.3390/pathogens10020236
4. Musuuza JS, Watson L, Parmasad V, Putman-Buehler N, Christensen L, Safdar N. Prevalence and outcomes of co-infection and superinfection with SARS-CoV-2 and other pathogens: a systematic review and meta-analysis. PLoS One. 2021;16:e0251170. https://doi.org/10.1371/journal.pone.0251170
5. Chong WH, Saha BK, Ananthakrishnan Ramani, Chopra A. State-of-the-art review of secondary pulmonary infections in patients with COVID-19 pneumonia. Infection. 2021;49:591–605. https://doi.org/10.1007/s15010-021-01602-z
6. Kang JS. Changing trends in the incidence and clinical features of *Pneumocystis jirovecii* pneumonia in non-HIV patients before and during the COVID-19 era and risk factors for mortality between 2016 and 2022. Life (Basel). 2023;13:1335. https://doi.org/10.3390/life13061335
7. Salzer HJF, Schäfer G, Hoenigl M, Günther G, Hoffmann C, Kalsdorf B, et al. Clinical, diagnostic, and treatment disparities between HIV-infected and non-HIV-infected immunocompromised patients with *Pneumocystis jirovecii* pneumonia. Respiration. 2018;96:52–65. https://doi.org/10.1159/000487713
8. Buonomo AR, Viceconte G, Fusco L, Sarno M, di Filippo I, Fanasca L, et al. Prevalence of *Pneumocystis jirovecii* colonization in non-critical immunocompetent COVID-19 patients: a single-center prospective study (JiroCOVID study). Microorganisms. 2023;11:2839. https://doi.org/10.3390/microorganisms11122839
9. Gentile I, Viceconte G, Lanzardo A, Zotta I, Zappulo E, Pinchera B, et al.; Federico Ii Covid-Team. *Pneumocystis jirovecii* pneumonia in non-HIV patients recovering from COVID-19: a single-center experience. Int J Environ Res Public Health. 2021;18:11399. https://doi.org/10.3390/ijerph182111399
10. Xiao Y, Su H, Ping P, Lin LP, Xiao GY. Clinicopathological characteristics of COVID-19 complicated with opportunistic infections in a case series of six patients. Academic Journal of Guangzhou Medical University. 2023;51:17–23.
11. Sun J, Ma J, Xue CX, Tian CX, Zhou L, Zhang XY, et al. Differential diagnosis and Chinese and western medicine treatment of novel coronavirus infection based on a case study combined with *Pneumocystis carinii* pneumonia. Jilin Journal of Chinese Medicine. 2023;43:1161–5.
12. Del Corpo O, Butler-Laporte G, Sheppard DC, Cheng MP, McDonald EG, Lee TC. Diagnostic accuracy of serum (1-3)-β-D-glucan for *Pneumocystis jirovecii* pneumonia: a systematic review and meta-analysis. Clin Microbiol Infect. 2020;26:1137–43. https://doi.org/10.1016/j.cmi.2020.05.024
13. Pappas PG, Kauffman CA, Andes DR, Clancy CJ, Marr KA, Ostrosky-Zeichner L, et al. Clinical practice guideline for the management of candidiasis: 2016 update by the Infectious Diseases Society of America. Clin Infect Dis. 2016;62:e1–50. https://doi.org/10.1093/cid/civ933

Address for correspondence: Tiecheng Yang, Department of Emergency, Emergency and Critical Care Medical Center, Beijing Shijitan Hospital, Capital Medical University, Tieyi Rd 10, Yangfangdian St, Haidian District, Beijing 100038, China; email: ytc3953@bjsjth.cn

Who is this person?

Here is a clue: He is honored by his name being used for a tickborne protozoan infection.

A) Emile Roux
B) Victor Babeș
C) George Duncan
D) Ronald Ross
E) Walter Reed

See next page for the answer.

Victor Babeș

Andrei Ionut Cucu, Antonio Perciaccante, Raffaella Bianucci

This is a photograph of Victor Babeş (1854–1926) (Figure 1), who discovered *Babesia* spp. microorganisms and was a prominent figure in the fields of pathology, virology, and microbiology in Romania (*1*–*3*). Born in Vienna, Austria, on July 28, 1854, he attended high school in Budapest, Hungary, before pursuing his medical studies in Budapest and Vienna. His father, Vincențiu Babeş (1821–1907), was an Imperial lawyer, teacher, president of the Supreme Court of Hungary, and a founding member of the Romanian Academic Society.

Victor Babeş began his career when he was 18 years of age in the pathology department at the University of Budapest and later earned his PhD in medical sciences. In 1885, he was appointed as an associate professor at the University of Budapest (*4*). He honed his skills in Europe's most renowned laboratories, studying with distinguished figures such as Rudolf Virchow (1821–1902), Friedrich Daniel von Recklinghausen (1833–1910), Karl Langer (1819–1887), Justus von Liebig (1803–1873), and Karl von Rockitansky (1804–1878). In the field of microbiology, he was mentored by giants such as Robert Koch (1843–1910) and Louis Pasteur (1822–1895) (*5*–*8*).

One of Dr. Babeş's greatest achievements was co-authoring the bacteriology treatise *Les bactéries et leur rôle dans l'anatomie et l'histologie pathologiques des maladies infectieuses* with André Victor Cornil (1837–1908); the work is considered a landmark of 19th Century medicine (*9*–*11*). The treatise gained substantial attention; all 3 editions sold out within 5 years. Louis Pasteur suggested that the book should be honored, praise that led the French Academy of Sciences to award the Montyon Prize to the authors (*12*,*13*).

Figure: Victor Babeș (1854–1926). Source: University of Kansas Medical Center, Clendening History of Medicine Museum (http://clendening.kumc.edu/dc/pc/babes.jpg).

In 1885, Dr. Babeş was appointed as a professor of histopathology in the Faculty of Medicine at the University of Budapest. In 1887, he moved to Bucharest, Romania, where he founded the pathology and bacteriology departments within the Faculty of Medicine at the University of Medicine and Pharmacy Carol Davila Bucharest and was a professor in the bacteriology department until 1926. In 1887, in accordance with the Ministry of Internal Affairs Law no. 1197, the Institute of Bacteriology and Pathology was established in Bucharest; the institute was led by Victor Babeş and now bears his name (Victor Babeş

Author affiliations: Universitatea Stefan cel Mare din Suceava, Iasi, Romania (A.I. Cucu); Spitalul Clinic de Urgență Prof Dr Nicolae Oblu, Iasi (A.I. Cucu); Azienda Sanitaria Universitaria Giuliano Isontina, Gorizia, Italy (A. Perciaccante); San Giovanni di Dio Hospital, Gorizia (A. Perciaccante); University of Turin, Turin, Italy (R. Bianucci); Université Paris-Saclay, Montigny-le-Bretonneux, France (R. Bianucci)

DOI: https://doi.org/10.3201/eid3009.231591

National Institute of Pathology). The Institute is the oldest medical science institute in Romania, initially conceived as a comprehensive medical institute similar to Institut Pasteur in Paris and has pathologic anatomy, bacteriology, veterinary pathology, rabies vaccination, and serology sections.

In 1888, Dr. Babeş established the second center for rabies vaccination in the world, the first having been created by Louis Pasteur in Paris. Furthermore, in 1888, Victor Babeş discovered microorganisms in the erythrocytes of cattle (now known as *B. bovis)* and sheep in Romania. He associated the presence of this microorganism with bovine hemoglobinuria, a sign of redwater fever. During 1889–1893, ticks were identified as the transmission vectors for *Babesia* spp. in Texas cattle (*14*). In 1893, the parasites were named *B. bovis*, *B. ovis*, and *B. bigemina*, the genus reflecting the name of their discoverer (*14*). The first case of human babesiosis was diagnosed in 1957 (*14*) in the small town of Strmec, Croatia, not far from Ljubljana, Slovenia.

Dr. Babeş pioneered the understanding of bacterial structures, discovering the metachromatic bodies of the diphtheria bacillus (*Corynebacterium diphtheriae*), which enabled the easiest bacteriologic diagnosis of diphtheria. In 1886, he was the first scientist to report the systemic invasion of organs by the diphteria bacillus and suggested antidiphtheria therapy. He was the first to describe leprosy and tuberculosis bacilli in actinomycotic forms (*2*–*4*,*12*) and demonstrated that some pathogens could be encapsulated and their structures could be observed under the microscope. He also accomplished the staining of microbial cilia.

During 1888–1889, Victor Babeş' studies laid the experimental and clinical groundwork for serotherapy in medicine, introducing the theory of seroimmunization involving the concurrent introduction of immunizing serum samples prepared with antigenic material in distinct body sections (*4*). In 1889, he published this method in the Annales de l'Institut Pasteur (*11*). In 1895, he formulated the principle of serovaccination. He prepared various serum samples and vaccines in his laboratory for mass prevention of certain communicable diseases. He prepared antidiphtheria serum samples by vaccinating horses and using a method to "offset dormant toxin through blood antitoxins," which was adopted by several laboratories (*4*,*12*).

Dr. Babeş identified rabies inclusions, which are pathognomonic lesions of rabies found in the cytoplasm of neurons in Ammon's horn of the hippocampus. Rabies inclusions were later rediscovered in 1903 by Aldechi Negri (1876–1912); the inclusions are now known as Babeş-Negri bodies (*8*). Moreover, Dr. Babeş demonstrated experimental rabies virus proliferation in the nerves of humans. In 1887, he observed that heating the rabies virus to 58°C for 2–14 minutes led to controlled attenuation, unlike conventional methods of drying or dilution. Thus, he created a rabies vaccine by heating the virus, which is known as the Romanian technique of immunization.

In 1912, he published the treatise Traité de la rage (published by Librairie J.-B. Baillière et fils in Paris), which received considerable acclaim from the medical scientific community. This extensive treatise on rabies is ≈700 pages long, encompasses all knowledge about rabies at that time, and includes ≈90 works solely on rabies.

Figure 2. Postage stamps issued in 2012 by the postal service of Romania (https://www.posta-romana.ro) to commemorate the 125th anniversary of the founding of the Victor Babeş National Institute. Source: Romfilatelia. Photography by Will Breedlove, August 2024.

In the field of epidemiology, he initiated a conference on leprosy and pellagra in Romania (*12*) and successfully coordinated fights against 4 cholera epidemics in Europe: Paris (1884), Budapest (1886), Central Europe (1892), and Bulgaria (1893) (*12*,*15*). In 1913, he prepared an anticholera vaccine to combat the cholera epidemic that had broken out among persons in the Army of Romania, who were campaigning in the Second Balkan War in Bulgaria. During 1916–1918, he continued to prepare biological products, remaining in the area occupied by the Central Powers.

In 1893, Victor Babeş became a full member of the Romanian Academy. During his lifetime, he was also appointed an officer of the French Legion d'Honneur and a corresponding member of the Paris Academy of Sciences (*7*).

Victor Babeş died on October 19, 1926, in Bucharest at 72 years of age. In 2012, the postal service of Romania (https://www.posta-romana.ro) issued 2 stamps to commemorate the 125th anniversary of the founding of the Victor Babeş National Institute (Figure 2). His contributions to medicine and science are substantial and should be remembered in the scientific realm of infectious diseases. Through his discoveries, which were published in >1,000 works in many different languages, he opened new horizons in the field of infectious disease pathology.

Acknowledgments

We thank Simon T. Donell for proofreading the text.

About the Author

Dr. Cucu is an associate professor of anatomy at the Faculty of Medicine and Biological Sciences at Stefan cel Mare University in Suceava and a consultant neurosurgeon at the Emergency Clinical Hospital Prof. Dr. N. Oblu in Iasi, Romania. His academic interests focus on interdisciplinary neurosurgery, surgical neuroanatomy, the history of neuroanatomy, icono-diagnosis, paleopathology, and innovative teaching methods in medical education.

References

1. Curcă D. The Romanian scientist: Prof. Victor Babes. Hist Med Vet. 2002;27:333–47.
2. Richou R. Victor Babes, his life, his work [in French]. Rev Pathol Gen Physiol Clin. 1964;64:281–2.
3. Calciu M. The 125th anniversary of the birth of V. Babeş (1854–1979). Contribution of Victor Babeş to the advancement of scientific phthisiology [in Romanian]. Rev Ig Bacteriol Virusol Parazitol Epidemiol Pneumoftiziol Pneumoftiziol. 1979;28:187–91.
4. Popa MI. Where pathology, microbiology and virology converge: Professor Victor Babeş. Rom Arch Microbiol Immunol. 2021;80:179–88. https://doi.org/10.54044/RAMI.2021.02.08
5. Babeş MV, Igiroşianu I. Babeş. Oameni de seamă. Bucharest (Romania): Tineretului Publishing House; 1961.
6. Victor Babeş, pagini alese. Bucharest: Editura de Stat pentru Literatura Ştiinţifică; 1954.
7. Victor Babeş, volum omagial. Bucharest: Editura de Stat pentru Literatura Medicală; 1949.
8. Babeş V, Babeş M, Horodniceanu F, Nicolau SS. Victor Babeş, opere alese. Bucharest: Editura Academiei Republicii Populare Romîne, 1954.
9. Cornil AV, Babes V. Les bactéries et leur rôle dans l'anatomie et l'histologie pathologiques des maladies infectieuses: ouvrage contenant les methods speéciales de la bactériologie [in French]. Paris: F. Alcan; 1885.
10. Stirbu A. Views of Victor Babes, on the problem of rabies [in Romanian]. Stud Cercet Inframicrobiol. 1963;14:81–91.
11. Rundfeldt C. Drug development: a case study based insight into modern strategies. Rijeka (Croatia): InTech; 2011.
12. Voinescu D, Mohan A, Constantinescu R, Ciurea AV. Nine decades after the death of the famous scientist Victor Babeş. Proc Rom Acad, Series B. 2016;18:243–50.
13. Prize Awards of the Paris Academy of Sciences. Nature. 1925;115:173–4.
14. Uilenberg G. *Babesia*—a historical overview. Vet Parasitol. 2006;138:3–10. https://doi.org/10.1016/j.vetpar.2006.01.035
15. Negru I. Concept of Prof. Victor Babeş of the training and education of the health officer [in Romanian]. Viata Med Rev Inf Prof Stiint Cadrelor Medii Sanit. 1983;31:211–4.

Address for correspondence: Andrei Ionut Cucu, Universitatea Stefan cel Mare din Suceava, Faculty of Medicine and Biological Sciences, 13 Universitatii Street, Suceava, Iasi 700309, Romania; email: andrei.cucu@usm.ro

Emerging *Leishmania donovani* Lineages Associated with Cutaneous Leishmaniasis, Himachal Pradesh, India, 2023

Patrick Lypaczewski,[1] Yogesh Chauhan,[1] Kayla Paulini,[1] Lovlesh Thakur, Shailja Chauhan, Ezrah Isaac Roy, Greg Matlashewski,[2] Manju Jain[2]

Author affiliations: McGill University, Montreal, Quebec, Canada (P. Lypaczewski, K. Paulini, E.I. Roy, G. Matlashewski); Central University of Punjab, Bathinda, India (Y. Chauhan, M. Jain); Cleveland State University Center for Gene Regulation in Health and Disease, Cleveland, Ohio, USA (L. Thakur); Indira Gandhi Medical College Cancer Hospital, Shimla, India (S. Chauhan)

DOI: https://doi.org/10.3201/eid3009.231595

The clinical manifestation of leishmaniasis has historically been determined by the *Leishmania* species involved. However, recent emergence of novel *Leishmania* lineages has caused atypical pathologies. We isolated and characterized 2 new *Leishmania donovani* parasites causing cutaneous leishmaniasis in Himachal Pradesh, India.

Leishmaniasis is a neglected tropical disease caused by the protozoan parasite *Leishmania*. The manifestation of the disease has historically been species-specific: *Leishmania donovani* and *Leishmania infantum* cause visceral leishmaniasis (VL), also called kala-azar, and many species such as *Leishmania tropica* and *Leishmania major* cause cutaneous leishmaniasis (CL) (*1*). In recent years, however, the existence of interspecies and intraspecies hybrids has emerged, and hybridization has been associated with a potential cause of CL in Sri Lanka (*2*) and Himachal Pradesh, India (*3*). In Sri Lanka, CL is mostly caused by an atypical *L. donovani* (*4*–*6*) and CL cases were recently observed to be associated with *L. donovani*/*L. major* hybrids or *L. donovani*/*L. tropica* hybrids (*2*). CL is an emerging disease in Himachal Pradesh, where a recently identified *L. donovani* intraspecies hybrid isolated from a CL patient belonged to the Indian subcontinent 1 (ISC1) Yeti clade (*3*). Further, the recent discovery of ISC1 *Leishmania* parasites in the neighboring region of West-Nepal supports the establishment of the ISC1 clade in the area (*7*). Therefore, continued monitoring for emergence of CL in Himachal Pradesh is necessary to identify new *L. donovani* lineages associated with cutaneous disease outcomes. We report 2 new cases of CL in Himachal Pradesh caused by *L. donovani* belonging to the ISC1 Yeti clade that are not hybrid parasites previously identified from this region (GenBank BioProject no. PRJNA701770) (Appendix Figure 1, https://wwwnc.cdc.gov/EID/article/30/9/23-1595-App1.pdf) (*3*). Genome surveillance of CL parasites coming from Himachal Pradesh can help identify gene sequences associated with CL disease outcomes and identify the origin and transmission of emerging *L. donovani* parasites.

We performed a phylogenetic analysis by adding LdHPCL71 and LdHPCL76 to a previously generated tree containing 685 whole-genome *L. donovani* isolates (*3*). As shown previously, the topology of the tree matches the geographic origin of the samples used (*2*). Consistent with the previous report from Himachal Pradesh (*3*), phylogenetic analysis of the new LdHPCL71 and LdHPCL76 CL lineages revealed that they also clustered within the ISC1 Yeti clade of *L. donovani* (Figure). Because the previously identified cutaneous lineage LdHPCL66 from Himachal Pradesh was an intraspecific hybrid (*3*), we next investigated whether the LdHPCL71 and LdHPCL76 parasites were also hybrids. We used VarScan (https://varscan.sourceforge.net) to identify all single-nucleotide polymorphisms (SNPs) by using the Sri Lanka CL *L. donovani* reference strain (*6*) and compared the SNP frequencies with previous data on hybrid parasites (Appendix Figure 2, panel A). We plotted the full genomic representation for all 36 chromosomes for each parasite by using Circos (https://circos.ca) (Appendix Figure 2, panel B).

The heterozygosity index of LdHPCL71 was 0.168 and of LdHPCL76 was 0.158, suggesting that they are not hybrids because the known hybrids have been shown to contain a large portion of heterozygous SNPs (*2*,*3*). In addition, the many SNPs seen (Appendix Figure 2, panel B) are homozygous, indicating the lineages are distant from the core *L. donovani* parasite population in India but neither parasite seems to be a hybrid. We compared the SNPs from each of the newly identified parasites with the SNPs from the previously isolated LdHPCL66 hybrids from the Yeti ISC1 group to determine if a subset of SNPs is common among the 3 lineages (Appendix Table). We found too many SNPs in common between the parasites to specifically associate any of them with the CL manifestations in patients because they are from 3 divergent lineages in an undersampled population.

Our data, combined with other reports of ISC1 spread (*7*), could support the theory that atypical *L. donovani* parasites are being increasingly encountered

[1]These first authors contributed equally to this article.

[2]These authors were co–principal investigators.

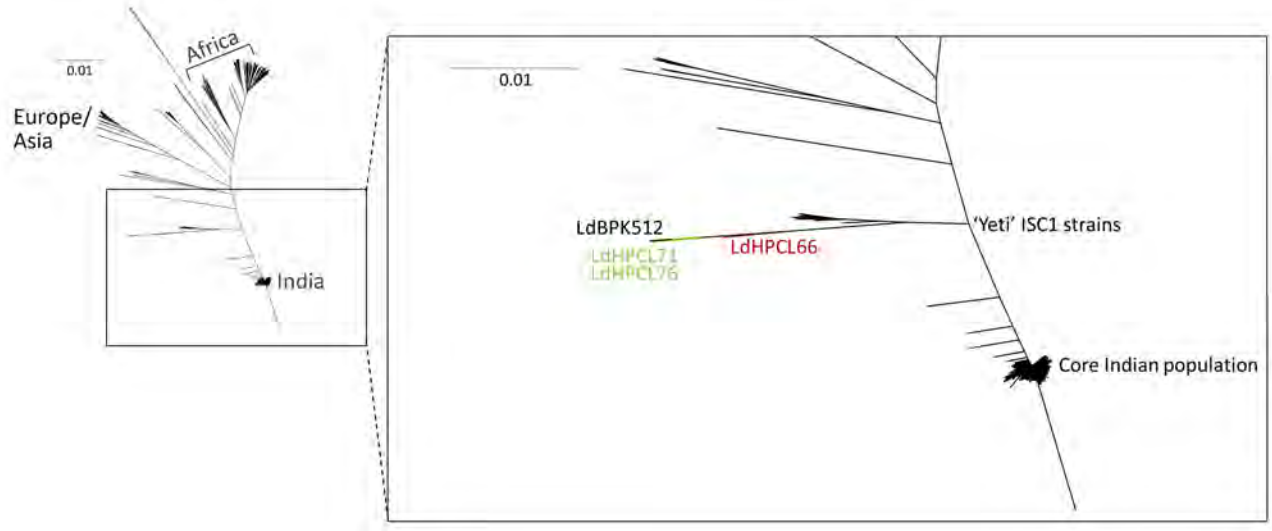

Figure. Phylogeny of *Leishmania donovani* lineages associated with cutaneous leishmaniasis, Himachal Pradesh, India, 2023. Novel *L. donovani* from this study (green) are compared with the global population of the 684 parasites previously reported in the *L. donovani* complex, including reference strains *L. donovani* LV9, *L. donovani* BHU 1220, and *L. donovani* BPK282A1. The previously isolated interspecific hybrid LdHPCL66 (red) falls halfway between the unique LDBPK512 and Yeti-ISC1 lineages. The novel LdHPCL71 and LdHPCL76 (green) nonhybrid parasites are more closely related to the unique LdBPK512 parasite. Scale bar indicates the modified Euclidian distance as calculated by TASSEL (https://tassel.bitbucket.io).

as a cause of CL in the Indian subcontinent. That hypothesis is further supported by a recent report on occurrence of CL cases in provinces in Nepal caused by *L. donovani* that are endemic and nonendemic for visceral disease (*8*). Of potential concern, this clade now includes both hybrid and nonhybrid parasites able to cause VL and CL. Emergence of such CL-causing *L. donovani* parasites highlights the urgent need for molecular surveillance as an integral part of the ongoing kala-azar elimination program in the Indian subcontinent. The ongoing regional strategic framework emphasizes the need to control post–kala-azar dermal leishmaniasis cases as a parasite reservoir to break the transmission cycle for sustaining the elimination program (*9*). On a similar note, CL cases caused by atypical *L. donovani* genotypes may also contribute to the transmission cycle of VL in some patients. Our observations support the argument that surveillance of atypical *L. donovani* lineages associated with CL should be included in VL elimination programs.

Acknowledgments

We thank Rentala Madhubala for generously gifting *L. donovani* and *L. major* standard cultures used as controls in initial species identification (data not shown).

Informed consent was obtained from the patients with due approval of the study by the Institutional Ethics Committee of Indira Gandhi Medical College, approval no. HFW (MS) G-5 (Ethics)/2014-10886.

G.M. and P.L. received support from the Canadian Institutes of Health Research (G.M. grant no. 153282, P.L. grant no. 187858). M.J. received a collaborative research grant from International Centre for Genetic Engineering and Biotechnology, Trieste, Italy (project no. CRP/IND19-01) under collaborative research project and Indian Council of Medical Research, ICMR (no. 6/9-7 272/KA/2021/ECD-II). Y.C. is supported by a fellowship from University Grant Commission, India. K.P. is supported by the Fonds de recherche du Québec (doctoral award).

About the Author

Dr. Lypaczewski is a researcher with the Department of Microbiology & Immunology at McGill University. His research interests are parasitic diseases and all aspects of microbial genetics, including sample collection, DNA extraction, sequencing, and bioinformatics.

References

1. Burza S, Croft SL, Boelaert M. Leishmaniasis. Lancet. 2018; 392:951–70. https://doi.org/10.1016/S0140-6736(18)31204-2
2. Lypaczewski P, Matlashewski G. *Leishmania donovani* hybridisation and introgression in nature: a comparative genomic investigation. Lancet Microbe. 2021;2:e250–8. https://doi.org/10.1016/S2666-5247(21)00028-8
3. Lypaczewski P, Thakur L, Jain A, Kumari S, Paulini K, Matlashewski G, et al. An intraspecies *Leishmania donovani* hybrid from the Indian subcontinent is associated with an atypical phenotype of cutaneous disease. iScience. 2022;25:103802. https://doi.org/10.1016/j.isci.2022.103802

4. Thakur L, Singh KK, Shanker V, Negi A, Jain A, Matlashewski G, et al. Atypical leishmaniasis: a global perspective with emphasis on the Indian subcontinent. PLoS Negl Trop Dis. 2018;12:e0006659. https://doi.org/10.1371/journal.pntd.0006659
5. Zhang WW, Ramasamy G, McCall LI, Haydock A, Ranasinghe S, Abeygunasekara P, et al. Genetic analysis of *Leishmania donovani* tropism using a naturally attenuated cutaneous strain. PLoS Pathog. 2014;10:e1004244. https://doi.org/10.1371/journal.ppat.1004244
6. Lypaczewski P, Hoshizaki J, Zhang WW, McCall LI, Torcivia-Rodriguez J, Simonyan V, et al. A complete *Leishmania donovani* reference genome identifies novel genetic variations associated with virulence. Sci Rep. 2018;8:16549. https://doi.org/10.1038/s41598-018-34812-x
7. Monsieurs P, Cloots K, Uranw S, Banjara MR, Ghimire P, Burza S, et al. Source tracing of *Leishmania donovani* in emerging foci of visceral leishmaniasis, Western Nepal. Emerg Infect Dis. 2024;30:611–3. https://doi.org/10.3201/eid3003.231160
8. Rai T, Shrestha S, Prajapati S, Bastola A, Parajuli N, Ghimire PG, et al. *Leishmania donovani* persistence and circulation causing cutaneous leishmaniasis in unusual-foci of Nepal. Sci Rep. 2023;13:12329. https://doi.org/10.1038/s41598-023-37458-6
9. Kumar A, Singh VK, Tiwari R, Madhukar P, Rajneesh, Kumar S, et al. Post kala-azar dermal leishmaniasis in the Indian sub-continent: challenges and strategies for elimination. Front Immunol. 2023;14:1236952. https://doi.org/10.3389/fimmu.2023.1236952

Address for correspondence: Greg Matlashewski, McGill University, 3775 University St, Rm 511, Montreal, QC H3A 2B4, Canada; email: greg.matlashewski@mcgill.ca

Powassan Virus Encephalitis after Tick Bite, Manitoba, Canada

Nathan Smith, Yoav Keynan,[1] Terry Wuerz,[1] Aditya Sharma[1]

Author affiliation: University of Manitoba, Winnipeg, Manitoba, Canada

DOI: https://doi.org/10.3201/eid3009.231344

[1]These senior authors contributed equally to this article.

A case of Powassan encephalitis occurred in Manitoba, Canada, after the bite of a black-legged tick. Awareness of this emerging tickborne illness is needed because the number of vector tick species is growing. No specific treatment options exist, and cases with illness and death are high. Prevention is crucial.

On October 2, 2022, a 60-year-old male hobbyist outdoor photographer in southern Manitoba, Canada, noticed a black-legged tick (*Ixodes scapularis*) attached to his neck (Figure). The patient sought treatment for possible Lyme disease and was prescribed doxycycline.

On October 16, 2 weeks after the tick bite, the patient had complaints of diarrhea, nausea, and malaise. He also had a fever that reached 40°C (104°F), a 10–15-pound weight loss, difficulty concentrating, and a bilateral headache, and he became bedbound from weakness and ataxia. He was admitted to a hospital in Winnipeg, Manitoba on November 1. He had a history of hypertension for which he was taking ramipril and right arm thrombosis for which he was taking apixaban.

The patient complained of radicular pain in his arms and legs requiring opioids. He recalled no recent travel, immunizations, or mosquito bites. Physical examination revealed tachycardia, confusion, dysarthria, and difficulty following commands. He did not have fever, rash, or nuchal rigidity. A neurologic examination demonstrated a bilateral intention tremor, twitching, dysmetria, and ataxia.

Laboratory testing of the patient's blood samples showed mild hypokalemia and leukopenia (4.1 cells/μL). Magnetic resonance imaging of the patient's brain revealed a punctate T2 hyperintensity in the right frontal lobe white matter. Electroencephalography revealed mild bilateral fronto-temporal cerebral dysfunction. Cerebrospinal fluid (CSF) examination showed 41 nucleated cells/mm^3 (89% lymphocytes) and a protein level of 1.41 g/L (reference range 0.2–0.4 g/L); glucose level was within reference range. Results of laboratory testing of the CSF was negative for West Nile virus IgM, Epstein-Barr virus, cytomegalovirus, herpes simplex virus 1 and 2, and varicella zoster virus; bacterial and viral cultures yielded negative results. PCR testing of the CSF was negative for human herpesvirus 6. Additional serum testing was negative for HIV, syphilis, hepatitis B and C, and Lyme disease. PCR testing on a stool sample was negative for enteroviruses.

We ordered Powassan virus (POWV) testing of convalescent serum, and results were positive for IgM. A 90% plaque reduction neutralization test

Figure. Black-legged tick (*Ixodes scapularis*) after removal with tweezers from a patient in Manitoba, Canada, who was later diagnosed with Powassan virus.

($PRNT_{90}$) resulted in antibody neutralization at a dilution of 1:80 on November 3 and then 1:160 on November 6. On the basis of clinical symptoms, timeline from tick attachment to symptom onset, and confirmatory $PRNT_{90}$, we made a diagnosis of Powassan encephalitis. After 1 week, the patient improved and was discharged. Repeat serologic testing on July 14, 2023, showed that $PRNT_{90}$ had decreased to 1:20.

POWV is a flavivirus transmitted by tick species that also act as reservoirs (*1*). The most consequential vectors are black-legged ticks, which are known to bite humans and can spread other tickborne pathogens such as *Borrelia burgdorferi* (Lyme disease), *Anaplasma phagocytophilum* (anaplasmosis), and *Babesia microti* (babesiosis) (*2*). Those pathogens require tick attachment periods ≥24 hours (*2*), but according to animal studies, the transmission time of POWV from vector to host can occur in 15 minutes (*2*), although transmission typically occurs after 3 hours in humans (*3*). No human-to-human transmission has been reported.

POWV is found in Canada, the United States, and Russia (*1*). In the northeastern United States, ≥200 cases have been reported. The highest incidence is in Wisconsin and Minnesota, both bordering Manitoba (*1*,*4*). Cases occur predominantly in May–November, when ticks are active (*4*). Only 21 cases have been reported in Ontario, New Brunswick, and Quebec (*1*), Canada. The true prevalence in Canada is unknown because POWV is not a reportable disease. Serologic surveys from 1968–1969 in British Columbia found antibodies in 0.129% of those tested and higher rates of 12.4% in outdoor workers (*5*). Studies in Ontario from the 1970s found antibodies in 0.70% of persons tested (*1*). The range of black-legged ticks is expanding up to 46 km annually, so exposure is likely increasing (*6*). No data on the prevalence of POWV in black-legged ticks in Manitoba have been published.

The incubation period of POWV is 7–34 days, after which 1–3 days of influenza-like prodrome occurs (*7*). Central nervous system infection with encephalitis is common (*7*). During 2011–2020, the United States reported 194 cases; 91.75% were neuroinvasive, and 10%–15% resulted in death (*4*,*7*). Fevers, weakness, headaches, and altered sensorium are the most common patient complaints reported (*7*,*8*). Other complaints include gastrointestinal involvement, focal neurologic signs, seizures, ataxia, twitching, tremors, and radiculitis (*7*). Magnetic resonance imaging findings commonly include T2/flair hyperintensities in the brainstem, cortex, and deep gray structures (*9*). Electroencephalography slowing has been described (*8*). Those findings are corroborated by autopsy results showing high POWV RNA levels in brain tissue (*10*). Neurologic sequelae occur in ≥50% of survivors. In the case we report, the patient reported persistent ataxia for months. Because no specific antiviral drug is available, disease management consists of supportive measures for airway protection and cerebral edema and analgesia for radiculitis.

A lack of reporting, limited awareness of POWV as a causative agent of encephalitis, expanding tick range, and incomplete knowledge of prevalence has led to a lack of action against this emerging virus. Prevention strategies include avoiding ticks, using insect repellant, treating clothing with 0.5% permethrin in endemic areas, and frequent tick checks.

About the Author

Dr. Smith is a second-year core internal medicine resident with the Max Rady College of Medicine at the University of Manitoba. Research interests include infectious disease and general internal medicine.

References

1. Corrin T, Greig J, Harding S, Young I, Mascarenhas M, Waddell LA. Powassan virus, a scoping review of the global evidence. Zoonoses Public Health. 2018;65:595–624. https://doi.org/10.1111/zph.12485
2. Eisen L. Pathogen transmission in relation to duration of attachment by *Ixodes scapularis* ticks. Ticks Tick Borne Dis. 2018;9:535–42. https://doi.org/10.1016/j.ttbdis.2018.01.002
3. Feder HM Jr, Telford S III, Goethert HK, Wormser GP. Powassan virus encephalitis following brief attachment

of Connecticut deer ticks. Clin Infect Dis. 2021;73:e2350–4. https://doi.org/10.1093/cid/ciaa1183
4. Centers for Disease Control and Prevention. Powassan virus [cited 2022 Dec 1]. https://www.cdc.gov/powassan/statistics.html.
5. Kettyls GD, Verrall VM, Wilton LD, Clapp JB, Clarke DA, Rublee JD. Arbovirus infections in man in British Columbia. Can Med Assoc J. 1972;106:1175–9.
6. Clow KM, Leighton PA, Ogden NH, Lindsay LR, Michel P, Pearl DL, et al. Northward range expansion of *Ixodes scapularis* evident over a short timescale in Ontario, Canada. PLoS One. 2017;12:e0189393. https://doi.org/10.1371/journal.pone.0189393
7. Kemenesi G, Bányai K. Tickborne flaviviruses, with a focus on Powassan virus. Clin Microbiol Rev. 2018;32:e00106–17. https://doi.org/10.1128/CMR.00106-17
8. El Khoury MY, Camargo JF, White JL, Backenson BP, Dupuis AP II, Escuyer KL, et al. Potential role of deer tick virus in Powassan encephalitis cases in Lyme disease–endemic areas of New York, USA. Emerg Infect Dis. 2013;19:1926–33. https://doi.org/10.3201/eid1912.130903
9. Piantadosi A, Rubin DB, McQuillen DP, Hsu L, Lederer PA, Ashbaugh CD, et al. Emerging cases of Powassan virus encephalitis in New England: clinical presentation, imaging, and review of the literature. Clin Infect Dis. 2016;62:707–13. https://doi.org/10.1093/cid/civ1005
10. Normandin E, Solomon IH, Zamirpour S et al. Powassan virus neuropathology and genomic diversity in patients with fatal encephalitis. Open Forum Infect Dis. 2020;7:ofaa392.

Address for correspondence: Nathan Smith, University of Manitoba, 561 Trent Ave, Winnipeg, MB R2K1G2, Canada; email: smithn4@myumanitoba.ca

Thelazia callipaeda Eyeworms in American Black Bear, Pennsylvania, USA, 2023

Caroline Sobotyk, Jaclyn Dietrich, Guilherme G. Verocai, Lauren Maxwell, Kevin Niedringhaus

Author affiliations: University of Pennsylvania School of Veterinary Medicine, Philadelphia, Pennsylvania, USA (C. Sobotyk, J. Dietrich, L. Maxwell, K. Niedringhaus); Texas A&M University College of Veterinary Medicine and Biomedical Sciences, College Station, Texas, USA (Guilherme G. Verocai)

DOI: https://doi.org/10.3201/eid3009.240679

We identified a *Thelazia callipaeda* eyeworm in an American black bear in Pennsylvania, USA, on the basis of its morphological features and molecular analysis. Our finding highlights emergence of a *T. callipaeda* worm sylvatic transmission cycle in the United States.

Thelaziosis is an emerging zoonotic disease caused by nematodes of the genus *Thelazia* (Spirurida, Thelazioidea). In the United States, 3 zoonotic species have been identified: *Thelazia gulosa* (*1*), *T. californiensis* (*2*), and most recently *T. callipaeda* (*3*). In Asia and Europe, *T. callipaeda* is considered the main agent of

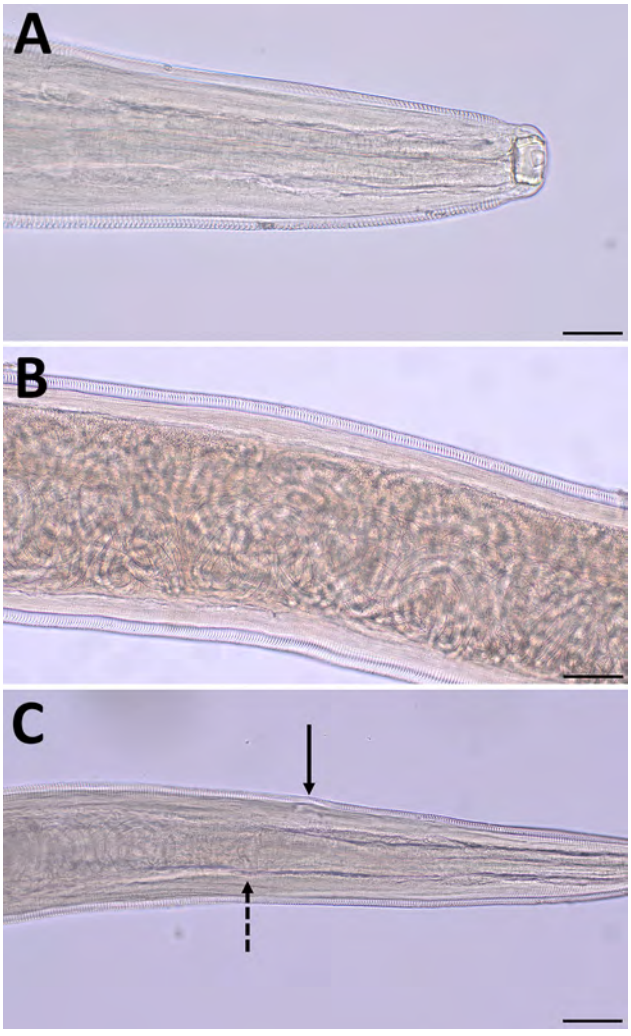

Figure 1. Morphologic features of adult female *Thelazia callipaeda* eyeworm isolated from an American black bear in Coolbaugh Township, Monroe County, Pennsylvania, USA, 2023. A) Anterior end showing the large, deep, cup-shaped buccal cavity. Scale bar indicates 50 μm. B) Midbody region showing the thin transverse cuticular striations pattern and numerous coiled first-stage larvae. Scale bar indicates 100 μm. C) Anterior end showing the location of the vulvar opening anterior to the esophageal-intestinal junction. Dashed black arrow indicates esophageal-intestinal junction; solid black arrow indicates the vulval opening. Scale bar indicates 100 μm.

thelaziosis in humans, domestic animals, and wild animals (*4*). Over the past decade, the geographic distribution and prevalence of *T. callipaeda* infection has increased worldwide in scale and intensity (*4*). The first autochthonous case in the United States was reported in 2018 in a domestic dog (*Canis lupus familiaris*) from New York with a history of unilateral epiphora and blepharospasm. Since then, additional cases in domestic dogs and cats have been reported, predominately from the northeastern United States (*3*,*5*).

T. callipaeda eyeworms are found in the conjunctival sac and lacrimal duct of the definitive host. They are transmitted when a male zoophilic secretophagous *Phortica variegata* fly ingests first-stage larvae from the host's lachrymal secretions. In the vector, the first-stage larvae molt to the infective third-stage larvae in the testes, migrate to the mouthparts, and are transferred to another host during subsequent feeding on lachrymal secretions (*4*).

The role of wildlife in the epidemiology and emergence of *T. callipaeda* eyeworms is not completely known. In Europe, cases of *T. callipaeda* eyeworm infection have been detected in a wide range of hosts, including wild carnivores, omnivores, and lagomorphs (*6*,*7*). Wild canids, particularly red foxes (*Vulpes vulpes*), seem to play a large role in

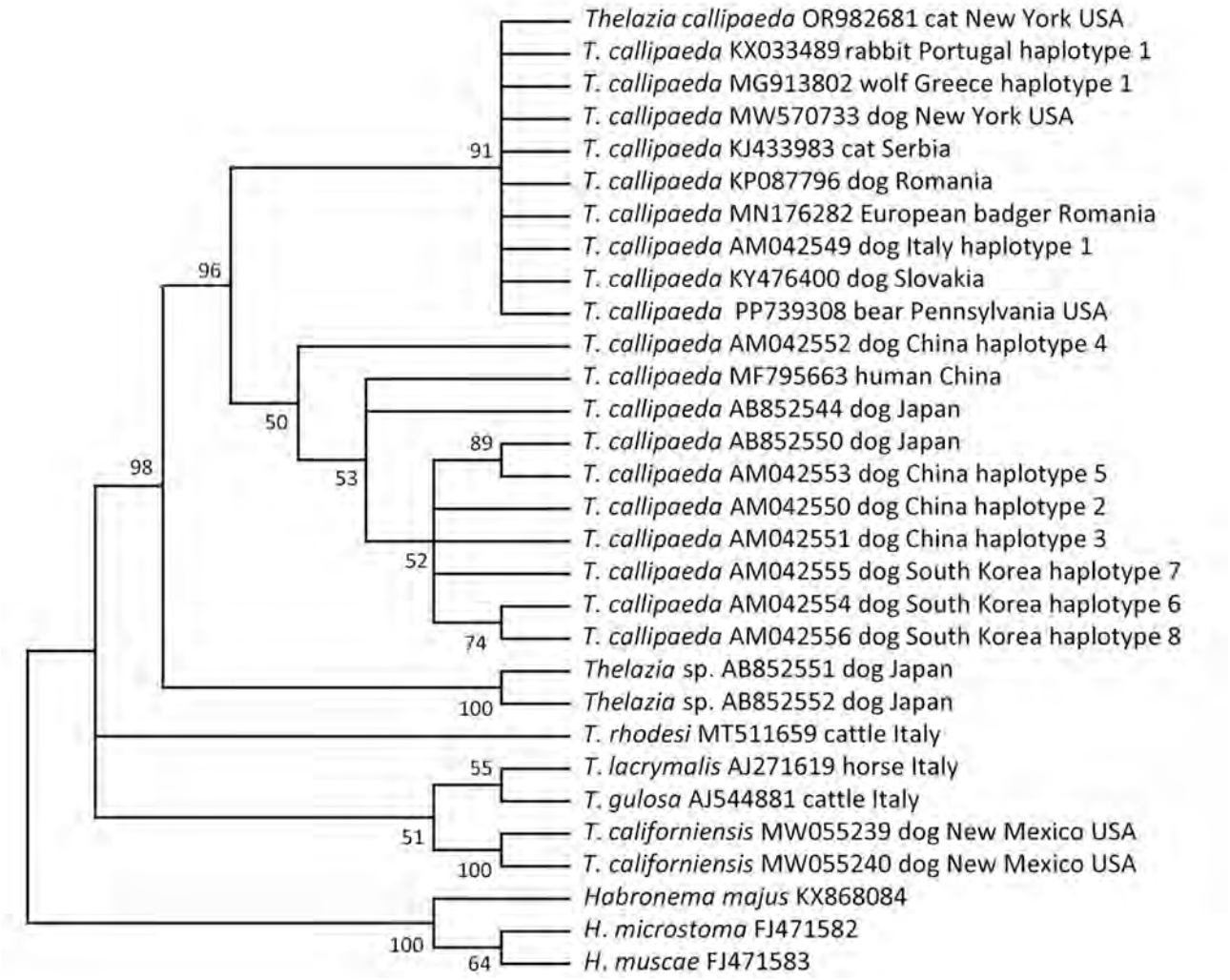

Figure 2. Phylogenetic relationship of *Thelazia callipaeda* isolate from an American black bear in Coolbaugh Township, Monroe County, Pennsylvania, USA, 2023 (GenBank accession no. PP739308), and other species of *Thelazia* available in GenBank (accession numbers shown). Analysis was performed by using the maximum-likelihood method (1,000 bootstrap replicates) in MEGA X version 11 (https://www.megasoftware.net). The best-fit nucleotide substitution model for the dataset was Tamura-Nei with a discrete gamma distribution, which was used to model evolutionary rate differences among sites (5 categories [+G, parameter = 0.2578]). That analysis involved 30 nucleotide sequences. There were 647 positions in the final dataset. Distances, defined as the number of nucleotide substitutions/site, were calculated by using that model. Branches corresponding to partitions reproduced in <50% of bootstrap replicates are collapsed.

maintaining the sylvatic cycle in thelaziosis-endemic areas of Europe (*7*). However, knowledge of the sylvatic transmission cycle of *T. callipaeda* eyeworms, along with their environmental and anthropogenic factors, remains limited. Considering the emergence of those zoonotic nematodes in non–thelaziosis-endemic areas and the need for more information about their ecology and epidemiology in the United States, we report a case of *T. callipaeda* eyeworm infection in an American black bear (*Ursus americanus*) and identify a new geographic location of transmission.

In November 2023, an adult, female American black bear was legally harvested in Coolbaugh Township, Monroe County, Pennsylvania. During processing of the bear for taxidermy preparation, multiple linear nematodes were observed behind the third eyelid. Nematodes were extracted and submitted for identification. Two additional harvested bears from Monroe and Pike Counties, Pennsylvania, were also reported to have similar ocular nematode infections, but specimens from those bears were not collected.

We identified 9 female and 4 male adult nematodes from the bear as *T. callipaeda* on the basis of morphologic and morphometric features (*8*). The nematodes were characterized by the presence of a cup-shaped buccal capsule and cuticular transverse striations, as well as the location of the vulvar opening anterior to the esophageal-intestinal junction on the female worms (Figure 1). Female nematodes were 1.16–1.46 cm long and 0.36–0.42 mm wide; male worms were 0.82–1.06 cm long and 0.31–0.42 mm wide. The number of transverse cuticular striations ranged from 160 to 400/mm in the cephalic, midbody, and caudal regions.

We extracted genomic DNA from a midbody fragment of a female adult worm and amplified, sequenced, and analyzed the partial cytochrome oxidase c subunit I (*cox*1) gene, as previously described (*2*). We generated a 623-bp *cox*1 sequence (GenBank accession no. PP739308), which showed 99%–100% maximum identity with *T. callipaeda* sequences available in GenBank. Phylogenetic analysis was performed by using the maximum-likelihood method and confirmed the taxonomic identification of *T. callipaeda*. The isolate clustered with all previous isolates from domestic animals in North America and with some isolates from Europe (Figure 2), indicating circulation of the newly introduced pathogen in wildlife habitats and transmission from domestic animals to wildlife.

The presence of adult *T. callipaeda* eyeworms in an American black bear suggests the establishment of a sylvatic transmission cycle in the United States and expansion of the number of definitive host species used by the zoonotic nematode. In the past decade, wild carnivores have been identified as primary definitive hosts associated with the sylvatic cycle in thelaziosis-endemic and non–thelaziosis-endemic areas of Europe and Asia (*7*). American black bears are the most widely distributed species of bear in North America, inhabiting diverse regions throughout Mexico, Canada, and the United States (*9*). Given the bears' extensive geographic distribution and frequent and close interaction with humans and pets (*10*), thelaziosis in the black bear population raises concerns about the rapidly increasing incidence and geographic range of *T. callipaeda* eyeworms in the United States. Although further research into the extent to which black bears play a role in the maintenance of the sylvatic cycle and transmission of *T. callipaeda* eyeworms is needed, the presence of the zoonotic nematode in such a wide range of hosts implicates exposure and risk for transmission to threatened and endangered species and direct or indirect risk for transmission to humans and domestic animals.

Acknowledgments

We thank the Pennsylvania Game Commission and Dillon Gruver for their continued support. We also acknowledge Shawn Lamparter's Wildlife Design for recognition and prompting submission of the specimens.

About the Author

Dr. Sobotyk is an assistant professor of clinical parasitology and director of the Clinical Parasitology Laboratory at the University of Pennsylvania, Philadelphia, PA. Her research focuses on zoonotic helminth infections in domestic and wild animals and improvement and development of diagnostic techniques for detecting parasitic infections of veterinary and public health relevance.

References

1. Bradbury RS, Breen KV, Bonura EM, Hoyt JW, Bishop HS. Case report: conjunctival infestation with *Thelazia gulosa*: a novel agent of human thelaziasis in the United States. Am J Trop Med Hyg. 2018;98:1171–4. https://doi.org/10.4269/ajtmh.17-0870
2. Sobotyk C, Foster T, Callahan RT, McLean NJ, Verocai GG. Zoonotic *Thelazia californiensis* in dogs from New Mexico, USA, and a review of North American cases in animals and humans. Vet Parasitol Reg Stud Rep. 2021;24:100553. https://doi.org/10.1016/j.vprsr.2021.100553
3. Schwartz AB, Lejeune M, Verocai GG, Young R, Schwartz PH. Autochthonous *Thelazia callipaeda* infection in dog, New York, USA, 2020. Emerg Infect Dis. 2021;27:1923–6. https://doi.org/10.3201/eid2707.210019
4. Otranto D, Mendoza-Roldan JA, Dantas-Torres F. *Thelazia callipaeda*. Trends Parasitol. 2021;37:263–4. https://doi.org/10.1016/j.pt.2020.04.013

5. Manoj RRS, White H, Young R, Brown CE, Wilcox R, Otranto D, et al. Emergence of thelaziosis caused by *Thelazia callipaeda* in dogs and cats, United States. Emerg Infect Dis. 2024;30:591–4. https://doi.org/10.3201/eid3003.230700
6. Papadopoulos E, Komnenou A, Karamanlidis AA, Bezerra-Santos MA, Otranto D. Zoonotic *Thelazia callipaeda* eyeworm in brown bears (*Ursus arctos*): a new host record in Europe. Transbound Emerg Dis. 2022;69:235–9. https://doi.org/10.1111/tbed.14414
7. Otranto D, Dantas-Torres F, Mallia E, DiGeronimo PM, Brianti E, Testini G, et al. *Thelazia callipaeda* (Spirurida, Thelaziidae) in wild animals: report of new host species and ecological implications. Vet Parasitol. 2009;166:262–7. https://doi.org/10.1016/j.vetpar.2009.08.027
8. Otranto D, Lia RP, Traversa D, Giannetto S. *Thelazia callipaeda* (Spirurida, Thelaziidae) of carnivores and humans: morphological study by light and scanning electron microscopy. Parassitologia. 2003;45:125–33.
9. Garshelis DL, Scheick BK, Doan-Crider DL, Beecham JJ, Obbard ME. The American black Bear (*Ursus americanus*). The IUCN Red List of Threatened Species. Washington (DC): International Union for Conservation of Nature. 2016:e. T41687A114251609.
10. Di Salvo AR, Chomel BB. Zoonoses and potential zoonoses of bears. Zoonoses Public Health. 2020;67:3–13. https://doi.org/10.1111/zph.12674

Address for correspondence: Caroline Sobotyk, University of Pennsylvania, School of Veterinary Medicine, Matthew J. Ryan Veterinary Hospital, Rm 4034, 3900 Delancey St, Philadelphia, PA 19104-6051, USA; email: csobotyk@vet.upenn.edu

Molecular Confirmation of *Taenia solium* Taeniasis in Child, Timor-Leste

Hanna Jin, Sung-Tae Hong, Merita Antonio Armindo Monteiro, Endang da Silva, Odete da Silva Viegas, Felix dos Santos Lopes, Dong Hee Kim, Sung Hye Kim

Author affiliations: Seoul National University, Seoul, South Korea (H. Jin, S.-T. Hong, D.H. Kim); Ministry of Health, Dili, Timor-Leste (M.A.A. Monteiro, E. da Silva, O. da Silva Viegas); World Health Organization Timor-Leste Country Office, Dili (F. dos Santos Lopes); Hanyang University College of Medicine, Seoul (S.H. Kim)

DOI: https://doi.org/10.3201/eid3009.240238

We report a case of *Taenia solium* taeniasis in a 10-year-old child in Timor-Leste, confirmed by molecular analysis, suggesting *T. solium* transmission to humans is occurring in Timor-Leste. Proactive measures are needed to improve public understanding of prevalence, geographic spread, and health implications of human taeniasis and cysticercosis in Timor-Leste.

The pork tapeworm, *Taenia solium*, causes human taeniasis and cysticercosis, which are considerable health problems in many developing countries (*1*). In Southeast Asia, *T. solium* infections are considered endemic, but epidemiologic data remain scarce (*2*). We report a case of *T. solium* taeniasis in Timor-Leste, confirmed by molecular methods.

In March 2019, as part of routine monitoring by the Timor-Leste Ministry of Health's national control program targeting soil-transmitted helminthiasis, in collaboration with the World Health Organization's country office, 1,121 fecal samples from school children in Timor-Leste were examined by using the Kato-Katz method. *Taenia* spp. eggs were identified in 4 samples. Subsequently, we conducted home visits for each affected child and administered a single dose of 10 mg/kg praziquantel (Shin Poong Pharmaceutical Co. Ltd, https://shinpoong.co.kr). We were able to collect expelled worm segments on the same day of treatment from a 10-year-old girl residing in Dili, the capital of Timor-Leste. Throughout most of her life, the child had remained in good health and had not manifested symptoms indicative of human taeniasis. Also, she had not traveled outside of the country.

The retrieved worm segments exhibited a flat, creamy white appearance, aligning with the typical macroscopic characteristics associated with *Taenia* spp. (Figure 1). Microscopic analysis of the segments revealed ≈50 gravid, 20 mature, and 20 immature proglottids of *T. solium*.

To determine the species through molecular analysis, we isolated genomic DNA from 1 segment by using the DNeasy Blood & Tissue Kit (QIAGEN, https://www.qiagen.com), according to the manufacturer's instructions. We performed PCR of genomic DNA to detect the parasite mitochondrial *cox-1* gene that encodes cytochrome c oxidase subunit I (Appendix, https://wwwnc.cdc.gov/EID/article/30/9/22-0154-App1.pdf) (*3*). We purified the PCR products by using DNA Clean & Concentrator-5 (Zymo Research, https://www.zymoresearch.com), according to the manufacturer's protocol. Sanger sequencing was subsequently performed by Bioneer Co., Ltd. (https://www.bioneer.co.kr), which used an ABI3730XL instrument (Applied Biosystems/Thermo Fisher Scientific,

Figure 1. Proglottids of *Taenia solium* collected from a patient in Dili, Timor-Leste, in case study of molecular confirmation of taeniasis in a child. We collected the expelled worm segments from a 10-year-old girl on the same day she was treated with 10 mg/kg praziquantel.

whttps://www.thermofisher.com). We deposited the derived sequence in GenBank (accession no. PP837933.1) and compared it with other *cox-1* sequences in GenBank by using BLAST (https://blast.ncbi.nlm.nih.gov). The sequence showed 98.85%–100% identity with the *T. solium* mitochondrial *cox-1* gene. We used *cox-1* sequences for phylogenetic reconstruction (Figure 2; Appendix). We aligned DNA sequences by using ClustalW (http://www.clustal.org) and conducted evolutionary analyses by using MEGA11 (*4*). The sequence isolated in this study was shown to be most homologous with an isolate from Tulear (also known as Toliara), Madagascar (GenBank accession no. FM958316.1) (*5*). Consequently, molecular evaluation confirmed the infection was caused by *T. solium*.

We report documented human *T. solium* taeniasis in Timor-Leste, an area where previous records of the parasite have been nearly absent (*6*). Clinically diagnosed neurocysticercosis in persons from Timor have been reported in Australia and Indonesia, suggesting the presence of *T. solium* in Timor-Leste (*7*,*8*). However, the only documentation of human taeniasis/cysticercosis within Timor-Leste is a case of oral cysticercosis in a person originally from Timor-Leste reported in Northern Ireland in 2015 (*9*). That particular patient exhibited symptoms of oral submucosal swelling and had relocated from Timor-Leste in 2006. Because no alternative sources of cysticercosis were identified, it is likely that the patient acquired the infection in Timor-Leste before migrating to Northern Ireland, a region where cysticercosis is not endemic (*9*). Similarly, a high probability exists that the child's infection in this case study originated within Timor-Leste, because she had not traveled outside of the country before the worm was detected. Through interviews, we found that she had regular interactions with confined pigs in her backyard and with free-ranging pigs within the village where she lived previously. However, the presence of *T. solium* cysticerci in those pigs and potential infection status remains undetermined.

The *cox-1* sequence from the worm isolated in Timor-Leste was closely related to sequences collected in Toliara in southern Madagascar. According to a previous study conducted in Madagascar, specimens from Toliara had diverged from parasites of the African/South American genotype (*5*). However, the lack of data limits what we can infer about *T. solium* in Timor-Leste. Further epidemiologic studies are needed to determine the extent of *T. solium* infection in pigs and to guide the implementation of control programs.

In conclusion, *T. solium* infections have been identified as endemic in Timor-Leste, a nation previously devoid of documented cases. Considering the widespread practice of backyard pig farming and the presence of free-roaming pigs across much of the country (*10*), veterinarians and clinicians should be vigilant in suspecting this emerging zoonotic parasite as a cause of taeniasis, not only in pig populations but also in humans. Furthermore, we urge health authorities in Timor-Leste to take proactive measures to enhance public understanding of the prevalence, geographic spread, and health implications of human taeniasis and cysticercosis within the nation.

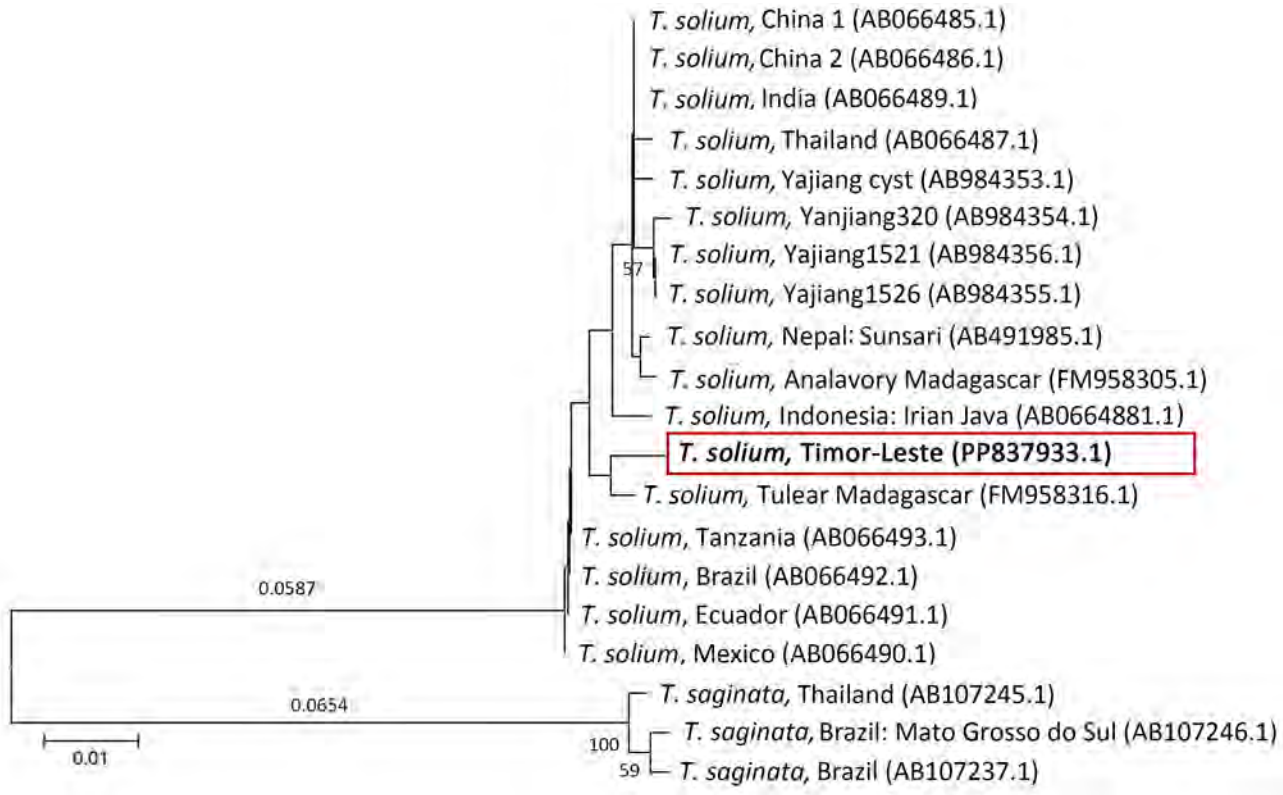

Figure 2. Phylogenetic analysis of the *cox-1* gene in case study of *Taenia solium* taeniasis in a child, Timor-Leste. Evolutionary history was inferred by using the neighbor-joining method and analysis was conducted by using MEGA11 (*4*). Red box and bold text indicates the sequence from this study. GenBank accession numbers are indicated in parentheses. Percentages of replicate trees in which the associated taxa clustered together in the bootstrap test (1,000 replicates) are shown below the branches. Tree is drawn to scale; branch lengths (above the branches) are in the same units as those of the evolutionary distances used to infer the phylogenetic tree. The evolutionary distances were computed by using the Kimura 2–parameter method. Analysis involved 20-nt sequences. Codon positions included were first + second + third + noncoding. All ambiguous positions were removed for each sequence pair (pairwise deletion option). A total of 480 positions were in the final dataset. Scale bar indicates nucleotide substitutions per site.

This work was partly supported by the Korea International Cooperation Agency's project of integrated control and elimination of neglected tropical diseases in Timor-Leste, the Education and Research Encouragement Fund of Seoul National University Hospital, and the research fund of Hanyang University (no. HY-202000000000495).

About the Author

Dr. Jin is a doctoral student in the Department of Tropical Medicine and Parasitology, Seoul National University College of Medicine, Seoul, South Korea. Her primary research interests focus on public health and neglected tropical diseases.

References

1. World Health Organization. WHO guidelines on management of *Taenia solium* neurocysticercosis. 2021 [cited 2024 Apr 17]. https://www.who.int/publications/i/item/9789240032231
2. Wu HW, Ito A, Ai L, Zhou XN, Acosta LP, Lee Willingham A III. Cysticercosis/taeniasis endemicity in Southeast Asia: current status and control measures. Acta Trop. 2017;165:121–32. https://doi.org/10.1016/j.actatropica.2016.01.013
3. Cho J, Jung BK, Lim H, Kim MJ, Yooyen T, Lee D, et al. Four cases of *Taenia saginata* infection with an analysis of COX1 gene. Korean J Parasitol. 2014;52:79–83. https://doi.org/10.3347/kjp.2014.52.1.79
4. Tamura K, Stecher G, Kumar S. MEGA11: molecular evolutionary genetics analysis version 11. Mol Biol Evol. 2021;38:3022–7. https://doi.org/10.1093/molbev/msab120
5. Michelet L, Carod JF, Rakontondrazaka M, Ma L, Gay F, Dauga C. The pig tapeworm *Taenia solium*, the cause of cysticercosis: biogeographic (temporal and spacial) origins in Madagascar. Mol Phylogenet Evol. 2010;55:744–50. https://doi.org/10.1016/j.ympev.2010.01.008
6. Ito A, Wandra T, Li T, Dekumyoy P, Nkouawa A, Okamoto M, et al. The present situation of human taeniases and cysticercosis in Asia. Recent Pat Antiinfect Drug Discov. 2014;9:173–85. https://doi.org/10.2174/1574891X10666150410125711
7. Walker J, Chen S, Packham D, McIntyre P. Five cases of neurocysticercosis diagnosed in Sydney. Southeast Asian J Trop Med Public Health. 1991;22:242–4.

8. Susilawathi NM, Suryapraba AA, Soejitno A, Asih MW, Swastika K, Wandra T, et al. Neurocysticercosis cases identified at Sanglah Hospital, Bali, Indonesia from 2014 to 2018. Acta Trop. 2020;201:105208. https://doi.org/10.1016/j.actatropica.2019.105208
9. Smyth J, Adams V, Napier S. Case report: getting it taped. Br Dent J. 2015;219:146. https://doi.org/10.1038/sj.bdj.2015.639
10. Australian Centre for International Agricultural Research. Evaluating the opportunities for smallholder livestock keepers in Timor-Leste—final report [cited 2024 May 1]. https://www.aciar.gov.au/publication/LS-2017-035-final-report

Address for correspondence: Sung Hye Kim, Department of Environmental Biology and Medical Parasitology, Institute for Health and Society, Hanyang University College of Medicine, 222 Wangshipni-ro, Seongdong-gu, Seoul 04763, South Korea; email: sunghyekim@hanyang.ac.kr

Optimizing Disease Outbreak Forecast Ensembles

Spencer J. Fox, Minsu Kim, Lauren Ancel Meyers, Nicholas G. Reich, Evan L. Ray

Author affiliations: University of Georgia, Athens, Georgia, USA (S.J. Fox); University of Massachusetts Amherst, Amherst, Massachusetts, USA (M. Kim, N.G. Reich, E.L. Ray); University of Texas at Austin, Austin, Texas, USA (L.A. Meyers); Dell Medical School, Austin (L.A. Meyers); Santa Fe Institute, Santa Fe, New Mexico, USA (L.A. Meyers)

DOI: https://doi.org/10.3201/eid3009.240026

On the basis of historical influenza and COVID-19 forecasts, we found that more than 3 forecast models are needed to ensure robust ensemble accuracy. Additional models can improve ensemble performance, but with diminishing accuracy returns. This understanding will assist with the design of current and future collaborative infectious disease forecasting efforts.

Real-time collaborative forecast efforts have become the standard to generate and evaluate forecasts for infectious disease outbreaks (*1*,*2*). Individual forecasts are aggregated into an ensemble prediction that has historically outperformed individual models and is the primary external communication used (*3*–*5*). Because of the focus on the singular ensemble model and the costs associated with producing individual forecasts, public health officials starting or maintaining a forecast hub face 2 key challenges: identifying target participation rates and optimizing ensemble performance of participating models. To guide this decision-making, we analyzed data from recent US-based collaborative outbreak forecast hubs to identify how the size and composition of an ensemble influences performance.

We analyzed hub forecasts for influenza-like illness (ILI) from 2010–2017 (*5*); for COVID-19 reported cases, hospital admissions, and deaths from 2020–2023 (*6*); and for influenza hospital admissions from 2021–2023 (*7*). For each hub, we identified time periods with maximal model participation that had at least 2 increasing and 2 decreasing epidemiologic phases and obtained forecasts for individual models that produced ≥90% of all possible forecasts (Appendix Table 1, Figure 1, https://wwwnc.cdc.gov/EID/article/30/9/24-0026-App1.pdf). For each ensemble size, $n_D \in \{1, \ldots, N_D\}$, where N_D is the disease-specific total number of models matching our inclusion criteria; we created unweighted ensemble forecasts for every combination of individual models of size n_D. We followed the hub forecast methodologies and made probabilistic forecasts for ILI by using a linear pool methodology (*5*), and we made quantile forecasts for all others by taking the median across all individual forecasts (Figure 1) (*8*). For each hub, we compared the ensemble performance against 2 hub-produced models. The first is a baseline model that produces naive forecasts and serves as a skill reference point; and the second is the published ensemble produced in real-time that is an unweighted ensemble of all submitted forecasts and is the current standard for performance (*3*,*5*). We summarized probabilistic ensemble forecast skill by using the log score for ILI forecasts and the weighted interval score for all others (*9*,*10*). We took the reciprocal of the log score so that lower values would indicate better performance similar to the weighted interval score (Appendix).

Looking across all ensemble sizes and combinations, we found that including more models improved average forecast performance and that all ensembles composed of >3 models outperformed the baseline model (Figure 2). Further increases to the ensemble size slightly improved the average forecast performance, but substantially decreased the variability of performance across ensembles. When we increased the ensemble size of influenza hospital admission forecasts from 4 to 7, the average

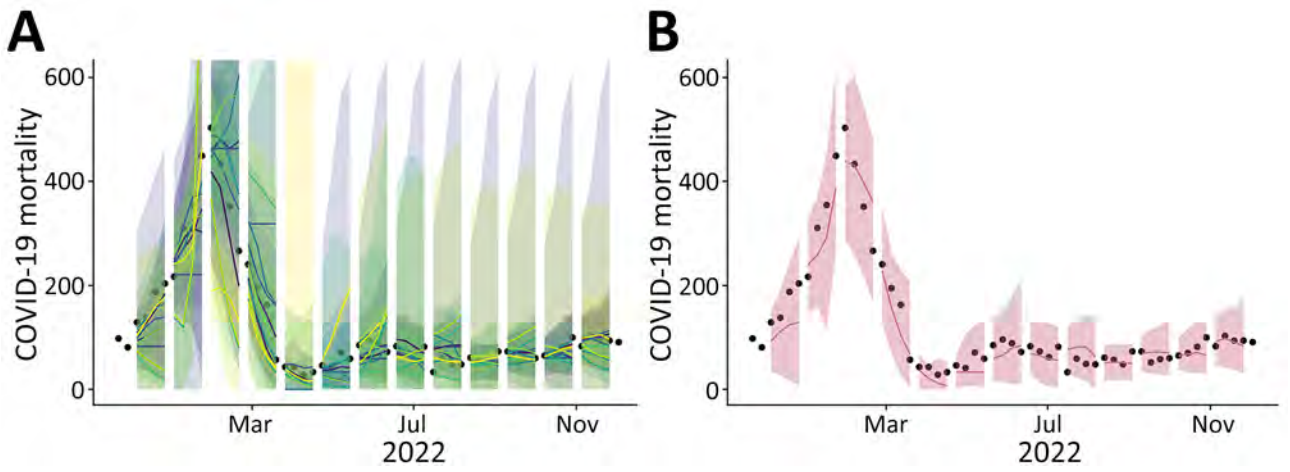

Figure 1. Comparison between individual and ensemble forecasts for COVID-19 mortality for Massachusetts, USA, from 1–4 weeks ahead, November 15, 2021–December 3, 2022, in study of optimizing disease outbreak forecasting ensembles. A) Individual forecasts of 10 models meeting inclusion criteria compared with weekly COVID-19 mortality estimates. B) An ensemble forecast constructed by taking the median across 10 individual forecasts compared with weekly COVID-19 mortality estimates. Black dots, weekly COVID-19 mortality estimates; colored lines, medians; ribbons, 95% prediction intervals.

performance improved by 2%, but the interquartile range decreased by 56.5%. Increasing the ensemble size therefore reduces the variability in expected performance of an ensemble.

To assist with decision-making regarding optimal ensemble assembly, we tested 2 approaches for model selection on the basis of past performance. We either ranked models by their individual performance and chose the top n_D models (individual rank) or we compared the performance of all ensemble combinations of size n_D and chose the models from the top performing ensemble (ensemble rank). Across all hubs, the individual rank methodology outperformed randomly assembled ensembles of

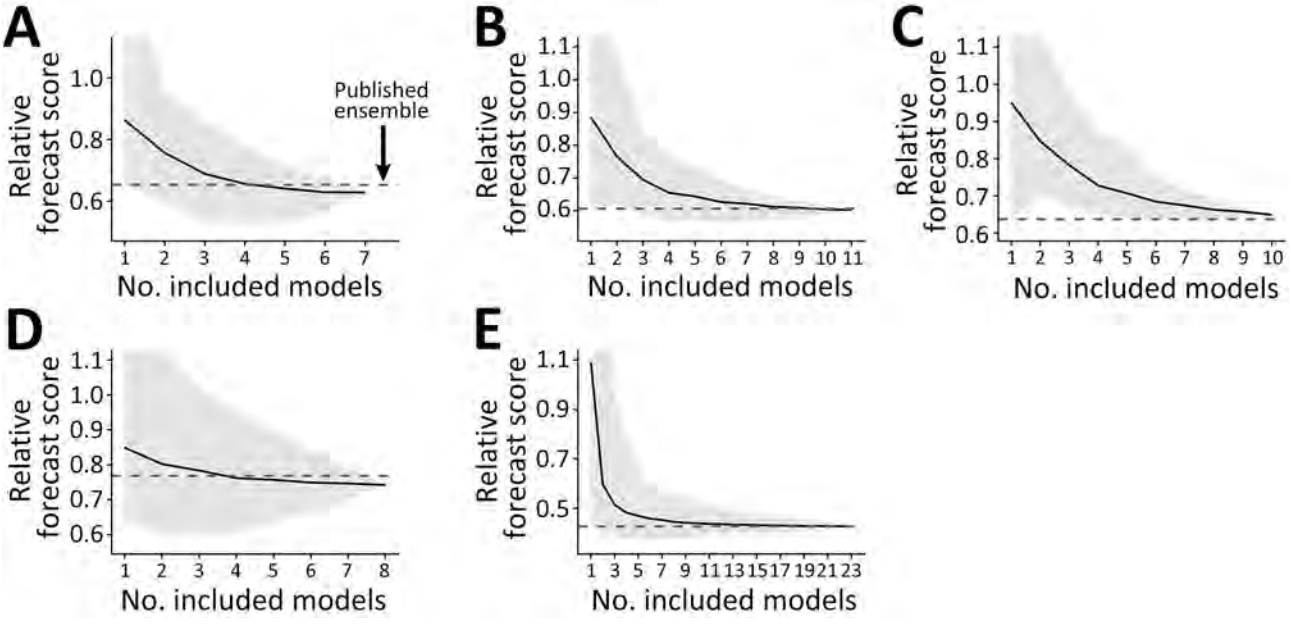

Figure 2. Summarized ensemble forecast scores from collaborative forecast efforts in study of optimizing disease outbreak forecasting ensembles. Scores correspond to the average forecast performance during testing periods across all dates, locations, and forecast horizons (Appendix Table 1, https://wwwnc.cdc.gov/EID/article/30/9/24-0026-App1.pdf). All scores are standardized by the baseline forecast model for that metric (Y = 1). Scores <1 indicate better accuracy than baseline. A) COVID-19 cases with 15 included models. B) COVID-19 admissions with 17 included models. C) COVID-19 deaths with 19 included models. D) Influenza admissions with 21 included models. D) Influenza-like illness with 23 included models. Solid black lines indicate mean scores; gray shading indicates minimum–maximum range. Horizontal purple dashed line indicates unweighted published ensemble used as standard.

the same size 63% (range 33.1%–87.2%) of the time, and the ensemble rank methodology outperformed randomly assembled ensembles of the same size 87.9% (range 70.9%–99.7%) of the time (Appendix Table 2, Figure 2). Performance of those ensembles is similar during both the training and testing periods, suggesting that ensemble performance is consistent through time (Appendix Figures 2, 3). Overall, ensemble rank outperforms individual rank for ensemble construction for 89.8% (range 66.7%–100%) of all sizes, and it provides a 6.1% (range 1.3%–11.9%) skill improvement (Appendix Table 2). The size 4 ensemble rank performed similarly to the published hub ensemble, although performance often declined with additional models (Appendix Figures 2, 3). Relative forecast performance across ensemble strategies was consistent when stratified by the ensemble size, forecast location, forecast date and phase of the epidemic, forecast target, and the skill metric (Appendix Figures 4–18).

Our results provide guidance for future collaborative forecast efforts. Hub organizers should target a minimum of 4 validated forecast models to ensure robust performance compared with baseline models. Adding more models reduces the variability in expected ensemble performance but might come with diminishing returns in average forecast skill. Organizers should use past ensemble performance rather than individual performance when selecting models to include in forecast ensembles; it is likely that further gains and different relationships between ensemble size and performance will come from weighted ensemble approaches (*8*). As public health officials and researchers look to expand collaborative forecast efforts, and as funding agencies allocate budgets across methodological and applied forecast efforts, our results can be used to identify target participation rates, assemble appropriate forecast models, and further improve ensemble forecast performance.

Acknowledgments

We thank the Council for State and Territorial Epidemiologists, Centers for Disease Control and Prevention, the Models of Infectious Disease Agent Study forecasting working groups, and the Scenario Modeling Hub. We also thank the Texas Advanced Computing Center at The University of Texas at Austin for providing high performance computing resources.

Funding for S.J.F. and L.A.M. was provided by the Council for State and Territorial Epidemiologists (grant no. NU38OT000297) and the Centers for Disease Control and Prevention (grant no. 75D30122C14776). Funding for M.K., E.L.R., and N.G.R. was provided by the National Institutes of General Medical Sciences (grant no. R35GM119582) and the Centers for Disease Control and Prevention (grant no. 1U01IP001122).

About the Author

Dr. Fox is an assistant professor at the University of Georgia in the department of epidemiology and biostatistics and the Institute of Bioinformatics. His research interests include statistical modeling of emerging infectious diseases and outbreak forecasting.

References

1. Reich NG, Lessler J, Funk S, Viboud C, Vespignani A, Tibshirani RJ, et al. Collaborative hubs: making the most of predictive epidemic modeling. Am J Public Health. 2022;112:839–42. https://doi.org/10.2105/AJPH.2022.306831
2. Biggerstaff M, Alper D, Dredze M, Fox S, Fung ICH, Hickmann KS, et al.; Influenza Forecasting Contest Working Group. Results from the Centers for Disease Control and Prevention's predict the 2013–2014 influenza season challenge. BMC Infect Dis. 2016;16:357. https://doi.org/10.1186/s12879-016-1669-x
3. Cramer EY, Ray EL, Lopez VK, Bracher J, Brennen A, Castro Rivadeneira AJ, et al. Evaluation of individual and ensemble probabilistic forecasts of COVID-19 mortality in the United States. Proc Natl Acad Sci U S A. 2022; 119:e2113561119. https://doi.org/10.1073/pnas.2113561119
4. Lutz CS, Huynh MP, Schroeder M, Anyatonwu S, Dahlgren FS, Danyluk G, et al. Applying infectious disease forecasting to public health: a path forward using influenza forecasting examples. BMC Public Health. 2019;19:1659. https://doi.org/10.1186/s12889-019-7966-8
5. Reich NG, Brooks LC, Fox SJ, Kandula S, McGowan CJ, Moore E, et al. A collaborative multiyear, multimodel assessment of seasonal influenza forecasting in the United States. Proc Natl Acad Sci U S A. 2019;116:3146–54. https://doi.org/10.1073/pnas.1812594116
6. Cramer EY, Huang Y, Wang Y, Ray EL, Cornell M, Bracher J, et al.; US COVID-19 Forecast Hub Consortium. The United States COVID-19 forecast hub dataset. Sci Data. 2022;9:462. https://doi.org/10.1038/s41597-022-01517-w
7. FluSight forecast -data 2022–2023 [cited 2023 Jul 12]. https://github.com/cdcepi/Flusight-forecast-data
8. Ray EL, Brooks LC, Bien J, Biggerstaff M, Bosse NI, Bracher J, et al. Comparing trained and untrained probabilistic ensemble forecasts of COVID-19 cases and deaths in the United States. Int J Forecast. 2023;39:1366–83. https://doi.org/10.1016/j.ijforecast.2022.06.005
9. Bracher J, Ray EL, Gneiting T, Reich NG. Evaluating epidemic forecasts in an interval format. PLOS Comput Biol. 2021;17:e1008618 https://doi.org/10.1371/journal.pcbi.1008618
10. Gneiting T, Raftery AE. Strictly proper scoring rules, prediction, and estimation. J Am Stat Assoc. 2007;102:359–78. https://doi.org/10.1198/016214506000001437

Address for correspondence: Spencer Fox, University of Georgia, 120 B.S. Miller Hall, Health Sciences Campus, 101 Buck Rd, Athens, GA 30602, USA; email: sjfox@uga.edu

Association of Intestinal Helminthiasis with Disseminated Leishmaniasis, Brazil

Brady Page, Alexsandro Lago, Edgar M. Carvalho

Author affiliations: University of California–San Diego, La Jolla, California, USA (B. Page); Scripps Research Institute, La Jolla (B. Page); Universidade Federal da Bahia, Salvador, Brazil (A. Lago, E.M. Carvalho); Instituto Nacional de Ciências e Tecnologia para Doenças Tropicais, Brasília, Brazil (E.M. Carvalho); Fundação Oswaldo Cruz, Salvador (E.M. Carvalho)

DOI: https://doi.org/10.3201/eid3009.240419

Disseminated leishmaniasis is an emerging clinical form of *Leishmania braziliensis* infection. Evidence shows that co-infection by *L. braziliensis* and intestinal helminths does not affect clinical manifestations or response to therapy in cutaneous leishmaniasis patients. We evaluated whether co-infection was associated with those aspects in disseminated leishmaniasis patients in Brazil.

American tegumentary leishmaniasis represents a group of neglected tropical diseases caused by protozoans of the genus *Leishmania* and transmitted to humans by phlebotomine sand flies. Brazil has one of the highest incidences of leishmaniasis in the world, where the predominating species is *Leishmania braziliensis* (*1*). The disease classically manifests as the localized ulcers of cutaneous leishmaniasis (CL), but in some instances, amastigotes metastasize from the site of inoculation and lead to disseminated leishmaniasis (DL), a severe and poorly understood form of disease characterized by the presence of up to several thousand skin lesions on multiple areas of the body; DL incidence has increased severalfold in recent decades (*1*).

No histopathologic or immunologic differences have been identified between CL and DL, but several host and parasite factors have been associated with the development of DL, including *L. braziliensis* strain and immune effector cell function (*2*,*3*). Although infection with intestinal helminths has been shown to modulate host immune response to bacterial and viral infections by inducing regulatory and Th2-type T cells, co-infection with *L. braziliensis* does not definitively affect clinical or therapeutic aspects of CL (*4*–*7*). However, a previous study showed an association between helminth infection and mucocutaneous leishmaniasis (*8*). To better clarify whether the presence of helminths contributes to *L. braziliensis* dissemination, we evaluated the influence of intestinal helminthiasis on clinical manifestations and response to therapy in DL patients in Brazil.

We recruited participants during January–December 2017 at a dedicated leishmaniasis center in the endemic region of Corte da Pedra in Bahia state, Brazil. Persons 5–70 years of age with skin lesions that had been present <60 days were eligible for enrollment. Criteria for diagnosis of CL were the presence of 1–9 well-demarcated cutaneous ulcers and detection by PCR of *L. braziliensis* DNA in a punch biopsy taken from a lesion. DL was defined as the presence of ≥10 cutaneous lesions located on ≥2 noncontiguous body parts and a positive PCR. At enrollment, participants provided a stool sample. We determined the presence

Table. Comparison of characteristics of patients with cutaneous and disseminated leishmaniasis, with and without intestinal helminthiasis, Brazil, 2017

	All patients			Patients with disseminated leishmaniasis		
Characteristic	Cutaneous leishmaniasis	Disseminated leishmaniasis	p value	With intestinal helminthiasis	Without intestinal helminthiasis	p value
Total no. patients	99	30		8	12	
Median age, y (range)	24 (13–56)	42 (18–69)	0.02*	37.5 (24–65)	49.5 (18–69)	0.6*
Sex, no. (%)						
M	76 (76.8)	15 (75)	1†	6 (75)	8 (67)	1†
F	23 (23.4)	5 (25)		2 (25)	4 (33)	
Median duration of illness, d (range)	40 (20–60)	30 (15–90)	0.18*	40 (20–90)	30 (15–90)	0.43*
Median no. lesions (range)	1 (1–8)	35.5 (11–1,500)	<0.05*	46 (11–1,500)	27 (12–102)	0.8*
Median area of largest lesion, mm^2 (range)	224 (15–3,016)	260.5 (16–16,160)	0.3*	240 (36–16,160)	260.5 (16–1,280)	0.57*
Helminths present, % (no.)	40 (40/99)	40 (8/20)	1†			
Median no. helminth ova present on fecal microscopy (range)	6 (1–4,000)	60 (1–288)	0.08*			
Cure rate at 90 d, % (no. patients)	65.9 (60/91)	30 (6/20)	0.003*	25 (2/8)	33 (4/12)	0.78*
Median time to cure, d (range)	65 (17–390)	154.5 (45–800)	<0.001*	184.5 (60–800)	140 (45–540)	0.46*

*Significance assessed by Mann-Whitney U test.
†Significance assessed by χ^2 test.

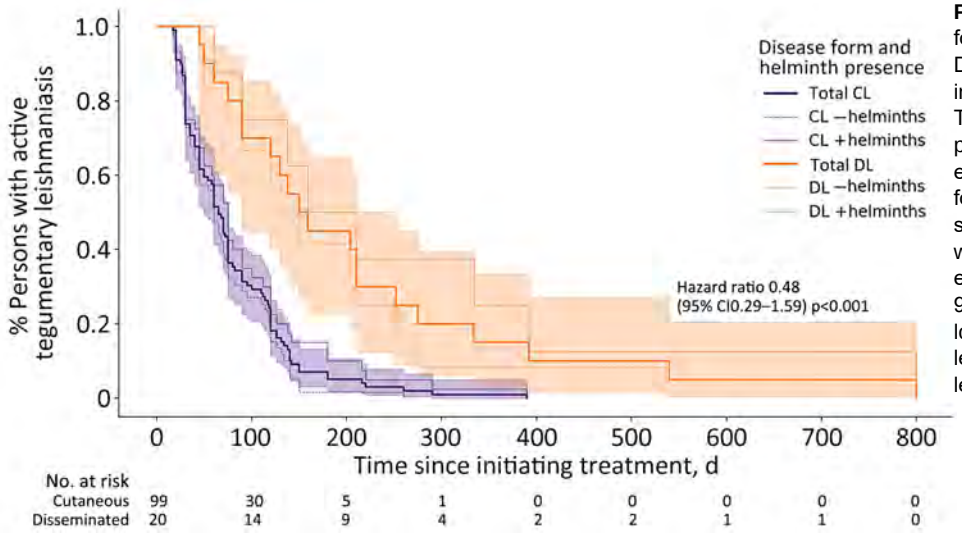

Figure. Kaplan-Meier estimates for clinical response of CL and DL stratified by the presence of intestinal helminths, Brazil, 2017. Thin dashed lines represent persons with stool parasitologic examinations that were negative for intestinal helminths; thin solid lines represent persons with positive stool parasitologic examinations; shading indicates 95% CIs. p value calculated with log-rank test. CL, cutaneous leishmaniasis; DL, disseminated leishmaniasis.

and quantification of intestinal helminth infection by the Kato–Katz method (*9*). All participants, regardless of enrollment status, were clinically evaluated and treated with 20 mg/kg/day of intravenous meglumine antimoniate for 20 days.

Initial clinical examination consisted of an evaluation of the size and number of cutaneous lesions. Upon 60-day and 90-day follow-up, we evaluated participants for the appearance of new lesions and response to treatment of existing lesions. We considered participants to be cured on the basis of the presence of complete re-epithelialization without elevated borders of all CL or DL lesions within 90 days after the initiation of antimonial treatment.

We enrolled a total of 99 persons with CL and 20 with DL. The median age of participants was 26 years (range 13–69 years); 76.5% of participants were male and 23.5% female (Table). Persons with DL were significantly older than patients with CL (42 vs. 24 years; p = 0.02), although we observed no correlation between age and time to cure in DL patients (R^2 0.06; p = 0.5) (Appendix Figure 1, https://wwwnc.cdc.gov/EID/article/30/9/24-0419-App1.pdf). Among persons with CL, age was correlated with time to cure but does not explain much of its variability (R^2 0.07; p = 0.04).

The prevalence of intestinal helminthiasis was 40.3% (48/119 patients); we observed no difference in prevalence between the CL and DL patients (Appendix Table). The most commonly identified organisms were *Necator americanus* (23/119 patients), *Trichuris trichiuris* (19/119 patients), and *Ascaris lumbricoides* (14/119 patients). The cure rate after 90 days of treatment was significantly lower in persons with DL compared with those with CL (30% vs. 65.9%; p = 0.003), and the median time to cure was significantly longer (154.5 vs. 65 days; p<0.001) (Figure). We observed no significant difference in the median number of lesions, median area of largest lesion, cure rate at 90 days, or median time to cure between DL patients with or without intestinal helminthiasis. We also observed no correlation between quantity of helminth ova in stool and time to cure in either group (R^2 0.01) (Appendix Figure 2).

Future investigation is needed to expound upon the immunologic and strain-specific parasitologic factors that may compromise the host Th1 immune response. A decrease in Th1-associated interferon-γ and tumor necrosis factor α production may precipitate the development of DL in a minority of patients.

The role of concomitant intestinal helminth infection in the clinical aspects and therapeutic response of CL and DL has thus far remained uncertain. We found a high prevalence of intestinal helminthiasis, but we observed no difference between the CL and DL groups and no effect on outcomes of either disease form. Persons with DL were significantly older than persons with CL, although there was no significant effect within age groups on therapeutic response. Cure rates among persons with DL treated with antimonials were characteristically low compared with persons with CL (*10*).

Acknowledgments

We thank the study participants and the team at the Health Post of Corte de Pedra, Bahia, Brazil, particularly Neuza Souza and Ednaldo Lago, for their invaluable contributions to recruitment, logistics, and parasitologic examinations.

About the Author

Dr. Page is an infectious diseases and critical care physician at the Scripps Research Institute and the University of California, San Diego. His research interests include the natural history, epidemiology, and management of infections that cause critical illness in resource-limited settings.

References

1. Queiroz A, Sousa R, Heine C, Cardoso M, Guimarães LH, Machado PR, et al. Association between an emerging disseminated form of leishmaniasis and *Leishmania* (*Viannia*) *braziliensis* strain polymorphisms. J Clin Microbiol. 2012;50:4028–34. https://doi.org/10.1128/JCM.02064-12
2. Machado PR, Rosa ME, Costa D, Mignac M, Silva JS, Schriefer A, et al. Reappraisal of the immunopathogenesis of disseminated leishmaniasis: in situ and systemic immune response. Trans R Soc Trop Med Hyg. 2011;105:438–44. https://doi.org/10.1016/j.trstmh.2011.05.002
3. Oliveira WN, Dórea AS, Carneiro PP, Nascimento MT, Carvalho LP, Machado PRL, et al. The influence of infection by different *Leishmania (Viannia) braziliensis* isolates on the pathogenesis of disseminated leishmaniasis. Front Cell Infect Microbiol. 2021;11:740278. https://doi.org/10.3389/fcimb.2021.740278
4. Page B, Lago A, Silva JA, Schriefer A, Lago J, Oliveira L, et al. Influence of intestinal helminth burden on clinical manifestations, therapeutic response, and *Leishmania braziliensis* load in patients with New World cutaneous leishmaniasis. Am J Trop Med Hyg. 2021;105:1060–6. https://doi.org/10.4269/ajtmh.20-1664
5. Gazzinelli-Guimaraes PH, Nutman TB. Helminth parasites and immune regulation. F1000 Res. 2018;7:7. https://doi.org/10.12688/f1000research.15596.1
6. O'Neal SE, Guimarães LH, Machado PR, Alcântara L, Morgan DJ, Passos S, et al. Influence of helminth infections on the clinical course of and immune response to *Leishmania braziliensis* cutaneous leishmaniasis. J Infect Dis. 2007;195:142–8. https://doi.org/10.1086/509808
7. Newlove T, Guimarães LH, Morgan DJ, Alcântara L, Glesby MJ, Carvalho EM, et al. Antihelminthic therapy and antimony in cutaneous leishmaniasis: a randomized, double-blind, placebo-controlled trial in patients co-infected with helminths and *Leishmania braziliensis*. Am J Trop Med Hyg. 2011;84:551–5. https://doi.org/10.4269/ajtmh.2011.10-0423
8. Azeredo-Coutinho RBG, Pimentel MI, Zanini GM, Madeira MF, Cataldo JI, Schubach AO, et al. Intestinal helminth coinfection is associated with mucosal lesions and poor response to therapy in American tegumentary leishmaniasis. Acta Trop. 2016;154:42–9. https://doi.org/10.1016/j.actatropica.2015.10.015
9. World Health Organization. Basic laboratory methods in medical parasitology. Geneva: The Organization; 1991. p. 9–25 [cited 2024 Jan 28]. https://iris.who.int/handle/10665/40793
10. Turetz ML, Machado PR, Ko AI, Alves F, Bittencourt A, Almeida RP, et al. Disseminated leishmaniasis: a new and emerging form of leishmaniasis observed in northeastern Brazil. J Infect Dis. 2002;186:1829–34. https://doi.org/10.1086/345772

Address for correspondence: Brady Page, University of California–San Diego, 9500 Gilman Dr, MC 0507, La Jolla, CA 92093-0507, USA; email: bpage@ucsd.edu

Confirmed Case of Autochthonous Human Babesiosis, Hungary

Dávid Sipos, Ágnes Kappéter, Barbara Réger, Gabriella Kiss, Nóra Takács, Róbert Farkas, István Kucsera, Zoltán Péterfi

Author affiliations: University of Pécs, Pécs, Hungary (D. Sipos, Á. Kappéter, B. Réger, G. Kiss, Z. Péterfi); University of Veterinary Medicine, Budapest, Hungary (N. Takács, R. Farkas); National Public Health Center, Budapest (I. Kucsera)

DOI: https://doi.org/10.3201/eid3009.240525

We report a case of autochthonous human babesiosis in Hungary, confirmed by PCR and partial sequencing of the *Babesia* spp. 18S rRNA gene. Babesiosis should be considered during the differential diagnosis of febrile illnesses, and peripheral blood smears to detect *Babesia* spp. should be part of the routine clinical workup.

Since the first description of human babesiosis caused by *Babesia divergens* protozoa in 1956 in the former Yugoslavia, 2 other zoonotic species, *B. venatorum* and *B. microti*, have been isolated in Europe. Unlike in North America, where most identified human cases have been caused by *B. microti*, the predominent pathogen causing babesiosis in Europe is *B. divergens* (*1*). The rising number of identified human infections in Europe has drawn attention to this emerging tick-borne zoonotic disease. In Europe, *B. microti* has been identified in 25 of 71 confirmed human babesiosis cases, of which 11 were autochthonous (*1*). Rodents and insectivores are reservoir hosts for *Babesia* spp. parasites, which are transmitted by widespread *Ixodes ricinus* ticks, well-known vectors of other zoonotic pathogens (*2*). We report a confirmed case of human babesiosis caused by *B. microti* infection in Hungary.

A 64-year-old man who lived in the countryside and worked as a farmer sought care at an emergency department on July 7, 2021, because of fatigue, nausea, vomiting, and a 10-kg weight loss during the past 2 months. His body temperature reached 38.9°C. He was unaware of having any chronic illnesses or tick infestations and did not have a blood transfusion or indicate a travel history outside of Hungary. Routine laboratory tests confirmed slightly elevated bilirubin (2.13 mg/dL), lactate dehydrogenase (760 U/L), alkaline phosphatase (170 U/L), gamma-glutamyl transferase (207 U/L), blood urea nitrogen (36.96 mg/dL), and creatinine (1.27 mg/dL) levels. He also had hyponatremia (120 mEq/L), prominent elevation of

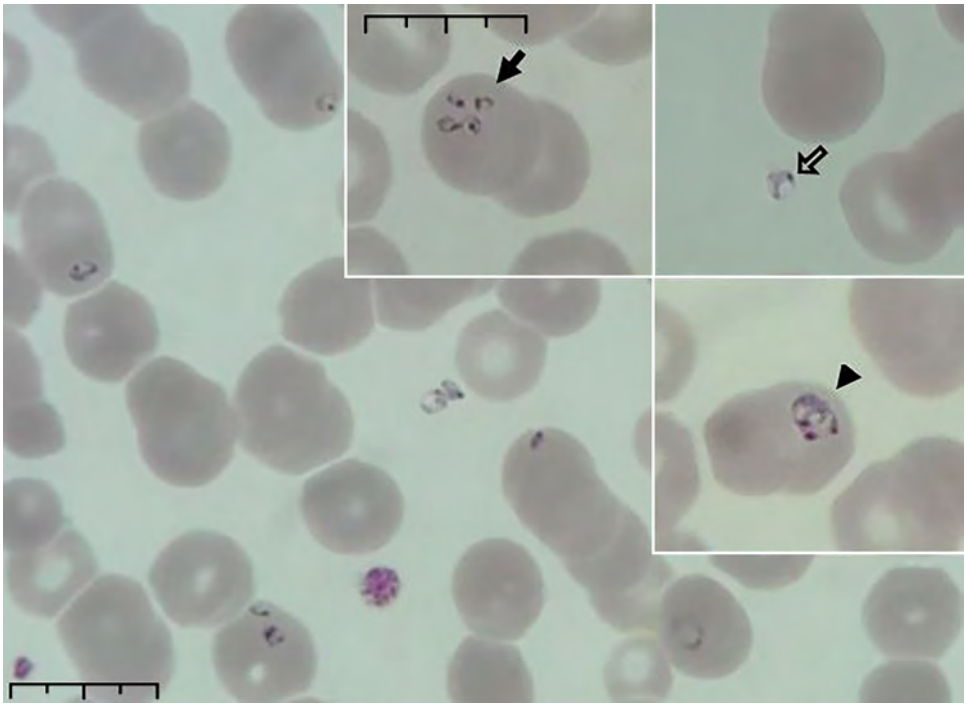

Figure 1. Peripheral blood smear from patient who had a confirmed case of autochthonous human babesiosis, Hungary. Smear shows erythrocytes infected with *Babesia* sp.; smear was stained with May-Grünwald Giemsa stain and examined by using light microscopy. In inset images, solid arrow indicates cells infected with multiple merozoites, open arrow indicates extracellular parasites, and arrowhead indicates vacuolated ring forms (trophozoites). Scale bars indicates 10 µm.

ultrasensitive C-reactive protein (218.8 mg/L), and new-onset diabetes, as well as slight anemia (hematocrit 37.9%) and an elevated procalcitonin level (1.94 ng/mL). A complete blood count examined by using an automated hematology analyzer (Sysmex, https://www.sysmex.com) showed elevated monocyte levels (25%) and thrombocytopenia (78×10^9 platelets/L). We examined peripheral blood smears by using automated and light microscopy, which confirmed intraerythrocytic ring forms with central vacuoles, some intraerythrocytic tetrades, and extraerythrocytic forms, suggesting babesiosis rather than malaria (Figure 1). Parasites infected 4.5% of erythrocytes. Because of microscopic findings and laboratory results, hospital staff tested blood haptoglobin level, which was 0.0 mg/dL, confirming suspected hemolysis.

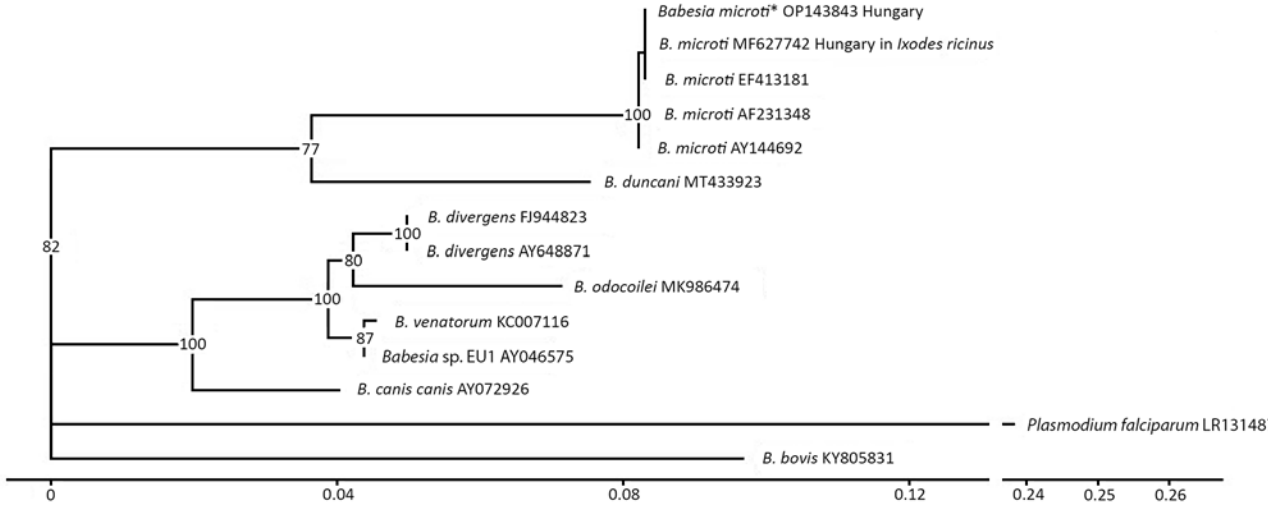

Figure 2. Phylogenetic analysis of *Babesia* spp. in confirmed case of autochthonous human babesiosis, Hungary. Asterisk indicates *B. microti* isolated from the patient in this case study. Phylogenetic tree was constructed by using Ggtree (*5*) according to multiple sequence alignments created by using MAFFT software (*6*). Best substitution model (3-parameter model, TPM2u) was selected by using functions of the phangorn version 2.11.1 R package (*7*) according to the Bayesian information criterion. Neighbor-joining tree was optimized by using the maximum-likelihood method. Bootstrap values were produced by 100 iterations and are indicated at branches. All data processing and plotting were performed in R version 4.4.1 (The R Project for Statistical Computing, https://www.r-project.org). GenBank accession numbers are indicated after the species name. Scale bar indicates nucleotide substitutions per site.

Other symptoms appeared during hospitalization, including left subcostal pain, decreased exercise tolerance, constipation, shivering, and new-onset torpidity; blurred vison occurred a few days after admission. Although malaria is not endemic in Hungary, we performed serologic tests for *Plasmodium* spp., which had negative results.

We performed PCR with primers BJ1 and BN2 to amplify a 459-bp fragment of the 18S rRNA gene of *Babesia* sp. (*3*) at the University of Veterinary Medicine, Budapest; the fragment was sequenced at the University of Szeged, Szeged, Hungary. We deposited the sequence in GenBank (accession no. OP143843.1). Nucleotide BLAST (https://blast.ncbi.nlm.nih.gov) analysis of the sequence showed 100% homology to *B. microti* detected in *I. ricinus* ticks and human blood (*4*). Although the sequence likely represents *B. microti*, further sequencing was not possible, and another closely related *Babesia* species cannot be excluded. We constructed a phylogenetic tree to compare the sequence with other *Babesia* spp. sequences found in GenBank (Figure 2).

Because of the advanced age of the patient and the clinical picture, we administered atovaquone/proguanil and azithromycin for 2 weeks (atovaquone is available in Hungary as an antimalaria drug). The patient became afebrile, and his condition improved. During follow-up examinations, fatigue and blurred vision gradually disappeared, and laboratory results improved. On the eighth day after treatment ended, we were unable to see any parasites through microscopic examination of blood. By the ninth week after treatment, lactate dehydrogenase, haptoglobin, and hemoglobin levels had normalized, and the patient fully recovered.

Although most human babesiosis cases have been imported in Europe, an increasing number of autochthonous *Babesia* spp. infections have been reported, possibly from a greater chance of tick contact because of human behavior changes (e.g., seeking outdoor activities) and a surge in vector population because of climate change. Furthermore, the number of immunocompromised hosts who have a more severe disease course and seek medical care is increasing as well.

In conclusion, although the 2 zoonotic species *B. divergens* and *B. microti* and their *I. ricinus* tick vector can be found in Hungary (*8*), imported or autochthonous human babesiosis cases had not been reported in this country. Babesiosis is not an endemic disease in Hungary; thus, clinicians rarely suspect this disease, despite the typical symptoms. Seroepidemiologic findings confirm the possibility of *Babesia* spp. transmission to humans in Europe. The increasing number of reported cases indicates that babesiosis should be considered in the differential diagnosis of patients manifesting fever in Europe. Furthermore, peripheral blood smears to detect this parasite should be a routine part of the workup for febrile illnesses, especially when disease-typical laboratory findings are present.

About the Author

Dr. Sipos is a medical doctor specializing in infectious diseases. His academic interests focus on infections of immunocompromised hosts and differential diagnosis of fever.

References

1. Hildebrandt A, Zintl A, Montero E, Hunfeld KP, Gray J. Human babesiosis in Europe. Pathogens. 2021;10:1165. https://doi.org/10.3390/pathogens10091165
2. Yabsley MJ, Shock BC. Natural history of zoonotic *Babesia*: role of wildlife reservoirs. Int J Parasitol Parasited Wildl. 2012;2:18–31. https://doi.org/10.1016/j.ijppaw.2012.11.003
3 Casati S, Sager H, Gern L, Piffaretti JC. Presence of potentially pathogenic *Babesia* sp. for human in *Ixodes ricinus* in Switzerland. Ann Agric Environ Med. 2006;13:65–70.
4. Moniuszko-Malinowska A, Swiecicka I, Dunaj J, Zajkowska J, Czupryna P, Zambrowski G, et al. Infection with *Babesia microti* in humans with non-specific symptoms in North East Poland. Infect. Dis. 2016;48:537–43. https://doi.org/10.3109/23744235.2016.1164339
5. Xu S, Li L, Luo X, Chen M, Tang W, Zhan L, et al. Ggtree: a serialized data object for visualization of a phylogenetic tree and annotation data. Imeta. 2022;1:e56. https://doi.org/10.1002/imt2.56
6. Katoh K, Standley DM. MAFFT multiple sequence alignment software version 7: improvements in performance and usability. Mol Biol Evol. 2013;30:772–80. https://doi.org/10.1093/molbev/mst010
7. Schliep K, Potts AJ, Morrison DA, Grimm GW. Intertwining phylogenetic trees and networks. Methods Ecol Evol. 2017;8:1212–20. https://doi.org/10.1111/2041-210X.12760
8. Sréter T, Kálmán D, Sréterné Lancz Z, Széll Z, Egyed L. *Babesia microti* and *Anaplasma phagocytophilum*: two emerging zoonotic pathogens in Europe and Hungary. Orv Hetil. 2005;146:595–600.

Address for correspondence: Dávid Sipos, University of Pécs, Rákóczi út 2, 7623 Pécs, Hungary; email: sipos.david@pte.hu

SARS-CoV-2 Dynamics in the Premier League Testing Program, United Kingdom

Adam J. Kucharski, Timothy W. Russell, Joel Hellewell, Sebastian Funk, Andrew Steele, W. John Edmunds, Mark Gillett

Author affiliations: London School of Hygiene & Tropical Medicine, London, UK (A.J. Kucharski, T.W. Russell, S. Funk, W.J. Edmunds); European Bioinformatics Institute at Wellcome Genome Campus, Hinxton, UK (J. Hellewell); Stride Health Group, London (A. Steele); The Football Association Premier League, London (M. Gillett)

DOI: https://doi.org/10.3201/eid3009.240853

During 2020–2022, players and staff in the English Premier League in the United Kingdom were tested regularly for SARS-CoV-2 with the aim of creating a biosecure bubble for each team. We found that prevalence and reinfection estimates were consistent with those from other studies and with community infection trends.

During the COVID-19 pandemic, frequent SARS-CoV-2 testing regardless of symptoms was used to reduce transmission risk in several workplace populations (*1*,*2*). In the process, data from those cohorts generated a range of scientific insights, including estimates of viral shedding dynamics and patterns of immune responses against novel variants of concern. Such testing programs in different settings are valuable for informing planning for future pandemics, especially given likely variation in behavior and therefore risk across subpopulations. Sports testing programs pose a particular challenge for infection control given the potential number of contacts made within and between teams and their support staff.

English Premier League (EPL) fixtures were suspended on March 19, 2020; such events included not only the games but also related social and behavioral aspects, such as fan mingling outside the venues and at concession stands. In May, a strategy was developed to allow games to resume while minimizing transmission risk, including not allowing fan attendance. A key principle of this strategy was a biosecure bubble for each team, which involved SARS-CoV-2 testing of core players and staff twice a week. Initially, PCR testing was used; during June–November 2021 and from January 2022 on, rapid antigen testing was used for screening (regular PCR was used during the Omicron wave in December 2021), and PCR testing was performed only after a positive rapid test result (Appendix, https://wwwnc.cdc.gov/EID/article/30/9/24-0853-App1.pdf). For this study, we examined PCR test results recorded during May 11, 2020–March 2, 2022.

During the study period, 178,588 PCR tests were obtained from 7,552 unique persons. Throughout late 2020 and early 2021, and during the early stages of the Omicron wave in late 2021, SARS-CoV-2 PCR positivity in the EPL broadly mirrored positivity in the UK Office for National Statistics Community Infection Survey (S. Abbott et al., unpub. data, https://doi.org/10.1101/2022.03.29.22273101) among 16–24- and 25–29-year age groups (Figure, panel A). One exception was early outbreaks in August 2020, as well as a period in early 2021 where prevalence in the EPL program was lower than community prevalence in the Community Infection Survey.

Regular testing can also provide insights into epidemiologic characteristics such as reinfection risk and viral shedding. Several persons recorded positive PCR tests for several weeks after their initial positive test; we identified 1 person with evidence of a reinfection during the Alpha wave (indicated by cycle threshold values >40 after 90 days postinfection) and another 3 persons with evidence of reinfection during the Delta wave (Figure, panel B). Those findings reinforce the importance of effective communication in ensuring appropriate interpretation of results, particularly if persons are being tested regardless of symptoms; a single positive PCR test does not necessarily indicate a recent infection, but a test conducted after symptom onset does. The estimated odds ratio for subsequent infection during the Alpha wave among those infected before December 1, 2020, was therefore 0.1 (95% CI 0.004–0.4), which is broadly consistent with other cohort studies that have estimated ≈85% risk reduction following an initial infection (*3*). We also found that cycle threshold values at time of first positive test were higher on average during the pre-Alpha period (mean value 33.7, SD 6; n = 106) than during the Alpha wave (mean 29.2, SD = 5.8; n = 223), reflecting the increased shedding for Alpha that has been observed in other studies (S. Funk et al., unpub. data).

In conclusion, we found that SARS-CoV-2 infection prevalence and reinfection estimates among EPL players and staff were consistent with those from other studies and with community infection trends. Such real-time insights could be further enhanced for

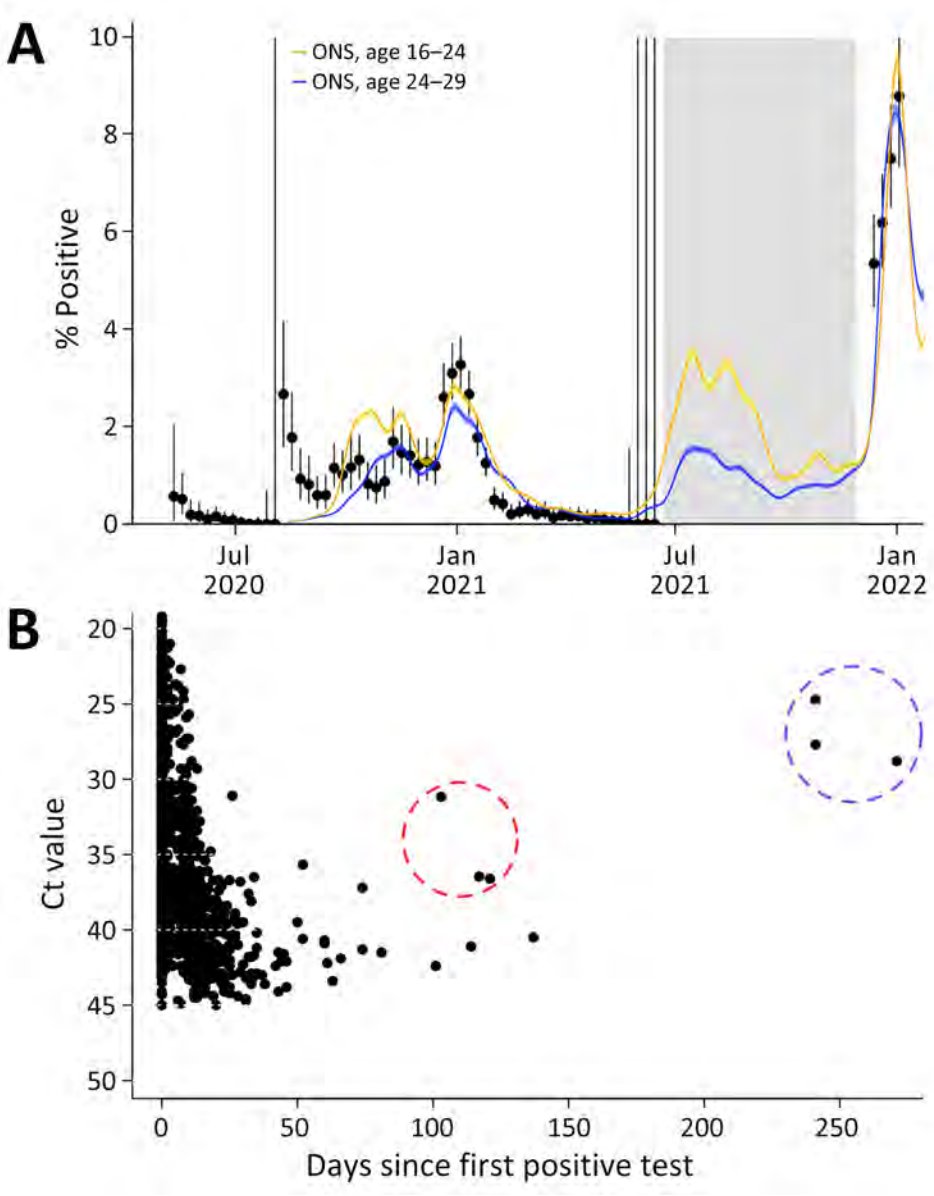

Figure. Infection dynamics in the English Premier League testing program for SARS-CoV-2, 2020–2022. A) Weekly PCR test positivity. Dots indicate infections; error bars indicate 95% CIs. Colored lines show inferred mean prevalence in the UK ONS Community Infection Survey. Gray shading shows period where the testing protocol was based on a rapid antigen test, with subsequent confirmatory PCR; hence, PCR positivity is not comparable because sampling was nonrandom. B) Distribution of individual Ct values over time since first positive test. Dashed circles indicate estimated reinfections: orange represents Alpha wave, in which 1 person was reinfected, as determined from 3 samples; purple represents Delta wave, in which samples indicate that 3 persons were reinfected. Ct, cycle threshold; ONS, Office for National Statistics.

future outbreaks or pandemics by adding sequencing or antibody testing.

S.F., A.J.K., and W.J.E. were supported by funding from the National Institute for Health and Care Research (NIHR) Health Protection Research Unit in Modelling and Health Economics, a partnership between the UK Health Security Agency (UKHSA), Imperial College London, and the London School of Hygiene & Tropical Medicine (NIHR200908). The views expressed are those of the authors and not necessarily those of the UK Department of Health and Social Care, NIHR, or UKHSA. A.J.K. and T.W.R. were supported by a Wellcome Trust Henry Dale Fellowship (no. 206250) and S.F. by a Wellcome Trust Senior Research Fellowship (no. 210758). The Premier League funded the original data collection.

About the Author

Dr. Kucharski is a professor of infectious disease epidemiology at London School of Hygiene & Tropical Medicine. His research focuses on making better use of data and analytics for understanding infectious disease dynamics, to inform epidemic preparedness and response.

References

1. Bailey C, Sanderson T, Townsley H, Goldman J, Black JRM, Young G, et al.; Crick COVID-19 Consortium. Independent SARS-CoV-2 staff testing protected academic and health-care institutions in northwest London. Lancet. 2023;402:21–4. https://doi.org/10.1016/S0140-6736(23)00917-0

2. Kissler SM, Fauver JR, Mack C, Olesen SW, Tai C, Shiue KY, et al. Viral dynamics of acute SARS-CoV-2 infection and applications to diagnostic and public health strategies. PLoS Biol. 2021;19:e3001333. https://doi.org/10.1371/journal.pbio.3001333
3. Hall VJ, Foulkes S, Charlett A, Atti A, Monk EJM, Simmons R, et al.; SIREN Study Group. SARS-CoV-2 infection rates of antibody-positive compared with antibody-negative health-care workers in England: a large, multicentre, prospective cohort study (SIREN). Lancet. 2021;397:1459–69. https://doi.org/10.1016/S0140-6736(21)00675-9

Address for correspondence: Adam Kucharski, London School of Hygiene & Tropical Medicine—Department of Infectious Disease Epidemiology, Keppel St, London WC1E 7HT, UK; email: adam.kucharski@lshtm.ac.uk

etymologia revisited

Paracoccidioides
[p′a rə kok-sid"e-oi' d′ez]

From the Greek (*para*/παρά + *kokkis* [coccidia]), Adolpho Lutz described *Paracoccidioides* in 1908. After analysis of oral and cervical lymph node lesions from infected patients, Lutz initially believed that he had detected *Coccidioides*. However, more extensive analysis showed that he had detected another fungus. Because of morphologic and clinical disease similarities, the name *Paracoccidioides* was suggested. The prefix para (near) indicates its similarity with *Coccidioides*.

Paracoccidioides is a thermally dimorphic fungus. It grows as an infective mycelium form (at 18°C–23°C) or a parasitic multibudding yeast form (at 35°C–37°C). It is composed of 2 species: *P. brasiliensis* and *P. lutzi*. They are the etiologic agents of paracoccidioidomycosis. This systemic infection is endemic to Latin America (southern Mexico to northern Argentina). The highest number of cases are found in Brazil, Colombia, and Venezuela. *Paracoccidioides* conidia and mycelia are found in soil and transmitted by inhalation.

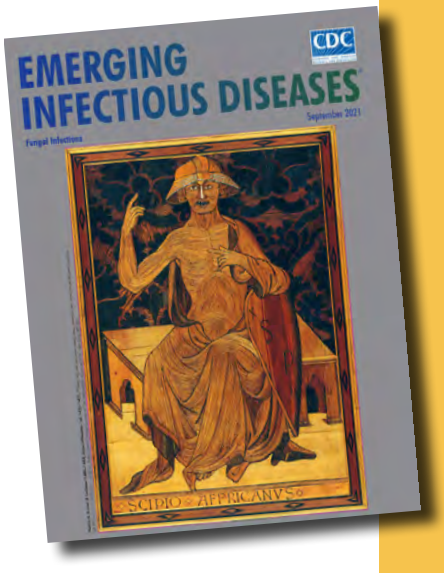

Sources

1. Bocca AL, Amaral AC, Teixeira MM, Sato PK, Shikanai-Yasuda MA, Soares Felipe MS. Paracoccidioidomycosis: eco-epidemiology, and clinical and therapeutic issues. Future Microbiol. 2013;8:1177–91. https://doi.org/10.2217/fmb.13.68
2. Chaves AF, Navarro MV, de Barros YN, Silva RS, Xander P, Batista WL. Updates in *Paracoccidioides* biology and genetic advances in fungus manipulation. J Fungi (Basel). 2021;7:116. https://doi.org/10.3390/jof7020116
3. Lutz A. A pseudococcidic mycose located in the mouth and observed in Brazil: contribution to the knowledge of American hypoblatomycoses [in Portuguese]. Revista Semanal de Medicina e Cirurgia. 1908;22:121–4.
4. Turland NJ, Wiersema JH, Barrie FR, Greuter W, Hawksworth DL, Herendeen PS, et al., editors. International code of nomenclature for algae, fungi, and plants (Shenzhen code) adopted by the Nineteenth International Botanical Congress Shenzhen, China, July 2017. Regnum Vegetabile 159. Glashütten (Germany): Koeltz Botanical Books; 2018 [cited 2021 May 17]. https://www.iapt-taxon.org/nomen/pages/intro/citation.html
5. Viera e Silva CR, de Mattos MC, Fujimore K. Scanning electron microscopy of *Paracoccidioides brasiliensis*. Study with and without pre-treatment with pooled sera from patients with 'South American blastomycosis'. Mycopathol Mycol Appl. 1974;54:235–51.

Originally published in September 2021

https//wwwnc.cdc.gov/eid/article/27/9/et-2709_article

Recognition of Antifungal-Resistant Dermatophytosis by Infectious Diseases Specialists, United States

Jeremy A.W. Gold, Kaitlin Benedict, Shawn R. Lockhart, Caitlyn Lutfy, Meghan Lyman, Dallas J. Smith, Philip M. Polgreen, Susan E. Beekmann

Author affiliations: Centers for Disease Control and Prevention, Atlanta, Georgia, USA (J.A.W. Gold, K. Benedict, S.R. Lockhart, C. Lutfy, M. Lyman, D.J. Smith); University of Iowa Carver College of Medicine, Iowa City, Iowa, USA (P.M. Polgreen, S.E. Beekmann)

DOI: https://doi.org/10.3201/eid3009.240118

Antifungal-resistant dermatophyte infections have recently emerged as a global public health concern. A survey of US infectious diseases specialists found that only 65% had heard of this issue and just 39% knew how to obtain testing to determine resistance. Increased clinician awareness and access to testing for antifungal-resistant dermatophytosis are needed.

Dermatophytosis (i.e., ringworm, tinea) is a common superficial fungal skin infection caused by dermatophyte molds (*1*). In the past decade, widespread outbreaks of antifungal-resistant dermatophytosis have occurred in South Asia because of the spread of *Trichophyton indotineae* fungus, which causes extensive pruritic plaques on the trunk, extremities, groin, and face in immunocompetent persons (*2*–*4*). Unlike typical dermatophyte skin infections, those involving *T. indotineae* fungus often do not resolve with over-the-counter topical antifungals or oral terbinafine (first-line systemic therapy) (*2*,*3*).

T. indotineae fungus has been detected in at least 11 US states, and recalcitrant dermatophytosis caused by antifungal-resistant *T. rubrum* fungus also has been reported (*2*,*5*,*6*). Affected patients have experienced diagnostic delays and received inappropriate therapies, including topical corticosteroids, which can worsen dermatophytosis (*2*). Antifungal-resistant dermatophytosis cases in the United States probably are underrecognized because this condition is not reportable to public health authorities in any state (https://www.cdc.gov/fungal/php/case-reporting) and most superficial fungal infections are not confirmed with diagnostic testing (*7*). Further, laboratory capacity to identify dermatophyte species and perform antifungal-susceptibility testing (AFST) may be limited, given that definitive identification of certain species, such as *T. indotineae,* requires advanced molecular techniques (e.g., using internal transcribed spacer region sequencing) and most clinical laboratories do not perform AFST for molds (*2*,*8*).

Antifungal-resistant dermatophytosis cases might require infectious diseases (ID) clinician consultation both to manage antifungal use and because of the potential effect of these infections on highly immunocompromised patients. Understanding ID clinicians' level of awareness regarding antifungal-resistant dermatophytosis and access to laboratory testing could improve strategies to increase disease recognition and facilitate early appropriate treatment. Therefore, we surveyed ID clinicians by using the Emerging Infections Network (EIN) (https://ein.idsociety.org), a sentinel network of ID physicians and other ID specialists.

During December 2023, EIN distributed a survey link to ≈3,000 member subscribers on 3 separate occasions ≈1 week apart. EIN queries are designated as non–human subjects research by the institutional review board of the University of Iowa.

In total, we received 158 responses (Table). The most common practice setting was university hospital (47%), followed by community hospital (16%) and nonuniversity teaching hospital (12%). Most respondents were adult ID physicians (80%), followed by pediatric ID physicians (12%), pharmacists (4%), nurse practitioners, physician assistants or physician associates (1%), or other (3%). Overall, 103 (65%) respondents had heard of antifungal-resistant dermatophytosis before receiving the survey; among those, most (58%) had heard of it through previous EIN listserv emails. Seventeen percent of respondents reported seeing or consulting on a patient who had dermatophytosis that was potentially resistant to treatment or concerning for resistance within the previous year.

Approximately half (47%) of respondents reported that if they saw a patient with potentially resistant dermatophytosis, they either would not be able to obtain laboratory testing to determine the species (16%) or were unsure whether they could obtain such testing (31%) (Table). Likewise, most respondents (61%) reported they would either not be able to obtain testing to determine if a dermatophyte was resistant to antifungals (16%) or were unsure whether they could obtain such testing (45%).

In summary, our survey found that approximately one third (35%) of ID clinicians had not heard of antifungal-resistant dermatophytosis. Only 53% of respondents reported knowing how to obtain access to dermatophyte speciation testing,

Table. Survey regarding 158 infectious diseases clinicians' awareness of antifungal-resistant dermatophyte infections and access to laboratory testing, United States, 2023

Survey query	No. (%) respondents
Primary setting of clinical practice	
University hospital	75 (47)
Community hospital	26 (16)
Non-university teaching hospital	19 (12)
Veterans Affairs hospital or Department of Defense	13 (8)
Outpatient setting only	8 (5)
Free-standing children's hospital	5 (3)
City, county, or public hospital	4 (3)
Other	4 (3)
Question not answered	4 (3)
Type of clinical practice	
Adult infectious diseases physician	126 (80)
Pediatric infectious diseases physician	19 (12)
Pharmacist	6 (4)
Nurse practitioner, physician assistant, or physician associate	2 (1)
Other	4 (3)
Question not answered	1 (1)
How did you hear about the issue of antifungal-resistant dermatophyte infections? (select all that apply)	
I had not previously heard of this issue	55 (35)
Answers among those who had heard of this issue, n = 103	
Emerging Infections Network emails	60 (58)
CDC webpage or *Morbidity and Mortality Weekly Report*	46 (45)
Scientific publication	28 (27)
News reports	18 (17)
From clinical colleagues	18 (17)
Clinician education website (e.g., Doximity and Medscape)	6 (6)
Point-of-care medical resource (e.g., UpToDate)	4 (4)
Social media	2 (2)
Other	6 (6)
In the past year, I have seen or consulted on a patient with a dermatophyte infection that was potentially resistant to treatment or concerning for resistance	
Yes	27 (17)
No	119 (75)
Unknown	12 (8)
If I saw a patient with a potentially resistant dermatophyte infection, I would be able to obtain laboratory testing to determine the species	
Yes	83 (53)
No	26 (16)
Unknown	49 (31)
I would be able to obtain testing to determine if a dermatophyte is resistant to antifungals	
Yes	62 (39)
No	25 (16)
Unknown	71 (45)

and even fewer (39%) reported knowing how to obtain testing for dermatophyte resistance (Table). Those findings probably reflect the relatively recent recognition of these infections in the United States and the fact that testing to identify *T. indotineae* and other resistant dermatophyte species is limited to select US mycology reference centers and public health laboratories (*2*,*8*).

Dermatophyte species identification and AFST are critical to guiding antifungal treatment decisions for patients with potentially resistant dermatophytosis and for monitoring population-level trends in resistance profiles to inform treatment guidelines (*8*). National guidelines for treating antifungal-resistant dermatophytosis are lacking, but the azole antifungal itraconazole has been used successfully for patients with dermatophytosis caused by *T. indotineae* and terbinafine-resistant *T. rubrum* fungi (*2*,*9*). However, clinicians should be aware of challenges with itraconazole, including pharmacokinetic variability (e.g., absorption), insurance coverage, drug–drug interactions, need for prolonged treatment (e.g., ≥6 weeks), and reports of emerging itraconazole-resistant *T. indotineae* and *T. rubrum* fungi (*2*,*6*,*9*,*10*).

One limitation of our survey is its low response rate and nonrepresentative nature. Furthermore, the survey might overestimate clinician awareness of antifungal-resistant dermatophytosis and laboratory testing access if clinicians experienced in this topic were likelier to respond. Despite those limitations, our survey highlights a need for increased awareness of antifungal-resistant dermatophytosis and

increased laboratory capacity to identify and perform susceptibility testing for dermatophytes to address this emerging public health concern.

Healthcare professionals can find information about recognizing, diagnosing, treating, and reporting emerging dermatophyte infections online (https://www.aad.org/member/clinical-quality/clinical-care/emerging-diseases/dermatophytes), including information about laboratories that can perform testing (https://www.aad.org/member/clinical-quality/clinical-care/emerging-diseases/dermatophytes/recognizing-trichophyton-indotineae#testing). Those websites were developed as a collaboration between the Centers for Disease Control and Prevention and the American Academy of Dermatology's Emerging Diseases Task Force.

This work was supported by Cooperative Agreement Number 5 (grant no. NU50CK000574), funded by the Centers for Disease Control and Prevention.

About the Author

Dr. Gold is a medical epidemiologist in the Mycotic Diseases Branch, Division of Foodborne, Waterborne, and Environmental Diseases, National Center for Emerging and Zoonotic Infectious Diseases, Centers for Disease Control and Prevention, Atlanta, Georgia, USA. His research interests include the epidemiology and prevention of fungal infections.

References

1. Gupta AK, Ryder JE, Chow M, Cooper EA. Dermatophytosis: the management of fungal infections. Skinmed. 2005;4:305–10. https://doi.org/10.1111/j.1540-9740.2005.03435.x
2. Caplan AS, Chaturvedi S, Zhu Y, Todd GC, Yin L, Lopez A, et al. Notes from the field: first reported U.S. cases of tinea caused by *Trichophyton indotineae*—New York City, December 2021–March 2023. MMWR Morb Mortal Wkly Rep. 2023;72:536–7. https://doi.org/10.15585/mmwr.mm7219a4
3. Verma SB, Panda S, Nenoff P, Singal A, Rudramurthy SM, Uhrlass S, et al. The unprecedented epidemic-like scenario of dermatophytosis in India: I. Epidemiology, risk factors and clinical features. Indian J Dermatol Venereol Leprol. 2021;87:154–75. https://doi.org/10.25259/IJDVL_301_20
4. Gupta AK, Renaud HJ, Quinlan EM, Shear NH, Piguet V. The growing problem of antifungal resistance in onychomycosis and other superficial mycoses. Am J Clin Dermatol. 2021;22:149–57. https://doi.org/10.1007/s40257-020-00580-6
5. Cañete-Gibas CF, Mele J, Patterson HP, Sanders CJ, Ferrer D, Garcia V, et al. Terbinafine-resistant dermatophytes and the presence of *Trichophyton indotineae* in North America. J Clin Microbiol. 2023;61:e0056223. https://doi.org/10.1128/jcm.00562-23
6. Gu D, Hatch M, Ghannoum M, Elewski BE. Treatment-resistant dermatophytosis: a representative case highlighting an emerging public health threat. JAAD Case Rep. 2020;6:1153–5. https://doi.org/10.1016/j.jdcr.2020.05.025
7. Benedict K, Wu K, Gold JAW. Healthcare provider testing practices for tinea and familiarity with antifungal-drug-resistant tinea—United States, 2022. J Fungi (Basel). 2022;8:831. https://doi.org/10.3390/jof8080831
8. Lockhart SR, Smith DJ, Gold JAW. *Trichophyton indotineae* and other terbinafine-resistant dermatophytes in North America. J Clin Microbiol. 2023;61:e0090323. https://doi.org/10.1128/jcm.00903-23
9. Khurana A, Agarwal A, Agrawal D, Panesar S, Ghadlinge M, Sardana K, et al. Effect of different itraconazole dosing regimens on cure rates, treatment duration, safety, and relapse rates in adult patients with tinea corporis/cruris: a randomized clinical trial. JAMA Dermatol. 2022;158:1269–78. https://doi.org/10.1001/jamadermatol.2022.3745
10. Burmester A, Hipler U-C, Uhrlaß S, Nenoff P, Singal A, Verma SB, et al. Indian *Trichophyton mentagrophytes* squalene epoxidase *erg1* double mutants show high proportion of combined fluconazole and terbinafine resistance. Mycoses. 2020;63:1175–80. https://doi.org/10.1111/myc.13150

Address for correspondence: Jeremy Gold, Centers for Disease Control and Prevention, 1600 Clifton Rd NE, Mailstop H24-11, Atlanta, GA 30329-4027, USA; email: jgold@cdc.gov

Corrections

Vol. 30, No. 5

The name of author Glenn Patriquin was misspelled in Case Series of Jamestown Canyon Virus Infections with Neurologic Outcomes, Canada, 2011–2016 (V. Meier-Stephenson et al.). The article has been corrected online (https://wwwnc.cdc.gov/eid/article/30/5/22-1258_article).

Vol. 30, No. 8

The name of author Carlos E. Sanz-Rodriguez was misspelled in Outbreak of Intermediate Species *Leptospira venezuelensis* Spread by Rodents to Cows and Humans in *L. interrogans*–Endemic Region, Venezuela (L. Caraballo et al.). The article has been corrected online (https://wwwnc.cdc.gov/eid/article/30/8/23-1562_article).

Thomas J. Gryczan (1949–2024)

Byron Breedlove, Barbara Segal

Thomas J. Gryczan, better known to his coworkers and many friends as Tom, worked from May 2005 until his death in March 2024 with the Centers for Disease Control and Prevention as a dedicated, highly focused technical writer-editor for *Emerging Infectious Diseases* (EID). During his tenure with the journal, Tom was recognized for his unwavering enthusiasm for work, willingness to share knowledge about science and publishing, and ability to handle challenging assignments and tight deadlines. Tom contributed to EID in many other ways, including mentoring new staff and helping coordinate and administer continuing medical education credits offered by the journal.

EID editor-in-chief Peter Drotman recalled Tom's knowledge was almost boundless. "One of the many places where he put his skills to good use was in assisting authors of the popular Etymologia entries in crafting their historical vignettes," Drotman said. "Tom edited more than 100 of those articles, all of which are uncredited. Tom was an ardent supporter of the goal of this EID feature, which is to enhance the knowledge of students of microbiology and infectious diseases about the heritage of our field and how the names we use came to be."

Tom held a bachelor's degree from Marist College in New York, a master's degree from Long Island University, and a PhD in microbiology from New York University. Before joining CDC, Tom worked as a researcher at the Public Health Research Institute, International Center for Public Health, at New Jersey Medical School at Rutgers University. Throughout his career, he authored 16 scholarly articles that have been cited 1,170 times to date.

In the mid-1980s, Tom embarked on a nearly four-decade career as a technical writer-editor, initially with Gordon & Breach Science Publishers in New York. After relocating to Atlanta, Georgia, he worked for the *American Journal of Tropical Medicine and Hygiene* and *Arthritis & Rheumatology*. He also worked as an editor for the American Cancer Society.

Tom's puns and bad jokes brought levity to many EID staff meetings, and he often delighted colleagues with homemade treats from his kitchen during EID's weekly gatherings, before the COVID-19 pandemic required social distancing. Beyond his professional pursuits, he had diverse interests, including gardening, bowling, roller skating, listening to disco music, cooking, reading nonfiction, studying history, and watching hockey and baseball.

Figure. Thomas J. Gryczan. Photo credit: Susan Twadell.

Tom was a born teacher and was knowledgeable in countless subject areas. One of Tom's daughters noted that "Tom was Google before there was a Google." For instance, he could list every World Series winner from the 1950s to 2023 and how many games were played in each series. He could also provide details on all the elements in the periodic table or recount historical events, including precise dates and locations. Colleagues recall many enthusiastic breakroom conversations with Tom on myriad subjects that invariably ended with learning new facts and insights. If someone mentioned a trivia interest, it then became Tom's thoroughly researched passionate interest as well. Despite his enthusiasm and extroverted personality, Tom was notably modest except when talking about family, and then he could not contain his pride.

We offer our condolences to Tom's surviving family members, including his wife, daughters, grandsons, and sisters, and to his many friends and acquaintances at CDC and around the world.

Author affiliation: Centers for Disease Control and Prevention, Atlanta, Georgia, USA

DOI: https://doi.org/10.3201/eid3009.240736

Winslow Homer (1836–1910). ***On the Trail*** **(1889)** (detail). Watercolor over graphite on wove paper, 12 5/8 in × 19 7/8 in /32.1 cm × 50.5 cm. Gift of Ruth K. Henschel in memory of her husband, Charles R. Henschel. National Gallery of Art, Washington, DC, USA. Open access image.

Views Most Would Never See

Byron Breedlove

Winslow Homer is regarded by many as the greatest American painter of the nineteenth century," noted art historian and curator H. Barbara Weinberg. Homer's skill at mastering watercolor and oil painting is what led to his being considered among America's foremost painters.

Homer was born in Boston, Massachusetts, USA, and grew up in nearby Cambridge. He received no formal artistic education, although his mother instructed him in watercolor. He initially apprenticed as a commercial printmaker in Boston and continued in that trade after moving to New York, New York, USA, in 1859. Commercial printmaking was a profession that Homer grew to dislike. In New York, he first freelanced as an illustrator for magazines, including *Harper's Weekly*, briefly took drawing classes at the National Academy of Design, and began to focus on painting.

During the US Civil War, when Homer was 25 years old, *Harper's Weekly* dispatched him as an artist-correspondent embedded with the Union army, and he gained widespread recognition for his work. "Homer gave people views of the war that most would never see," according to Keely Orgeman, the Seymour H. Knox, Jr., Associate Curator of Modern and Contemporary Art at the Yale University Art Gallery, quoted in an article in *Yale News*.

Homer spent 1867 abroad in France, starting to paint in watercolor in 1873, and in 1875 he ended his career as a magazine illustrator to focus on painting. In 1881, Homer moved to the seaside village of Cullercoats, England, an experience that preceded his permanent move in 1883 to the fishing village of Prouts Neck, Maine, USA. On that coastal peninsula, Homer's studio, converted from a stable, provided him both the solitude and scenery he craved.

In a 1923 collection of Homer's work, painter and art writer Nathaniel Pousette-Dart asserted, "Certainly no artist in whose work the influence of contemporary painters is less apparent ever lived. He shunned exhibits and rarely contributed his own pictures to them…. He lived during the greater part of his life like a hermit." Although Homer lived in Prouts Neck

Author affiliation: Centers for Disease Control and Prevention, Atlanta, Georgia, USA

DOI: https://doi.org/10.3201/eid3009.AC3009

for the rest of his life, he frequently wintered in Florida and Bermuda and often visited Boston and the Adirondack region of upstate New York. Among his favorite subjects were fishermen and hunters.

This month's cover image, *On the Trail,* is among Homer's New York paintings. The dappled light and gossamer layers of leaves, rendered as splotches of yellow, orange, and green, suggest early autumn, show the artist's mastery at rendering scenes from the natural world. An attentive young hunter peers into the thick forest, clutching his eager dogs, anticipating an unsuspecting deer. The quiet intensity Homer conveys diverges from more dramatic scenes in many of his other hunting-themed paintings. The National Gallery of Art notes, "These works celebrate the pleasures and beauty of life in the Adirondacks but also confront the more brutal realities of hunting. In one series, Homer depicted a practice called hounding, in which dogs were used to drive deer into a lake."

In *On the Trail*, the fate of the unseen deer remains unsettled; perhaps it escaped in the underbrush. Regardless, the young hunter would likely have given little thought to health threats in such sylvan settings, particularly from ticks. Health threats from tickborne pathogens were not as widespread or recognized then as they are now. Homer's hunter, dogs, and unseen deer would have been less likely than modern hunters and hikers to encounter ticks that transmit diseases. Epidemiologist Katharine Walters and colleagues, in their article "Genomic Insights into the Ancient Spread of Lyme Disease across North America Deforestation" note that urbanization, climate change, and increased deer populations have altered the ecology and landscape, enabling ticks to flourish and spread.

Ticks are vectors for numerous bacterial diseases, including anaplasmosis, bartonellosis, ehrlichiosis, Lyme disease, and spotted fever rickettsioses. They are also vectors for viral diseases including Bourbon virus disease, Colorado tick fever, Crimean-Congo hemorrhagic fever, Heartland virus disease, and Powassan encephalitis. Tick bites may also transmit parasitic diseases such as babesiosis, a disease caused by microscopic parasites that infect red blood cells. Most cases of babesiosis are caused by *Babesia microti*, transmitted in North America by bites from *Ixodes scapularis* ticks. The ticks that cause that parasitic disease, now endemic to many places Homer lived and visited in the northeastern United States, have expanded their range from Virginia to Maine and the upper midwestern states. As reported in this issue of *Emerging Infectious Diseases*, including in a new report from Hungary and another in the Netherlands, nonimported human babesiosis is increasing its range in Europe.

Articles about *Mansonella ozzardi*, a filarial worm transmitted by biting midges and black flies, in raccoons in urban areas of Costa Rica and emergence of *Thelazia callipaeda*, an ocular nematode of carnivores and humans, in black bears in Pennsylvania, USA, document the work of researchers on the trail of potential spillover pathogens. Through his art, Homer afforded views of the Civil War, the ocean, and the woods that most people would never experience. Through their epidemiologic sleuthing, researchers tracking emerging vector-borne health threats provide public health authorities with views most would never have and help respond to those threats.

Bibliography

1. Centers for Disease Control and Prevention. About babesiosis [cited 2024 Aug 7]. https://www.cdc.gov/babesiosis/about/index.html
2. Centers for Disease Control and Prevention. Lyme disease [cited 2024 Aug 7]. https://www.cdc.gov/lyme/index.html
3. Gray EB, Herwaldt BL. Babesiosis Surveillance - United States, 2011-2015. MMWR Surveill Summ. 2019;68:1–11. https://doi.org/10.15585/mmwr.ss6806a1
4. McDonald AA. As embedded artist with the Union army, Winslow Homer captured life at the front of the Civil War [cited 2024 Aug 5]. https://news.yale.edu/2015/04/20/embedded-union-troops-winslow-homer-documented-civil-war-art
5. National Gallery of Art. Winslow Homer in the National Gallery of Art [cited 2024 Aug 1]. https://www.nga.gov/features/slideshows/winslow-homer-in-the-national-gallery-of-art.html
6. Potter P. Painting nature on the wing. Emerg Infect Dis. 2006;12:180–1. https://doi.org/10.3201/eid1201.AC1201
7. Pousette-Dart N. Distinguished American artists. Winslow Homer. New York: Frederick A. Stokes Company; 1923. p. vii, viii.
8. Quesada J, Alfaro-Segura P, Solano-Barquero A, Vega K, Rojas-Sánchez E, Jiménez M, et al. Zoonotic *Mansonella ozzardi* in raccoons, Costa Rica, 2019–2022. Emerg Infect Dis. 2024;30:1930–3.
9. Sipos D, Kappéter Á, Réger B, Kiss G, Takács N, Farkas R, et al. Confirmed case of autochthonous human babesiosis, Hungary. Emerg Infect Dis. 2024;30:1972–4.
10. Sobotyk C, Dietrich J, Verocai GG, Maxwell L, Niedringhaus K. *Thelazia callipaeda* eyeworms in American black bear, Pennsylvania, USA. 2023. Emerg Infect Dis. 2024;30:1961–4.
11. Spoorenberg N, Köhler CF, Vermeulen E, Jurriaans S, Cornelissen M, Persson KEM, et al. Autochthonous human babesiosis caused by *Babesia venatorum*, the Netherlands. Emerg Infect Dis. 2024;30:1934–8.
12. Walter KS, Carpi G, Caccone A, Diuk-Wasser MA. Genomic insights into the ancient spread of Lyme disease across North America. Nat Ecol Evol. 2017;1:1569–76. https://doi.org/10.1038/s41559-017-0282-8
13. Weinberg HB. Winslow Homer (1836–1910). In: Heilbrunn timeline of art history. New York: The Metropolitan Museum of Art; 2000 [cited 2024 Aug 2]. http://www.metmuseum.org/toah/hd/homr/hd_homr.htm

Address for correspondence: Byron Breedlove, EID Journal, Centers for Disease Control and Prevention, 1600 Clifton Rd NE, Mailstop H16-2, Atlanta, GA 30329-4018, USA; email: wbb1@cdc.gov

EMERGING INFECTIOUS DISEASES®

Upcoming Issue • October 2024
Vectorborne Diseases

- Temporal Characterization of Prion Shedding in Secreta of White-Tailed Deer in Longitudinal Study of Chronic Wasting Disease, United States
- Population Structure and Antimicrobial Resistance in *Campylobacter jejuni* and C. coli Isolated from Humans with Diarrhea and Poultry, East Africa
- Fatal Renal Abscess Caused by *Porphyromonas gingivalis* and Subcapsular Hemorrhage, Japan
- Dengue Virus Serotype 3 Origins and Genetic Dynamics, Jamaica
- Challenges from Migration of *Amblyomma maculatum* Ticks and *Rickettsia parkeri* into the Northeastern United States
- One Health Investigation into Mpox and Pets, United States
- Associations between Minority Health Social Vulnerability Index Scores, Rurality, and Histoplasmosis Incidence, Eight US States
- Age- and Gender-Specific Differences in Lyme Disease Health-Related Behaviors, Ontario, Canada, 2015–2022

Complete list of articles in the October issue at https://wwwnc.cdc.gov/eid/#issue-314

Earning CME Credit

To obtain credit, you should first read the journal article. After reading the article, you should be able to answer the following, related, multiple-choice questions. To complete the questions (with a minimum 75% passing score) and earn continuing medical education (CME) credit, please go to http://www.medscape.org/journal/eid. Credit cannot be obtained for tests completed on paper, although you may use the worksheet below to keep a record of your answers.

You must be a registered user on http://www.medscape.org. If you are not registered on http://www.medscape.org, please click on the "Register" link on the right hand side of the website.

Only one answer is correct for each question. Once you successfully answer all post-test questions, you will be able to view and/or print your certificate. For questions regarding this activity, contact the accredited provider, CME@medscape.net. For technical assistance, contact CME@medscape.net. American Medical Association's Physician's Recognition Award (AMA PRA) credits are accepted in the US as evidence of participation in CME activities. For further information on this award, please go to https://www.ama-assn.org. The AMA has determined that physicians not licensed in the US who participate in this CME activity are eligible for AMA PRA Category 1 Credits™. Through agreements that the AMA has made with agencies in some countries, AMA PRA credit may be acceptable as evidence of participation in CME activities. If you are not licensed in the US, please complete the questions online, print the AMA PRA CME credit certificate, and present it to your national medical association for review.

Article Title

Clinical Aspects and Disease Severity of *Streptococcus dysgalactiae* Subspecies *equisimilis* Bacteremia, Finland

CME Questions

1. Which of the following was the most common clinical presentation of *Streptococcus dysgalactiae* subspecies *equisimilis* (SDSE) bacteremia in the current study?

A. Endocarditis
B. Purulent skin infection
C. Cellulitis
D. Pneumonia

2. Which of the following statements regarding antibiotic therapy of SDSE bacteremia in the current study is most accurate?

A. Most patients received second-generation cephalosporins
B. Most SDSE isolates were resistant to penicillins
C. One-quarter of SDSE isolates were resistant to cephalosporins
D. All SDSE isolates were sensitive to erythromycin

3. Which of the following statements regarding outcomes of the current cohort study of patients with SDSE bacteremia is most accurate?

A. The 30-day case-fatality rate was 6%
B. A shorter duration of symptoms before admission was associated with a higher risk for mortality
C. Nearly 30% of patients were admitted to the intensive care unit (ICU)
D. <5% of patients required surgical intervention

4. Which of the following objective tools was most helpful in predicting the risk for severe SDSE disease in the current study?

A. Pulse rate and respiratory rate
B. Platelet level and procalcitonin level
C. White blood cell count and C-reactive protein
D. Hemoglobin level and blood pressure

Earning CME Credit

To obtain credit, you should first read the journal article. After reading the article, you should be able to answer the following, related, multiple-choice questions. To complete the questions (with a minimum 75% passing score) and earn continuing medical education (CME) credit, please go to http://www.medscape.org/journal/eid. Credit cannot be obtained for tests completed on paper, although you may use the worksheet below to keep a record of your answers.

You must be a registered user on http://www.medscape.org. If you are not registered on http://www.medscape.org, please click on the "Register" link on the right hand side of the website.

Only one answer is correct for each question. Once you successfully answer all post-test questions, you will be able to view and/or print your certificate. For questions regarding this activity, contact the accredited provider, CME@medscape.net. For technical assistance, contact CME@medscape.net. American Medical Association's Physician's Recognition Award (AMA PRA) credits are accepted in the US as evidence of participation in CME activities. For further information on this award, please go to https://www.ama-assn.org. The AMA has determined that physicians not licensed in the US who participate in this CME activity are eligible for AMA PRA Category 1 Credits™. Through agreements that the AMA has made with agencies in some countries, AMA PRA credit may be acceptable as evidence of participation in CME activities. If you are not licensed in the US, please complete the questions online, print the AMA PRA CME credit certificate, and present it to your national medical association for review.

Article Title

Mortality Rate and Cause of Death in Adults with Extrapulmonary Nontuberculous Mycobacteria Infection, Denmark

CME Questions

1. What was the rate of increased mortality associated with extrapulmonary nontuberculous mycobacterial (E-NTM) disease after adjustment for comorbidity in the current study?

A. 2% (no significant difference vs control participants)
B. 34%
C. 115%
D. 488%

2. Which of the following causes of death were more common in the control vs E-NTM disease cohorts in the current study?

A. Respiratory disease and cardiovascular disease
B. Hematologic malignancy and respiratory disease
C. Hematologic malignancy and solid malignant neoplasms
D. Cardiovascular disease and solid malignant neoplasms

3. Which of the following causes of death was most important in driving the difference between the E-NTM disease and control cohorts in the current study?

A. HIV
B. Hematologic malignancy
C. End-stage kidney disease
D. Respiratory disease

4. Which of the following statements regarding mortality in the E-NTM vs control cohorts in the current study is most accurate?

A. E-NTM disease was associated with a higher risk for death among women vs men
B. E-NTM disease was associated with a higher risk for death among men vs women
C. E-NTM disease was associated with a higher risk for death only among persons born outside Denmark
D. E-NTM disease was associated with its highest risk for death during the first 3 years of follow-up